POLYPUBLIE
Polytechnique Montréal

Titre: Title:	Experimental and Thermodynamic Study on the Mg-X (X : Ag, Ca, In, Li, Na, Sn, Sr and Zn) Multicomponent Systems
Auteur: Author:	Jian Wang
Date:	2014
Type:	Mémoire ou thèse / Dissertation or Thesis
Référence: Citation:	Wang, J. (2014). Experimental and Thermodynamic Study on the Mg-X (X : Ag, Ca, In, Li, Na, Sn, Sr and Zn) Multicomponent Systems [Ph.D. thesis, École Polytechnique de Montréal]. PolyPublie. https://publications.polymtl.ca/1361/

Document en libre accès dans PolyPublie
Open Access document in PolyPublie

URL de PolyPublie: PolyPublie URL:	https://publications.polymtl.ca/1361/
Directeurs de recherche: Advisors:	Patrice Chartrand, In-Ho Jung, & Mamoun Medraj
Programme: Program:	Génie métallurgique

UNIVERSITÉ DE MONTRÉAL

EXPERIMENTAL AND THERMODYNAMIC STUDY ON THE Mg-X (X: Ag, Ca, In, Li, Na, Sn, Sr and Zn) MULTICOMPONENT SYSTEMS

JIAN WANG

DÉPARTEMENT DE GÉNIE CHIMIQUE

ÉCOLE POLYTECHNIQUE DE MONTRÉAL

THÈSE PRÉSENTÉE EN VUE DE L'OBTENTION

DU DIPLÔME DE PHILOSOPHIAE DOCTOR

(GÉNIE MÉTALLURGIQUE)

JANVIER 2014

Cette thèse intitulée:

EXPERIMENTAL AND THERMODYNAMIC STUDY ON THE Mg-X (X: Ag, Ca, In, Li, Na, Sn, Sr and Zn) MULTICOMPONENT SYSTEMS

présentée par : WANG Jian

en vue de l'obtention du diplôme de : Philosophiae Doctor

a été dûment acceptée par le jury d'examen constitué de :

M. PELTON Arthur, Ph. D., président

M. CHARTRAND Patrice, Ph. D., membre et directeur de recherche

M. JUNG In-Ho, Ph. D., membre et codirecteur de recherche

M. MEDRAJ Mamoun, Ph. D., membre et codirecteur de recherche

M. BALE Christopher, Ph. D., membre

M. LAROUCHE Daniel, Ph. D., membre

DEDICACE

To my Beloved Family

ACKNOWLEDGEMENTS

Résumé

Les alliages de magnésium, considérés à l'heure actuelle comme les plus légers des matériaux métalliques structurels, sont utilisés dans les industries automobile, électronique et aérospatiale. Ils présentent une faible densité, une résistance mécanique par rapport au poids très élevée, de bonnes propriétés de transformation, ainsi que la possibilité d'être recyclés presque complètement.

Jusqu'à présent, plusieurs séries d'alliages de magnésium ont été développées pour diverses applications, notamment les séries Mg-Al, Mg-Zn, Mg-Mn, Mg-terres rares, etc. Ces alliages de magnésium présentent certaines faiblesses, notamment une résistance à la corrosion médiocre, une faible résistance à la déformation à température élevée, ainsi qu'une faible robustesse.

Pour toutes ces raisons, il apparait nécessaire d'améliorer les propriétés des alliages actuels en développant de nouveaux alliages à base de magnésium pour répondre à la demande de l'industrie. La technologie de microalliage est largement utilisée pour améliorer les propriétés mécaniques des alliages. Des recherches récentes montrent que l'ajout de métaux comme Li, Na, Ca, Zn, Ag, Au, Sr et Sn au cours de la fabrication peuvent améliorer les propriétés mécaniques des alliages à base de magnésium.

En développant de nouveaux alliages, il est important de comprendre leur constitution (microstructure) et leur comportement thermodynamique. L'obtention de telles informations par le biais des techniques expérimentales est lourde et coûteuse. Les diagrammes de phase, sous forme de graphique visualisant l'état d'équilibre, dans un système, en fonction de la température, de la pression et des constituants, se révèlent être un moyen utile pour la conception et le traitement des matériaux. De plus, la modélisation thermodynamique des systèmes multi-composants par une approche de type CALPHAD (« Calculation of Phase Diagrams ») est un moyen très efficace d'étude des équilibres de phases. Avec l'aide des calculs thermochimiques, non seulement les systèmes binaires et ternaires sont étudiés, mais également les systèmes multi-composants.

Dans le cadre de projets en cours dans notre groupe de recherche pour développer une banque de données thermodynamiques des alliages multi-composants à base de magnésium, l'objectif

principal du présent travail est d'obtenir des modèles pour les énergies de Gibbs des phases et d'établir une banque de données des paramètres thermodynamiques de ces modèles qui soit cohérente pour le système multi-composant à base de magnésium, avec des éléments comme Ag, Ca, In, Li, Na, Sn, Sr et Zn, afin de fournir une explication à la conception du système des alliages de magnésium, en utilisant la modélisation informatique et des recherches expérimentales. De nombreux systèmes binaires et ternaires du système à composants multiples Mg-X (X: Ag, Ca, In, Li, Na, Sn, Sr et Zn) ont été évalués de façon critique puis optimisés de façon systématique.

Premièrement, les mesures des équilibres de phase sur cinq systèmes ternaires du système Mg-Sn-X (X: Ag, Au, Zn, Ca et Sr) ont été effectuées dans le présent travail. Les équilibres de phases dans la région riche en Mg des systèmes ternaires Mg-Sn-In (à 415 ^{o}C et à 330 ^{o}C), Mg-Sn-Ag (à 415 ^{o}C et à 330 ^{o}C) et Mg-Sn-Zn (à 300 ^{o}C) ont été déterminés par diffraction aux rayons X, microanalyse par sonde électronique, et par des expériences de d'équilibre et de trempe. Les sections isoplèthes ternaires avec 5% In et 10% Sn du système Mg-In-Sn, 10% Sn et 30% Ag du système Mg-Sn-Ag et 10% Sn du système Mg-Sn-Zn, ont été déterminées par calorimétrie différentielle à balayage (DSC). Aucun composé ternaire n'a été retrouvé dans les sections isothermes des systèmes Mg-Sn-In, Mg-Sn-Ag et Mg-Sn-In. Les sections isothermes des systèmes ternaires Mg-Sn-Ca et Mg-Sn-Sr dans la région riche en magnésium à 350 ^{o}C et à 415 ^{o}C ont été déterminées par analyse dispersive de l'énergie (technique EDS), par microscopie électronique à balayage, et par des essais de trempe. L'existence des phases ternaires MgSnCa et MgSnSr a été confirmée dans cette étude. Deux nouvelles phases ternaires Mg_5Sn_3Sr et $Mg_{25}Sn_{24}Sr_{14}$ ont été retrouvées dans les sections isothermes Mg-Sn-Sr à 415 ^{o}C et 350 ^{o}C.

Deuxièmement, la modélisation des propriétés thermodynamiques et des équilibres de phases des 19 systèmes binaires (Mg-In, Mg-Ag, Ag-Zn, Ag-Ca, Ag-Li, In-Na, Na-Sn, Li-Sn, Na-Zn, In-Zn, Sn-Sr, Ca-Li, Ca-Sn, In-Sn, Ca-In, Ca-Na, Ag-In, Ag-Na et Ag-Sn) et des 13 systèmes ternaires (Mg-Sn-X (X: Ag, In, Li, Zn, Ca, et Sr), Mg-Zn-In, Mg-Ag-In, Mg-Ca-Li, Mg-Ca-Sr, Mg-Sn-In et In-Sn-Zn)) a été effectuée dans cette étude. Cette description, basée sur une revue critique de la littérature et l'optimisation de type CALPHAD des paramètres des modèles d'énergie de Gibbs des phases, s'est focalisée sur les propriétés du solide (composés intermétalliques, formes cristallographiques, températures de fusion, enthalpie de formation, températures de transition de phases, etc.) et du liquide (enthalpie de mélange intégrale, enthalpie de mélange partielle,

activités des composants, capacités calorifiques, solubilités du solide, etc.) ainsi que sur les données expérimentales des diagrammes de phases. Le modèle Quasichimique Modifié par Approximation de Paires (MQMAP) a été appliqué à la solution liquide qui a montré un degré élevé d'ordonnancement à courte distance. Les phases solides ont été modélisées à l'aide du formalisme basé sur l'énergie des composés (Compound Energy Formalism). Une banque de données thermodynamiques cohérente contenant les paramètres des modèles de chaque phase a été établie pour les systèmes multi-composants Mg-X(X: Ag, Ca, In, Li, Na, Sn, Sr et Zn).

Troisièmement, quelques applications de la banque de données thermodynamiques sont présentées. De plus, les études expérimentales de formabilité du verre métallique des alliages Mg-Zn-X (Ag, Sr, In, *etc*) sélectionnés, pour des applications avec la présente banque de données thermodynamiques, ont été effectuées avec la collaboration de Mr. Yi-Nan Zhang de l'Université de Concordia. Les équilibres de phase Mg-Zn-Sr à 300 ºC dans l'intervalle 0-30 % Sr ont été mesurés par des méthodes d'échantillonnage et de diffusion des couples d'échantillons. Quatre nouveaux composés ternaires ont été retrouvés dans cette section isotherme. La formabilité du verre des deux séries d'alliages Mg-Zn-Sr, de composition Mg88-xZnxSr2 (28≤x≤38) et Mg85-yZnySr5 (23≤y≤37) a été étudiée expérimentalement dans ce travail. La banque de données thermodynamiques des systèmes multi-composants Mg-X (X: Ag, Ca, In, Li, Na, Sn, Sr and Zn) fournira une ligne directrice claire pour la sélection et la conception des alliages à base de magnésium, ce qui permettra d'éviter des expériences improductives portant sur des alliages qui ont moins de potentiels pour des applications pratiques.

ABSTRACT

Magnesium alloys, as the current lightest structural metallic materials, have been widely used in automotive, electronic consumer, and aerospace industries. This interest in the use of magnesium alloys arises from their low density and potentially high strength/weight ratios, good processing properties, as well as the possibility of nearly complete recycling. Hitherto, several series of magnesium alloys have been developed for different applications. These alloys include Mg-Al, Mg-Zn, Mg-Mn, and Mg-Rare-earths, *etc*. However, magnesium alloys display shortcomings. Among them are poor corrosion behavior, low creep resistance at elevated temperatures, and low strength. Consequently, improvements are still needed in the properties of current alloys and in the development of new Mg-based alloys to meet the requirements of industry. Microalloying has been widely used for improving the mechanical properties of alloys. Current research shows that additions of Li, Na, Ca, Zn, Ag, In, Sr, and Sn can improve the mechanical properties of Mg-based alloys, by forming secondary precipitates in the Mg matrix.

In developing new magnesium alloys, it is important to understand their constitution (microstructure) and thermodynamic behaviour. Obtaining such information solely through experiment is cumbersome and costly. Phase diagrams, as a visual representation of the state of equilibrium in a system as a function of temperature, pressure and component composition, have been proved to be a useful aid for materials design and processing. Thermodynamic modeling on multi-component systems by the CALPHAD approach has been shown to be a very efficient way of investigating phase equilibria. With the help of computational thermochemistry, not only binary and ternary systems, but also multi-component systems, can be investigated properly.

As part of ongoing projects in our group to develop a thermodynamic database for Mg-based multicomponent alloys, the main objective of the present work is to establish such a database with added Ag, Ca, In, Li, Na, Sn, Sr and Zn. This is expected to provide a guide for magnesium alloy design, through computational modeling and experimental investigations. Numerous binary and ternary systems in the Mg-X (X: Ag, Ca, In, Li, Na, Sn, Sr and Zn) multicomponent system have been critically evaluated and systematically optimized in the present work.

First, phase equilibria measurements on the five ternary systems: Mg-Sn-X (X: Ag, In, Zn, Ca, and Sr) system have been carried out. Phase equilibria in the Mg-rich region of the Mg-Sn-In (415 and 330 ^{o}C), Mg-Sn-Ag (415 and 330 ^{o}C), and Mg-Sn-Zn (300 ^{o}C) ternary systems were

inverstigated by quenching, electron probe micro-analysis (EPMA), and X-ray diffraction (XRD). Ternary isoplethal sections at constant compositions were inverstigated using differential scanning calorimetry (DSC). These were Mg-In-Sn (5 at. %, 10 at. % Sn), Mg-Sn-Ag (10 at. % Sn, 30 at.% Ag0 and Mg-Sn-Zn (10 at.% Sn). No ternary compounds were found in these three isothermal sections. Iisothermal sections of the Mg-Sn-Ca and Mg-Sn-Sr systems in the Mg-rich region (350 and 415 ^{o}C) were inverstigated by quenching key samples. SEM and EDS were used for phase composition analysis. The existence of the ternary phases MgSnCa and MgSnSr was confirmed, and two new ternary phases (Mg_5Sn_3Sr and $Mg_{25}Sn_{24}Sr_{14}$) were found in Mg-Sn-Sr isothermal sections at 415 and 350 ^{o}C.

Second, thermodynamic descriptions of 19 binary systems (Mg-In, Mg-Ag, Ag-Zn, Ag-Ca, Ag-Li, In-Na, Na-Sn, Li-Sn, Na-Zn, In-Zn, Sn-Sr, Ca-Li, Ca-Sn, In-Sn, Ca-In, Ca-Na, Ag-In, Ag-Na and Ag-Sn) and 12 ternary systems (Mg-Sn-X, X: Ag, In, Li, Zn, Ca, and Sr, Mg-Zn-In, Mg-Ag-In, Mg-Ca-Li, Mg-Ca-Sr, Mg-Sn-In, and In-Sn-Zn) have been carried out in the present work. These were based on literature review of the solid solutions including intermetallic compounds (crystal structures, melting points, enthalpies of formation, transformation temperatures, *etc*.). The same has been done for liquid solutions (liquidus curves, integral enthalpies of mixing, partial enthalpies of mixing, activities of the components, heat capacities, *etc*.). The Modified Quasichemical Model in the Pair Approximation (MQMPA) was used for modeling the liquid solution, which exhibits a high degree of short-range order. The solid phases are modeled with the Compound Energy Formalism (CEF). A self-consistent thermodynamic database was constructed for the Mg-X (X: Ag, Ca, In, Li, Na, Sn, Sr and Zn) multicomponent system.

Third, some applications with the complete thermodynamic database are shown. A study of alloy design for Mg-based multicomponent systems was carried out. The effects of In, Li and Na additions on the properties of Mg-Sn based alloys was also studied.

Futhermore, an experimental study of metallic glass formability in selected Mg-Zn-X ternary systems have been done with the collaboration of Mr. Yi-Nan Zhang of Concordia University. Phase equilbria in the Mg-Zn-Sr ternary system, at 300 ^{o}C in the composition range 0-30 at. % Sr, were measured in the present work using key samples and the diffusion-couple technique. Four new ternary compounds were found in this isothermal section. The glass formability of two

series of Mg-Zn-Sr alloys of compostions $Mg_{88-x}Zn_xSr_2$ ($28 \leq x \leq 38$) and $Mg_{85-y}Zn_ySr_5$ ($23 \leq y \leq 37$) were studied experimentally in the present work.

Use of the thermodynamic database of the Mg-X (X: Ag, Ca, In, Li, Na, Sn, Sr and Zn) multicomponent system provides clear guidelines for selection of Mg-based alloys for design, thereby avoiding tedious and time-consuming experiments.

CONDENSÉ EN FRANÇAIS

Les alliages de magnésium sont actuellement les matériaux métalliques structuraux les plus légers et à ce titre ils ont été utilisés dans l'automobile, l'électronique grand public et l'industrie aérospatiale. L'intérêt pour l'utilisation des alliages de magnésium vient de leur faible densité et de leur rapport résistance/poids potentiellement élevé, de leurs bonnes propriétés de transformation, ainsi que de la possibilité de les recycler presque complètement. Jusqu'à présent, plusieurs séries d'alliages de magnésium ont été développées pour différentes applications, qui comprennent les séries Mg-Al, Mg-Zn, Mg-Mn, et Mg-terre rare *etc*. Mais les alliages de magnésium ont encore des défauts tels qu'une faible résistance à la corrosion, une faible résistance au fluage à la température d'évaluation, une faible résistance,… Par conséquent, il est encore nécessaire d'améliorer les propriétés des alliages actuels et de développer de nouveaux alliages à base de Mg pour répondre à la demande de l'industrie. La méthode de microalliage a été largement utilisée pour améliorer les propriétés mécaniques d'un alliage. Des recherches récentes montrent que des additions de Li, Na, Ca, Zn, Ag, In, Sr et Sn peuvent améliorer les propriétés mécaniques des alliages à base de Mg avec des précipités secondaires dans la matrice de Mg.

En développant de nouveaux alliages, il est important de comprendre leur constitution (microstructure) et leur comportement thermodynamique. L'obtention de telles informations uniquement à travers des techniques expérimentales est lourde et coûteuse. Les diagrammes de phases, sous forme de graphique visuel de l'état d'équilibre dans un système en fonction de la température, de la pression et des composants constitutifs, se sont avérés être une feuille de route utile pour la conception et la transformation des matériaux. De plus, il a été démontré que la modélisation thermodynamique de systèmes multi-composants par l'approche de type CALPHAD (« Calculation of Phase Diagrams ») est un moyen très efficace pour étudier les équilibres de phases. A l'aide de calculs thermochimiques, non seulement des systèmes binaires et ternaires, mais aussi des systèmes multi-composants peuvent être étudiés correctement.

Dans le cadre de projets en cours dans notre groupe pour développer une base de données thermodynamiques pour des alliages multi-composants à base de Mg, l'objectif principal du présent travail est d'établir une base de données thermodynamiques cohérente pour le système

multi-composant à base de Mg ayant comme additifs Ag, Ca, In, Li, Na, Sn, Sr et Zn de façon à assurer la compréhension et l'orientation nécessaires à la conception d'alliages de magnésium à travers la modélisation par ordinateur et des études expérimentales. De nombreux systèmes binaires et ternaires du système multi-composant Mg-X (X : Ag, Ca, In, Li, Na, Sr et Zn) ont été évalués de façon critique et optimisés de manière systématique.

Les objectifs prioritaires de ce travail sont les suivants :

(1) Une évaluation critique des données expérimentales et une description thermodynamique seront menées pour les 19 systèmes binaires : Mg-In, Mg-Ag, Ag-Zn, Ag-Ca, Ag-Li, In-Na, Na-Sn, Li-Sn, Na-Zn, In-Zn, Sn-Sr, Ca-Li, Ca-Sn, In-Sn, Ca-In, Ca-Na, Ag-In, Ag-Na et Ag-Sn.

(2) Les mesures expérimentales seront axées sur les 5 systèmes ternaires : Mg-Sn-X (X : Ag, In, Zn, Ca et Sr)

(3) Une description thermodynamique des 13 systèmes ternaires suivants sera effectuée : Mg-Sn-X (X : Ag, In, Li, Zn, Ca et Sr), Mg-Zn-In, Mg-Ag-In, Mg-Ca-Li, Mg-Ca-Sr, Mg-Sn-In, et In-Sn-Zn.

Les objectifs secondaires du présent travail sont les suivants :

(1) Utilisation de calculs de base de données thermodynamiques pour analyser le comportement en solidification d'alliages sélectionnés à base de Mg-Sn à des températures élevées.

(2) Analyse de l'effet combiné de Ag, Li, Ca, In, Sr et Zn sur les alliages sélectionnés à base de Mg-Sn.

En outre, l'étude expérimentale de la formabilité de verre métallique à partir d'alliages Mg-Zn-X (X : Ag, Sr, In, *etc*) sélectionnés en guise d'application de la présente base de données thermodynamiques a été réalisée en collaboration avec M. Yi-Nan Zhang de l'Université Concordia.

Dans le chapitre 1, un aperçu de la littérature sur le développement d'alliages à base de Mg et la méthode CALPHAD est présenté. Ensuite, les objectifs incluant l'énoncé du problème et la sélection sont décrits.

Dans le chapitre 2, une description générale des méthodes utilisées dans le présent travail, incluant la méthode CALPHAD de calcul thermodynamique (« Calculation of Phase Diagram »),

et les techniques expérimentales de mesure du diagramme de phases sont introduites. Le Modèle Quasichimique Modifié dans l'Approximation des Paires (MQMAP) est utilisé pour la description des propriétés thermodynamiques de la solution liquide, et le « Compound Energy Formalism » (CEF) a été utilisé pour décrire l'énergie de Gibbs des phases de solution solide. Dans le travail expérimental, les techniques de touche - échantillon, de couple de diffusion et de Calorimétrie Différentielle à Balayage (DSC) sont utilisées pour les mesures d'équilibres de phases. Les techniques de Microsonde Electronique (EPMA), de Microscopie Electronique à Balayage (SEM) et de diffraction des rayons X (XRD) sont utilisées pour la microstructure, la structure cristalline des phases et l'analyse de la composition des phases.

Dans le chapitre 3, l'organisation de cette thèse est décrite.

Dans le chapitre 4, l'article intitulé « Evaluation thermodynamique et optimisation des systèmes binaires Na-X (X : Ag, Ca, In, Sn, Zn) à l'aide de la méthode Calphad et des calculs ab-initio », publié dans « The Journal of Chemical Thermodynamics », est présenté. Le chapitre 4 est principalement axé sur l'évaluation des données expérimentales et sur l'optimisation thermodynamique des équilibres de phases des sous-systèmes binaires Na-X (X : Ag, Ca, In, Sn et Zn) à base de Na. Cet article comporte une revue critique de la littérature approfondie et une optimisation thermodynamique de ces cinq sous-systèmes binaires (Na-X avec X = Ag, Ca, In, Sn et Zn) combinée à des calculs ab-initio de l'enthalpie de formation de composés binaires sélectionnés. Les calculs ab-initio ont été effectués par M. N. Miao indépendamment, en collaboration. Les paramètres thermodynamiques des fonctions d'énergie de Gibbs pour toutes les phases permettent de reproduire avec une bonne précision les données expérimentales retenues lors de l'analyse critique. Il a été démontré dans les optimisations actuelles des systèmes binaires Na-Sn et Na-In que le Modèle Quasichimique Modifié dans l'Approximation des Paires (MQMAP) pour la phase liquide, qui prend en compte l'ordre à courte distance entre les paires premiers-voisins, est capable de très bien reproduire les données expérimentales avec les courbes typiques d'enthalpie intégrale de mélange en forme de "V" (et les inflexions associées dans les courbes d'enthalpie partielle de mélange), de même que les courbes typiques d'entropie intégrale de mélange en forme de « m » (plus réalistes).

Dans le chapitre 5, l'article intitulé « Optimisations thermodynamiques du système binaire Li-Sn et du système ternaire Mg-Sn-Li » est présenté. Il a été soumis pour publication dans le journal

« CALPHAD : Computer Coupling of Phase Diagrams and Thermochemistry » (Wang, et al., 2013). Dans cet article, une évaluation critique des données expérimentales et l'optimisation thermodynamique du système ternaire Mg-Sn-Li a été réalisée à l'aide de calculs ab-initio et de la méthode CALPHAD. A partir des données expérimentales et des résultats prédits à partir des calculs ab-initio (les calculs ab-initio ont été terminés par M. Han indépendamment), les paramètres du modèle thermodynamique pour tous les solides et la phase liquide du système binaire Li-Sn et du système ternaire Mg-Li-Sn ont été optimisés. Nous avons également présenté dans l'article une comparaison entre une optimisation précédente du système binaire Li-Sn à l'aide du modèle de mélange aléatoire de Bragg-Williams (BWM) pour la phase liquide et la présente optimisation à l'aide du Modèle Quasichimique Modifié dans l'Approximation des Paires (MQMAP) pour la phase liquide. Nous avons ainsi montré l'avantage important du MQMAP pour modéliser les propriétés thermodynamiques des solutions liquides, en particulier dans les systèmes très ordonnés.

Dans le chapitre 6, le troisième article intitulé « Etude expérimentale et thermodynamique du système quaternaire Mg-Sn-In-Zn » soumis pour publication dans le journal « Journal of Alloys and Compounds » (Wang, et al., 2013) est présenté. Dans ce chapitre, les équilibres de phases dans la région riche en Mg du système ternaire Mg-Sn-In à 415°C et à 330°C, et les sections ternaires isoplèthes Mg-Sn-In à 10 % molaire de Sn et à 5 % molaire de In ont été étudiés. Les équilibres de phases dans la région riche en Mg du système ternaire Mg-Sn-Zn à 300°C ont également été déterminés dans le présent travail ; ils sont en accord avec les données expérimentales antérieures de Godecke et Sommer (Godecke & Sommer, 1994) et de Gladyshevsky et Cherkashin (Gladyshevsky & Cherkashin, 1959) à l'intérieur de l'erreur expérimentale. La section isoplèthe ternaire Mg-Sn-Zn à 10 % molaire de Sn a aussi été mesurée dans le présent travail à l'aide de mesures de DSC. Tous les résultats expérimentaux issus d'études antérieures et le présent travail s'accordent raisonnablement. Toutes les données expérimentales pour les sous-systèmes binaires Mg-In, Zn-In et In-Sn ainsi que pour les sous-systèmes ternaires Mg-Sn-In, Mg-Sn-Zn et In-Sn-Zn ont été évaluées de manière critique et ont été optimisées thermodynamiquement dans le présent travail à l'aide du MQMAP pour la phase liquide. L'avantage important du MQMAP pour modéliser les propriétés thermodynamiques des solutions liquides, en particulier dans les systèmes très ordonnés, a été très bien démontré dans les travaux précédents (Chartrand & Pelton, 2000b ; Jin, et al., 2010, 2011). Enfin, une base de

données thermodynamiques auto-cohérente pour le système quaternaire Mg-Sn-In-Zn a été préparée dans le présent travail ; il s'agit d'un travail important pour la construction de la base de données thermodynamiques du système multi-composant Mg-X (X : Ag, Ca, In, Li, Na, Sn, Sr et Zn).

Dans le chapitre 7, le quatrième article intitulé « Etude expérimentale et thermodynamique du système quaternaire Mg-Sn-Ag-In » soumis pour publication dans le journal « Journal of Phase Equilibria and Diffusion » (Wang, et al., 2013) est présenté. Les équilibres de phases mesurés dans le système ternaire Mg-Sn-Ag sont présentés dans cet article. Une optimisation thermodynamique du système quaternaire Mg-Sn-Ag-In a été réalisée à l'aide de la méthode CALPHAD. Une évaluation critique et thermodynamique des systèmes binaires Ag-Mg, Ag-Sn et Ag-Mg est présentée. Pour le système binaire Ag-Mg, en comparaison avec l'optimisation précédente de Lim *et al.* (Lim et al., 1997), les phases ordonnées bcc (bcc_A2 et bcc_B2) et fcc (fcc_A1 et fcc_L12) ont été modélisées avec une structure de deux sous-réseaux, et la structure cristalline de symétrie a été prise en compte lors de l'ajustement des paramètres thermodynamiques. De plus, toutes les phases et leur solubilité à l'état solide rapportées dans le travail précédent ont été prises en compte. Dans le présent travail, après une évaluation critique de toutes les données expérimentales disponibles, une réoptimisation thermodynamique stricte du diagramme de phases du système binaire Ag-In a été effectuée à partir des données précédentes et des données expérimentales obtenues récemment, et toutes les phases existant de manière réaliste ont été considérées. Les équilibres de phases dans les systèmes ternaires Mg-Ag-In, Mg-Sn-Ag et Ag-In-Sn ont été optimisés thermodynamiquement dans le présent travail à partir des données expérimentales disponibles ; ils sont également présentés dans le présent chapitre. Enfin, en utilisant notre optimisation thermodynamique précédente du système ternaire Mg-Sn-In décrite dans le chapitre 7, nous avons préparé une banque de données thermodynamiques auto-cohérente pour le système quaternaire Mg-Sn-Ag-In à l'aide des données expérimentales limitées rapportées (Kolesnichenko, et al., 1989).

Dans le chapitre 8, le travail intitulé « Etude expérimentale et thermodynamique du système quinaire Mg-Sn-Ca-Li-Sr », qui sera soumis pour publication dans un avenir proche, est présenté. Dans ce chapitre, les équilibres de phases mesurés dans les systèmes ternaires Mg-Sn-Ca et Mg-Sn-Sr sont présentés. Les équilibres de phases dans la zone riche en Mg des systèmes ternaires Mg-Sn-Ca et Mg-Sn-Sr ont été mesurés à 415°C et à 350°C dans le présent travail. L'existence

des phases ternaires MgSnCa et MgSnSr a été confirmée. Deux nouvelles phases ternaires, Mg_5Sn_3Sr et $Mg_{25}Sn_{24}Sr_{14}$, ont été mises en évidence dans les sections isothermes Mg-Sn-Sr à 415^oC et à 350^oC. D'autres expériences sont nécessaires pour déterminer la structure cristalline et la stabilité thermique des composés nouvellement trouvés. La présente évaluation critique et optimisation thermodynamique des sous-systèmes binaires Ca-Sn, Sn-Sr et Ca-Li et des sous-systèmes ternaires Mg-Sn-Ca, Mg-Sn-Sr, Mg-Ca-Sr et Mg-Ca-Li est présentée. Enfin, une base de données thermodynamiques auto-cohérente pour le système quinaire Mg-Sn-Ca-Li-Sr a été préparée ; elle s'insère dans le développement de la base de données thermodynamiques finale pour le système multi-composant Mg-X (X : Ag, Ca, In, Li, Na, Sn, Sr et Zn).

Le chapitre 9 s'intitule « Optimisation thermodynamique des systèmes binaires Ag-X (X : Ca, Li, Zn) et Ca-In ». Il sera soumis pour publication à l'avenir. Puisque l'objectif final de la présente recherche est de développer une base de données thermodynamiques pour le système multi-composant Mg-X (X : Ag, Ca, In, Li, Na, Sn, Sr et Zn), l'évaluation et l'optimisation des sous-systèmes binaires restants sont résumées dans le chapitre 9. Dans ce chapitre, l'évaluation expérimentale et l'optimisation thermodynamique des sous-systèmes binaires Ag-Ca, Ag-Li, Ag-Zn et Ca-In sont présentées.

Le chapitre 10 est une discussion générale de cette étude. Des exemples d'application de la base de données thermodynamiques résultante sont donnés.

Enfin, un travail de recherche en collaboration avec M. Yi-Nan Zhang de l'Université Concordia est présenté dans l'Annexe ; il s'agit d'une partie très intéressante et importante du présent travail de recherche portant sur le développement d'une base de données thermodynamiques pour le système multi-composant Mg-X (X : Ag, Ca, In, Li, Na, Sn, Sr et Zn). Ce travail s'intitule « Etude expérimentale et thermodynamique du système ternaire Mg-Zn-Sr et application au verre métallique" et est présenté en annexe ; il sera soumis pour publication dans un avenir proche. Ce travail consiste en la mesure d'équilibres de phases dans la section isotherme à 300^oC, et l'aptitude au formage de verre métallique du système ternaire Mg-Zn-Sr a été étudiée thermodynamiquement à l'aide de la présente base de données thermodynamiques. Selon les résultats des calculs, une série d'alliages a été étudiée dans le présent travail avec la coulée de filage-fraisage, la diffraction des rayons X (XRD), et la DSC pour l'étude du formage de verre métallique.

Les principales contributions de cette thèse de recherche en ingénierie des matériaux comprend :

Tout d'abord, des mesures d'équilibres de phases dans les 5 systèmes ternaires Mg-Sn-X (X : Ag, In, Zn, Ca et Sr) ont été effectuées. Les équilibres de phases dans la région riche en Mg des systèmes ternaires Mg-Sn-In (à 415°C et à 330°C), Mg-Sn-Ag (à 415°C et à 330°C), et Mg-Sn-Zn (à 300°C) ont été déterminés. Les sections isoplèthes ternaires des systèmes Mg-Sn-In (à 5 % molaire de In et à 10 % molaire de Sn), Mg-Sn-Ag (à 10 % molaire de Sn et à 30 % molaire de Ag), et Mg-Sn-Zn (à 10 % molaire de Sn) ont été mesurées. Les sections isothermes des systèmes ternaires Mg-Sn-Ca et Mg-Sn-Sr dans la région riche en Mg à 350°C et à 415°C ont été déterminées. L'existence des phases ternaires MgSnCa et MgSnSr a été confirmée. Deux nouvelles phases ternaires, Mg_5Sn_3Sr et $Mg_{25}Sn_{24}Sr_{14}$, ont été mises en évidence dans les sections isothermes Mg-Sn-Sr à 415°C et à 350°C.

Deuxièmement, la description thermodynamique de 19 systèmes binaires (Mg-In, Mg-Ag, Ag-Zn, Ag-Ca, Ag-Li, In-Na, Na-Sn, Li-Sn, Na-Zn, In-Zn, Sn-Sr, Ca-Li, Ca-Sn, In-Sn, Ca-In, Ca-Na, Ag-In, Ag-Na et Ag-Sn) et de 13 systèmes ternaires (Mg-Sn-X avec {X : Ag, In, Li, Zn, Ca et Sr}, Mg-Zn-In, Mg-Ag-In, Mg-Ca-Li, Mg-Ca-Sr, Mg-Sn-In et In-Sn-Zn) a été effectuée dans le présent travail à partir d'une revue de la littérature pour les solides (composés intermétalliques, structure cristalline, point de fusion, enthalpie de formation, température de transformation, *etc*), les propriétés du liquide (enthalpie intégrale de mélange, enthalpie partielle de mélange, activités des composants, capacités calorifiques, solubilité à l'état solide,…) et les données de diagrammes de phases expérimentales. Le Modèle Quasichimique Modifié dans l'Approximation des Paires (MQMAP) a été utilisé pour la solution liquide, qui présente un degré élevé d'ordre à courte distance. Les phases solides sont modélisées à l'aide du « Compound Energy Formalism » (CEF). Une base de données thermodynamiques auto-cohérente a été préparée pour le système multi-composant Mg-X (X : Ag, Ca, In, Li, Na, Sn, Sr et Zn).

En outre, les équilibres de phases à 300°C dans la gamme de composition 0-30 % molaire de Sr du système ternaire Mg-Zn-Sr ont été mesurés dans le présent travail à l'aide des techniques de touche - échantillon et de couple de diffusion, en collaboration avec M. Yi-Nan Zhang de l'Université Concordia. Quatre nouveaux composés ternaires ont été trouvés dans cette section isotherme. Le formage de verre pour deux séries d'alliages Mg-Zn-Sr avec la composition Mg88-xZnxSr2 (28 ≤ x ≤ 38) et Mg85-yZnySr5 (23 ≤ y ≤ 37) a été étudié expérimentalement.

La base de données thermodynamiques pour le système multi-composant Mg-X (X : Ag, Ca, In, Li, Na, Sn, Sr et Zn) fournira des lignes directrices claires pour la sélection et la conception d'alliages à base de Mg, évitant ainsi des expériences à long terme improductives avec des alliages ayant moins de potentiel pour des applications pratiques.

TABLE OF CONTENTS

LIST OF TABLES

LIST OF FIGURES

LIST OF SYMBOLS

at.%	Atomic percent
a_i	Activity of component i
a_{ji}^{φ}	Coefficient of the stoichiometry matrix composed of the constituents of phase φ
b_i	The total amount of the ith system component
C_p	Molar heat capacity (J/mol-K)
$C_p^{A_m B_n}$	Molar heat capacity of the compound $A_m B_n$ (J/mol-K)
G	The total Gibbs energy (J)
G_i^0	Standard Gibbs energy of i (J/mol)
G^{total}	Total Gibbs energy of system (J/mol)
ΔG	Gibbs energy change (J/mol)
ΔG_{mix}^{ex}	Molar excess Gibbs energy (J/mol)
G^{φ}	Molar Gibbs energy of phase φ (J/mol)
G_T^{φ}	The contribution to the total molar Gibbs energy by temperature (*T/K*) (J/mol)
G_P^{φ}	The contribution to the total molar Gibbs energy by pressure (*P/Pa*) (J/mol)
G_m^{φ}	The magnetic contribution to the total molar Gibbs energy (J/mol)
g_i^o	Molar Gibbs energy of component i (J/mol)
$\Delta H_{298.15K}^o$	Molar enthalpy of formation at 298.15 K (J/mol)
H_i^o	Standard enthalpy of element i (J/mol)
$^iL_{i,j:*}$	The interaction energies between i and j atoms (J/mol)
n	Number of moles of component (mol)
n_i	Number of moles of component i (mol)
n_{ij}	Number of moles of *i-j* pairs in a solution (mol)
n_j^{φ}	The amount of the jth constituent of phase φ (mol)
n_{φ}	The number of moles of φ phase (mol)
Δg_{AB}	Gibbs energy change for the formation of half mole of $(A-B)$ (J/mol)

g_{AB}^{ij}	Excess Gibbs energy of A and B (J/mol)
R	Ideal gas constant (8.31451 J/mol-K in FactSage)
S_i^o	Standard entropy of component i (J/mol-K)
ΔS^{config}	Configurational entropy of mixing of a solution (J/mol-K)
T	Absolute temperature (K)
T_M	Melting temperature (K)
T_g	Glass transition temperature (K)
T_{rg}	Reduced glass transition temperature (K)
$wt.\ \%$	Weight percent
x_i^{φ}	Mole fraction of element i in φ phase
X_i	Mole fraction of i
X_{ij}	Pair fraction of i-j pairs
y_i^{I} and y_i^{II}	Site fractions of elements i
Y_i	"Coordination-equivalent" fraction of i
γ_i	Activity coefficient of component i
Z_i	Coordination number of i, when all the nearest neighbors of an i are i's
Z_{ij}	Coordination number of i, when all the nearest neighbors of an i are j's
φ	Constituted phase of system
μ_i^{φ}	Chemical potential of component i (J/mol)

LIST OF ABBREVIATIONS

BWM	Bragg-Williams Model
CALPHAD	CALculation of PhAse Diagram
CEF	Compound Energy Formalism
DFT	Density Functional Theory
DSC	Differential Scanning Calorimentry
DTA	Differential Thermal Analysis
EDS	Energy Dispersive X-Ray Spectrometry
EMF	Electromotive Force
EPMA	Electron Probe Microanalysis
ES	Excess Stability function
FNN	First-nearest-neighbor pairs
GGA	Generalized Gradient Approximation
LDA	Local Density Approximation
LRO	Long-Range Order
MQM (MQMPA)	Modified Quasichemical Model in the Pair Approximation
MP	Monkhorst–Pack
PBE	Perdew-Burke-Ernzerhof gradient approximation
PAW	Projector Augmented plane Wave
SEM	Scanning Electron Microscopy
SRO	Short-Range Order
SGTE	Scientific Group Thermodata Europe
VASP	Vienna Ab initio Simulation Package
XRD	X-Ray Diffraction

LIST OF APPENDICES

CHAPITRE 1   INTRODUCTION

1.1   Literature review

Magnesium based alloys are widely used in the automotive and aeronautic industries because magnesium is the lightest structural material with a density about 1.80 g/cm^3. This interest in the use of magnesium alloys arises from their low density and potentially high strength/weight ratios, and good processing properties, as well as of near completely recycling possibilities (Polmear, 1994). Their high strength-to-weight ratio makes them even more attractive than steels in many applications (Kainer & Kaiser, 2003). Moreover, magnesium is the eighth most aboundance element on earth, and it can be extracted from sea water ($MgCl_2$), which makes Mg-based alloys relatively cheap. Consenquently, new Mg based alloys with a lower cost and superior properties are desirable if wider applications of Mg based alloys in structural applications are to be developed. Hitherto, several series of magnesium alloys have been developed for different applications. These include the Mg-Al, Mg-Zn, Mg-Mn, and Mg-Rare-earth series *etc*. The common alloying elements and their potential properties for Mg alloys are listed in Table 1.1.

The Mg-Al series, as one group of the more popular Mg-based alloys, is widely used because of its high strength-to-weight ratio, specific rigidity, good corrosion resistance and good ductility. The AM (Mg-Al-Mn based) and AZ (Mg-Al-Zn based) series offer very good performance as structural materials at ambient temperature. However, the existence of creep-induced precipitation of the $Al_{12}Mg_{17}$ phase greatly destroys the creep performance of Al-containing Mg alloys at elevated temperatures (above 150 $^{\circ}$C). This has made them inadequate for engine blocks or high temperature applications (Baril, et al., 2003). Therefore, many new Mg-based alloys (Al free series) are under development.

The Mg-Zn series is the first hardenable Mg-based alloy developed for structural materials (Avedesian & Baker, 1999). The high solid solubility of Zn in the Mg (hcp) phase and the considerable amount of secondary precipitates in the Mg matrix can produce a very good age-hardening effect (Gao & Nie, 2007). Unfortunately, the Mg-Zn series has the same problem as the Mg-Al series (but not the AE series), that is, poor mechanical properties at elevated temperatures which restrict its applications.

Table 1.1 Common alloying elements and their potential effects on properties of Mg alloys

Alloying element	Abbreviation letter (ASTM code)	Potential properties for Mg alloys
Al	A	Aluminium increases the tensile strength and hardness, improves castibalility
RE	E	Rare-earths increase the creep resistance, corrosion resistance, and high-temperature strength
Zr	K	Zirconium is the grain refining agent, which can increase the tensile strength without loss of ductility
Li	L	Lithium reduces density and increases ductility
Mn	M	Manganese increases the yield strength and improves salt water corrosion resistance and MgAl and MgAlZn alloys.
Ag	Q	Silver increases the age hardening response and high temperature properties of thorium or rare-earths containing alloys
Si	S	Silicon increases the fluidity of molten alloys, increases the creep resistance
Sn	T	Tin can increase the high temperature creep resistance , the tensile strength and corrosion resistance
Y	W	Yttrium improves high temperature strength and creep resistance
Zn	Z	Zinc increases the tensile strength and hardness, improves castibalility

Mg-Sn based alloys have stable microstructures and good mechanical properties at high temperatures due to the high solubility of Sn in the Mg (hcp) phase and the potential to precipitate a cubic secondary phase (Mg_2Sn) in the magnesium matrix (Kang, et al., 2007; Gibson, et al., 2010). This makes Mg-Sn alloys very interesting for the development of creep resistant magnesium alloys at high temperatures. In fact, previous investigations indicate that Mg-Sn alloys with additionnal alloying elements have comparable or even better creep properties than AE42 alloys (Leil, et al., 2007). In addition, it is known that Sn can improve corrosion resistance when it is used as an alloying element (Jung, et al., 2007). Moreover, at its present market price, Sn is a reasonably cheap alloying element compared with other alloying elements like rare earths (RE). However, a long-term ageing is necessary for Mg-Sn alloys to reach their peak hardness, which is not very practical for industrial applications (Van der Planken, 1969). Hence, it is necessary to improve the age hardening response and creep resistance behaviour of Mg-Sn alloys by considering at new microalloying additives. To date, many additional alloying elements such as Ag, Ca, Li, Na, Zn, Sr, In etc. and rare-earth elements have been considered (Mendis, et al., 2006; Sasaki, et al., 2006).

As discussed above, although many series of Mg-based alloys have been developed, there is still a neede to improve the properties of the current alloys and develop new Mg-based alloys to meet the demands of the industry.

In developing new alloys, it is important to understand their constitution (microstructure) and their thermodynamic behaviour. Obtaining all information solely through experimental techniques is cumbersome and costly. Fortunately, thermodynamic modeling of multi-component systems by the CALPHAD method (Calculation of Phase Diagrams) approach (Lukas, et al., 2007) has been shown to be a very efficient way to investigate phase equilibria with minimum time and cost (Ohtani & Ishida, 1998). In the thermodynamic "optimization (modeling)" of a chemical system, all available thermodynamic and phase equilibrium data are critically assessed and evaluated simultaneously. One set of model equations is obtained for the Gibbs energies of all of phases as functions of temperature and composition. From these equations, all the thermodynamic properties and phase diagrams can be back-calculated. Model parameters phases in lower-order subsystems can be used to predict the thermodynamic properties of the same phases in the higher-order systems, because bond energies are mostly additive. Through this, all calculated data are rendered self-consistent and consistent with thermodynamic principles. Thermodynamic data, such as activity data or calorimetric data, can aid in the evaluation of the phase diagram, while thermodynamic properties can be deduced from phase diagram measurements. Discrepancies in the available data can often be resolved, and interpolations and extrapolations can be made in a thermodynamically correct manner (Jung, et al., 2004).

1.2 CALPHAD method

In materials science, one of the important goals for engineers is to control and design alloy microstructure in order to achieve the desired properties and performances (Lukas, et al., 2007). The microstructure of an alloy depends on temperature, pressure, chemical composition and thermal history (thermal processing) of the material. One of the most important guides for the materials scientist is the appropriate phase diagram, which may be regarded as a road map, describing the state of equilibrium in the system under various experimental conditions, i.e. temperature, pressure and chemical composition. According to thermodynamics, the phase assemblage with the lowest Gibbs energy determines the equilibrium state at given conditions (Lukas, et al., 2007). With the help of computational thermo-chemistry, not only binary and

ternary systems, but also multi-component systems can be investigated properly (Lukas, et al., 2007). Thus thermodynamic equilibrium aids in the investigation of annealing conditions (annealing alloys composition, annealing temperature, *etc.*) for alloys, while the thermodynamic information plays a major role in transition states (non-equilibrium conditions)

Phase diagrams, as a visual graph of the state of equilibrium in a system as functions of temperature, pressure and constituent components, have been proved to be useful guides for materials design and processing. They can also be used to better understand transformation mechanisms. The relationship between Gibbs energy constraints and the thermodynamic equilibrium conditions of a system were first established by Roozeboom (Roozeboom, 1900). Further elaboration developed quickly. Kaufman and Bernstein (Kaufman & Bernstein, 1970) summarized the features of the calculation of phase diagrams with computers and named this method CALPHAD in 1970. Since then, along with the development of computer technology, the CALPHAD community has grown continuously larger. Several large thermodynamic databases, containing parameters of thermodynamic models for the calculation of system properties have been established (Iikubo, et al., 2011; Ohnuma, et al., 1999). The CALPHAD method, based on the theory of Gibbs energy minimization of the system, is not only a mathematic optimization of the phase diagram but is theoretically meaningful. The thermodynamic optimization of the phase diagram with the CALPHAD method is a systematic approach. A brief introduction to the CALPHAD method is shown in Figure 1.1.
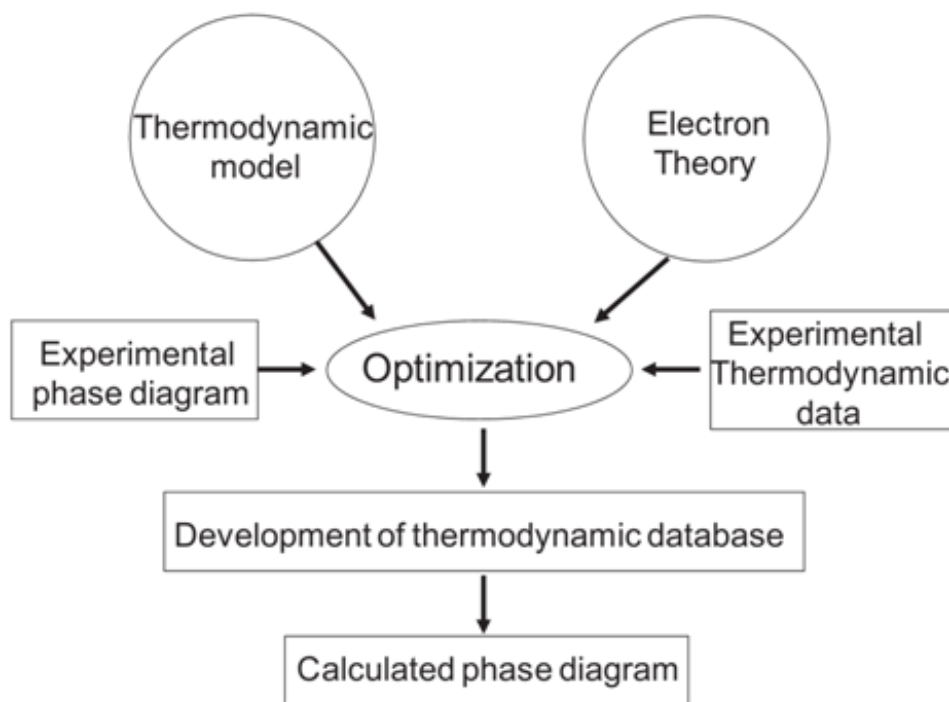
Figure 1.1 Approach of the CALPHAD method

The total Gibbs energy of a system reaches its minimum value when phase equilibrium is established at fixed conditions of temperature and pressure, and at a constant composition in the system components. The process can be expressed as follows:

$$G^{total} = \sum_{n=0}^{n} n\, G^{\varphi} = minimum \tag{1.1}$$

where n is the number of moles of phase φ, and G^{φ} is the molar Gibbs energy of phase φ. A thermodynamic description of the Gibbs energy of a chemical system with the CALPHAD method involves various mathematical functions of temperature, pressure and composition dependences for the different phases.

Under a given set of constraints (pressure, temperature and elemental balance), the Gibbs energy minimization algorithms search and obtain a set of mole numbers of each phase φ and compositions of each solution phase which minimize the total Gibbs energy of given system.

The Gibbs energy function of each phase is made dependent on temperature, pressure and internal solution component compostion and can be described by several different models derived from statistical thermodynamics.

The Gibbs energy of a disordered solution in a binary A-B system can be described as:

$$G_m = n_A G_A^o + n_B G_B^o - T\Delta S^{config} + \Delta G_{mix}^{ex} \tag{1.2}$$

where G_A^o and G_B^o are the molar Gibbs energies of the pure components *A* and *B*, $-T\Delta S^{config}$ is the configurational mixing contribution to the Gibbs energy, and ΔG_{mix}^{ex} is the excess Gibbs energy.

The configurational entropy change in Eq. 1.2 can be described by a Bragg-Williams model (BWM) (Dinsdale, 1991), where the atoms of *A* and *B* are assumed to mix randomly in the solution and the excess Gibbs energy can be expressed by a polynomial. However, a large number of interaction parameters are often needed in this simple polynomial based model to represent adequately all the thermodynamic properties of solution when strong short-range ordering is observed. The same problems also arise in representing the thermodynamic properties of the higher-order solutions (in a ternary, quaternary system) when the binary parameters are used to extrapolate the Gibbe energy. Large arbitrary ternary parameters are often needed in these higher-order solutions to reproduce the available data.

Considering the short-range ordering characteristic in liquid solutions, Pelton and co-workers (Pelton et al., 1997; Pelton & Blander, 1986; Pelton & Chartrand, 2001; Pelton, et al., 2000) developed the Modified Quasichemical Model (MQM) by improving the configurational entropy term of the model, taking into account short-range ordering.

The important advantages of the MQM compared with the BWM for modeling the thermodynamic properties of liquid solutions, particularly in high-order systems, has been well demonstrated in previous work (Jung, et al., 2007; Kang, et al., 2008; Shukla, et al., 2008; Wasiur-Rahman & Medraj, 2009). The short-range ordering behavior of liquid phases were well described in MQM, which is very difficult with the BWM. More parameters needed, and the "V-shaped" enthalpy of mixing and "m-shaped" entropy of mixing are not well reproduced in BWM. Because the MQM takes the short range ordering (SRO) into account, it allows the reproduction of the nearly straight "V" shape of enthalpy mixing curves and "m" shape of entropy mixing curves. The SRO is tentatively treated in the BWM with excess terms in the mixing entropy. The

MQM rather treats the SRO configurationnaly, and it is hence not dependent on extrapolation in higher order systems. Thus, the MQM will usually provide better extrapolations into dilute solutions and more realistic entropy of mixing curves in higher order systems. There here will be significant differences in the predicted thermodynamic properties of ternary and higher order systems by using the binary parameters based on the MQM or the BWM even if the optimations of the binary systems look quite similar.

The Compound Energy Formalism (CEF) was introduced by Hillert and Staffansson (Hillert, 1998; Hillert, 2001; Hillert & Staffansson, 1970) to describe the Gibbs energy of solid phases with sub-lattices (long range ordering, LRO). Ideal mixing (Bragg-Williams mixing) of species on each sub-lattice is assumed.

1.3 Objectives

1.3.1 Problem statement and objective selection

As discussed above, the development of Mg-based alloys of lower cost and superior mechanical properties would be very beneficial to the transportation sector, in the context of energy efficiency. However, shortcomings of magnesium alloys in corrosion resistance, creep resistance and plastic deformation, and the high cost of additives with rare-earth elements must be overcome.

Three approaches were historically used to improve the strength of alloys: (1) solution hardening; (2) phase transformation (precipitation hardening); and (3) grain refining. Consequently, superior mechanical properties of Mg-based alloys can be obtained by improving the solubility of additives in the Mg (hcp) phase, increasing the amount of precipitates in the Mg matrix, and using better grain refiners.

The maximum solubilities of the main alloying elements in the Mg (hcp) phase are listed in Table 1.2. As shown in Table 1.2, the elements with large solid solubility can be divided into three groups:

1) Toxic and radioactive elements: Cd, Tl, Pb, Th, *etc*.

2) High cost elements: rare-earth elements, Sc, *etc*.

3) Low cost or environment-friendly elements: Li, Ag, Zn, In, Sn, *etc*.

Thus Li, Ag, Zn, In, and Sn in the third group with large solid solubility in the Mg (hcp) phase should be the first choice of additives used for solution hardening of new Mg-based alloys as Mg-X (X: Ag, In, Li, and Sn).

Additionally, for precipitation strengthening, distribution of heterogeneities on the Mg lattice will be beneficial for the nucleation of strengthening precipitates in the Mg (hcp) matrix. The effectiveness of heterogeneities depends on the following conditions (Mendis, et al., 2006):

(1) Large driving force for heterogeneity formation (i.e. an ordering or short-range ordering tendency among the microalloying elements).

(2) There should not be no repulsive tendency among the solutes forming the strengthening precipitates.

Table 1.2 The solubility of main alloying elements in Mg (hcp) phase

Alloying element	Solubility in hcp(Mg)		Precipitation phase	Alloying element	Solubility in hcp(Mg)		Precipitation phase
	at.%	wt. %			at.%	wt. %	
Li	17.0	5.5	N	Sc	15	24.5	MgSc
Al	11.6	12.7	Mg17Al12	Pb	7.75	41.9	Mg2Pb
Ag	3.8	15.0	Mg3Ag	Tu	6.3	31.8	?
Y	3.35	12.4	Mg24Y5	Tb	4.6	24.0	Mg24Tb5
Zn	2.5	6.2	MgZn	Sn	3.35	14.5	Mg2Sn
Nd	0.1	0.6	Mg41Nd5	Ga	3.1	8.4	Mg5Ga2
Zr	1.0	3.8	Zr	Yb	1.2	8.0	Mg2Yb
Mn	1.0	2.2	Mn	Bi	1.1	8.9	Mg3Bi2
Th	0.52	4.75	Mg23Th6	Ca	0.82	1.35	Mg2Ca
Ce	0.1	0.5	Mg12Ce	Sm	1.0	6.4	Mg6.2Sm
Cd	100	100	Mg3Cd	Au	0.1	0.8	?
In	19.4	53.2	Mg3In	Ti	0.1	0.2	Ti
Tl	15.4	60.5	Mg5Tl2				

In selecting microalloying additives (Y) for the Mg-(X: Li, Ag, In, Zn, Sn) system as Mg-(X: Li, Ag, In, Zn, Sn)-(Y), the additive Y is required to have a very strong tendency toward ordering (or short-range ordering) with the first group elements X (X: Li, Ag, In, Zn, Sn), which will allow

the additives X and Y to form small precipitates preferentially on the Mg hcp lattice during cooling from the solution treatment temperature or during final heat treatment.

With theese guides for the first group of elements X (X: Li, Ag, In, Zn, Sn), the concise methodology for selecting microalloying additives for the Mg-X-Y (X: Li, Ag, In, Zn, Sn) system give the elements Y listed in Table 1.3. The enthalpies of formation of the most stable compounds in the Mg-X/Y and X-Y systems are shown in Figure 1.2. The more negative the enthalpy of formation, the stronger the tendency to have ordering.

As shown in Figure 1.2 and Table 1.3, the elements Na, Sr, Ca, and Li from IA and IIA group in the periodic table, having extremely negative enthalpy of formation with first group additives, should be the best potential candidates for the second group to form precipitates in the Mg matrix.
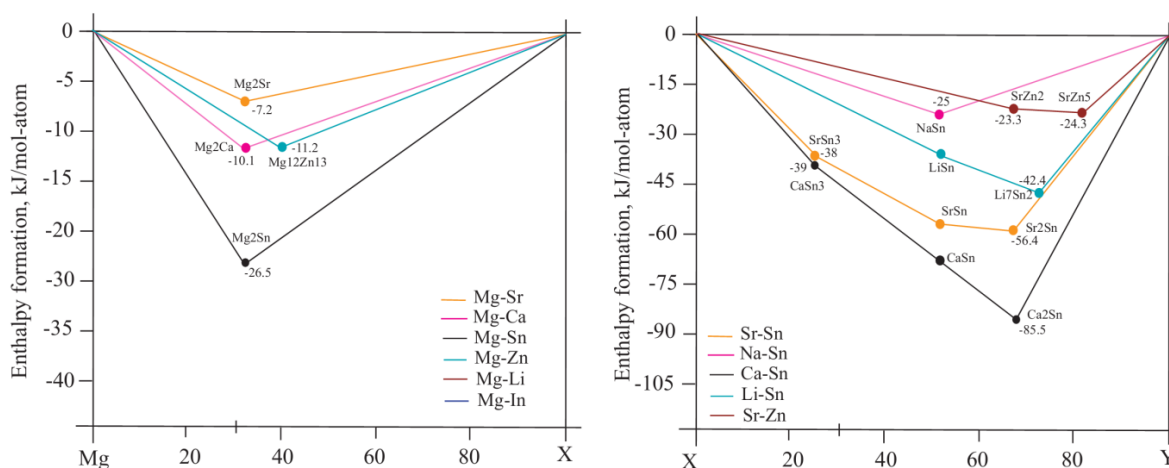
Figure 1.2 Enthalpy of formation of Mg-X and X-Y most stable compounds

Table 1.3 The concise methodology for selecting microalloying additives for Mg-X (X: Li, Ag, In, Zn, Sn)-(Y) system

Tendency to from ordering structure X-Y system	Tendency to form immiscibility Mg-Y systems	Possible choices for Y alloying elements
Ag-Ca, Ag-Ce, Ag-Mg, Ag-Sb, Ag-Sn, Ag-Sr, Ga-Li, Li-In, Li-Zn, In-Mg	Mg-Na, Mg-Cr, Mg-Hf, Mg-Mn, K-Mg, Mg-V, Mg-Zr	Na, Sr, Ca, Li

1.3.2 Objectives of the present research

According to the strategy described in the previous section, the Mg-X (X: Ag, Ca, In, Li, Na, Sn, Sr, and Zn) system was selected as one potential candidate for the development of new Mg-based alloys. In order to study these alloys, a better grasp of the phase equilibria of the binary and the important ternary subsystems is imperative. Obtaining such information solely through experimental techniques is very cumbersome and costly, and does not link the experimental phase equilibrium results to the important thermodynamic properties of the phases. Fortunately, thermodynamic modeling of multi-component systems by the CALPHAD approach has been shown to be a very efficient way to investigate phase equilibria with minimum time and cost (Ohtani & Ishida, 1998). Consequently, it is mandatory to construct the thermodynamic models (and database of model parameters) for the phases of the multi-component systems. The thermodynamic models and the associated database will provide clear guidelines for selection and design of Mg-based alloys, thus avoiding unproductive long-term experimental work. The thermodynamic database of this targeted system will be constructed with 36 binary sub-systems, 84 ternary sub-systems and 126 quaternary sub-systems.

As part of ongoing projects in our group to develop a thermodynamic database for Mg-based multi-component alloys, the main objective of the present work is to establish a consistent thermodynamic database for the Mg-based multi-component systems. This includes additives of Ag, Ca, In, Li, Na, Sn, Sr and Zn which will aid system design of magnesium. Numerous binary and ternary systems in the Mg-X (X: Ag, Ca, In, Li, Na, Sn, Sr and Zn) multi-component system will be critically evaluated and systematically optimized.

The thermodynamic optimization study status of binary sub-systems of the Mg-X (X: Ag, Ca, In, Li, Na, Sn, Sr, and Zn) multicomponent system is shown in Table 1.4. As shown in this Table, the 14 sub-binary systems: Mg-Ca (Aljarrah & Medraj, 2008b; Anctil, 2003), Mg-Li (Spencer, 2006), Mg-Na (Chartrand, 2003), Mg-Sn (Jung, et al., 2007), Mg-Sr (Aljarrah,et al., 2007; Aljarrah & Medraj, 2008a, 2008b), Mg-Zn (Aljarrah, et al., 2007; Ghosh, et al., 2012; Spencer, 2006; Wasiur-Rahman & Medraj, 2009), Ca-Sr (Aljarrah & Medraj, 2008a; Anctil, 2003), Ca-Zn (Spencer, et al., 2008; Wasiur-Rahman & Medraj), Li-Na (Chartrand, 2003), Li-Sr (Chartrand, 2003), Na-Sr (Chartrand, 2003), Li-Zn (Spencer, 2006), Sn-Zn (Ghosh, et al., 2012) and Sr-Zn (Spencer, et al., 2008) have been critically evaluated and thermodynamicaly optimized with the

Modified Quasichemical Model in the Pair Approximation (MQMPA) for the liquid phase. And 11 sub-binary systems: Ag-Mg (Lim, et al., 1997), Ag-Zn (Gomez-Acebo, 1998), Ag-Ca (Huang, et al., 2008), In-Zn (Lee, 1996), Ca-Sn (Ohno, et al., 2006), In-Sn (Lee, 1996; Liu, et al., 2002), Ca-Na (Zhang, et al., 2003), Ag-Sr (Liu & Liang, 2006), Ag-In (Liu, et al., 2002), Ag-Sn (Liu, et al., 2002), Li-Sn and Ag-Na (Hao et al., 2012) have been optimized with the BWM for the liquid phase.

Table 1.4 The current thermodynamic optimization status of binary sub-systems of the Mg-X (X: Ag, Ca, In, Li, Na, Sn, Sr and Zn) multi-component system

System	Experimental data	Thermodynamic optimization	System	Experimental data	Thermodynamic optimization
Mg-Ca	Y	[a] MQM	Ag-Ca	Y	BWM
Mg-Li	Y	MQM	Ag-Li	Y	N
Mg-Na	Y	MQM	In-Na	Y	N
Mg-Sn	Y	MQM	Na-Sn	Y	N
Mg-Sr	Y	MQM	Li-Sn	Y	BWM
Mg-Zn	Y	MQM	Na-Zn	Y	N
Ca-Sr	Y	MQM	In-Zn	Y	BWM
Ca-Zn	Y	MQM	Sn-Sr	Y	BWM
Li-Na	Y	MQM	Ca-Li	Y	BWM
Li-Sr	Y	MQM	Ca-Sn	Y	BWM
Na-Sr	Y	MQM	In-Sn	Y	BWM
Sr-Zn	Y	MQM	Ca-In	Y	N
Li-Zn	Y	MQM	Ca-Na	Y	BWM
Sn-Zn	Y	MQM	Ag-Na	Y	N
Ag-Sr	Y	MQM	Ag-Sn	Y	BWM
Mg-Ag	Y	[b] BWM	Ag-In	Y	BWM
Ag-Zn	Y	BWM	In-Li	N/A	N
Mg-In	Y	N	In-Sr	N/A	N
[a] Modified Quasichemical model, [b] Bragg-Willams model					

However, for most of the assessed systems with a BWM for the liquid phase, even with a large number of model parameters, the assessed results were still inconsistent with experimental data. This was possibly due to the limitation of the choice of BWM for liquid solution (as discussed in section 1.2). Moreover, a critical review of the experimental data was not performed in some previous work. Although the optimized parameters of liquid solutions described with BWM can be used with the FactSage thermodynamic database for the liquid phase (Pelton & Chartrand, 2001), there will be some difficults in extrapolating to high-order systems with the BWM

parameters. For example, in a ternary system *A-B-C*, *A-B* maybe an ideally mixing system. The *B-C* and *A-C* binary systems may have high short range ordering tendencies. When *C* is added to a binary solution of *A-B*, there will be a high tendency to form *B-C* and *A-C* ordering pairs instead still keep the *A-B* pairs (ideally mixing pairs) in this tenary solution. However, if the liquid solution *A-B* is modeled with BWM, the *A-B* pairs composition is fixed at $x_A = x_B = 0.5$, which means that the forming of short-range ordering pairs of *B-C* and *A-C* will be affected. This problem was pointed out by Kang and Pelton (Kang & Pelton, 2010) in Mg-Al-Sn system.

As discussed above, in order to construct a self-consistent thermodynamic database of the Mg-X (X: Ag, Ca, In, Li, Na, Sn, Sr and Zn) multi-component system, all the 11 binary systems mentioned above modeled with BWM and the remaning 8 binary systems except In-Sr and In-Li will have to be completely re-evaluated and optimized in the present study using MQM for the liquid phase. The In-Sr and In-Li binary systems, for which few experimental data are available, will not be included in this work.

As mentioned above, there is a total of 84 sub-ternary systems in the Mg-X (X: Ag, Ca, In, Li, Na, Sn, Sr and Zn) multi-component system. For the present investigation, the priority ternary sub-systems are those containing Mg. The optimization status of 28 ternary sub-systems with Mg in the Mg-X multi-component systems are listed in Table 1.5.

As listed in Table 1.5, most of the present selected ternary systems have neither been investigated experimentally nor modeled thermodynamically. Consequently, phase equilibria will be measured for selected key alloys for these ternary systems. Due to the large number of undetermined systems, and depending on present research interests, the priority systems for experimental measurement in the Mg-rich portion are selected as Mg-Sn-X (X: Ag, In, Zn, Ca, and Sr) and Mg-Zn-Sr. Thermodynamic optimizations of these systems (except Mg-Zn-Sr system) will also be carried out. In order to construct a comprehensive thermodynamic database, several ternary subsystems without Mg will also be optimized in the present work.

Table 1.5 The current thermodynamic optimization status of the ternary sub-systems of the Mg-X multi-component system

System	Experimental data		Thermodynamic optimization
Mg-Li-Sn	[a]IS	370 ^{o}C	N
	[b]VS	Li:Sn (1:1, 3:1, 9:1), Mg97Li3-Mg4Sn (wt. %)	
Mg-Zn-Sn	IS	400 ^{o}C	BWM
	VS	Mg$_2$Sn-MgZn$_2$, Mg$_2$Sn-Zn, *etc.*	
Mg-Li-Ca	IS	150 ^{o}C	BWM
	VS	Mg$_2$Ca-Li$_2$Ca, CaMg-13Li (at. %)	
Mg-Ca-Sn	IS	N/A	BWM
	VS	Mg$_2$Sn-Mg$_2$Ca, Mg-CaSn, Mg$_2$Sn-Ca$_2$Sn, 7Ca53Sn-Mg	
Mg-Zn-Li	IS	300 ^{o}C	BWM
	VS	N/A	
Mg-Zn-Sr	IS	N/A	N
	VS	N/A	
Mg-Sn-Sr	IS	N/A	N
	VS	N/A	
Mg-Ca-Sr	IS	500 ^{o}C	N
	VS	79.6Mg20.4Ca-53.7Mg46.3Sr (wt. %)	
Mg-Sn-In	IS	N/A	N
	VS	N/A	
Mg-Sn-Ag	IS	550 ^{o}C, 450 ^{o}C	N
	VS	10 Sn, 10 Ag (wt. %)	
Mg-Ag-In	IS	280 ^{o}C	N
	VS	50 In, 10 Ag, 30 Mg (wt. %)	
Mg-Ca-Zn	IS	300 ^{o}C	N
	VS	2 Ca, 4Ca, Zn$_2$Mg-Mg$_2$Ca, *etc.* (at. %)	
Mg-Ag-Ca	N/A		N
Mg-Sn-Na	N/A		N
Mg-Zn-Na	N/A		N
Mg-Ag-Sr	N/A		N
Mg-Sr-Na	N/A		N
Mg-Sr-Li	N/A		N
Mg-Sr-In	N/A		N
Mg-Na-Li	N/A		N
Mg-Na-In	N/A		N
Mg-Li-In	N/A		N
Mg-Ca-In	N/A		N
Mg-Ca-Na	N/A		N
Mg-Zn-In	N/A		N
Mg-Ag-Zn	N/A		N
Mg-Ag-Li	N/A		N
Mg-Ag-Na	N/A		N
[a] Isothermal section, [b] Vertical section			

Thus, the present objectives can be divided into the following groups as:

The priority objectives in the present work therefore include

(1) Critical evaluation of experimental data and thermodynamic description on 19 binary systems: Mg-In, Mg-Ag, Ag-Zn, Ag-Ca, Ag-Li, In-Na, Na-Sn, Li-Sn, Na-Zn, In-Zn, Sn-Sr, Ca-Li, Ca-Sn, In-Sn, Ca-In, Ca-Na, Ag-In, Ag-Na and Ag-Sn.

(2) Experimental measurements will be focused on five ternary systems: Mg-Sn-X (X: Ag, In, Zn, Ca, and Sr)

(3) Thermodynamic description of 12 ternary systems: Mg-Sn-X (X: Ag, In, Li, Zn, Ca, and Sr), Mg-Zn-In, Mg-Ag-In, Mg-Ca-Li, Mg-Ca-Sr, Mg-Sn-In, and In-Sn-Zn.

And the secondary objectives in the present work include:

(1) Use of the thermodynamic database for calculations to analyze the solidification behavior of selected Mg-Sn based alloys at elevated temperatures.

(2) Alloy design with the Ag, Li, Ca, In, Sr, Sn, and Zn additions for Mg based alloys will be carried out with the present thermodynamic database.

In addition, an experimental study of the phase equilibria measurement and metallic glass forming ability of selected Mg-Zn-X (Ag, Sr, In, *etc*) alloys will be done with the collaboration of Mr. Yi-Nan Zhang from Concordia University.

CHAPITRE 2   METHODOLOGY

In this chapter, a general description of the methodologies used in the present work, including of the CALPHAD method and the techniques of phase diagram experimental measurements will be introduced. The literature related to specific systems presented in papers is not reviewed in this chapter, but will be given in the following chapters 4 to 7 respectively.

2.1   Thermodynamic models

The thermodynamic database of the Mg-X (X: Ag, Ca, In, Li, Na, Sn, Sr and Zn) multi-component system will be developed by means of the FactSage thermodynamic software (Bale et al., 2009; Bale et al., 2002).

2.1.1   Pure element and stoichiometric phases

The molar Gibbs energy of pure stoichiometric phases (including the different allotropic forms of elements) G^{φ} can be described by:

$$G^{\varphi} = G_T^{\varphi} + G_P^{\varphi} + G_m^{\varphi} \tag{2.1}$$

where G_T^{φ} is the contribution to the total Gibbs energy by temperature (T), G_P^{φ} is the contribution to the total Gibbs energy by pressure (P), for the selected system at pressure more than 1 atm (the Gibbs energy contribution from pressure at 1 atm is included in the $G(T)$ function). G_m^{φ} is the magnetic contribution to the total Gibbs energy; for non-magnetic phases, the magnetic contribution to the total Gibbs energy is zero.

The temperature and composition dependence of G_T^{φ} can be expressed as:

$$G_T^{\varphi} = H_T^{\varphi} - S_T^{\varphi}T \tag{2.2}$$

$$H_T^{\varphi} = \Delta H_{298.15K}^{\varphi} + \int_{298.15K}^{T} C_P dT \tag{2.3}$$

$$S_T^{\varphi} = S_{298.15K}^{\varphi} + \int_{298.15K}^{T} (C_P / T) dT \tag{2.4}$$

where $\Delta H^{\varphi}_{298.15K}$ is the molar enthalpy of formation of the stable allotropic form from pure element ($\Delta H^{\varphi}_{298.15K}$ of stable allotropic form of pure element at 298.15 K and 1 atm is assumed as 0 J·mol⁻¹; reference state), and $S^{\varphi}_{298.15K}$ is the molar entropy at 298.15 K. C_p is the molar heat capacity, which usually be expressed by the polynomial with temperature (T) as:

$$C_P = a + b \times T + c \times T^{-2} + d \times T^2 + ... \tag{2.5}$$

In the present study, the Gibbs energy of all allotropic forms of the pure elements Ag, Ca, In, Li, Mg, Na, Sn, Sr, and Zn were taken from the SGTE database (Dinsdale, 1991). As there are no experimental data of heat capacity of all the intermetallics in the present Mg-X (X: Ag, Ca, In, Li, Na, Sn, Sr and Zn) multi-components system, the heat capacities of all the intermetallics were evaluated using the Neumann-Kopp rule: "Each element (in the solid state) has essentially the same specific or atomic heat in compounds as it has in the free state" (Kopp, 1865). For example, in case a compound $A_m B_n$ formed with pure element A and B by the reaction: $mA + nB \leftrightarrow A_m B_n$, the following equation can be used to construct the heat capacity $C_p^{A_m B_n}$ of the compound $A_m B_n$:

$$C_p^{A_m B_n} = mC_P^A + nC_P^B \tag{2.6}$$

where C_P^A and C_P^B are the heat capacities of stable allotropic forms of the pure elements A and B.

As heat capacity curves of solid In, Na, Li and Sn from the SGTE database (Dinsdale, 1991) show maxima just above their melting temperatures, the resultant heat capacities of intermetallics phases directly obtained from the Neumann-Kopp rule also exhibit maxima in the temperature range 350-550 K. This is in the stable liquid region. Several intermetallic phases in the present system melt at temperatures substantially higher than those of the pure elements from which they are formed. An example is In_5Na_3 with a melting point at 444 °C, in which the melting temperatures of Na (bcc) and In (tetragonal) are 97.1 °C and 156.6 °C respectively. The heat capacity of intermetallic phases considered here obtained by the Neumann-Kopp rule, showed a maxima about 506 K. This is scarcely physically plausible as no magnetism is involved. In order to resolve this, the heat capacity functions of solid In, Na, Li and Sn were modified above their melting temperatures (that is, in their metastable regions) to make sure that the heat capacity curves of intermetallics phases involving these four elements increase with temperature up to their own melting temperatures. During this modification, the C_p values and the slope of the C_p

curves at melting points for the pure elements were first fixed, and then another C_p values at high temperature (around 2500 K) was fixed for which the slope at this point is set to zero. The new function values a, b, c, and d shown in Eq. 2.5 will be fixed based on these four conditions. The input conditions were made with small adjustments render reasonable the extrapolated. This modification does not influence pure solid phases of In, Na, Li and Sn elements themselves below their melting temperatures. The modified heat capacity functions are given Table 2.2, and the comparison between the C_p curves from the SGTE database (Dinsdale, 1991) are shown in Figure 2.1.
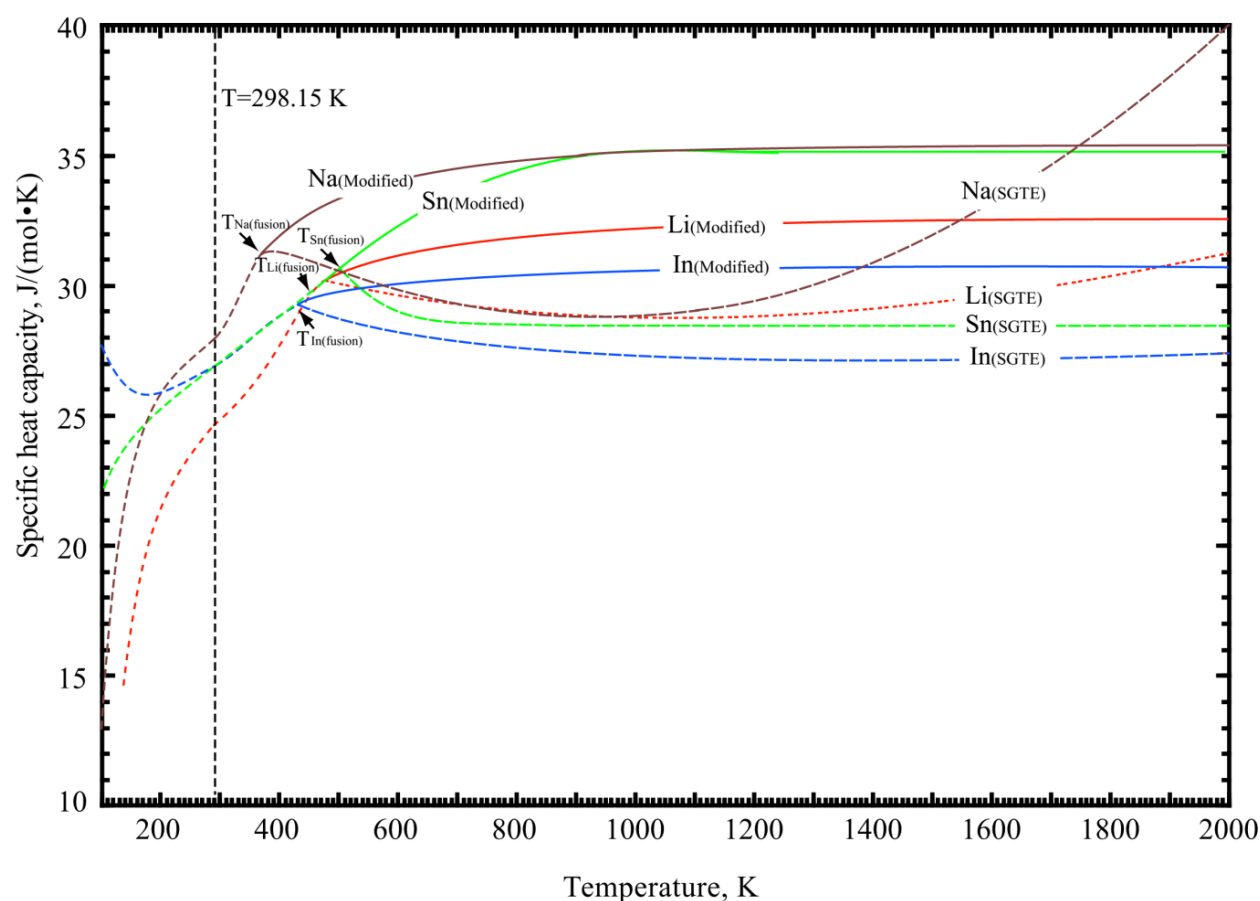
Figure 2.1 Comparison between the C_p curves from SGTE database and the modified results for In, Li, Na and Sn in the solid state.

2.1.2 Liquid solution

The Modified Quasichemical Model in the Pair Approximation (MQMPA) (Pelton & Chartrand, 2001; Pelton, et al., 2000) was developed for the modeling of liquid solution exhibiting a high degree of short-range order. As discussed in section 1.3, for more realistic description of the liquid solution and construction of a self-consistent thermodynamic database, the thermodynamic properties of the liquid phase were modeled by the MQMPA in the present work. A detailed description of the MQMPA and its associated notation is given in the refered papers (Pelton & Chartrand, 2001; Pelton, et al., 2000). The same notation given by the source authors is used in the present work. A brief description of MQMPA is given as follows:

For the binary *A-B* system, the following quasichemical pair exchange reaction can be considered:

$$(A - A)_{pair} + (B - B)_{pair} = 2(A - B)_{pair}, \ \Delta g_{AB} \tag{2.7}$$

where $i - j$ pair represents a first-nearest-neighbor pair of atoms. The Gibbs energy change for the formation of one mole of *(A-B)* according to reaction (2.7) is $\Delta g_{AB}/2$. Let n_A and n_B be the number of moles of A and B, n_{AA}, n_{BB}, and n_{AB} be the number of moles of *(A-A)*, *(B-B)*, and *(A-B)* pairs. Z_A and Z_B are the coordination numbers of A and B. Then the Gibbs energy of the solution can be expressed as:

$$G = (n_A G_A^o + n_B G_B^o) - T\Delta S^{config} + (n_{AB}/2)\,\Delta g_{AB} \tag{2.8}$$

where G_A^o and G_B^o are the molar Gibbs energies of the pure component A and B, and ΔS^{config} is the configurational entropy of mixing given by randomly distributing the *(A-A)*, *(B-B)*, and *(A-B)* pairs in the one-dimensional Ising approximation. The expression for ΔS^{config} is:

$$\begin{aligned}
\Delta S^{config} = &-R(n_A \ln X_A + n_B \ln X_B) \\
&- R(n_{AA} \ln \frac{X_{AA}}{Y_A^2} + n_{BB} \ln \frac{X_{BB}}{Y_B^2} + n_{AB} \ln \frac{X_{AB}}{2Y_A Y_B})
\end{aligned} \tag{2.9}$$

where X_{AA}, X_{BB} and X_{AB} are the mole fractions of the *(A-A)*, *(B-B)*, and *(A-B)* pairs; Y_A and Y_B are the coordination-equivalent fractions of A and B:

$$X_{ij} = \frac{n_{ij}}{n_{AA} + n_{BB} + n_{AB}} \quad (i, j = A \text{ or } B) \tag{2.10}$$

$$Y_i = \frac{Z_i n_i}{Z_A n_A + Z_B n_B} \qquad (i = A \text{ or } B) \tag{2.11}$$

Moreover, the following elemental balance equations can be written:

$$Z_A n_A = 2n_{AA} + n_{AB} \tag{2.12}$$

$$Z_B n_B = 2n_{BB} + n_{AB} \tag{2.13}$$

It should be pointed out that there is no exact expression for the configurational entropy in three dimensions. Although Eq. (2.9) is only an approximate expression in three dimensions, it is exact one-dimensionally (when $Z=2$) (Pelton, et al., 2000). As explained in this reference, one is forced by the approximate nature of Eq. (2.9) to use nonphysical values for the coordination numbers in order to yield good fits between the experimental and calculated data. The mathematical approximation of the one-dimensional Ising model of Eq. (2.9) can be partially compensated by selecting values of Z_A and Z_B which are smaller than the experimental values (Kang, et al., 2008) . The MQMPA model is sensitive to the ratio of coordination numbers, but less sensitive to their absolute values. From a practical standpoint for the development of large thermodynamic database values of Z_A and Z_B of the order of 6 have been found necessary for the solutions with a small or medium degree of ordering (*i.e.* alloy solutions).

Δg_{AB} is the model parameter to reproduce the Gibbs energy of liquid phase of the *A-B* binary system, which is expanded as a polynomial in terms of the pair fractions, as follows:

$$\Delta g_{AB} = \Delta g_{AB}^o + \sum_{i \geq 1} g_{AB}^{io} (X_{AA})^i + \sum_{j \geq 1} g_{AB}^{oj} (X_{BB})^j \tag{2.14}$$

where Δg_{AA}^o, g_{AB}^{io} and g_{AB}^{oj} are the adjustable model parameters which can be function of the temperature, and the X_{AA} and X_{BB} are the molar fractions of *A-A* and *B-B* pairs. The equilibrium state of the system is obtained by minimizing the total Gibbs energy at constant elemental composition, temperature and pressure. The equilibrium pair distribution is calculated by setting:

$$\left(\frac{\partial G}{\partial n_{AB}} \right)_{n_A n_B} = 0 \tag{2.15}$$

which gives the ''equilibrium constant'' for the ''quasichemical pair reaction'' of Eq. (2.4):

$$\frac{X_{AB}^2}{X_{AA}X_{BB}} = 4\exp\left(\frac{-\Delta g_{AB}}{RT}\right) \tag{2.16}$$

Moreover, the model permits Z_A and Z_B to vary with composition as follows (Pelton, et al., 2000):

$$\frac{1}{Z_A} = \frac{1}{Z_{AA}^A}\left(\frac{2n_{AA}}{2n_{AA}+n_{AB}}\right) + \frac{1}{Z_{AB}^A}\left(\frac{n_{AB}}{2n_{AA}+n_{AB}}\right) \tag{2.17}$$

$$\frac{1}{Z_B} = \frac{1}{Z_{BB}^B}\left(\frac{2n_{BB}}{2n_{BB}+n_{AB}}\right) + \frac{1}{Z_{AB}^B}\left(\frac{n_{AB}}{2n_{BB}+n_{AB}}\right) \tag{2.18}$$

where Z_{AA}^A and Z_{AB}^A are the values of Z_A when all nearest neighbours of an atom A are As, and when all nearest neighbours of an atom A are Bs, and where Z_{BB}^B and Z_{AB}^B are defined similarly. The composition of maximum short range ordering (SRO) is determined by the ratio of the coordination numbers Z_{AB}^A / Z_{AB}^B.

For the multi-component system A-B-C-D…, the detailed thermodynamic description of the MQMPA for the liquid solution has been given by Pelton and Chartrand (Pelton & Chartrand, 2001). The same notation will be used in the present thermodynamic optimization. A brief expression of MQMPA for multi-component liquid solutions may be given as follows.

The components (A-B-C-D…) of a multi-component solution can be considered distributed over the sites of a quasi-lattice. In the pair approximation, the pair-exchange reactions are considered as:

$$(M - M) + (N - N) = 2(M - N); \qquad \Delta g_{MN} \tag{2.19}$$

where (M and $N=A, B, C, D, …$) and $(M$-$N)$, $(M$-$M)$ and $(N$-$N)$ are the first-nearest-neighbor pairs (FNN). $\Delta g_{MN}/2$ is the non-configurational Gibbs energy change of the formation of one mole of $(M$-$N)$ pairs. Then, for n moles of M element, the balance constrains for the multi-component solution between coordination number and mass can be expressed as:

$$n_M Z_M = 2n_{MN} + \sum_{N \neq M} n_{MN} \tag{2-20}$$

where n_{MM} and n_{NM} are the number of moles of $(M$-$M)$ and $(M$-$N)$ pairs, respectively.

The relationship among the pair fractions X_{MN}, overall mole (or site) fractions X_M and "coordination-equivalent" fractions Y_M are as follows:

$$X_{MN} = n_{MN} / \sum n_{ij} \qquad\qquad (i, j = A, B, C,...) \qquad\qquad\qquad (2\text{-}21)$$

$$X_M = n_M / \sum n_i \qquad\qquad (i, j = A, B, C,...) \qquad\qquad\qquad (2\text{-}22)$$

$$Y_M = Z_M n_M / \sum Z_i n_i = Z_M n_M / \sum Z_j n_j \qquad\qquad (i, j = A, B, C,...) \qquad\qquad (2\text{-}23)$$

The Gibbs energy of the solution can be expressed as:

$$G = \sum g_M^o n_i - T\Delta S^{config} + \sum_{N>M} \sum n_{MN} (\Delta g_{MN} / 2) \qquad\qquad (2\text{-}24)$$

where g_M^o is the molar Gibbs energy of pure component M, and ΔS^{config} is an approximate expression for the configurational entropy of mixing, which given by randomly mixing the M-N pairs. ΔS^{config} is given by:

$$\Delta S^{config} = -R\sum (n_M \ln X_M) - R\left(\sum n_{MN} \ln(X_{MN} / Y_M^2) + \sum_{M>N}\sum n_{MN} / 2Y_M Y_N \right) \qquad (2\text{-}25)$$

Δg_{MN} is given by a polynomial in pair fractions, in symmetric or asymmetric models (Figure 2.2) for constructing the total Gibbs energy function based on the thermodynamic properties of the subsystems.
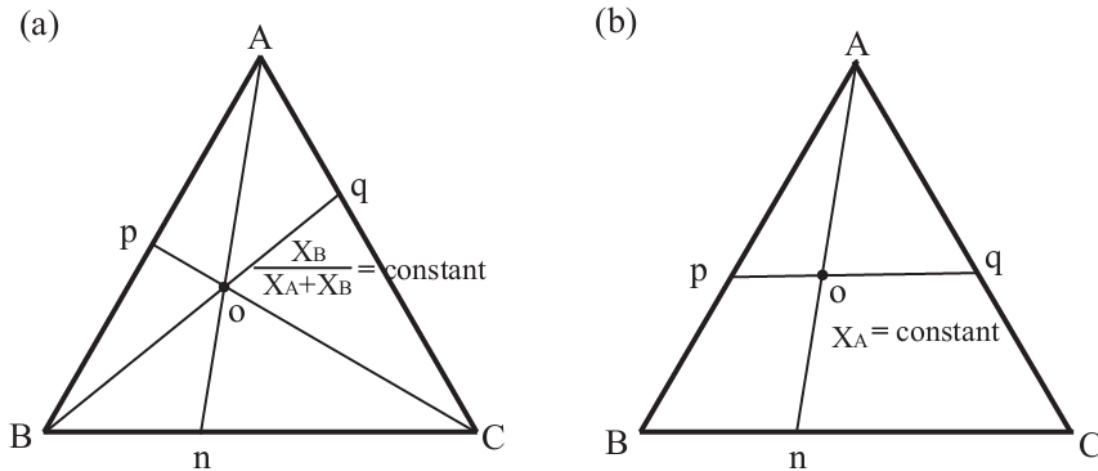
Figure 2.2 Symmetric (a) and asymmetric (b) models for interpolation from binary systems to ternary system (Pelton & Chartrand, 2001)

For the ternary system *A-B-C*, if the thermodynamic properties of each binary subsystems are quite symmetric, the symmetric model Kohler-type (shown in Figure 2.2(a)) (Patrice Chartrand & Pelton, 2000a; Kohler, 1960) the interpolation would be used. The interpolation formulae of Δg_{AB} in the ternary solution can be expressed as:

$$
\Delta g_{AB} = \Delta g_{AB}^0 + \sum_{i+j \geq 1} g_{AB}^{ij} \left(\frac{X_{AA}}{X_{AA} + X_{AB} + X_{BB}} \right)^i \left(\frac{X_{BB}}{X_{AA} + X_{AB} + X_{BB}} \right)^j
$$
$$
+ \sum_{\substack{i \geq 0, \\ j \geq 0, \\ k \geq 1}} g_{AB(C)}^{ijk} \left(\frac{X_{AA}}{X_{AA} + X_{AB} + X_{BB}} \right)^i \left(\frac{X_{BB}}{X_{AA} + X_{AB} + X_{BB}} \right)^j Y_C^k
$$

(2.26)

where the empirical ternary coefficients $g_{AB(C)}^{ijk}$ result from the optimization on the ternary system.

If the thermodynamic properties of the binary subsystems are quite asymmetric, as illustrated in Figure 2.2(b), the Toop (Toop, 1965) interpolation will be introduced. As shown in Figure 2.2(b), component *A* is an asymmetric component for the *A-B* system. The Gibbs energy of formation of nearest-neighbor pairs *(A-B)* is assumed to be constant as component *B* is replaced by constituent element *C* in the *A-B-C* ternary system. The interpolation formulae of Δg_{AB} and Δg_{AC} in the ternary solution is given as follows:

$$
\Delta g_{AB} = \Delta g_{AB}^0 + \sum_{(i+j) \geq 1} g_{AB}^{ij} X_{AA}^i (X_{BC} + X_{BB} + X_{CC})^j
$$
$$
+ \sum_{\substack{i \geq 0, \\ j \geq 0, \\ k \geq 1}} g_{AB(C)}^{ijk} X_{AA}^i (X_{BC} + X_{BB} + X_{CC})^j \left(\frac{Y_C}{Y_B + Y_C} \right)^k
$$

(2.27)

where the binary terms are constant along the line *pq* and equal to their values at point *o* in Figure 2.2(b). The interpolation formulae of Δg_{BC} can be given by a similar expression (Eq. 2.26). For example, the thermodynamic properties of liquid Ag-In, Ag-Sn and In-Sn solutions introduce asymmetry into ternary system. The minimum enthalpy of mixing of Ag-Sn liquid at 1000 ^{o}C is about -3 kJ/mol, while the minima of Ag-In and In-Sn are -4 kJ/mol and -150 J/mol respectively. Consequently, the Toop interpolation (Ag was treated as the asymmetric component) was used for liquid Ag-In-Sn ternary system.

Here it should be noted that the thermodynamic properties of a multi-component solution can be extrapolated using one of the techniques proposed by Kohler, Toop, or Muggianu et al. from optimized binary parameters. The thermodynamic characteristics and structural properties of the solution will be considered for the selection of the most appropriate geometric model. Some of geometric models (64 possible geometric models in total) (Pelton, 2001) for extrapolatiing the ternary thermodynamic properties from the optimized parameters of the binary subsystems are shown in Figure 2.3.

(a) Kohler Model

$\dfrac{X_B}{X_A+X_B}=\text{constant}$

(b) Kohler/Toop Model

$X_A = \text{constant}$

(c) Muggianu Model

$(1+X_A-X_B)/2=\text{constant}$
or $X_A-X_B=\text{constant}$
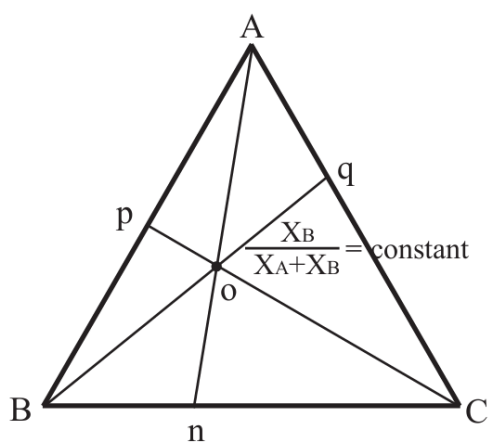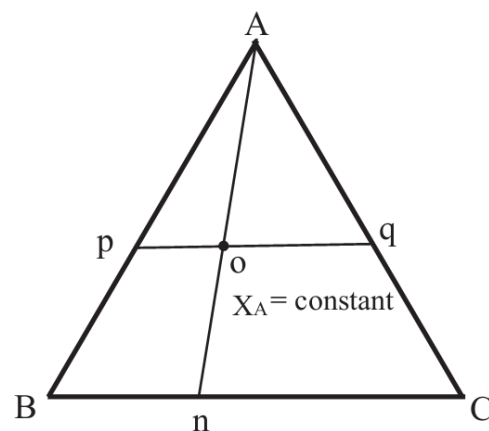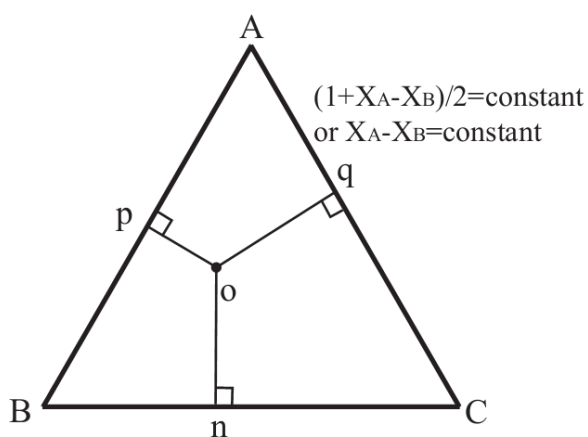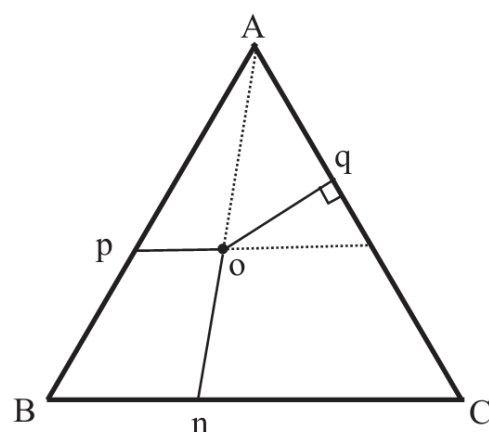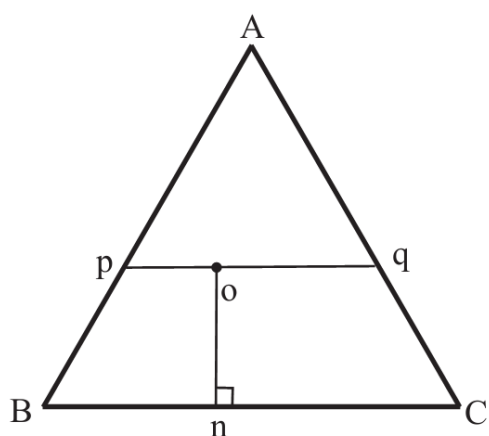
(d) A Weird Model

(e) Toop/Muggianu Model
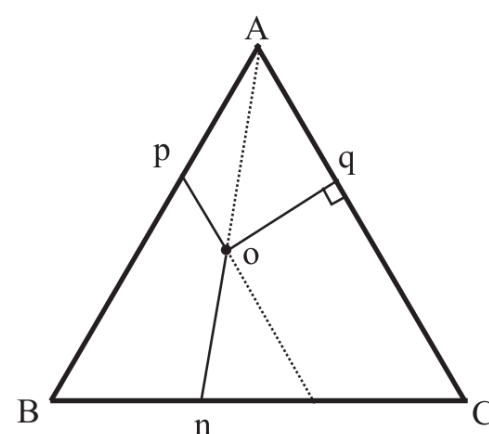
(f) Another Weird model

Figure 2.3 Some geometric extrapolation models for a multi-components solution from the optimized parameters of the sub-systems (Pelton, 2001)

2.1.3 Solid solution

The Compound Energy Formalism (CEF) introduced by Hillert (Hillert, 2001) was used to describe the Gibbs energy of solid solution phases considering their sub-lattice structures. Ideal mixing of the sub-lattice species on each sub-lattice site is assumed. The Gibbs energy expression then depends on the particular choice of lattice stoichiometries and on which species is mixing on any given lattice. Taking the laves_C14 phase as example, the molar Gibbs energy of A_2B (laves_*C14*) olid solution phase using the CEF with the sub-lattice model of $(A, B)_2 (A, B)$ can be expressed as follows:

$$
\begin{aligned}
G^{A,B} &= y_A^I y_B^{II} {}^0G_{A:B}^{A,B} + y_A^I y_A^{II} {}^0G_{A:A}^{A,A} + y_B^I y_A^{II} {}^0G_{B:A}^{B,A} + y_B^I y_B^{II} {}^0G_{B:B}^{B,B} \\
&\quad + 2RT(y_A^I \ln y_A^I + y_B^I \ln y_B^I) + RT(y_A^{II} \ln y_A^{II} + y_B^{II} \ln y_B^{II}) \\
&\quad + 2y_A^I y_B^I \left(\sum_i {}^iL_{A,B:A} y_A^{II} (y_A^I - y_B^I)^i + \sum_i {}^iL_{A,B:B} y_B^{II} (y_A^I - y_B^{II})^i \right) \\
&\quad + y_A^{II} y_B^{II} \left(\sum_i {}^iL_{A:A,B} y_A^I (y_A^{II} - y_B^{II})^i + \sum_i {}^iL_{B:A,B} y_B^I (y_A^{II} - y_B^I)^i \right)
\end{aligned}
\tag{2.28}
$$

where y_*^I and y_*^{II} are the site fractions of component A or B on the first and second sublattices, respectively. ${}^0G_{m:n}^{m,n}$ represent the Gibbs free energies of the m_2n ($n = A$ or $B, m = A$ or B) compound ("end-member") when the first and second sublattices are occupied by component A or B, respectively. Note that this compound, in the laves_*C14* structure, can be stable or metastable. The items ${}^iL_{A,B:*}$ and ${}^iL_{*:A,B}$ are the interaction energies between A and B atoms while the first and second sublattices are occupied by component A or B respectively. They can be expressed as:

$$
{}^iL_{A,B:*} = a_i + b_iT
\tag{2.29}
$$

$$
{}^iL_{*:A,B} = c_i + d_iT
\tag{2.30}
$$

The parameters a_i, b_i, c_i and d_i are evaluated parameters. ${}^iL_{A,B:A,B}$ is the reciprocal interaction parameter when the first sub-lattice is occupied by A and B, and the second sub-lattice is occupied by A and B, concurrently.

2.1.4 Phase equilibria calculation of multi-component system

In a multi-component system, the total Gibbs energy G of all phases can be expressed as:

$$G = \sum_{\varphi}^{p} n_{\varphi} G^{\varphi}$$
(2.31)

G^{φ} is the molar Gibbs energy of phase φ (at its given T, P and composition), and n_{φ} is the number of moles of φ phase.

For the calculation of phase equilibria, it is necessary to minimize the total Gibbs energy, G, of all the phases that take part in this equilibrium (Kattner, 1997), as:

$$\frac{\partial G}{\partial x_i^{\varphi}} = 0$$
(2.32)

where x_i^{φ} is the mole fraction of element i in φ phase.

From the condition that the Gibbs energy at thermodynamic equilibrium reveals a minimum for given temperature, pressure, and composition, Gibbs (Gibbs, 1948) derived the well-known equilibrium conditions that the chemical potential, μ_i^{φ}, of each component i, is the same in all equilibrated phases:

$$\mu_i^1 = \mu_i^2 = ... = \mu_i^{\varphi} \;\; (i = 1,.....,n)$$
(2.33)

Equation (2.33) results in i nonlinear equations that can be used in numerical calculations.

Then, the integral total Gibbs energy at equilibrium in Eq. 2.31 can be expressed:

$$G = \sum_{\varphi=1}^{\varphi} \sum_{i=1}^{N_{\varphi}} n_{i(\varphi)} \mu_{i\varphi}$$
(2.34)

The total G in Eq. 2.34 is minimized under mass balance constraints by the Solgasmix algorithm using Lagrangian multipliers at constant temperature, pressure and elemental composition (Eriksson, 1979; Peters, 1988; Piro & Simunovic, 2012). When the system components are represented by the chemical elements, the total mass of element i system components can be written as:

$$b_i = \sum_{\varphi} \sum_{i} n_j^{\varphi} a_{ji}^{\varphi} \;\;\;\;\; (i = 1,2,3,......)$$
(2.35)

where n_j^φ is the amount of the jth constituent of phase φ, a_{ji}^φ is a coefficient of the stoichiometry matrix composed of the constituents of phase φ , and b_i is the total amount of the ith system component.

Under given set of constraints, like constant temperature, pressure, and overall composition, the Gibbs energy minimization algorithms search and obtain a set of mole numbers of each phase φ and compositions of each solution phase which minimize the total Gibbs energy of given system.

2.1.5 Themodynamic evaluation and optimization procedure

The thermodyanmic parameter optimization procedure within the CALPHAD method (as shown in Figure 2.4) involves obtaining all reported or estimated data related to the thermodynamic properties of phases and phase equilibria. In a second step, a critical review of the data is performed and a thermodynamic model is selected for every phase. Then, the optimization procedure of each selected model is carried out. This is performed to reproduce simultaneously all critically assessed experimental data. As shown in Figure 2.4, the experimental review, model selection procedures will be repeated several times to obtain final self-consistency results.

The present project will be divided into two main parts: 1) obtaining key experimental data and 2) thermodynamic optimization of all the systems of interest. Obtaining the the key input data for the limited experimental information systems is a challenge in the present work. First-principle calculations is usually used for thermodynamic properties estimation, and key experiment work is used for phase equilibria measurement. As for the optimization of selected systems, many techniques and tactics will be considered, such as:

1) which proper thermodynamic model should be chosen for each phase,

2) how to assess the data according to the quality and credibility of the experimental methods,

3) how to extrapolate or interpolate the thermodynamic data in the ranges needed.
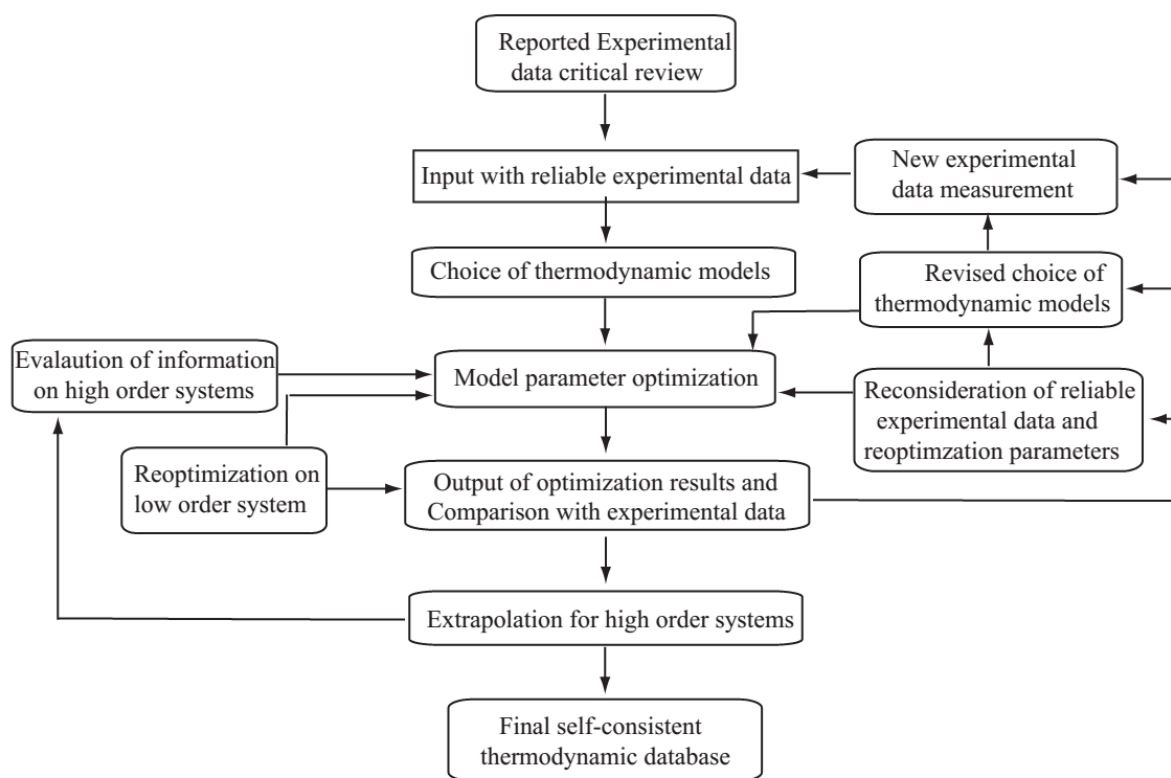
Figure 2.4 Schematic diagram of the optimization procedure of model parameters

The whole procedure of thermodynamic optimization can be divided by the following steps:

1) Gathering and critical review of the reported experimental data, including estimated data from First-Principles Calculations

The reported experimental data on a chemical system A-B-(C) related to the thermodynamic properties of phases includes the enthalpyof mixing, entropy of mixing, Gibbs energy of mixing, chemical potential and activity *etc*. The experimental data of phase equilibira include the phase equilibrium composition, liquidus and solidus curves, phase crystal structure and phase transformation temperature, *etc*. Reported experimental data result from various experimental methods and different investigators. Consequently, some of the experimental data will be very reliable, while others will be less so. Thus, a critical evaluation of all the available experimental

data simultaneously eliminates contradictory or unreliable data. Measurement methods, experimental procedure details (starting materials, experimental procedures, experimental apparatus, *etc.*) and the data source (authors generating the most reliable results are often well known) will be taken into account into the final evaluation decision. For example, the data of enthalpy of formation of the phases obtained from calorimetry usually are more reliable than those obtained from electromotive force (EMF) measurements. Experimental contaminants should be considered also, such as the use of Al_2O_3 crucibles for Mg-, Li-, Ca-, and Sr-containing alloys in high temperature operations.

New experiments are usually required when the reported experimental data are limited or controversial.

2) Choice of an appropriate thermodynamic model for each phase

To construct an accurate and reliable multi-component dataset, the choice of appropriate thermodynamic models for describing the Gibbs energy of phases is critical. In order to obtain a better and more scientific description of the thermodynamic properties, the MQM with consideration of realistic characteristics of the liquid solution is used for liquid solution modeling in the present work.

The solid solutions were modeled with the Compound Energy Formalism model (CEF), and the choice of sub-lattice model is based on crystal structure and solid solubility of each phase. The sublatice structure of solid solution may be modified and adjusted, based on previous optimization results.

3) Optimization the model parameters of phases in each subsystem

The model parameters of phases are optimized, based on the input of evaluated experimental data and selected thermodynamic models. The FactSage^{TM} thermodynamic software (Bale et al., 2002; Bale, et al., 2009) was used in the present work,

The number of optimized model parameters will be set according to the author's experience. Usually, more experimental data are available for the liquid solution than for solid phases. Thus, the thermodynamic parameters of the model for the liquid phase can be optimized first in an reasonable range of values. Then, typically, the enthalpy of formation of the solid solutions and stoichiometric phases can be fixed, based on the pre-optimizaton results of the liquid phase and

the reported experimental data. Finally, the entropy of formation of solid solutions and stoichiometric phases can be adjusted to achieve a global result. These three main steps are usually repeated a few times, based on the previous optimized parameters, to obtain a satisfying result. Here it should be pointed out that the number of parameters per phase will be minimized to achieve acceptable optimization results, as too many parameters often lead to uncertainties in extrapolation into higher order systems.

2.2 Experimental methodology

As discussed in the Section 1.3.2, the phase equilibrium experimental measurements with key-samples and diffusion-couple methods on 6 ternary systems will be performed on the Mg-Sn-X (X: Ag, In, Zn, Ca, and Sr) and the Mg-Zn-Sr systems. The details of the experimental procedures used in the present work are described here.

2.2.1 Preparation of materials

The starting materials supplied by Alfa Aesar company are Mg ingot of 99.8 wt. %, 99.9 wt. % for Ag pieces, 99.5 wt. % for Ca pieces, 99.5 wt. % for Sn shots, Sr ingot with the purity of 99 wt. %, and Zn pieces with purity 99.99 wt. %, and the purity of Ta foil used for protecting samples is 99.5 wt. % with 0.15 mm thickness.

2.2.2 Sample preparation and annealing

During the weighing procedure, all the pure metals were ground to remove the oxidation layer and then washed with ultrasound in high purity ethanol solution. Pure Ca and Sr were kept under oil after weighing due to their high reactivity with the atmosphere. Then all the samples were melted using induction furnaces at Concordia University. Before melting, pure Ca and Sr were removed from the oil and washed with high purity ethanol to remove the oil. All the samples were melted in a cube shaped Ta foil crucible (by the induction furnace) under an argon atmosphere and re-melted at least 3 times in order to obtain a good homogenous microstructure. During the melting procedure, all the samples were held at around 200 ^{o}C for few minutes to vaporize the ethanol or oil. Also, the loss in the fusion of the elements with high vapor pressures has been estimated through sample weighing, and the melting losses was found to be less than 5 wt. % for each sample. The Figure 2.5 shows a schematic diagram of the structure of the furnace.
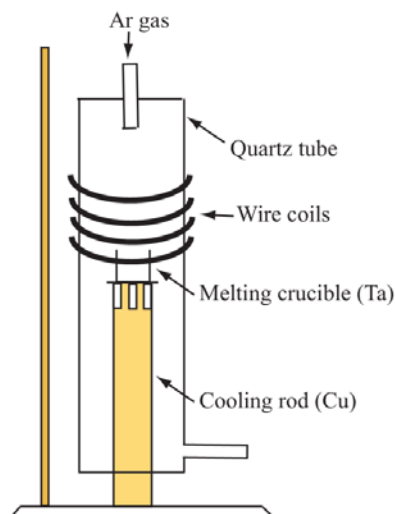
Figure 2.5 Schematic diagram of the structure of the induction melting furnace

After the melting procedure is completed, the key samples were cut into several pieces, and sealed into a quartz tube with Ta foil wrapped under argon. The sealed samples were put into heat furnaces at set temperatures in the range 415-300 ^{o}C for several weeks for annealing. The set temperatures of the furnace was adjusted with two thermo-couples (E-type) in horizonal and vertical directions. The samples were then quenched with cold water within the quartz tube at the end of the annealing period.

2.2.3 Characterization of quenched key samples

The quenched key samples were sealed into resin and polished with 240#~1500# sand paper and polishing paste. For the very reactive of present experimental alloys, the polishing solutions were 99.5 wt. % ethanol for Mg-Sn-X (X: Zn, In, Ag) and Mg-Zn-Sr samples, and mineral oil for Mg-Sn-Ca and Mg-Sn-Sr samples.

Electron probe microanalysis (EPMA) of the quenched samples was performed with the JEOL 8900 probe at McGill University using wavelength-dispersive spectrometry (WDS). An accelerating voltage of 15 kV was used with a 20 nA beam current, a spot size of 2 µm and counting times of 20 s on peaks and 10 s on backgrounds. Raw data were reduced with the PRZ correction using pure Mg, Sn, In and Zn metal standards. Five points in different area of each phase were measured during the EPMA composition analysis. The error limit of the EPMA measurements results is about ±3 %.

Scanning Electron Microscopy (SEM) with Energy Dispersive X-Ray Spectrometry (EDS) was used to analyze the phase compositions of the Mg-Sn-Ca and Mg-Sn-Sr samples. All the samples were put into SEM within 2 minutes after the final polishing, because of their reaction with oxgen and moisture. The analyses of the Mg-Sn-Ca and Mg-Sn-Sr samples were obtained by a Philips XL30 FE-SEM at Mcgill using an accelerating voltage of 15-20 KV. Five points in different areas of each phase were measured, and the error limit of the EDS measurements results is about ±5 %.

The constituent phases of the quenched samples were identified by X-ray diffraction (XRD). All the tested key samples were crushed and ground into powder in an Al_2O_3 crucible. XRD patterns were obtained with the PANanalytical Xpert Pro powder X-ray diffractometer at Concordia University using CuKα radiation at 45 kV and 40 mA. The spectra were acquired from 20 to 120º 2θ with a 0.02º step size. The collected patterns were analyzed with the X'Pert HighScore Plus analysis software using the Pearson's crystal database (Willars, 1997).

Liquidus and polymorphic transformation temperatures were measured by differential scanning calorimetry (DSC) using the SETARAM instrumentation at Concordia University. The samples (typically 50 to 70 mg) were prepared in cylindrical shape, and the bottom surface was polished to be very flat in order to obtain good contact with the crucible. Experiments were carried out with sintered Al_2O_3 crucibles under flowing argon gas. The melting point of each sample was obtained with high heating and cooling rates (10 ^{o}C/min) in several heating steps from 550 to 700 ^{o}C. Then all the samples were measured with heating and cooling rates of 5 ^{o}C/min up to about 20 ^{o}C above their melting temperature in three cycles. Finally, the thermal arrest data were retained if there was no significant difference between the runs in each of the three cycles. The error limit of the DSC measurements is about ±2 ^{o}C.

CHAPITRE 3   ORGNIZATION OF THE ARTICLES

The results obtained in the present work are presented in the following chapters. The chapters are associated with published or submitted articles in peer-reviewed journals. A brief discription is given below on the organization of the presentation of the research results in the following chapters.

Na can potentially be an alloying element that improves the precipitation hardening of Mg-Na-X based systems because there are many stable Na-X (In, Sn, Zn, *etc.*) binary intermetallic phases and ternary intermetallics. Consequently, the thermodynamic optimization of Na-X system are very important to understanding the phase equilibria relation in the designed alloys. The first article presented, in the Chapter 4, is entitled "Thermodynamic evaluation and optimization of the Na-X binary systems (X; Ag, Ca, In, Sn, Zn) using combined Calphad and first-principles method of calculation" was published in the Jounral of Chemical of Thermodynamics (Wang, et al, 2013). Chapter 4 is focused mainly on experimental data evaluation and thermodynamic optimization of phase equilibria of Na-containing binary sub-systems Na-X (X: Ag, Ca, In, Sn, and Zn) as a part of Mg-X (X: Ag, Ca, Li, Na, In, Sn, Sr and Zn) multi-component system study. This article contains a thorough critical literature review and thermodynamic optimization of these five binary sub-systems combined with first-principles calculations of the enthalpy of formation of selected binary compounds. The first-principles calculations were performed by Mr. N. Miao as an independent collaboration. The thermodynamic parameters of the Gibbs energy functions for all phases allows reproduction within good accuracy of the experimental data retained from the critical analysis. It is shown in the present optimizations of the Na-Sn and Na-In binary systems that the Modified Quasichemical Model in Pair Apporximation (MQMAP) for the liquid phase, which takes SRO with a first-neareast-neighbour pairs into account, is able to reproduce the experimental data very well. This includes with the typical "V"-shaped integral enthalpy of mixing curves (and the associated inflections in the partial enthalpy of mixing curves), as well as the typical "m"-shaped integral entropy of mixing curves.

 Mg-Sn based alloys are of great interest in current Mg alloy development. Due to the shortcomings of Mg-Sn based alloys, many additives in Mg-Sn based alloys are being investigated. Chapters 5, 6, 7, and 8 contain with the present experimental and thermodynamic results on the Mg-Sn based systems with selected additives Ag, In, Zn, Li, Ca and Sr.

The article entitled "Thermodynamic optimization of the binary Li-Sn and the ternary Mg-Sn-Li systems" is presented in Chapter 5, which was submitted to the journal CALPHAD: Computer Coupling of Phase Diagrams and Thermochemistry (Wang, et al., 2013). In this article, a critical experimental data evaluation and thermodynamic optimization of the Mg-Sn-Li ternary system was conducted using a coupled First-principles calculations and the CALPHAD method. The first-principles calculations were finished by the one author of the Mr. Han. Based on the experimental data and the results from the First-principle calculations, the thermodynamic model parameters for all solid and liquid phases for binary Li-Sn and ternary Mg-Sn-Li systems were optimized. A comparison is made between the previous optimization of the Li-Sn binary system with Bragg-Williams random mixing approxiomation model (BWM) for the liquid phase and the present optimization with the MQM for the liquid phase.

The third article presented in Chapter 6 is entitled "Experimental and thermodynamic study of Mg-Sn-In-Zn quaternary system" was accepted by the Journal of Alloys and Compounds (Wang, et al., 2013). In this chapter, the phase equilibria in the Mg-rich region of the Mg-Sn-In ternary system at 415 ^{o}C and 330 ^{o}C, and the Mg-Sn-In ternary isoplethal sections at 10 Sn and 5 In (at. %) were studied. Phase equilibria data in the Mg-rich region of the Mg-Sn-Zn ternary system at 300 ^{o}C also have been determined in the present work, which are in agreement with the previous experimental data of Godecke and Sommer (Godecke & Sommer, 1994) and Gladyshevsky and Cherkashin (Gladyshevsky & Cherkashin, 1959). The ternary isoplethal section Mg-Sn-Zn at constant composition of 10 at. % Sn also has been measured in the present work by using DSC. All the reported experimental results from previous investigators and the present work are in reasonable agreement. All the experimental data of the Mg-In, Zn-In and In-Sn binary sub-systems and Mg-Sn-In, Mg-Sn-Zn, and In-Sn-Zn ternary sub-systems were critically evaluated and thermodynamically optimized in the present work, using the MQM for liquid phase. The important advantage of the MQM for modeling the thermodynamic properties of liquid solutions, particularly in high-order systems, has been demonstrated in previous work (Chartrand & Pelton, 2000b; Jin, et al., 2010, 2011). Finally, a self-consistent thermodynamic database for the Mg-Sn-In-Zn quaternary system has been constructed in the present work. This is an important part of the thermodynamic database of the Mg-X (X: Ag, Ca, In, Li, Na, Sn, Sr, and Zn) multicomponent system.

The fourth article presented in Chapter 7 is entitled "Experimental and thermodynamic study of the Mg-Sn-Ag-In quaternary system" and was submitted to the Journal of Phase Equilibria and Diffusion (Wang et al., 2013). The present experimental results of the phase equilibria of Mg-Sn-Ag ternary system are given. A thermodynamic optimization of the quaternary system was carried out using the CALPHAD method. A critical evaluation and thermodynamic assessment on the Ag-Mg, Ag-Sn and Ag-Mg binary systems in the present work are shown. In the Ag-Mg binary system, with reference to the previous optimization by Lim et al. (Lim, et al., 1997), the ordered phases bcc (bcc_A2 and bcc_B2) and fcc (fcc_A1 and fcc_L12) were modeled with two sublattices. The crystal structure symmetry symmetry was considered during setting of the thermodynamic parameters. Furthermore, all the phases and solid solubility limits reported in the previous work were taken into account. In the present work, after a critical evaluation of all the available experimental data, a strict thermodynamical re-optimization on the phase diagram of Ag-In binary system was carried out. This was based on the previous data and recent updated experimental data, and all the pertinent existing phases were considered in the present work. The phase equilibria of the Mg-Ag-In, Mg-Sn-Ag and Ag-In-Sn ternary systems were also optimized in the present work; This was based on the available experimental data also shown in the present chapter. Together with our previous thermodynamic optimization of Mg-Sn-In ternary system in the chapter 6, a self-consistent thermodynamic database for the Mg-Sn-Ag-In quaternary system has been constructed and evaluated with the limited reported experimental data (Kolesnichenko, et al., 1989).

The results in Chapter 8 and entitled "Experimental and thermodynamic study on Mg-Sn-Ca-Li-Sr quinary system" will be submitted for publication in the near future. In this chapter, the experimental phase equilibrium results of the Mg-Sn-Ca and Mg-Sn-Sr ternary systems are presented. The cirirical evaluation and thermodynamic optimization results on the Ca-Sn, Sn-Sr, and Ca-Li binary sub-systems, and Mg-Sn-Ca, Mg-Sn-Sr, Mg-Ca-Sr, and Mg-Ca-Li ternary sub-systems are presented. Finally, a self-consistent thermodynamic database for the Mg-Sn-Ca-Li-Sr quinary system was constructed as part of the final thermodynamic database of the Mg-X (X: Ag, Ca, In, Li, Na, Sn, Sr, and Zn) multicomponent system.

Chapter 9 is entitled "Thermodynamic optimization on Ag-X (X: Ca, Li, Zn and Ca-In) binary systems", which will be submitted for publication in the future. As the part objective for developing the thermodynamic database of Mg-X (X: Ag, Ca, In, Li, Na, Sn, Sr, and Zn) multi-

component system in the present research, the evaluation and optimization results of the rest sub-binary systems are summarized in the chapter 9. In this chapter, the experimental evaluation and thermodynamic optimization results of the Ag-Ca, Ag-Li, Ag-Zn and Ca-In binary sub-systems are presented.

Chapter 10 is a general discussion of the present work. Some examples of the application of the multicomponent thermodynamic database are given. The study of alloy design on Mg-X multi-component system are carried out by present thermodynamic database. And the effect of In, Li and Na on Mg-Sn based alloy was also studied in the present chapter.

Finally, some collaborative work with Mr. Yi-Nan Zhang of Concordia University appear in Appendix 1. The results of this work will be pertinent and valuable in assessing the complete multicomponent database. The report entitled "Experimental and thermodynamic study on Mg-Zn-Sr ternary system and its application for metallic glass" is presented in Apendix 1, and will be submitted for future publication. In this part, the work involves measured phase equilbria of the isothermal section at 300 ^{o}C. The glass forming ability in the Mg-Zn-Sr ternary system was studied with the present thermodynamic database. Folowinging to the calculated results, a series of alloys were studied in the present work with spinning-milling casting, XRD, and DSC for these glass formatibilty properties.

The calculated entropy of mixing of all binary systems optimized in the present work are present in appendix 2 with previously calculated results.

CHAPITRE 4 ARTICLE 1: THERMODYNAMIC EVALUATION AND OPTIMIZATION OF THE (NA+X) BINARY SYSTEMS (X=AG, CA, IN, SN, ZN) USING COMBINED CALPHAD AND FIRST-PRINCIPLES METHODS OF CALCULATION

Jian Wang[a], Naihua Miao[b], Patrice Chartrand[a*], In-Ho Jung[c]

[a] *Center for Research in Computational Thermochemistry (CRCT), Dept. of Chemical Engineering, Ecole Polytechnique, Montréal, Québec, Canada H3C 3A7*

[b] *Physique Théorique des Matériaux, Institut de Physique, Université de Liège, Bât. B5a 3/5, Allée du 6 août, 17, B-4000, Sart Tilman, Belgium*

[c] *Department of Mining and Materials Engineering, McGill University, H.W. Wong Building, 3610 University Street, Montréal, Québec, H3A 2B2, Canada*

[*] *Corresponding author. Center for Research in Computational Thermochemistry (CRCT), Dept. of Chemical Engineering, Ecole Polytechnique, Montréal, Québec, Canada, H3C 3A7. Tel: +1 514 340-4711 ext. 4089; fax: +1 514 340-5840. E-mail address: patrice.chartrand@polymtl.ca*

Abstract

Critical evaluations and optimizations of the (Na + X) binary systems (X: Ag, Ca, In, Sn, Zn) are presented. The enthalpies of formation of $Ag_2Na(cF24\_Fd\bar{3}m)$, $InNa(cF16\_Fd\bar{3}m)$, $NaZn_{13}(cF112\_Fd\bar{3}m)$ and $InNa_2(oC48\_C222_1)$ were estimated from First-Principles calculations. The Modified Quasichemical Model in the Pair Approximation (MQMPA) was used for the liquid solution which exhibits a high degree of short-range order. The solid phases are modeled with the Compound Energy Formalism (CEF). All available and reliable experimental data are reproduced within experimental error limits. The integration of finite temperature First-Principles calculations provides a useful and effective assistance to the Calphad modeling approach. Finally, the short-range ordering behavior of (Na + In) and (Na + Sn) in the liquid solution is studied.

4.1 Introduction

The low density of magnesium alloys is a strong driving force for their applications in the automotive and aeronautical industries. Compared to other structural materials, such as aluminum alloys and steels, the use of magnesium alloys can potentially reduce the weight of vehicles and their fuel consumption. A major alloying element in Mg alloys is aluminum, but most of the Mg-Al based alloys, except the AE series, have poor mechanical properties at high temperature, which restricts their applications. The current trend is to improve Mg-based alloys for high temperature applications. Mg–Sn based alloys have stable microstructures and good mechanical properties at high temperature due to the high solubility of Sn in hcp(Mg) and to the potential precipitation of a cubic second phase (Mg2Sn) in the magnesium-rich matrix [1, 2]. Previous investigations [1-3] indicate that (Mg + Sn) alloys with additional alloying elements have comparable or even better creep properties than AE42 alloys. In addition, it is known that Sn can improve the corrosion resistance [4, 5]. Unfortunately, the behavior of (Mg + Sn) alloys during ageing after quenching requires quite long aeging times to reach the peak hardness, which is not practical for industrial applications [6]. Hence, it is necessary to improve the age hardening response and creep resistant behavior of (Mg + Sn) alloys. Adding microalloying elements can potentially achieve this goal, with many alloying elements such as Ag, Ca, Li, Na, Zn, Sr, In and rare-earth elements being considered [7-9]. For precipitation hardenable alloys, Mendis et al. [7, 8] proposed a qualitative thermo-kinetic criteria for choosing microalloying additions (In, Li, Na, and Zn). In the case of (In + Li) additions, the increase in number density is closer to one order of magnitude and the hardening increment is about 150% (270% with Na) [8]. A similar result has also been reported by Sasaki et al. [9] with (Na + Zn) additions. Gibson et al. [10] reported that (Mg + Sn + Zn + Na) alloys show secondary creep rates five orders of magnitudes lower than binary (Mg + Sn) alloys and approximately three orders of magnitudes lower than ternary (Mg + Sn + Zn) alloys. Park et al. [11] reported that the addition of Ag to (Mg + Zn) alloys can increase the tensile strength in a double aging condition. Mendis et al. [12] studied the effects of additives of Ag and Ca on the (Mg + Zn) alloys, and pointed out that the hardness was enhanced due to the refinement of precipitates. Thus a systematical study on the role of additives Ag, Na, In, Ca and Zn for the mechanical properties improvement of (Mg + Sn) based alloys is necessary.

In order to design new (Mg + Sn)-based alloys and to understand the relationship between their microstructures and mechanical properties, a better knowledge of the phase relationships in (Mg + Sn)-based alloys is imperative, starting with phase equilibria. Obtaining such information by the sole mean of experimental techniques is cumbersome and costly. Fortunately, thermodynamic modeling of multi-component systems by the CALPHAD (Calculation of Phase Diagrams) [13] approach has been shown to be a very efficient way to investigate phase equilibria [14]. Coupled phase-field calculations, ab initio calculations, and physical properties modeling permit one to estimate material properties [15]. In the present work, the (Na + X) binary systems (X = Ag, Ca, In, Sn, and Zn) were studied, as part of a wider thermodynamic database development project for (Mg + Sn + X) multi-component systems (X: Ag, Ca, In, Li, Na, Sr, and Zn).

The available experimental data on phase equilibria and on the thermodynamic properties of the condensed phases has been critically reviewed. Due to the lack of thermodynamic data for several compounds in the (Na + X) binary systems (X = Ag, Ca, In, Sn, and Zn), and due to the experimental difficulties (high vapour pressures) of measuring this type of data in such chemical systems, first-principles calculations were used to obtain the enthalpy of formation for several solid phases in the present study. Using the CALPHAD technique, a consistant set of model parameters has been obtained for all condensed phases in the (Na + X) binary systems (X = Ag, Ca, In, Sn, and Zn). The parameters will be added to a thermodynamic database for Mg alloys.

4.2 Thermodynamic models

In the present work, all the thermodynamic optimizations of the (Na + X) binary systems (X = Ag, Ca, In, Sn, and Zn) have been carried out by means of the FactSage thermodynamic software [16]. The phases considered are listed in table 4.1, along with the model used to describe their thermodynamic properties. The thermodynamic parameters of the pure elements are the recommanded SGTE values [17].

Table 4.1 Binary phases considered in the present work in the (Na + X) binary systems (X= Ag, Ca, In, Sn, and Zn)

Phase	Strukturbericht	Prototype	Pearson symbol	Space group	Model[a]
Liquid	-	-	-	-	MQM
fcc	A1	Cu	cF4	$Fm\bar{3}m$	CEF
bcc	A2	W	cI2	$Im\bar{3}m$	CEF
hcp	A3	Mg	hP2	$P6_3/mmc$	CEF
bct	A5	Sn	tI4	$I4_1/amd$	CEF
tet	A6	In	tI2	$I4/mmm$	CEF
Ag_2Na	C15	Cu_2Mg	cF24	$Fd\bar{3}m$	CEF
In_9Na_5	-	-	-	-	ST
InNa	B32	NaTl	cF16	$Fd\bar{3}m$	ST
$InNa_2$	-	-	-	-	ST
In_5Na_3	-	-	-	-	ST
$Na_{15}Sn_4$	$D8_6$	$Cu_{15}Si_4$	cI76	$I\bar{4}3d$	ST
$NaSn_3$	-	-	-	-	ST
Na_9Sn_4	-	Na_9Sn_4	oC52	$Cmcm$	ST
Na_4Sn_3	-	-	-	-	ST
$\beta NaSn$	-	-	-	-	ST
$\alpha NaSn$	-	NaPb	tI64	$I4_1/acd$	ST
$NaSn_2$	-	-	-	-	ST
$NaSn_3$	-	-	-	-	ST
$NaSn_4$	-	-	-	-	ST
$NaSn_6$	-	-	-	-	ST
$NaZn_{13}$	$D2_3$	$NaZn_{13}$	cF112	$Fd\bar{3}m$	ST

[a] MQM: Modified Quasichemical Model with Pair approximation [19]; CEF: Compound Energy Formalism; ST: Stoichiometric compound

4.2.1 Liquid phase

The thermodynamic properties of the liquid phase were modeled using the Modified Quasichemical Model in the Pair Approximation (MQMPA) developed by Pelton et al. [18, 19]. A detailed description of the MQMPA and its associated notation is given in refs. [18, 19]. The same notation is used in the present work, and a brief description of MQMPA is given as follows:

For the binary $(A + B)$ system, the quasichemical pair exchange reaction can be considered:

$$(A - A)_{pair} + (B - B)_{pair} = 2(A - B)_{pair,} \quad \Delta g_{AB} \tag{4.1}$$

where $i - j$ pair represents a first-nearest-neighbor pair of atoms. The Gibbs energy change for the formation of one mole of $(A - B)$ pairs according to Reaction (1) is $\Delta g_{AB}/2$. Let n_A and n_B be the number of moles of A and B, n_{AA}, n_{BB}, and n_{AB} be the number of moles of $A - A$, $B - B$, and $A - B$ pairs. Z_A and Z_B are the coordination numbers of A and B. Then the Gibbs energy of the solution is given by:

$$G = (n_A G_A^o + n_B G_B^o) - T\Delta S^{config} + (n_{AB} / 2)\Delta g_{AB} \tag{4.2}$$

where G_A^o and G_B^o are the molar Gibbs energies of the pure component A and B, and ΔS^{config} is the configurational entropy of mixing given by randomly distributing the $A - A$, $B - B$ and $A - B$ pairs in the one-dimensional Ising approximation. The expression for ΔS^{config} is:

$$\begin{aligned}\Delta S^{config} = &-R(n_A \ln X_A + n_B \ln X_B) \\ &- R(n_{AA} \ln \frac{X_{AA}}{Y_A^2} + n_{BB} \ln \frac{X_{BB}}{Y_B^2} + n_{AB} \ln \frac{X_{AB}}{2Y_A Y_B})\end{aligned} \tag{4.3}$$

where X_{AA}, X_{BB} and X_{AB} are the mole fractions of the $A - A$, $B - B$ and $A - B$ pairs respectively; Y_A and Y_B are the coordination-equivalent fractions of A and B:

$$X_{ij} = \frac{n_{ij}}{n_{AA} + n_{BB} + n_{AB}} \quad (i, j = A \text{ or } B) \tag{4.4}$$

$$Y_i = \frac{Z_i n_i}{Z_A n_A + Z_B n_B} \quad (i = A \text{ or } B) \tag{4.5}$$

Moreover, the following elemental balance equations can be written:

$$Z_A n_A = 2n_{AA} + n_{AB} \tag{4.6}$$

$$Z_B n_B = 2n_{BB} + n_{AB} \tag{4.7}$$

It may be noted that there is no exact expression for the configurational entropy in three dimensions. Although Eq. (4.3) is only an approximate expression in three dimensions, it is exact one-dimensionally (when $Z = 2$) [19]. As explained in [19], one is forced by the approximate

nature of Eq. 3 to use non-exact values for the coordination numbers in order to yield good fits between the experimental data and calculated ones. The mathematical approximation of the one-dimensional Ising model of Eq. (4.3) can be partially compensated by selecting values of Z_A and Z_B which are smaller than the experimental values [20]. As is known, the MQMPA model is sensitive to the ratio of coordination numbers, but less sensitive to their absolute values. From a practical standpoint for the development of large thermodynamic databases, values of Z_A and Z_B of the order of 6 have been found necessary for the solutions with a small or medium degree of ordering (*i.e.* alloy solutions).

Δg_{AB} is the model parameter to reproduce the Gibbs energy of liquid phase of the $A-B$ binary system, which is expanded as a polynomial in terms of the pair fractions, as follows:

$$\Delta g_{AB} = \Delta g_{AB}^{o} + \sum_{i \geq 1} g_{AB}^{io} (X_{AA})^{i} + \sum_{j \geq 1} g_{AB}^{oj} (X_{BB})^{j} \tag{4.8}$$

where Δg_{AA}^{o}, g_{AB}^{io} and g_{AB}^{oj} are the adjustable model parameters which can be function of the temperature. The equilibrium state of the system is obtained by minimizing the total Gibbs energy at constant elemental composition, temperature and pressure. The equilibrium pair distribution is calculated by setting:

$$\left(\frac{\partial G}{\partial n_{AB}} \right)_{n_A, n_B} = 0 \tag{4.9}$$

This gives the ''equilibrium constant'' for the ''quasichemical pair reaction'' of Eq. (1):

$$\frac{X_{AB}^{2}}{X_{AA} X_{BB}} = 4 \times \exp\left(-\frac{\Delta g_{AB}}{RT} \right) \tag{4.10}$$

Moreover, the model permits Z_A and Z_B to vary with composition as follows [19]:

$$\frac{1}{Z_A} = \frac{1}{Z_{AA}^{A}} \left(\frac{2n_{AA}}{2n_{AA} + n_{AB}} \right) + \frac{1}{Z_{AB}^{A}} \left(\frac{n_{AB}}{2n_{AA} + n_{AB}} \right) \tag{4.11}$$

$$\frac{1}{Z_B} = \frac{1}{Z_{BB}^{B}} \left(\frac{2n_{BB}}{2n_{BB} + n_{AB}} \right) + \frac{1}{Z_{AB}^{B}} \left(\frac{n_{AB}}{2n_{BB} + n_{AB}} \right) \tag{4.12}$$

where Z_{AA}^{A} and Z_{AB}^{A} are the values of Z_A when all nearest neighbours of an atom A are As, and when all nearest neighbours of an atom A are Bs respectively. Z_{BB}^{B} and Z_{AB}^{B} are defined similarly.

The composition of maximum short-range ordering (SRO) is determined by the ratio of the coordination numbers Z_{AB}^A / Z_{AB}^B. The values of the coordination numbers chosen in the present study are listed in Table 4. 2.

Table 4.2 Optimized model parameters of the MQM for the liquid phase in the (Na + X) binary systems (X= Ag, Ca, In, Sn, and Zn)

Coordination numbers [a]				Gibbs energies of pair exchange reactions
i	j	Z_{ij}^i	Z_{ij}^j	
Ag	Na	6	6	$\Delta g_{Ag,Na} / (J \cdot mol^{-1}) = -974.9 - 1427.2 X_{AgAg} + 7740.4 X_{NaNa}$
Ca	Na	6	6	$\Delta g_{Ca,Na} / (J \cdot mol^{-1}) = 8075.1 + 2050.2 X_{CaCa} - 3138 X_{NaNa}$
In	Na	6	7.5	$\Delta g_{In,Na} / (J \cdot mol^{-1}) = -9706.9 + 4.60(T/K) + (2301.2 - 0.628(T/K)) X_{InIn}$ $+ (3556.4 + 3.347(T/K)) X_{NaNa}$
Sn	Na	5.6	4.4	$\Delta g_{Na,Sn} / (J \cdot mol^{-1}) = -21924.2 + 8.703(T/K) + (1631.8 - 0.460(T/K)) X_{NaNa}$ $+ (2175.7 - 1.172(T/K)) X_{SnSn}$
Zn	Na	6	6	$\Delta g_{Na,Zn} / (J \cdot mol^{-1}) = 11338.6 - 3.35(T/K) + (4184 - 5.02(T/K)) X_{NaNa}$ $+ (2092 + 1.26(T/K)) X_{ZnZn}$
[a] For all pure elements (Na, Ag, Ca, In, Sn, and Zn), $Z_{ij}^j = 6$				

4.2.2 Solid Solutions

The Compound Energy Formalism (CEF) was introduced by Hillert to describe the Gibbs energy of solid phases with sub-lattices, and ideal mixing on each sub-lattice is assumed [21]. In the present work, all solid solutions (hcp, bct, bcc and fcc) and the ordered intermetallic solutions in the (Na + X) binary systems (X = Ag, Ca, In, Sn, and Zn) were modeled with the CEF with their sublattice stoichiometry based on the reported crystal structures. Taking the $Ag_2Na(cF24\_Fd\bar{3}m)$ solution for example, its Gibbs energy expression, based on the CEF, is obtained by mixing Ag and Na on two sublattices with a stoichiometry ratio of 2:1, as in $(Ag, Na)_2(Ag, Na)$. The Gibbs energy of the laves_C15 solution can be expressed as:

$$G^{Ag_2Na} = y_{Ag}^I y_{Na}^{II}\ {}^0G_{Ag:Na}^{Ag_2Na} + y_{Ag}^I y_{Ag}^{II}\ {}^0G_{Ag:Ag}^{Ag_2Na} + y_{Na}^I y_{Na}^{II}\ {}^0G_{Na:Na}^{Ag_2Na} + y_{Na}^I y_{Ag}^{II}\ {}^0G_{Na:Ag}^{Ag_2Na}$$
$$+ 2RT(y_{Ag}^I \ln y_{Ag}^I + y_{Na}^I \ln y_{Na}^I) + RT(y_{Ag}^{II} \ln y_{Ag}^{II} + y_{Na}^{II} \ln y_{Na}^{II})$$
$$+ y_{Ag}^I y_{Na}^I y_{Ag}^{II}\ {}^nL_{Ag,Na:Ag} + y_{Ag}^I y_{Na}^I y_{Na}^{II}\ {}^nL_{Ag,Na:Na} + y_{Ag}^I y_{Ag}^{II} y_{Na}^{II}\ {}^nL_{Ag:Na,Na}$$
$$+ y_{Na}^I y_{Ag}^{II} y_{Na}^{II}\ {}^nL_{Na:Ag,Na} \tag{4.13}$$

where y_*^I and y_*^{II} are the site fractions of elements Ag or Na on the first and second sublattices, respectively. The values of ${}^0G_{*:*}^{Ag_2Na}$ represent the Gibbs free energies of the end-members of the Ag_2Na solution when the first and second sublattices are completely occupied by one of the four permutations of Ag and Na, in the laves_C15 structure. $L_{Ag,Na:*}$ and $L_{*:Ag,Na}$ are the second-nearest neighbor interaction parameters between Ag and Na when the other sublattice is fully occupied by either Na or Ag, and they can be expressed as linear functions of temperature:

$${}^nL_{Ag,Na:*} = a_n + b_n T \tag{4.14}$$

and

$${}^nL_{*:Ag,Na} = a_n' + b_n' T \tag{4.15}$$

The parameters a_n, b_n, a_n' and b_n' are evaluated, and they were set as "0" in the present work.

4.2.3 Stoichiometric phases

The molar Gibbs energies of pure elements and stoichiometric phases can be described by:

$$G_T^o = H_T^o - TS_T^o \tag{4.16}$$

$$H_T^o = \Delta H_{298.15K}^o + \int_{298.15K}^T CpdT \tag{4.17}$$

$$S_T^o = S_{298.15K}^o + \int_{298.15K}^T (Cp/T)dT \tag{4.18}$$

where $\Delta H_{298.15K}^o$ is the molar enthalpy of formation of a given species from pure elements ($\Delta H_{298.15K}^o$ of element stable at 298.15 K and 1 atm is assumed as 0 J·mol^{-1}; reference state), $S_{298.15K}^o$ is the molar entropy at 298.15 K and C$_p$ is the molar heat capacity. As there are no heat capacity experimentals of intermetallics, the heat capacities were evaluated using Neumann–Kopp rule [22]. Both heat capacities of solid In, Na and Sn from SGTE database shows maximum just above their melting temperatures (that is in the liquid stable region). Several intermetallic phases

in the studied system have their melting temperature substantially higher that the pure elements they are formed from. The resultant heat capacities of intermetallic phases, from the Neumann–Kopp rule, had also maximum at about 506 K, which is not likely in reality. In order to resolve this, we modified the heat capacities of solid In, Na and Sn above their melting temperature to make sure that the heat capacities of intermetallics can increase with temperatures until their melting temperatures (Table 4.5). This is solely applied in the Neumann–Kopp rule, not for the pure elements. Hence, this proposed modification does not influence the pure In, Na and Sn elements.

4.3   First-principles calculations method

First-principles total energy calculations were performed based on density functional theory (DFT), in order to estimate the thermodynamic properties of pure intermetallic phases. The projector augmented-wave (PAW) method [23-26] was used to solve the Kohn-Sham equations. We employed the PAW pseudopotentials with the following electronic configurations: Na $3s^1$, Ag $4d^{10}5s^1$, In $5s^25p^1$ and Zn $3d^{10}4s^2$. The generalized gradient approximation (GGA) [27] and Perdew Burke Ernzerhof functional (PBE) [28] were used for exchange correlation functions. The cutoff energy for plane wave basis set was 700 eV. The following k-points and Monkhorst–Pack (MP) scheme [29] were adopted as Brillouin Zone sampling: 12×12×12 for Na and Ag, 15×15×10 for In, 11×11×6 for Zn, 6×6×6 for Ag_2Na, 8×8×8 for $InNa$, 4×6×4 for $InNa_2$, and 2×2×2 for $NaZn_{13}$. The relaxation convergences for ions and electrons were $1×10^{-5}$ eV and $1×10^{-6}$ eV, respectively. The initial crystal structures have been built on the basis of the experimental crystallographic data and the optimized lattice parameters along with the compiled data from Pearson's handbook [30] are summarized in table 4.3. All the lattice parameters obtained in present work are in good agreement with the reported experimental data.

The total energy was calculated for the optimized crystal structures. The formation energy E_{form} for a given crystal A_xB_y was obtained according to $E_{\text{form}} = E_{\text{total}}^{(AxBy)} - xE_{\text{total}}^{(A)} - yE_{\text{total}}^{(B)}$, where $E_{\text{total}}^{(AxBy)}$, $E_{\text{total}}^{(A)}$ and $E_{\text{total}}^{(B)}$ were the total energy of A_xB_y, A and B crystals, respectively. The calculated heat of formation of the phases of Ag_2Na ($cF24\_Fd\bar{3}m$), $InNa$ ($cF16\_Fd\bar{3}m$), $NaZn_{13}$ ($cF112\_Fd\bar{3}m$) and $InNa_2$ ($oC48\_C222_1$) at 0 K also are summarized in table 4.3.

Table 4.3 Crystallographic data and calculated standard enthalpy of formation, ΔH_f^o of solid phases

Phase	Pearson symbol	Space group	Lattice parameter (nm)			Reference	ΔH_f (kJ·mol-atom^{-1})	
			a	b	c		FPC	Calphad
Ag_2Na	cF24	$Fd\bar{3}m$	0.7923	0.7923	0.7923	[30]	-10.55[a]	-10.36[a]
			0.8027	0.8027	0.8027	Present work		
$InNa$	cF16	$Fd\bar{3}m$	0.7332	0.7332	0.7332	[30]	-14.56[a] / -23.8[b]	-15.44[a]
			0.7460	0.7460	0.7460	Present work		
$InNa_2$	oC48	$C222_1$	1.3855	0.8836	1.1762	[30]	-11.04[a]	-10.52[a]
			1.3944	0.8851	1.1741	Present work		
In_5Na_3	-	-	-	-	-	[30]	-	-17.03[a]
In_9Na_5	-	-	-	-	-	[30]	-	-16.24[a]
$NaZn_{13}$	cF112	$Fd\bar{3}m$	1.2836	1.2836	1.2836	[30]	-3.25[a]	-3.15[a]
			1.2292	1.2292	1.2292	Present work		
[a] ΔH_f^o were calculated in this work using FPC (T= 0 K) and Calphad (T=298.15 K) methods separately, [b] ΔH_f^o were calculated by Ozisik et al. [60] using FPC (T= 0 K) occurring in the (Na + X) binary systems (X= Ag, Ca, In, Sn, and Zn)								

4.4 Critical evaluation and thermodynamic optimization of binary systems

4.4.1 The (Na + Ag) system

Pelton [31] critically reviewed the reported experimental phase equilibrium and thermodynamic data in the (Na + Ag) binary system. Only one intermetallic compound Ag_2Na is reported [32]. The Ag-liquidus curve was studied by Quercigh [33], Kienast and Verma [32], and Mathewson [34] with thermal analysis methods. There is a good agreement between the different data sets, except in the Ag-rich portion (> 75 at. % Ag) reported by Kienast and Verma [32], which are about 30-50 K higher than that of the two refs. [33, 34]. Pelton calculated that the experimental liquidus points of Kienast and Verma do not respect the theoretical limiting slope of the liquidus in this region of composition [31]. At lower temperatures (273 K to 550 K) the liquidus was determined by solubility measurements by Lamprecht and Crowther [35] and for 373 K to 823 K by Weeks [36]. Both reported dataset are in good agreement. The solubility of Na in fcc (Ag) was reported as 1 at. % by Mathewson [34] using chemical analysis. But the author also reported that

this value is most probably much too high, because of the presence of mechanically entrained Na in the samples. The ratio of atomic radii of Ag and Na indicates that solid solubility should be very limited. The X-ray study by Kienast and Verma [32] shows the existence of a Ag_2Na phase with the laves_C15 crystal structure which is similar to the Au_2Na phase reported in the (Au + Na) binary system [37]. The temperature of the peritectic reaction $liquid + fcc \leftrightarrow Ag_2Na$ was reported as 595.15 K by Kienast and Verma [32] using thermal arrest observations. There is no experimental data reported on the thermodynamic properties of the liquid phase or of the Ag_2Na compound.

All the experimental data discussed above were taken into account in the present thermodynamic optimization. The enthalpy of formation of Ag_2Na ($cF24\_Fd\bar{3}m$) at 0 K was calculated by first-principles calculations and is used in present work (table 4.3).

The calculated phase diagram of the (Na + Ag) system is shown in Figure 4.1, compared with the reported experimental data [32-34]. As discussed above, it was considered not necessary to use complex thermodynamic functions to fit the disputable experimental data of Kienast and Verma [32] in the range of Na contents below 25 at. %. The metastable misciblility gap of the liquid phase at low temperature was also calculated by using present optimized thermodynamic parameters as shown in Figure 4.1. The calculated consolute temperature of the metastable miscibility gap of the liquid is at 1013 K and 41.73 at. % Ag (the consolute point of the (Na + Cu) liquid miscibility gap is above 1273 K [38] – note that the (Na + Au) binary system has 3 stable compounds [37]). The stoichiometric compound Ag_2Na was modeled using a two-sublattics model $(Ag, Na)_2(Ag, Na)$ based on its reported crystal structure (laves_C15) [39]. The temperature of the peritectic reaction $liquid + fcc \leftrightarrow Ag_2Na$ is calculated at 595.15 K as reported by Kienast and Verma [32]. The calculated entropy of mixing of the liquid phase at 1273 K along with the ideal entropy mixing curves are shown in Figure 4.2. The optimized thermodynamic parameters of the present study are summarized in Tables 4.2 and 4.4.

Table 4.4 Optimized parameters of solid solutions in the (Na + X) binary systems (X= Ag, Ca, In, Sn, and Zn)

Ag_2Na phase, $(Ag,Na)_2(Ag,Na)$:

$G_{Ag:Ag} / (J \cdot mol^{-1}) = 3 \times {}^0G_{Ag}^{fcc} + 45000.0;$ $\quad G_{Na:Na} / (J \cdot mol^{-1}) = 3 \times {}^0G_{Na}^{bcc} + 45000.0$

$G_{Na:Ag} /(J \cdot mol^{-1}) = 2 \times {}^0G_{Na}^{bcc} + {}^0G_{Ag}^{fcc} + 45000.0;$ $\quad G_{Ag:Na} /(J \cdot mol^{-1}) = 2 \times {}^0G_{Ag}^{fcc} + {}^0G_{Na}^{bcc} - 31380.0 + 50.21(T/K)$

---

fcc_A1 phase, $(Ag,Ca,In,Na,Sn,Zn)(Va)_3$:

$G_{Ag:Va} / (J \cdot mol^{-1}) = {}^0G_{Ag}^{fcc};$ $\quad G_{Ca:Va} / (J \cdot mol^{-1}) = {}^0G_{Ca}^{fcc};$ $\quad G_{Na:Va} / (J \cdot mol^{-1}) = {}^0G_{Na}^{bcc} - 50.0 + 1.30(T/K)$

$G_{In:Va} / (J \cdot mol^{-1}) = {}^0G_{In}^{tet} + 123.0 - 0.30(T/K);$ $\quad G_{Sn:Va} / (J \cdot mol^{-1}) = {}^0G_{Sn}^{bct} + 4150.0 - 5.20(T/K)$

$G_{Zn:Va} / (J \cdot mol^{-1}) = {}^0G_{Zn}^{hcp-Zn} + 2969.8 + 1.57(T/K),$

$L_{Ag,Na:Va} / (J \cdot mol^{-1}) = 46024.0;$ $\quad L_{Ca,Na:Va} / (J \cdot mol^{-1}) = 20920.0;$ $\quad L_{Zn,Na:Va} / (J \cdot mol^{-1}) = 20920.0$

---

bcc_A2 phase, $(Ag,Ca,In,Na,Sn,Zn)(Va)_3$:

$G_{Ag:Va} / (J \cdot mol^{-1}) = {}^0G_{Ag}^{fcc} + 3400.0 + 1.05(T/K);$ $\quad G_{Ca:Va} / (J \cdot mol^{-1}) = {}^0G_{Ca}^{fcc} + 1405.0 + 2.25(T/K)$

$G_{Na:Va} / (J \cdot mol^{-1}) = {}^0G_{Na}^{bcc};$ $\quad\quad\quad\quad G_{In:Va} / (J \cdot mol^{-1}) = {}^0G_{In}^{tet} + 800.0 - 0.80(T/K);$

$G_{Sn:Va} / (J \cdot mol^{-1}) = {}^0G_{Sn}^{bct} + 4400.0 - 6.00(T/K);$ $\quad G_{Zn:Va} / (J \cdot mol^{-1}) = {}^0G_{Zn}^{hcp-Zn} + 2886.0 - 2.50(T/K)$

$L_{Ag,Na:Va} / (J \cdot mol^{-1}) = 20920.0;$ $\quad L_{Ca,Na:Va} / (J \cdot mol^{-1}) = 29330.0 - 10.50(T/K);$ $\quad L_{Zn,Na:Va} / (J \cdot mol^{-1}) = 20920.0$

---

tet_A6 phase, $(Ag,Ca,In,Na,Sn,Zn)(Va)_3$:

$G_{Ag:Va} / (J \cdot mol^{-1}) = {}^0G_{Ag}^{fcc} + 15000.0;$ $\quad G_{Ca:Va} / (J \cdot mol^{-1}) = {}^0G_{Ca}^{fcc} + 15000.0$

$G_{Na:Va} / (J \cdot mol^{-1}) = {}^0G_{Na}^{bcc} + 50208.0;$ $\quad G_{In:Va} / (J \cdot mol^{-1}) = {}^0G_{In}^{tet}$

$G_{Sn:Va} / (J \cdot mol^{-1}) = {}^0G_{Sn}^{bct} + 5388.0 - 8.25(T/K);$ $\quad G_{Zn:Va} / (J \cdot mol^{-1}) = {}^0G_{Zn}^{hcp-Zn} + 17505.0$

${}^0L_{In,Na:Va} / (J \cdot mol^{-1}) = -103428.0;$ $\quad {}^1L_{In,Na:Va} / (J \cdot mol^{-1}) = -29706.0$

$L_{Zn,Na:Va} / (J \cdot mol^{-1}) = 20920.0$

$hcp\_A3(Zn)$ phase, $(Ag,Ca,In,Na,Sn,Zn)(Va)_3$:

$G_{Ag:Va} / (J \cdot mol^{-1}) = {}^0G_{Ag}^{fcc} + 2000.0;$ $\quad G_{Ca:Va} / (J \cdot mol^{-1}) = {}^0G_{Ca}^{fcc} + 2000.0$

$G_{Na:Va} / (J \cdot mol^{-1}) = {}^0G_{Na}^{bcc} + 2000.0;$ $\quad G_{In:Va} / (J \cdot mol^{-1}) = {}^0G_{In}^{tet} + 2000.0$

$G_{Sn:Va} / (J \cdot mol^{-1}) = {}^0G_{Sn}^{bct} + 2000.0;$ $\quad G_{Zn:Va} / (J \cdot mol^{-1}) = {}^0G_{Zn}^{hcp-Zn}$

$L_{Zn,Na:Va} / (J \cdot mol^{-1}) = 10000.0$
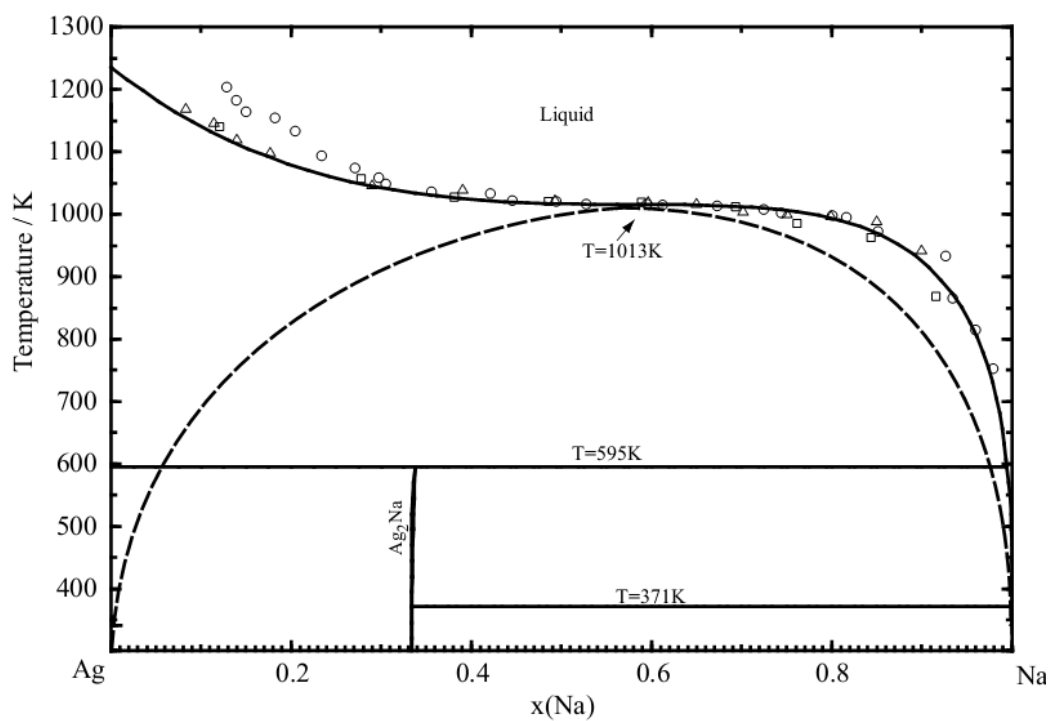
Figure 4.1 Calculated (Ag + Na) phase diagram system. Experimental data are from Kienast and Verma [32] (○), Quercigh [33] (□), and Mathewson [34] (△)
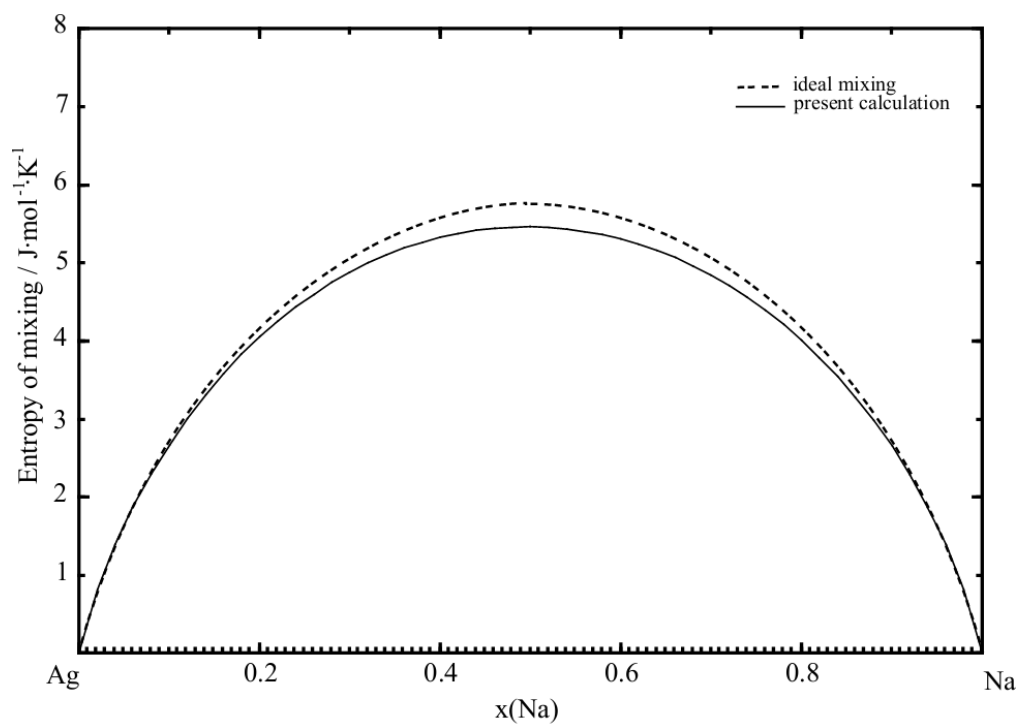
Figure 4.2 Calculated entropy of mixing of the (Na + Ag) binary liquid at 1273 K

4.4.2 The (Na + Ca) system

The (Na + Ca) system was first studied by Muthmann et al. [40], and Lorenz and Winzer [41, 42]. Later Rinck et al. [43] determined the limits of the miscibility gap of the liquid phase via the reaction Ca + 2NaCl = CaCl$_2$ + 2Na at various temperatures. The liquidus curves and the temperature of the monotectic reaction were also measured using thermal analysis techniques. The reported value of the melting temperature of Ca as 1082.15 K (instead of 1115.15 K) by Lorenz and Winzer [41, 42] suggests that there was some contamination in their samples, therefore the liquidus data reported by Rinck et al. [43] are considered more reliable. Thus, Pelton [44] evaluated the (Na + Ca) phase diagram mainly based on the experimental data of Rinck et al. [43]. There is no reported experimental thermodynamic properties data on the (Na + Ca) binary system. The (Na + Ca) binary system was thermodynamic optimized by Zhang et al. [45] with Bragg–Williams random mixing approximation model for the liquid phase.

The optimized phase diagram of the (Na + Ca) system of the present work, compared with reported experimental data, is shown in Figure 4.3. The calculated monotectic reaction temperature is 983.15 K with the compostions of the two liquids in equilibrium being 22.5 and 96.5 at.% Na, which is in a good agreement with the experimental data of 22.1 and 95.9 at.% Na at 983.15 K as reported by Rinck et al. [43]. And the calculated maximum solubility of Na in bcc Ca is 8.0 at.% compared to 7.5 at.% reported by Pelton [44] using the limiting slopes of the calcium liquidus. The calculated maximum temperature of the liquid miscibility gap is 1433 K at 69 at. % Na in the present work. The calculated entropy of mixing of liquid phase at 1473 K is shown in Figure 4. 4 along with the calculated entropy of mixing calculated with an ideal solution model and the model proposed by Zhang et al. [45]. The entropy of mixing proposed by Zhang et al. [45] is substantially larger than the ideal solution entropy, which is dubious for this relatively simple system (see in Figure 4.4). All the optimized thermodynamic parameters of the present study are summarized in Table 4.2 and table 4.4.
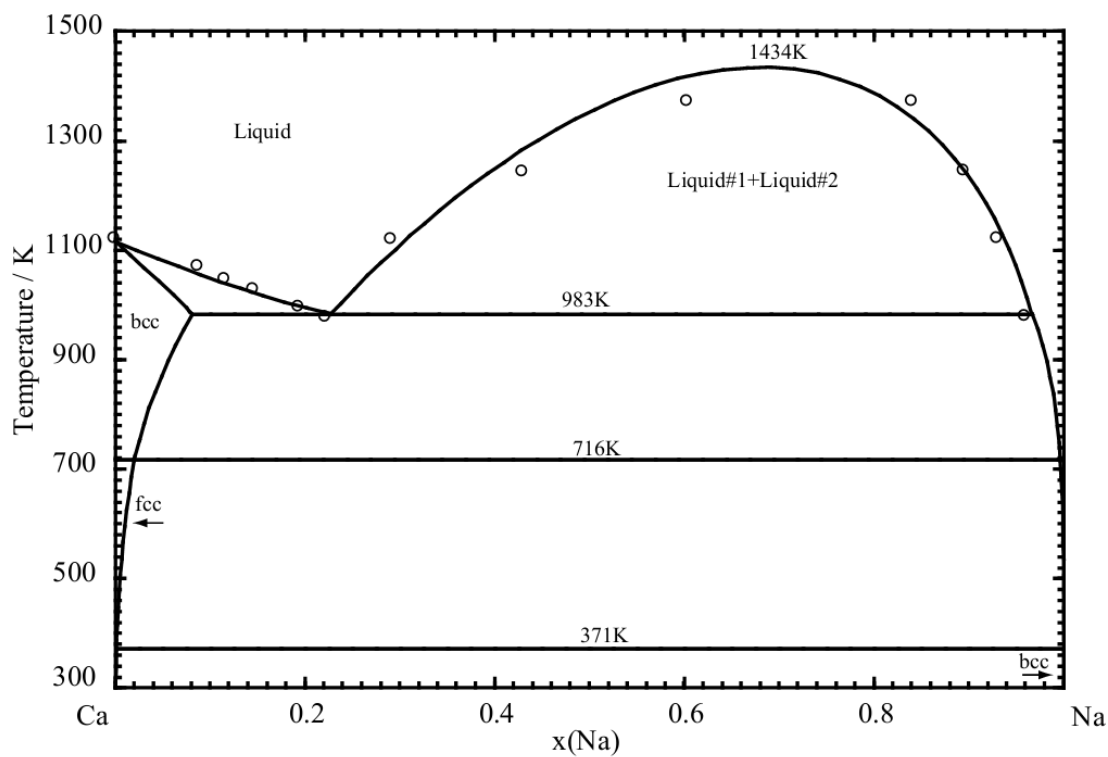
Figure 4.3 Calculated (Na + Ca) phase diagram. Experimental data are from Rinck et al. [43] (○)
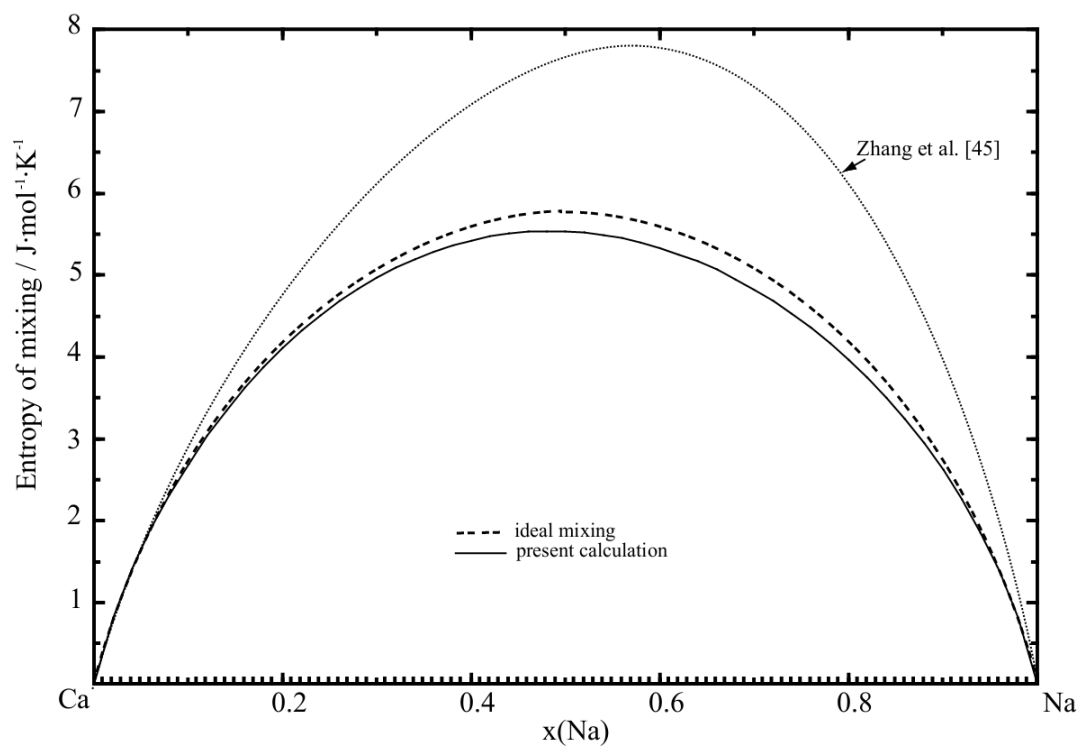
Figure 4.4 Calculated entropy of mixing of the (Ca + Na) binary liquid at 1473 K.

4.4.3 The (Na + In) system

Phase equilibria of (Na + In) binary system in the composition of 0-51 at. % Na region was investigated by Heberlein [46] using thermal analysis and metallographic techniques. The temperature of the peritectic reaction $Liquid + In_8Na_5 \leftrightarrow tet(In)$ was reported at 433.15 K. The solubility of In in liquid Na was measured by Davies [47] by using thermal analysis. The same author also reported that the temperature of the the eutectic reaction $Liquid \leftrightarrow bcc(Na) + InNa$ is 368.15 K. Phase equilibria over the complete composition range was investigated by Lamprecht and Crowther [48], Thummel and Klemm [49], and Neething [50] using thermal analysis and X-ray methods. The shape of the liquidus curve in the Na-rich region (up to 90 at. % Na) reported by Lamprecht and Crowther [48] is very close a straight line, and similar results were also reported by Davies [47]. Davies [47] and Neething [50] reported that the temperature of the peritectic reaction $Liquid + In_8Na_5 \leftrightarrow tet(In)$ is 428.15 K, while the eutectic reaction $Liquid \leftrightarrow tet(In) + In_8Na_5$ was rather reported by Lamprecht and Crowther [48]. A stoichiometric compound with a congrunent melting point at 713.15 K was reported by Lamprecht and Crowther [48] with the formula of In_3Na_2. But later Thummel and Klemm [49] proved that the formula of this compound is rather In_8Na_5 using a X-ray method. The compound $InNa$ was studied by Thummel and Klemm [49] using a X-ray method. The temperature of the peritectic reaction $Liquid + In_8Na_5 \leftrightarrow NaIn$ was reported to be about 618±5 K by Lamprecht and Crowther [48], and by Thummel and Klemm [49]. A third compound was reported by Lamprecht and Crowther [48] with the formula $InNa_3$, and by Thummel and Klemm [49] with the formula of $InNa_2$, based on the thermal measurenent and crystal analysis results in the Na-rich portion. Because of the controversy among the reported results [46-50], especially for the existence of the compound $InNa_2$, Sevov and Corbett [51] reinvestigated the (Na + In) system experimentally by using X-ray and electrical resistivity techniques: four compounds with the compositions $In_{27.4}Na_{15}$, $InNa$, $InNa_2$ and $In_{11.8}Na_7$ were reported. The assessed phase diagram of the (In + Na) system was modified by Sevov and Corbett [51] based on the compilation of Larose and Pelton [52] the compound In_3Na_2 （or In_8Na_5）was replaced by two different compounds with the following stoichiometry $In_{27.4}Na_{15}$ and $In_{11.8}Na_7$. In the present work the chemical formula In_9Na_5 and In_5Na_3

were used for the thermodynamic modeling of the "$In_{27.4}Na_{15}$" and "$In_{11.8}Na_7$" phases reported by Sevov and Corbett [51].

The activity of Na in liquid (In + Na) alloys has been measured by many investigators [53-58] using EMF techniques: all the reported data are in good agreement. The enthalpies and entropies of mixing, obtained from the temperature dependence of the electromotive force (EMF), are also in good agreement. The enthalpy of mixing of the liquid phase was also measured by Kleinsteuber [54] and by Bushmanov and Yatsenko [59] using differential scanning microcalorimeters at 773 K. Their reported data are also in good agreement with the results derived from electromotive forces (EMF). The isothermal enthalpy of mixing curve show a "V"-shape with a minima near 40 to 50 at. % Na, and the isothermal entropy of mixing curve exhibits a "m"-shape with a minimum near the ame composition, all of which indicate a tendency to ordering in the liquid phase around this compostion range. Accordingly, in the present work the coordination numbers of In and Na in the melt were set to $Z_{InNa}^{In} = 6$ and $Z_{InNa}^{Na} = 7.5$ (table 2) in order to fix the maximum ordering composition near 44 at. % Na. No experimental thermodynamic data were reported for the solid phases. The enthalpy formation of *InNa* was calculated by Ozisik et al. [60] by using First-Principles calculations.

The calculated phase diagram of the (Na + In) system is shown in Figure 4.5 along with the reported experimental data [46-50]. According to the results of Ozisika et al. [60], *InNa$_2$* is stable from room temperature to about 513 K. The compound *InNa$_2$* is calculated to decompose peritectically at 523.15 K in the present work. The calculated curves for the entropies of mixing of liquid (Na + In) alloys at 723.15 K and 773.15 K are presented in Figure 4.6 with the reported experimental points derived from the temperature dependance of emf measurements. The curves show the classic "m"-shape associated to short-range order with a minimum entropy value near 45 at. % Na. At the same composition, a clear minimum appears in the enthalpy of mixing curve, as shown in Figure 4.7. The calculated curves for the activity of Na and In (reference: liquid (Na) and liquid (In)) in liquid (In + Na) alloys at different temperatures are shown in Figure 4.8 along with the reported measurements using EMF techniques. The calculated enthalpies of formation for the solid phases at 298.15 K are shown in Figure 4.9 and Tables 4.3 compared the estimations from first-principles calculations. All the optimized thermodynamic parameters of the present study are summarized in Tables 4.2, 4.4 and 4.5.
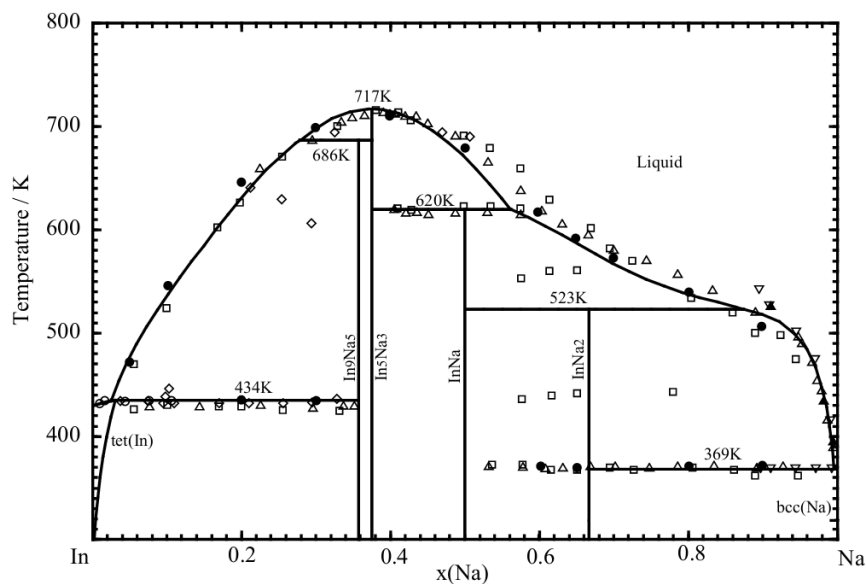
Figure 4.5 Calculated (In + Na) phase diagram. Experimental data are from Heberlein [46] (◇), Davies [47] (▽), Lamprecht and Crowther [48] (△ thermal analysis and ▲ solubility measurement), Thummel and Klemm [49] (□), Neething [50] (○ solubility measurement and ● thermal analysis)
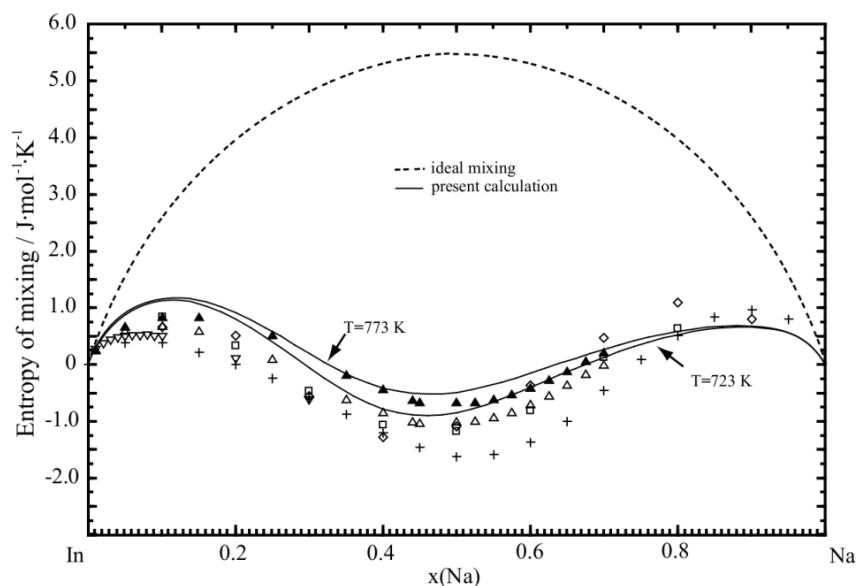
Figure 4.6 Calculated entropy mixing of (In + Na) binary liquid at 723 K and 773 K. Experimental data are from Iwasw et al. [53] (□ T=728 K), Rais et al. [55] (▲ T=773 K and △ T=723 K), Bartleett et al. [56] (+ T=713 K), Morachevskii et al. [57] (◇ T=850 K), Maiorova and Morachevskii [58] (▽ T=800 K)
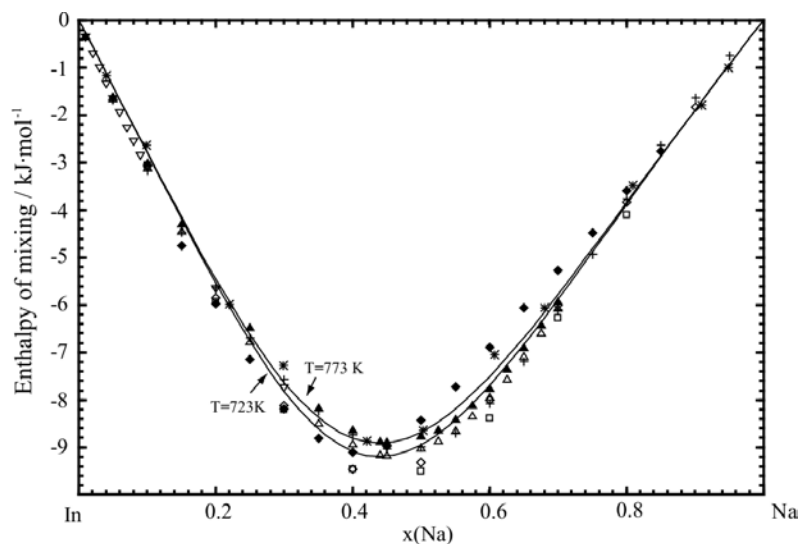
Figure 4.7 Calculated entropy mixing of (In+ Na) binary liquid at 723 K and 773 K. Experimental data are from Iwasw et al. [53] (□ T=728 K), Kleinsteuber [54] (✳ T=773 K), Rais et al. [55] (▲ T=773 K) and (△ T=723 K), Bartleett et al. [56] (+ T=713 K), Morachevskii et al. [57] (◇ T=850 K), Maiorova and Morachevskii [58] (▽ T=800 K), Bushmanov and Yatsenko [59] (◆ T=773 K)
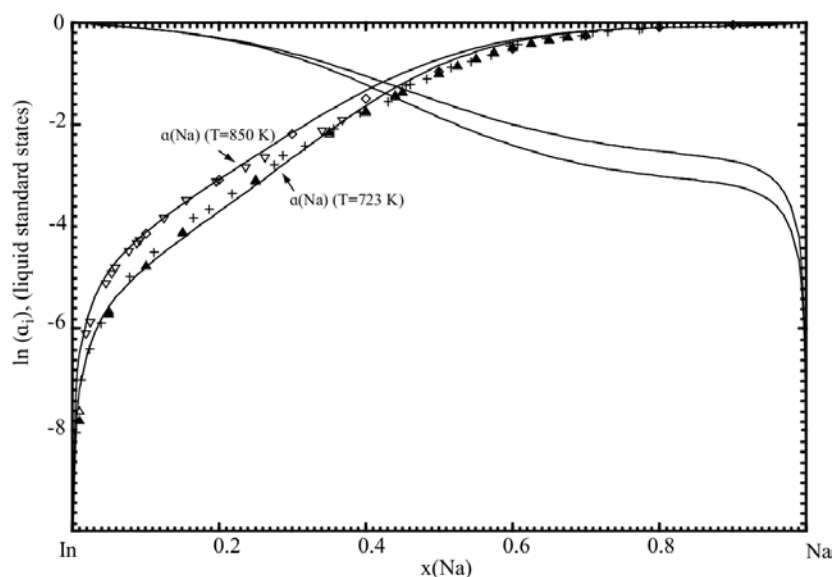
Figure 4.8 Calculated activities of In and Na (liquid standard states) in (In + Na) binary liquid at 723 K and 850 K. Experimental are from Iwasw et al. [53] (□ T=728 K), Rais et al. [55] (▲ T=773 K) and (△ T=723 K), Bartleett et al. [56] (+ T=713 K), Morachevskii et al. [57] (◇ T=850 K), Maiorova and Morachevskii [58] (▽ T=800K)
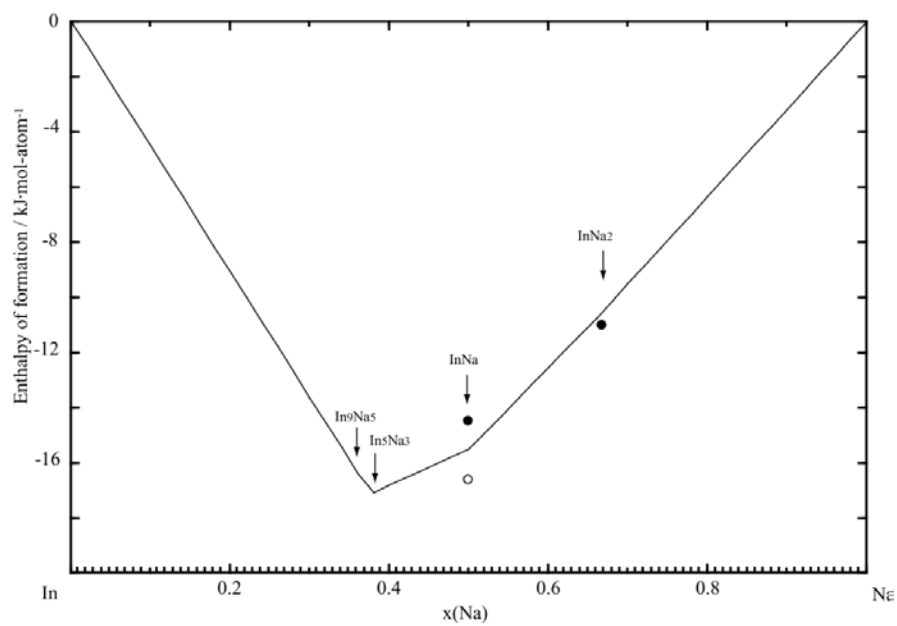
Figure 4.9 Calculated enthalpy of formation of (In + Na) binary alloys at 298.15 K

Table 4.5 Optimized parameters of stoichiometric compounds of Na-X (X: Ag, Ca, In, Sn, Zn) systems

Compound	ΔH°_{298K} (kJ·mol^{-1})	S°_{298K} (J·mol^{-1}·K^{-1})	C_p (J·mol^{-1}·K^{-1})
In_9Na_5	- 227.104	660.742	$C_p^{In_9Na_5} = 9 \times {}^*C_p(In) + 5 \times {}^*C_p(Na)$
In_5Na_3	-136.957	369.028	$C_p^{In_5Na_3} = 5 \times {}^*C_p(In) + 3 \times {}^*C_p(Na)$
$InNa$	-30.958	91.703	$C_p^{InNa} = {}^*C_p(In) + {}^*C_p(Na)$
$InNa_2$	-31.638	144.250	$C_p^{InNa_2} = {}^*C_p(In) + 2 \times {}^*C_p(Na)$
$Na_{15}Sn_4$	-298.210	903.198	$C_p^{Na_{15}Sn_4} = 4 \times {}^*C_p(Sn) + 15 \times {}^*C_p(Na)$
Na_3Sn	-71.804	187.185	$C_p^{Na_3Sn} = {}^*C_p(Sn) + 3 \times {}^*C_p(Na)$
Na_9Sn_4	-276.211	594.299	$C_p^{Na_9Sn_4} = 4 \times {}^*C_p(Sn) + 9 \times {}^*C_p(Na)$
Na_4Sn_3	-156.992	331.224	$C_p^{Na_4Sn_3} = 3 \times {}^*C_p(Sn) + 4 \times {}^*C_p(Na)$
$\beta NaSn$	-52.080	92.545	$C_p^{\beta NaSn} = {}^*C_p(Sn) + {}^*C_p(Na)$
$\alpha NaSn$	-48.080	92.545	$C_p^{\alpha NaSn} = {}^*C_p(Sn) + {}^*C_p(Na)$
$NaSn_2$	-52.970	141.249	$C_p^{NaSn_2} = 2 \times {}^*C_p(Sn) + {}^*C_p(Na)$
$NaSn_3$	-51.900	197.574	$C_p^{NaSn_3} = 3 \times {}^*C_p(Sn) + {}^*C_p(Na)$
$NaSn_4$	-51.960	249.059	$C_p^{NaSn_4} = 4 \times {}^*C_p(Sn) + {}^*C_p(Na)$
$NaSn_6$	-51.753	352.308	$C_p^{NaSn_6} = 6 \times {}^*C_p(Sn) + {}^*C_p(Na)$
$NaZn_{13}$	-44.108	571.090	$C_p^{NaZn_{13}} = 13 \times C_p(Zn, hcp) + {}^*C_p(Na)$

$${}^*C_p(Na) / (J \cdot mol^{-1} \cdot K^{-1}) = 51.0393608 - 0.144613266(T/K) - 264308(T/K)^{-2} + 0.000261829698(T/K)^2;$$
$$200K < T < 370.87K$$
$$= 36.02 - 0.0003196(T/K) - 647000 \times (T/K)^{-2} + 3.908 \times 10^{-8}(T/K)^2;$$
$$370.88K < T < 2300K$$

$${}^*C_p(In) / (J \cdot mol^{-1} \cdot K^{-1}) = 21.8386 + 0.01145132(T/K) + 45812(T/K)^{-2} + 1.2721926 \times 10^{-5}(T/K)^2;$$
$$298K < T < 429.78K$$
$$= 31.05 - 0.0001919(T/K) - 312000(T/K)^{-2} + 3.374 \times 10^{-8}(T/K)^2$$
$$429.79K < T < 38000K$$

$${}^*C_p(Sn) / (J \cdot mol^{-1} \cdot K^{-1}) = 25.858 - 0.0010237(T/K) - 36880(T/K)^{-2} + 1.9156602 \times 10^{-5}(T/K)^2;$$
$$249K < T < 250K$$
$$= 15.961 + 0.0377404(T/K) + 123920(T/K)^{-2} - 1.8727002 \times 10^{-5}(T/K)^2;$$
$$251K < T < 1000K$$
$$= 35.098 ; \quad 1000K < T < 3000K$$

4.4.4 The (Na + Sn) system

Mathewson [61] studied phase equilibria in the (Na + Sn) binary system over the entire composition range using thermal analysis and microscopic methods. Five compounds were reported: Na_4Sn, Na_2Sn, Na_4Sn_3, $NaSn$ and $NaSn_2$. Hume-Rothery [62] re-investigated the phase equilibria in the (Na + Sn) system for the whole composition range using thermal and optical microscope methods: four more compounds were identified, namely Na_3Sn, $NaSn_3$, $NaSn_4$ and $NaSn_4$. The melting points of Na_2Sn and $NaSn$ were reported [62] at 751.15 K and 851.15 K respectively, in good agreement with Mathewson's results [61] (750.15 K and 849.15 K). According to the thermal analysis results by Hume-Rothery [62], the compound Na_4Sn_3 is melting incongruently at 751.15 K and decomposes at 630.15 K. However, this compounds was reported to be stable from 751.15 K down to room temperature by Mathewson [61]. The solubility of Sn in liquid Na has been determined by Lamprecht et al. [63] in the temperature range 373-533 K by radiochemical analysis, and by Hubberstey [64] and Hubbberstey and Pulham [65] using EMF, thermal analysis and resistance measurement methods. Their results [63-65] are in good agreement. The reported maximum solubility of Sn in bcc (Na) and of Na in bct (Sn) are less than 0.01 atomic percent [66]. The compounds Na_4Sn and Na_2Sn reported in the work of Mathewson [61] and Hume-Rothery [62] were characterized as $Na_{15}Sn_4$ [67-69] and Na_9Sn_4 [68, 69] by using single-crystal and X-ray methods.

The thermodynamic properties of (Na + Sn) molten alloys were determined by EMF measurements by several authors. Hauffe and Vierk [70] measured the activity of Na in liquid (Na + Sn) alloys at 753 K. Delimars and Konomuu [71] reported the activities at 773 K. The activity of Na in liquid phase at 873 K were studied by Morachevskii and Lantratov [72], who derived from their EMF measurements the enthalpy mixing of the liquid at 873 K. The temperature dependence of the EMF related to the activity of Na in the liquid was determined between 623 K and 773 K by Yuan and Kroger [73], who also reported the enthalpy of formation of the compound $NaSn$ as -25±1.6 kJ·mol-atom[-1]. Hubberstey [64] measured and calculated the thermodynamic properties of dilute liquid (Na + Sn) alloys between 573 K and 773 K. Maiorova and Morachevskii [58] reported the thermodynamic properties of dilute sodium solutions in molten Sn at 800 K. Rivier and Pelton [74] measured the activity of Na using a EMF tenchnique

in liquid (Na + Sn) alloys in the compostition range 0-30 at. % Na from 523-723 K. The derived enthalpy mixing, Gibbs energy and entropy mixing of liquid (Na + Sn) alloys were reported by Rais et al. [55] at 773 K and 856 K, by Tamaki et al. [75] at 673 K and 873 K, and by Alqasmi and Egan [76] at 1073 K based on their EMF measurements. The thermodynamic properties of liquid (Na + Sn) alloys were studied by Saboungi and Corbin [77], Itho and Kozuka [78], and Fang and Wendt [79], using EMF techniques with the beta-alumuina cell. The enthalpy of mixing of liquid (Na + Sn) alloys were measured by direct calorimetry at 773 K [54] and at 883 K [80]. The reported enthalpy of mixing data for liquid (Na + Sn) alloys, obtained either by EMF methods or by calorimetric methods, are in relatively good agreement considering the experimental errors (figure 5.11). The enthalpy of formation of the solid compounds was determined by direct calorimetry at 298.15 K [81] and by solution calorimetry at the same temperature by Biltz [82], and Biltz and Holverscheit [83]. Later Mckisson and Bromley [80] measured the heat of formation of the binary compounds using a high-temperature calorimeter. A complete review of the (Na + Sn) phase diagram data was published by Sangster and Bale [84].

The local structure of liquid (Na + Sn) alloys has been studied by several investigators both theoretically and experimentally [55, 73, 75, 79, 85]. All the reported results show that there is a high degree of short-range ordering near the composition 42-45 at. % Na. This behavior is also evidence by the composition of the minimum in the entropy of mixing and the enthalpy of mixing curves for the liquid phase.

In the present work, the coordination numbers of Na and Sn in the liquid solution were set based on the the maximum short-range ordering (SRO) composition of 43 at.% Na: $Z_{SnNa}^{Sn} = 5.7$ and $Z_{SnNa}^{Na} = 4.3$ (table 4.2). The calculated enthalpy and entropy of mixing curves for the liquid solution at 773 K and 856 K with the experimental data from Rais et al. [55] and Kleinsteuber [54] are shown in Figures 4.10 and 4.11. The "m"-shaped entropy curve and the "V"-shaped enthalpy curve support the fact that the liquid exhibits strong SRO. The calculated free Gibbs energy of liquid phase at at 773 K and 856 K is shown in Figure 4.12.
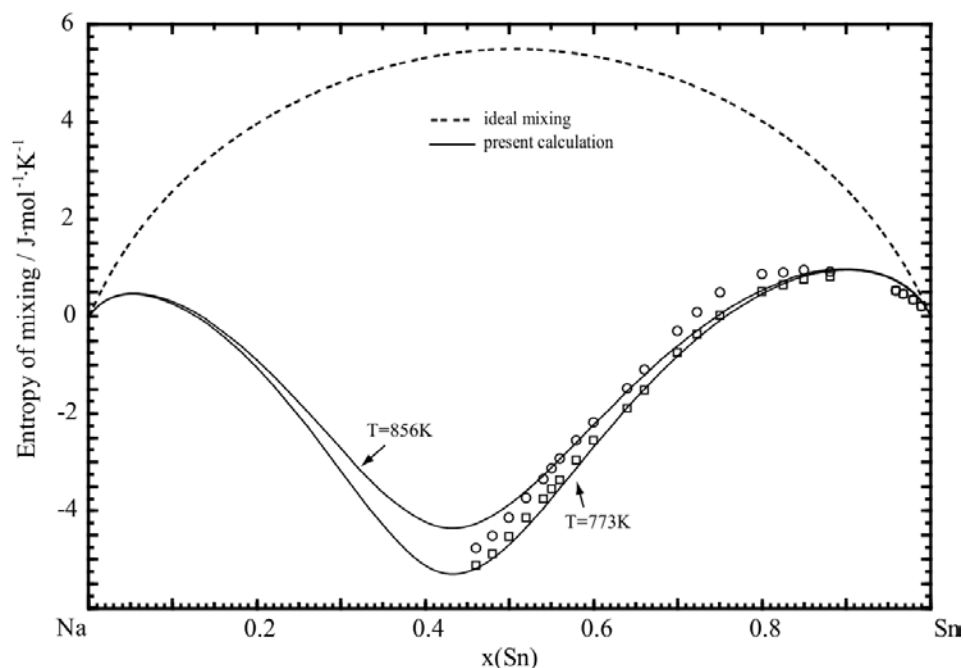
Figure 4.10 Calculated mixing of entropy of (Na + Sn) binary liquid at 773 K and 856 K. Experimental data are from Rais et al. [55] (□ T=856 K and ○ T=773 K)
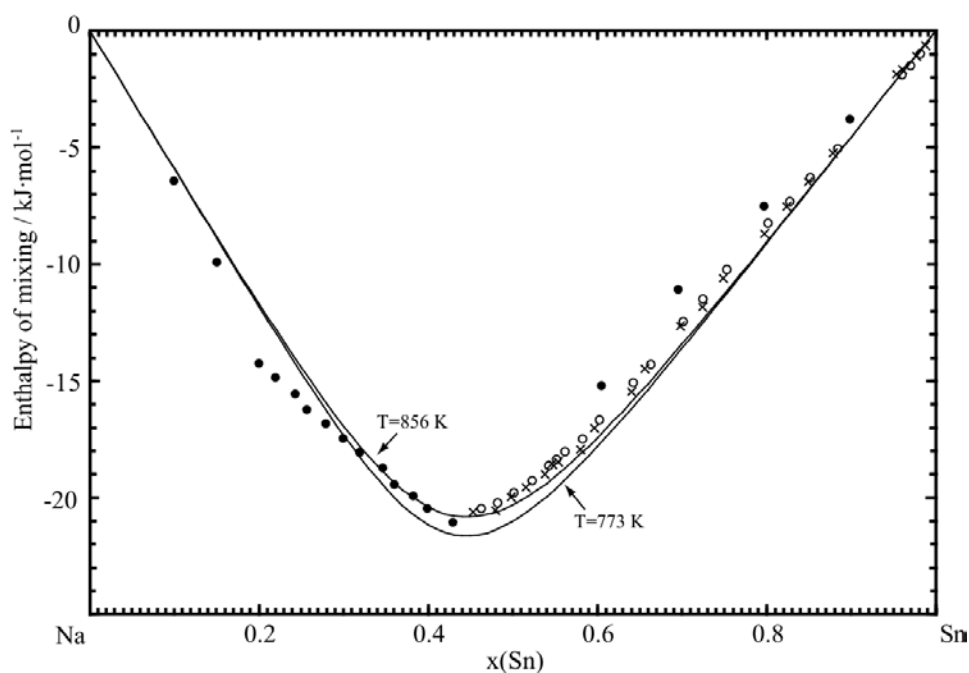
Figure 4.11 Calculated mixing of enthalpy of (Na + Sn) binary liquid 773 K and 856 K. Experimental data are from Kleinsteuber [54] (● T=773 K), and Rais et al. [55] (○ T=856 K and ✕ T=773 K)
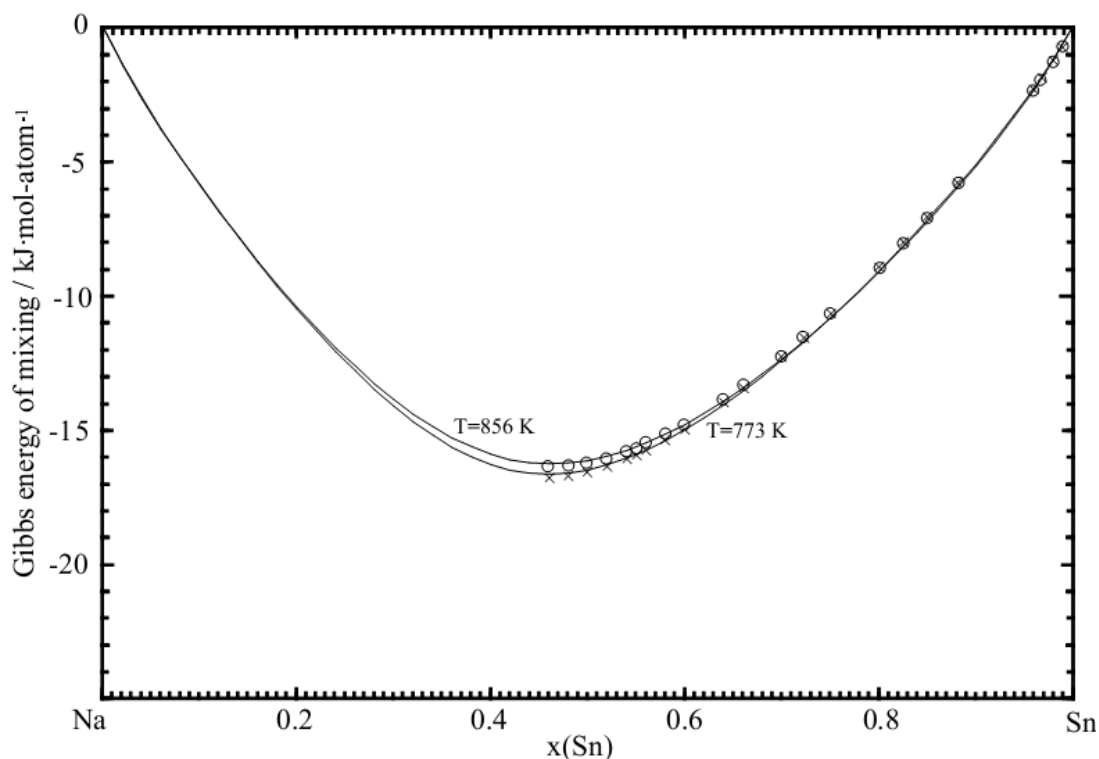
Figure 4.12 Calculated Gibbs energy of mixing of (Na + Sn) binary liquid at 773 K and 856 K. Experimental data are from Rais et al. [55] (○ T=856 K and × T=773 K)

The calculated (Na + Sn) phase diagram is shown in Figure 4.13 along with the experimental data [61-65]. In the present work, the allotropic transition temperature of $\alpha NaSn \leftrightarrow \beta NaSn$ was fixed at 756.15K with $\Delta H^{\circ}_{trans} = 4.0 \, \text{kJ} \cdot \text{mol}^{-1}$. The calculated activity of Na in the liquid phase (liquid standard state) compared with reported experimental data are shown in Figure 4.14 and Figure 4.15. The calculated heat of formation of binary intermetallics is shown in Figure 4.16 compared with reported data [80-83]. The optimized enthalpies of formation are in agreement with the experimental data except for those of Blitz and Holverscheit [83]. All the optimized thermodynamic parameters of the present study are summarized in Tables 4.2, 4.4 and 4.5.
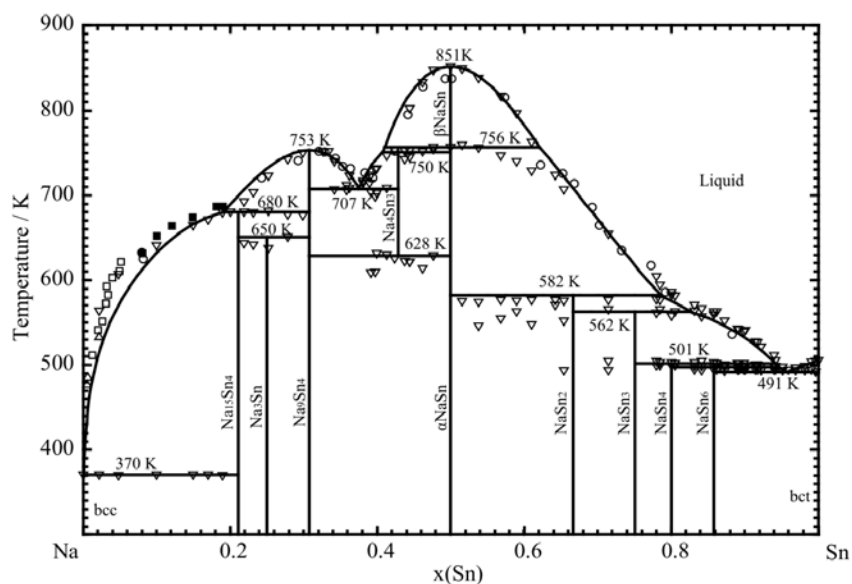
Figure 4.13 Calculated (Sn + Na) phase diagram. Experimental data are from Mathewson [61] (thermal analysis ○), Hume-Rothery [62] (thermal analysis ▽), Lamprecht et al. [63] (thermal analysis △), Hubberstey [64] (resistance measurement ■), Hubberstey and Pulham [65] (radiochemical analysis □)
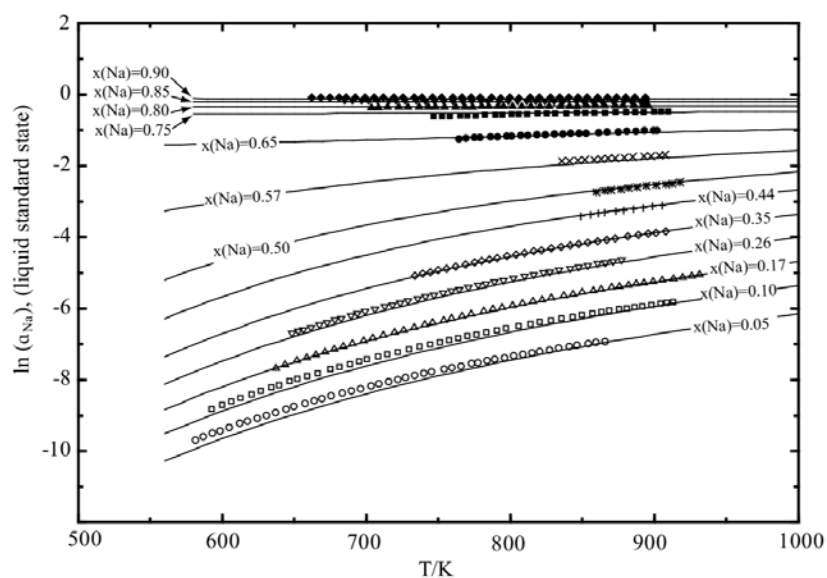
Figure 4.14 Calculated activity of Na (liquid standard state) in (Na + Sn) bianry liquid versus (T/K). Experimental data are from Tamaki et al. [75] (○ x=0.05 Na, □ x=0.10 Na, △ x=0.17 Na, ▽ x=0.26 Na, ◇ x=0.35 Na, + x=0.44 Na, ✳ x=0.50 Na, × x=0.57 Na, ● X=0.65 Na, ■ x=0.75 Na, ▲ x=0.80 Na, ▼ x=0.85 Na, ◆ x=0.90 Na)
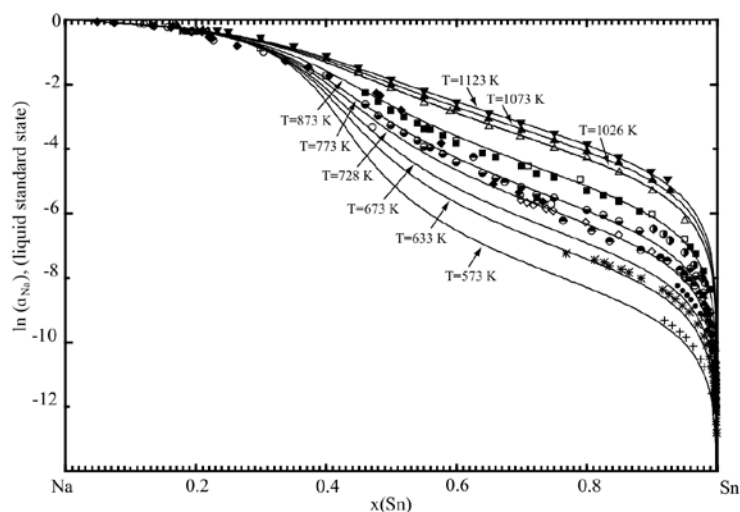
Figure 4.15 Calculated activity of Na (liquid standard state) in (Na + Sn) binary liquid for temperature range from 573 K to 1123 K. Experimental data are from Rais et al. [55] (◒ T=773 K and ▪ T=856 K), Maiorova and Morachevskii [58] (◗ T=800 K), Hauffe and Vierk [70] (◆ T=753 K), Delimarskii and Konomuu [71] (○ T=773 K), Morachevskii and Lantratov [72] (□ T=873 K), Yuan and Kroger [73] (◕ T=773 K), Rivier and Pelton [74] (✳ T=633 K), Alqasmi and Egan [76] (▼ T=1123 K, ▲ T=1073 K, and △ T=1026 K), Saboungi and Corbin [77] (● T=673 K, + T=573 K), Itoh and Kozuka [78] (◇ T=628 K)
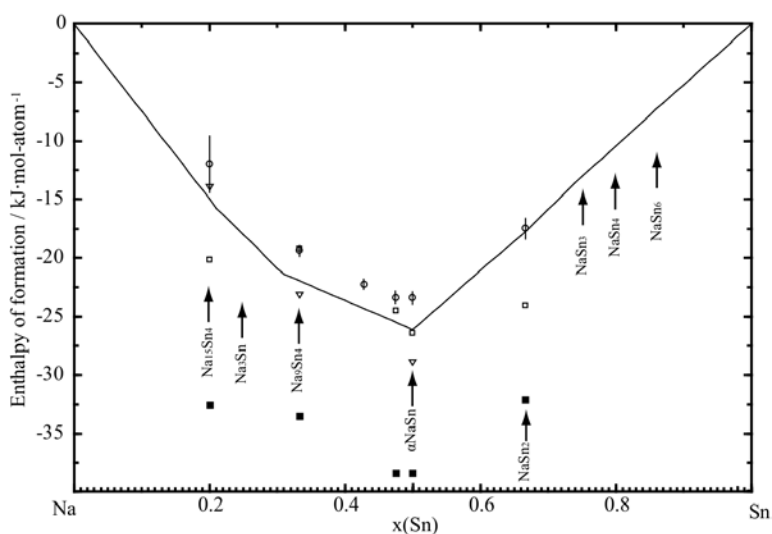
Figure 4.16 Calculated enthalpy of formation of (Na + Sn) stable compounds at 298.15 K. Experimental data are from Mckisson and Bromley [80] (○ T=880 K), Kubaschewski and Seith [81] (□ T=298.15 K), Biltz [82] (▽ T=298.15 K), Biltz and Holverscheit [83] (▪ T=298.15 K)

4.4.5 The (Na + Zn) system

The equilibrium phase diagram of the (Na + Zn) system was studied earlier by Mathewson [86] using thermal analysis and micrography techinques. Two invariant reactions were reported at 830.15 K and 370.15 K, together with the solubility curve of Na in Zn-rich liquid. Zintl and Haucke [87] reported a compound with the stoichiometry $NaZn_{13}$ using X-ray diffraction, which was comfirmed by other workers [35, 88]. Morachevskii et al. [88] studied the Zn-rich region using the breaks in the EMF curves as a function of temperature obtained by concentration cells with an aluminosilicate glass as the solid electrolyte. The results of Mathewson [86] and Morachevskii et al. [88] are in very close agreement. Cetin and Ross [89] studied the liquid-liquid miscibility gap boundary in the composition range of 10–90 at. % Zn by using thermal analysis techniques. The temperature of the syntectic reaction $Liquid\,\#1 + Liquid\,\#2 \leftrightarrow NaZn_{13}$ is reported at 821 K with liquid compositions of 11 and 93 at. % Zn (Cetin and Ross [89]) from cooling curves. The temperature of the eutectic reaction $Liquid \leftrightarrow NaZn_{13} + bcc(Na)$ determined by Cetin and Ross [89] at 371.15 K, is in very good agreement with the result of Mathewson [86]. Hausler [90] studied the invariant reaction temperatures and the liquidus curves near the Zn-rich region by thermal analyses with different alloy compositions. The experimental results showed that the two invariant temperatures are 830 K and 370 K respectively.

The activity of Na in the liquid phase at 873 K was measured by Hausler [90], Lantratov et al. [91] and Morachevskii et al. [88] using EMF techniques. The reported curve for the activity of Na shows a strong positive deviation from the ideal solution behavior, indicating the presence of the miscibility gap in the liquid phase.

The optimized phase diagram is shown in Figure 4.17 along with the reported experimental data [86, 88-90]. In the present optimization, the calculated temperature of the syntectic reaction $Liquid\,\#1 + Liquid\,\#2 \leftrightarrow NaZn_{13}$ is 821 K with the compositions of 2 liquidus at 11 at. % and 93 at. % Zn respectively, in a good agreement with the reported data [35, 86, 89]. The consolute temperature of the miscibility gap in the liquid phase is calculated at 1090 K and 57 at. % Zn. The calculated enthalpy of formation of $NaZn_{13}$ is given in Table 4.3. The calculated activity of Na in the liquid phase (references: liquid (Na) and liquid (Zn)) is shown in Figure 4.18. The

thermodynamic parameters obtained for the (Na + Zn) binary system are listed in Tables 4.2, 4.4 and 4.5.
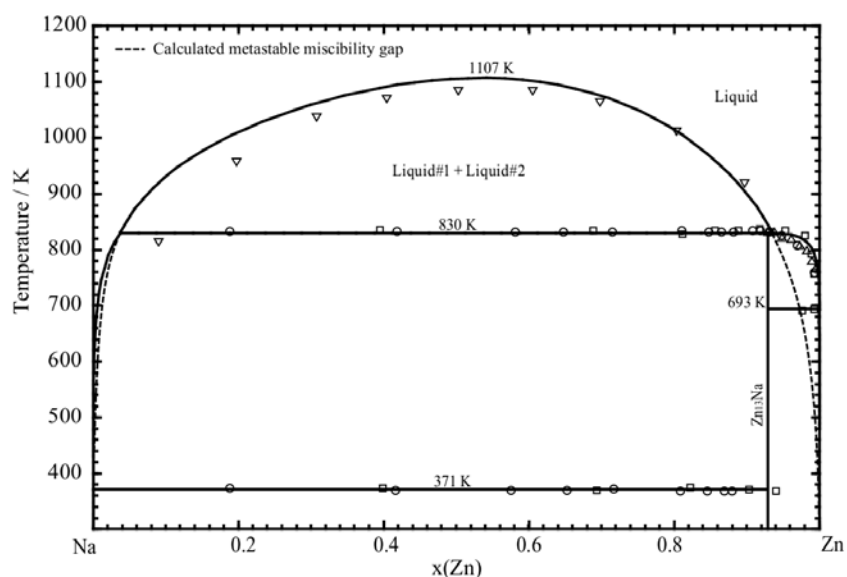
Figure 4.17 Calculated (Na + Zn) phase diagram. Experimental data are from Mathewson [86] (○ thermal analysis and optical micorgraphy), Morachevskii et al [88] (△ EMF), Cetin and Ross [89] (▽ thermal analysis), Hausler [90] (□ thermal analysis)
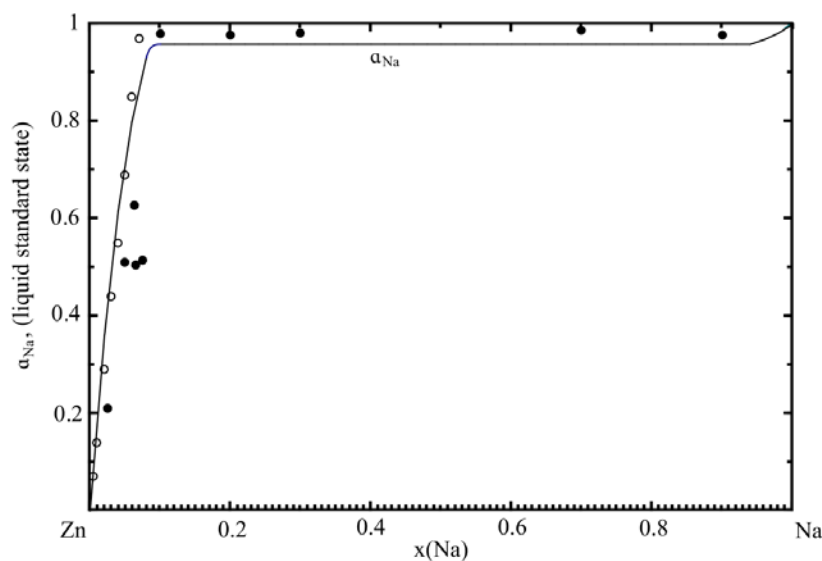
Figure 4.18 Calculated activity of Na (liquid standard state) in (Zn + Na) binary liquid at 873K. Experimental data are from Morachevskii et al. [88] (○ T=873 K), Lantratov et al. [91] (● T=873 K)

4.5 Short-range ordering in (Na + In) and (Na + Sn) liquid alloys

The structure of molten (Na + Sn) alloys was investigated by Alblas et al. [92] and Akinlade [93] who reoprted strong ordering behavior in the liquid at the Na_4Sn_3 composition from neutron diffraction measurements. A similar ordering behavior in the liquid alloy appeared for the (Na + In) system at the composition of Na_2In_3 [94]. These ordering behaviors can be expected from the strong negative Gibbs energy and enthalpy of liquid phase in (Na + In) and (Na + Sn) systems, as described above. The modified Quasichemical Model (MQM) used for liquid phase of (Na + In) and (Na + Sn) binary system in the present study can be allowed to calculate the bonding structure of the liquid solutionas pair fractions. According to the present calculate results shown in Figure 4.19, the maximum amount of (Na + Sn) pairs in molten Na-Sn alloys is 0.68 at $x_{Na} \approx 57\%$ and 1073 K, and the maximum amount of (Na + In) pairs is 0.57 at $x_{Na} = 45\%$ and 1073 K.
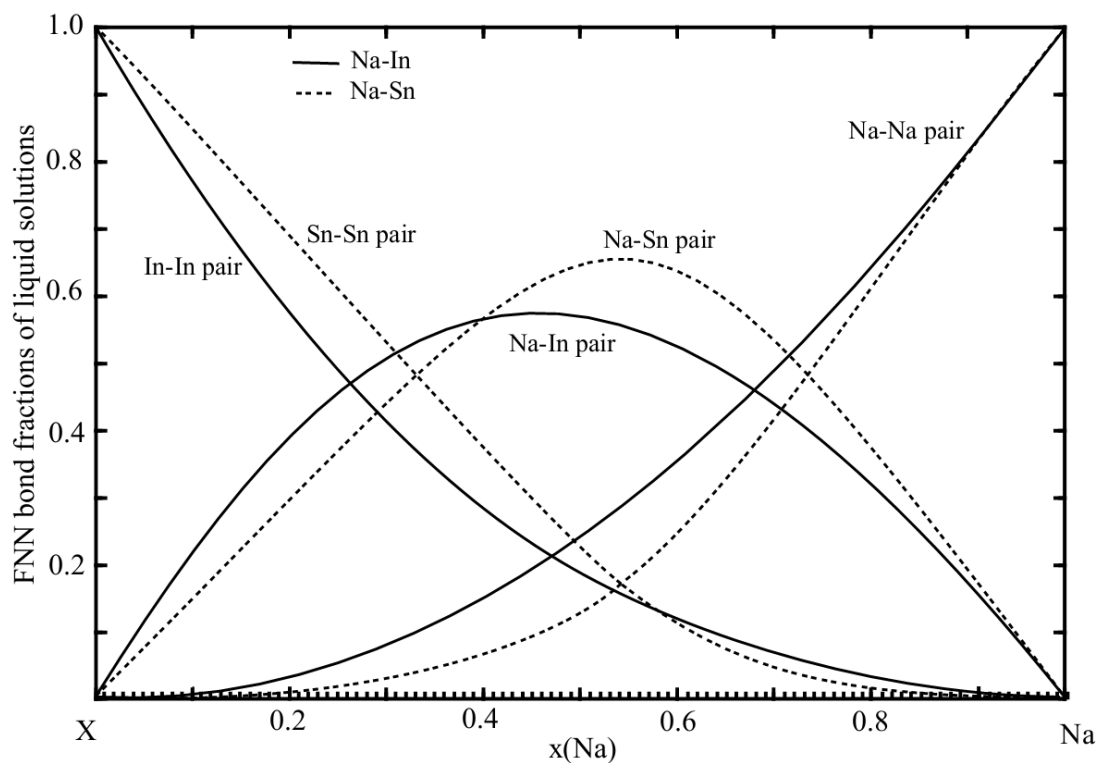
Figure 4.19 Calculated First nearest-neighbour bond fractions in (Na + In) and (Na + Sn) binary liquid solutions at 1073 K

One of the best indicators of a tendency toward ordering is the excess stability function (ES) defined by Darken [95] as:

$$ES = \left(\frac{\partial^2 G^E}{\partial X_i^2} \right)_{T,P} \tag{19}$$

The calculated excess stability functions for the liquid phase in (Na + In) and in (Na + Sn) alloys are shown in Figure 4.20. Quite strong peaks in the excess stability functions can be observed at $x_{Na} \approx 59\%$ for (Na + Sn) system, and at $x_{Na} \approx 41\%$ for (Na + In) system.
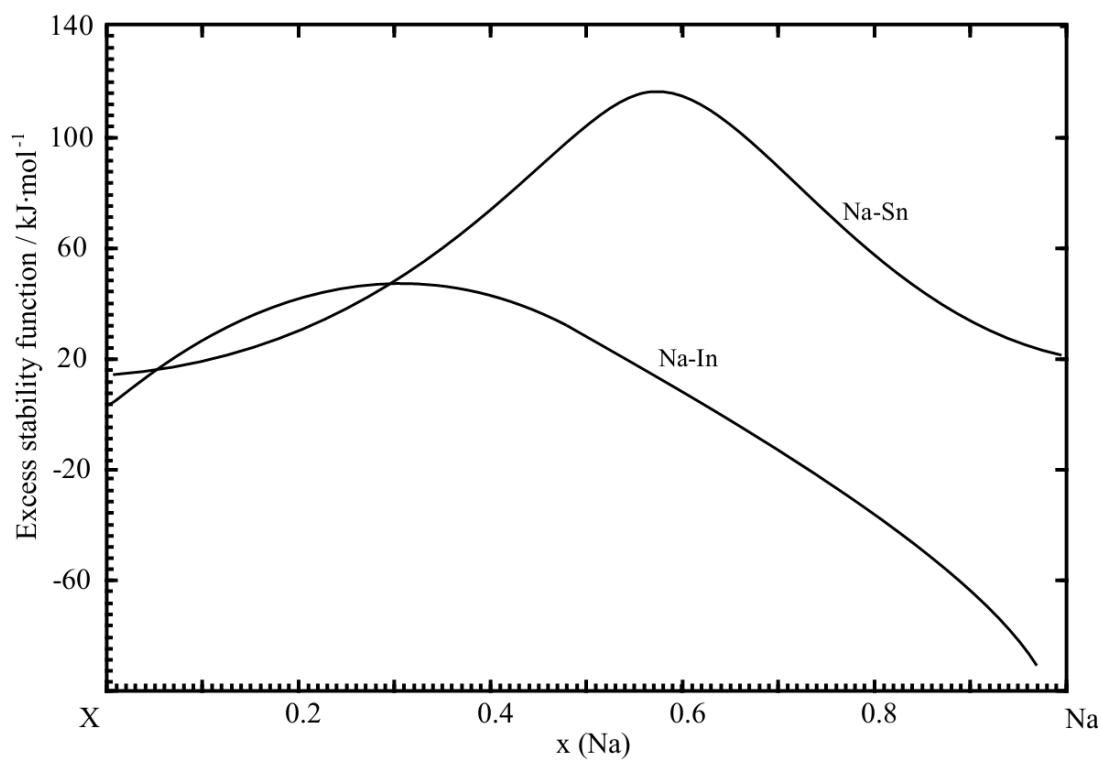
Figure 4.20 Calculated excess stability functions (Na + In) and (Na + Sn) binary liquid solutions at 1073 K

Another indication of short range ordering in liquid solution is the variation of ΔC_p function with temperature and composition from the thermodynamic relationship,

$$\Delta C_p = T \frac{\partial}{\partial T} (\Delta S_m) \tag{20}$$

the calculated ΔC_p function for the liquid solution of (Na + Sn) and (Na + In) system at 773K is shown in Figure 4.21. These calculated ordering behaviors are in good agreement with the experimental observation [93, 94].
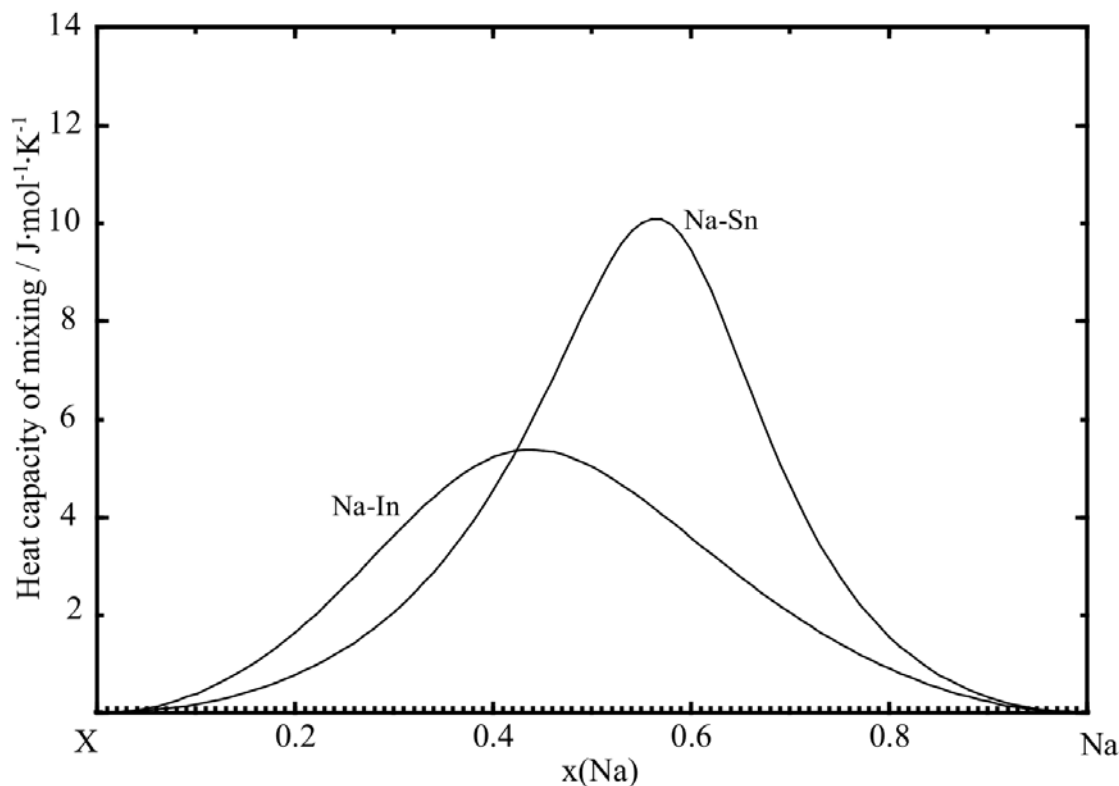
Figure 4.21 Calculated heat capacity of mixing of (Na + In) and (Na + Sn) binary liquid solutions at 773 K

4.6   Conclusion

Finite temperature first-principles calculations can produce reasonable and useful thermodynamic data for intermetallic compounds. The enthalpies of formation of the Ag_2Na, $InNa$, $InNa_2$ and $NaZn_{13}$ compounds at 0 K were calculated by first-principles calculations in the present work and intergrated in the present thermodynamic optimization by using Calphad method.

A critical evaluation and optimization of the (Na + X) binary systems (X = Ag, Ca, In, Sn, and Zn) has been presented combined with the assistant of first-principles calculations method. The thermodynamic parameters of the Gibbs energies functions for all phases permit to reproduce within good accuracy the experimental data retained from the critical analysis.

The (Na + In) and (Na + Sn) binary liquid alloys exhibit a substantially large degree of short-range ordering (SRO) in the liquid phase. It has shown that the the Modified Quasichemical Model (MQM) for liquid phase, which takes the SRO into account with a first-neareast-neighbour pair equilibrium, is able to reproduce the experimental data very well with the resultant typical "V"-shaped integral enthalpy of mixing curves (and the associated inflections in the partial enthalpy of mixing curves), as well as the typical "m"-shaped integral entropy of mixing curves more realsitic.

Acknowledgements

References

[1] M.A. Gibson, X. Fang, C.J. Bettles, C.R. Hutchinson, Scripta Mater., 63 (2010) 899-902.

[2] D.H. Kang, S.S. Park, Y.S. Oh, N.J. Kim, Mater. Sci. Eng. A, 449-451 (2007) 318-321.

[3] T.A. Leil, Y.D. Huang, H. Dieringa, N. Hort, K.U. Kainer, J. Buršík, Y. Jirásková, K.P. Rao, Mater. Sci. Forum, 2007, pp. 69-72.

[4] N. Hort, Y. Huang, T.A. Leil, P. Maier, K.U. Kainer, Adv. Eng. Mater., 8 (2006) 359-364.

[5] T.A. Leil, N. Hort, W. Dietzel, C. Blawert, Y. Huang, K.U. Kainer, K.P. Rao, Trans. Nonferr. Metal. Soc. China, 19 (2009) 40-44.

[6] K. Van der Planken, J. Mater. Sci. Lett., 4 (1969) 927.

[7] C.L. Mendis, C.J. Bettles, M.A. Gibson, C.R. Hutchinson, Mater. Sci. Eng. A, 435-436 (2006) 163-717.

[8] C.L. Mendis, C.J. Bettles, M.A. Gibson, S. Gorsse, R. Hutchinson, Philosophical Magazine Letters, 86 (2006) 443-456.

[9] T.T. Sasaki, K. Oh-ishi, T. Ohkubo, K. Hono, Scripta Mater., 55 (2006) 251-254.

[10] M.A. Gibson, X. Fang, C.J. Bettles, C.R. Hutchinson, Scripta Mater., 63 (2010) 899-902.

[11] S.C. Park, J.D. Lim, D. Eliezer, K.S. Shin, Mater. Sci. Forum, 419-422 (2003) 159-164.

[12] C.L. Mendis, K. Oh-ishi, K. Hono, Scripta Mater., 57 (2007) 485-488.

[13] N. Saunders, A.P. Miodownik, CALPHAD (Calculation of Phase Diagrams): A Comprehensive Guide, Pergamon, 1998.

[14] H. Ohtani, K. Ishida, Thermochimica Acta, 314 (1998) 69-77.

[15] J.C. Zhao, B.P. Bewlay, M.R. Jackson, L.A. Peluso, Structural Intermetallics 2001 TMS, Warrendale PA, 2001, pp. 483-491.

[16] C.W. Bale, P. Chartrand, S.A. Degterov, G. Eriksson, K. Hack, R. Ben Mahfoud, J. Melancon, A.D. Pelton, S. Petersen, CALPHAD: Computer Coupling of Phase Diagrams and Thermochemistry, 26 (2002) 189-228.

[17] A.T. Dinsdale, CALPHAD: Computer Coupling of Phase Diagrams and Thermochemistry, 15 (1991) 317-425.

[18] A.D. Pelton, P. Chartrand, Metall. Mater. Trans. A, 32 (2001) 1355-1360.

[19] A.D. Pelton, S.A. Degterov, G. Eriksson, C. Robelin, Y. Dessureault, Metall. Mater. Trans. B: Process Metallurgy and Materials Processing Science, 31 (2000) 651-659.

[20] Y.-B. Kang, A.D. Pelton, P. Chartrand, C.D. Fuerst, CALPHAD: Computer Coupling of Phase Diagrams and Thermochemistry, 32 (2008) 413-422.

[21] M. Hillert, J. Alloys Compounds, 320 (2001) 161-176.

[22] H. Kopp, Phil. Trans. Roy. Soc. A, 155 (1865) 71-202.

[23] P.E. Blöchl, Phys. Rev. B, 50 (1994) 17953-17979.

[24] G. Kresse, J. Furthmüller, Computational Mater. Sci., 6 (1996) 15-50.

[25] G. Kresse, D. Joubert, Phys. Rev. B, 59 (1999) 1758-1775.

[26] G. Kresse, J. Furthmüller, Phys. Rev. B, 54 (1996) 11169-11186.

[27] J.P. Perdew, Y. Wang, Phys. Rev. B, 45 (1992) 13244-13249.

[28] J.P. Perdew, K. Burke, M. Ernzerhof, Phys. Rev. Lett., 77 (1996) 3865-3868.

[29] H.J. Monkhorst, J.D. Pack, Phys. Rev. B, 13 (1976) 5488.

[30] P. Villars, K. Cenzual, Materials Park (OH): ASM International, (2007).

[31] A.D. Pelton, Bulletin of Alloy Phase diagram, New York, 1986, 133-136.

[32] G. Kienast, J. Verma, Z. Anorg. allg. Chem., 310 (1961) 143-169.

[33] E. Quercigh, Z. Anorg. allg. Chem., 68 (1910) 301-306.

[34] C.H. Mathewson, Int. Z. Metallogro., 1 (1911) 51-63.

[35] G.J. Lamprecht, P. Crowther, Trans. AIME, 242 (1968) 2169-2171.

[36] J.R. Weeks, Trans. ASM, 62 (1969) 304.

[37] A.D. Pelton, Bulletin of Alloy Phase diagram, New York, 1986, 136-139.

[38] A.D. Pleton, Bulletin of Alloy Phase diagram, New York, 1986, 25-27.

[39] P. Willars, Pearson's Handbook Desk Edition, ASM international, Materials park, OH, 1997.

[40] W. Muthmann, L. Weiss, J. Metzger, Justus Liebigs Annalen der Chemie, 355 (1907) 137-143.

[41] R. Lorenz, R. Winzer, Z. Anorg. allg. Chem., 179 (1929) 281-286.

[42] R. Lorenz, R. Winzer, Z. Anorg. allg. Chem., 181 (1929) 193-202.

[43] A. Rinck, E. Kaempf, A. Steinmann, Z. Anal. Chem., 83 (1931) 67-70.

[44] A.D. Pelton, J. Phase Equilib. Diff., 6 (1985) 35-37.

[45] S.J. Zhang, D.W. Shin, Z.K. Liu, CALPHAD: Computer Coupling of Phase Diagrams and Thermochemistry, 27 (2003) 235-241.

[46] M.F.W. Heberlein, Trans. ASM, 44 (1952) 545-548.

[47] H.A. Davies, Trans. Metall. Soc. AIME, 239 (1967) 928-929.

[48] G.J. Lamprecht, P. Crowther, J. Inorg. Nucl. Chem., 31 (1969) 925-931.

[49] R. Thummel, W. Klemm, Z. Anorg. Allg. Chem., 376 (1970) 44-63.

[50] A.J. Neething, S.a.a.e.b. Report (Ed.), PEL230, Pretoria, Pelindaba, 1974, pp. 21.

[51] S.C. Sevov, J.D. Corbett, J. solid state chemistry, 103 (1993) 114-130.

[52] S. Larose, A.D. Pelton, J. Phase Equilib. Diff., 12 (1991) 371-376.

[53] M. Iwase, S. Sugino, E. Ichise, J. Chem. Thermodyn., 17 (1985) 601-609.

[54] T. Kleinsteuber, Ludwig-Maximilian university, Munich, 1961.

[55] A. Rais, N.E. Cusack, F.E. Neale, J. Phys. F: Met. Phys., 12 (1982) 1091-1100.

[56] H.E. Bartlett, A.J. Neethling, P. Crowther, J. Chem. Thermodyn., 2 (1970) 523-534.

[57] A.G. Morachevskii, M.A. Bykova, E.A. Maiorova, Z. Prikl. Khim., 44 (1971) 2317-2319.

[58] E. Maiorova, A.G. Morachevskii, Z. Prikl. Khim., 49 (1976) 2537-2539.

[59] V.D. Bushmanov, S.P. Yatsenko, Z. Prikl. Khim., 55 (1981) 2951-2952.

[60] H.B. Ozisik, K. Colakoglu, E. Deligoz, H. Ozisik, Computational Mater. Sci., 50 (2011) 1070-1076.

[61] C.H. Mathewson, Z. Anorg. Chem., 46 (1905) 94-112.

[62] W. Hume-Rothery, J. Chem. Soc. Fara. Trans. 1, (1928) 947-963.

[63] G.J. Lamprecht, P. Crowther, D.M. Kemp, J. Phys. Chem., 71 (1967) 4209-4212.

[64] P. Hubberstey, J. Electrochem. Soc., 110 (1972) 967-970.

[65] P. Hubberstey, R.J. Pulham, J. Chem. Soc. Dalton Trans., 14 (1974) 1541-1544.

[66] N.L. Pokrovskii, T.G. Smirnova, Phys. Met. Metallog. USSR, 12 (1961) 751-780.

[67] W. Muller, K. Volk, Z. Naturforsch. B, 30 (1975) 494-496.

[68] W. Muller, K. Volk, Z. Naturforsch. B, 33 (1978) 709-710.

[69] O.Y. Gukov, Y.Y. Gukova, Deposited document SPSTL 777 Khp-D80, (1980).

[70] K. Hauffe, A.L. Vierk, Z. Elektrochem. angewandte Phys. Chem., 53 (1948) 151-191.

[71] Y.K. Delimarskii, A.A. Konomuu, Z. Fiz. Khim., 28 (1954) 1169-1173.

[72] A.G. Morachevskii, M.F. Lantratov, Z. Obsh. Khim. 29 (1959) 2109-2113.

[73] D. Yuan, F.A. Kroger, J. Phys. Chem., 73 (1969) 2390-2492.

[74] M. Rivier, A.D. Pelton, J. Electrochem. Soc., 125 (1978) 1377-1382.

[75] S. Tamaki, T. Ishiguro, S. Takeda, J. Phys. F: Met. Phys., 12 (1982) 1613-1624.

[76] R. Alqasmi, J.J. Egan, Berichte der Bunsen-gesellschaft fur Physikalische Chemie, 87 (1983) 815-817.

[77] M.L. Saboungi, T.P. Corbin, J. Phys. F: Met. Phys., 14 (1984) 13-21.

[78] M. Itoh, Z. Kozuka, J. Mater. Sci., 26 (1991) 5221-5228.

[79] Q. Fang, H. Wendt, J. App. Electrochem., 26 (1996) 343-352.

[80] R.L. Mckisson, L.A. Bromley, Transaction of American Institute of Mining, Metallurgical, and Petroleum Engineers 4(1952) 33-38.

[81] O. Kubaschewski, W. Seith, Z. Metallk., 30 (1938) 7-9.

[82] V.W. Biltz, Z. Metallk., 29 (1937) 72-79.

[83] V.W. Biltz, W. Holverscheit, Z. Anorg. allg. Chem., 140 (1924) 261-267.

[84] J. Sangster, C.W. Bale, J. Phase Equilib. Diff., 19 (1998) 76-80.

[85] D. Adhikari, B.P. Singh, I.S. Jha, J. Molecular Liquids, 167 (2012) 52-56.

[86] C.H. Mathewson, Z. Anorg. Chem., 48 (1906) 195-200.

[87] E. Zintl, W. Haucke, Acta Crystallogr., 5 (1937) 637-644.

[88] A.G. Morachevskii, E.A. Maiorova, O.I. Vorobeva, Elektrokhim., 18 (1982) 148-150.

[89] H. Cetin, R.G. Ross, J. Phase Equilib. Diff., 12 (1991) 6-9.

[90] W. Hausler, Z. Metallk., 51 (1960) 95.

[91] M.F. Lantratov, A.G. Morachevskii, M.I. Antonova, Z. Prikl. Khim., 36 (1963) 1278-1283.

[92] B.P. Alblas, W. Van der Lugt, J. Dijkstra, W. Geertsma, C. Van Dijk, J. Phys. F: Met. Phys., 13 (1983) 2465-2470.

[93] O. Akinlade, Physics and Chemistry of Liquids: An International Journal 29 (2006) 9-21.

[94] O. Akinlade, Z. Metallk., 85 (1996) 487-491.

[95] L. Darken, Met. Soc. Trans. AIME, 239 (1967) 80-89.

CHAPITRE 5   ARTICLE 2: THERMODYNAMIC OPTIMIZATION OF THE BINARY LI-SN AND THE TERNARY MG-SN-LI SYSTEMS

Submitted to CALPHAD (22th May, 2013) titled as "Thermodynamic evaluation and optimization of the Mg-Sn-Li ternary system using a coupled first-principles calculations and CALPHAD method and its application to Mg-based alloy design".

Revised and resubmitted to CALPHAD (5th November, 2013) titled as "Thermodynamic optimization of the binary Li-Sn and the ternary Mg-Sn-Li systems".

Jian Wang[a], Jiajia Han[b], In-Ho Jung[c], Daniel Bairos[c], Patrice Chartrand*[a]

[a] Center for Research in Computational Thermochemistry (CRCT), Dept. of Chemical Engineering, Ecole polytechnique de Montréal, Montréal, Québec, Canada H3C 3A7

[b] Department of Materials Science and Engineering, College of Materials, Xiamen University, Xiamen 361005, P. R. China

[c] Department of Mining and Materials Engineering, McGill University, H.W. Wong Building, 3610 University Street, Montreal, Quebec, H3A 2B2, Canada

*Corresponding author: Center for Research in Computational Thermochemistry (CRCT), Dept. of Chemical Engineering, Ecole Polytechnique, Montréal, Québec, Canada, H3C 3A7. Tel: +1 514 340-4711 ext. 4089; fax: +1 514 340-5840. E-mail address: patrice.chartrand@polymtl.ca

Abstract

The critical re-optimization of the Li-Sn binary system and optimization of Mg-Sn-Li ternary system in Mg-rich portion have been conducted using a coupled first-principles calculations and CALPHAD method. The enthalpies of formation of LiSn, Li_7Sn_3, Li_5Sn_2, $Li_{13}Sn_5$, Li_7Sn_2, Li_2Sn_5, and Li_2MgSn phases at 0 K were evaluated by first-principles calculations. Based on the experimental data and the results from first-principles calculations, thermodynamic model parameters for all solid and liquid phase for binary Li-Sn and ternary Mg-Li-Sn were optimized. In particular, the strong ordered binary liquid Li-Sn solution and ternary liquid Mg-Li-Sn solution

were well described by the Modified Quasichemical Model (MQM) taking into account the short range ordering of atoms with the pair approximation.

Keywords: Mg-Sn-Li system, Alloy design, ab-initio calculations, Phase diagram and prediction (including CALPHAD)

5.1   Introduction

Magnesium, as the lightest structural metal with a density of about 1.8 g/cm^3, is particularly attractive for the automotive and aeronautical industries for weight reduction and improvement of fuel efficiency [1]. Although Mg-Al based alloys, including the AM (Mg-Al-Mn) and AZ (Mg-Al-Zn) series, are the most widely used structural Mg alloys offering very good performances at room temperature, most of Mg-Al based alloys have poor mechanical properties at evaluated temperatures because of the low thermal stability of the $Mg_{17}Al_{12}$ phase which is the main secondary phase in Mg-Al based alloys. Therefore, new Mg-based alloys (Al free series) are under development, aiming at low costs and advanced mechanical properties.

Mg-Sn based alloys maintain a stable microstructure and good mechanical properties at high temperatures due to the formation of the thermally stable Mg_2Sn phase. Previous investigations [2-4] indicate that Mg-Sn alloys with additional alloying elements have comparable or better creep resistance properties than AE42 alloys. In addition, it is known that Sn can improve corrosion resistance [5, 6]. However, Mg-Sn alloys require long ageing times to reach their peak hardness, which is less practical for industrial applications [7]. Consequently, it is necessary to improve the age hardening response and creep resistance behavior of Mg-Sn alloys. Micro-alloying can potentially achieve this goal. Many alloying elements forming stable precipitates such as Ag, Ca, Li, Na, Zn, Sr, In, and rare-earth elements can be considered for this purpose. Mendis et al.[8, 9] reported a qualitative thermo-kinetic criteria for choosing micro-alloying elements to improve the mechanical properties of Mg-Sn based alloys. They reported that with the In + Li additions, the number density of Mg_2Sn precipitation was increased by 270 %, which resulted in a hardening increment by about 150 % [9]. Although Mendis et al. showed the potential of the Mg-Sn-Li system for new high temperature Mg-Sn alloys, the accurate phase equilibria of the Mg-Sn-Li system were not well reported in previous literature, particularly for the Mg-rich side.

The purpose of the present study is the thermodynamic optimization of the Mg-Sn-Li system, in particular for the Mg-rich region. In the thermodynamic "optimization (modeling)" of a chemical system, all available thermodynamic and phase equilibrium data are evaluated simultaneously to obtain a self-consistent set of modeling equations for the Gibbs energies of all of the phases as functions of temperature and composition. From these equations, all of the thermodynamic properties and the phase diagrams can be back-calculated. Through this, all phase equilibrium and thermodynamic data are rendered self-consistent and consistent with thermodynamic principles. First-principles calculations based on density functional theory can successfully calculate the enthalpy of formation of intermetallic phases, which can be incorporated into CALPHAD type assessments [10].

In order to build a thermodynamic database for the ternary Mg-Sn-Li system, all three binary sub-systems should be firstly assessed and optimized. Two sub-systems Mg-Sn [11] and Mg-Li [12] have been optimized by our group using the Modified Quasichemical Model (MQM) for liquid phase, which takes into account the short-range order (SRO) in the liquid phase. SRO is strong in Mg-Sn and Li-Sn binary liquid alloys, due to their very negative enthalpy of mixing. The Li-Sn binary system has been thermodynamically optimized by Gasior et al. [13], Yin et al. [14] and Du et al. [15]. However, the reproduction of phase diagram and thermodynamic properties still left some room for further improvement. In all cases, the liquid phase was described by the Bragg-Williams model (BWM) [16], which assumes random mixing of elements and neglects SRO resulting in many temperature-dependent parameters. In addition, an inverse miscibility gap in liquid Li-Sn is calculated above 3650 $^\circ$C from the assessed parameters of Du et al. [15], another sign that neglecting SRO in this system results in improper extrapolation. Thus, in the present study, re-optimization of the Li-Sn binary system using the MQM for liquid phase was performed to use the same model for liquid phase and improve the prediction capability of the model in the ternary liquid alloy from the binary model parameters for liquid solution. As there are no available thermodynamic properties for the ternary compound Li_2MgSn, first-principles calculations were performed to calculate the enthalpy of formation of this compound. The first-principles calculations are also used to calculate the enthalpy of the binary Li-Sn compounds in order to resolve the discrepancy between existing calorimetric data for the formation enthalpies of these binary compounds. This work is part of a comprehensive research

program to develop a thermodynamic database for the Mg-X (X: Ag, Ca, In, Li, Na, Sn, Sr, Zn) based alloys for automotive applications.

5.2   Literature review

5.2.1 Li-Sn system

Hansen and Anderko [17], Hultgren et al. [18] and Smith and Moser [19] previously reviewed the phase equilibria and thermodynamic data in the Li-Sn binary system. Later, Sangster and Bale [20] made a critical review of all the available experimental data of the Li-Sn system including phase equilibrium and thermodynamic data. A brief review of the phase diagram and thermodynamic experimental data is given below.

Phase diagram data

All reported experimental data of the phase equilibria in the Li-Sn system are plotted in Fig. 5.1. The phase diagram of the Li-Sn system was first investigated using a thermal analysis technique by Masing and Tammann [21] over the entire composition range. The authors claimed the existence of three compounds: Li_2Sn_5, Li_3Sn_2 and Li_4Sn. Baroni [22] reported similar results using thermal and roentgenographic analyses. Later, through the careful thermal and thermo-resisto metric analyses, Grube and Meyer [23] revealed a more complex feature of the phase diagram and reported six intermetallic phases: $LiSn_2$, $LiSn$, Li_2Sn, Li_5Sn_2, Li_7Sn_2 and Li_4Sn. It is important to note that the melting temperatures of all intermetallic compounds, except for $LiSn_2$ reported by Grube and Mayer, are substantially higher than those reported by previous studies [21, 22]. All authors [21-23] agree that no detectable amount of Li is dissolved in the β-Sn phase from a resistometric method, which is in agreement with a later study by Jenckel and Roth [24] who used hardness curves and resistometric methods (the reported solubility of Li in solid β-Sn is < 0.1 at. %). Grube and Meyer [23] reported that Li_7Sn_2 contains about 1 at. % excess solubility Sn at 715 °C and the same was later confirmed by Bailey et al. [25]. Bailey et al. [25] re-investigated and refined the liquidus region between LiSn and Li_7Sn_2 using DTA and metallographic observations. They confirmed the crystal structure of LiSn [26], Li_5Sn_2 [27], Li_7Sn_2 [28] and corrected the stoichiometry and the crystal structure of Li_2Sn to 'Li_7Sn_3' [29], Li_4Sn to '$Li_{22}Sn_5$' [30] and $LiSn_2$ to 'Li_2Sn_5' [31]. Many of these compounds were found to be isostructural with compounds formed in the Li-Pb system [30]. Frank and Müller [32] prepared

and characterized a compound not previously observed by thermal techniques, $Li_{13}Sn_5$. Foster et al. [33] and Barsoum and Lukas [34] performed EMF measurements to investigate the thermodynamic properties of liquid and solid compounds. The liquidus compositions extrapolated from their experiments are also in good agreement with the results of Grube and Meyer [23]. Dadd et al. [35] performed extensive work on the liquidus on Li-rich portion using equilibrium resistivity-temperature experiments at the temperature range between 306 and 472 °C and found quite different liquidus results from previous studies [22, 23]. This may be due to Sn dissolution into Fe crucibles (maximum solubility of about 8 at. %) under their experimental condition, as pointed out by Dadd et al. [35]. Recently, Gasior et al. [13] studied the phase diagram of the Li-Sn system by EMF method for a composition range of 2.4 to 95.2 at. % Li. The seven previously reported compounds were confirmed, and one more new phase, named Li_8Sn_3,
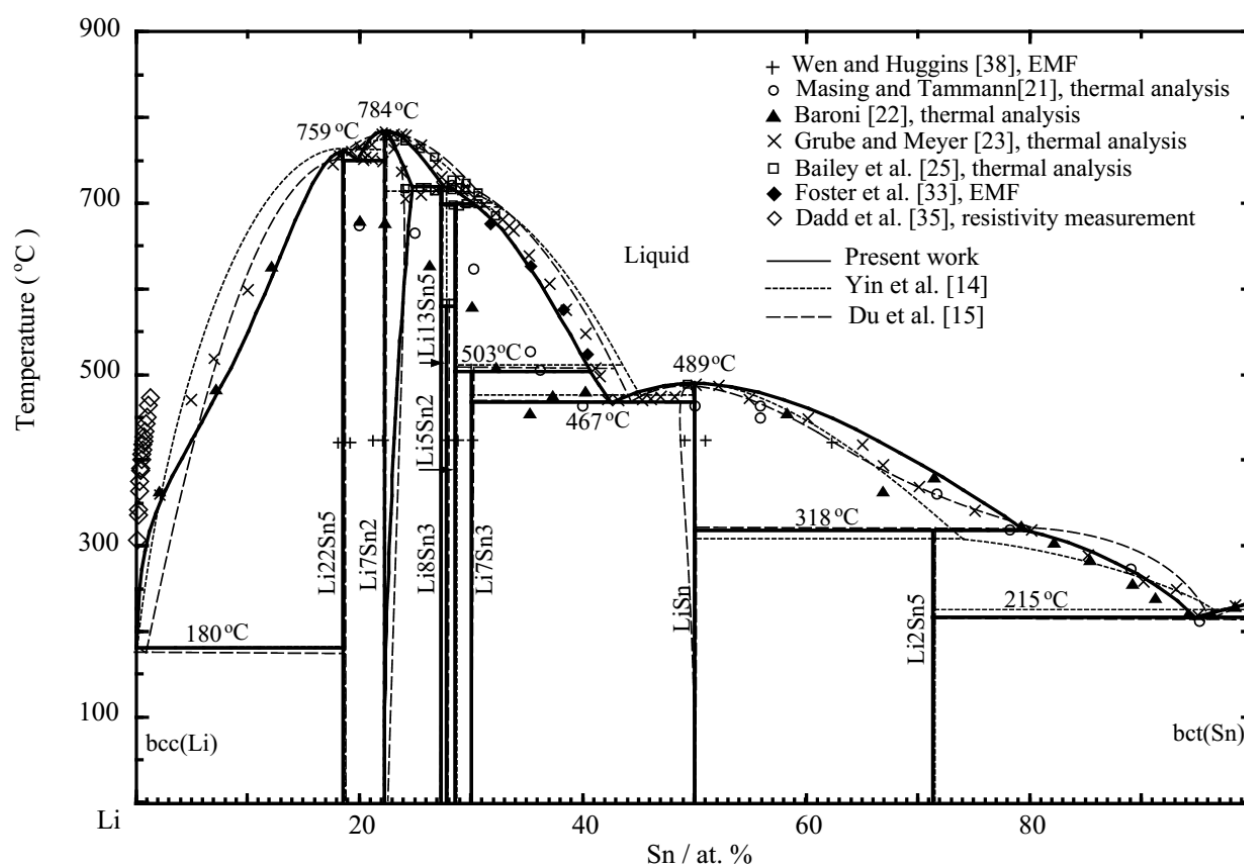
Figure 5.1 Calculated phase diagram of the Li-Sn system in the present study along with experimental data [21-23, 25, 33, 35, 38] and the previous assessment results [14, 15]

was found in their work. Goward et al. [36] and Lupu et al. [37] reinvestigated the $Li_{22}Sn_5$ compound using X-ray techniques, and reported that $Li_{22}Sn_5$ has a cubic crystal structure with the formula of $Li_{341}Sn_{80}$.

In the present optimization work, eight stable compounds discussed above were taken into account: Li_2Sn_5, $LiSn$, Li_7Sn_3, Li_5Sn_2, $Li_{13}Sn_5$, Li_7Sn_2, Li_8Sn_3 and $Li_{22}Sn_5$ (for the sake of simplicity, the recently reported $Li_{341}Sn_{80}$ formula of $Li_{22}Sn_5$ compound was not used in this study).

Thermodynamic data

Foster et al. [33] carried out EMF measurements for Li-Sn alloys with $0.1 < x_{Li} < 0.65$ at temperatures ranging from 527 °C to 777 °C. As results of the experiments, the activity values for Li in liquid Li-Sn and the standard Gibbs energy of formation of Li_5Sn_2 were determined. Wen and Huggins [38] performed a similar research using a galvanic cell of Al at $0 < x_{Li} < 0.86$ in the temperature range from 360 °C to 590 °C, and reported the activities of Li in liquid and two phase regions: thermodynamic properties such as Gibbs energy, enthalpy and entropy of liquid and solid intermetallic phases at 415 °C were derived from their data. Recently, Gasior et al. [13] also performed an extensive thermodynamic study in this system ($0.025 < x_{Li} < 0.952$) at a temperature range from 382 °C to 700 °C using several different EMF cells. Morachevskii et al. [39], Yatsenko and Saltykova [40], Moser et al. [41] also used a similar EMF technique to determine the thermodynamic properties of the Li-Sn system.

Thermodynamic properties of liquid Li-Sn were also determined using the vapor pressure of Li. Baradel et al. [42] used the Knudsen effusion cell at 700 °C and 850 °C over a wide Li composition range ($0 < x_{Li} < 0.9$). Fischer and Johnson [43] used the transpiration apparatus for liquid Li-Sn ($0.1 < x_{Li} < 0.9$) at 1200 °C to determine the activity of Li. Recently, Fürtauer et al. [44] determined the integral molar enthalpies of mixing of Li-Sn molten alloys at 500 °C and 800 °C by using drop calorimetry. The enthalpy of formation of solid Li-Sn intermetallic compounds and liquid alloys were determined using a calorimetry technique. Kubaschewski and Seith [45] determined ΔH°_{298} of solid Li-Sn compounds using a drop calorimeter. Sommer et al. [46] used a solution calorimeter with a Sn bath to determine ΔH^f_{800K} of $LiSn$, Li_5Sn_2, Li_7Sn_2, $Li_{22}Sn_5$ alloys from liquid Li and Sn. Moser et al. [41] measured the enthalpies of liquid Li-Sn ($0.01 < x_{Li} < 0.5$ and $0.87 < x_{Li} < 0.99$) using a high temperature calorimeter in the temperature range 691 and 938

K and reported very negative values for the enthalpy of mixing with a minimum of -40 kJ/mol at $x_{Li} \approx 0.8$. The heat content of Li_7Sn_2 alloy with the temperature dependence was determined by Singh and Sommer [47] by calorimetry. The heat fusion of Li_7Sn_2 alloy was reported as 8.3±0.5 kJ/mol by Singh and Sommer [47].

The thermodynamic properties of Li-Sn intermetallic phases were studied by Courtney et al. [48] and Chou et al. [49] using first-principles calculations. But differences between the calculated data are more than 5 kJ/mol-atoms for many intermetallic phases (Fig. 5.2) and therefore it is worthwhile to perform new first-principles calculations in the present work.
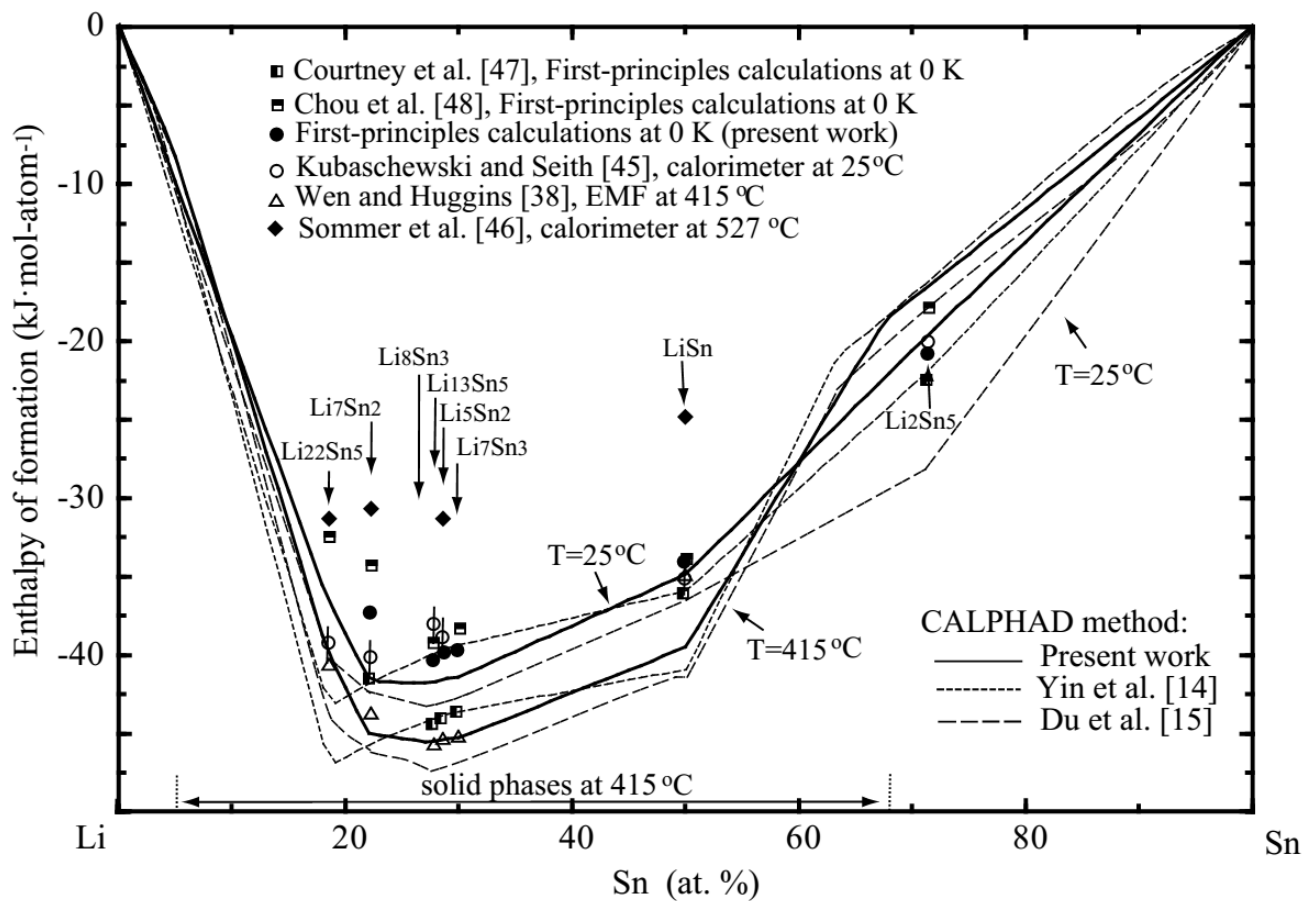
Figure 5.2 Enthalpies formation of the Li-Sn system. Reference states: Li (bcc) and Sn (bct) at 25 °C, and Li (liquid) and Sn (liquid) at 415 °C and 527 °C

Mg-Sn-Li system

Teslyuk et al. [50] studied the isothermal phase equilibria of the Mg-Sn-Li ternary system ($0 < X_{Sn} < 50$ at.%) at 370 ^{o}C using annealed alloys followed by optical microscopy and X-ray analysis. In their study, two ternary compounds Li$_2$MgSn (NaTl-type, fcc cubic structure) and Li$_4$MgSn (unknown crystal structure) with small solubilities of Li and Sn were reported. In addition, they reported that the binary Mg$_2$Sn and Li$_{22}$Sn$_5$ phases are extending into the ternary system with 18 at. % Li solubility in Mg$_2$Sn and with 5 at. % Mg in Li$_{22}$Sn$_5$, respectively. Sviderskaya et al. [51] investigated the liquidus and solidus of several isoplethal sections of the system, Mg-Li10Sn90, Mg-Li25Sn75, Mg-Li50Sn50, and Mg70Li30-Mg20Sn80 (wt. %) using a DSC technique and microscopic analysis. As results, Sviderskaya et al. [51] extrapolated two ternary invariant reactions of Liquid + Li$_2$MgSn $\leftrightarrow$ hcp + Mg$_2$Sn at 609±2 ^{o}C and Liquid $\leftrightarrow$ hcp + bcc + Li$_2$MgSn at 580 ^{o}C based on their thermal analysis results. Padezhnova and Guzei [52] investigated the isothermal sections of the Mg-rich region of ternary Mg-Sn-Li system at the temperature range between 200 ^{o}C and 500 ^{o}C using electrical resistance measurements, micro-hardness and optical microscopy methods. No thermodynamic study has been conducted for ternary liquid and solid phases.

5.3 Methodologies

5.3.1 Thermodynamic modeling

In the present work, the thermodynamic optimizations of the Li-Sn and Mg-Sn-Li systems have been carried out. All thermodynamic calculations were performed using the FactSage thermodynamic software [54]. The thermodynamic properties of the liquid phase were described using the MQM with the Pair Approximation developed by Pelton et al. [55, 56]. All crystal structures of solid phases considered in the Mg-Sn-Li system are summarized in Table 5.1 along with the thermodynamic model used to describe their thermodynamic properties. The binary Mg-Sn [11, 57-59] and Mg-Li [12, 60-62] systems have been previously optimized several times with different liquid models such as BWM, MQM, and Associated Model (AM). In order to obtain the best predictions of the thermodynamic properties of the liquid solution in the ternary field of composition, the Mg-Sn, Li-Sn and Mg-Li binary liquid solutions should have their

thermodynamic properties described by the MQM, even if the Mg-Li binary liquid looks rather ideal (enthalpy of mixing with a minimum near -3.5 kJ/mol at 50 at.% Li).

Table 5.1 Structural parameters and thermodynamic models for all phases in the Mg-Sn-Li system

Phase	Pearson symbol	Space group	Lattice parameters, in Å			Model[a]
			a	b	c	
Liquid	-	-	-	-	-	MQM
fcc	cF4	$Fm\bar{3}m$	-	-	-	CEF
bct	tI4	$I4_1/mmm$	-	-	-	CEF
bcc	cI2	$Im\bar{3}m$	-	-	-	CEF
hcp	hP2	$P6_3/mmc$	-	-	-	CEF
$Li_{22}Sn_5$	cF432	$F\bar{4}3m$	19.6902 [36] 19.6907 [37]			CEF
Li_8Sn_3	-	-	-	-	-	CEF
Li_2Sn_5	tP14	P_4/mbm	10.407[b] (1.3%)[c] 10.274 [72]		3.126[b] (0 %)[c] 3.126 [72]	ST
Li_5Sn_2	hR7	$R\bar{3}m$	4.723[b] (-0.4%)[c] 4.741 [72]		19.803[b] (-0.2%)[c] 19.833 [72]	ST
Li_7Sn_2	oC36	$Cmmm$	9.805[b] (-0.03%)[c] 9.802 [72]	13.858[b] (-0.4%)[c] 13.803 [72]	4.722[b] (-0.6%)[c] 4.752 [72]	CEF
Li_7Sn_3	mP20	$P2_1/m$	8.55[b] (-0.13%)[c] 8.561 [72]	4.730[b] (-0.2%)[c] 4.721[71]	9.473[b] (-0.23%)[c] 9.451 [72]	ST
$Li_{13}Sn_5$	hP18	$P\bar{3}m1$	4.695[b] (-0.06%)[c] 4.701 [72]		17.110[b] (-0.08%)[c] 17.124 [72]	ST
LiSn	mP6	$P2/m$	5.167[b] (-0.09%)[c] 5.172 [72]	3.229[b] (1.48%)[c] 3.182 [72]	7.808[b] (0.85%)[c] 7.742 [72]	ST
Li_2MgSn	cF16	$Fm\bar{3}m$	6.760[b] (-0.06%)[c] 6.764 [72]			CEF
Li_4MgSn	-	-	-	-	-	ST
Mg_2Sn	cF24	$Fd\bar{3}m$	6.762 [72]			CEF

[a] MQM: Modified Quasichemical Model; CEF: Compound Energy Formalism; ST: Stoichiometric Compound. [b] The parameters calculated in the present work using first-principle calculations. [c] The calculated difference of present results compared to experimental data.

The reason is that $[Mg-Li]_{pairs}$ must dissociate upon mixing with $[Sn-Sn]_{pairs}$ (i.e. mixing with Sn) to form [Mg-Sn]pairs and $[Li-Sn]_{pairs}$, which are much more favored energetically. Imposing a random distribution of $[Mg-Li]_{pairs}$ by the use of a BW binary description for the Mg-Li liquid solution would overestimate the amount of $[Mg-Li]_{pairs}$ and result in a lower quality prediction of the ternary liquid properties compared to a MQM description of the same binary system which

would dissociate more of the [Mg-Li]$_{pairs}$ to favor the [Mg-Sn]$_{pairs}$ and [Li-Sn]$_{pairs}$ upon mixing with Sn. Consequently, in order to construct a self-consistent thermodynamic database for liquid, the optimization results carried out by Jung et al. [11] and Spencer [12], where the MQM was used for the description of liquid Mg-Sn and Mg-Li, were taken for the present optimization of the Mg-Sn-Li ternary system.

Stoichiometric phase

The molar Gibbs energies of pure elements and stoichiometric phases can be described by:

$$G_T^o = H_T^o - TS_T^o \tag{5.1}$$

$$H_T^o = \Delta H_{298.15K}^o + \int_{T=298.15K}^{T} C_p dT \tag{5.2}$$

$$S_T^o = S_{298.15K}^o + \int_{T=298.15K}^{T} (C_p / T) dT \tag{5.3}$$

where $\Delta H_{298.15K}^o$ is the molar enthalpy of formation of a given species from pure elements ($\Delta H_{298.15K}^o$ of element stable at 298.15 K and 1 atm is assumed as 0 J·mol^{-1}; reference state), and $S_{298.15K}^o$ is the molar entropy at 298.15 K and C_p is the molar heat capacity.

In the present study, the Gibbs energies of pure elements were taken from the SGTE database [16]. As there are no experimental heat capacity of Li-Sn intermetallics, the heat capacities were evaluated using the Neumann–Kopp rule [62]. Both heat capacities curves of solid Li and Sn from SGTE database show maxima just above their melting temperatures (see Figure 5. 3 (a)). This is because the heat capacity of liquid was used to estimate that of solid above the melting temperature in order to prevent the diversion of heat capacity of these low melting elements above their melting temperatures. However, as several intermetallic phases in the present Li-Sn and Mg-Sn-Li systems have their melting temperatures substantially higher than that of Li and Sn, the resultant heat capacities curves of intermetallic phases, constructed simply from the Neumann–Kopp rule, also can have maxima at about 500 K as shown in Figure 5. 3 (b), which are less likely in reality. In order to resolve this, we modified the heat capacities of solid Sn and Li (only for the applications of Neumann-Kopp rule for intermetallic phases) above their melting temperatures to make sure that the heat capacities of intermetallics can increase with

temperatures until their melting temperatures. The optimized model parameters for stoichiometric compounds are listed in Table 5. 2.

Table 5.2 Optimized thermodynamic model parameters for the Mg-Sn-Li ternary system [a]

Phase, model and thermodynamic parameters (J·mol^{-1}, or J·mol^{-1}·K^{-1}))	Reference
bcc_A2 phase $(Li,Mg,Sn)(Va)_3$: $L_{Li,Mg:Va} = -17154.4 + 7.53 \times T$, $^1L_{Li,Mg:Va} = -3347.2 + 1.26 \times T$, $^2L_{Li,Mg:Va} = 3347.2$ $G_{Mg:Va} = {}^oG_{Mg}^{hcp} + 3100.0 + 2.10 \times T$, $G_{Sn:Va} = {}^oG_{Sn}^{bct} + 4400.0 - 6.00 \times T$, $G_{Li:Va} = {}^oG_{Li}^{bcc}$	[12]
bct_A5 phase $(Li,Mg,Sn)(Va)_3$: $G_{Mg:Va} = {}^oG_{Mg}^{hcp} + 15000.0$, $G_{Sn:Va} = {}^oG_{Sn}^{bct}$, $G_{Li:Va} = {}^oG_{Li}^{bcc} + 15000.0$	
hcp_A3(Mg) phase $(Li,Mg,Sn)(Va)_3$: $G_{Mg:Va} = {}^oG_{Mg}^{hcp}$, $G_{Sn:Va} = {}^oG_{Sn}^{bct} + 3900.0 - 4.40 \times T$, $G_{Li:Va} = {}^oG_{Li}^{bcc} - 154.0 + 2.00 \times T$	
$L_{Li,Mg:Va} = -6694.4 + 0.42 \times T$, $^1L_{Li,Mg:Va} = -3932.9$, $^2L_{Li,Mg:Va} = 4100.3$	[12]
$^1L_{Mg,Sn:Va} = 48116.0$	[11]
$^0L_{MgSn(Li):Va} = {}^0L_{MgLi(Sn):Va} = {}^0L_{LiSn(Mg):Va} = -292880.0$	This work
Mg_2Sn phase $(Li,Mg)_2(Sn)$: $G_{Mg:Sn} = -102589.8 + 367.50 \times T - 68.331 \times T \ln T - 0.0178986 \times T^2 + 3.33829 \times 10^{-7} \times T^3 + 95940.0 / T$ $G_{Li:Sn} = 2 \times G_{Li} + G_{Sn} - 37656.0$, $L_{Li,Mg:Sn} = -121336.0$	[11] This work
$Li_{22}Sn_5$ phase $(Li,Mg)_{22}(Sn)_5$: $G_{Li:Sn} = 22 \times G_{Li} + 5 \times G_{Sn} - 990630.4 + 123.50 \times T$, $G_{Mg:Sn} = 22 \times {}^oG_{Mg}^{hcp} + 5 \times G_{Sn} - 167360.0$ $^0L_{Li,Mg:Sn} = -125520.0$	This work This work
Li_7Sn_2 phase $(Li,Sn)_7(Li,Sn)_2$: $G_{Li:Li} = 9 \times G_{Li} + 15000.0$, $G_{Sn:Sn} = 9 \times G_{Sn} + 15000.0$ $G_{Li:Sn} = 7 \times G_{Li} + 2 \times G_{Sn} - 37630.9 + 8.79 \times T$, $G_{Sn:Li} = 2 \times G_{Li} + 7 \times G_{Sn}$ $^1L_{Li,Sn:Sn} = 25940.8 + 75.31 \times T$	This work This work This work
Li_8Sn_3 phase $(Li)_8(Sn)_3$: $G_{Li:Sn} = 8 \times G_{Li} + 3 \times G_{Sn} - 460807.0 + 62.99 \times T$	This work
$Li_{13}Sn_5$ phase $(Li)_{13}(Sn)_5$: $G_{Li:Sn} = 13 \times G_{Li} + 5 \times G_{Sn} - 752999.3 + 101.32 \times T$	This work
Li_5Sn_2 phase $(Li)_5(Sn)_2$: $G_{Li:Sn} = 5 \times G_{Li} + 2 \times G_{Sn} - 291829.7 + 37.90 \times T$	This work
Li_7Sn_3 phase $(Li)_7(Sn)_3$: $G_{Li:Sn} = 7 \times G_{Li} + 3 \times G_{Sn} - 415271.0 + 56.54 \times T$	This work
$LiSn$ phase $(Li)_1(Sn)_1$: $G_{Li:Sn} = G_{Li} + G_{Sn} - 69986.0 + 9.02 \times T$	This work
Li_2Sn_5 phase $(Li)_2(Sn)_5$: $G_{Li:Sn} = 2 \times G_{Li} + 5 \times G_{Sn} - 137949.0 + 0.60 \times T$	This work
Li_4MgSn phase $(Li)_4(Mg)(Sn)$: $G_{Li:Mg:Sn} = 4 \times G_{Li} + G_{Mg}^{hcp} + G_{Sn} - 214001.0 + 45.23 \times T$	This work
Li_2MgSn phase $(Li)_2(Li,Mg)(Li,Sn)$: $G_{Li:Mg:Sn} = 2 \times G_{Li} + G_{Mg}^{hcp} + G_{Sn} - 145680.0 + 7.53 \times T$	This work

Table 5.2 (Continued) Optimized thermodynamic model parameters for the Mg-Sn-Li ternary system [a]

$G_{Li:Li:Sn} = 3 \times G_{Li} + G_{Sn}, G_{Li:Mg:Li} = 3 \times G_{Li} + G_{Mg}^{hcp}, G_{Li:Li:Li} = 4 \times G_{Li}$	This work
$^0L_{Li:Li,Mg:Sn} = -184096.0 + 50.63 \times T;$ $^1L_{Li:Li,Mg:Sn} = -171554.0 + 46.02 \times T$	This work
$^0L_{Li:Mg:Li,Sn} = -142256.0 + 63.18 \times T;$ $^1L_{Li:Mg:Li,Sn} = -129704 + 58.58 \times T$	This work
$G_{Li} = \int_{298}^{T} C_{p_{Li}} dt - T \times \int_{298}^{T} \dfrac{C_{p_{Li}}}{T} dt + \Delta H_{Li}^{298K} - TS_{Li}^{298K}$ $\qquad (\Delta H_{Li}^{298K} = 0; \ S_{Li}^{298K} = 29.12)$ $G_{Sn} = \int_{298K}^{T} C_{p_{Sn}} dt - T \times \int_{298K}^{T} \dfrac{C_{p_{Sn}}}{T} dt + \Delta H_{Sn}^{298K} - TS_{Sn}^{298K}$ $\qquad (\Delta H_{Sn}^{298K} = 0; \ S_{Sn}^{298K} = 51.19)$ $C_{p_{Sn}} = 15.961 + 0.0377404 \times T + 123920/T^{-2} - 1.8727002E\text{-}5 \times T^2 \qquad$ 298 K<T<1000 K $\qquad\quad = 35.098 \qquad\qquad\qquad\qquad\qquad\qquad\qquad\qquad\qquad$ 1000 K<T<3000 K	
$^*Cp_{Li} = 38.940488 - 0.070933862 \times T - 319988/T^{-2} + 0.000119218896 \times T^2 \qquad$ 298K<T<454K $\qquad\quad = 32.94 - 0.0002179 \times T - 598200/T^{-2} + 4.656E\text{-}8 \times T^2 \qquad$ 455K<T<3000K	
[a] $C_{p_{Sn}}$ and $C_{p_{Li}}$ are modified heat capacity in the present work, all other thermodynamic data for pure elements are taken from SGTE database	
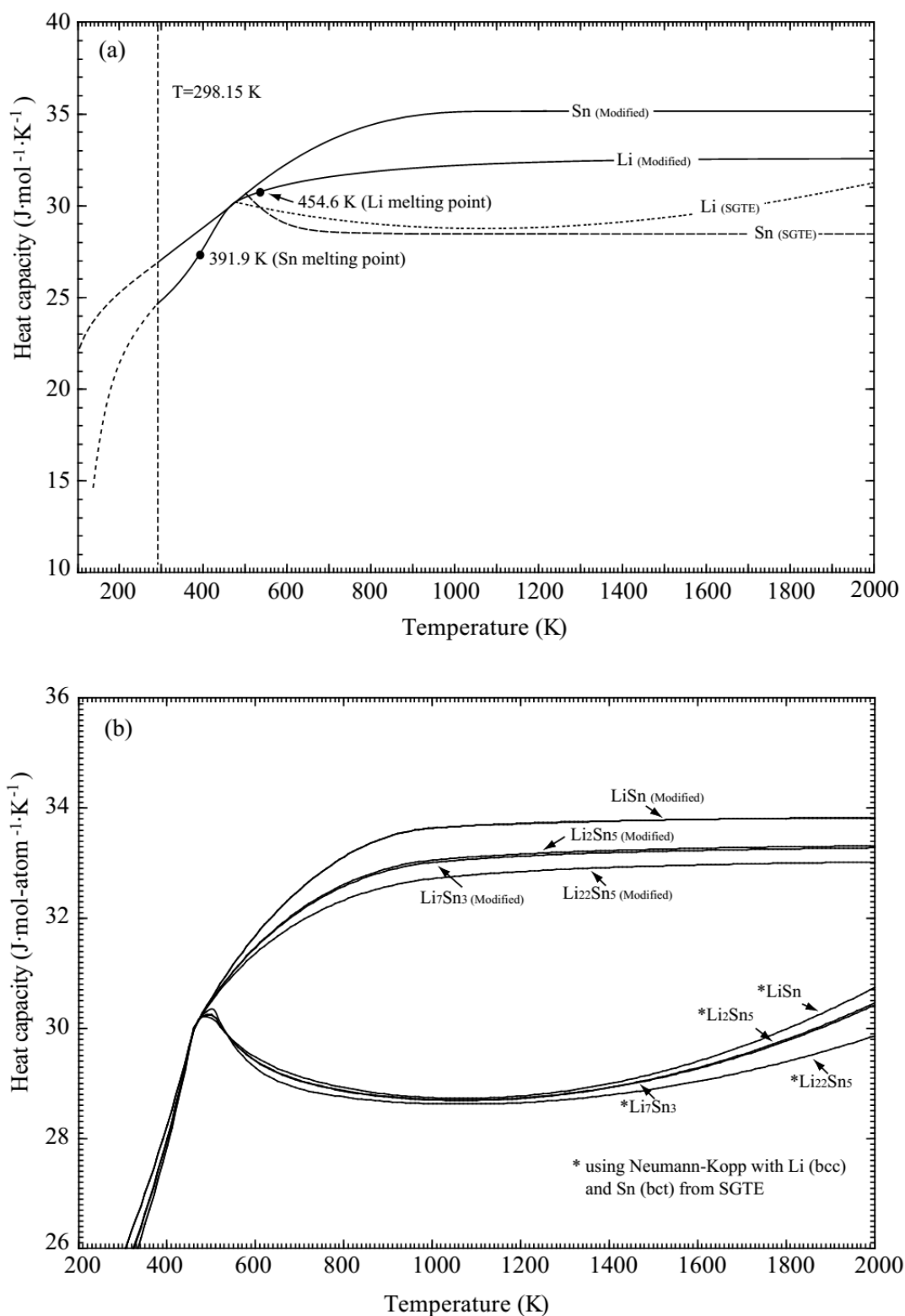
Figure 5.3 Heat capacities of (a) pure elements, Li and Sn, and (b) Li-Sn compounds evaluated in the present study using the Neumann–Kopp rule with modified heat capacities of Li and Sn

Solid solutions

hcp (Mg-rich), bct (Sn-rich), bcc (Li-rich), Mg_2Sn, Li_7Sn_2, $Li_{22}Sn_5$ and Li_2MgSn phases were modeled with the Compound Energy Formalism (CEF) [63] with their sublattice structures based on the reported crystal structures (Table 5. 1). For example, according to the solid solubility of Li in the Mg_2Sn phase reported by Teslyuk et al. [50], Mg is substituted by Li, thus the Mg_2Sn solid solution was modeled with the sublattice structure of $(Mg,Li)_2(Sn)$, and the Gibbs energy expression can be expressed as follows:

$$G^{Mg_2Sn} = y_{Mg}^I y_{Sn}^{II} G_{Mg:Sn}^o + y_{Li}^I y_{Sn}^{II} G_{Li:Sn}^o + 2RT(y_{Mg}^I \ln y_{Mg}^I + y_{Li}^I \ln y_{Li}^I)$$
$$+ y_{Li}^I y_{Mg}^I y_{Sn}^{II} \, {}^n L_{Li,Mg:Sn}$$

(5. 4)

where y_{Mg}^I and y_{Li}^I are the site fractions of the elements Mg and Li on the first sublattice and y_{Sn}^{II} the site fraction of Sn in the second sublattice (in this case, $y_{Sn}^{II} = 1$). $G_{Mg:Sn}^o$ and $G_{Li:Sn}^o$ are the Gibbs energies of the end members Mg_2Sn and Li_2Sn, respectively. $L_{Mg,Li:Sn}$ is the excess interaction energy between Mg and Li atoms occupying the first sublattice, which can be expressed as:

$${}^n L_{Mg,Li:Sn} = (a_n + b_n T)(y_{Li}^I - y_{Mg}^I)^n$$

(5. 5)

The Gibbs energies of end members and $L_{Mg,Li:Sn}$ are the model parameters evaluated in the present work. The optimized model parameters for solid solutions are listed in Table 5.2.

Liquid phase

The thermodynamic properties of liquid phase were modeled by the MQM with the pair approximation developed by Pelton et al. [54, 55]. A detailed description of the MQM can be found elsewhere [54, 55]. The same notation is used in the present work, and a brief description of MQM is given as follows:

For the binary *A-B* system, the following quasichemical pair exchange reaction can be considered:

$$(A-A) + (B-B) = 2(A-B), \quad \Delta g_{AB}$$

(5. 6)

where $(i-j)$ represents a first-nearest-neighbor pair of atoms. The Gibbs energy change for the formation of one mole of $(A-B)$ according to reaction (5. 6) is $\Delta g_{AB}/2$. Let n_A and n_B be the number of moles of A and B respectively, and n_{AA}, n_{BB}, and n_{AB} be the number of moles of $A-A$, $B-B$, and $A-B$ pairs, respectively. Z_A and Z_B are the coordination numbers of A and B. Then the Gibbs energy of the solution is given by:

$$G = (n_A G_A^o + n_B G_B^o) - T\Delta S^{config} + (n_{AB}/2)\Delta g_{AB} \tag{5. 7}$$

where G_A^o and G_B^o are the molar Gibbs energies of the pure component A and B, and ΔS^{config} is the configurational entropy of mixing given by randomly distributing the $A-A$, $B-B$ and $A-B$ pairs in the one-dimensional Ising approximation. The expression for ΔS^{config} is:

$$\Delta S^{config} = -R(n_A \ln X_A + n_B \ln X_B) - R(n_{AA} \ln\frac{X_{AA}}{Y_A^2} + n_{BB} \ln\frac{X_{BB}}{Y_B^2} + n_{AB} \ln\frac{X_{AB}}{2Y_A Y_B}) \tag{5. 8}$$

where X_{AA}, X_{BB} and X_{AB} are the mole fractions of the $A-A$, $B-B$ and $A-B$ pairs; Y_A and Y_B are the coordination-equivalent fractions of A and B:

$$X_{ij} = \frac{n_{ij}}{n_{AA} + n_{BB} + n_{AB}} \quad (i, j = A \text{ or } B) \tag{5. 9}$$

$$Y_i = \frac{Z_i n_i}{Z_A n_A + Z_B n_B} \quad (i = A \text{ or } B) \tag{5. 10}$$

Moreover, the following elemental balance equations can be written:

$$Z_A n_A = 2n_{AA} + n_{AB} \tag{5. 11}$$

$$Z_B n_B = 2n_{BB} + n_{AB} \tag{5. 12}$$

Δg_{AB} is the model parameter to reproduce the Gibbs energy of liquid phase of the $A-B$ binary system, which is expanded as a polynomial in terms of the pair fractions, as follows:

$$\Delta g_{AB} = \Delta g_{AB}^o + \sum_{i\geq 1} g_{AB}^{io}(X_{AA})^i + \sum_{j\geq 1} g_{AB}^{oj}(X_{BB})^j \tag{5. 13}$$

where Δg_{AA}^o, g_{AB}^{io} and g_{AB}^{oj} are the adjustable model parameters which can be functions of the temperature. The equilibrium state of the system is obtained by minimizing the total Gibbs

energy at constant elemental composition, temperature and pressure. The equilibrium pair distribution is calculated by setting:

$$\left(\frac{\partial G}{\partial n_{AB}}\right)_{n_A,n_B}=0 \tag{5. 14}$$

This gives the ''equilibrium constant'' for the ''quasichemical pair reaction'' of Eq. 5. 7:

$$\frac{X_{AB}^2}{X_{AA}X_{BB}}=4\times\exp\left(-\frac{\Delta g_{AB}}{RT}\right) \tag{5. 15}$$

Moreover, the model permits Z_A and Z_B to vary with composition as follows [55]:

$$\frac{1}{Z_A}=\frac{1}{Z_{AA}^A}\left(\frac{2n_{AA}}{2n_{AA}+n_{AB}}\right)+\frac{1}{Z_{AB}^A}\left(\frac{n_{AB}}{2n_{AA}+n_{AB}}\right) \tag{5. 16}$$

$$\frac{1}{Z_B}=\frac{1}{Z_{BB}^B}\left(\frac{2n_{BB}}{2n_{BB}+n_{AB}}\right)+\frac{1}{Z_{AB}^B}\left(\frac{n_{AB}}{2n_{BB}+n_{AB}}\right) \tag{5. 17}$$

where Z_{AA}^A and Z_{AB}^A are the values of Z_A when all nearest neighbours of an atom A are As, and when all nearest neighbours of an atom A are Bs, and where Z_{BB}^B and Z_{AB}^B are defined similarly. The composition of maximum short range ordering (SRO) is determined by the ratio of the coordination numbers Z_{AB}^A / Z_{AB}^B.

The optimized model parameters and coordination numbers chosen considering the short range ordering in each binary liquid solution are listed in Table 5. 3.

Table 5.3 Optimized model parameters of the MQM for the Mg-Sn-Li liquid solution

Coordination numbers [a]				Gibbs energies of pair exchange reactions (J·mol⁻¹)	Reference
i	j	Z_{ij}^i	Z_{ij}^j		
Mg	Li	4	6	$\Delta g_{MgLi}=-5439.2+3.933\times T+(-920.5+0.628\times T)X_{LiLi}+(2510.4-2.26\times T)X_{MgMg}$	[12]
Mg	Sn	4	8	$\Delta g_{MgSn}=-15263.2-0.88\times T+(3347.2+0.42\times T)X_{MgMg}$	[11]
Li	Sn	4	12	$\Delta g_{LiSn}=-28869.6+2.09\times T+(2301.2-1.13\times T)X_{LiLi}-(418.4+0.67\times T)X_{SnSn}$	This work
[a] For all pure elements (Mg, Li, and Sn), $Z_{ii}^i=6$					

5.3.2 First-principles calculations

The total energies and structures were found through the first-principles calculations based on density functional theory (DFT) [64] using Vienna *ab initio* simulation package (VASP) with the projector augmented wave (PAW) construction for the pseudopotential [65-68]. In this study, the PAW pseudopotentials with electronic configurations of Li $1s^2 2s^1$, Sn $4d^{10} 5s^2 5p^2$, and Mg $2p^6 3s^2$ were employed. The generalized gradient approximation (GGA) [69] and Perdew Burke Ernzerhof functional (PBE) [70] were used for exchange correlation functions. The cutoff energy for plane wave basis set was 600 eV for Li-Sn alloys and 700 eV for Mg-Sn-Li alloys. The following *k*-points and Monkhorst–Pack (MP) scheme [71] were adopted as Brillouin Zone sampling: $19 \times 19 \times 19$ for Li, $15 \times 15 \times 15$ for Sn, $15 \times 15 \times 10$ for Mg, $10 \times 16 \times 6$ for LiSn, $6 \times 6 \times 16$ for Li_2Sn_5, $10 \times 10 \times 10$ for Li_5Sn_2, $6 \times 6 \times 10$ for Li_7Sn_2, $6 \times 10 \times 6$ for Li_7Sn_3, $10 \times 10 \times 3$ for $Li_{13}Sn_5$, and $9 \times 9 \times 9$ for Li_2MgSn. The relaxation convergences for ions and electrons were 1×10^{-5} eV and 1×10^{-6} eV, respectively. For some low-symmetric structures, the Gamma centered MP grid was used.

The total energy was calculated for the optimized crystal structures. The formation energy E_{form} for a given crystal A_xB_y was obtained according to $E_{form} = E_{total}^{(AxBy)} - x E_{total}^{(A)} - y E_{total}^{(B)}$, where $E_{total}^{(AxBy)}$, $E_{total}^{(A)}$ and $E_{total}^{(B)}$ were the total energy of A_xB_y, A and B crystals, respectively. The calculated lattice parameters and enthalpy of formations for binary and ternary intermetallic phases are presented in Tables 5. 1 and 5. 4, respectively.

Table 5.4 Calculated enthalpies of formation at 0 K for binary Li-Sn and ternary Li-Sn-Li stoichiometric compounds from first-principle calculations in this study (kJ·(mol-atom)$^{-1}$)

Compound	First-principles calculations
LiSn	-34.4
$Li_{13}Sn_5$	-40.5
Li_7Sn_3	-39.9
Li_7Sn_2	-37.5
Li_5Sn_2	-40.2
Li_2Sn_5	-21.0
Li_2MgSn	-35.7

5.4   CALPHAD critical evaluation and optimization

5.4.1 Li-Sn system

For the thermodynamic modeling of Li-Sn system, a large number of thermodynamic property data both for solid and liquid phases are available. In addition, the phase diagram of the system is also in general well studied. All these experimental data were simultaneously used to obtain the most reliable model parameters for all phases in the system. During the thermodynamic modeling, inconsistencies between experimental data were also identified. The results of thermodynamic modeling are presented below in comparison with experimental data.

Fig.5.1 shows the calculated phase diagram of the Li-Sn system using the optimized model parameters in the present study along with all available phase diagram experimental data from literature [21-23, 25, 33, 35, 38]. The calculated phase diagrams of Yin et al. [14] and Du et al. [15] are also superimposed with dotted/dashed lines for comparison purposes. The invariant reactions of the binary system are summarized in Table 5.5. As discussed above, the experimental phase diagram at Li concentration of x_{Li}= 0.6~0.8 by Masing and Tammann [21] and Baroni [22] are inconsistent with later experimental results [23, 25, 33]. Thus, the liquidus determined by Grube and Mayer [23], Bailey et al. [25], Foster et al. [33] were mainly used in the present thermodynamic optimization.

As the liquidus determined by Dadd et al. [35] in the Li-rich side is erroneous due the possible contamination by the Fe crucible, their data were not considered in the present optimization. No noticeable mutual solubility of Li and Sn has been reported, so we left ideal (all ^iL terms = 0) the binary interaction parameters for the bcc_A2 (Li-Sn) and bct_A5 (Sn-Li) solutions in the present optimization. Considering the non-stoichiometry in Li_7Sn_2 (excess Sn of about 2 at.% at 716°C [25]), this phase were modeled using the CEF with $(Li,Sn)_7(Li,Sn)_2$ sublattice structure. The other compounds in the Li-Sn system were considered as stoichiometric compounds. The phase diagram calculated using the present optimized model parameters is in good agreement with all reliable experimental data. In the present thermodynamic modeling of liquid phase, only 6 model parameters including 3 small temperature-dependent terms were used to reproduce the phase diagram and all the thermodynamic data related to liquid solution.

Table 5.5 Invariant reactions of the Li-Sn system calculated in the present work

Reaction	Temperature (^{o}C)	Reaction type	Composition (Sn at. %)			Reference
liquid $\leftrightarrow$ bcc(Li)+Li$_{22}$Sn$_5$	181	Eutectic	-	-	18.5	[20]
	180		0.011	0.001	18.5	This work
liquid $\leftrightarrow$ Li$_{22}$Sn$_5$	758	Congruent			18.5	[20]
	759				18.5	This work
liquid $\leftrightarrow$ Li$_7$Sn$_2$+Li$_{22}$Sn$_5$	752	Eutectic	20.3	22.2	18.5	[20]
	749		19.8	22.2	18.5	This work
liquid $\leftrightarrow$ Li$_7$Sn$_2$	783	Congruent		22.2		[20]
	784			22.4		This work
liquid+Li$_7$Sn$_2$ $\leftrightarrow$ Li$_8$Sn$_3$	716	Peritectic	30.0	24.0	27.3	[13]
	719		27.5	24.8	27.3	This work
Li$_8$Sn$_3$+Li$_5$Sn$_2$ $\leftrightarrow$ Li$_{13}$Sn$_5$	579	Peritectoid	27.3	28.6	27.8	[13]
	579		27.3	28.6	27.8	This work
liquid+Li$_8$Sn$_3$ $\leftrightarrow$ Li$_5$Sn$_2$	698	Peritectic	31.0	27.3	28.6	[13]
	698		30.2	27.3	28.6	This work
liquid+Li$_5$Sn$_2$ $\leftrightarrow$ Li$_7$Sn$_3$	502	Peritectic	41.0	28.6	30.0	[20]
	503		40.7	28.6	30.0	This work
liquid $\leftrightarrow$ Li$_7$Sn$_3$+LiSn	470	Eutectic	43.0	30.0	50.0	[20]
	467		42.6	30.0	50.0	This work
liquid $\leftrightarrow$ LiSn	487	Congruent		50.0		[20]
	489			50.0		This work
liquid+LiSn $\leftrightarrow$ Li$_2$Sn$_5$	320	Peritectic	79.0	50.0	71.4	[20]
	318		79.6	50.0	71.4	This work
liquid+Li$_2$Sn$_5$ $\leftrightarrow$ bct(Sn)	214	Peritectic	95.0	71.4	100	[20]
	216		94.9	71.4	100	This work

In Figure 5.2, the optimized enthalpies of formation of the intermetallic phases at 25 ^{o}C (references: bcc (Li) and bct(Sn)) and 415 ^{o}C (references: liquid (Li) and liquid (Sn)) are compared with experimental data from direct calorimeter measurements [45, 46] and EMF measurement results [38]. The enthalpies of formation at 0 K for six binary intermetallic compounds (LiSn, Li$_7$Sn$_3$, Li$_5$Sn$_2$, Li$_{13}$Sn$_5$, Li$_7$Sn$_2$, Li$_2$Sn$_5$) in the Li-Sn system were calculated using first-principles calculations in the present work. The calculated lattice parameters of intermetallic phases in the Li-Sn and Mg-Sn-Li systems from this study are summarized in Table 5.1 in comparison with available experimental data [36, 37, 72]. The calculated values of the

enthalpy of formation using first-principle calculations are in reasonable agreement with the experimental data by Kubaschewski and Seith [45] but not with the data by Sommer et al. [46], and they are mostly in between the calculated values by Courtney et al. [48] and Chou et al. [49]. The calculated enthalpy of formation from optimized model parameters is in good agreement with direct calorimetric experimental data by Kubaschewski and Seith [45] at 25 ^{o}C and indirect EMF data by Wen and Huggins [38] at 415 ^{o}C. However, the experimental data reported by Sommer et al. [46] based on their calorimeter measurements were not consistent with the experimental data by Kubaschewski and Seith [45] and Wen and Huggins [38], which are also not reproduced in the present study. Sommer et al. [46] mentioned that the error in direct reaction calorimetry by Kubaschewski and Seith [45] would involve more experimental error and therefore their experimental data would be more accurate. However, we found that the experimental data of Sommer et al. [46] cannot be reproduced with other data such as Gibbs energy of formation data (Fig. 5.5) and also far from first-principles calculations results. Previous optimized enthalpy results by Yin et al. [14] and Du et al. [15] are also in reasonable agreement with the experimental data of Kubaschewski and Seith [45] except Li_2Sn_5 by Du et al. [15].

In Fig. 5. 4, the enthalpy of fusion of Li_7Sn_2 determined by Singh and Sommer [47] is compared with calculated results from the present study and the previous optimizations. The present optimization can well reproduce the enthalpy of fusion of Li_7Sn_2 compound of about -8.3 kJ·mol-atom^{-1}, while the results of previous work [14, 15] are almost twice larger than the experimental enthalpy of fusion. It should be also noted that the slopes of heat content of solid and liquid Li_7Sn_2 are well reproduced in the present optimization, which indicates the heat capacity of solid Li_7Sn_2 is accurate enough. The heat of fusion of Li_7Sn_2 in our evaluation is in good agreement with the data reported by Singh and Sommer [47]. At the same time, the melting and liquidus points of Li_7Sn_2 from Grube and Meyer [23] are also well reproduced, giving more weigth to our evaluation, and less to the evaluations of Yin et al. [14] and Du et al. [15] who chose to fit the liquidus points of Bailey et al. [25] near the Li_7Sn_2 composition.
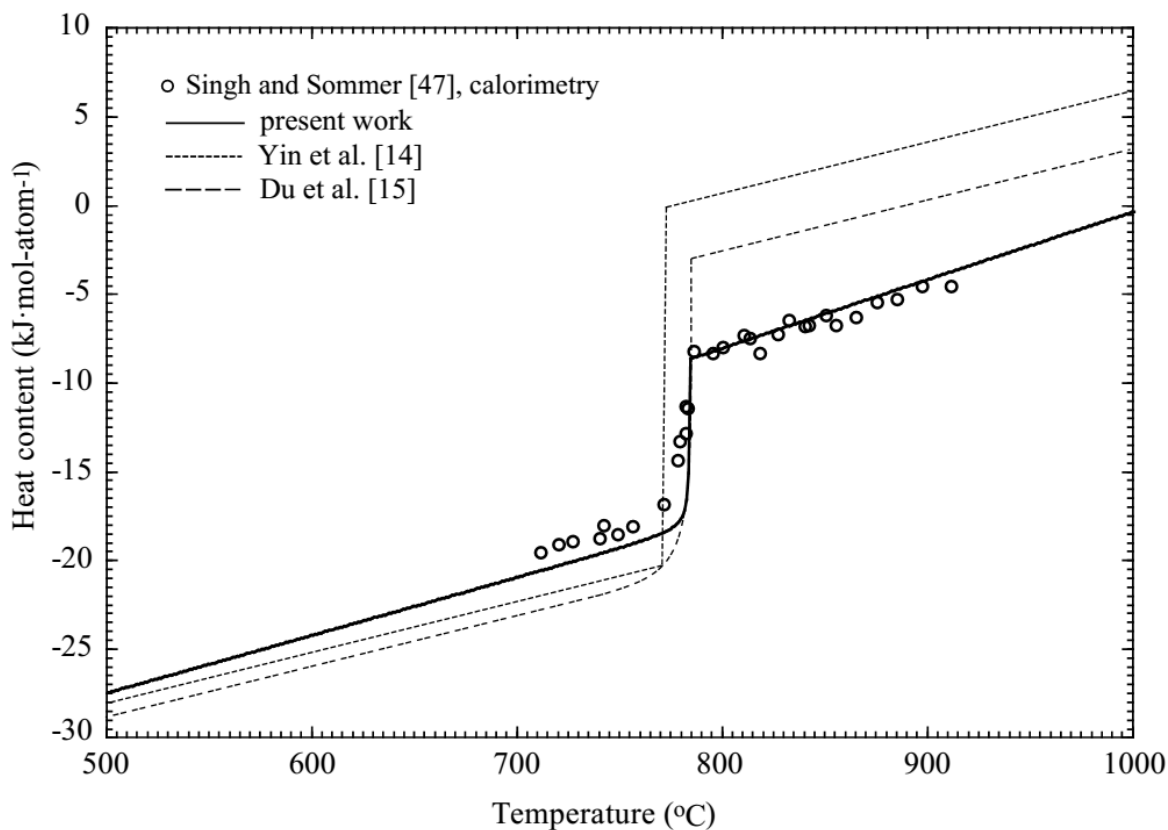
Figure 5.4 Variation of heat content of Li_7Sn_2 phase during its melting

The calculated Gibbs energies of formation for intermetallic phases from the present study are shown in Fig. 5.5 along with the experimental data [19, 33, 38]. The review data of Smith and Moser [19] based on the previous study are also plotted in Fig. 5 for comparison. In general, the calculated Gibbs energies of formation of Li-Sn compounds in the present study are in good agreement with available experimental data.
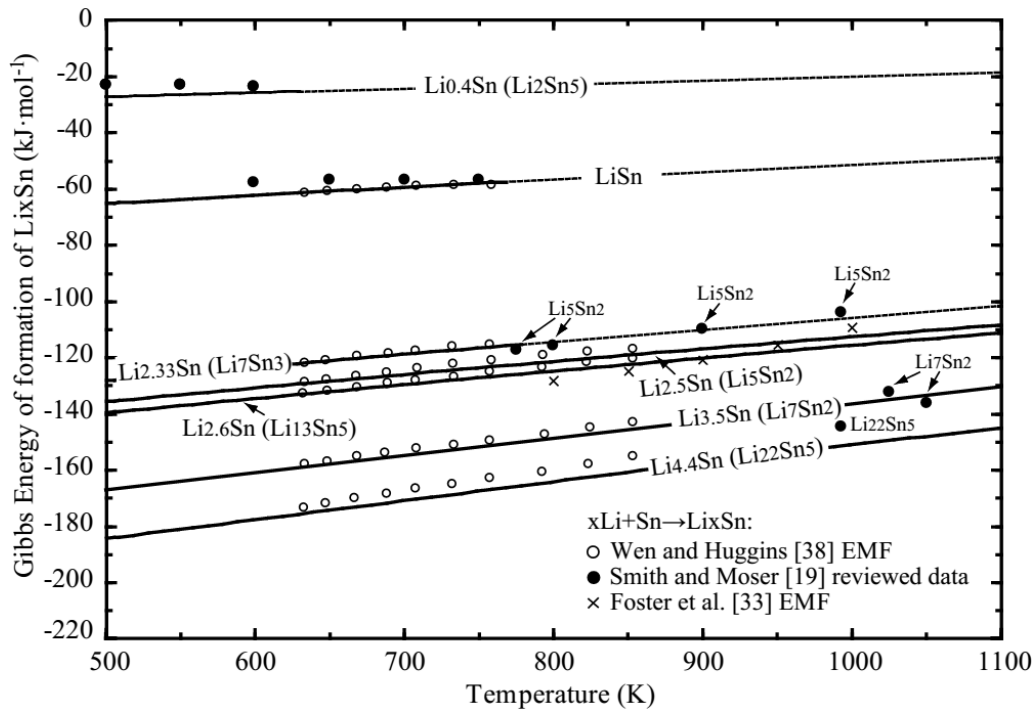
Figure 5.5 Calculated Gibbs energies of formation for Li-Sn intermetallic phases compared with experimental data and review data [19, 33, 38]

The calculated enthalpy and entropy of mixing (from liquid standard states) of the Li-Sn system at several temperatures are shown in Figs. 5.6 and 5.7 in comparison with the experimental data obtained from EMF measurements [34, 38, 40, 41] and drop calorimetry [44]. As can be seen in Fig. 5.6, the experimental enthalpies of mixing are well reproduced in the present study for all temperatures. In particular, the experimental enthalpy of mixing of liquid solution with the minimum of about -35 kJ to -40 kJ/g-atom at $X_{Sn} = 0.2 \sim 0.25$ is well reproduced by the present MQM model with coordination numbers $Z_{LiSn}^{Li} = 4$ and $Z_{LiSn}^{Sn} = 12$. However, the previous two assessments by Yin et al. [14] and Du et al. [15] cannot reproduce the enthalpy data of liquid
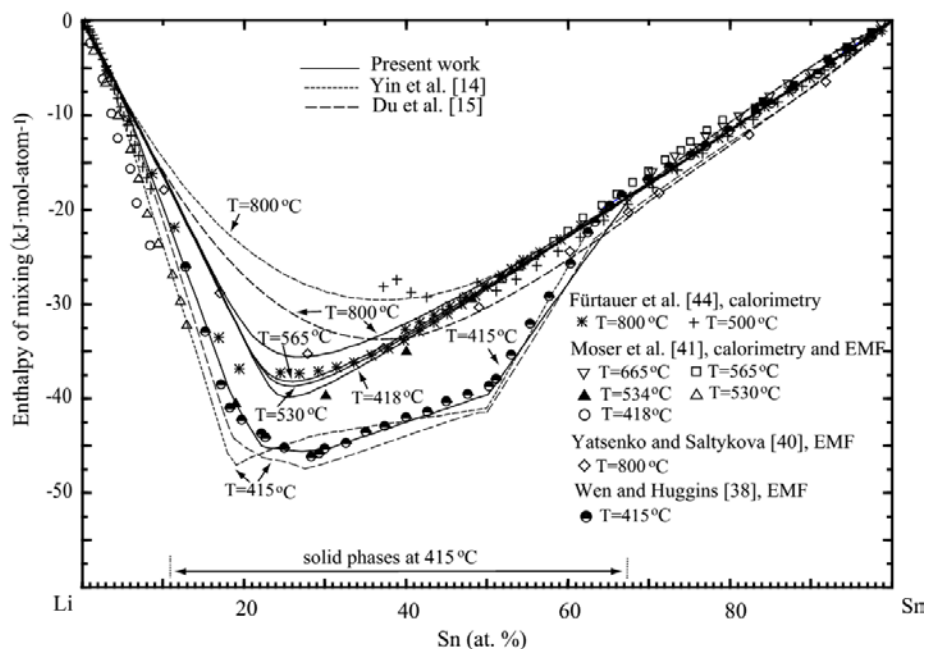
Figure 5.6 Calculated enthalpies of mixing of the Li-Sn system at various temperatures along with experimental data [38, 40, 41, 44]
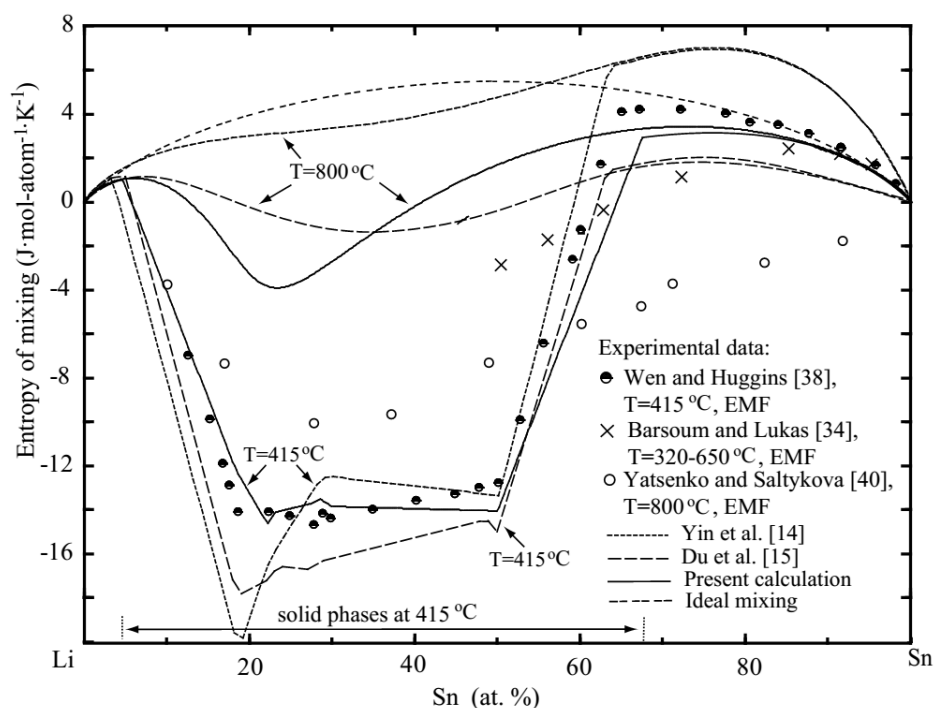
Figure 5.7 Calculated entropies of mixing of the Li-Sn system at various temperatures along with experimental data [34, 38, 40]

phase properly (in the liquid region at 800°C) although their assessed results for temperatures in liquid+solid regions are in quite good agreement with experimental data. The data for the entropy of mixing from Wen and Huggins [38] in Fig. 5. 7 are well reproduced in the present study, while the results by Yatsenko and Saltykova [40] were difficult to reproduce. Yin et al. [14] and Du et al. [15] failed to correctly reproduce the entropy of mixing of the liquid.

The activities and activity coefficients of Li and Sn (liquid standard states) in liquid solution are plotted in Figs. 5.8 and 5.9. The experimental data [39, 40, 43] are well reproduced in the present study. The previous assessment results by Du et al. [15] are also reasonably reproducing the experimental data. However, the results by Yin et al. [14] are rather less satisfactory in particular for the activity coefficient of Li.
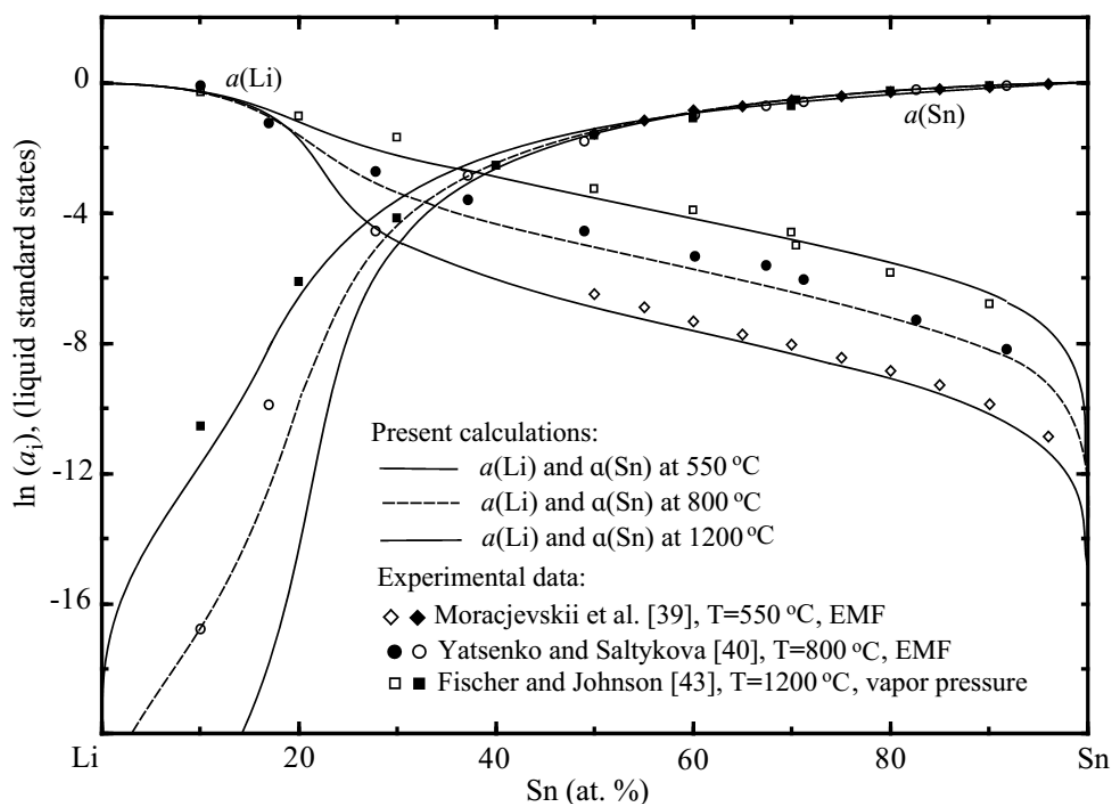
Figure 5.8 Calculated activities of Li and Sn (liquid standard states) in liquid Li-Sn solution at various temperatures along with experimental data [39, 40, 43]
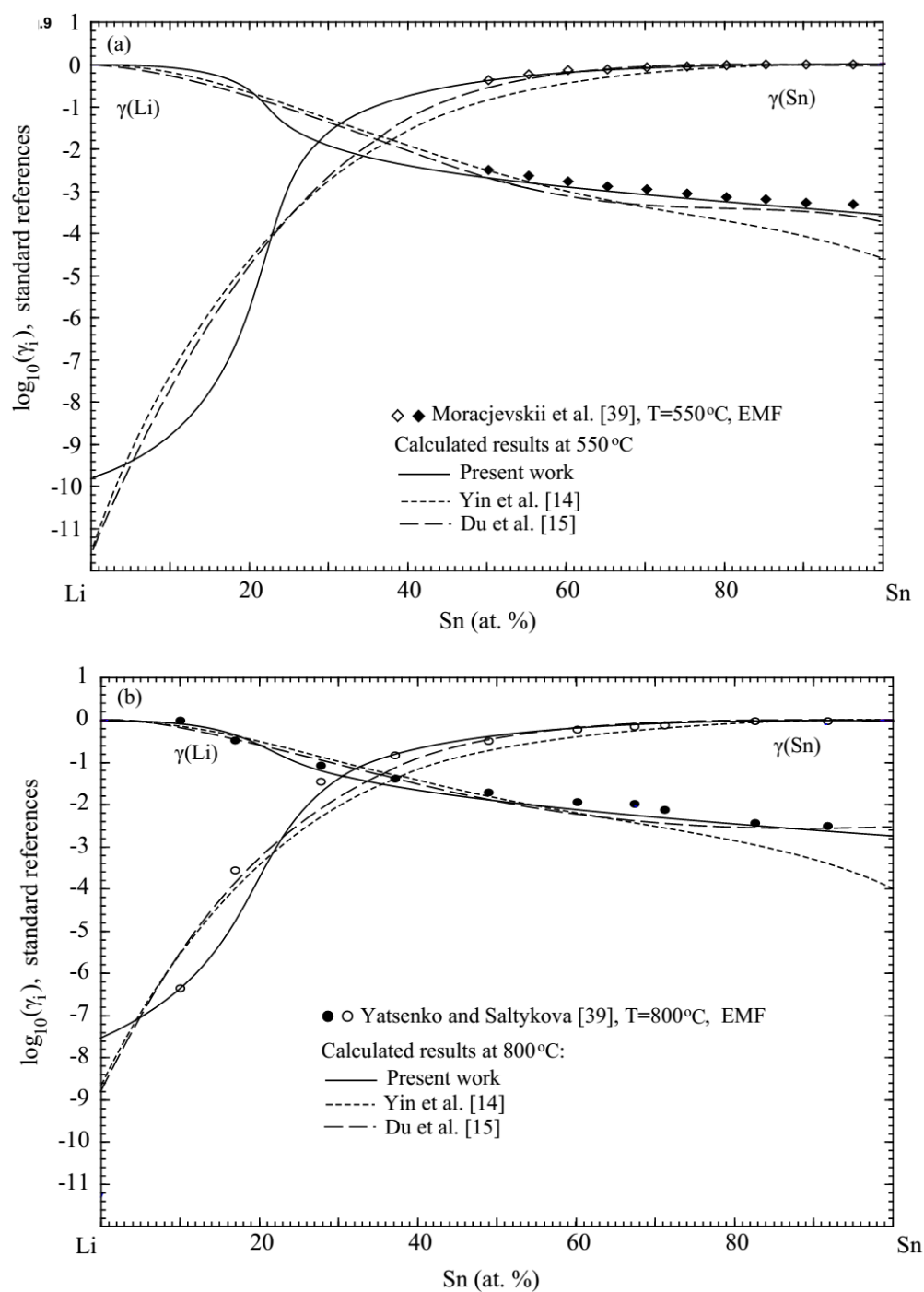
Figure 5.9 Calculated activity coefficients of Li and Sn (liquid standard states) in liquid Li-Sn solution at (a) 550 $^{\circ}$C and (b) 800 $^{\circ}$C in comparison with experimental data and previous optimizations [14, 15]

The structure of molten Li-Sn alloys was investigated by Alblas et al. [73], who found a strong ordering behavior in liquid solution at "Li$_4$Sn" composition from neutron diffraction measurements. Van der Marel et al. [74] measured the electrical resistivity of Li-Sn liquid alloys showing a strong maximum at Li$_4$Sn composition. This is also a good indication of short range ordering in liquid solution near Li$_4$Sn composition. This strong short range ordering behavior of liquid Li-Sn can be expected from the strong negative Gibbs energy and enthalpy of liquid phase. The Modified Quasichemical Model (MQM) employed for liquid phase in the present study can allow calculating the structure of liquid solution from the optimized model parameters. One of the best indicators of a tendency for ordering of liquid solution is the excess stability function (ES) defined by Darken [75]:

$$ES = \left(\frac{\partial^2 G^E}{\partial X_i^2} \right)_{T,P} \tag{5.18}$$

Another indication of short range ordering in liquid solution is the variation of ΔC_p function with composition. From the thermodynamic relationship,

$$\Delta C_p = T \frac{\partial}{\partial T} (\Delta S_m) \tag{5.19}$$

The calculated excess stability function and ΔCp function for liquid Li-Sn solution at 800 ^{o}C are presented in Figure 5.10. Strong short range ordering behavior is calculated, from both graphs, near Li$_4$Sn composition, which is in good agreement with the experimental observations [73, 74].
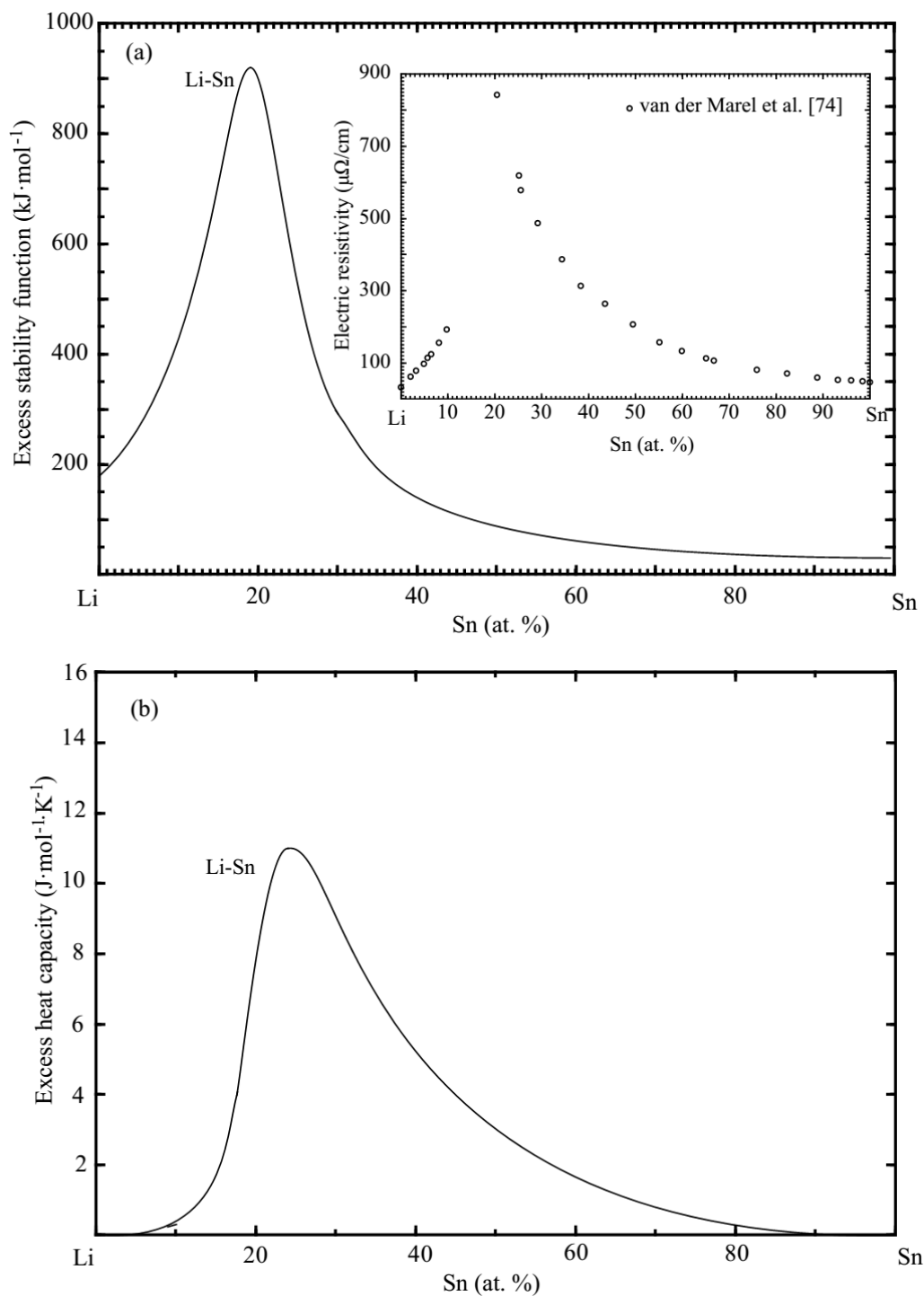
Figure 5.10 Calculated short range ordering behavior of liquid Li-Sn solution at 800 $^{\circ}$C. (a) Excess stability functions and (b) excess heat capacity. The experimental results of van der Marel et al. [74] are inserted in (a)

5.4.2 Mg-Sn-Li tenary system

The available experimental data of phase equilibria in the ternary Mg-Sn-Li system are still limited. The liquidus and sub-solidus phase equilibria of this ternary system are mostly determined for the composition range for Mg > 50 at. %. No thermodynamic data for ternary solid phases and the liquid solution are available. Therefore, in the present study, the Gibbs energy of liquid phase was predicted by the MQM from optimized binary model parameters using a 'Kohler' [76] interpolation technique. No ternary parameters were introduced for liquid phase. Then, the Gibbs energies of solid phases (the Mg_2Sn solution and the two ternary compounds) were optimized to reproduce all available phase diagram data. In this way, the available experimental phase diagram data were well reproduced. The optimized results are described below.

The calculated isothermal section of the Mg-Sn-Li ternary phase diagram at 370 ^{o}C along with experimental data by Teslyuk et al. [50] is shown in Figure 5.11.
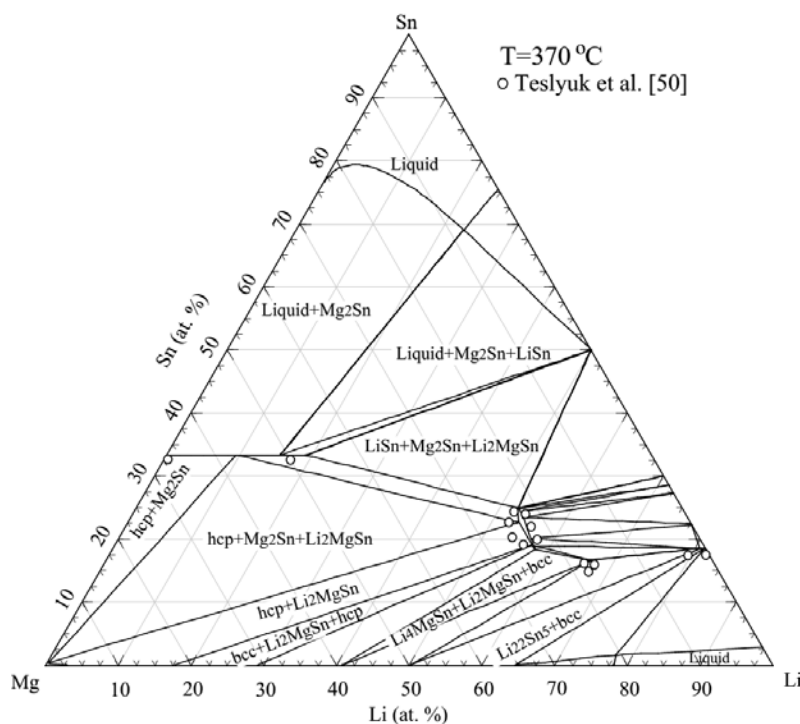
Figure 5.11 Calculated isothermal section of the Mg-Sn-Li system at 370 ^{o}C along with experimental data [50]

The isothermal sections from 200 °C to 500 °C are also calculated in Figure 5.12 along with the experimental data by Padezhnova and Guzei [52]. Two ternary phases, Li_2MgSn and Li_4MgSn, are found in the ternary system, as described previously. The enthalpy of formation of the stoichiometric Li_2MgSn phase (end member of solid solution Li_2MgSn phase) at 0 K was calculated using first-principles calculations (Table 5.4). This calculated value (-35.7 kJ/g-atom) was used as input for ΔH^o_{298K} in the CALPHAD modeling. The value of ΔS^o_{298K} for the same compound was optimized to reproduce the phase equilibria after fixing its heat capacity using Neumann-Kopp rule. The optimized values for ΔH^o_{298K} is -36.42 kJ/g-atom and for ΔS^o_{298K} is -1.88 J/g-atom-K, this last value being reasonably low. In order to reproduce the non-stoichiometry of the Li_2MgSn phase, the Gibbs energy of the Li_2MgSn phase was described using the CEF with a three-sublattice structure $(Li)_2(Li,Mg)(Li,Sn)$. It should be noted that the homogeneity range of Li_2MgSn solution phase does not encompass the Li_2MgSn composition. The ternary Li_4MgSn phase was treated as a stoichiometric compound due to its very limited non-stoichiometry and the lack of structural data. Unfortunately, the enthalpy of formation of Li_4MgSn could not be calculated from first principle calculations in the present study because the crystal structure of this compound is not known yet. Therefore, the values of ΔH^o_{298K} and ΔS^o_{298K} for the Li_4MgSn phase were roughly constrained to satisfy (i) the phase equilibria for the determined isothermal sections in the temperature range between 200 °C and 500 °C and (ii) its stability at room temperature. The optimized values are ΔH^o_{298K} = -35.46 kJ/g-atom and ΔS^o_{298K} = -3.87 J/g-atom-K, which seem reasonable in comparison to the optimized values for Li_2MgSn. The homogeneity ranges of Mg_2Sn and $Li_{22}Sn_5$ were modeled with the CEF considering the sublattice structures of $(Mg,Li)_2(Sn)$ and $(Li,Mg)_{22}(Sn)_5$, respectively. The Gibbs energies for the pseudo end-members, Li_2Sn and $Mg_{22}Sn_5$ of respective solid solutions were evaluated from the Gibbs energies of elements and an interaction parameter was used for each solution to reproduce its inhomogeneity range.

In Figure 5.13, four isoplethal sections are calculated along with the reported experimental data [51]. As can be seen from Fig. 5.13, the liquidus and solidus determined by Sviderskaya et al. [51] using thermal analysis technique are well reproduced even without any additional ternary parameters for liquid phase.
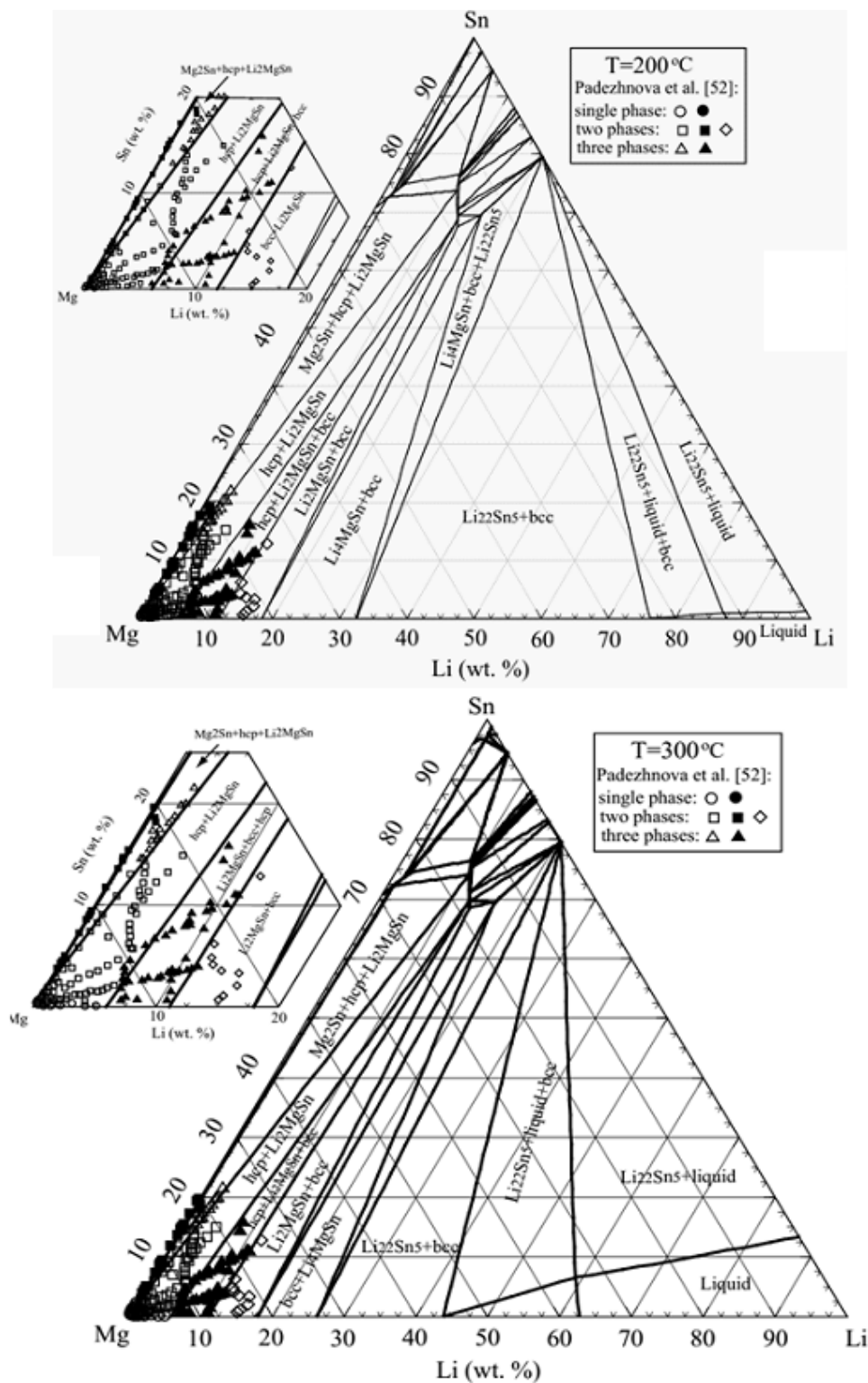
Figure 5.12 Calculated isothermal sections of the Mg-Sn-Li system at 200 °C, 300 °C, 400 °C and 500 °C along with experimental data [52] (Continued to next page)
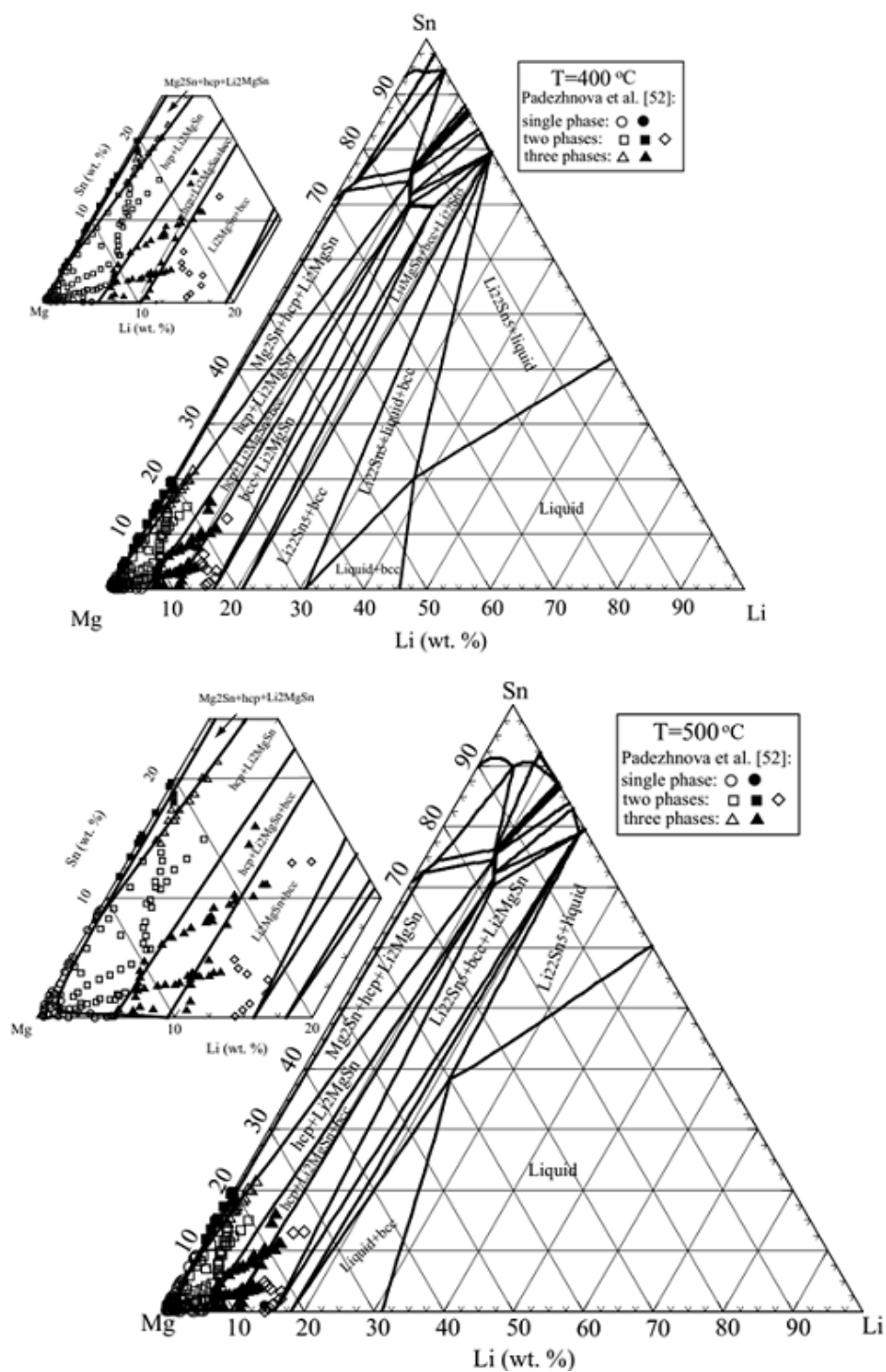
Figure 5.12 (Continued) Calculated isothermal sections of the Mg-Sn-Li system at 200 °C, 300 °C, 400 °C and 500 °C along with experimental data [52]
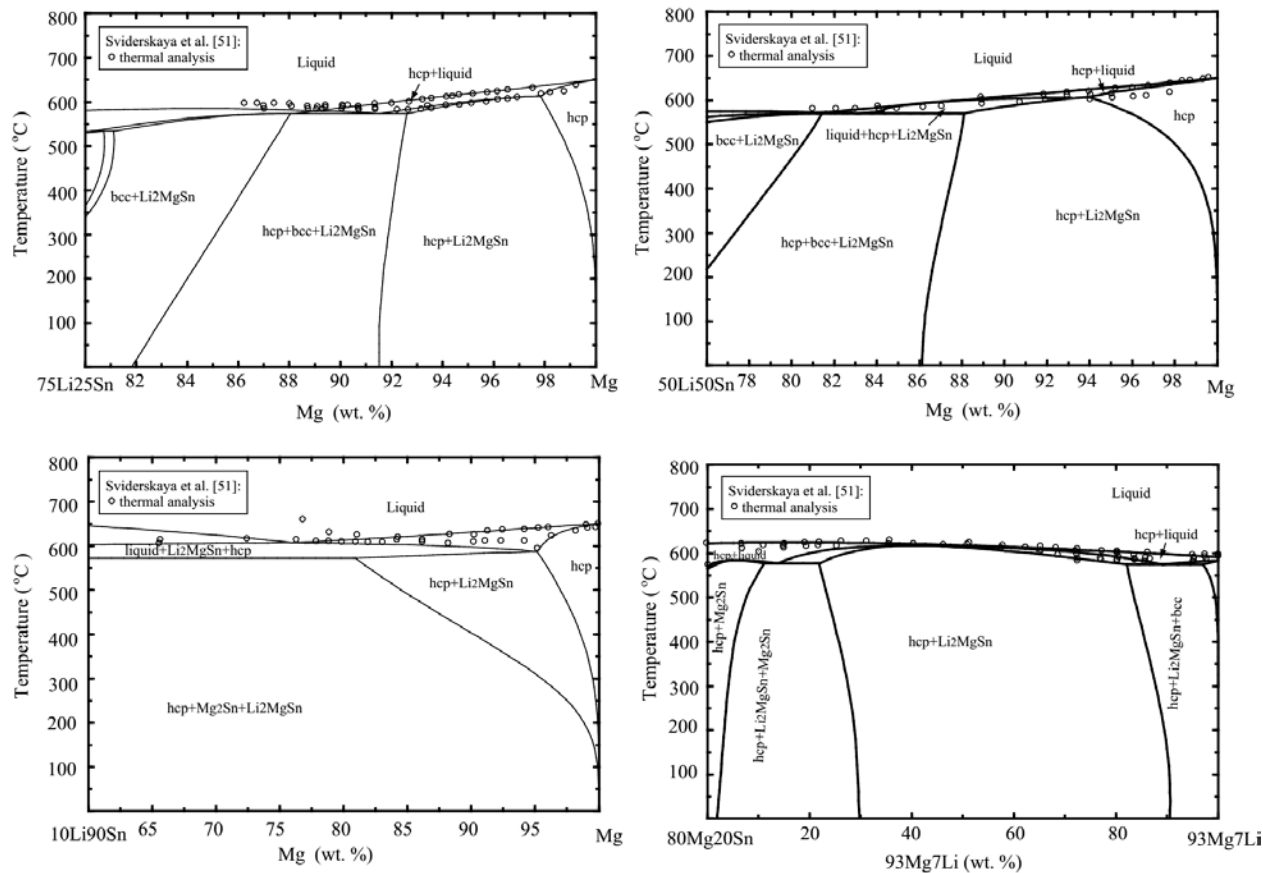
Figure 5.13 Calculated isopleths of the Mg-Sn-Li system. (a) Mg-Li/Sn(7.5:2.5 in weight), (b) Mg-Li/Sn(5:5 in weight), (c) Mg-Li/Sn (1:9 in weight), and (d) Mg/Sn(8:2 in weight) – Mg/Li(9.3:0.7 in weight) along with experimental data [51]

The liquidus projection of the Mg-Sn-Li ternary system is predicted in Fig. 5.14. All predicted ternary invariant reactions are summarized in Table 5.6. Two invariant reactions were reported by Sviderskaya et al. [51] using their thermal analysis and optical microscopic determination: (i) eutectic reaction: Liquid ↔ hcp + bcc + Li_2MgSn at 580 ^{o}C and (ii) peritectic reaction: Liquid + Li_2MgSn ↔ hcp + Mg_2Sn at 609 ^{o}C. In the present study, the eutectic reaction, Liquid ↔ hcp + bcc + Li_2MgSn, are calculated at 573 ^{o}C, which is close to the experimental temperature. However, we could not reproduce the peritectic reaction proposed by Sviderskaya et al. [51]. Instead, the present optimization suggested the eutectic reaction of Liquid ↔ hcp + Mg_2Sn + Li_2MgSn at 572 ^{o}C. In order to reproduce such peritectic behavior, the liquidus shape of Mg_2Sn

solution should be changed significantly, and the stability region of Li$_2$MgSn should be expanded in particular toward Mg$_2$Sn side. However, this is constrained by the isothermal phase diagram results in Fig. 5.13. Therefore, the peritectic reaction could not be reproduced in the present optimization. In fact, the experimental results presented in the paper of Sviderskaya et al. [51] are also very limited to clearly conclude the suggested peritectic reaction is correct. According to the present thermodynamic calculation, the melting temperature of Li$_2$MgSn phase is predicted to be 783 $^{\circ}$C. Li$_4$MgSn phase is predicted to have no primary solidification region, which is decomposed at 476 $^{\circ}$C (observed experimentally at 370 $^{\circ}$C, existence above this temperature is uncertain) according to present optimization
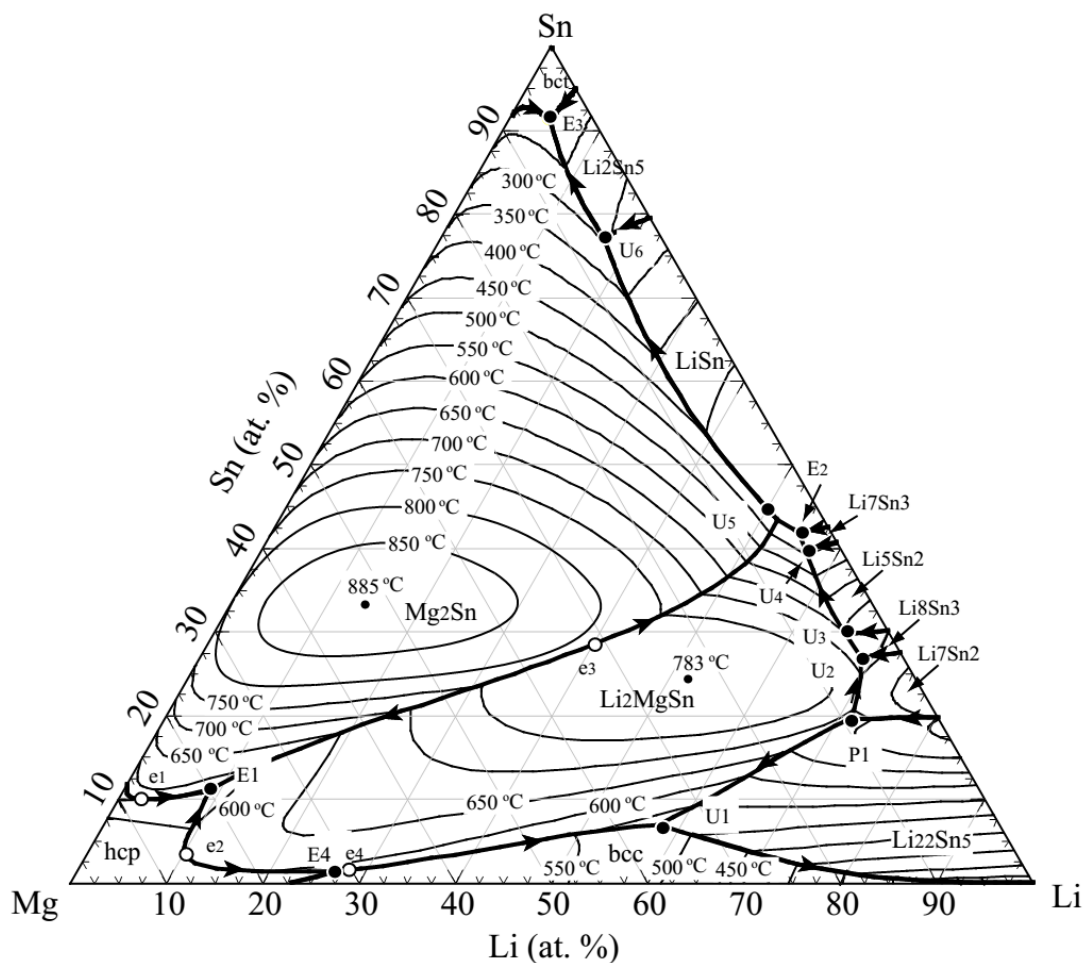
Figure 5.14 Predicted liquidus projection of the Mg-Sn-Li system

Based on the reproduction of most of available experimental data, the present thermodynamic modeling can be accurate enough in Mg-rich region of the Mg-Sn-Li system. Although we

believe the predicted phase equilibria in the wider range of composition of Mg-Sn-Li system be reasonable, it is necessary to carry out the phase diagram experiment to confirm these predictions in particular for Li-rich region.

Table 5.6 Predicted invariant reactions of the Mg-Sn-Li system in the present study

Label	Temperature (°C)	Reaction	Composition of Liquid (at. %)		
			Mg	Li	Sn
e1	585	$L \leftrightarrow hcp + Mg_2Sn$	85.88	3.85	10.27
e2	618	$L \leftrightarrow hcp + Li_2MgSn$	85.58	11.32	3.10
e3	762	$L \leftrightarrow Mg_2Sn + Li_2MgSn$	32.30	40.98	26.73
e4	573	$L \leftrightarrow bcc + Li_2MgSn$	70.87	27.23	1.90
E1	572	$L \leftrightarrow hcp + Mg_2Sn + Li_2MgSn$	79.99	8.89	11.12
E2	452	$L \leftrightarrow Li_7Sn_3 + Li_2MgSn + LiSn$	11.35	71.96	16.69
E3	203	$L \leftrightarrow bct + Mg_2Sn + Li_2Sn_5$	4.46	4.17	91.37
E4	573	$L \leftrightarrow bcc + Li_2MgSn + hcp$	71.91	26.75	1.34
P1	676	$L + Li_{22}Sn_5 + Li_7Sn_2 \leftrightarrow Li_2MgSn$	9.53	71.05	19.42
U1	508	$L + Li_2MgSn \leftrightarrow Li_{22}Sn_5 + bcc$	33.60	59.87	6.52
U2	674	$L + Li_7Sn_2 \leftrightarrow Li_2MgSn + Li_8Sn_3$	4.71	68.60	27.03
U3	654	$L + Li_8Sn_3 \leftrightarrow Li_5Sn_2 + Li_2MgSn$	4.54	65.63	29.83
U4	485	$L + Li_5Sn_2 \leftrightarrow Li_7Sn_3 + Li_2MgSn$	3.68	56.40	39.92
U5	453	$L + Li_7Sn_3 \leftrightarrow Mg_2Sn + LiSn$	5.16	51.62	43.52
U6	295	$L + LiSn \leftrightarrow Li_2Sn_5 + Mg_2Sn$	6.00	16.77	77.23

5.5 Summary

Thermodynamic optimizations of the Li-Sn and Mg-Sn-Li systems have been conducted based on the critical evaluation of all the phase diagram and thermodynamic experimental data reported in literature. First principles calculations were also carried out to calculate the formation enthalpies of binary Li-Sn intermetallic phases and the ternary Li_2MgSn compound. In the thermodynamic optimization, the Gibbs energy of the liquid phase was described by the Modified Quasichemical

Model taking into account the short range ordering, and solid solution phases were described by the Compound Energy Formalism considering the crystal structures of solids. The present thermodynamic models with optimized model parameters can accurately predict the critically assessed phase equilibria and thermodynamic properties in Mg-rich region of the ternary Mg-Sn-Li system, which can be applied to new Mg-Sn based alloy design.

Acknowledgement

References

[1] M. K. Kulekci, Magnesium and its alloys applications in automotive industry, The International Journal of Advanced Manufacturing Technology, 2008; 39: 851-65.

[2] M. A. Gibson, X. Fang, C. J. Bettles, C. R. Hutchinson, The effect of precipitate state on the creep resistance of Mg-Sn alloys, Scripta Mater., 2010; 63: 899-902.

[3] D. H. Kang, S. S. Park, Y. S. Oh, N. J. Kim, Effect of nano-particles on the creep resistance of Mg-Sn alloys, Mater. Sci. Eng. A, 2007; 449-451: 318-21.

[4] T. A. Leil, Y. D. Huang, H. Dieringa, N. Hort, K. U. Kainer, J. Buršík, Y. Jirásková, K. P. Rao, Effect of heat treatment on the microstructure and creep behavior of Mg-Sn-Ca Alloys, Mater. Sci. Forum; 2007, 69-72.

[5] N. Hort, Y. Huang, T. A. Leil, P. Maier, K. U. Kainer, Microstructural investigations of the Mg-Sn-xCa System, Adv. Eng. Mater., 2006; 8: 359-64.

[6] T. A. Leil, N. Hort, W. Dietzel, C. Blawert, Y. Huang, K. U. Kainer, K. P. Rao, Microstructure and corrosion behavior of Mg-Sn-Ca alloys after extrusion, T. Nonferr. Metal. Soc., 2009; 19: 40-4.

[7] K. Van der Planken, Solution hardening of lead single crystals at liquid air temperature, J. Mater. Sci., 1969; 4: 499-508.

[8] C. L. Mendis, C. J. Bettles, M. A. Gibson, C. R. Hutchinson, An enhanced age hardening response in Mg-Sn based alloys containing Zn, Mater. Sci. Eng. A, 2006; 435-436: 163-717.

[9] C. L. Mendis, C. J. Bettles, M. A. Gibson, S. Gorsse, R. Hutchinson, Refinement of precipitate distributions in an age-hardenable Mg-Sn alloy through microalloying, Philo. Magaz. Lett., 2006; 86: 443-56.

[10] L. Kaufman, P. E. A. Turchi, W. Huang, Z. K. Liu, Thermodynamics of the Cr-Ta-W system by combining the Ab Initio and CALPHAD methods, CALPAHD, 2001; 25: 419-433.

[11] I. -H. Jung, D. H. Kang, W. J. Park, N. J. Kim, S. H. Ahn, Thermodynamic modeling of the Mg-Si-Sn system, CALPHAD, 2007; 31: 192-200.

[12] P. J. Spencer, Mg-Li system, Thermodynamic database, CRCT editor, Montreal; 2006.

[13] W. Gasior, Z. Moser, W. Zakulski, Thermodynamic studies and the phase diagram of the Li-Sn system, J. Non-Cryst. Solids, 1996; 205-207: 379-382.

[14] F. C. Yin, X. P. Su, Z. Li, J. H. Wang, Thermodynamic assessment of the Li-Sn (Lithium-Tin) system, J. Alloy. Comp., 2005; 393: 105-108.

[15] Z. M. Du, Z. Q. Jiang, C. P. Guo, Thermodynamic optimizing of the Li-Sn system, Z. Metallkd., 2006; 97: 10-16.

[16] A. T. Dinsdale, SGTE data for pure elements, CALPHAD, 1991; 15: 317-425.

[17] M. Hansen, K. Anderko, Constitution of Binary Alloys, New York: McGraw-Hill; 1958.

[18] R. Hultgren, P. D. Desai, D. T. Hawkins, M Gleiser, KK Kelley, Selected vaules of the thermodynamic properties of binary alloys, American Society for Metals, Metals Park, Ohio; 1973.

[19] J. F. Smith, Z. Moser, Thermodynamic properties of binary Li systems, J. Nucl. Mater., 1975; 95: 158-174.

[20] J. Sangster, C. W. Bale, The Li-Sn system, J. Phase Equilib. Diff., 1998; 19: 70-75.

[21] G. Masing, G. Tammann, Bechavior of Li toward Na, K, Sn, Cd, and Mg, Z. Anorg. Allg. Chem., 1910; 67: 193-199.

[22] A. Baroni, Alloys of Li, Thermal and X-ray analysis of the system Li-Sn, Atti. Rend. Accad. Lincei, Roma, 1932; 16: 153-158.

[23] G. Grube, E. Meyer, Electrical conductivity and phase diagram of binary alloys: 16. the Li-Sn, Z. Elektrochem., 1934; 40: 771-777.

[24] E. Jenckel, L. Roth, The solubility of several metals in Sn and their influence on the recovery temperature, Z. Metallkd., 1938; 30: 135-144.

[25] D. M. Bailey, W. H. Skelton, J. E. Smith, Li-Sn phase pelationships between Li_7Sn_2 and Li-Sn, J. Less-common Met., 1979; 64: 233-240.

[26] W. Müller, H. Schiifer, The crystal structure of LiSn, Z. Naturforschung B, 1973; 28: 246-248.

[27] U. Frank, W. Müller, H. Schafer, The crystal structure of Li_5Sn_2, Z. Naturforschung B, 1975; 30: 1-5.

[28] U. Frank, W. Müller, H. Schafer, The crystal structure of Li_7Sn_2, Z. Naturforschung B, 1975; 30: 6-9.

[29] W. Müller, Preparation and crystal structure of Li_7Sn_3, Z. Naturforschung B, 1974; 29: 304-307.

[30] E. I. Gladyshevskii, G. I. Oleksiv, P. I. Kripyakevich, New examples of the structural type $Li_{22}Pb_5$, Kristallografiya, 1964; 9: 338-341.

[31] D. A. Hansen, L. J. Chang, Crystal structure of Li_2Sn_7, Acta Crystallogr. B, 1969; 25: 2392-2395.

[32] U. Frank, W. Müller, Preparation and crystal structure of $Li_{13}Sn_5$ and the structural relations between the phases of the systems Li-Sn and Li-Pb, Z. Naturforschung B, 1975; 30: 316-322.

[33] M. S. Foster, C. E. Crouthamel, S. E. Wood, Thermodynamics of binary slloys. II. The Li-Sn System, J. Phys. Chem., 1966; 70: 3042-3045.

[34] M. W. Barsoum, H. L. Lukas, Thermodynamics of molten lithium-tin alloys, Metall. Trans., 1988; 19A: 637-644.

[35] A. T. Dadd, E. Hubberstey, E. G. Roberts, Solutions of group IV elements in liquid Li, J.Chemi. Soci., Fara. Trans. 1, 1982; 78: 2735-2741.

[36] G. Goward, N. Taylor, D. Souza, L. Nazar, The true crystal structure of $Li_{17}M_4$ (M= Ge, Sn, Pb)-revised from $Li_{22}M_5$, J. Alloy. Comp., 2001; 329: 82-91.

[37] C. Lupu, J. -G. Mao, J. W. Rabalais, A. M. Guloy, J. W. Richardson, X-ray and neutron diffraction studies on "$Li_{4.4}Sn$", Inorg. Chem., 2003; 42: 3765-3771.

[38] C. J. Wen, R. A. Huggins, Thermoodynamic study of the Li-Sn System, J. Electrochem. Soc., 1981; 128: 1181-1187.

[39] A. G. Morachevskii, L. N. Gerasimenko, A. I. Demidov, O. A. Drozdova, Thermodynamic properties of molten Li-Sn alloys, Elektrokhimi., 1972; 8: 1622-1624.

[40] S. E. Yatsenko, E. A. Saltykova, Thermodynamic properties of alloys of the Li-Sn System, Khim. Thermodin. Termokhim., 1979; 190-191.

[41] Z. Moser, W. Gasior, E. Sommer, G. Schwitzgebel, B. Predel, Calorimelric and emf studies on liquid Li-Sn alloys, Metall. Mater. Trans. B, 1986; 17: 791-796.

[42] P. Baradel, A. Vermande, I. Ansara, E. Desre, Thermodynamic investigation of liquid Li-Sn alloys, Rev. Int. Hautes Temp. Refract., 1971; 8: 201-204.

[43] A. K. Fischer, S. A. Johnson, Liquid-vapor equilibria and thermodynamics of Li-Sn aystem, J. Chemi. Eng. Data, 1972; 17: 280-283.

[44] S. Fürtauer, E. Tserenjav, A. Yakymovych, H. Flandorfer, Calorimetric studies of Cu-Li, Li-Sn, and Cu-Li-Sn, J. Chemi. Thermodyn., 2013; 61: 105-116.

[45] O. Kubaschewski, W. Seith, Heats of Formation of Nonferrous Alloys, Z. Metallkd., 1938; 30: 7-9.

[46] E. Sommer, B. Fischer, B. Predel, Determination of the formarion enthalpies of Na alloys o f Li with In, Tl, Sn, Pb and Bi, HU Borgstedt (editor), Material Behavior and Physical Chemistry in Liquid Metal Systems, New York: Plenum Press; 1982.

[47] R. N. Singh, F. Sommer, Temperature dependence of the thermodynamic functions of strongley interacting liquid alloys, J. Phys.: Condensed Matter., 1992; 4: 5345-58.

[48] I. Courtney, J. Tse, O. Mao, J. Hafner, J. Dahn, Ab initio calculation of the lithium-tin voltage profile, Phys. Rev. B, 1998; 58: 15583-15588.

[49] C. -Y. Chou, H. Kim, G. S. Hwang, A Comparative first-principles study of the structure, energetics, and properties of Li-M (M= Si, Ge, Sn) Alloys, J. Phys. Chemi. C, 2011; 115: 20018-20026.

[50] M. Y. Teslyuk, E. V. Mel'nik, A. N. Malinkovich, M. F. Mitrofanova, Magnesium-lithium-tin ternary system in the 0-50 atom percent tin region, Visnik L'vivs'kogo Derzhavnogo Universitetu, Seriya Khimichna, 1969; 11: 25-30.

[51] Z. A. Sviderskaya, E. M. Padezhnova, L. S. Guzei, Phase diagram of the magnesium-lithium-tin system in the magnesium-rich region, Metall. Tsvet. Metal. Splavov., 1972; 48-52.

[52] E. M. Padezhnova, L. S. Guzei, Magnesium-based solid solutions in the magnesium-lithium-tin system, Strukt. Svoistva Legk. Splavov., 1971; 11-16.

[53] C. W. Bale, P. Chartrand, S. A. Degterov, G. Eriksson, K. Hack, R. Ben Mahfoud, J. Melancon, A. D. Pelton, S. Petersen, Factage thermochemical software and databases , CALPHAD, 2002; 26: 189-228.

[54] A. D. Pelton, P. Chartrand, The modified quasi-chemical model: Part II. multicomponent solutions, Metall. Mater. Trans. A, 2001; 32: 1355-1360.

[55] A. D. Pelton, S. A. Degterov, G. Eriksson, C. Robelin, Y. Dessureault, The modified quasi-chemical model: Part I. binary solutions, Metall. Mater. Trans. B, 2000; 31: 651-659.

[56] P. Ghosh, M. D. Mezbahul-Islam, M. Medraj, Critical assessment and thermodynamic modeling of Mg-Zn, Mg-Sn, Sn-Zn and Mg-Sn-Zn system, CALPHAD, 2012; 36: 28-43.

[57] C. Niu, C. Li, Z. Du, C. Guo, S. Chen, A thermodynamic assessment of the Bi-Mg-Sn ternary system, CALPHAD, 2012; 39: 37-46.

[58] F. Meng, J. Wang, L. Liu, Z. Jin, Thermodynamic modeling of the Mg-Sn-Zn ternary system, J. Alloy. Comp., 2010; 508: 570-581.

[59] N. Saunders, A review and thermodynamic assessment of the Al-Mg and Mg-Li Systems, CALPHAD, 1990; 14: 61-70.

[60] W. Gasior, Z. Moser, W. Zakulski, G. Schwitzgebel, Thermodynamic studies and the phase diagram of the Li-Mg system, Metall. Mater. Trans. A, 1996; 27: 2419-2428.

[61] P. Wang, Y. Du, S. Liu, Thermodynamic optimization of the Li-Mg and Al-Li-Mg systems, CALPHAD, 2011; 35: 523-532.

[62] H. Kopp, Investigations of the specific heat of solid bodies, Philo. Trans. Royal Society A, 1865; 155: 71-202.

[63] M. Hillert, The compound energy formalism, J. Alloy. Comp., 2001; 320: 161-76.

[64] W. Kohn, L. J. Sham, Self-consistent equations including exchange and correlation effects, Phys. Rev. B, 1965; 140: 1133-1138.

[65] G. Kresse, J. Furthmüller, Efficiency of ab-initio total energy calculations for metals and semiconductors using a plane-wave basis set, Comput. Mater. Sci., 1996; 6: 15-50.

[66] G. Kresse, J. Furthmüller, Efficient iterative schemes for ab initio total-energy calculations using a plane-wave basis set, Phys. Rev. B, 1996; 54: 11169-11186.

[67] G. Kresse, D. Joubert, From ultrasoft pseudopotentials to the projector augmented-wave method, Phys. Rev. B, 1999; 59: 1758-1775.

[68] P. E. Blöchl, Projector augmented-wave method, Phys. Rev. B, 1994; 50: 17953-17979.

[69] J. P. Perdew, Y. Wang, Accurate and simple analytic representation of the electron-gas correlation energy, Phys. Rev. B, 1992; 45: 13244-13249.

[70] J. P. Perdew, K. Burke, M. Ernzerhof, Generalized gradient approximation made simple, Phys. Rev. Lett., 1996; 77: 3865-3868.

[71] H. J. Monkhorst, J. D. Pack, Special points for brillouin-zone integrations, Phys. Rev. B, 1976; 13: 5188-5192.

[72] P. Willars, Pearson's handbook desk edition, Materials park, OH: ASM international; 1997.

[73] B. P. Alblas, W. Van der Lugtt, J. Dijkstra, C .Van Dijk, Structure of liquid Li-Sn alloys, J. Phys. F: Met. Phys., 1984; 14: 1995-2006.

[74] C. Van der Marel, A. B. Van Oosten, W. Geertsma, W. Van der Lugt, The electrical resistivity of liquid lithium-tin, sodium-tin, and sodium-lead alloys: strong effects of chemical interactions, J. Phys.: F Metal Phys., 1982; 12: 2349-2361.

[75] L. S. Darken, Thermodynamics of binary metallic solutions, Trans. Metall. Soci. AIME, 1967; 239(1): 80-89.

[76] A. D. Pelton, A general "geometric" thermodynamic model for multicomponent solutions, CALPHAD, 2001; 25: 319-328.

CHAPITRE 6   ARTICLE 3: EXPERIMENTAL AND THERMODYNAMIC STUDY OF THE MG-SN-IN-ZN QUATERNARY SYSTEM

Jian Wang[a], Pierre Hudon[b], Dmytro Kevorkov[c], Patrice Chartrand [a*], In-Ho Jung[b], Mamoun Medraj[c]

[a]Center for Research in Computational Thermochemistry (CRCT), Dept. of Chemical Engineering, École Polytechnique, Montréal, Québec, Canada, H3C 3A7

[b]Department of Mining and Materials Engineering, McGill University, 3610 University Street, Montreal, Quebec, H3A 0C5, Canada

[c]Department of Mechanical Engineering, Concordia University, 1455 De Maisonneuve Blvd. West, Montreal, Quebec, H3G 1M8, Canada

*Corresponding author: Center for Research in Computational Thermochemistry (CRCT), Dept. of Chemical Engineering, Ecole Polytechnique, Montréal, Québec, Canada, H3C 3A7. Tel: +1 514 340-4711 ext. 4089; fax: +1 514 340-5840. E-mail address: patrice.chartrand@polymtl.ca

Abstract

Phase equilibria in the Mg-rich region of the Mg-Sn-In (at 415 ^{o}C and 330 ^{o}C), and Mg-Sn-Zn (at 300 ^{o}C) ternary systems were determined by quenching experiments, electron probe micro-analyzer (EPMA), and X-ray diffraction (XRD) techniques. The ternary isoplethal sections with constant 5 In and 10 Sn at. % of Mg-In-Sn system, and 10 Sn at. % of Mg-Sn-Zn system were determined by differential scanning calorimetry (DSC), No ternary compounds were found in the Mg-Sn-Zn and Mg-Sn-In isothermal sections. Critical evaluation and thermodynamic optimization of the Mg-Sn-In-Zn quaternary system were carried out using CALPHAD (Calculation of Phase Diagrams) technique. The Modified Quasichemical Model in the Pair Approximation (MQMPA) was used for modeling the liquid solution, which exhibits a high degree of short-range ordering behavior. The solid phases were modeled with the Compound Energy Formalism (CEF). All available and reliable experimental data were reproduced within

experimental error limits. A self-consistent thermodynamic database was constructed for the Mg-Sn-In-Zn quaternary system, which can be used as a guide for Mg-based alloys development.

Keywords: A. Metals and alloys, C. Phase diagram, D. Thermodynamic modeling, D. Electron Probe Micro Analyzer, SEM

6.1 Introduction

Magnesium-based alloys are very attractive to the automotive and aeronautic industries thanks to their low density (approximately 1.80 g/cm^3), which is lower than Al based alloys (~2.80 g/cm^3) and steels (~7.90 g/cm^3). In addition, Mg-based alloys have good processing properties and are almost completely recyclable [1, 2]. Up to now, several series of magnesium alloys were developed, which includes the Mg-Al, Mg-Mn, Mg-Rare-Earths, and Mg-Zn series. The Mg-Zn series is the first hardenable Mg-based alloy developed for structural materials. The high solid solubility of Zn in Mg (hcp) phase and the considerable amount of secondary precipitates in the Mg matrix can produce a very good age-hardening effect [3]. Unfortunately, the Mg-Zn series has the same problem than the Mg-Al series (but the AE series), that is poor mechanical properties at elevated temperature which restricts its applications. On the other hand, Mg-Sn based alloys have stable microstructures and good mechanical properties at high temperature due to the high solubility of Sn in Mg (hcp) and the potential to precipitate a cubic structure second phase (Mg$_2$Sn) in the magnesium-rich matrix [4, 5]. Moreover, the solubility of Sn in Mg (hcp) drops sharply from about 15 wt. % at 561 ^{o}C to 0.45 at 200 ^{o}C, which provides the wide heat treatment temperature range necessary to obtain good mechanical properties through ageing process. Unfortunately, Mg-Sn alloys require quite long ageing times to reach peak hardness, which is not practical for industrial applications [6]. In addition to Sn, another element, In, is also known to improve the mechanical properties of Mg-based alloys. According to Mendis *et al.* [7, 8], and Becerra and Pekguleryuz [9], Indium is quite beneficial to the mechanical properties of Mg based alloys. In brief, Zn, Sn, and In are good candidates to develop new Mg-based alloys but up to now, experimental research on the Mg-Zn-Sn-In quaternary system and especially the effects associated to the addition of In to Mg-Zn-Sn ternary alloys, is quite limited.

Obtaining phase equilibrium information by the sole mean of experimental techniques is cumbersome and costly. Fortunately, thermodynamic modeling of multi-component systems by

the CALPHAD (Calculation of Phase Diagrams) [10] approach has proven to be a very efficient way to investigate and develop new alloys [11]. In order to obtain Mg-Sn-In-Zn alloys with good mechanical properties at high temperatures and better understand the relationships existing between phase equilibria and alloy microstructures, the thermodynamic database of the Mg-Sn-In-Zn system was constructed in the present work experimentally and thermodynamically.

6.2   Literature review

6.2.1 The In-Mg system

Phase equilibria in the Mg-rich portion (0 to 20 at. % In) of the In-Mg binary system was first studied by Hume-Rothery and Raynor [12] by means of thermal analysis and metallographic observation methods. The liquidus and solidus curves were determined and a large solid solution field located between 18.6 and 19.4 at. % In in the Mg (hcp) phase was reported. The whole composition range of the In-Mg binary system was examined by Hancke [13] by using XRD; four intermediate phases were reported: Mg_5In_2 (body-centered rhombic), Mg_2In (hexagonal), $MgIn$ (body-centered tetragonal) and $MgIn_3$. Later, the constitution of In-Mg alloys between 20 to 50 at. % In was studied by Raynor [14] by using optical microscopy, electrolytic measurements, and XRD. The peritectic reaction *liquid + Mg (hcp) ↔ β* was found to occur at 302 ^{o}C at a liquid composition of 23.2 at. % In. Two intermediate phases, β_1 and β_2, were found, and the solubility in β_1 was found to lie between 23.5 and 25 at. % In. Raynor [14] also found that β_1 and β_2 have very complex crystal structures, and noted that the crystal structure of β_1 is different from that of Mg_5In_2 [13]). Moreover, Raynor [14] pointed out that β_2 may actually correspond to Mg_2In, as reported earlier by Hancke [13]. Two ordering transformations, $\beta \rightarrow \beta'(L1_2)$ and $\beta \rightarrow \beta''(L1_0)$, are mentioned in Raynor's work [14]. Graham and Raynor [15] investigated several In-Mg binary alloys by using XRD and metallography, and the peritectic reaction $fcc + liquid \leftrightarrow tet(In)$ was found to occur at 333.5 ^{o}C. Ino *et al.* [16] investigated the ordering phase transformation in the In-Mg system between 36.8 and 56.3 at. % In using XRD and thermal analysis. According to them, the $\beta \rightarrow \beta'(L1_2)$ and $\beta \rightarrow \beta''(L1_0)$ transformations go through two phase regions of $\beta + \beta'(L1_2)$ and $\beta + \beta''(L1_0)$, respectively. Phase equilibria in the In-Mg binary system was afterwards investigated up to 40 at. % Mg by Hiraga *et al.* [17] by using

XRD, thermal analysis, and calorimetry. The solid solubility of magnesium in indium was found to reach about 5 at. %. The peritectic reaction $fcc + liquid \leftrightarrow tet(In)$ was reported to occur at 160 ^{o}C by Hiraga *et al.* [17], which is quite different from the temperature observed earlier by Graham and Raynor (333.5 ^{o}C) [15]. In the In-rich portion, a new ordered phase, γ', with a Cu$_3$Au-type structure, was reported by Hiraga *et al.* [17] based on thermal and X-ray analysis. The In-rich region was reinvestigated by Pickwick *et al.* [18] and Feschotte [19] by using differential thermal analysis (DTA), electrical resistivity measurements, and metallographic observation methods. The temperatures of the peritectic reactions $liquid + hcp(Mg) \leftrightarrow \beta$ and $fcc + liquid \leftrightarrow tet(In)$ were observed to occur at 305±0.5 ^{o}C and 160 ^{o}C, respectively, which is in good agreement with the data of Hiraga *et al.* [17]. Pickwick *et al.* [18] also observed that the intermediate fcc solid solution is homogeneous over a wide range, from 23 to 86 at. % In. Watanabe [20] re-examined the In-Mg system near the Mg$_3$In composition and the β_3 phase, reported as Mg$_5$In$_2$ in Hancke's work [13], was confirmed. According to Watanabe [20], the β_3 phase is only stable below 210 ^{o}C and decomposes to β' and β_2 above this temperature. The whole thermodynamic and phase equilibra data of the In-Mg binary system were compiled by Nayeb-Hashemi and Clark [21]. Seven binary compounds were considered: β, β_1, β_2, β_3, β', β'' and γ', where β' and γ' are ordered phases with the fcc Ll_2 structure ($AuCu_3$), and β'' is another ordered fcc phase with the Ll_0 structure ($AuCu$).

The thermodynamic properties of activities of In and Mg, enthalpy and entropy mixing of the In-Mg liquid phase were studied by calorimetric measurements [22, 23], EMF measurements [23-27], and vapour pressure measurements [28]. Ehrlich [22] reported the experimental enthalpy of mixing of the In-Mg liquid phase at 650 ^{o}C using direct calorimetric measurements. Moser and Castanet [23, 27] studied the In-Mg liquid solution by an EMF technique based on the concentration cell: $Mg_{(s)} \| (MgCl_2-LiCl-KCl) \| Mg-In_{(liq.)}$. And the activities, enthalpy mixing and Gibbs energy of mixing at 577 ^{o}C were derived in their work [23, 27] based on the results from EMF measurements. Slaby and Terpilowshki [24, 25] investigated the Mg-In liquid phase using EMF measurements with the type of cell: $Mg_{(s)} \| (0.58LiCl+0.42KCl+0.05MgBr_2) \| Mg_xIn_{1-x}$. The enthalpy of mixing, entropy of mixing, and the activity of In and Mg in the liquid phase at 650 ^{o}C were extrapolated by Slaby and Terpilowshki [24, 25] based on their measurements obtained

from EMF techniques. Nebell [26] studied the In-Mg liquid phase in the temperature range from 450 ^{o}C to 650 ^{o}C by measuring the EMF of the galvanic cells: $Mg_{(s)}\|(MgF_2\text{-}LiCl\text{-}KCl)\|Mg\text{-}In_{(liq.)}$ and derived the enthalpy and entropy mixing properties. The enthalpy mixing results at 650 ^{o}C reported by Nebell [26] are in good agreement with the results reported by Moser and Castanet [23, 27], but more positive (about 2 kJ/mol at 60 at. % Mg) than the data from Slaby and Terpilowshki [24, 25]. Chirulli *et al.* [28] investigated the activity of Mg in the liquid phase at 627 ^{o}C by using a torsion-effusion apparatus. Moser and Castanet [27] reported the experimental enthalpy of mixing of the In-Mg liquid phase at 650 ^{o}C, 675 ^{o}C and 735 ^{o}C using direct calorimetric measurements, their results are in good agreement with each other, but a little bit positive than the data reported by Slaby and Terpilowshki [24, 25] and negative than the data reported by Nebell [26] and Moser and Castanet [23, 27].

Thermodynamic optimization of the Mg-In binary system was not carried out previously. Consequently, the Mg-In binary system was optimized in the present work for the first time.

6.2.2 The In-Sn system

The phase diagram of the In-Sn binary system has been investigated by several authors [29-36]. The present accepted phase diagram, constituted with two intermetallic phases, $\beta(InSn)$ and $\gamma(InSn)$, plus the bct(Sn) and tet(In) terminal solid solution, is compiled mainly from the reported results of Heumann and Alpaut [34] who used differential thermal analysis (DTA), X-ray, dilatometric measurements and microscopic observations, and the reported results of Cakir and Alpaut [35] who used EMF measurements. The liquidus curve was determined by Heumann and Alpaut [34] using DTA measurements. Two peritectic reactions $liquid + tet \leftrightarrow \beta(InSn)$ and $liquid + bct \leftrightarrow \gamma(InSn)$ and one eutectic reaction $liquid \leftrightarrow \gamma(InSn) + \beta(InSn)$ were reported with at 143 ^{o}C, 224 ^{o}C and 120 ^{o}C respectively [34]. Predel and Godecke [29] determined the phase equilibria in the Sn-rich region with DTA measurements. The phase diagram of the In-Sn binary system in the whole composition range was determined by Evans and Prince [30] using DTA measurements. Kaplun [31] determined the phase equilibria in the composition range from 0 to 60 Sn (at. %) using thermal analysis. The solid phases were determined by Wojtaszek and Kuzyk [32, 33] using electrical resistance ratio measurements. All the reported experimental data show a reasonable agreement.

Activity data for In and Sn in the In-Sn liquid phase at different temperatures have been determined by Vassiliev *et al.* [37], Heumann and Alpaut [34], Terpilowski [38] using EMF techniques. Zivkovic *et al.* [39] investigated the enthalpies of mixing of In-Sn liquid phase using Oelsen calorimetry, and derived the the activities of In and Sn in the In-Sn liquid phase at 327 ^{o}C. The enthalpy of mixing of the liquid phase was determined with a calorimetric method by Wittig and Scheidt [40], Kleppa [41], Yazawa *et al.* [42], Bros and Laffitte [43], Rechchach *et al.* [44] in the temperature range from 248 ^{o}C to 500 ^{o}C. Their results are in a reasonable agreement with the experimental error bar of $\pm$10 J/mol. The enthalpy of formation and activity of In in the solid phases for the temperature range from 75 ^{o}C to 125 ^{o}C were determined by Cakir and Alpaut [35] using EMF measurements, and by Alpaut and Heumann [45] using quantitative thermal analysis, respectively.

The In-Sn binary system was optimized by Lee *et al.* [36] with BWM for liquid phase in 1997, their optimization are in good agreement with the reported experimental data at that time. In order to construct a self-consistent thermodynamic database of Mg-Sn-In-Zn quaternary system, the In-Sn system was re-optimized with the Modified Quasichemical Model in the Pair Approximation (MQMPA) [46, 47] for liquid phase, and with the recently reported experimental data in the present work.

6.2.3 The In-Zn system

Experimental phase equilibrium and thermodynamic data of the In-Zn system were evaluated and compiled by Dutkiewicz and Zakulski [48]. The phase diagram is constituted of a simple eutectic, liquid $\leftrightarrow$ tet(In) + hcp(Zn), and was first investigated by Wilson and Peretti [49] using the visual polythermal method and optical microscopy. Soon after, Valentiner [50] and Rhines and Grobe [51] modified the phase diagram based on new data obtained by thermal analysis. The phase relations were then determined by Svirbely and Selis [52], Oelsen and Zuhlke [53], Bohl and Hildebrandt [54], and Moser [55] by performing EMF or calorimetric measurements. All the liquidus experimental data are in a good agreement except for the early data collected by Wilson and Peretti [49]. The eutectic temperature was reported to lie in the range of 141.5 to 144 ^{o}C. The temperature of 143.5 ^{o}C reported by Rhines and Grobe [51], which is based on accurate measurements of the cooling curves, was accepted as the most reliable value. According to the metallographic examinations of Dutkiewicz and Moser [56], In-Zn alloys with 3.1, 3.8 and 4.8 at.

% Zn are solidifying with hypoeutectic, eutectic and hypereutectic microstructures, respectively. Considering all the available experimental data, the eutectic composition is located between 3.46 and 3.8 at. % Zn. The maximum solubility of Zn in the tet(In) phase was found to be 2.09 at. % Zn by Rhines and Grobe [51], which is virtually identical to the 2.1 at. % Zn reported later by Nishimura *et al.* [57]. The solubility of In in the Zn (hcp) terminal solid solution is very limited; less than 0.2 at. % In [57].

The enthalpy of mixing of the liquid phase was investigated by Oelsen and Zuhlke [53], Kleppa [58], and Wittig and Muller [59] using calorimetric measurements, and derived by Svirbely and Selis [52], Bohl and Hildebrandt [54], Moser [55], Jung [60] based on their results from EMF measurements, and by Ferro *et al.* [61] and Hagiwara *et al.* [62] based on their results obtained from a Knudsen torsion-effusion and isopiestic measurements respectively. And all their results are in good agreement except the data reported by Bohl and Hildebrandt [54]. The activity of Zn in the liquid phase at different temperatures was studied by several investigators [52, 54, 55] using EMF measurements, and studied by Ferro *et al.* [61] and Hagiwara *et al.* [62] using Knudsen torsion-effusion and isopiestic measurements methods. All the reported thermodynamic experimental data are in a reasonable agreement.

The thermodynamic optimization of In-Zn binary system was carried by Lee *et al.* [63] with BMW for liquid phase. In order to construct a self-consistent thermodynamic database of Mg-Sn-In-Zn quaternary system, the In-Zn system was re-optimized with the MQMPA for liquid phase in the present work.

6.2.4 The Mg-Sn-In system

The phase equilibria in the isothermal section at 300 $^{\circ}$C was investigated by Kinzhibalo [64] using XRD. According to him, there is no stable ternary compound in this isothermal section. The activity of Mg in the Mg-Sn-In ternary liquid alloys were studied by Moser and Castanet [65] and by Zakulski *et al.* [66] using EMF measurements with the cell of the type: *Mg*(liq., s)‖(*MgCl₂-LiCl-KCl*)‖*Mg-In-Sn*(liq.,liq.+s).

In order to obtain an accurate and self-consistent thermodynamic optimization of Mg-Sn-In ternary system, the phase equilibria measurements are needed. Consequently, the isothermal sections at 415 and 330 $^{\circ}$C, and isoplethal sections at 10 Sn and 5 In (at. %) were studied in the

present work firstly, and then a thermodynamic optimization of Mg-Sn-In ternary was carried out.

6.2.5 The Mg-Sn-Zn system

Phase equilibria in the Mg-Sn-Zn ternary system was first studied by Otani [67] using thermal analysis and optical microscopy. Seven ternary isoplethal sections were reported. However, it should be noted that Otani [67] employed an outdated phase diagram for the Mg-Zn system; the currently accepted phase diagram, with five intermediate compounds, was updated by Agarwal *et al.* [68]. Phase equilibria in the $MgZn_2$-Mg_2Sn-Zn-Sn region were investigated by Godecke and Sommer [69] using thermal analysis and metallographic methods. The liquidus projection and six isoplethal sections were determined. According to Otani [67] and Godecke and Sommer [69], no stable ternary compound exists in the Mg-Sn-Zn system. The ternary solubility of Sn in Mg-Zn binary compounds and of Zn in Mg_2Sn was studied by Mingolo *et al.* [70] and Sirkin *et al.* [71] using Mossbauer spectroscopy and XRD. According to them, there is a limited solid solubility of Sn in Mg-Zn binary compounds and of Zn in Mg_2Sn. For Gladyshevsky and Cherkashin [72], the ternary solubility of Sn in $MgZn_2$ reaches 3.6 wt. % at 400 °C. Later, Godecke and Sommer [69] measured a maximum solubility of about 0.7 wt. % by using thermal analysis and optical microscopy, which is in a reasonable agreement with Gladyshevsky and Cherkashin [72] and our own results considering experimental errors.

Although, many experimental results of the phase equilibria measurements were reported in previously [67-72], the phase equilibra information of isothermal sections is still lacking. Furthermore, the data of solid solubility for Sn in Mg-Zn binary compound is also limited, which is important for studying the solidification behavior of the Mg based alloys. Consequently, the ternary isothermal section of Mg-Zn-Sn at 330 °C was firstly studied in the present work.

A thermodynamic assessment of the Mg-Zn-Sn ternary system was obtained by Ghosh *et al.* [73] and by Meng *et al.* [74], and their optimization results are in a reasonable agreement with all the reported data. In order to obtain an accurate and self-consistent thermodynamic optimization of Mg-Sn-In-Zn ternary system, the thermodynamic optimization was carried out in the present work with the MQMPA for liquid solution, taking into account the current experimental data and those reported in the literature [67-72].

6.2.6 The In-Sn-Zn system

The liquidus projection and numerous isoplethal sections of the In-Sn-Zn system were determined by Yoon *et al.* [75] using DSC, scanning electron microscopy (SEM) and XRD. Xie *et al.* [76] measured the isoplethal sections at Sn/Zn molar ratios of 2:1, 1:1 and 1:2 and ternary isoplethal section at constant 10 at. % In by using DTA, XRD and EPMA. Recently, Sabbar *et al.* [77] determined with DSC six isoplethal sections with In/Sn molar ratios of 5:95, 15:85, 1:2, 52:48, 2:1 and 85:15.

Moser [78] reported the activity of Zn in In-Sn liquid solutions with 3 wt.% Zn by using EMF measurements at 441 $^{\circ}$C, 484 $^{\circ}$C and 532 $^{\circ}$C. Fiorani *et al.* [79] studied the enthalpy of mixing of the In-Sn-Zn liquid phase by using a Calvet-type drop calorimeter. Nakamura *et al.* [80] studied the thermodynamic properties of the In-Sn-Zn liquid phase with the In/Sn molar ratios of 1:1, 3:1 and 1:3 by using EMF measurements. Later, Anres *et al.* [81] measured the enthalpy of mixing of the In-Sn-Zn liquid phase with the In/Sn molar ratios of 1:3, 1:1, 3:1, and Zn/In molar ratios of 1:3 and 1:1 at 440 °C and 634 °C by using a direct-reaction calorimeter. Recently, Rechchach *et al.* [44] reported the enthalpy of mixing of the In-Sn-Zn liquid phase with the In/Sn ratios of 1.795, 0.506, 0.999, 2.01, and 5.702 at 500 °C by using a direct-reaction calorimeter. A thermodynamic modeling of the In-Sn-Zn ternary system was obtained by Xie *et al.* [82] and by Cui *et al.* [83] both using a BWM for liquid phase. In order to get a self-consistent and more critical evaluated thermodynamic database for the Mg-Sn-In-Zn quaternary system, the In-Sn-Zn ternary system was critical evaluated and re-optimized using MQMPA for the liquid phase.

6.3 Thermodynamic modeling

In the present work, the thermodynamic optimization of the Mg-Sn-In-Zn quaternary system was carried out by means of the FactSage thermodynamic software [84]. All phases considered in the Mg-Sn-In-Zn quaternary system are listed in Table 6.1, along with the model used to describe their thermodynamic properties. The binary systems Mg-Sn, Mg-Zn and Sn-Zn have been critical evaluated and parameters of their thermodynamic models have been optimized by Jung *et al.* [85], Spencer [86] and Ghosh *et al.* [73] using MQMPA for the liquid solution. Consequently, all the thermodynamic parameters of Mg-Sn, Mg-Zn and Sn-Zn binary systems were taken from

their work [73, 85, 86] without further modification for the present optimization of the Mg-Sn-In-Zn quaternary system.

6.3.1 Liquid phase

The thermodynamic properties of the liquid phase were modeled using the Modified Quasichemical Model in the Pair Approximation (MQMPA) developed by Pelton *et al.* [46, 47]. A detailed description of the MQMPA and its associated notation is given in refs. [46, 47]. The same notation is used in the present work, and a brief description of MQMPA is given as follows:

For the binary $(A + B)$ system, the quasichemical pair exchange reaction can be considered:

$$(A-A)_{pair} + (B-B)_{pair} = 2(A-B)_{pair,} \quad \Delta g_{AB} \tag{6.1}$$

where $i - j$ pair represents a first-nearest-neighbor pair of atoms. The Gibbs energy change for the formation of one mole of *(A-B)* pairs according to Reaction (6.1) is $\Delta g_{AB}/2$. Let n_A and n_B be the number of moles of A and B, n_{AA}, n_{BB}, and n_{AB} be the number of moles of A-A, B-B and A-B pairs. Z_A and Z_B are the coordination numbers of A and B. Then the Gibbs energy of the solution is given by:

$$G = (n_A G_A^o + n_B G_B^o) - T\Delta S^{config} + (n_{AB}/2)\Delta g_{AB} \tag{6.2}$$

where G_A^o and G_B^o are the molar Gibbs energies of the pure component A and B, and ΔS^{config} is the configurational entropy of mixing given by randomly distributing the A-A, B-B and A-B pairs in the one-dimensional Ising approximation. The expression for ΔS^{config} is:

$$\Delta S^{config} = -R(n_A \ln X_A + n_B \ln X_B)$$
$$- R(n_{AA} \ln \frac{X_{AA}}{Y_A^2} + n_{BB} \ln \frac{X_{BB}}{Y_B^2} + n_{AB} \ln \frac{X_{AB}}{2Y_A Y_B}) \tag{6.3}$$

where X_{AA}, X_{AB} and X_{BB} are the mole fractions of the A-A, B-B and A-B pairs respectively; Y_A and Y_B are the coordination-equivalent fractions of A and B:

$$X_{ij} = \frac{n_{ij}}{n_{AA} + n_{BB} + n_{AB}} \quad (i, j = A \text{ or } B) \tag{6.4}$$

$$Y_i = \frac{Z_i n_i}{Z_A n_A + Z_B n_B} \quad (i = A \text{ or } B) \tag{6.5}$$

Table 6.1 Optimized phases and thermodynamic models used in the present work.

Phase	Pearson symbol	Strukturbericht designation	Space group	Prototype	Model[a]
Liquid	-	-	-	-	MQMPA
fcc	cF4	A1	$Fm\bar{3}m$	Cu	CEF
bct	tI4	A5	$I4_1/mmm$	Sn	CEF
bcc	cI2	A2	$Im\bar{3}m$	W	CEF
hcp	hP2	A3	$P6_3/mmc$	Mg	CEF
hcp (Zn)	hP2	A3	$P6_3/mmc$	Mg	CEF
tet	tI2	A6	$F4/mmm$	In	CEF
β'	cP4	$L1_2$	$Pm3m$	$AuCu_3$	CEF
β_1	hR16	-	$R3m$	-	CEF
β_2	hP9	-	$P\bar{6}2m$	Mg_2Tl	ST
β_3	oI28	$D8_g$	$Ibam$	Mg_5Ga_2	ST
β''	tP4	$L1_0$	$P4/mmm$	AuCu	CEF
γ'	cP4	$L1_2$	$Pm3m$	$AuCu_3$	CEF
$Mg_{12}Zn_{13}$	-	-	-	-	ST
Mg_2Zn_3	mC110	-	$B2/m$	-	ST
$MgZn_2$	hP12	C14	$P6_3/mmc$	$MgZn_2$	ST
Mg_2Zn_{11}	cP39	$D8_c$	$Pm\bar{3}$	Mg_2Zn_{11}	ST
$Mg_{51}Zn_{20}$	oI142	$D7_b$	$Immm$	Ta_3B_4	ST
Mg_2Sn	cF12	C1	$Fm\bar{3}m$	CaF_2	ST
$\beta(InSn)$	tI2	A6	$F4/mmm$	In	CEF
$\gamma(InSn)$	hP5	-	$P6/mmm$	-	CEF

[a] MQMPA: Modified Quasichemical Model in the Pair Approximation;
CEF: Compound Energy Formalism;
ST: Stoichiometric Compound

Moreover, the following elemental balance equations can be written:

$$Z_A n_A = 2n_{AA} + n_{AB} \tag{6.6}$$

$$Z_B n_B = 2n_{BB} + n_{AB} \tag{6.7}$$

It may be noted that there is no exact expression for the configurational entropy in three dimensions. Although Eq. (6.3) is only an approximate expression in three dimensions, it is exact one-dimensionally (when $Z = 2$) [47]. As explained in [47], one is forced by the approximate

nature of Eq. 6.3 to use non-exact values for the coordination numbers in order to yield good fits between the experimental data and calculated ones. The mathematical approximation of the one-dimensional Ising model of Eq. (6.3) can be partially compensated by selecting values of Z_A and Z_B which are smaller than the experimental values [87] . As is known, the MQMPA model is sensitive to the ratio of coordination numbers, but less sensitive to their absolute values. From a practical standpoint for the development of large thermodynamic databases, values of Z_A and Z_B of the order of 6 have been found necessary for the solutions with a small or medium degree of ordering (i.e. alloy solutions).

Δg_{AB} is the model parameter to reproduce the Gibbs energy of liquid phase of the A-B binary system, which is expanded as a polynomial in terms of the pair fractions, as follows:

$$\Delta g_{AB} = \Delta g_{AB}^{o} + \sum_{i \geq 1} g_{AB}^{io}(X_{AA})^{i} + \sum_{j \geq 1} g_{AB}^{oj}(X_{BB})^{j} \tag{6.8}$$

where Δg_{AA}^{o} , g_{AB}^{io} and g_{AB}^{oj} are the adjustable model parameters which can be function of the temperature. The equilibrium state of the system is obtained by minimizing the total Gibbs energy at constant elemental composition, temperature and pressure. The equilibrium pair distribution is calculated by setting:

$$\left(\frac{\partial G}{\partial n_{AB}} \right)_{n_A, n_B} = 0 \tag{6.9}$$

This gives the ''equilibrium constant'' for the ''quasichemical pair reaction'' of Eq. (6.1):

$$\frac{X_{AB}^{2}}{X_{AA}X_{BB}} = 4 \times \exp\left(-\frac{\Delta g_{AB}}{RT} \right) \tag{6.10}$$

Moreover, the model permits Z_A and Z_B to vary with composition as follows [47]:

$$\frac{1}{Z_A} = \frac{1}{Z_{AA}^{A}} \left(\frac{2n_{AA}}{2n_{AA} + n_{AB}} \right) + \frac{1}{Z_{AB}^{A}} \left(\frac{n_{AB}}{2n_{AA} + n_{AB}} \right) \tag{6.11}$$

$$\frac{1}{Z_B} = \frac{1}{Z_{BB}^{B}} \left(\frac{2n_{BB}}{2n_{BB} + n_{AB}} \right) + \frac{1}{Z_{AB}^{B}} \left(\frac{n_{AB}}{2n_{BB} + n_{AB}} \right) \tag{6.12}$$

where Z_{AA}^{A} and Z_{AB}^{A} are the values of Z_A when all nearest neighbors of an atom A are As, and when all nearest neighbors of an atom A are Bs respectively. Z_{BB}^{B} and Z_{AB}^{B} are defined similarly. The composition of maximum short-range ordering (SRO) is determined by the ratio of the

coordination numbers Z^A_{AB}/Z^B_{AB}. The values of the coordination numbers chosen in the present study are listed in Table 6. 2.

Table 6.2 Optimized model binary parameters of the MQMPA for the liquid phase for the Mg-Sn-In-Zn quaternary system.

Coordination numbers [a]				Gibbs energies of pair exchange reactions (J/mol-atoms)	Reference
i	j	Z^i_{ij}	Z^j_{ij}		
Mg	In	3	6	$\Delta g_{Mg,In} = -9790.6 - 2092X_{InIn} - 209.2X^2_{InIn}$	This work
Mg	Sn	4	8	$\Delta g_{Mg,Sn} = -15263.2 - 0.88 \times T + (3347.2 + 0.42 \times T)X_{MgMg}$	[85]
Mg	Zn	6	6	$\Delta g_{Mg,Zn} = -6778.1 + 3.14 \times T - (1966.5 - 2.01 \times T)X_{MgMg} - (3974.8 - 1.67 \times T)X_{ZnZn}$	[86]
In	Zn	6	4	$\Delta g_{In,Zn} = 5104.5 - 2.22 \times T + (962.3 - 0.71 \times T)X_{ZnZn}$	This work
In	Sn	6	6	$\Delta g_{In,Sn} = -175.7 - 138.1X_{InIn} - 133.9X_{SnSn}$	This work
Sn	Zn	6	6	$\Delta g_{Sn,Zn} = 2259.4 + (2175.7 - 4.18 \times T)X_{SnSn} + (5355.5 - 5.86 \times T)X_{ZnZn}$	[73]

[a] For all pure elements (Mg, Li, and Sn), $Z^i_{ii} = 6$
Note: T in K.

The Gibbs energy of the liquid solution in a ternary system can be interpolated from the Gibbs energies of the three sub-binary systems with different interpolation techniques based on the nature of this ternary system, and small external model parameters will be introduced into the models to get more self-consistent results with the experimental data if they are necessary. The Gibbs energy of all ternary liquid phases are calculated using an asymmetric "Kohler-like" [88] type of ternary interpolation technique.

6.3.2 Solid Solutions

The Compound energy formalism (CEF) was introduced by Hillert [89] to describe the Gibbs energy of solid phases with sub-lattices. Ideal mixing of species on each sub-lattice is assumed. In the present work, all the solid solutions (hcp, bct, tet and Zn (hcp)) and the ordered intermetallic solutions in the Mg-Sn-In-Zn quaternary system were modeled with the CEF based on their crystal structure. The Gibbs energy expressions are based on the each sub-lattice model, and the details were descript in the Hillert's work [89].

6.3.3 Stoichiometric phases

The molar Gibbs energies of pure elements and stoichiometric phases can be described by:

$$G_T^o = H_T^o - TS_T^o \tag{6.13}$$

$$H_T^o = \Delta H_{298.15K}^o + \int_{T=298.15K}^{T} Cp \ dT \tag{6.14}$$

$$S_T^o = S_{298.15K}^o + \int_{T=298.15K}^{T} (Cp/T)dT \tag{6.15}$$

where $\Delta H_{298.15K}^o$ is the molar enthalpy of formation of a given species from pure elements ($\Delta H_{298.15K}^o$ of element stable at 298.15 K and 1 atm is assumed as 0 J·mol^{-1}; reference state), $S_{298.15K}^o$ is the absolute third law molar entropy at 298.15 K and C_p is the molar heat capacity.

In the present study, the Gibbs energy of pure elements were taken from the SGTE database [90]. As there are no experimental heat capacity data for Ag-In, Ag-Sn and Ag-Mg intermetallics, their heat capacities were evaluated using the Neumann–Kopp rule [91]. The heat capacity of solid In and Sn from the SGTE database show a maximum just above their melting points (that is in the liquid stable region). Consequently, the heat capacity of several intermetallic phases in the studied system obtained with Neumann–Kopp rule had also a maximum at about 506 K, which is not likely. In order to resolve this, the heat capacity of solid In and Sn above their melting points were adjusted in the present work, which makes it possible for the heat capacity of intermetallics to increase with temperature until the melting point. This was solely applied when the Neumann–Kopp rule was employed and does not influence pure In and Sn.

6.4 Experimental procedures

Mg-Sn-In and Mg-Sn-Zn ternary alloys were prepared with pure Mg (99.8 wt. %), Sn (99.9 wt. %), In (99.99 wt. %) and Zn (99.5 wt. %) from Alfa Aesar and melted in a frequency induction furnace under argon atmosphere. In order to minimize the interaction of sample with the crucibles, cubic-shaped crucibles with Ta foil (99.5 wt. % purity, 0.15 mm thickness) were prepared. Each alloy was remelted three times in the crucible in order to obtain a homogeneous alloy; the loss due to evaporation was less than 5 wt. % for each sample. Mg-Sn-In samples were sealed into quartz capsules under argon atmosphere and equilibrated at 415 ^{o}C for 20 days and at

330 °C for 35 days, respectively. The Mg-Sn-Zn samples were sealed into quartz capsules under argon atmosphere, and equilibrated at 330 °C for 50 days. These temperatures were chosen because they correspond to the temperatures at which heat treatment is usually performed on Mg alloys. Quenching was carried out in water without breaking the quartz tubes.

Electron probe microanalysis (EPMA) of the quenched samples was performed with the JEOL 8900 probe at McGill University using wavelength-dispersive spectrometry (WDS). An accelerating voltage of 15 kV was used with a 20 nA beam current, a spot size of 2 µm and counting times of 20 s on peaks and 10 s on backgrounds. Raw data were reduced with the PRZ correction using pure Mg, Sn, In and Zn metal standards.

The constituent phases of the quenched samples were identified by X-ray diffraction (XRD). XRD patterns were obtained with the PANanalytical Xpert Pro powder X-ray diffractometer at Concordia University using CuKα radiation at 45 kV and 40 mA. The spectra were acquired from 20 to 120º 2θ with a 0.02º step size. The collected patterns were analyzed with the X'Pert HighScore Plus analysis software using the handbook "Pearson's crystal data, crystal structure database for inorganic compounds" [92].

Liquidus and polymorphic transformation temperatures were measured by differential scanning calorimetry (DSC) using the SETARAM instrumentation at Concordia University. Experiments were carried out by using sintered Al_2O_3 crucibles under flowing argon gas with heating and cooling rates of 5 °C/min. No reaction was observed between the samples and the sintered Al_2O_3 crucibles.

6.5   Experiment and optimization results

6.5.1 Experimental results

The Mg-Sn-In system

BSE (back-scattered electron) images of typical ternary Mg-Sn-In alloys are shown in the Figs. 6. 1 a-b. Phase identification was based on the EPMA and XRD results. In the Mg78Sn10In12 (at. %) alloy quenched from 415 °C, the three-phase equilibrium microstructure hcp(Mg)-Mg$_2$Sn-fcc was observed (Fig. 6.1a). Isothermal sections of the Mg-Sn-In ternary system in the Mg-rich region at 415 °C and 330 °C were measured and no ternary compound was found in. All the

phase equilibrium compositions determined in the present work are listed in Table 6. 3. The solid solubility of In in Mg$_2$Sn is less than 0.4 at. %, and the solid solubility of Sn in the fcc and β$_1$ Mg-In binary compounds is 0.15 and 0.38 at. %, respectively. Since these values are within the error limits of the EPMA measurements, the solubilities are considered negligible. The isoplethal sections in the Mg-In-Sn system at constant 10 Sn and 5 In (at. %) were measured by the DSC technique. The DSC curve of Mg78Sn10In12 alloy is shown in Fig. 6. 2 (a). Three exothermic peaks were observed in the cooling spectrum, which were well repeated during heating with two endothermic peaks and one weak liquid peak. All the thermal singles obtained from the DSC measurements are presented in Table 6. 4.
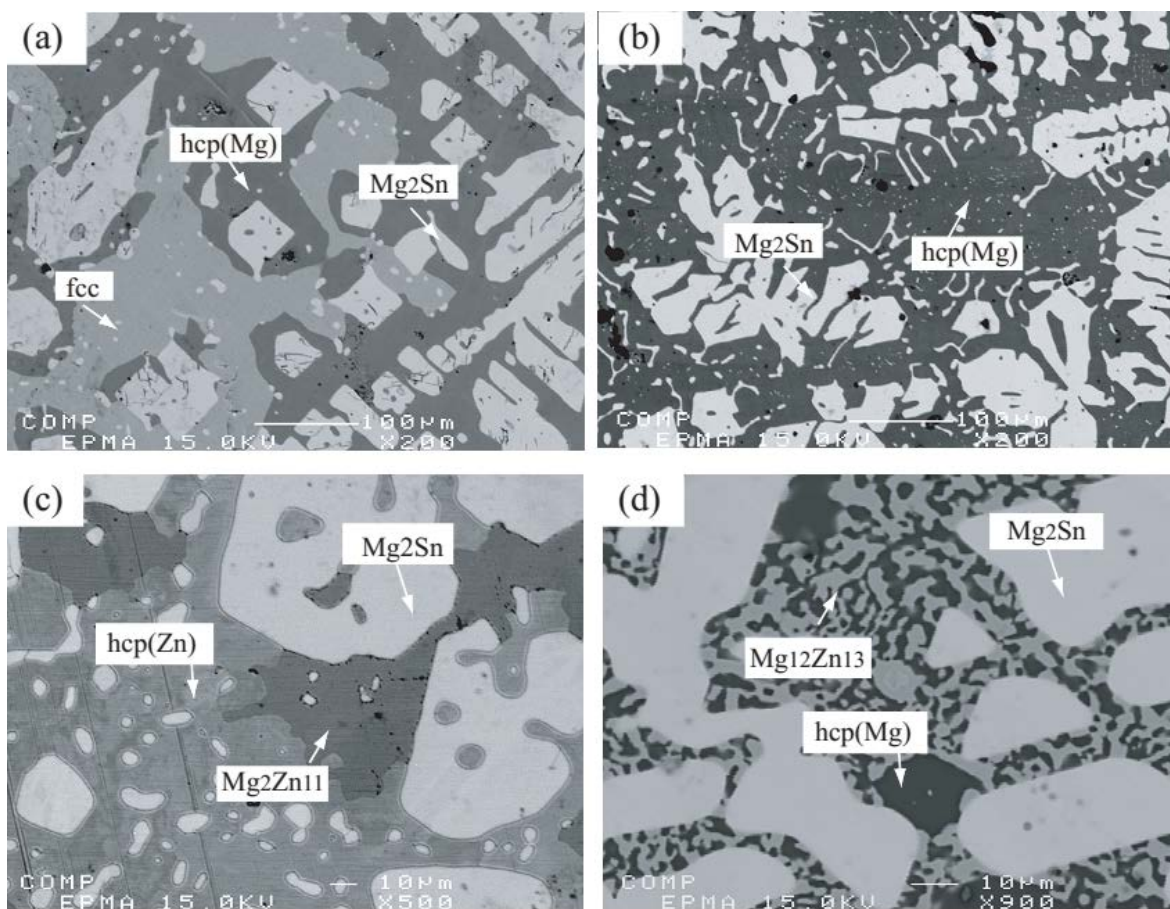
Figure 6.1 Typical ternary BSE images obtained from (a) Mg78Sn10In12 (at. %) alloy annealed at 415 ^{o}C for 20 days; (b) Mg80Sn10In10 (at. %) alloy annealed at 330 ^{o}C for 35 days; (c) Mg25Sn10Zn65 (at. %) alloy annealed at 300 ^{o}C for 50 days; (d) Mg70Sn10Zn20 (at. %) alloy annealed at 300 ^{o}C for 50 days.
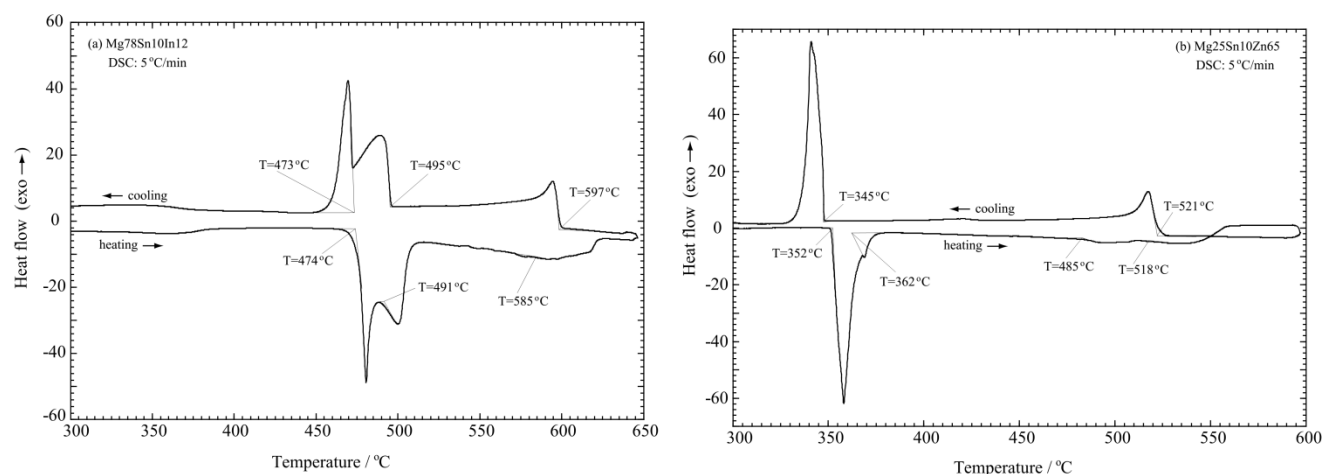
Figure 6.2 The DSC curves of (a) Mg88Sn10Zn12 and (b) Mg25Sn10Zn65 alloys obtained in the present work

Table 6.3 Equilibria compositions in the Mg-Sn-X (X: In, Zn) ternary systems as measured in the present work

System	Temp. (°C)	Alloy Nominal comp. (at. %)	Phase equilibira Phase 1/Phase 2/Phase 3	Composition (at. %)								
				Phase 1			Phase 2			Phase 3		
				Mg	Sn	In	Mg	Sn	In	Mg	Sn	In
Mg-Sn-In	415	Mg80Sn10In10	hcp (Mg)/Mg$_2$Sn/-	84.77	0.39	14.84	67.81	31.91	0.28	—	—	—
		Mg78Sn10In12	hcp (Mg)/Mg$_2$Sn/fcc	80.55	0.34	19.11	67.82	31.79	0.39	77.73	0.15	22.12
		Mg70Sn10In20	Mg$_2$Sn/fcc/-	67.32	32.26	0.42	70.34	0.35	29.31	—	—	—
		Mg65Sn10In25	Mg$_2$Sn/fcc/-	67.30	32.50	0.20	64.07	0.15	35.78	—	—	—
	330	Mg80Sn10In10	hcp (Mg)/Mg$_2$Sn/-	84.73	0.15	15.12	67.76	31.93	0.31	—	—	—
		Mg78Sn10In12	hcp (Mg)/Mg$_2$Sn/β$_1$	81.59	0.10	18.31	67.50	32.15	0.35	75.11	0.38	24.51
		Mg70Sn10In20	Mg$_2$Sn/β'(L1$_2$)/-	67.83	31.87	0.30	70.92	0.13	28.95	—	—	—
		Mg65Sn10In25	Mg$_2$Sn/fcc/-	67.68	31.96	0.36	62.53	0.15	37.32	—	—	—
				Mg	Sn	Zn	Mg	Sn	Zn	Mg	Sn	Zn
Mg-Sn-Zn	300	Mg70Sn10Zn20	hcp (Mg)/Mg$_2$Sn/Mg$_{12}$Zn$_{13}$	98.00	0.23	1.77	67.95	32.02	0.03	50.44	0.6	48.96
		Mg50Sn10Zn40	Mg$_2$Sn/Mg$_2$Zn$_3$/Mg$_{12}$Zn$_{13}$	67.42	32.46	0.12	42.73	0.02	57.25	50.80	0.04	49.16
		Mg45Sn10Zn45	Mg$_2$Sn/Mg$_2$Zn$_3$/-	67.87	32.09	0.04	38.99	3.17	57.84	—	—	—
		Mg25Sn10Zn65	Mg$_2$Sn/Mg$_2$Zn$_{11}$/hcp(Zn)	67.09	32.84	0.07	18.90	3.98	77.12	0.95	1. 5	97.55

Table 6.4 Thermal signals obtained from DSC measurements with the corresponding interpretation from the thermodynamic calculations for the Mg-Sn-In ternary system

System	Sample (at. %)	Thermal signals (°C)		Interpretation	
		Heating	Cooling	Calculated phase boundary or invariant reaction with temp. (°C)	
Mg-Sn-In	Mg80Sn10In10	596	592	583	liquid/liquid+Mg_2Sn
		524	513	533	liquid+Mg_2Sn/liquid+Mg_2Sn+hcp
		473	471	474	liquid+hcp $\leftrightarrow$ Mg_2Sn+fcc
	Mg78Sn10In12	603	599	591	liquid/liquid+Mg_2Sn
		490	495	521	liquid+Mg_2Sn/liquid+Mg_2Sn+hcp
		476	472	474	liquid+hcp $\leftrightarrow$ Mg_2Sn+fcc
	Mg70Sn10In20	614	614	608	liquid/liquid+Mg_2Sn
		448	452	463	liquid+Mg_2Sn/liquid+Mg_2Sn+fcc
		359	373	359	Mg_2Sn+fcc/Mg_2Sn+β'
	Mg65Sn10In25	596	604	607	liquid/liquid+Mg_2Sn
		389	397	427	liquid+Mg_2Sn/liquid+Mg_2Sn+fcc
		326	324	329	Mg_2Sn+fcc/Mg_2Sn+β'+fcc
	Mg90Sn5In5	572	558	592	liquid/liquid+hcp
		539	537	552	liquid+hcp/liquid+Mg_2Sn
	Mg85Sn10In5	584	580	563	liquid/liquid+Mg_2Sn
		532	542	541	liquid+Mg_2Sn+hcp/hcp+Mg_2Sn
	Mg40Sn55In5	490	480	557	liquid/liquid+Mg_2Sn
		193	185	185	liquid+Mg_2Sn/liquid+Mg_2Sn+γ(InSn)
		182	-	172	liquid+Mg_2Sn+γ(InSn)/Mg_2Sn+γ(InSn)
Mg-Sn-Zn	Mg50Sn10Zn40	-	616	608	liquid/liquid+Mg_2Sn
		524	543	553	liquid+Mg_2Sn/liquid+Mg_2Sn+$MgZn_2$
		399	-	413	liquid+Mg_2Sn+$MgZn_2$ /liquid+Mg_2Zn_3+Mg_2Sn
		343	348	350	liquid+Mg_2Zn_3+Mg_2Sn /Mg_2Zn_3+Mg_2Sn+$Mg_{12}Zn_{13}$
		337	-	-	-
		333	330	-	-
	Mg45Sn10Zn45	-	624	604	liquid/liquid+Mg_2Sn
		558	562	565	liquid+Mg_2Sn/liquid+Mg_2Sn+$MgZn_2$
	Mg35Sn10Zn55	542	564	575	liquid/liquid+Mg_2Sn
		344	352	357	liquid+$MgZn_2$ $\leftrightarrow$ Mg_2Zn_{11}+Mg_2Sn
		337	332		-
	Mg25Sn10Zn65	516	523	509	liquid/liquid+Mg_2Sn
		485	-	480	liquid+Mg_2Sn/liquid+Mg_2Sn+$MgZn_2$
		368	-	-	-
		351	347	357	liquid+$MgZn_2$ $\leftrightarrow$ Mg_2Zn_{11}+Mg_2Sn

The Mg-Sn-Zn system

We experimentally determined the isothermal section at 300 ^{o}C of the Mg-Sn-Zn ternary system. No ternary compound was found. BSE (Back-scattered electron) images of typical ternary Mg-Sn-Zn alloys are shown in Figs. 6. 1c-d. In the key sample of Mg25Sn10Zn65 (at. %) quenched from 300 ^{o}C, a three-phase equilibrium microstructure $Mg_2Zn_{11}+Mg_2Sn+hcp$ (Zn) was observed (Fig. 6. 1c). And three-phase equilibrium microstructure of $Mg_2Sn+Mg_{12}Zn_{13}+hcp$ (Mg) was observed in the key sample of Mg70Sn10Zn20 as shown in Fig. 6.1d. The ternary isoplethal with constant 10 Sn (at. %) was determined in the present work with DSC technique, The DSC curve of Mg25Sn10Zn65 alloy is shown in Fig. 6. 2b, two exothermic peaks were observed in the cooling spectrum, one strong endothermic peak and three weak peaks were observed in the heating spectrum. The final liquid peaks are well repeated during heating and cooling occurring at 518 ^{o}C and 521 ^{o}C. The endothermic peak occurring at 485 ^{o}C should be overlapped in the cooling spectrum because it is close to the first exothermic reaction occurring at 521 ^{o}C. All the thermal signals obtained from the DSC measurements are presented in Table 6. 4. All the phase equilibria compositions determined in the present work are listed in Table 6. 3. As for the Mg-Sn-In ternary system, there is limited solubility of Zn in the Mg_2Sn compound (less than 0.2 at. %), and the solid solubility of Sn in the Mg-Zn binary compounds is in the composition range from 0.0 to 4±2 at. %.

6.5.2 Thermodynamic optimization

The In-Mg system

All the experimental data discussed above were used in the present thermodynamic optimization of the In-Mg binary system. The calculated phase diagram is shown in Fig. 6.3 with experimental data [12, 14, 17-20]. In the present work, the γ' and β' phases were treated as a single fcc solution and modeled with the two sub-lattice structure of $(In, Mg)_3(In, Mg)$ as $L1_2$, and the β'' phase was modeled with a two sub-lattice structure of $(In, Mg)(In, Mg)$ as $L1_0$. The calculated peritectic reaction liquid+hcp(Mg) $\leftrightarrow \beta$ is 484 ^{o}C, which agrees well with the experimental data [14, 18, 19]. All the calculated invariant reactions are listed in Table 6. 5 and are in a good agreement with the experimental data [12, 14, 17-20].
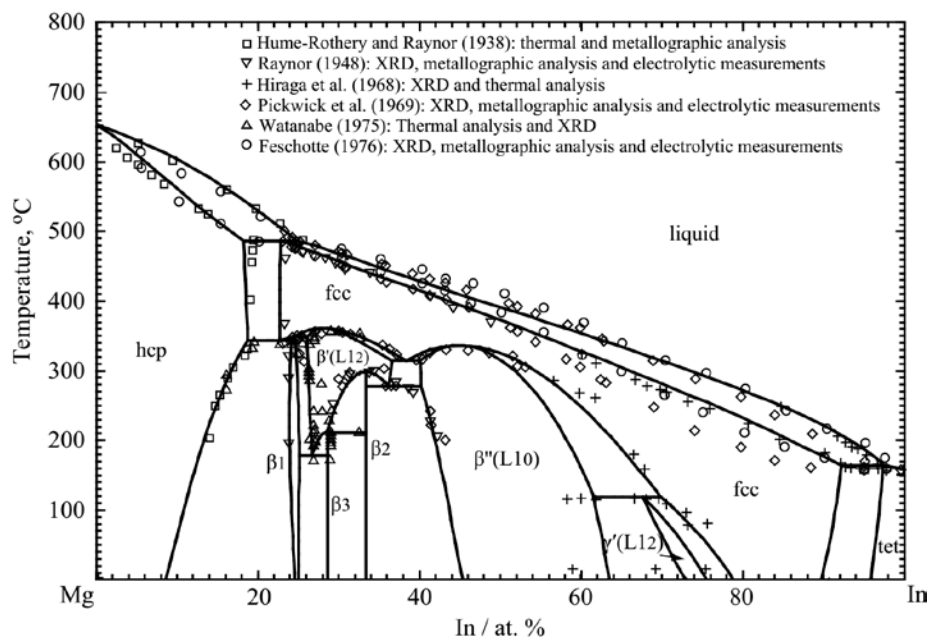
Figure 6.3 Calculated Mg-In binary phase diagram compared with the reported experimental data [12, 14, 17-20]

Table 6.5 The calculated results of invariant reactions in the In-Mg system compared with experimental data

Reaction	Reaction type	Temperature, (°C)	Composition (In at. %)			Reference
liquid+hcp ↔ *fcc*	Peritectic	484	25	19.4	23	[29, 32-33]
		483	24.8	18.3	22.7	This work
fcc ↔ β_1 + *hcp*	Eutectoid	334	23.2	19	24	[35]
		335	22.4	18.4	24	This work
liquid+*fcc* ↔ *tet*	Peritectic	160±1	97	93.5	95	[32]
		160	96.5	86	94	[33]
		161	97.8	92.5	97.4	This work
fcc + β' ↔ β_1	Peritectiod	337	23.9	26	24.4	[35]
		340	23.5	25.7	24.3	This work
β' ↔ β_1 + β_3	Eutectoid	202	27.5	26.2	28.6	[35]
		167	26.4	25.1	28.6	This work
β'+ β_2 ↔ β_3	Peritectoid	210	27.6	33.8	28.6	[35]
		211	28.1	33.3	28.5	This work
β' ↔ β_2	Congruent	298		34		[29, 35]
		298		33.3		This work
β' ↔ β_2 + β''	Eutectoid	276	37.8	33.5	38.2	[31]
		281	36	33.3	40	This work
β''+ *fcc* ↔ γ'	Peritectoid	114	58.5	70	69.5	[32]
		111	60.5	67.3	69.5	This work

The calculated enthalpy of mixing of the liquid phase at 675 ^{o}C is shown in Fig. 6.4 along with the experimental data [22-27]. As shown in this figure, the data extrapolated from EMF measurements have large error limits compared to the experimental data obtained from direct calorimetric measurements. Consequently, in the present work, the optimization was mainly based on the experimental data [22, 27] obtained by calorimetric methods. The calculated activities of Mg and In in the liquid phase at 650 ^{o}C are shown in Fig. 6. 5 in comparison with experimental data [24, 26-28].

No experimental thermodynamic data exist for intermetallic compounds. Therefore, their heat capacities were obtained with the Neumann–Kopp rule [91], with the "Zero" enthalpy of formation at 25 ^{o}C, firstly. And then the enthalpy and entropy of formation were then adjusted by fitting the phase diagram. The calculated enthalpies of formation of compounds in the In-Mg system at 25 ^{o}C are shown in the Fig. 6.6. All the thermodynamic parameters optimized in the present work are listed in Tables 6.2 and 6. 6.
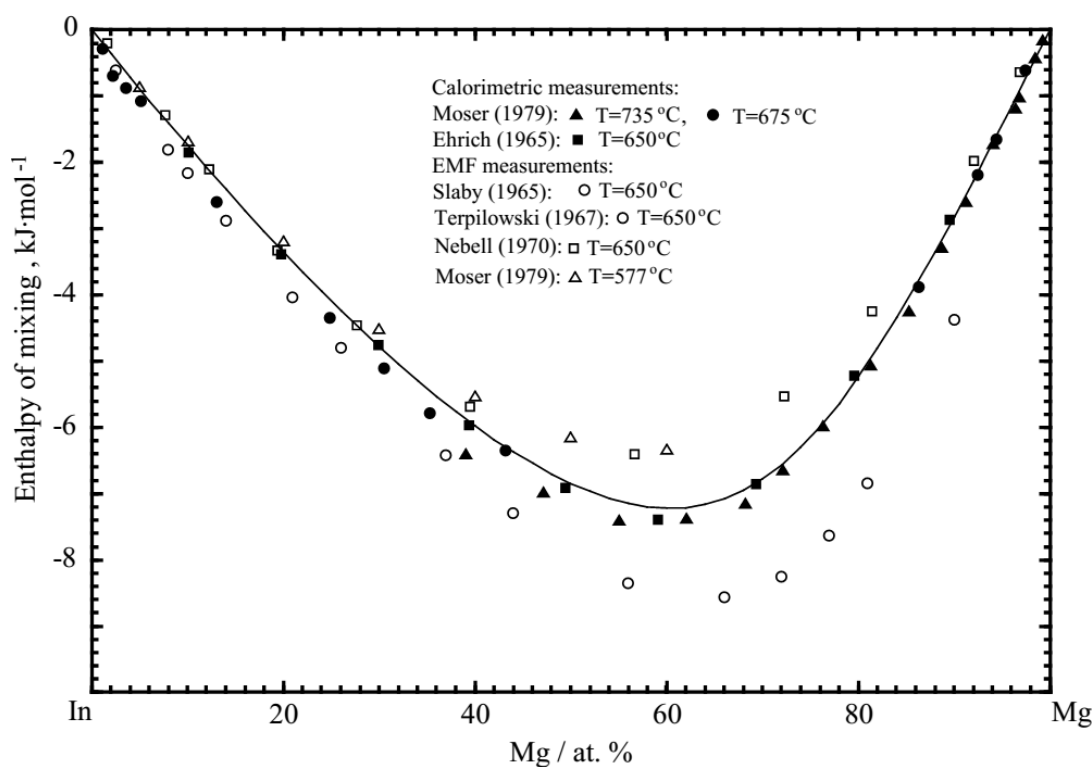
Figure 6.4 Calculated enthalpy of mixing of the In-Mg liquid phase at 675 ^{o}C in comparison with the reported experimental data [22-27]
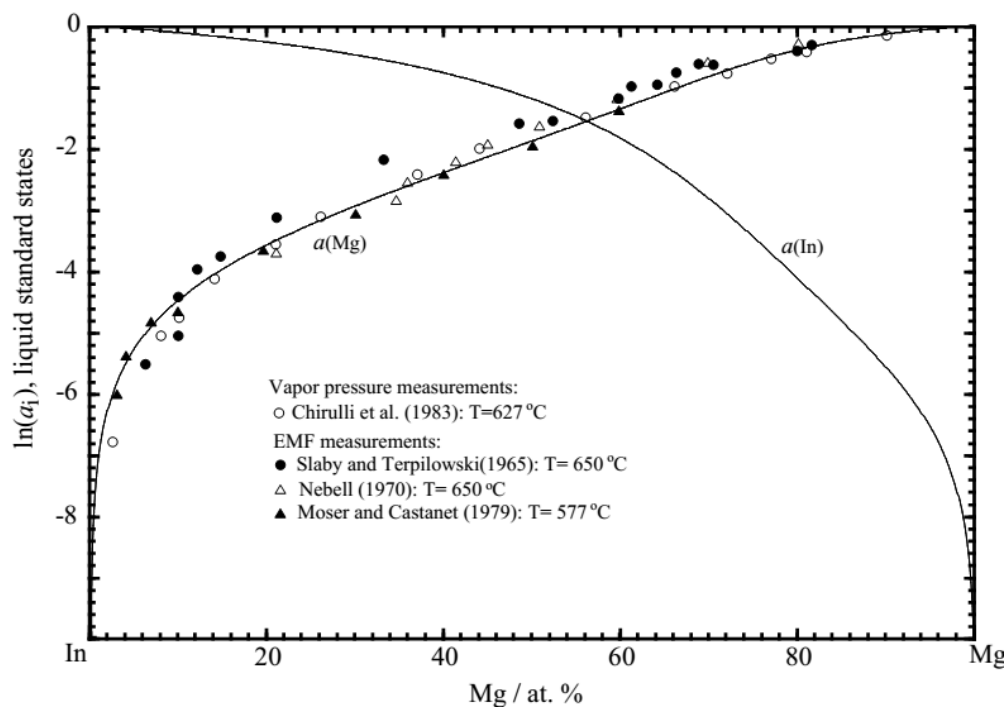
Figure 6.5 Calculated activities of Mg and In in the liquid phase at 650 $^{\circ}$C in comparison with the reported experimental data [24, 26-28]
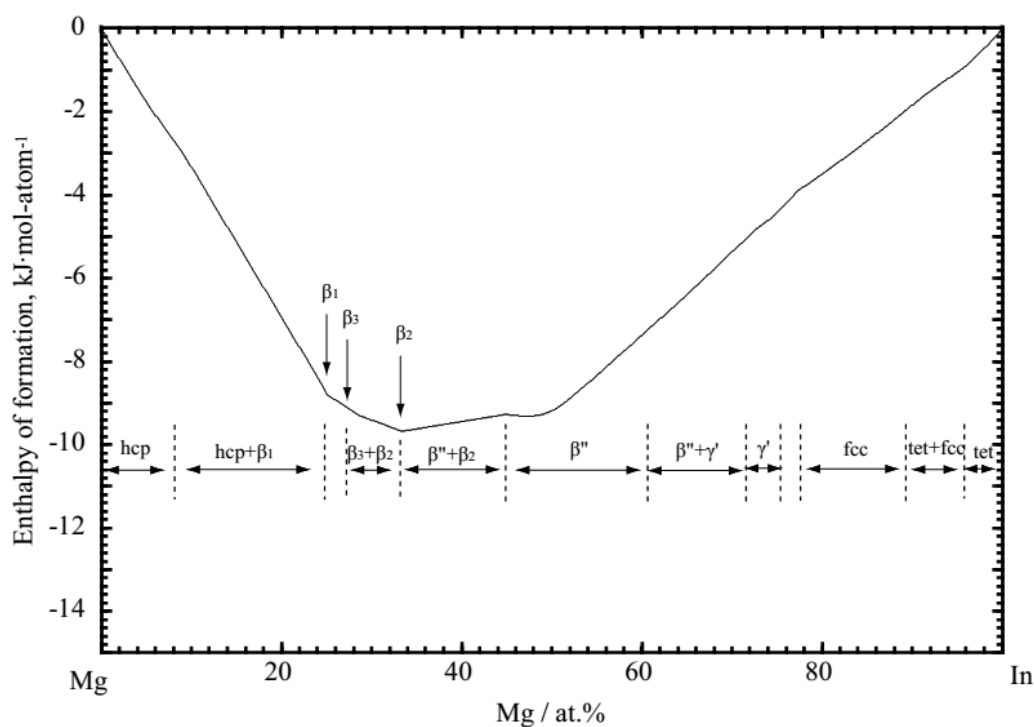
Figure 6.6 Calculated enthalpy of formation of solid phases of the In-Mg binary system 25 $^{\circ}$C

Table 6.6 Optimized model parameters for the quaternary Mg-Sn-In-Zn liquid phase and solid solutions

Phase, model and thermodynamic parameters (J·mol⁻¹, or J·mol⁻¹·K⁻¹)	reference
Liquid phase, MQMPA	
$g_{InSn(Mg)}^{001} = -9204.8,$	This work
$g_{InSn(Zn)}^{001} = -2928.8,\ g_{InZn(Sn)}^{001} = 1255.2,\ g_{ZnSn(In)}^{001} = 1255.2$	This work
$g_{MgSn(Zn)}^{001} = -3765.6 + 3.14 \times T,\ g_{MgZn(Sn)}^{001} = -5439.2 + 2.30 \times T,\ g_{ZnSn(Mg)}^{001} = -1255.2 + 2.72 \times T$	This work
hcp_A3(Mg) phase, $(In,Mg,Sn,Zn)(Va)_3$:	
$G_{Mg:Va} = {}^0G_{Mg}^{hcp},\ G_{Zn:Va} = {}^0G_{Zn}^{hcp-Zn} + 2969.0 - 1.57 \times T$	
$G_{Sn:Va} = {}^*G_{Sn} + 3900.0 - 4.4 \times T,\ G_{In:Va} = {}^*G_{In} + 533.0 - 0.69 \times T,$	This work
${}^1L_{Mg,Sn:Va} = 48116.0,$	[85]
${}^0L_{In,Zn:Va} = 6945.4,\ \ {}^0L_{Mg,In:Va} = -28325.7 + 6.07 \times T,\ {}^1L_{Mg,In:Va} = -10460.0 + 5.44 \times T$	This work
fcc_A1 phase, $(In,Mg,Sn,Zn)(Va)_3$:	
$G_{Mg:Va} = {}^0G_{Mg}^{hcp} + 2600.0 + 0.90 \times T,\ G_{Zn:Va} = {}^0G_{Zn}^{hcp-Zn} + 2969.0 + 1.57 \times T$	
$G_{In:Va} = {}^*G_{In} + 123.0 - 0.30 \times T,\ G_{Sn:Va} = {}^*G_{Sn} + 4150.0 - 5.20 \times T$	
${}^0L_{In,Zn:Va} = 33472.0,\ \ {}^0L_{In,Sn:Va} = 10460.0,\ \ {}^0L_{Sn,Zn:Va} = 12552.0,$	This work
${}^0L_{In,Mg:Va} = -29957.4 - 1.88 \times T,\ \ {}^1L_{In,Mg:Va} = -13723.5 - 1.46 \times T,\ {}^2L_{In,Mg:Va} = -6276.0$	This work
hcp_A3(Zn) phase, $(In,Mg,Sn,Zn)(Va)_3$:	
$G_{Mg:Va} = {}^0G_{Mg}^{hcp},\ G_{Zn:Va} = {}^0G_{Zn}^{hcp-Zn},$	
$G_{In:Va} = {}^*G_{In} + 2000.0, G_{Sn:Va} = {}^*G_{Sn} + 2000.0$	This work
${}^0L_{Mg,Zn:Va} = -3056.8 + 5.64 \times T,\ {}^1L_{Mg,Zn:Va} = 3127.3 - 5.66 \times T$	[86]
${}^0L_{Sn,Zn:Va} = 35020.1$	[73]
${}^0L_{In,Zn:Va} = 35020.1,\ {}^0L_{In,Sn:Va} = 33472.0$	This work
bct(Sn) phase, $(In,Mg,Sn,Zn)(Va)_3$:	
$G_{Mg:Va} = {}^0G_{Mg}^{hcp} + 15000.0,\ G_{Zn:Va} = {}^0G_{Zn}^{hcp-Zn} + 4184.0,$	This work
$G_{In:Va} = {}^*G_{In} + 2092.0, G_{Sn:Va} = {}^*G_{Sn}$	This work
${}^0L_{Sn,Zn:Va} = 5999.9 + 22.50 \times T,\ \ {}^0L_{In,Sn:Va} = 460.2$	This work
tet(In) phase, $(In,Mg,Sn,Zn)(Va)_3$:	
$G_{In:Va} = {}^*G_{In}, G_{Sn:Va} = {}^*G_{Sn} + 15000.0, G_{Mg:Va} = {}^0G_{Mg}^{hcp} + 15000.0, G_{Zn:Va} = {}^0G_{Zn}^{hcp} + 17505.9$	This work
${}^0L_{In,Zn:Va} = -12552.0 - 20.08 \times T,\ \ {}^0L_{In,Sn:Va} = 836.8 - 1.67 \times T,\ {}^0L_{Sn,Zn:Va} = 14644.0$	This work
${}^0L_{In,Mg:Va} = -26359.2 + 18.83 \times T$	This work
$MgZn_2$ phase, $(Mg,Zn)_2(Mg,Zn)$:	
$G_{Mg:Mg} = 3 \times {}^0G_{Mg}^{hcp} + 23372.7,\ G_{Mg:Zn} = 2 \times {}^0G_{Mg}^{hcp} + 1 \times {}^0G_{Zn}^{hcp} + 6535.5 - 8.84 \times T,$	[86]
$G_{Zn:Zn} = 3 \times {}^0G_{Zn}^{hcp} + 15000.0,\ \ G_{Zn:Mg} = 2 \times {}^0G_{Zn}^{hcp} + 1 \times {}^0G_{Mg}^{hcp} - 35359.6 + 8.84 \times T$	
To be continued	

Table 6.6 (continued) Optimized model parameters for the quaternary Mg-Sn-In-Zn liquid phase and solid solutions

Phase, model and thermodynamic parameters (J·mol^{-1}, or J·mol^{-1}·K^{-1})	reference
$\beta''(L1_0)$ phase, (Mg,In)(Mg,In) : $G_{Mg:Mg} = {}^0G_{Mg}^{hcp} + 2600.0 + 0.90 \times T, G_{In:In} = {}^*G_{In} + 123.0 - 0.30 \times T,$ $G_{Mg:In} = G_{In:Mg} = {}^*G_{In} + {}^0G_{Mg}^{hcp} - 4479.4 - 0.59 \times T,$ $L_{Mg,In:Mg} = L_{Mg:Mg,In} = -21756.0 + 0.63 \times T, L_{Mg,In:In} = L_{In:Mg,In} = 627.6 - 0.42 \times T,$	This work
$\beta', \gamma'(L1_2)$ phase, (Mg,In)$_3$(Mg,In) : $G_{Mg:Mg} = 4 \times {}^0G_{Mg}^{hcp} + 10400 + 3.6 \times T, G_{In:In} = 4 \times {}^*G_{In} + 492 - 1.20 \times T,$ $G_{Mg:In} = {}^*G_{In} + 3 \times {}^0G_{Mg}^{hcp} + 7923.0 \times + 2.4T, G_{In:Mg} = 3 \times {}^*G_{In} + {}^0G_{Mg}^{hcp} - 35540.5 - 1.09 \times T$ ${}^0L_{In:Mg,In} = -32049.4 + 2.93 \times T, {}^1L_{In:Mg,In} = 7949.6,$	This work
$\beta_1(hR16)$ phase, (Mg,In)$_3$(Mg,In) : $G_{Mg:Mg} = 4 \times {}^0G_{Mg}^{hcp} + 6694.4, G_{In:In} = 4 \times {}^*G_{In},$ $G_{Mg:In} = {}^*G_{In} + 3 \times {}^0G_{Mg}^{hcp} - 35145.6 + 3.18 \times T, G_{In:Mg} = 3 \times {}^*G_{In} + {}^0G_{Mg}^{hcp}$	This work
$\gamma(InSn)$ phase, (In,Sn)(Va)$_3$: $G_{In:Va} = {}^*G_{In} + 10292.6 - 7.64 \times T, G_{Sn:Va} = {}^*G_{Sn} + 924.7 - 1.76 \times T,$ ${}^0L_{In,Sn:Va} = -15480.8 + 18.74 \times T$	This work
$\beta(InSn)$ phase, (In,Sn)(Va)$_3$: $G_{In:Va} = {}^*G_{In}, G_{Sn:Va} = {}^*G_{Sn} + 5015.5 - 7.50 \times T,$ ${}^0L_{In,Sn:Va} = 292.0 - 3.14 \times T ,{}^1L_{In,Sn:Va} = 627.6 + 0.29 \times T$	This work
Mg_2Sn phase, (Mg)$_2$(Sn) : $G = -102589.8 + 367.5 \times T - 68.331 \times T \ln T - 0.0178986 \times T^2 + 3.33829 \times 10^{-7} \times T^3 + 95940 / T$	[85]
Mg_2Zn_3 phase, (Mg)$_2$(Zn)$_3$: $G = 2 \times G_{Mg}^{hcp} + 3 \times G_{Zn}^{hcp} - 54406.2 + 13.60 \times T$	[86]
Mg_2Zn_{11} phase, (Mg)$_2$(Zn)$_{11}$: $G = 2 \times G_{Mg}^{hcp} + 11 \times G_{Zn}^{hcp} - 73818.3 + 18.46 \times T$	[86]
$Mg_{12}Zn_{13}$ phase, (Mg)$_{12}$(Zn)$_{13}$: $G = 12 \times G_{Mg}^{hcp} + 13 \times G_{Zn}^{hcp} - 236980.8 + 59.23 \times T$	[86]
$Mg_{51}Zn_{20}$ phase, (Mg)$_{51}$(Zn)$_{20}$: $G = 51 \times G_{Mg}^{hcp} + 20 \times G_{Zn}^{hcp} - 335741.5 + 35.40 \times T$	[86]
$InMg_2$ phase, (In)(Mg)$_2$: $G = 2 \times G_{Mg}^{hcp} + {}^*G_{In} - 29022.6 + 1.09 \times T$	This work
In_2Mg_5 phase, (In)$_2$(Mg)$_5$: $G = 5 \times G_{Mg}^{hcp} + 2 \times {}^*G_{In} - 65022.3 + 5.14 \times T$	This work

$${}^*G_{In} = \int {}^*Cp_{In}dt - T \times \int \frac{{}^*Cp_{In}}{T} dt, \qquad {}^*G_{Sn} = \int {}^*Cp_{Sn}dt - T \times \int \frac{{}^*Cp_{Sn}}{T} dt$$

$${}^*C_p(Sn) = 25.858 - 0.0010237 \times T - 36880/T^{-2} + 1.9156602 \times 10^{-5} \times T^2 \qquad 249K < T < 250K$$
$$= 15.961 + 0.0377404 \times T + 123920/T^{-2} - 1.8727002 \times 10^{-5} \times T^2 \qquad 251K < T < 1000K$$
$$= 35.098 \qquad 506K < T < 3000K$$
$${}^*C_p(In) = 21.8386 + 0.01145132 \times T + 45812 \times T^{-2} + 1.2721926 \times 10^{-5} \times T^2 \qquad 298K < T < 429.78K$$
$$= 31.05 - 0.0001919 \times T - 312000 \times T^{-2} + 3.374 \times 10^{-8} \times T^2 \qquad 429.79K < T < 3800K$$

140

The In-Sn system

The calculated In-Sn binary phase diagram is shown in the Fig. 6.7 along with experimental data [30-32, 34]. The calculated temperatures of the peritectic reactions $liquid + tet \leftrightarrow \beta(InSn)$ and $liquid + bct \leftrightarrow \gamma(InSn)$ are 119 ^{o}C and 223 ^{o}C, respectively, which is in good agreement with the experimental temperature of Heumann and Alpaut [34] (120 ^{o}C and 224 ^{o}C).
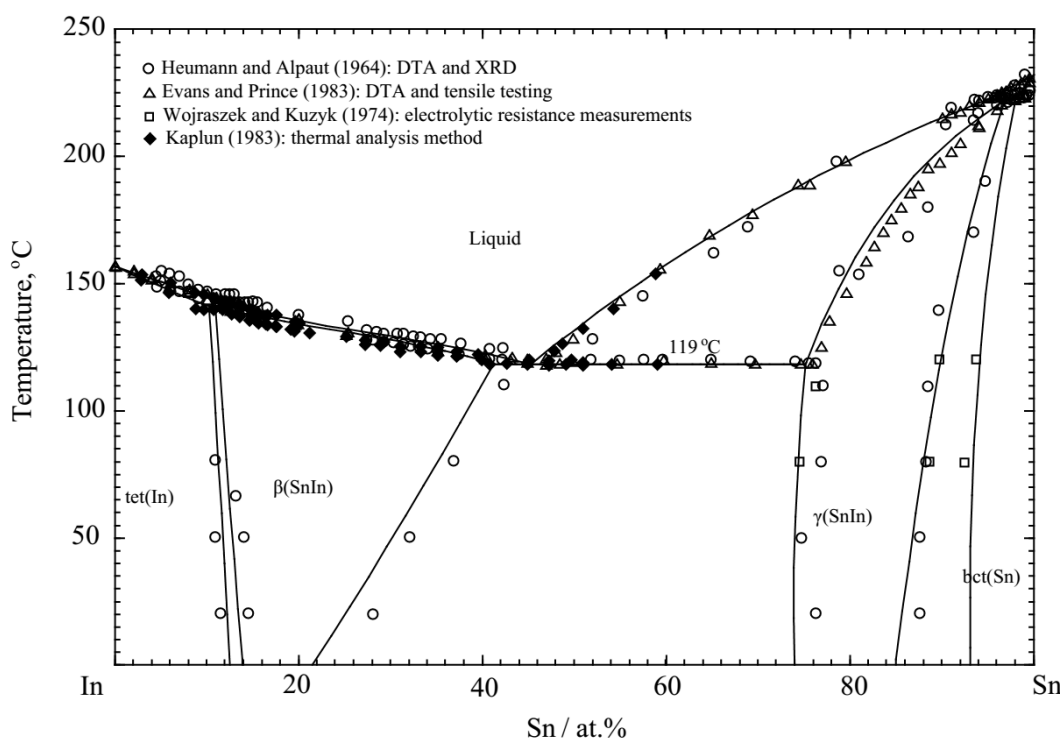
Figure 6.7 Calculated In-Sn phase diagram in comparison with the reported experimental data [30-32, 34]

The calculated enthalpy of mixing of the liquid phase at 450 ^{o}C and the calculated activity of In and Zn in the liquid at 427 ^{o}C are depicted in Figs. 6.8 and 6.9. The agreement between our calculated results and the experimental data obtained by emf and calorimetric measurements is quite good. Fig. 9 shows the calculated activity of In and Zn in the liquid phase at 427 ^{o}C along with the experimental data [37-39]. And the calculated activity of In in the solid phases at 100 ^{o}C (reference state tet(In)) is shown in Fig. 6. 10 in comparison with the experimental data [35]. The calculated enthalpy of formation of solid phases at 100 ^{o}C is shown in Fig. 6. 11 along with the

experimental data [35, 45]. All the thermodynamic parameters optimized in the present work are listed in Tables 6. 2 and 6.6.
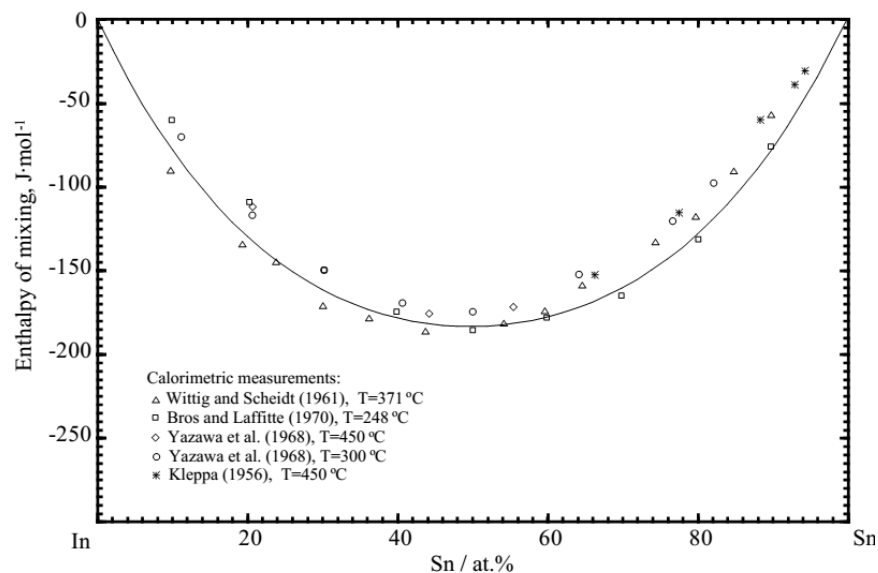
Figure 6.8 Calculated enthalpy of mixing of liquid In-Sn binary alloys at 450 ^{o}C in comparison with the reported experimental data [40-43]
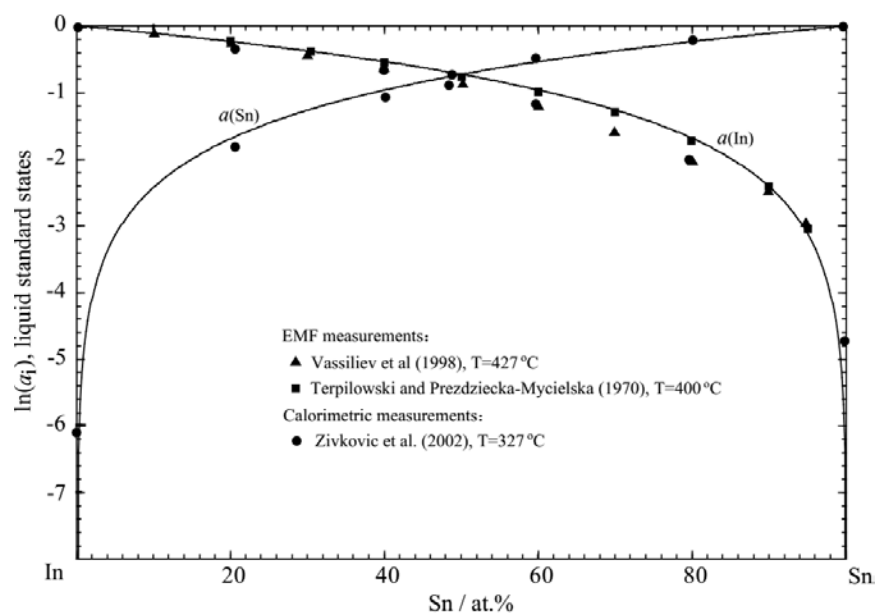
Figure 6.9 Calculated activity of In and Sn in the liquid phase at 427 ^{o}C in comparison with the reported experimental data [37-39]
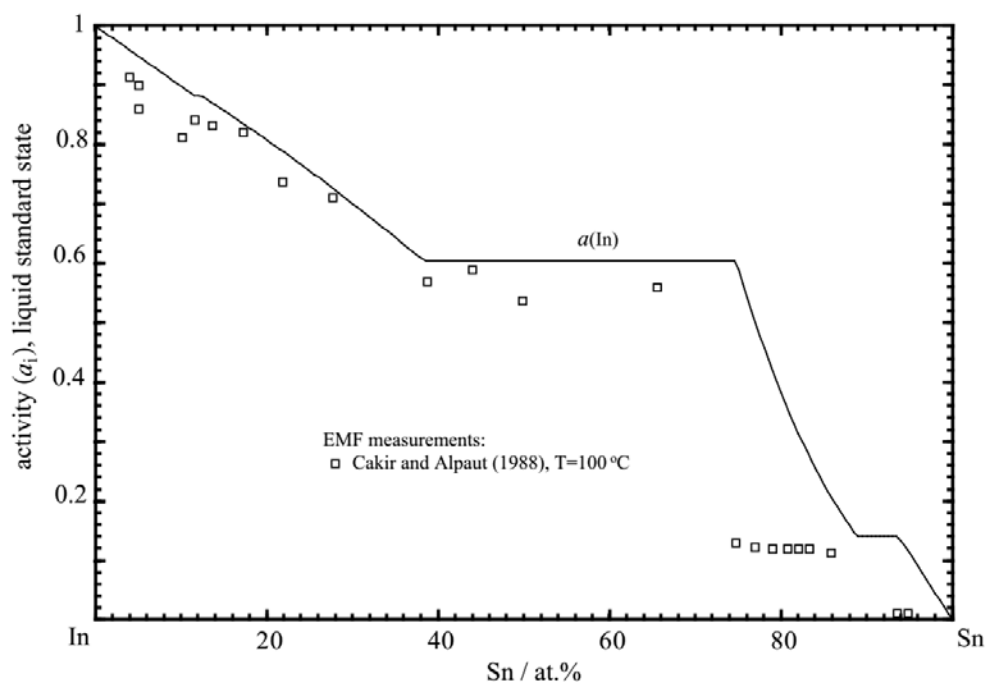
Figure 6.10 Calculated activity of In in solid In-Sn binary alloys at 100 ^{o}C (reference state tet(In)) in comparison with the reported experimental data [35]
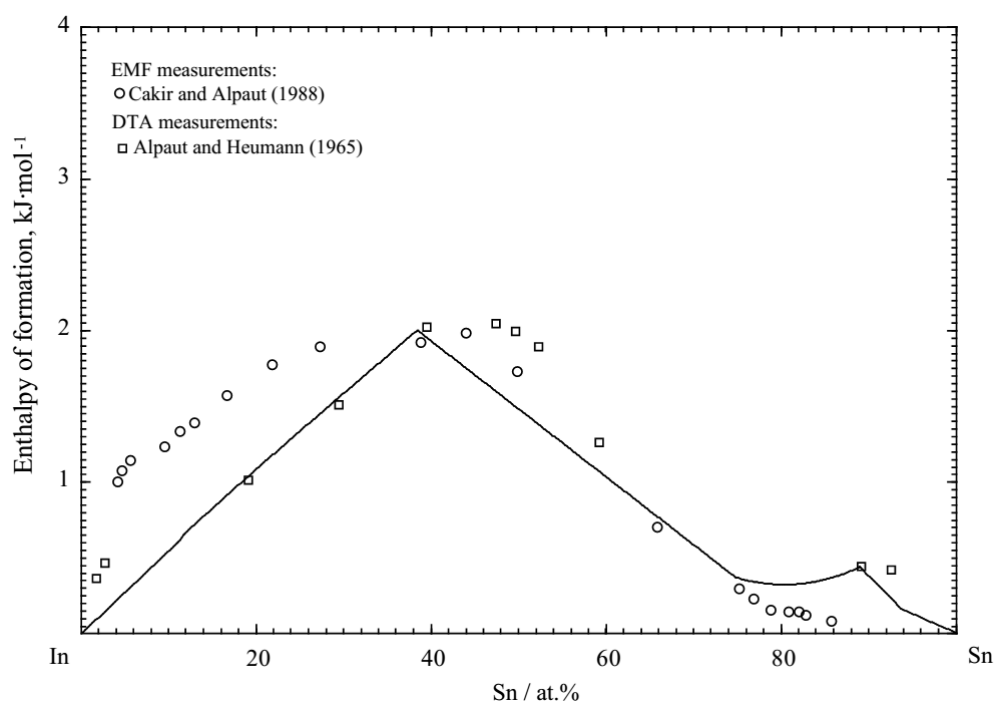
Figure 6.11 Calculated heat of formation of solid In-Sn binary alloys at 100 ^{o}C in comparison with the reported experimental data [35, 45]

The In-Zn system

The calculated In-Zn phase diagram along with the experimental data discussed above [50-53, 56] is shown in Fig. 6.12. The liquid phase has a tendency to form a metastable miscibility gap, which is depicted by a dotted line in Fig. 6.12. The consolute temperature of the miscibility gap is very close to the stable liquidus line, which was predicted by Oelsen and Zuhlke [53]. In the present work, the eutectic $liquid + tet(In) \leftrightarrow hcp(Zn)$ is calculated to lie at 144 ^{o}C and 4.5 at. % Zn, which is in reasonable agreement with experimental data [51].
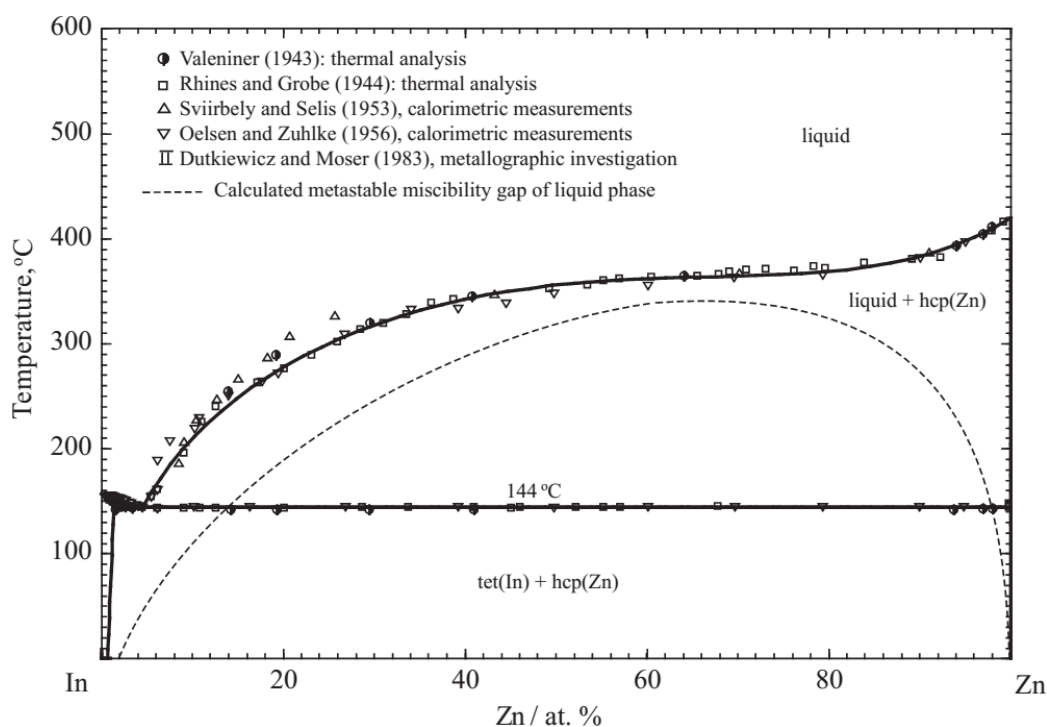
Figure 6.12 Calculated In-Zn phase diagram along with the reported experimental data [50-53]

The calculated enthalpy mixing of the liquid phase at 450 ^{o}C is shown in Fig. 6.13 along with the experimental data [52-55, 58, 59]. Fig. 6.14 shows the calculated activity of Zn in the liquid phase in the temperature range from 423 ^{o}C to 857 ^{o}C in comparison with the experimental data [52-55, 60-62]. The calculated results have a good agreement with the experimental data. All the thermodynamic parameters optimized in the present work are listed in Tables 6.2 and 6.6.
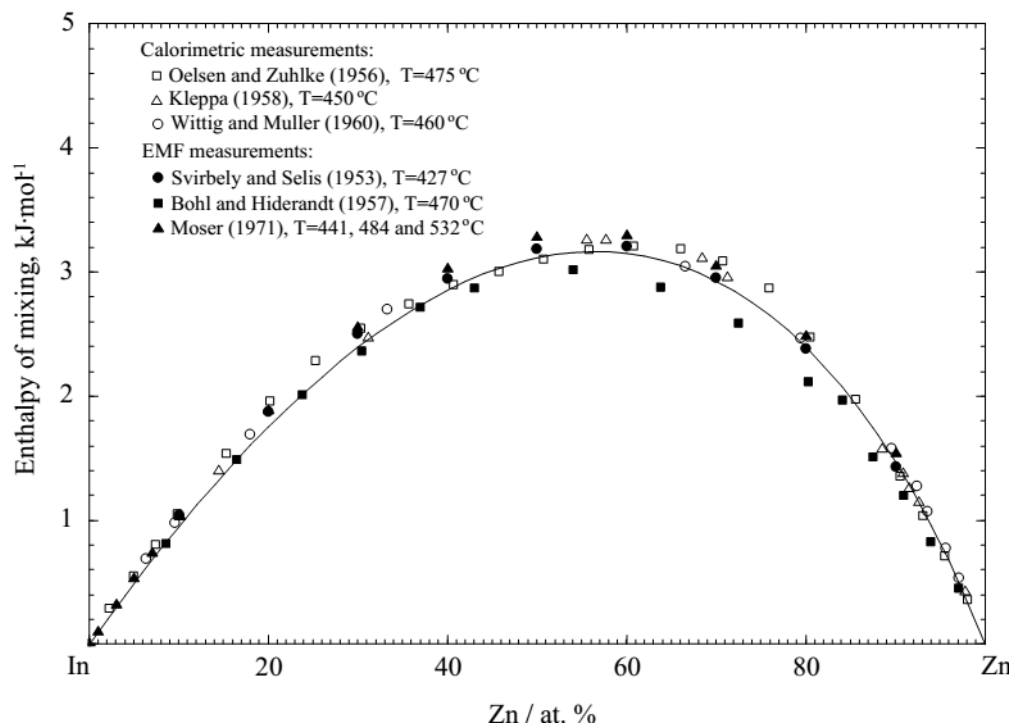
Figure 6.13 Calculated enthalpy of mixing of liquid In-Zn binary alloys at 450 °C along with the reported experimental data [52-55, 58, 59]
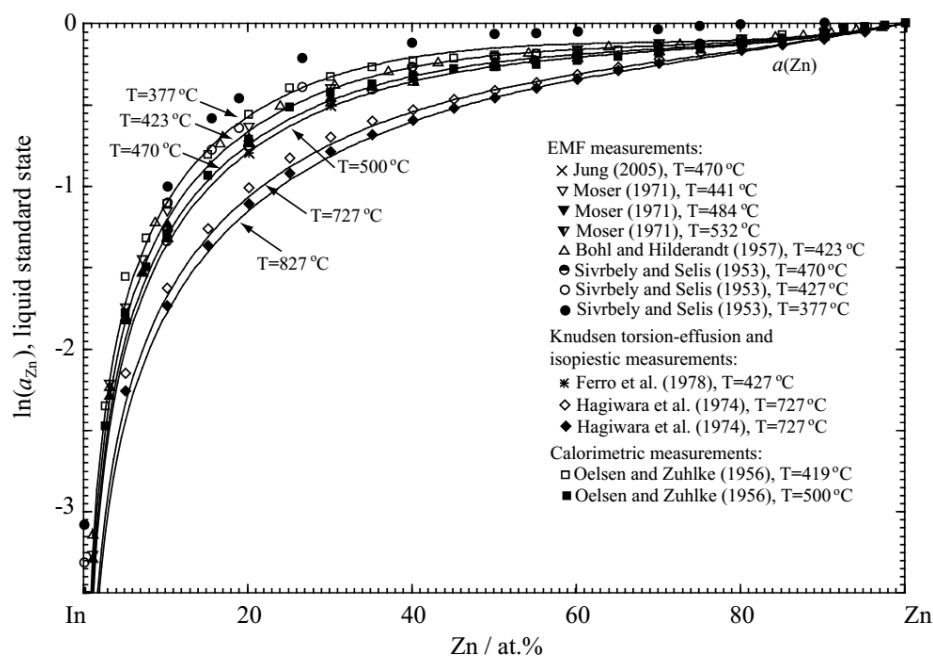
Figure 6.14 Calculated activity of Zn in liquid In-Zn binary alloys at temperatures from 423 °C to 857 °C in comparison with the reported experimental data [52-55, 60-62]

The Mg-Sn-In ternary system

According to our experimental results, there is a very limited ternary solubility of Sn in Mg-In binary compounds, and of In in Mg_2Sn. Consequently, we assumed that there is no ternary solubility in binary compounds in the present thermodynamic optimization. The calculated isothermal sections of the Mg-Sn-In ternary system at 415 ^{o}C and 330 ^{o}C are shown in Figs. 6.15 a-b along with the experimental data obtained in the present work. The calculated ternary isoplethal sections at 10 Sn and 5 In (at. %) are shown in Fig. 6.16a-b in comparison with our experimental data.

The calculated phase boundaries and invariant reactions are listed in Table 6.3 together with our DSC experimental data. A good agreement between the calculated results and experimental data can be seen. The calculated activity of Mg in the liquid phase with the Sn/In molar ratios of 0.25, 1.00, and 0.75 versus temperature are shown in Fig. 6.17a-c. low Mg contents, our calculated results are in a good agreement with the experimental data of Zakulski *et al.* [66]. The calculated liquidus projection of the Mg-Sn-In ternary system is shown in Fig. 6.18. There are a total of four ternary peritectic (U type) reactions and of one ternary eutectic (E type) in the calculated Mg-Sn-In system. The calculated invariant reactions of the liquidus projection of the Mg-Sn-In ternary system are listed in Table 6.7. All the optimized ternary thermodynamic parameters of Mg-Sn-In ternary system in the present work are listed in Tables 6.2 and 6.6.

The present calculated results at low Mg compositions are in a good agreement with the experimental data [76]. For the discrepancy between the calculated results and experimental data at high Mg composition, further experiments should be performed to verify the results of [76]. The calculated liquidus projection of the Mg-Sn-In ternary system is shown in Fig. 6.17. There are a total of four ternary peritectic (U type) reactions and of one ternary eutectic (E type) reaction in the calculated Mg-Sn-In ternary system. The calculated invariant reactions of the liquidus projection of the Mg-Sn-In ternary system are listed in Table 6.7. All the ternary thermodynamic parameters optimized of Mg-Sn-In ternary system in the present work are listed in Tables 6.5 and 6.6.
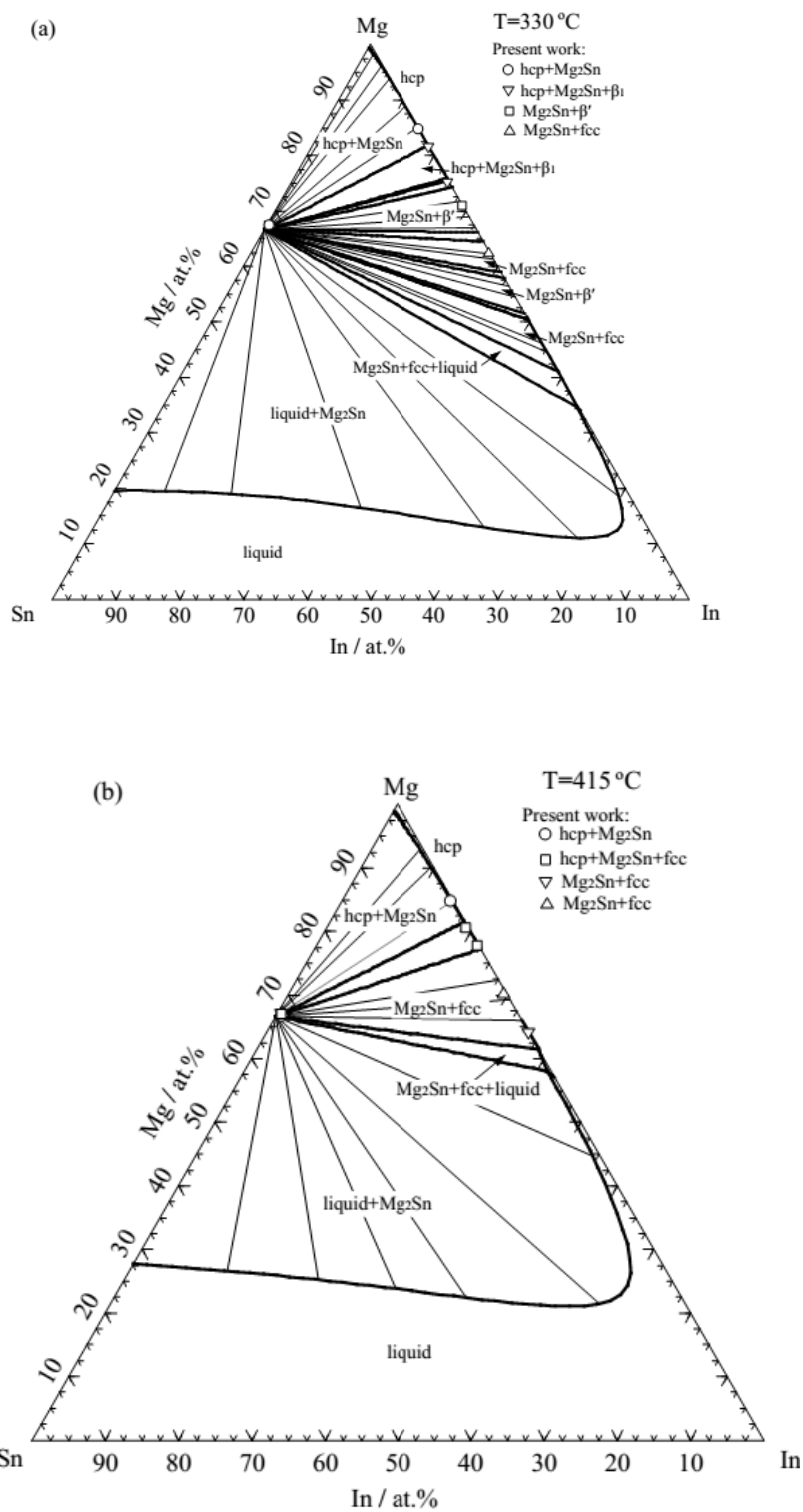
Figure 6.15 Calculated isothermal sections of the Mg-Sn-In ternary system at (a) 415 °C and (b) 330 °C along with the present experimental data obtained by EPMA measurements
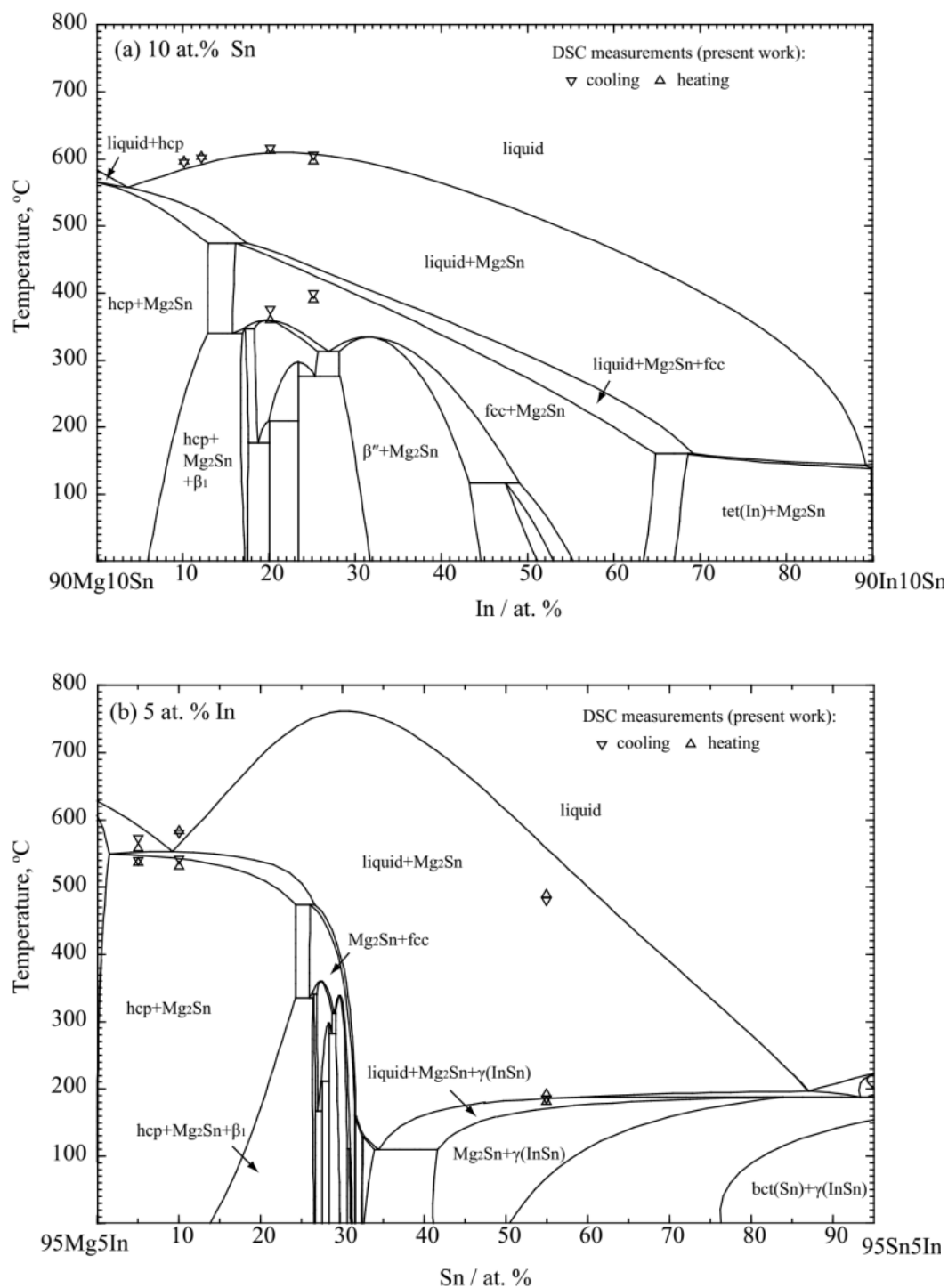
Figure 6.16 Calculated ternary isoplethal sections of the (a) 10 Sn and (b) 5 In (at. %) in comparison with the present experimental data
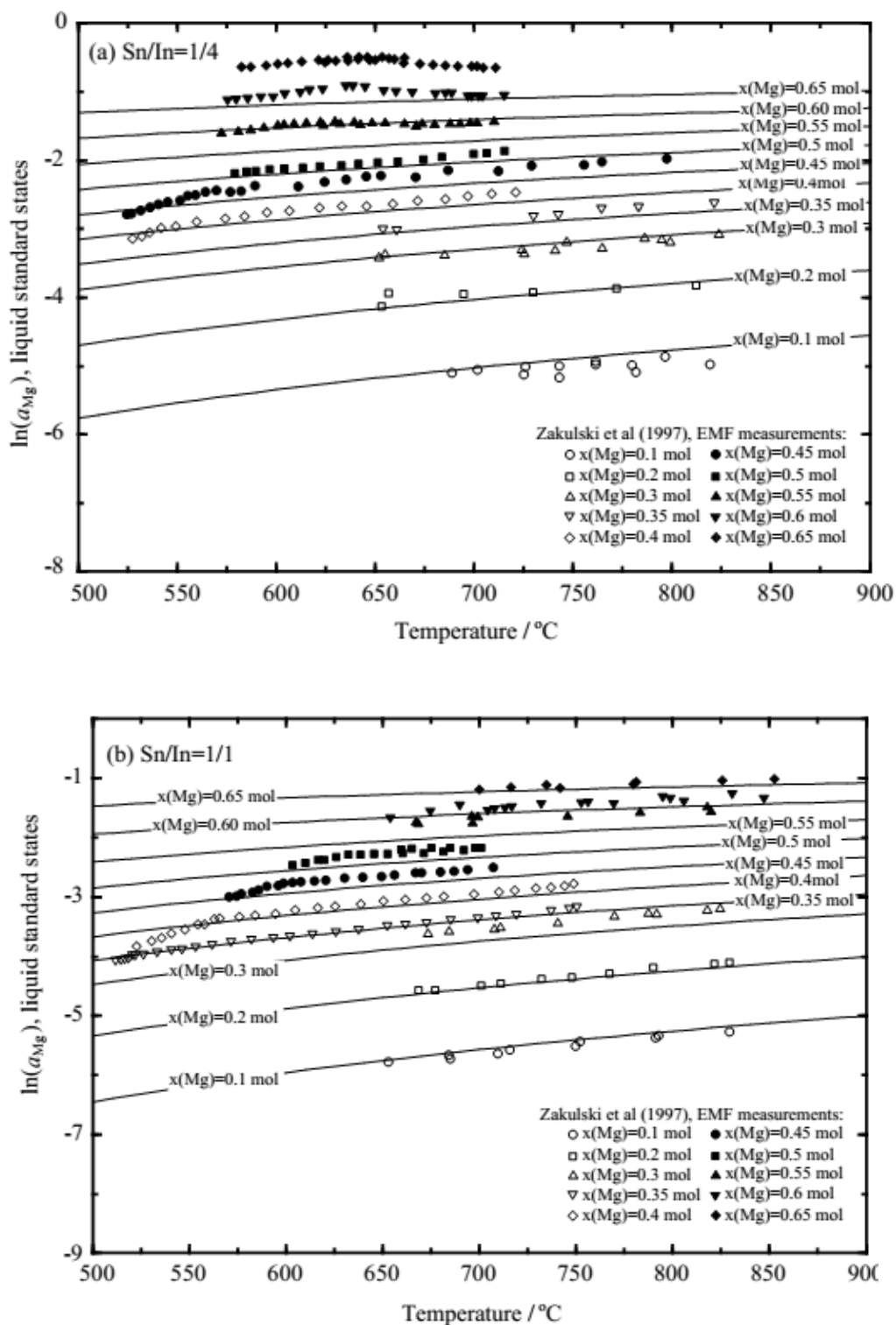
Figure 6.17 Calculated activity of Mg (liquid reference states) with the (a) 0.25, (b) 1, (c) 3/1 in liquid Mg-In-Sn ternary alloys versus temperature along with the reported experimental data (corrected for the Mg(s)/Mg(liq.) fusion below 650 °C) [66]
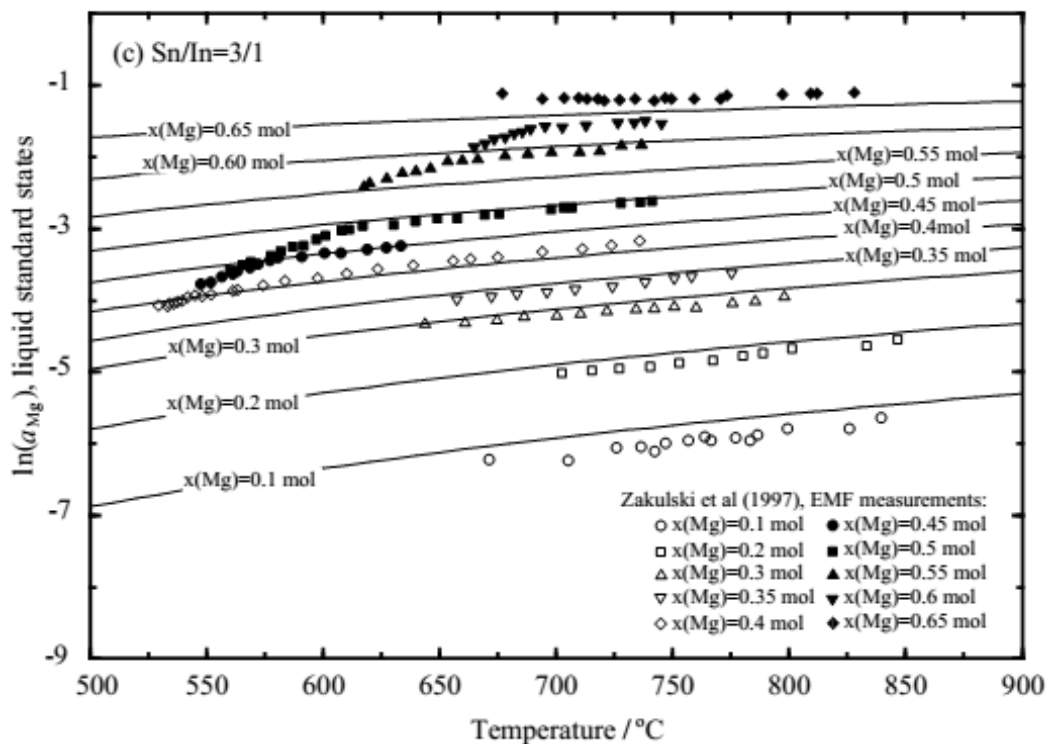
Figure 6.17 (Continued) Calculated activity of Mg (liquid reference states) with the (a) 0.25, (b) 1, (c) 3/1 in liquid Mg-In-Sn ternary alloys versus temperature along with the reported experimental data (corrected for the Mg(s)/Mg(liq.) fusion below 650 °C) [66]
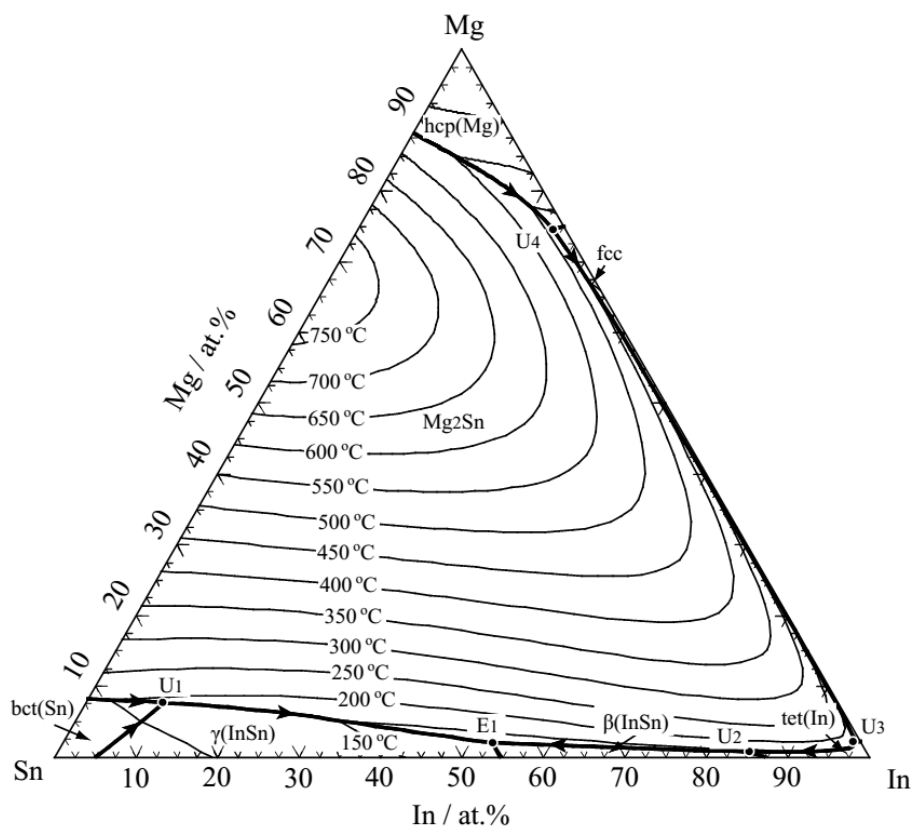
Figure 6.18 Calculated liquidus projection of the Mg-Sn-In ternary system

Table 6.7 Calculated invariant reactions in the liquidus projection of the Mg-Sn-In ternary system

Label	Temperature (°C)	Reaction	Composition of liquid (at. %)		
			Mg	In	Sn
E1	110	$L \leftrightarrow \gamma(InSn) + \beta(InSn) + Mg_2Sn$	2.02	52.69	45.30
U1	188	$L + bct(Sn) \leftrightarrow \gamma(InSn) + Mg_2Sn$	7.65	9.52	82.82
U2	136	$L + tet(In) \leftrightarrow \beta(InSn) + Mg_2Sn$	0.81	84.34	14.85
U3	160	$L + fcc \leftrightarrow tet(In) + Mg_2Sn$	2.28	97.13	0.59
U4	474	$L + hcp \leftrightarrow fcc + Mg_2Sn$	74.62	23.88	1.50

The Mg-Sn-Zn ternary system

As discussed above, there is a limited solid solubility of either Zn in Mg_2Sn or Sn in Mg-Zn binary compounds. As a result, the ternary solubility for the terminal binary compounds in the present optimization did not considered. The present calculated ternary isothermal sections at 300, 340 and 500 ^{o}C are shown in Figs. 6.19a-c. Other calculated isoplethal sections are depicted in Figs. 6.20a-l along with their related experimental data [67, 69]. The calculated ternary isoplethal section at constant 10 Sn (at. %) is shown in Fig. 6.21 along with our DSC experimental data. The present calculations are in good agreement with all the available experimental data. The calculated liquidus projection of the Mg-Sn-Zn ternary system is shown in Fig. 6.22. The calculated invariant reactions in the liquidus projection of the Mg-Sn-Zn ternary system are listed in Table 6.8. All the ternary thermodynamic parameters optimized of Mg-Sn-Zn ternary system are listed in Tables 6.2 and 6.6.
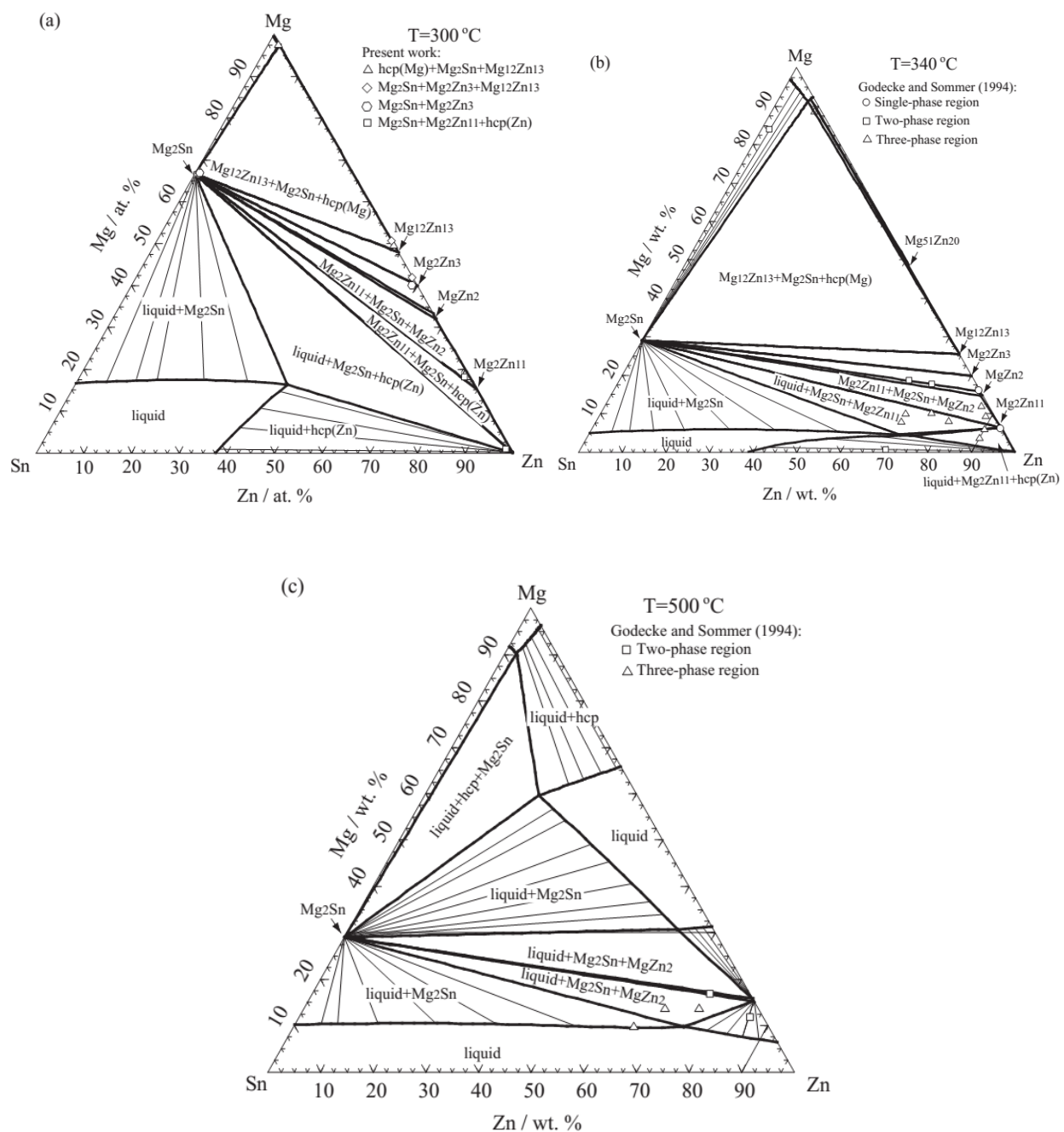
Figure 6.19 Calculated isothermal sections of the Mg-Sn-Zn ternary system at (a) 300 °C, (b) 340 °C and (c) 500 °C compared with present and reported experimental data [69]

Figure 6.20 Calculated isoplethal sections of the Mg-Sn-Zn ternary system (a) Mg$_2$Sn-Zn, (b) Mg$_2$Sn-MgZn$_2$, (c) Mg2Sn98-Mg2Zn98, (d) Mg10Sn90-Mg10Zn90, (e) Mg48Sn52-Mg48-Zn52, (f) Mg97Zn3-Sn97Zn3, (g) Mg30Zn70-Mg30Sn70, (h) Mg10Zn90-Sn10Zn90, (i) Mg98Sn2-Zn98Sn2, (j) Mg90Sn10-Zn90Sn10, (k) Mg60Sn40-Zn60Sn40, and (l) Mg15Sn85-Zn15Sn85 along with the reported experimental data [67, 69]

Figure 6. 20 Calculated isoplethal sections of the Mg-Sn-Zn ternary system (a) Mg$_2$Sn-Zn, (b) Mg$_2$Sn-MgZn$_2$, (c) Mg2Sn98-Mg2Zn98, (d) Mg10Sn90-Mg10Zn90, (e) Mg48Sn52-Mg48-Zn52, (f) Mg97Zn3-Sn97Zn3, (g) Mg30Zn70-Mg30Sn70, (h) Mg10Zn90-Sn10Zn90, (i) Mg98Sn2-Zn98Sn2, (j) Mg90Sn10-Zn90Sn10, (k) Mg60Sn40-Zn60Sn40, and (l) Mg15Sn85-Zn15Sn85 along with the reported experimental data [67, 69]

Figure 6.21 Calculated isoplethal section at 10 at. % Sn in the Mg-Sn-Zn system along with the experimental data obtain in the present work from DSC measurements

Table 6.8 Calculated invariant reactions in the liquidus projection of Mg-Sn-Zn ternary system

Label	Temperature (°C)	Reaction	Composition of liquid (at. %)		
			Mg	Zn	Sn
e1	566	$L \leftrightarrow MgZn_2 + Mg_2Sn$	38.98	54.63	6.39
E1	177	$L \leftrightarrow bct(Sn) + hcp\_Zn + Mg_2Sn$	8.07	15.12	76.81
U1	335	$L + Mg_2Zn_{11} \leftrightarrow hcp\_Zn + Mg_2Sn$	13.30	40.32	16.38
U2	357	$L + MgZn_2 \leftrightarrow Mg_2Zn_{11} + Mg_2Sn$	12.19	79.20	8.61
U3	414	$L + MgZn_2 \leftrightarrow Mg_2Zn_3 + Mg_2Sn$	64.66	34.41	0.93
U4	349	$L + Mg_2Zn_3 \leftrightarrow Mg_{12}Zn_{13} + Mg_2Sn$	70.03	28.56	4.18
U5	345	$L + Mg_{51}Zn_{20} \leftrightarrow Mg_{12}Zn_{13} + hcp$	71.54	28.25	2.08
E2	344.6	$L \leftrightarrow Mg_{12}Zn_{13} + Mg_2Sn + hcp$	71.53	28.08	3.94
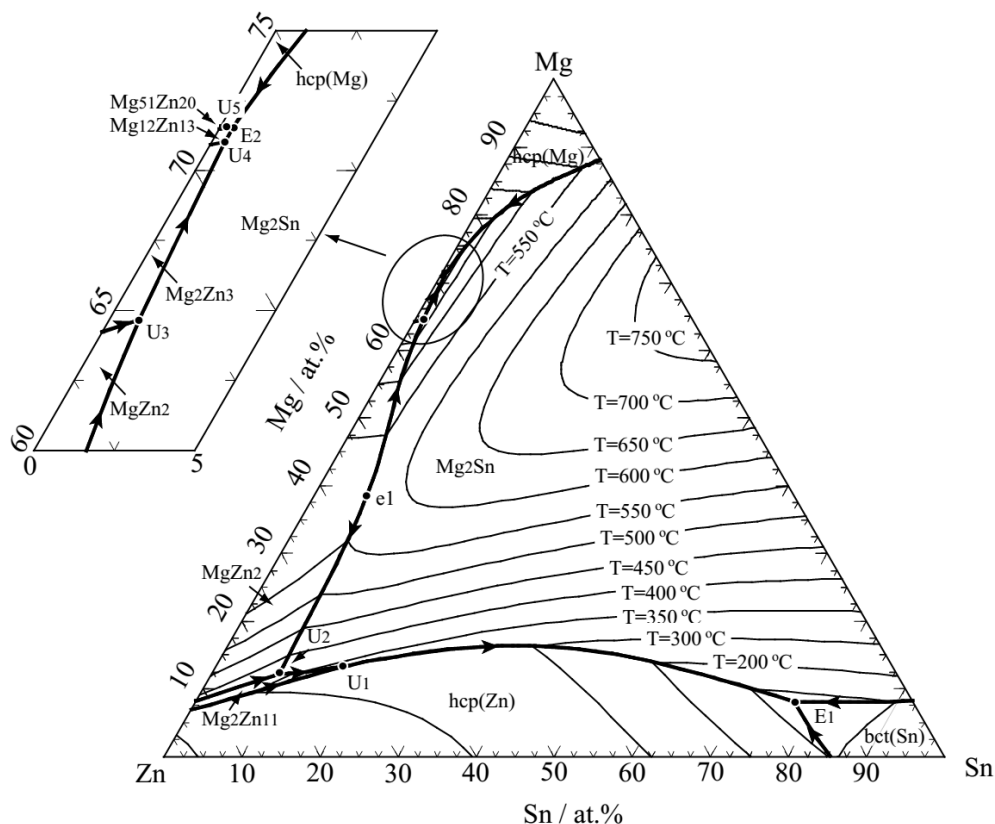
Figure 6.22 Calculated liquidus projection of the Mg-Sn-Zn ternary system

The In-Sn-Zn ternary system

The calculated isoplethal sections of the In-Sn-Zn ternary system for the Sn/Zn molar ratios of 2:1, 1:1 and 1:2 are shown in Fig. 6.23a-c along with the experimental data reported by Xie *et al.* [76]. Fig. 6.24 a-f shows the calculated isoplethal sections of the In-Sn-Zn ternary system for the In/Sn molar ratios of 5:95, 15:85, 1:2, 52:48, 2:1, and 85:15 along with the experimental data of Sabbar *et al.* [77]. All the present calculated results are in good agreement with the experimental data [76, 77], except isoplethal section of In/Sn=15/85 (Fig. 6.24 (b)). The singals observed in the isoplethal section of In/Sn=15/85 around 115 °C by Sabbar *et al.* [77] may due to the Scheil-Gulliver cooling effect.
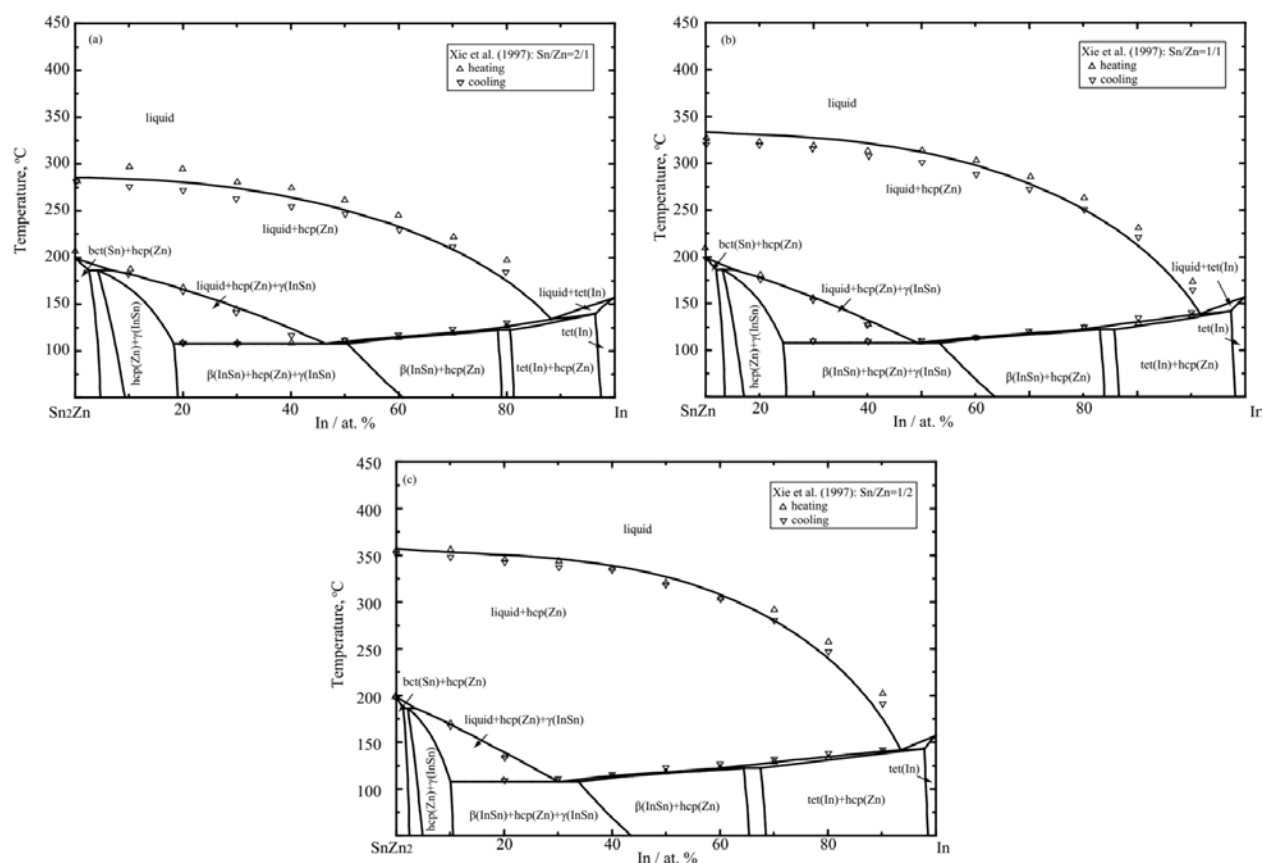
Figure 6.23 Calculated isoplethal sections of the In-Sn-Zn ternary system for Sn/Zn molar ratios of (a) 2:1, (b)1:1 and (c)1:2 in comparison with the reported experimental data [76]
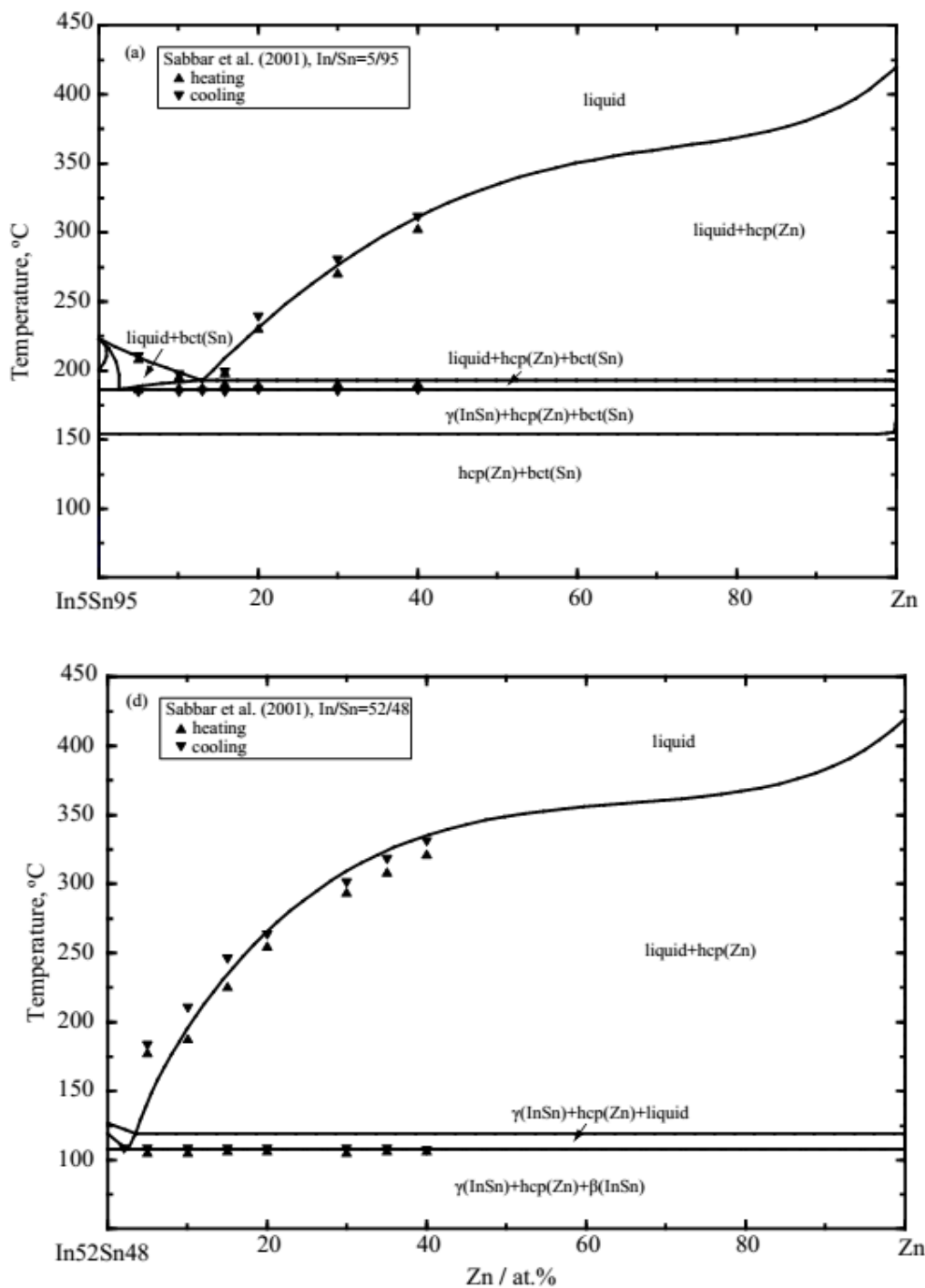
Figure 6.24 Calculated isoplethal sections of the In-Sn-Zn ternary system for In/Sn molar ratios of (a) 5:95, (b) 15:85, (c) 1:2, (d) 52:48, (e) 2:1, and (f) 85:15 in comparison with the reported experimental data [77]
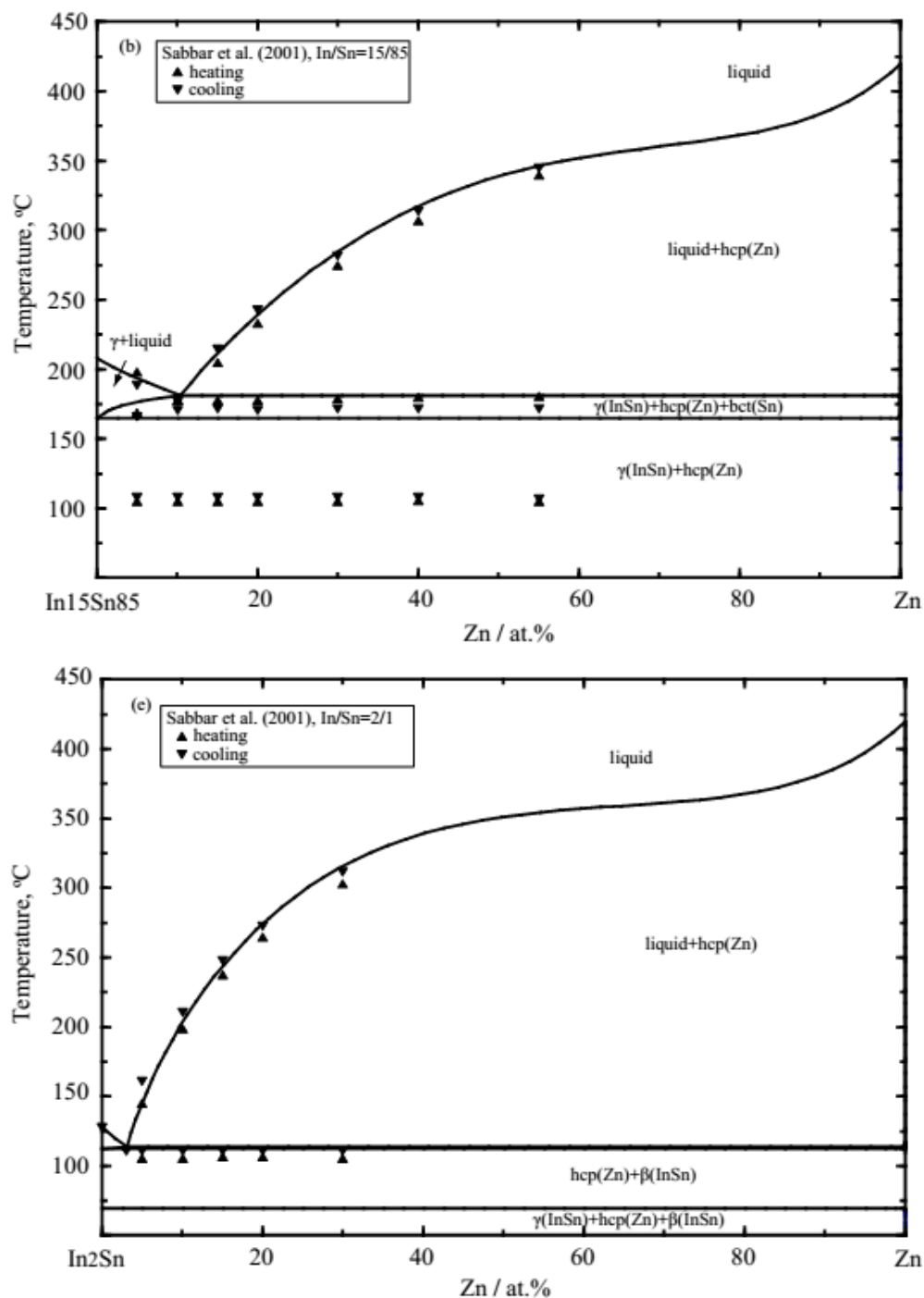
Figure 6.24 Calculated isoplethal sections of the In-Sn-Zn ternary system for In/Sn molar ratios of (a) 5:95, (b) 15:85, (c) 1:2, (d) 52:48, (e) 2:1, and (f) 85:15 in comparison with the reported experimental data [77]
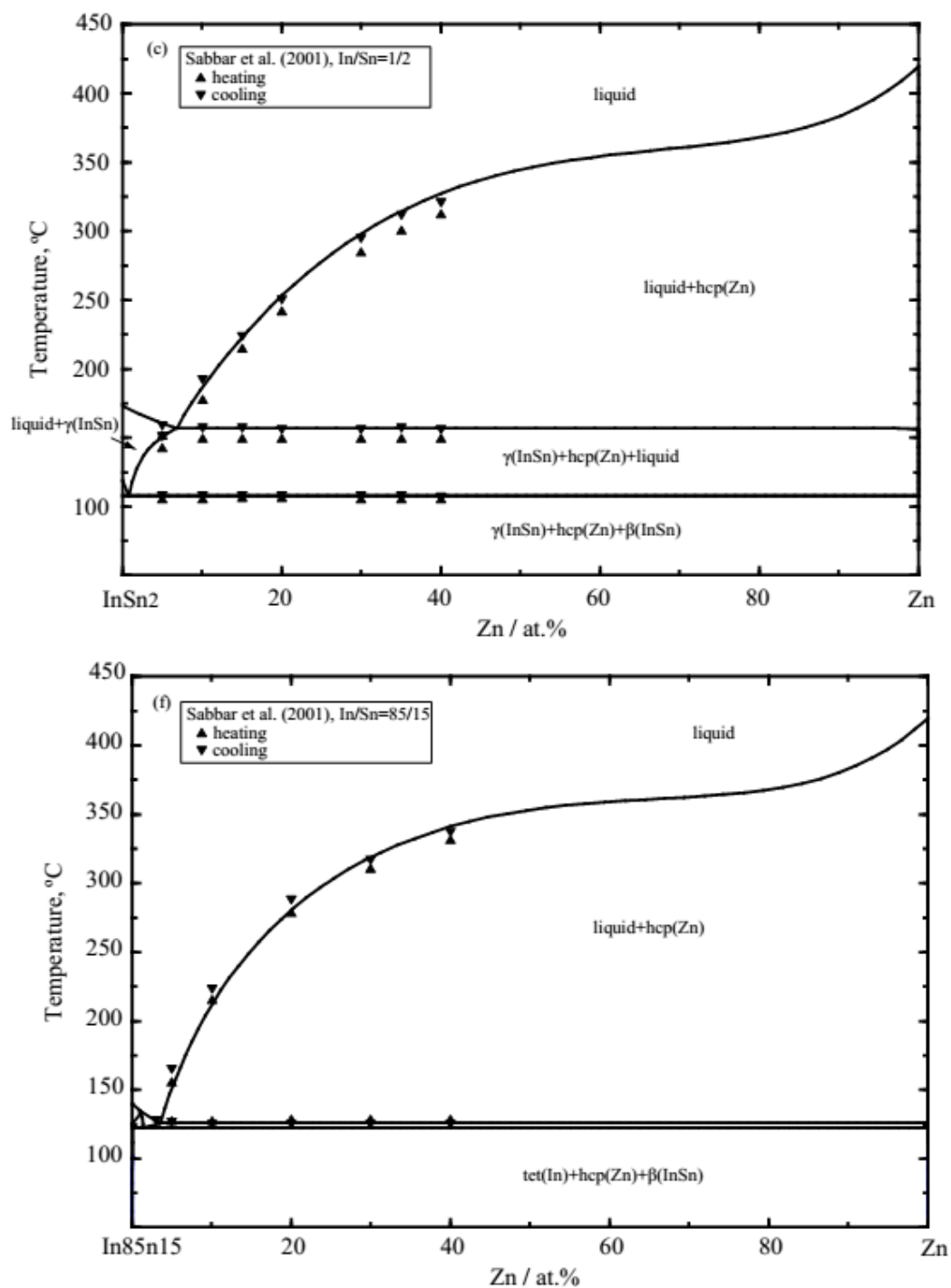
Figure 6.24 Calculated isoplethal sections of the In-Sn-Zn ternary system for In/Sn molar ratios of (a) 5:95, (b) 15:85, (c) 1:2, (d) 52:48, (e) 2:1, and (f) 85:15 in comparison with the reported experimental data [77]

The calculated Scheil cooling simulations of alloys with the components of $(In15Sn85)_{1-x}Zn_x$ ($0 \leq x \leq 60$ at. %) using the present thermodynamic database show a reaction: liquid $\leftrightarrow \gamma$ (InSn) + β(InSn) + hcp(Zn) occurring at 106 $^{\circ}$C during the solidification process. This may due to the solidification of γ (InSn) with a large solid solubility range (~74 to 85 at. % Sn in Sn-In binary system) during the cooling process (as shown in Fig. 6. 24b), which changes the solidification behavior of liquid from equilibrium to Scheil-Gulliver status. This demonstrates that the signal reported by [77] can be due to this nonequilibrium reaction. The calculated ternary isoplethal sections at 10 In (at. %), 9 Zn (wt. %) and 6 Zn (wt. %) are shown in Fig. 6.25 (a)-(c) in comparison with the experimental data [76, 93].

The calculated mixing enthalpies of the ternary liquid phase for the In/Sn molar ratio of 1:1 and In/Zn molar ratio of 52:48 and 1:1 at various temperatures are shown in Fig. 6.26 (a) and (b) along with experimental data [44, 79, 81]. The calculated partial molar enthalpy of mixing of Zn in liquid In-Sn-Zn alloys at 500 $^{\circ}$C in comparison with the experimental data [44] is shown in Fig. 6.27. The calculated activity of Zn in the liquid phase (liquid standard state) for the In/Sn molar ratios of 1:3, 1:1 and 3:1 are shown in Fig. 6.28 along with experimental data from Nakamura *et al.* [80]. Fig. 6.29 shows the calculated activity of Zn in the liquid phase (liquid standard state) at 3 Zn (at. %) compared with the experimental data reported by Moser [78]. The calculated liquidus projection of the In-Sn-Zn ternary system is shown in Fig. 6.30. The calculated invariant reactions in the liquidus projection of the In-Sn-Zn ternary system are listed in Table 6.9. All the optimized ternary thermodynamic parameters of In-Sn-Zn ternary system in the present work are listed in Tables 6.2 and 6.6.
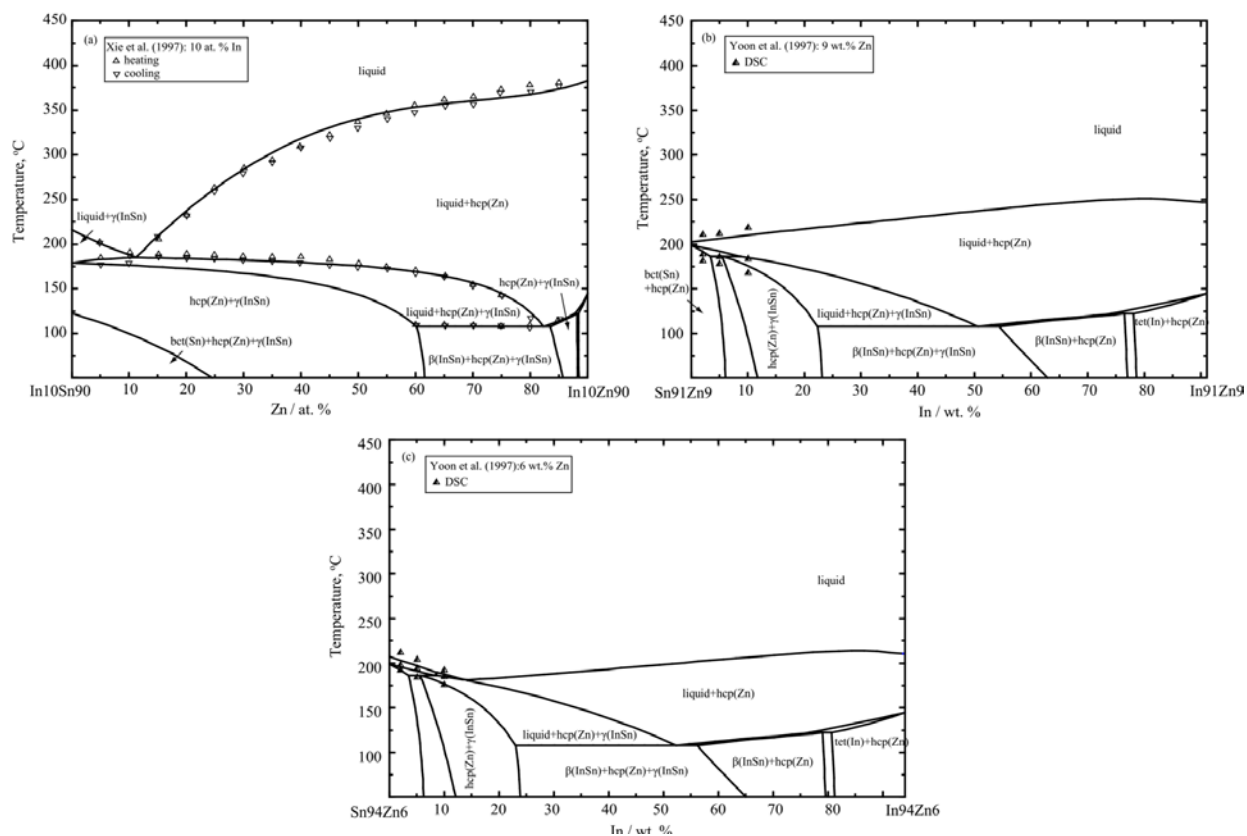
Figure 6.25 Calculated isoplethal sections of the In-Sn-Zn system at constant (a) 10 In (at. %), (b) 9 Zn (wt. %), (c) 6 Zn (wt. %) in comparison with the reported experimental data [76, 93].
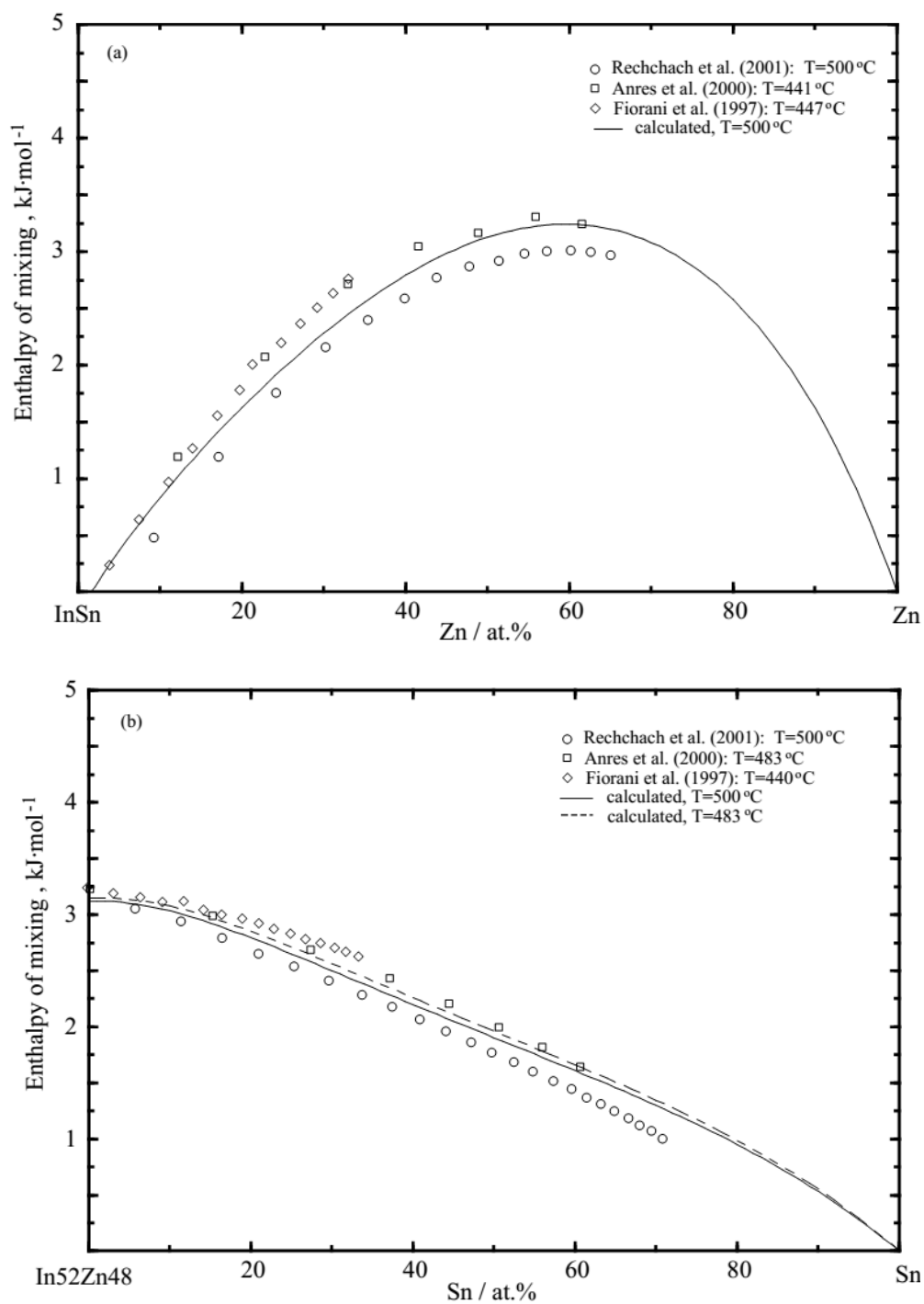
Figure 6.26 Calculated mixing enthalpies of ternary liquid In-Sn-Zn alloys (a) with the In/Sn molar ratio of 1:1, and (b) the In/Zn molar ratio of 52:48 and 1:1 at various temperatures along with the reported experimental data [44, 79, 81]
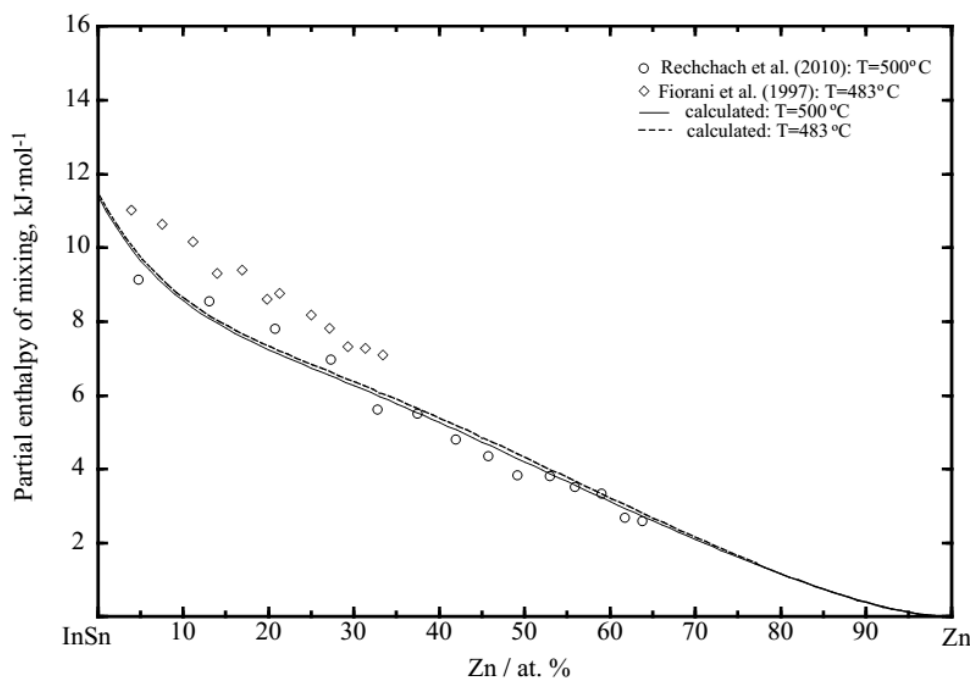
Figure 6.27 Calculated partial molar enthalpy of mixing of Zn in liquid In-Sn-Zn alloys at 500 °C compared with the reported experimental data [44]
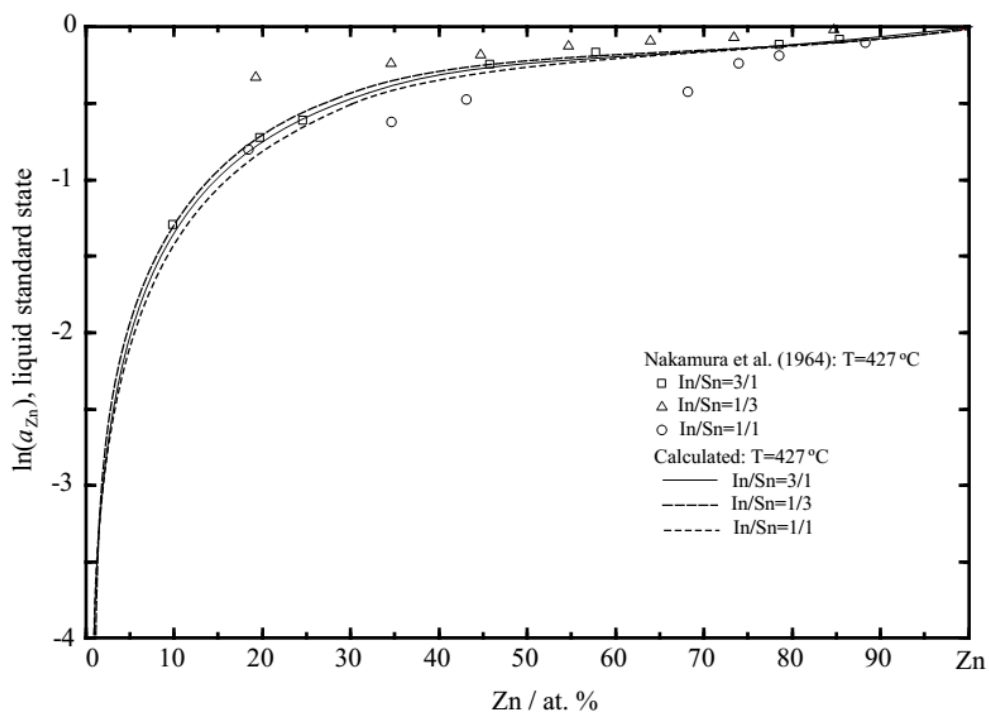
Figure 6.28 Calculated activity of Zn in the In-Sn-Zn liquid phase with the In/Sn molar ratios of 1:3, 1:1 and 3:1 along with the reported experimental data [80]
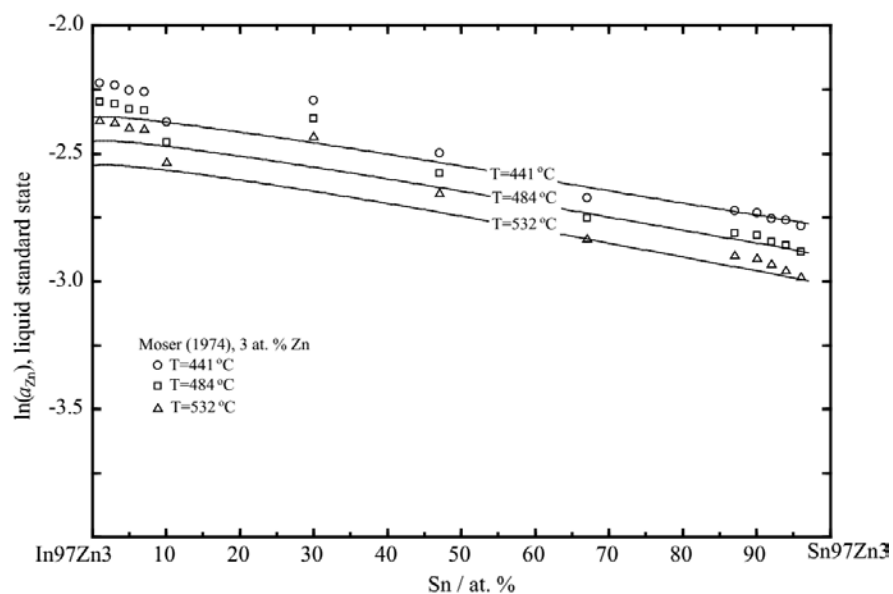
Figure 6.29 Calculated activity of Zn in the In-Sn-Zn liquid phase at constant 3 Zn (at. %) in comparison with the reported experimental data [78]
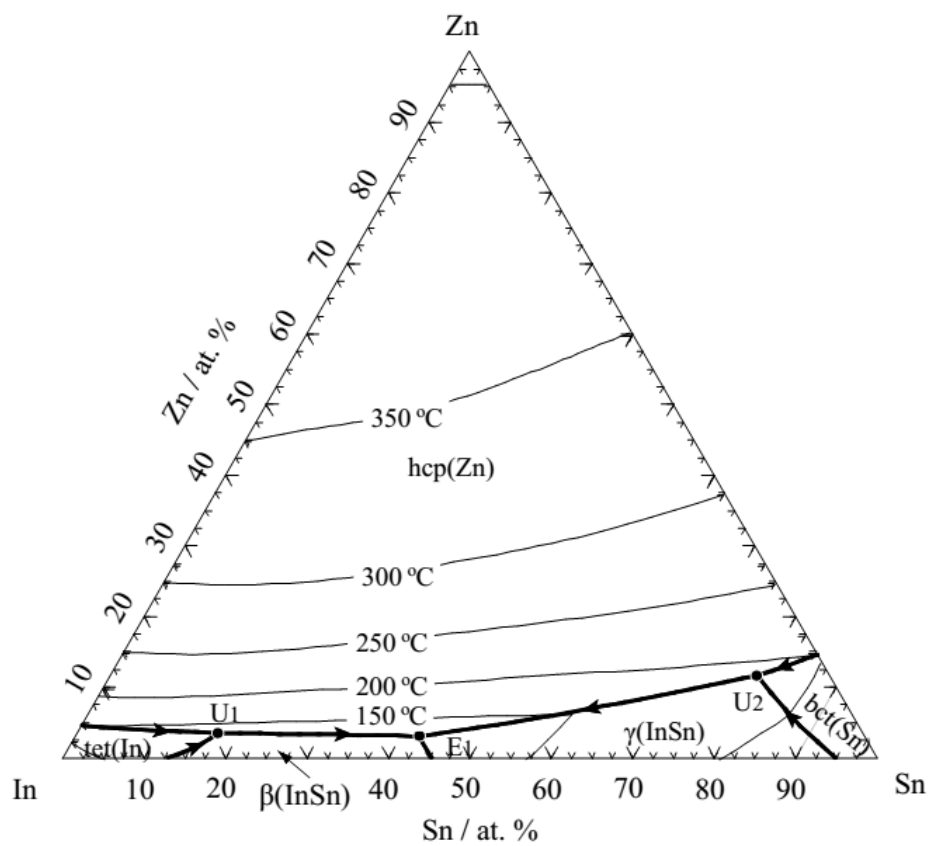
Figure 6.30 Calculated liquidus projection of the In-Sn-Zn ternary system

Table 6.9 Calculated invariant reactions in the liquidus projection of the In-Sn-Zn ternary system

Label	Temperature (^{o}C)	Reaction	Composition of liquid (at. %)		
			In	Zn	Sn
E1	107	$L \leftrightarrow \beta(InSn) + \gamma(InSn) + hcp(Zn)$	54.78	3.07	42.16
U1	121	$L + tet(In) \leftrightarrow \beta(InSn) + hcp(Zn)$	79.10	3.52	17.38
U2	186	$L + bct(Sn) \leftrightarrow \gamma(InSn) + hcp(Zn)$	8.88	11.68	79.44

The Mg-In-Zn and Mg-Sn-In-Zn systems

No experimental phase diagram and thermodynamic data exist for the Mg-In-Zn ternary system. According to the similar Mg-Sn-In and Mg-Sn-Zn systems, one's should expect some limited ternary solubility for In in Mg-Zn binary compounds and for Zn in Mg-In binary compounds. Mg-Zn and Mg-In liquids have quite similar negative deviations from ideal mixing while In-Zn liquid has a nearly ideal mixing behavior. In the present work, the thermodynamic properties of the ternary liquid were extrapolated with the symmetric Toop-like [88] technique within the MQMPA model. Our calculated isothermal sections of the Mg-In-Zn ternary system at 300 and 350 ^{o}C are shown in 6.31. The calculated liquidus projection of the Mg-In-Zn ternary system is shown in Fig. 6.32 and the calculated invariant reactions are listed in Table 6.10.

No experimental data exist for the Mg-Sn-In-Zn quaternary system. Consequently, our thermodynamic optimization was performed by extrapolating the thermodynamic parameters employed for the bounding subsystems and no additional model parameter was used. The calculated isothermal sections of Mg-Sn-Zn with 1 and 3 wt. % In at 300 ^{o}C and 400 ^{o}C are shown in Fig. 6.33.

Table 6.10 Calculated invariant reactions in the liquidus projection of the Mg-In-Zn ternary system

Label	Temperature (°C)	Reaction	Composition of liquid (at. %)		
			Mg	Zn	In
e1	377	$L \leftrightarrow fcc + MgZn_2$	61.90	12.46	25.64
E1	147	$L \leftrightarrow tet(In) + MgZn_2 + Mg_2Zn_{11}$	0.45	4.25	95.00
E2	366.3	$L \leftrightarrow hcp + MgZn_2 + Mg_2Zn_3$	67.46	21.24	11.30
U1	145	$L + hcp(Zn) \leftrightarrow Mg_2Zn_{11} + MgZn_2 + tet(In)$	0.41	4.68	94.91
U2	153	$L + fcc \leftrightarrow tet(In) + MgZn_2$	2.35	2.53	95.12
U3	366.4	$L + fcc \leftrightarrow hcp + MgZn_2$	67.07	19.61	13.32
U4	349	$L + Mg_{51}Zn_{20} \leftrightarrow hcp + Mg_2Zn_3$	71.05	28.42	0.53
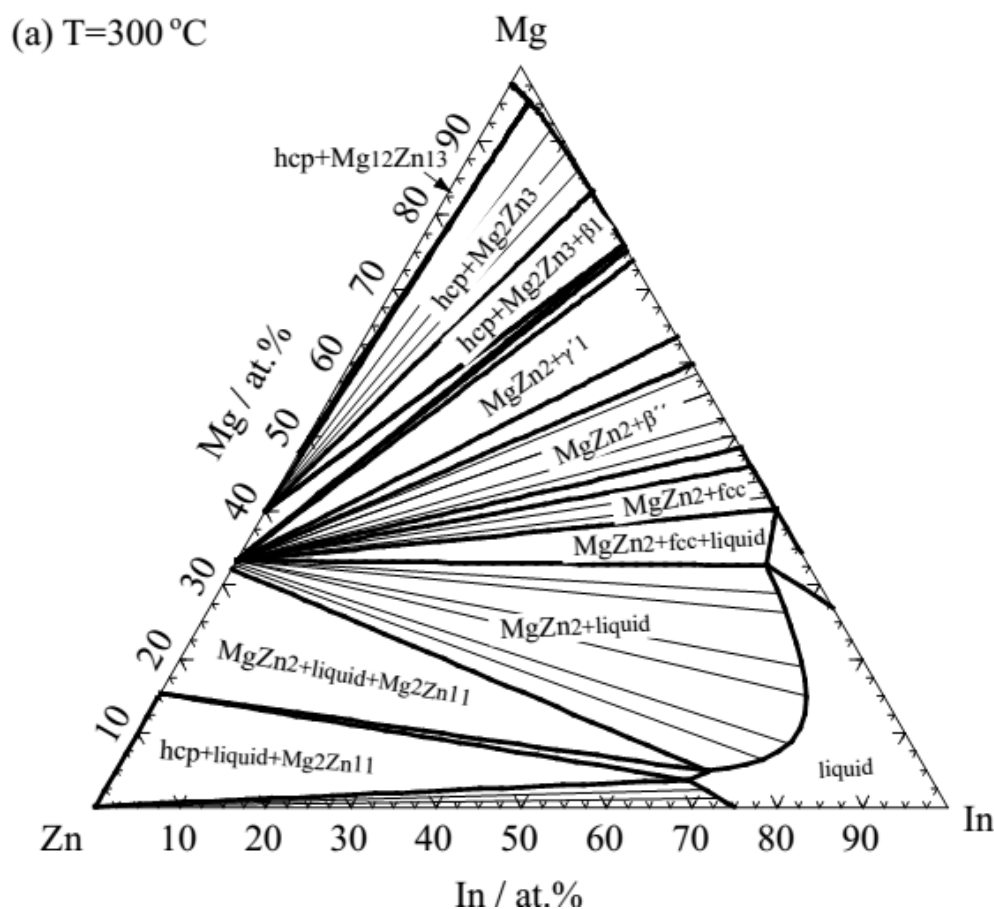
Figure 6.31 Calculated isothermal sections at (a) 300 °C, and at (b) 350 °C of the Mg-In-Zn ternary system
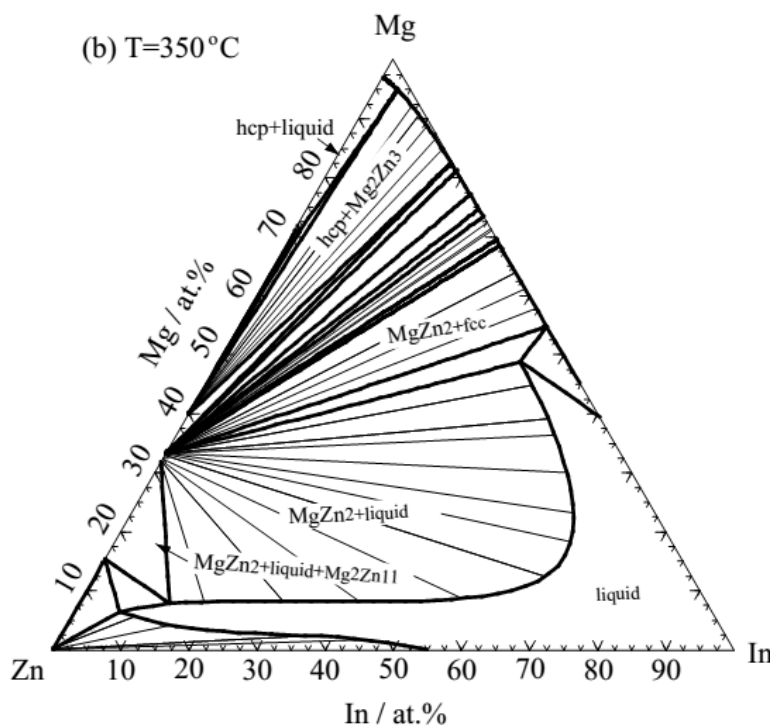
Figure 6.31 (Continued) Calculated isothermal sections at (a) 300 °C, and at (b) 350 °C of the Mg-In-Zn ternary system
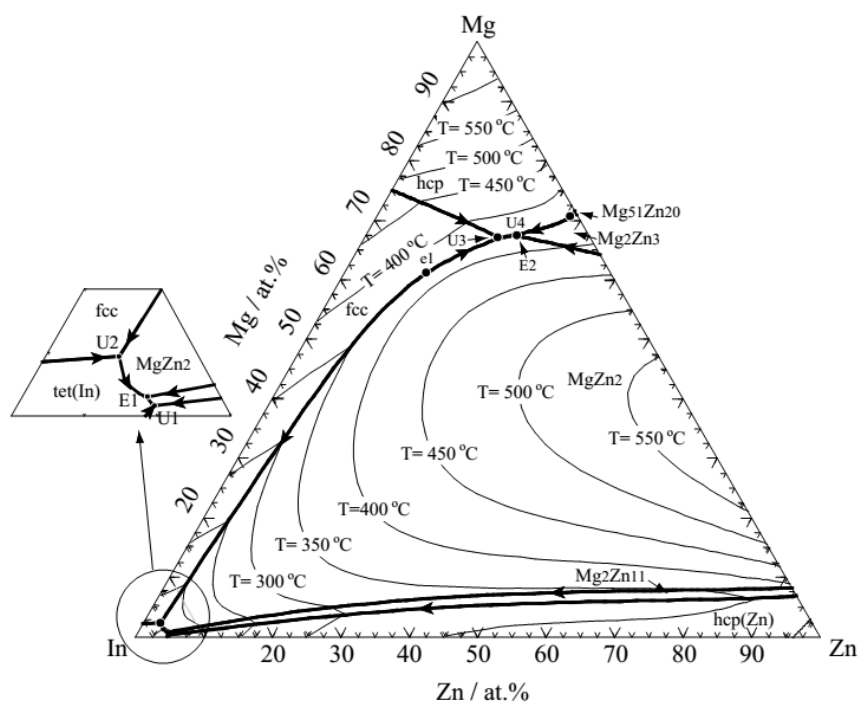
Figure 6.32 Calculated liquidus projection of the Mg-In-Zn ternary system
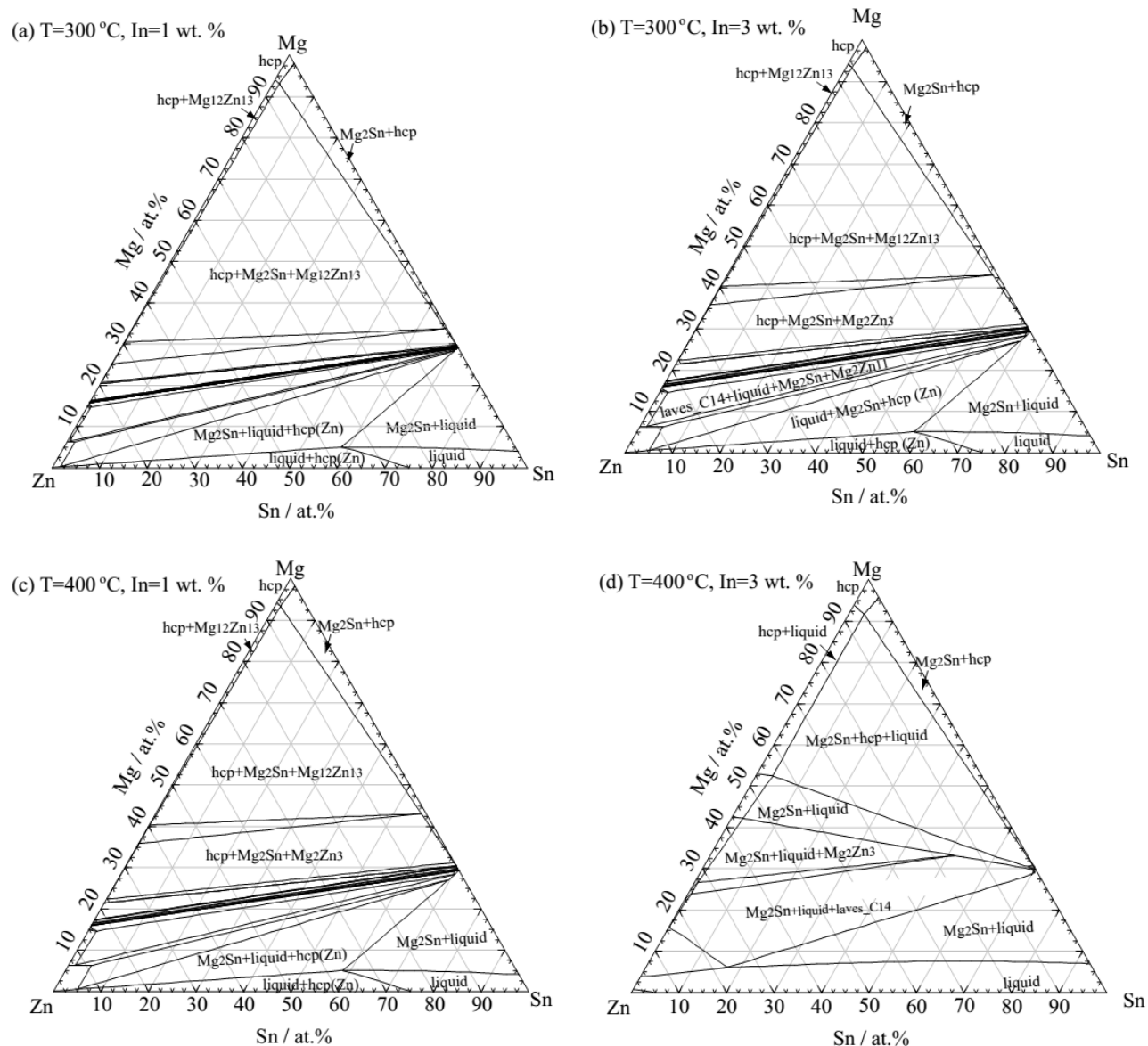
Figure 6.33 Calculated isothermal sections of Mg-Sn-Zn with 1 and 3 In (wt. %) at 300 °C and 400 °C

6.6 Conclusions and discussions

Phase equilibria in the Mg-rich portion of the Mg-Sn-In ternary system at 415 °C and 330 °C, and the Mg-Sn-In ternary isoplethal sections at 10 Sn and 5 In (at. %) were investigated in the present work. No evidence of the existence of ternary compounds was found in the present work. The present results show that the solid solubility of In in the Mg_2Sn phase and of Sn in the Mg-In

binary intermetallic phases are very limited. In consideration of the high solid solubility of In in the hcp (Mg) terminal phase (Fig. 6.3), all the added In should dissolve into the hcp (Mg) phase upon addition to Mg-Sn alloys. A critical thermodynamic optimization of the Mg-Sn-In ternary system was carried in the present work based in part on the data obtained in the present experimental measurements. Hence, a systematic study of the relationship among the phase equilibria, the solidification process and the microstructures of the Mg-Sn based alloys with In addition can be carried out with the present thermodynamic database.

Phase equilibria in the Mg-rich portion of the Mg-Sn-Zn ternary system at 300 $^{\circ}$C have been determined in the present work. Same as for the Mg-Sn-In ternary system, no stable ternary compound was found in this isothermal section. There is a limited solubility in all the terminal sub-binary compounds which is in agreement with the previous experimental data from Godecke and Sommer [69] and Gladyshevsky and Cherkashin [72] within the experimental error limits. The ternary isoplethal section Mg-Sn-Zn at constant 10 Sn (at. %) has been determined in the present work using DSC measurements. All the reported experimental results from previous investigators and from the present work are in a reasonable agreement. A self-consistent database of parameters of thermodynamic models for phases in the Mg-Sn-Zn ternary system was obtained in the present work after a critical evaluation of all the available experimental data. The present optimization results are in more global agreement with all the experimental data in comparison with the previous optimization performed by Meng *et al.*[74] using an "associate model" with the introducing of the associate or molecule of Mg_2Sn into the liquid phase. For many optimized binary systems, the optimization results are mathematically very similar with the two models of MQM and associate model. However, the associate model does not correctly predict the properties of ternary and high ordered system, which was discussed and proved by Kang and Pelton [94].

All available experimental data for the Mg-In binary system were critically evaluated. A thermodynamic optimization of the phase diagram was carried out for the first time. As shown in the previous section, the present optimization reproduces all available experimental data very well. Unfortunately, no thermodynamic data exist for the intermetallic phases and new experiments are clearly needed to fully validate the present optimized results. A critical evaluation of all available experimental data and a thermodynamic re-optimization of the Zn-In and In-Sn binary systems were carried by using the MQMPA for the liquid phase.

A self-consistent thermodynamic database for the Mg-Sn-In-Zn quaternary system has been constructed in the present work, which provides an efficient and convenient way to study and develop new Mg based alloys. As shown in Fig. 6.33, a small addition of In toMg-Zn-Sn alloys a small addition of In to Mg-Zn-Sn alloys will increase the In content of Mg (hcp), which will improve the strength of the alloys.

Acknowledgement

References

[1] K.U. Kainer, F. Kaiser, Magnesium alloys and technology, Wiley Online Library, 2003.

[2] I. Polmear, Magnesium alloys and applications, Mater. Sci. Tech. Lond., 10 (1994) 1-16.

[3] X. Gao, J. Nie, Characterization of strengthening precipitate phases in a Mg–Zn alloy, Scripta Mater., 56 (2007) 645-648.

[4] M.A. Gibson, X. Fang, C.J. Bettles, C.R. Hutchinson, The effect of precipitate state on the creep resistance of Mg–Sn alloys, Scripta Mater., 63 (2010) 899-902.

[5] D.H. Kang, S.S. Park, Y.S. Oh, N.J. Kim, Effect of nano-particles on the creep resistance of Mg-Sn alloys, Mater. Sci. Eng. A, 449-451 (2007) 318-321.

[6] K. Van der Planken, Solution hardening of lead single crystals at liquid air temperature, J. Mater. Sci., 4 (1969) 927.

[7] C.L. Mendis, C.J. Bettles, M.A. Gibson, C.R. Hutchinson, An enhanced age hardening response in Mg–Sn based alloys containing Zn, Mater. Sci. Eng. A, 435-436 (2006) 163-717.

[8] C.L. Mendis, C.J. Bettles, M.A. Gibson, S. Gorsse, R. Hutchinson, Refinement of precipitate distributions in an age-hardenable Mg–Sn alloy through microalloying, Phil. Maga. Lett., 86 (2006) 443-456.

[9] A. Becerra, M. Pekguleryuz, Effects of zinc, lithium, and indium on the grain size of magnesium, J. Mater. Res., 24 (2009) 1722-1729.

[10] N. Saunders, A.P. Miodownik, CALPHAD (Calculation of Phase Diagrams): A Comprehensive Guide, Pergamon, 1998.

[11] H. Ohtani, K. Ishida, Application of the CALPHAD method to material design, Thermochim. Acta, 314 (1998) 69-77.

[12] W. Hume-Rothery, G.V. Raynor, The constitution of the magnesiym-rich alloys in the systems Al-Mg, Ga-Mg, In-Mg, and Tl-Mg, J. Inst. Met., 63 (1938) 204-216.

[13] W. Hancke, Alloys of magnesium with gallium, indium and thallium, Naturwissenschaften, 26 (1938) 577-578.

[14] G.V. Raynor, The constitution of the In-Mg alloys in the region 20 to 50 atomic precent of In, Trans. Fara. Soci., 44 (1948) 15-28.

[15] J. Graham, G.V. Raynor, Indium-rich indium-magnesium and indium-lithium alloys, Philosophical Magazine, 2 (1957) 1354-1363.

[16] N. Ino, M. Hirabayashi, S. Ogawa, X-ray and thermal analysis of the ordered-disordered transition in Mg-In alloys, Trans. Jpn. Inst. Met., 6 (1965) 172-178.

[17] K. Hiraga, M. Koiwa, M. Hirabayashi, Constitution of the indium-rich portion of the indium-magnesium system, J. Less-common Met., 15 (1968) 109-118.

[18] K.M. Pickwick, W.A. Alexander, E.H. Gamble, The constitution of In-Mg alloys containing 23-100 atomic pre cent Indium, Canad. J. Chem., 47 (1969) 3417-3427.

[19] P. Feschotte, The Mg-In binary system, J. Less-common Met., 46 (1976) 51-54.

[20] Y. Watanabe, Consititution og the Mg-In system near the composition of Mg3In and phase transition of beta1 phase, Acta Metall., 23 (1975) 691-696.

[21] A.A. Nayeb-hashemi, J.B. Clark, The In-Mg system, Bulletin of Alloy phase diagrams, 6 (1985) 149-160.

[22] K. Ehrlich, Ludwig-maximilians university, Munchen, 1965.

[23] Z. Moser, R. Castanet, EMF and calorimeteric measurements of the Mg-In liquid solutions, Czech. Conf. Calorimetry, Inst, Inorg. Chem., Czech. Acad. Sci. Prague, A3 (1977) 1-4.

[24] H. Slaby, J. Terpilowski, Thermodynamic properties of liquid Mg-In solutions, Bull. Acad. Polon. Sco., XIII (1965) 319-322.

[25] J. Terpilowski, H. Slaby, Thermodynamic properties of liquid Mg-In solutions, Roczniki, Chem. Ann. Soc. Chim. Polon, 41 (1967) 1845-1855.

[26] H. Nebell, Thermodynamic properyies of liquid Mg-Pb, Mg-In and Mg-Ga alloys, Rev. Roum. Chim., 15 (1970) 59-65.

[27] Z. Moser, R. Castanet, EMF and calorimetric measurements on the Mg-In liquid solutions, Metall. Mater. Trans. B, 10 (1979) 483-487.

[28] G. Chirulli, D. Ferro, V. Piacente, Magnesium activity in liquid In-Mg alloy from vapour pressure measurements, Thermochim. Acta, 62 (1983) 171-177.

[29] B. Predel, T. Godecke, Das Dreistoffsystem zinn-indium-thallium, Z. Metallkd., 66 (1975) 654.

[30] D.S. Evans, A. Prince, Materials research society symposium proceeding 19, Elsecier, North-holland, 1983, pp. 389.

[31] A.B. Kaplun, Phase transformations near the liquidus temperature in the indium-tin system, Teplofiz. Svoistva Rastvorov., 1983, pp. 65-69.

[32] Z. Wojtaszek, H. Kuzyk, Phase digram of the In-Sn system in the range 60-100 atomic % tin, Zeszyty Naukowe Uniwersytety Jagiellonskiego, Prace Chemiczne, 19 (1974) 281-287.

[33] Z. Wojtaszek, H. Kuzyk, Phase digram of the In-Sn system in the range 0-60 atomic per cent of tin, Zeszyty Naukowe Uniwersytety Jagiellonskiego, Prace Chemiczne, 21 (1976) 27-32.

[34] T. Heumann, O. Alpaut, The phase diagram of In-Sn, J. less-common Met., 6 (1964) 108-117.

[35] O. Cakir, O. Alpaut, thermodynamic properties of solid In-Sn alloys, J. less-common Met., 141 (1988) 11-27.

[36] B.-J. Lee, C.-S. Oh, J.-H. Shim, Thermodynamic assessments of the Sn-In and Sn-Bi binary systems, J. Electron. Mater., 25 (1996) 983-991.

[37] V. Vassiliev, Y. Feutelais, M. Sghaier, B. Legendre, liquid state electrochemical study of the system In-Sn, Thermochim. Acta, 315 (1998) 129-134.

[38] J. Terpilowski, E. Prezdziecka-Mycielska, Thermodynamic properties of liquid metallic solutions. IV. The system In-Sb, Archiv. Hutnictwa, 5 (1960) 281-290.

[39] D. Zivkovic, A. Mitovski, L. Balanovic, D. manasujevic, Z. Zivkovic, Thermodynamic analysis of liquid In-Sn alloys using Oelsen calorimetry, J. Therm. Anal. Calorim., 102 (2010) 827-830.

[40] F.E. Wittig, P. Scheidt, Energetics of metallic systems. XIV. Heats of mixing in the binary systems of indium and thallium with tin and lead, Z. Physikali. Chem., 28 (1961) 120-142.

[41] O.J. Kleppa, A calorimetric investigation of some binary and ternary liquid alloys rich in tin, J. Phys. Chem. B, 60 (1956) 842-846.

[42] A. Yazawa, T. Kawashima, K. Itagaki, Measurements of heats of mixing in molten alloys with the adiabatic calorimeter, Nippon Kinzoku Gakkaishi, 32 (1968) 1281-1287.

[43] J.P. Bros, M. Laffitte, Enthalpies of formation of In-Sn alloys in the liquid state, J. Chem. Thermodyn., 2 (1970) 151-152.

[44] M. Rechchach, A. Sabbar, H. Flandorfer, H. Ipser, Enthalpies of mixing of liquid In-Sn and In-Sn-Zn alloys, Thermochim. Acta, 502 (2010) 66-72.

[45] O. Alpaut, T. Heumann, Thermodynamic properties of solid indium-tin alloys, Acta Metall., 13 (1965) 543-548.

[46] A. D. Pelton, P. Chartrand, The modified quasi-chemical model: Part II. Multicomponent solutions, Metall. Mater. Trans. A, 32 (2001) 1355-1360.

[47] A. D. Pelton, S. A. Degterov, G. Eriksson, C. Robelin, Y. Dessureault, The modified quasichemical model I-binary solutions, Metall. Mater. Trans. B, 31 (2000) 651-659.

[48] J. Dutkiewicz, W. Zakulski, The In-Zn system, Bulletin of Alloy phase diagrams, 5 (1984) 284-289.

[49] C.L. Wilson, E.A. Peretti, Zn-In alloy system, Ind. Eng. Chem. Process des. Develop., 26 (1936) 204-205.

[50] V.S. Valentiner, On the In-Zn and In-Cd system, Z. Metallkd., 35 (1943) 250-253.

[51] F.N. Rhines, A. Grobe, Constitution of the system In-Zn, Trans. Metall. Soci. AIME, 156 (1944) 253-262.

[52] W.T. Svirbely, S.M. Selis, A thermodynamic study of the Zn-In system, J. Am. Chem. Soc., 75 (1953) 1532-1535.

[53] W. Oelsen, E.A. Zuhlke, The calorimetry and thermodynamics of the In-Zn system, Archiv. Eisenhuettenwesen, 27 (1956) 743-752.

[54] R.W. Bohl, V.D. Hildebrandt, Electrode potential studies of liquid-solid equilibrium in Zn-Cd and Zn-In alloys, J. Am. Chem. Soc., 79 (1957) 2711-2727.

[55] Z. Moser, Determination of the thermodynamic properties in Zn-In liquid solutions, Rev. Roum. Chim., 16 (1971) 327-341.

[56] J. Dutkiewicz, Z. Moser, Bull. Acad. Polon. Sci. Tech. Sco., 31 (1983) 27.

[57] G.S. Nishimura, R.S. Fidler, R.T. M., S.R. William, Classification of the indium-zinc eutectic, Canad. Metall. Quart., 8 (1969) 319-322.

[58] O.J. Kleppa, Thermodynamic analysis of binary liquid alloys of Group IIB metals. I. The systems zinc-cadmium, zinc-gallium, zinc-indium, and zinc-tin, Acta Metall., 6(1958) 225-232.

[59] F.E. Wittig, E. Muller, The heats of mixing of the binary liquid systems of Znic and cadmium with indium and thallium, Z. Metallkd., 51 (1960) 226-238.

[60] W.G. Jung, Activity measurement in liquid Zn-(In,Sn) alloy using EMF method, Korean J. Mater. Res., 15 (2005) 47-54.

[61] D. Ferro, B.M. Nappi, V. Piacente, P.L. Cignini, Znic activity in In-Zn alloys measured by the Knudsen Torsion-effusion method, High Temp. Sci., 10 (1978) 131-142.

[62] H. Hagiwara, S. Sugino, H. Fujiwara, Thermodynamic properties of liquid In-Zn solutions, Bulletin University Osaka, 23 (1974) 41-50.

[63] B.-J. Lee, Thermodynamic assessments of the Sn-Zn and In-Zn binary systems, CALPHAD, 20 (1996) 471-480.

[64] V. Kinzhibalo, Ternary systems of Magnesium with elements of groups IIIA-VA, Fazov. Rano. Metall. Splava., 6 (1981) 73-78.

[65] Z. Moser, R. Castanet, Thermodynamic studies on liquid Mg-In-Sn ternary solutions, INKA-confi.-79-003-023, IAEA-Sm-236/35, 1979, pp. 263-271.

[66] W. Zakulski, Z. Moser, F. Sommer, Thermodynamic study of liquid Mg-In-Sn alloys, J. Phase Equilib. Diff., 18 (1997).

[67] B. Otani, Constitution of the phase equilibrium diagram of the magne-sium-zinc-tin system, Tetsu to Hagane, 19 (1933) 566-574.

[68] R. Agarwal, S.G. Fries, H.L. Lukas, G. Petzow, F. Sommer, T.G. Chart, G. Effenberg, The Mg-Zn system, Z. Metallkd., 83 (1992) 216-223.

[69] T. Godecke, F. Sommer, Stable and metastable phase equilibria in MgZn$_2$-Zn and Mg$_2$Sn-MgZn$_2$-Sn-Zn alloys, Z. Metallkd., 85 (1994) 683-691.

[70] M. Mingolo, B. Arcondo, E. Nassif, H. Sirkin, Changes in the glass forming ability of Mg-Zn-Sn alloys due to the presence of an intermetallic compound, Z. Naturforsch. A, A41 (1986) 1357-1360.

[71] H. Sirkin, N. Mingolo, E. Nassif, B. Arcondo, Increase of the glass-forming composition range of Mg-based binary alloys by addition of tin, J. Non-Cryst. Solids, 93 (1987) 323-330.

[72] E.I. Gladyshevsky, E.E. Cherkashin, Solid solutions based on metallic compounds, Zh. Neorg. Khim., 1 (1959) 1394-1401.

[73] P. Ghosh, M.D. Mezbahul-Islam, M. Medraj, Critical assessment and thermodynamic modeling of Mg-Zn, Mg-Sn, Sn-Zn and Mg-Sn-Zn system, CALPHAD, 36 (2012) 28-43.

[74] F. Meng, J. Wang, L. Liu, Z. Jin, Thermodynamic modeling of the Mg-Sn-Zn ternary system, J. Alloy. Comp., 508 (2010) 570-581.

[75] S.W. Yoon, J.R. Soh, H.M. Lee, B.-J. Lee, Thermodynamics-aided alloy design and evaluation of Pb-free solder Sn-Bi-In-Zn system, Acta Mater., 45 (1997) 951-960.

[76] Y. Xie, H. Schicketanz, A. Mikura, The In-Sn-Zn system, Berich. Bunsen-Gesellschaft Physi. Chem., 102 (1998) 1334-1338.

[77] A. Sabbar, A. Zrineh, M. Gambino, J.P. Bros, B. Arcondo, Contribution a l'etude du diagramme d'equilibre des phases du systeme ternaire indium-etain-zinc, Thermochim. Acta, 369 (2001).

[78] Z. Moser, Thermodynamic Studies of the Zn-Sn-In System in Dilute Liquid Solutions Z. Metallkd., 65 (1974) 106-111.

[79] J.M. Fiorani, C. Naguet, J. Hertz, A. Bourkba, L. Bouirden, Z. Metallkd., 88 (1997) 711.

[80] Y. Nakamura, M. Shimoji, K. Niwa, Thermodynamic studies on liquid ternary Zn-In-Sn solutions, Trans. Jpn. Inst. Met., 5 (1964) 28-32.

[81] P. Anres, M. Alaoui-elbelghiti, M. Gambino, J.P. Bros, Enthalpy of formation of the In-Sn-Zn liquid system, Thermochim. Acta, 346 (2000) 49-56.

[82] Y. Xie, Z.Y. Qiao, A. Mikula, The Sn-In-Zn system, CALPHAD, 25 (2001) 3-10.

[83] Y. Cui, X.J. Liu, I. Ohnuma, R. kainuma, H. Ohtani, K. Ishida, Thermodynamic calculation of the In-Sn-Zn ternary system, J. Alloy. Comp., 320 (2001) 234-241.

[84] C.W. Bale, P. Chartrand, S.A. Degterov, G. Eriksson, K. Hack, R. Ben Mahfoud, J. Melancon, A.D. Pelton, S. Petersen, Factage thermochemical software and databases, CALPHAD, 26 (2002) 189-228.

[85] I.-H. Jung, D.H. Kang, W.J. Park, N.J. Kim, S.H. Ahn, Thermodynamic modeling of the Mg-Si-Sn system, CALPHAD, 31 (2007) 192-200.

[86] P.J. Spencer, Mg-Zn system, database, CRCT (Ed.), Montreal, 2006.

[87] Y.-B. Kang, A.D. Pelton, P. Chartrand, C.D. Fuerst, Critical evaluation and thermodynamic optimization of the Al-Ce, Al-Y, Al-Sc and Mg-Sc binary systems, CALPHAD, 32 (2008) 413-422.

[88] A.D. Pelton, A general "geometric" thermodynamic model for multicomponent solutions, CALPHAD, 25 (2001) 319-328.

[89] M. Hillert, The compound energy formalism, J. Alloy. Comp., 320 (2001) 161-176.

[90] A.T. Dinsdale, SGTE data for pure elements, CALPHAD, 15 (1991) 317-425.

[91] H. Kopp, Investigations of the specific heat of solid bodies, Philo. Trans. Roy. Soci. A, 155 (1865) 71-202.

[92] P. Villars and K. Cenzual, (2007). Pearson's crystal data, crystal structure database for inorganic compounds. Materials Park (OH): ASM International.

[93] S.W. Yoon, J.R. Soh, B.J. Lee, H.M. Lee, Design and reliability of solders and solders interconnections, in: R.K. Mahidhara, D.R. Frear, S.M.L. Saty, K.L. Murty, P.K. Liaw, W. Winterbottom (Eds.), Min. Met. Mater. Soc., 1997, pp. 121.

[94] Y.-B. Kang, A.D. Pelton, Modeling short-range ordering in liquids: The Mg-Al-Sn system, CALPHAD, 34 (2010) 180-188.

CHAPITRE 7   ARTICLE 4: EXPERIMENTAL AND THERMODYNAMIC STUDY OF THE MG-SN-AG-IN QUATERNARY SYSTEM

Jian Wang[a], Pierre Hudon[b], Dmytro Kevorkov[c], Patrice Chartrand[a*], In-Ho Jung[b], Mamoun Medraj[c]

[a]*Center for Research in Computational Thermochemistry (CRCT), Dept. of Chemical Engineering, École Polytechnique, Montréal, Québec, Canada, H3C 3A7*

[b]*Department of Mining and Materials Engineering, McGill University, 3610 University Street, Montreal, Quebec, H3A 0C5, Canada*

[c]*Department of Mechanical Engineering, Concordia University, 1455 De Maisonneuve Blvd. West, Montreal, Quebec, H3G 1M8, Canada*

* Corresponding author. Center for Research in Computational Thermochemistry (CRCT), Dept. of Chemical Engineering, École Polytechnique, Montréal, Québec, Canada, H3C 3A7. Tel: +1 514 340-4711 ext. 4089; fax: +1 514 340-5840. E-mail address: patrice.chartrand@polymtl.ca

Abstract

Phase equilibria in the Mg-rich region of the Mg-Sn-Ag ternary system were determined by quenching experiments, differential scanning calorimetry (DSC), electron probe micro-analysis (EPMA), and X-ray diffraction (XRD) techniques. No ternary compounds were found in the studied isothermal sections. A critical evaluation of the available experimental data and a thermodynamic optimization of the Mg-Sn-Ag-In quaternary system were carried out using the CALPHAD (Calculation of Phase Diagrams) method. The Modified Quasichemical Model in the Pair Approximation (MQMPA) was used for the liquid solution, which exhibits a high degree of short-range order. The solid phases were modeled with the Compound Energy Formalism (CEF). All available and reliable experimental data were reproduced within experimental error limits. A self-consistent thermodynamic database was constructed for the Mg-Sn-Ag-In quaternary system, which can be used as a guide for Mg-based alloys development.

7.1 Introduction

Magnesium alloys, with a density around 1.74 g/cm^3 which is nearly 1.6 and 4.5 times less dense than aluminum alloys and steel, is an exceptionally lightweight structural materials. The low density of magnesium alloys is a strong driving force for their applications in the transportation industry with the associated reductions in weight of vehicles and fuel consumption. Magnesium and its alloys have some advantageous properties as high thermal conductivity, high dimensional stability, high damping characteristics, high machinability, and they are also completely recyclable [1], which makes them suitable for automobile and computer parts, aerospace components, and household equipment parts. Up to now, several series of magnesium alloys have been developed for different applications, such as Mg-Al based, Mg-Zn based, Mg-RE based alloys. Unfortunately, most of these series have a number of undesirable properties (especially at evaluated temperatures) including poor corrosion resistance, poor creep resistance, and low wear resistance, which restricts their applications. The current trend, instead, is to improve Mg-based alloys for high temperature applications. To this end, Mg-Sn based alloys are good candidates because they have stable microstructures and good mechanical properties at high temperatures due to the high solubility of Sn in hcp Mg and to the possibility to precipitate a cubic second phase (Mg$_2$Sn) in the magnesium-rich matrix [2, 3]. Previous investigations [2-4] also indicate that Mg-Sn alloys with additional alloying elements have comparable or even better creep properties than AE42 alloys. Moreover, it is known that Sn can improve the corrosion resistance [5, 6]. Unfortunately, the behavior of Mg-Sn alloys after quenching require quite long time to reach the peak hardness, which is not practical for industrial applications [7]. Hence, it is necessary to improve the age hardening response and creep resistance behavior. Adding microalloying elements such as In, Ag, Ca, Li, Na, Zn, Sr and rare-earth elements can potentially achieve this goal [8-10]. Among these, In and Ag are of interest. Mendis *et al.* [8, 9], for example, proposed a qualitative thermo-kinetic criteria for choosing microalloying elements that can be applied to precipitation hardenable alloys. Indium was one of these elements and the authors [8, 9] were able to show that additions of In + Li to Mg-Sn alloys increase the number density by approximately one order of magnitude, resulting in 150 % hardening increment [9]. In

the case of Ag, its addition to Mg-Sn alloys can improve the mechanical properties [11, 12], greatly affects the grain refinement and corrosion resistance [13, 14], and bias the age hardening response which enhances the mechanical properties. Recently, Son *et al.* [15] also found that the addition of Ag leads to the formation of fine submicron-sized Mg-Ag particles, grain refinement, and weaker basal texture. The addition of In and Ag to Mg-Sn based alloys is thus quite beneficial.

In order to design new Mg-Sn-based alloys and to understand the relationships between their microstructures and mechanical properties, a better knowledge of the phase relations in Mg-Sn-based alloys is imperative. Obtaining such information by the sole mean of experimental techniques is cumbersome and costly. Fortunately, thermodynamic modeling of multi-component systems by the CALPHAD (Calculation of Phase Diagrams) [16] approach is a very efficient way to investigate phase equilibria [17]. Coupled phase-field calculations, *ab initio* calculations, and physical properties modeling permit one to estimate material properties [18]. In the present work, phase relations in the Mg-rich portion of the Mg-Sn-Ag ternary system were determined and the thermodynamic optimization of Mg-Sn-Ag-In quaternary system was carried out as part of a wider thermodynamic database development project for the Mg-X (X: Ag, Ca, In, Li, Na, Sn, Sr and Zn) multi-component system.

7.2   Literature review

7.2.1 The Ag-Mg system

The Ag-Mg system was critically reviewed by Nayeb-Hashemi and Clark [19]. There are five solid phases: fcc (Ag), hcp (Mg), bcc_B2, Ag_3Mg and $AgMg_3$ in the Ag-Mg system. The liquidus was first determined by Zemczuznyj [20] using thermal analysis; four invariant reactions: L $\leftrightarrow$ $AgMg_3$ + hcp (Mg), L $\leftrightarrow$ bcc_B2 + fcc (Ag), L $\leftrightarrow$ bcc_B2, and L + bcc_B2 $\leftrightarrow$ $AgMg_3$ were reported at 472 ^{o}C, 759 ^{o}C, 820 ^{o}C and 492 ^{o}C, respectively. Andrews and Hume-Rothery [21], Payne and Haughton [22], and Hume-Rothery and Butchers [23] determined the liquidus by thermal analysis and results are all in good agreement with each other. The $AgMg_3$ phase was first reported by Ageew and Kuznezow [24] by studying several alloys using metallographic methods and the structure was found to be hexagonal with 8 atoms per unit cell. However, results from later investigators [25-27] suggest that Mg_3Ag has a more complex structure. An X-ray

diffraction analysis performed by Prokofev *et al*. [28] demonstrated that $AgMg_3$ appear to be constituted of ε (bct) at high temperature and ε' (fcc) at low temperature. Later, Kolesnichenko *et al.* [29] rather found that the phase $AgMg_4$ must be the one described earlier as $AgMg_3$; according to them, its structure is hexagonal. Kolesnichenko *et al.* [29] also pointed out that the structural formula of ε' (fcc) is $Ag_{17}Mg_{54}$. Recently, phase equilibria in the Ag-Mg system were studied by Lim *et al.* [30] using DSC, XRD, and scanning electron microscopy (SEM); the existence of $AgMg_4$ and $Ag_{17}Mg_{54}$ was then confirmed. The phase relations and the polymorphic transition temperature of the ordering phase Ag_3Mg (fcc_L12) were determined by Gangulee and Bever [31].

The enthalpy of formation of the liquid phase at 1050 ^{o}C was measured by Kawakami [32] using calorimetric measurement method. The activity of Mg in the Ag-Mg liquid phase was determined by Gran *et al.* [33] by measuring the vapor pressure at 1300 and 1400 ^{o}C and with a gas equilibration technique at 1500 and 1600 ^{o}C. The enthalpies of formation of the bcc_B2 and fcc phases over the temperature range of 350 to 500 ^{o}C were measured by Kachi [34, 35] by performing emf measurements. The enthalpy of formation of the bcc_B2 phase between 39 and 54.8 Mg (at. %) at 0 ^{o}C was measured by Robinson and Bever [36] by tin-solution calorimetry. Later, Jena and Bever [37] measured the enthalpy of formation of the bcc_B2 phase at 78, 195 and 273 K with the same equipment. The partial molar enthalpy, entropy and free Gibbs energy changes of the bcc_B2 phase were derived by Trzebiatowski and Terpilowski [38] based on their emf results. The enthalpies of formation of the fcc and Ag_3Mg phases at 0 ^{o}C were determined by Gangulee *et al.* [31] by solution calorimeter. All the reported results of the enthalpy of formation of solid phases are in good agreement.

7.2.2 The Ag-In system

Weibke and Eggers [39] investigated the phase relations in the whole Ag-In binary system by means of thermal analysis, X-ray analysis, and photomicrography. According to their experimental results, the Ag-In phase diagram is constituted of six solid phases: fcc, bcc, γ (hcp), δ (Ag_5In_2), and ε and φ ($AgIn_3$). The bcc phase is only stable in the temperature range of 660 to 667 ^{o}C and possesses a narrow solid solubility field, from 25 to 29 at. % In. Hume-Rothery *et al.* [40] studied the solubility limit of indium in the terminal phase of fcc (Ag) with temperature. Owen and Roberts [41] determined carefully the fcc phase boundaries below the melting point

and their results are in good agreement with the ones reported by Weibke and Eggers [39] and Hume-Rothery [40]. Hellner [42] studied the crystal structure and the solubility range of the intermetallic phases with X-ray analysis and pointed out that an ordered phase, γ' (MgCd$_3$-type), exists in Ag$_3$In below 187 $^{\circ}$C. The φ (AgIn$_3$) phase reported by Weibke and Eggers [39] was confirmed as AgIn$_2$ (with a CuAl$_2$-type crystal structure) by Hellner [42]. Campbell and Wagemann [43] re-investigated the phase equilibra in the whole composition range of the Ag-In system by DTA, XRD, photomicrography and EPMA. The existence of the bcc phase was confirmed between 660 and 695 $^{\circ}$C and the hcp phase was found to decompose at 670 $^{\circ}$C following the peritectoid reaction fcc + bcc $\leftrightarrow$ hcp. In the Ag-rich area below 300 $^{\circ}$C, a primitive cubic phase, α', was reported to exist below about 73.8 at. % Ag. The homogeneity region of the ε phase was reported to lie between 67 and 70 at. % Ag by Campbell and Wagemann [43]. Uemura and Satow [44] investigated the order-disorder transition of Ag$_3$In by using specific heat capacity measurements, electrical resistivity, magnetic susceptibility and X-ray analysis. The order-disorder transition of the hcp phase was observed to occur at 214 $^{\circ}$C. Satow *et al.* [45] studied the phase transition of AgIn$_2$ with the help of the same techniques and found that the cubic phase transforms to the hcp one at 222 $^{\circ}$C. Based on the experimental results of the time, Barren [46] compiled and presented a new phase diagram for the Ag-In binary system. Later, Moser *et al.* [47] investigated the phase relations in the Ag-In binary system by using diffusion couple measurements, DSC and metallographic methods. Their experimental results are in good agreement with previous data. Recently, Jendrzejczyk and Fitzner [48] determined the liquidus of the Ag-In binary system over whole composition range using emf measurements.

The heat of formation of the solid and liquid alloys of the Ag-In system at 450 $^{\circ}$C were measured by Kleppa [49] using calorimetric measurements. Prezdziecka-Mycielska *et al.* [50] and Nozaki *et al.* [51] derived the partial and integral values of excess enthalpy, excess free Gibbs energy and excess entropy of liquid Ag-In alloys at 727 and 827 $^{\circ}$C based on the emf measurements results. Beja [52] determined the enthalpy mixing of the liquid phase at 755 $^{\circ}$C using calorimetric measurements method. Itagaki and Yazawa [53] measured the heat of mixing at 970 $^{\circ}$C in Ag-In liquid alloys by adiabatic calorimetry; the minimum value recorded was -4.54 kJ·mol-atom^{-1} at 66 Ag at. %. Alcock *et al.* [54] and Qi *et al.* [55] derived the enthalpy of mixing, Gibbs energy of mixing and entropy of mixing of liquid Ag-In alloys at 1027 $^{\circ}$C based on the results of vapor pressure measurements with the Knudsen cell and mass spectrometer. Their results are in good

agreement with previous works. The activity of In in the liquid phase at 777, 800, and 977 $^{\circ}$C were determined by Kameda *et al.* [56] from emf measurements. The integral molar enthalpy of liquid Ag-In at 470 and 1007 $^{\circ}$C were measured by Castanet *et al.* [57] by drop calorimetry. Recently, Jendrzejczyk and Fitzner [48] derived the activities, Gibbs energy of mixing and enthalpy of mixing of liquid Ag-In alloys based emf measurements using solid oxide galvanic cells with zirconia electrolyte. The heat of formation of the fcc phase at 44 $^{\circ}$C was measured by Orr and Hultgren [58] by means of calorimetric measurements method. The activity of In in the fcc phase at 727 $^{\circ}$C was measured by Masson and Pradhan [59] with vapor pressure measurement method.

7.2.3 The Ag-Sn system

The liquidus of the Ag-Sn binary system was determined by Heycock and Neville [60-62] by employing samples prepared in heavy iron blocks covered by paraffin, to prevent the oxidation of tin, and by thermal analysis. Peternko [63] investigated the system with thermal analysis and metallographic methods and reported the existence of a new intermetallic compound, Ag_3Sn, with a peritectic melting temperature of 480 $^{\circ}$C following the reaction liquid + fcc $\leftrightarrow$ Ag_3Sn. Puschin [64] studied molten Ag-Sn alloys with the emf method and observed the existence of a new phase, named ζ (Ag_6Sn or Ag_5Sn), in the Ag-rich region. Murphy [65] investigated the whole Ag-Sn system with thermal analysis and metallographic methods and determined the solid solubility boundaries of the fcc, ζ and Ag_3Sn phases. Murphy [65] also found that the solid solubility of Ag in the terminal bct (Sn) phase was less than 0.1 at. % Ag at 206 $^{\circ}$C. Hume-Rothery *et al.* [66] and Hume-Rothery and Eutchers [67] determined the liquidus of the Ag-Sn binary system by thermal analysis; their results are in good agreement with previous investigations [60-63]. Hanson *et al.* [68] employed thermal analysis and carefully determined the liquidus between 0 to 6 at. % Ag. The eutectic liquid $\leftrightarrow$ Ag_3Sn + bct (Sn) was located at 3.5 at. % Ag and 221 $^{\circ}$C. The solid solubility of fcc was determined by Owen and Roberts [69] with XRD; their results are in good agreement with the previous work of Murphy [65]. Umansky [70] re-investigated the whole Ag-Sn system with XRD and confirmed the existence of the fcc, ζ and Ag_3Sn phases. The solid solubility range of the fcc phase was also measured. The solubility of Ag in the terminal phase bct (Sn) was determined by Vnuk *et al.* [71] with the help of hardness measurements on several heat treated alloys, and the maximum solid solubility of Ag in bct (Sn)

was found to be 0.09 at.% Ag at the eutectic temperature of 221 ^{o}C. All the available experimental phase equilibria data of the Ag-Sn binary system were compiled by Karakay and Thompson [72].

Frantik and McDonald [73] derived the activity, partial molar Gibbs energy and integral Gibbs energy of molten Ag-Sn alloys based on their experimental data obtained by emf measurements method. Yanko *et al.* [74] studied the activity of dilute Ag-Sn liquid solutions with the emf method in the temperature range of 250 to 412 ^{o}C. Both of their results were shown that the Ag-Sn solution is not an ideal mixing solution. Kleppa [75] measured the enthalpy of formation of solid and liquid Ag-Sn phases at 450 ^{o}C using calorimetric measurement method. The positive enthalpy of mixing of Ag-Sn liquid solution was determined in the composition range from 0 to 40 at. % Ag at 450 ^{o}C, which is in agreement with the derived data by Frantik and McDonald [73]. Nozaki *et al.* [76] derived the partial and integral molar excess Gibbs energy, excess entropy and excess enthalpy of molten Ag-Sn alloys based on the experimental data obtained using emf measurements method, and the activity of Sn in the liquid phase at 827 ^{o}C was reported in their work. Elliott and Lemons [77] determined the activity of Ag and Sn in the dilute Ag-Sn liquid solution using emf measurements method. Itagaki and Yazawa [53] measured the enthalpy of mixing of the liquid phase in Ag-Sn alloys at 970 ^{o}C using adiabatic calorimetry. An "N" type enthalpy of mixing with the positive value part in the composition range from 0 to 50 Ag (at. %) and negative part with a minimum value of -2777 J·mol-atom^{-1} at 76.4 at. % Ag were reported in their work, which are in good agreement with the previous one reported by Kleppa [75]. Castanet and Laffitte [78] reoprted the enthalpy of mixing of Ag-Sn liquid phase at 1007 ^{o}C using calorimetric measurements method, which are in agreement with the data reported by Itagaki and Yazawa [53] and Kleppa [75]. Chowdhury and Ghosh [79] derived the activity of Sn and Ag in liquid phase in the composition range from 20 to 90 Sn (at. %) in the temperature range of 552 to 838 ^{o}C using emf measurements method. The reported activity of Sn in liquid solution at 627 ^{o}C are in good agreement with the data reported by Frantik and McDonald [73]. Okajima and Sakao [80] reported the activity of Ag in the liquid phase at 500, 560 and 620 ^{o}C using emf measurements method. The activity of Sn in the liquid phase at 827 and 727 ^{o}C were determined by Iwase *et al.* [81] using the emf measurements method with two different solid-oxide galvanic cells. And the derived activity of Sn in liquid solution in the work of Iwase *et al.* [81] are self-consistent, but are not in agreement with the previous reported results [73, 79, 80]. The activity of

Sn in the liquid phase at 600 and 700 ^{o}C were measured by Kameda *et al.* [82] using the emf measurements method. The enthalpy of formation of solid phases were measured by Flandorfer *et al.* [83] with calorimetric measurements method. Rakotomavo *et al.* [84] studied the enthalpy of mixing of liquid phase at 1100 ^{o}C with calorimetric measurements method. Laurie *et al.* [85] reported the partial enthalpy mixing of Ag-Sn liquid phase at 554 ^{o}C using emf measurement and calorimetric measurement methods. The activity of Ag and Sn in liquid phase and partial moral enthalpy of the Ag-Sn liquid phase were derived by Yamaji and Kato [86] based on their experimental data obtained by using emf measurements method and mass spectrometer measurements, which are in agreement with the reported data from Iwase *et al.* [81], but are not in agreement with the reported results [73, 79, 80]. All the reported results of the enthalpy of mixing of Ag-Sn liquid solution measured by calorimetric measurements method [53, 75, 78, 84, 85] are in a reasonable agreement.

7.2.4 The Mg-Ag-Sn, Mg-Ag-Sn and Ag-In-Sn systems

Kolesnichenko *et al.* [87] measured the isothermal section of the Mg-Ag-In system at 280 ^{o}C and the ternary isopleths with 50 In, 10 Ag and 30 Mg (wt. %) using XRD and metallographic methods.

Raynor and Frost [88] determined the isothermal sections in the Ag-rich area of the Mg-Ag-Sn system at 450 and 550 ^{o}C using optical microscopy and XRD. The isothermal section at 450 ^{o}C was also measured by Karonik *et al.* [89] by means of thermal analysis, optical microscopy, and XRD. The solubility of Sn in Mg_3Ag was found to be about 7 wt. %. Karonik *et al.* [89] also determined the ternary isoplethal sections at constant Sn of 10 and Ag of 10 wt. %.

Phase relations in the Ag-In-Sn system were studied by Korhonen and Kivilahti [90] with DSC, SEM, and optical microscopy, but no experimental data are tabulated or illustrated in their work. Liu *et al.* [91] reinvestigated phase equilibria in the system with DSC and metallography and determined the isothermal sections at 180, 250, 400, and 600 ^{o}C as well as ternary isoplethal sections with constant Ag of 10, 20, 30, and 40, and constant In of 20 and 40 (wt. %). Vassilev *et al.* [92] measured the isothermal section at 280 ^{o}C and a ternary isoplethal section at constant Ag of 2.5 (at. %) using DSC, XRD and SEM. Miki *et al.* [93] determined the activity of Ag in the liquid solution using Knudsen cell with mass spectrometry but none of his data are tabulated.

Gather *et al.* [94] measured the enthalpy of mixing of the liquid phase by heat flow calorimetry with different molar ratios of Sn/In (1/4, 2/3, 3/2 and 4/1).

7.3 Thermodynamic modeling

All the thermodynamic assessment status of sub-systems of Mg-Sn-Ag-In quaternary system are listed in Table 7.1. The Mg-Sn phase diagram was critically evaluated and optimized by Jung et al. [95, 96] using the Modified Quasichemical Model in the Pair Approximation (MQMPA) for the liquid phase. Similarly, the In-Mg and In-Sn binary systems and the Mg-In-Sn ternary system were critically evaluated and optimized in our previous work [97] by using the MQMPA as well for the liquid phase. In order to construct a self-consistent thermodynamic database of Mg-base system, the thermodynamic parameters reported for the Mg-Sn [95], In-Mg [97], In-Sn [97], and Mg-In-Sn [97] systems were thus used in the present work for the optimization of the whole Mg-Sn-Ag-In quaternary system.

Table 7.1 Thermodynamic optimization status of sub-systems of Mg-Sn-Ag-In quaternary system

System	Reference	
	[a]BW for liquid solution	[b]MQMPA for liquid solution
Ag-Mg	Lim *et al.* [30]	N/A
Ag-In	Moser *et al.* [47], Liu *et al.* [91]	N/A
Ag-Sn	Oh *et al.* [98]	N/A
In-Mg	N/A	Wang *et al.* [97]
In-Sn	Liu *et al.* [91]	Wang *et al.* [97]
Mg-Sn	Meng *et al.* [99]	Jung *et al.* [95, 96]
Mg-Sn-Ag	N/A	N/A
Mg-Sn-In	N/A	Wang *et al.* [97]
Mg-Ag-In	N/A	N/A
Sn-Ag-In	Liu *et al.* [91]	N/A

[a]BW: Bragg-Willams model; [b]MQMPA: Modified Quasichemical Model in the Pair Approximation

The remaining binary systems, the Ag-Mg, Ag-In and Ag-Sn systems, were previously optimized by Lim *et al.* [30], Moser *et al.* [47], and Oh *et al.* [98], respectively, using the Bragg-Williams

Model (BWM) [100] for the liquid phase, which neglects short-range order. However, these assessments are inconsistent with some experimental data. For example, in the optimized work of the Ag-Mg system by Lim *et al.* [30], Mg_3Ag and $Mg_{54}Ag_{17}$ are treated as a single stoichiometric compound, $Mg_{54}Ag_{17.}$ In addition, although the bcc phase is modeled using two energy contribution parts, ordered bcc_B2 and disordered bcc_A2, the parameters of the ordered bcc_B2 part are given without considering the symmetry of the crystal structure. Another example is the Ag-In binary system optimized by Moser *et al.* [47]: the bcc and Ag_3In phases are missing. Moreover, no critical review of the experimental data is performed in the assessments of Lim *et al.* [30] and Moser *et al.* [47]. Consequently, in the present work, all available phase diagram and thermodynamic data of the Ag-Mg, Ag-In and Ag-Sn binary systems were critically re-evaluated and optimized using the MQMPA for the liquid phase with the FactSage thermodynamic software [101]. All phases considered in the Mg-Sn-Ag-In quaternary system are summarized in Table 7.2 along with the model used to describe their thermodynamic properties.

7.3.1 Stoichiometric phases

The molar Gibbs energies of pure elements and stoichiometric phases can be described by:

$$G_T^o = H_T^o - TS_T^o \tag{7.1}$$

$$H_T^o = \Delta H_{298K}^o + \int_{T=298.15K}^{T} C_p dT \tag{7.2}$$

$$S_T^o = S_{298K}^o + \int_{T=298.15K}^{T} (C_p / T)dT \tag{7.3}$$

where $\Delta H_{298.15K}^o$ is the molar enthalpy of formation of a given species from pure elements (the $\Delta H_{298.15K}^o$ of any element stable at 298.15 K and 1 atm is assumed as 0 J·mol^{-1} at the reference state), $S_{298.15K}^o$ is the molar entropy at 298.15 K, and C_p is the molar heat capacity.

In the present study, the Gibbs energy of pure elements were taken from the SGTE database [100]. As there are no experimental heat capacity data for Ag-In, Ag-Sn and Ag-Mg intermetallic phases, their heat capacities were evaluated using the Neumann–Kopp rule [102]. The heat capacity curves of solid In and Sn from the SGTE database show a maximum just above their melting points (that is in the liquid stable region). Several intermetallic phases in the studied

system have their melting points substantially higher than the pure elements from which they are formed. The heat capacity functions of intermetallic phases obtained with the Neumann–Kopp rule had also such a maximum, which is little plausible.

Table 7.2 Structural parameters and thermodynamic model used in present work

Phase	Pearson symbol	Strukturbericht designation	Space group	Prototype	Model[a]
Liquid	-	-	-	-	MQMPA
fcc	$cF4$	A1	$Fm\bar{3}m$	Cu	CEF
bct	$tI4$	A5	$I4_1/mmm$	Sn	BW
bcc_A2	$cI2$	A2	$Im\bar{3}m$	W	BW
hcp	$hP2$	A3	$P6_3/mmc$	Mg	BW
tet	$tI2$	A6	$F4/mmm$	In	BW
Mg_2Sn	$cF12$	C1	$Fm\bar{3}m$	CaF_2	ST
Ag_3Sn	$oP8$	D0a	$Pmmm$	Cu_3Ti	CEF
bcc_B2	$cP2$	B2	$Pm\bar{3}m$	CsCl	CEF
Ag_3Mg	$cP4$	$L1_2$	$Pm\bar{3}m$	$AuCu_3$	CEF
$AgMg_3$	$hP8$	$D0_{18}$	$P6_3/mmc$	$AsNa_3$	CEF
$AgMg_4$	$hP*$	-	-	-	ST
$Ag_{17}Mg_{54}$	-	-	-	-	CEF
β'	$cP4$	$L1_2$	$Pm3m$	$AuCu_3$	CEF
β_1	$hR16$	-	$R3m$	-	CEF
β_2	$hP9$	-	$P\bar{6}2m$	Mg_2Tl	ST
β_3	$oI28$	$D8_g$	$Ibam$	Mg_5Ga_2	ST
β''	$tP4$	$L1_0$	$P4/mmm$	AuCu	CEF
γ'	$cP4$	$L1_2$	$Pm3m$	$AuCu_3$	CEF
$\beta(InSn)$	$tI2$	A6	$F4/mmm$	In	BW
$\gamma(InSn)$	$hP5$	-	$P6/mmm$	-	BW
Ag_2In	$cP52$	$D8_3$	$P\bar{4}3m$	Cu_9Al_4	CEF
Ag_3In	$cP*$	-	$Pm\bar{3}m$	-	ST
$AgIn_2$	$tI12$	C16	$I4/mcm$	Al_2Cu	ST

[a] MQMPA: Modified Quasichemical Model in the Pair Approximation; CEF: Compound Energy Formalism; BW: Bragg-Willams model; ST: Stoichiometric compound

In order to resolve this problem, we modified the heat capacity functions of solid In and Sn above their melting points, that is extrapolated into the liquid region, to make sure that the heat capacity curves of intermetallic phases increase with temperature until their own melting points. This was solely applied when the Neumann–Kopp rule was employed for intermetallic phases and does not influence pure solid In and Sn which keep their SGTE Gibbs energy functions.

7.3.2 Solid solutions

The Compound Energy Formalism (CEF) was introduced by Hillert [103] to describe the Gibbs energy of solid solutions. In this model, ideal mixing is assumed on each sub-lattice. In the present work, the Ag$_3$Mg, Ag$_3$Sn, AgMg$_3$, Ag$_{17}$Mg$_{54}$, β', β_1, β'', γ', and Ag$_2$In phases were modeled with the CE. The stoichiometry of the sublattices was based on the crystal structures reported in the literature (Table 2). The Gibbs energy expression of the Ag$_2$In phase, for example, based on the CEF, is obtained by mixing In and Ag on two sublattices with a stoichiometric ratio of 2:1 as (Ag)$_2$ (Ag, In). The Gibbs energy of the Ag$_2$In solution is then expressed as:

$$
\begin{aligned}
G^{Ag_2In} = {} & y_{Ag}^I y_{In}^{II} G_{Ag:In}^o + y_{Ag}^I y_{Ag}^{II} G_{Ag:Ag}^o + RT(y_{Ag}^{II} \ln y_{Ag}^{II} + y_{In}^{II} \ln y_{In}^{II}) \\
& + y_{Ag}^I y_{Ag}^{II} y_{In}^{II} \, {}^n L_{Ag:Ag,In}
\end{aligned}
\tag{7.4}
$$

where y_{Ag}^{II} and y_{In}^{II} are the site fractions of Ag and In on the second sublattice. $G_{Ag:In}^o$ and $G_{Ag:Ag}^o$ are the Gibbs energy of Ag$_2$In and Ag$_2$Ag, respectively. ${}^n L_{Ag:Ag,In}$ is the interaction energy between Ag and In on the second sublattice. Similarly, the Gibbs energy functions of all other solid solutions are described according to the structure of their sublattice using the CEF.

The sublattice model, developed by Hillert [103], allows the description of a variety of solid solutions with mathematical functions, particularly for the ordered phase. The sublattice formalism applied to the A2 and B2 phases was introduced by Dupin and Ansara [104] and the same notations were used in the present work. The Gibbs energy functions of the bcc_A2 and bcc_B2 phases were model as single bcc phases with sublattice structures as disordered (Ag, In, Mg, Sn)(Va)$_3$ and ordered (Ag, In, Mg, Sn)(Ag, In, Mg, Sn)(Va)$_3$ parts. The molar Gibbs energy of these disordered and ordered parts can be expressed as:

$$
G^{bcc} = {}^{dis}G^{bcc\_A2} + {}^{ord}G^{bcc\_B2}
\tag{7.5}
$$

where $^{dis}G^{bcc\_A2}$ is the Gibbs energy contribution of the bcc phase from the disordered part (bcc_A2), which can be expressed as follows:

$$^{dis}G^{bcc\_A2} = \sum_{i=Ag,In,Mg,Sn} x_i \, ^oG_i^{bcc\_A2} + RT(x_{Ag}\ln x_{Ag} + x_{In}\ln x_{In} + x_{Mg}\ln x_{Mg} + x_{Sn}\ln x_{Sn})$$
$$+ x_i x_j \sum_{n=0}^{n}(x_i - x_j)^n \, ^nL_{i,j}^{dis} + x_i x_j x_k \, ^mL_{i,j,k}^{dis} \quad (7.6)$$
$$_{m=0,1,\,and\,2}$$

In this expression, $^nL_{i,j}^{dis}$ and $^mL_{i,j,k}^{dis}$ are the binary and ternary interaction parameters of the disordered part of the bcc phase (bcc_A2).

In equation 7.5, $^{ord}G^{bcc\_B2}$ is the Gibbs energy contribution of the bcc phase from the ordered part (bcc_B2), which can be expressed as follows:

$$^{ord}G^{bcc\_B2} = \sum_{i\neq j} {}^oG_{i:j}^{bcc\_B2} + RT(x_i^I \ln x_i^I + x_j^I \ln x_j^I + ...) + RT(x_i^{II}\ln x_i^{II} + x_j^{II}\ln x_j^{II} + ...) + \Delta^{ord}G^{bcc\_B2} \quad (7.7)$$

where $^oG_{i:j}^{bcc\_B2}$ is the Gibbs energy of the hypothetical compound ij, and $\Delta^{ord}G^{bcc\_B2}$ is the excess Gibbs energy of ordered part (bcc_B2), which is constituted of the binary and ternary interaction parameters $\Delta^{ord}G_{binary}^{bcc\_B2}$ and $\Delta^{ord}G_{ternary}^{bcc\_B2}$, which are expressed as:

$$\Delta^{ord}G_{binary}^{bcc\_B2} = y_i^I y_j^I \sum_{n=0}^{n}(y_i^I - y_j^I)^n \, ^nL_{i,j:i}^I + y_i^{II} y_j^{II} \sum_{n=0}^{n}(y_i^{II} - y_j^{II})^n \, ^nL_{i:i,j}^{II} \quad (7.8)$$

$$\Delta^{ord}G_{ternary}^{bcc\_B2} = y_i^I y_j^I \sum_{n=0}^{n}(y_i^{II} - y_j^{II})^n \, ^nP_{i,j:k}^I + y_i^{II} y_j^{II} \sum_{n=0}^{n}(y_i^{II} - y_j^{II})^n \, ^nP_{k:i,j}^{II}$$
$$_{i\neq j\neq k}$$
$$+ (y_i^I y_j^I y_k^I \, ^nP_{i,j,k:l}^I + y_i^{II} y_j^{II} y_k^{II} \, ^nP_{l:i,j,k}^{II}) \quad (7.9)$$
$$_{l=i,\,j,\,or\,k\ and\ i\neq j\neq k}$$

where $^nL_{i,j:i}^I$ and $^nL_{i:i,j}^{II}$ are the binary interaction parameters of the ordered part bcc_B2, and $^nP_{i,j:k}^I$, $^nP_{k:i,j}^{II}$, $^nP_{i,j,k:l}^I$, and $^nP_{l:i,j,k}^{II}$ are the ternary interaction parameters of the ordered part bcc_B2. Due to the crystallographic symmetry of the bcc_B2 phase, the following relations are introduced:

$$^oG_{i:j}^{bcc\_B2} = {}^oG_{j:i}^{bcc\_B2}; \quad ^nL_{i,j:k}^I = {}^nL_{k:i,j}^{II}; \quad ^nP_{i,j:k}^I = {}^nP_{k:i,j}^{II}, \quad ^nP_{i,j,k:l}^I = {}^nP_{l:i,j,k}^{II} \quad (7.10)$$

Also, relations exist for the parameters between the ordered and disordered solutions which are used in the present work and are described in details in the reference [104].

The disorder solid solutions hcp (Mg-rich), bct (Sn-rich), tetatrahedral (In-rich), bcc, $\beta(InSn)$, and $\gamma(InSn)$ were modeled with one sublattice as (Ag, Mg, Sn), a sub-regular solution approximation is used for the excess Gibbs energy and the configurational entropy if of Bragg-Williams type.

7.3.3 Liquid phase

The thermodynamic properties of the liquid phase were modeled using the Modified Quasichemical Model in the Pair Approximation (MQMPA) developed by Pelton *et al.* [105, 106]. A detailed description of the MQMPA and its associated notation are given in refs. [105, 106].

7.4 Experimental procedures

Mg-Sn-Ag ternary alloys were prepared with pure Mg (99.8 wt. %), Sn (99.9 wt. %), and Ag (99.9 wt. %) from Alfa Aesar and melted in a frequency induction furnace under high purity argon atmosphere. In order to minimize the interaction of the samples with the crucibles, Ta cubic-shaped crucibles were made using Ta foil (99.5 wt. % purity, 0.15 mm thickness). Each alloy was remelted three times in its crucible in order to obtain a homogeneous alloy; the melting loss was less than 5 wt. % for each sample. Mg-Sn-Ag samples were then sealed into quartz capsules under argon atmosphere and equilibrated at 415 $^{\circ}$C for 20 days and at 350 $^{\circ}$C for 35 days, respectively. These temperatures were chosen because they correspond to the temperatures at which heat treatment is usually performed on Mg alloys. Quenching was carried out in water without breaking the quartz tubes. The alloys preparation was done at Concordia University

Electron probe microanalysis (EPMA) of the quenched samples was performed with the JEOL 8900 probe at McGill University using wavelength-dispersive spectrometry (WDS). An accelerating voltage of 15 kV was used with a 20 nA beam current, a spot size of 2 µm and counting times of 20 s on peaks and 10 s on backgrounds. Raw data were reduced with the PRZ correction using pure Mg, Sn, and Ag metal standards. The experimental error limit of EPMA measurement is about 0~3 at. %.

Liquidus and polymorphic transformation temperatures were measured by differential scanning calorimetry (DSC) using the SETARAM instrumentation under a continuous flow of purified

argon at Concordia University. Experiments were carried out by using sintered Al_2O_3 crucibles under flowing argon gas with heating and cooling rates of 5 ^{o}C/min. No reaction was observed between the samples and the sintered Al_2O_3 crucibles.

7.5 Experimental and thermodynamic optimization results

7.5.1 Experimental determination of the Mg-Sn-Ag ternary system

Equilibrium compositions measured at 415 and 350 ^{o}C in the Mg-rich area of the Mg-Sn-Ag system are summarized in Table 7.3. Sums of elemental compositions are always close to 100 wt. % which indicates that Mg loss by evaporation was small. No ternary compound was found in the measured sections.

The solubility of Ag in Mg_2Sn at 415 and 350 ^{o}C is very limited (less than 0.1 at. %). The solubility of Sn in Mg_3Ag at 415 and 350 ^{o}C is about 2.5 to 3 at. %. With Sn additions, the ternary equilibrium hcp (Mg) + Mg_2Sn + Mg_3Ag was observed in both isothermal sections. On the other hand, in the Mg-Ag system, no binary equilibrium involving hcp (Mg) + Mg_3Ag was detected. Typical ternary Mg-Sn-Ag alloys are shown in the back-scattered electron (BSE) images of Fig.7.1.

Table 7.3 Equilibrium compositions of the Mg-Sn-Ag ternary system as determined in the present work

T (ºC)	Alloy Nominal comp. (at. %)	Phase equilibria Phase 1/Phase 2/Phase 3	Phase Compositions (at. %)								
			Phase 1			Phase 2			Phase 3		
			Mg	Sn	Ag	Mg	Sn	Ag	Mg	Sn	Ag
415	88Mg10Sn2Ag	hcp (Mg)/Mg$_2$Sn/Mg$_3$Ag	97.14	1.00	1.86	67.59	32.39	1.86	76.56	2.56	20.88
	80Mg10Sn10Ag	hcp (Mg)/Mg$_2$Sn/Mg$_3$Ag	96.85	1.02	2.13	67.55	32.43	2.13	75.34	2.31	22.35
	70Mg10Sn30Ag	bcc_B2/Mg$_2$Sn/Mg$_3$Ag	55.13	0.03	44.84	67.86	31.93	44.84	74.28	2.43	23.29
	50Mg20Sn30Ag	bcc_B2/Mg$_2$Sn	35.83	11.44	52.73	67.32	32.41	52.73	—	—	—
	45Mg25Sn30Ag	bcc_B2/Mg$_2$Sn/liquid	33.79	13.76	52.45	67.28	32.47	52.45	—	—	—
350	88Mg10Sn2Ag	hcp (Mg)/Mg$_2$Sn/Mg$_3$Ag	98.32	0.58	1.10	67.51	32.42	1.10	75.20	3.41	21.39
	80Mg10Sn10Ag	hcp (Mg)/Mg$_2$Sn/Mg$_3$Ag	98.34	0.57	1.09	67.86	32.10	1.09	76.02	2.18	21.80
	70Mg10Sn30Ag	bcc_B2/Mg$_2$Sn/Mg$_3$Ag	55.29	0.83	43.88	67.55	32.10	43.88	72.96	3.33	23.71
	50Mg20Sn30Ag	bcc_B2/Mg$_2$Sn	35.85	11.21	52.94	67.54	32.20	52.94	—	—	—
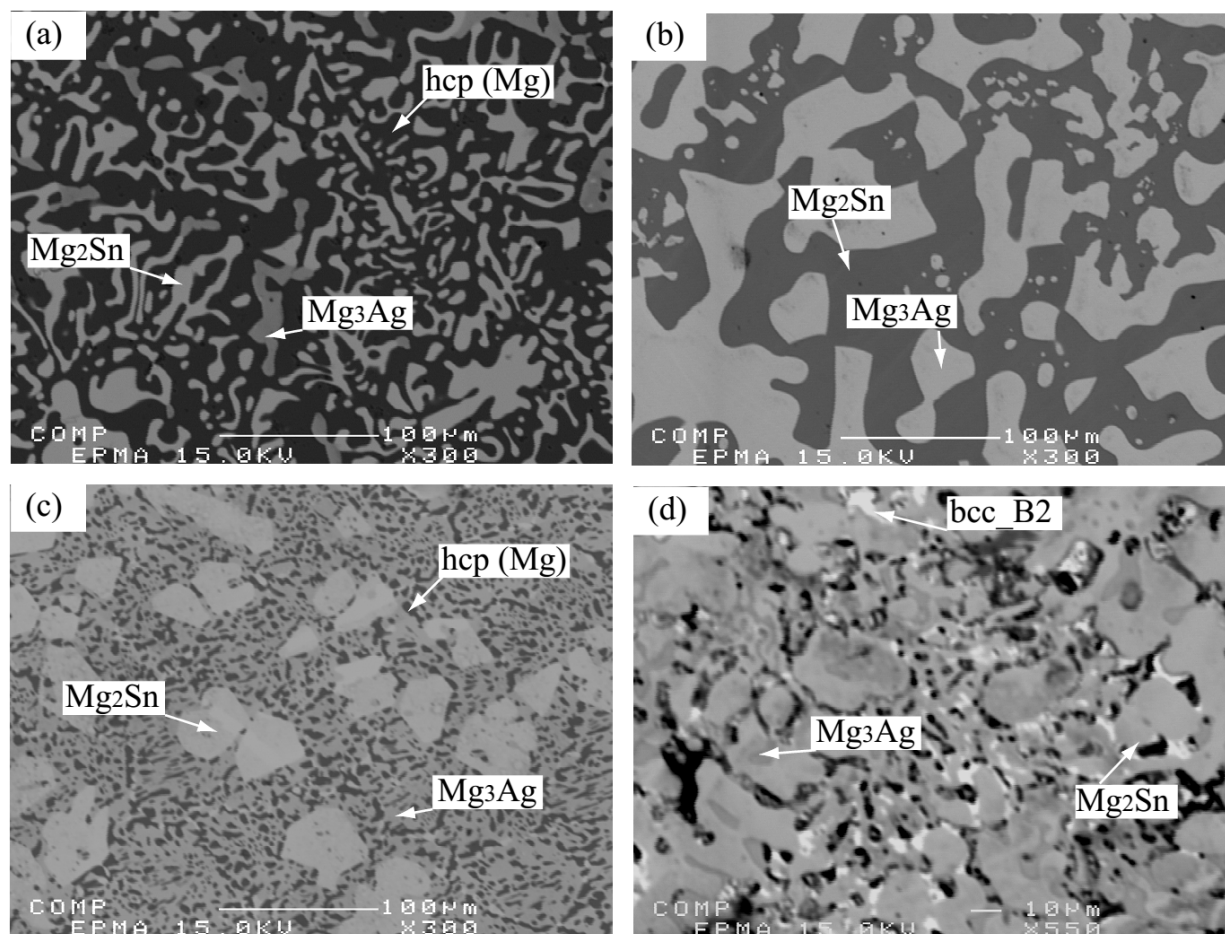
Figure 7.1 BSE images of typical ternary alloys: (a) Mg88Sn10Ag2 (at. %) alloy annealed at 415 ^{o}C for 25 days; (b) Mg50Sn20Ag30 (at. %) alloy annealed at 415 ^{o}C for 25 days; (c) Mg80Sn10Ag10 (at. %) alloy annealed at 350 ^{o}C for 40 days; (d) Mg60Sn10Ag30 (at. %) alloy annealed at 350 ^{o}C for 40 days

The constituted phases in annealed samples were examined with XRD technique, and the selected XRD patterns of samples Mg50Sn20Ag30 and Mg80Sn10Ag10 are shown in Fig. 7.2. As shown in Fig. 7.1(c), the containing of hcp (Mg) phase is small in comparison with Mg$_2$Sn and Mg$_3$Ag phase. The weak diffraction patterns of hcp (Mg) phase were observed in the XRD result as shown in the Fig. 7.2(b). These two present results are self-consistent.
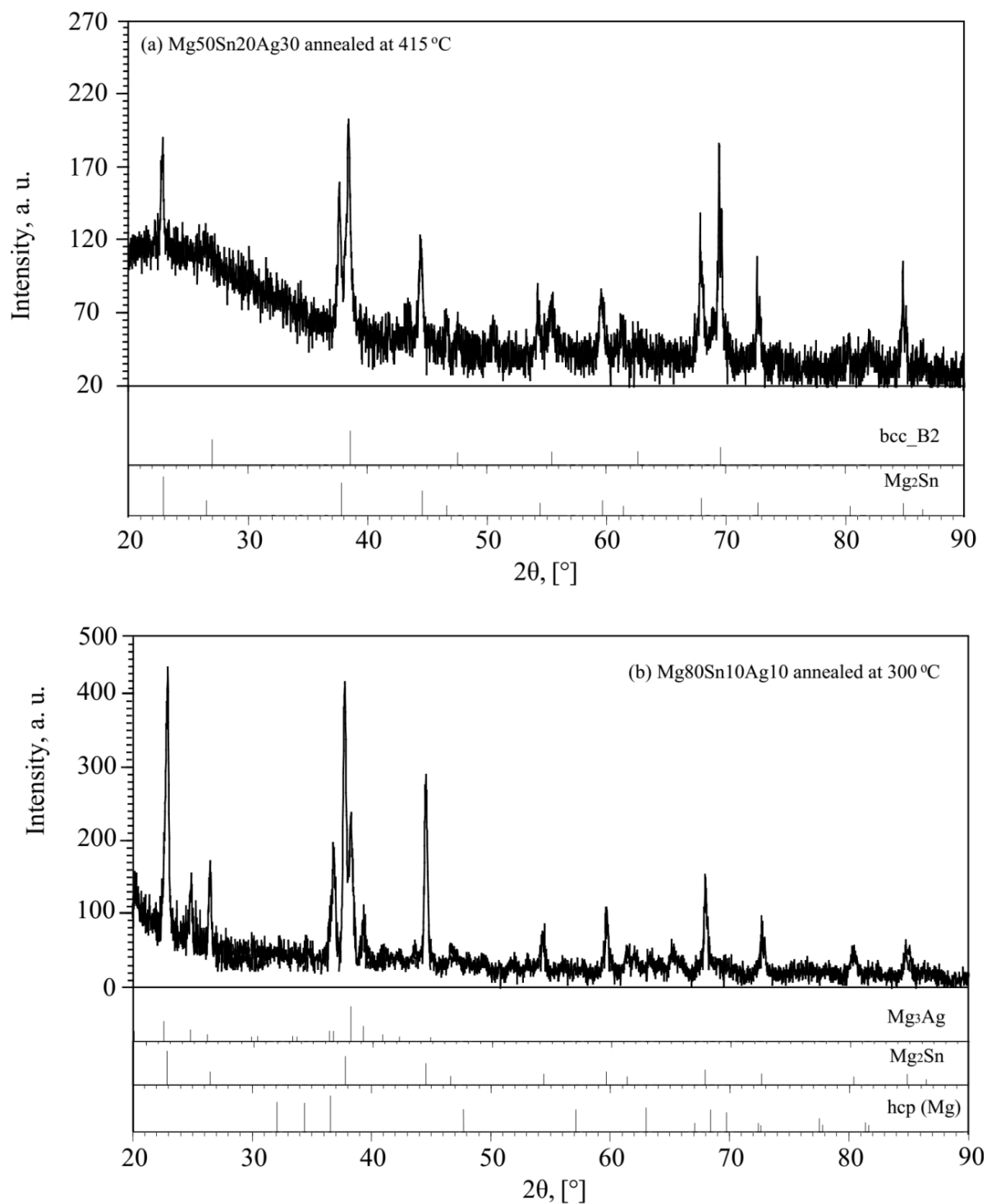
Figure 7.2 XRD patterns of selected annealed samples: (a) Mg50Sn20Ag30 alloy annealed at 415 °C for 25 days, and (b) Mg80Sn10Ag10 alloy annealed at 350 °C for 40 days

The ternary isoplethal sections with the constant Sn of 10 and Ag of 30 (at. %) were measured in the present work by DSC technique. The DSC curve of the Mg80Sn10Ag10 alloy is shown in Fig. 7.3. Three strong exothermic peaks and one weak peak were observed in the cooling spectrum, which were well repeated during heating with two endothermic peaks and one weak liquid peak. All the thermal signals obtained from DSC measurements are listed in Table 7.4. As shown in Figure 7.3, the difference signals observed between the heating and cooling cycles may due to the supercooling effect. Although both heating and cooling data were shown in the present work, it should be noted that the data from heating cycle have the high priority.
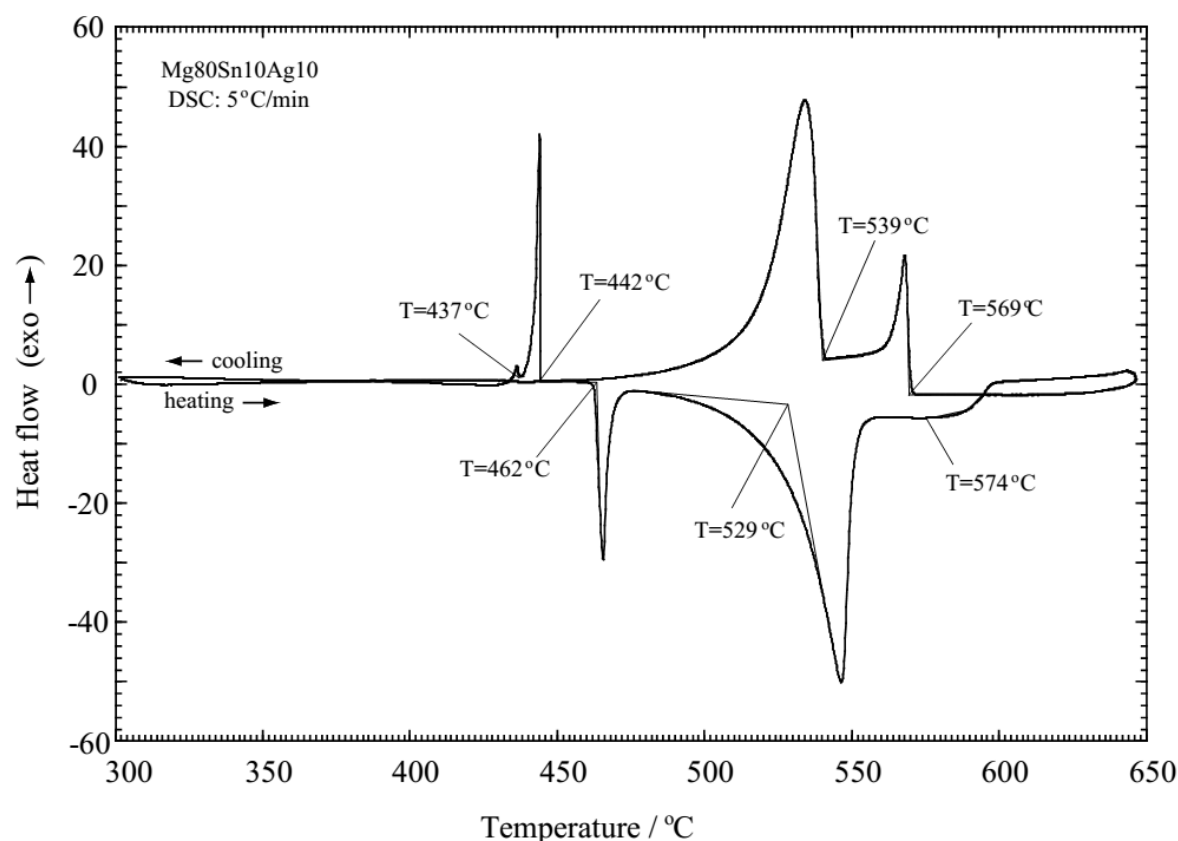
Figure 7.3 The DSC curves of Mg80Sn10Ag10 alloy obtained in the present work

Table 7.4 Thermal signals obtained from DSC measurements of the Mg-Sn-Ag ternary system

Sample (at. %)	Thermal signal (°C)	
	Heating	Cooling
Mg88Sn10Ag2	568; 527; 462	569; 531; 444; 438
Mg80Sn10Ag10	574; 529; 462	569; 539; 442; 437
Mg60Sn10Ag30	678; 622	681; 625
Mg50Sn20Ag30	602; 562; 413	608; 573; 416
Mg45Sn25Ag30	528; 415; 375; 199	533; 420; 191

7.5.2 Thermodynamic optimization results

The Ag-Mg system

The calculated phase diagram of the Ag-Mg binary system is shown in Fig. 7.4 along with reported experimental data [20-24, 29-31]. Ordering of the bcc_B2 (AgMg), Ag_3Mg and Mg_3Ag phases was treated with two sublattices as $(Ag, Mg)_m(Ag, Mg)_n$. Moreover, basing on the reported results of phase transition and solid solubility of the $Mg_{54}Ag_{17}$ compound by Kolesnichenko *et al.* [29], $Mg_{54}Ag_{17}$ was as treated as a high temperature stable phase with a narrow solid solubility by using the two sublattices as $(Ag, Mg)_{17}(Mg)_{54}$ in the present work. The calculated temperature of the eutectic reaction liquid $\leftrightarrow Mg_{54}Ag_{17}$ + hcp is 471 °C, which is in a good agreement with the temperature of 472 °C measured by Kolesnichenko *et al.* [29]. All the invariant reactions of the calculated Ag-Mg phase diagram are listed in Table 7.5.

The calculated enthalpy of mixing of the liquid phase is presented in Fig. 7.5 and compared with the experimental data of Kawakami [32], which show a minimum near $x_{Mg} = 0.5$. Consequently in the present work, the coordination numbers for short-range ordering in the liquid solution were fixed as $Z^{Ag}_{AgMg} = 7$ and $Z^{Mg}_{AgMg} = 7$ (as listed in Table 7.6). The calculated ΔG^{xs}_{Mg} versus $(1 - x_{Mg})^2$ of the liquid phase at 1400 °C, along with the experimental data of Gran *et al.* [33], are depicted in Fig. 7.5. The calculated enthalpy of formation of the solid phases at 25 °C is shown in Fig. 7.6 together with the experimental data [31, 34-36].

As shown in the figures, our calculated results are in a good agreement with experimental data. All the thermodynamic parameters used in the present study are listed in Tables 7.6 and 7.7.
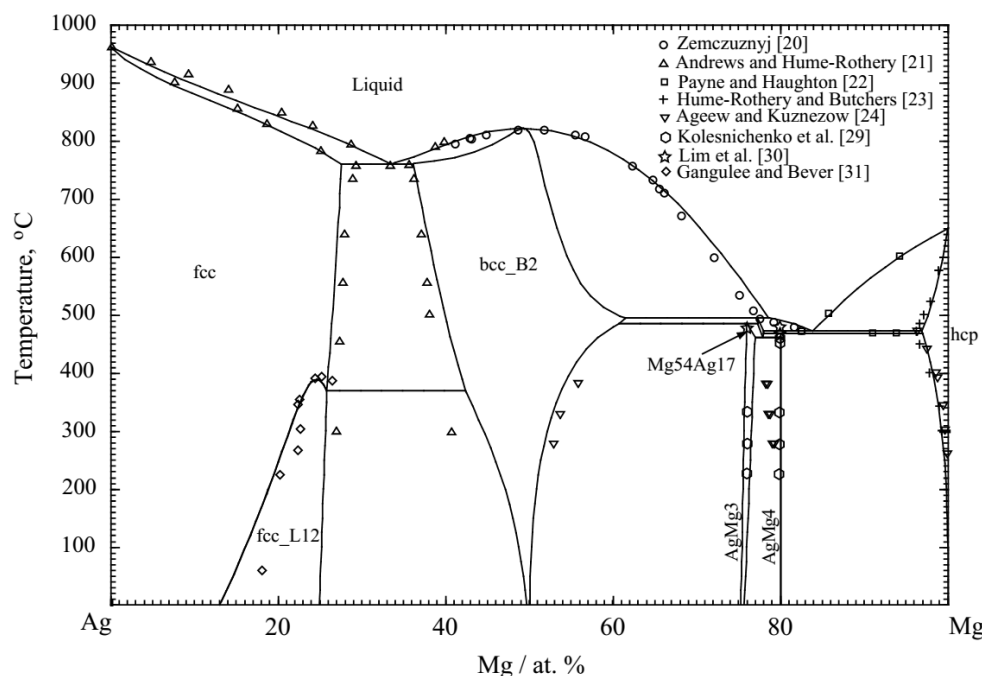
Figure 7.4 Calculated phase diagram of Ag-Mg binary system compared with experimental data [20-24, 29-31]

Table 7.5 Calculated invariant reactions in the Ag-Mg system compared with reported experimental values

Reaction	Reaction type	T (°C)	Composition (Mg at. %)			Reference
$liquid \leftrightarrow fcc + bcc\_B2$	Eutectic	759	33.4	29.3	35.5	[19]
		761	33.5	27.6	36.1	This work
$liquid \leftrightarrow bcc\_B2$	Congruent	820	50.0	50.0	-	[19]
		822	49.3	49.3	-	This work
$liquid + bcc\_B2 \leftrightarrow Mg_{54}Ag_{17}$	Peritectic	494	77.4	65.4	-	[19, 29]
		494	78.6	61.4	77.2	This work
$bcc\_B2 + Mg_{54}Ag_{17} \leftrightarrow AgMg_3$	Peritectiod	484	-	-	-	[30]
		483	60.6	76.2	77.2	This work
$liquid \leftrightarrow Mg_{54}Ag_{17} + hcp$	Eutectic	472	82.4	-	96.2	[19,29]
		472	83.8	78.0	97.0	This work
$Mg_{54}Ag_{17} + hcp \leftrightarrow AgMg_4$	Peritectoid	465	-	-	-	[29]
		469	77.0	96.0	80.0	[30]
		467	78.0	96.9	80.0	This work
$Mg_{54}Ag_{17} \leftrightarrow AgMg_4 + AgMg_3$	Eutectoid	464	77.5	80.0	77.9	This work
$fcc \leftrightarrow fcc\_L12 + bcc\_B2$	Eutectoid	370	25.8	25.8	42.3	This work
$fcc \longleftrightarrow Ag_3Mg$	Congruentiod	392	-	-	-	[19]
		390	24.4	24.4	-	This work
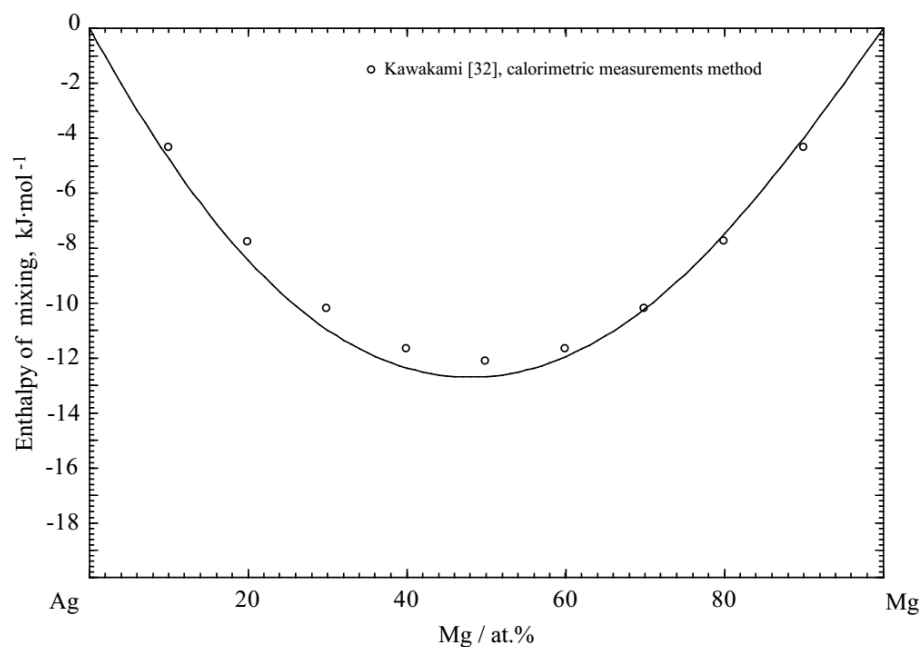
Figure 7.5 Calculated enthalpy mixing of liquid phase of Ag-Mg system at 1050 °C compared with experimental data [32]
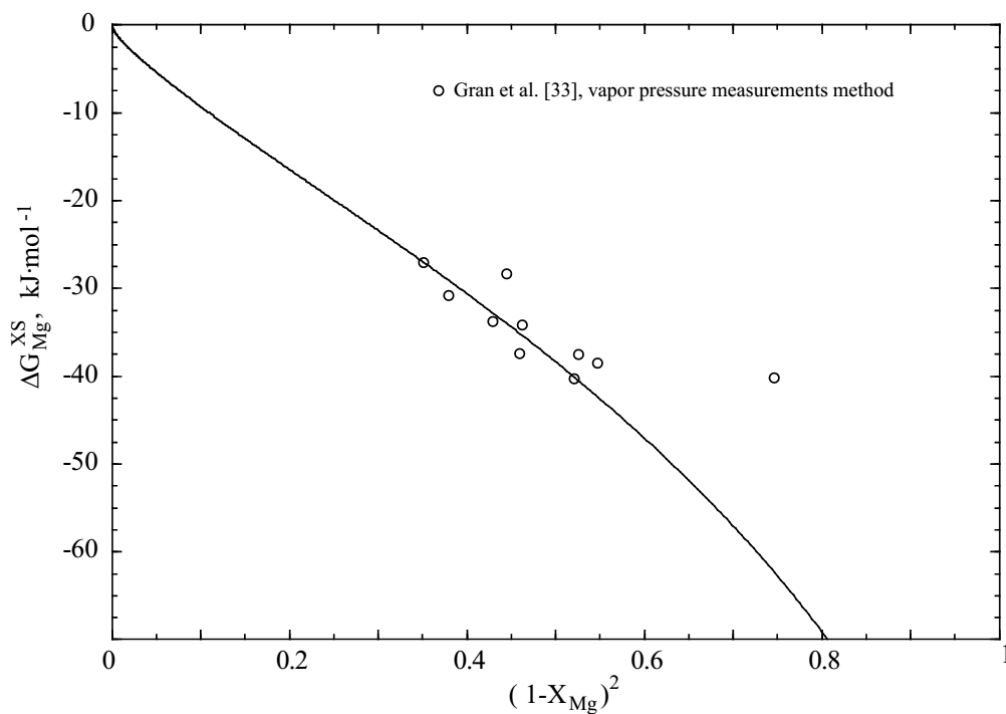
Figure 7.6 Calculated ΔG_{Mg}^{xs} versus $(1-x_{Mg})^2$ of liquid phase at the temperature of 1400 °C along with the experimental data [33]
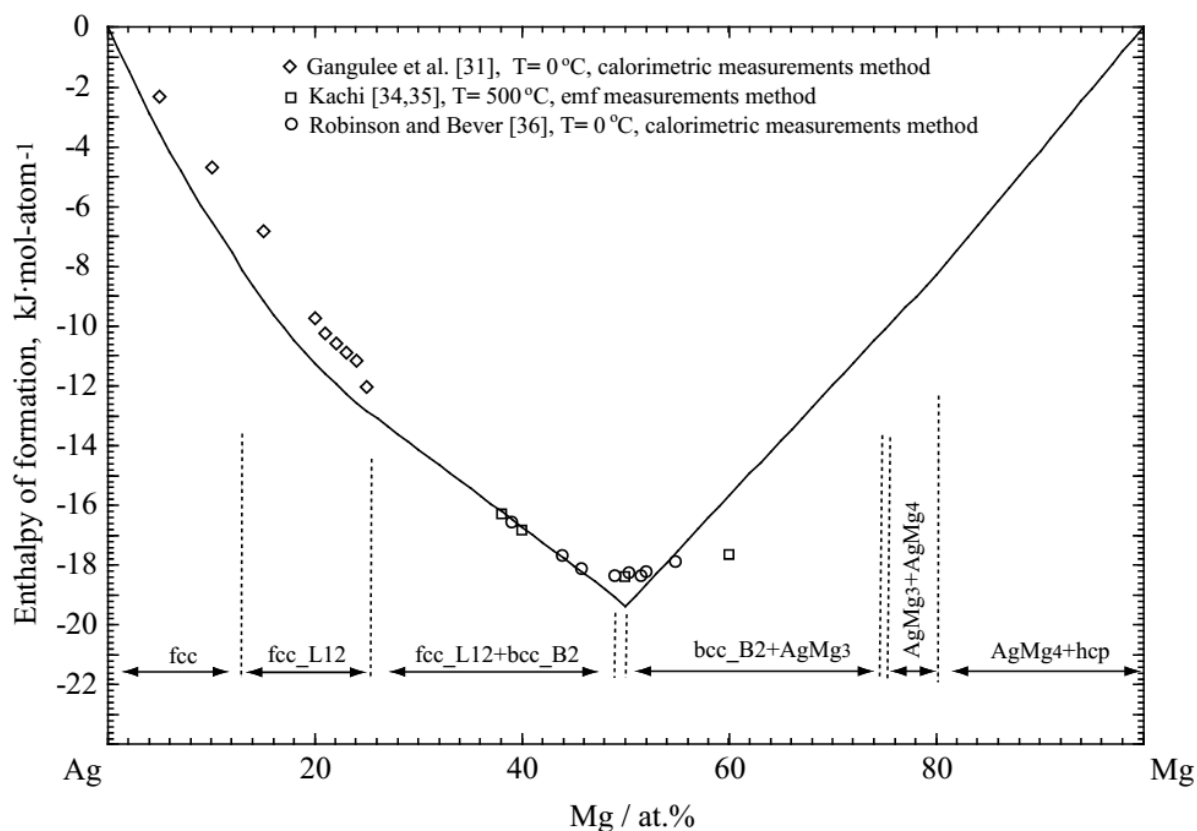
Figure 7.7 Calculated heat formation of solid phases at 25 °C compared with experimental data [31, 34-36]

Table 7.6 Optimized model binary parameters of the MQM for liquid Mg-Sn-Ag-In alloys

Coordination numbers [a]				Gibbs energies of pair exchange reactions (J·mol⁻¹)	Reference
i	j	Z_{ij}^i	Z_{ij}^j		
Mg	In	3	6	$\Delta g_{MgIn} = -9790.6 - 2092 X_{InIn} - 209.2 X_{InIn}^2$	[97]
Mg	Sn	4	8	$\Delta g_{MgSn} = -15263.2 - 0.88 \times T + (3347.2 + 0.42 \times T) X_{MgMg}$	[95]
Mg	Ag	7	7	$\Delta g_{MgAg} = -11129.4 + 0.08 \times T + (-3933.0 + 0.13 \times T) X_{AgAg} - 2594.1 X_{MgMg}$	This work
Ag	In	3	7	$\Delta g_{AgIn} = -7112.8 - 1.26 \times T + 1255.2 X_{AgAg} + (2825.8 - 0.84 \times T) X_{InIn}$	This work
Ag	Sn	3	7	$\Delta g_{AgSn} = -3723.8 - 2.30 \times T + (-3347.2 + 1.26 \times T) X_{AgAg} + (6276 - 3.35 \times T) X_{SnSn}$	This work
Sn	In	6	6	$\Delta g_{SnIn} = -175.7 - 138.1 X_{SnSn} - 133.9 X_{InIn}$	[97]

[a] For all pure elements (Mg, Ag, In and Sn), $Z_{ii}^i = 6$

Table 7.7 Optimized model parameters for phases in the quaternary Mg-Sn-Ag-In system

Phase, model and thermodynamic parameters (J·mol^{-1} or J·mol^{-1}·K^{-1})	Reference
Liquid phase,	
$q^{001}_{InSn(Mg)} = -9204.8,$	This work
$q^{001}_{AgIn(Mg)} = q^{001}_{AgMg(In)} = q^{001}_{MgIn(Ag)} = 251.0 - 7.32 \times T$	This work
$q^{001}_{AgIn(Sn)} = 2301.2 - 2.93 \times T,\ q^{001}_{AgSn(In)} = 2301.2 - 0.42 \times T, q^{001}_{InSn(Ag)} = 2301.2 - 2.51 \times T$	This work
$q^{001}_{AgMg(Sn)} = -5020.8,\ q^{001}_{AgSn(Mg)} = -12552.0$	This work
hcp_A3(Mg) phase, (Ag,In,Mg,Sn) :	
$G_{Mg} = {}^0G^{hcp}_{Mg},\ G_{Ag} = {}^0G^{fcc}_{Ag} + 300 - 0.3 \times T$	
$G_{Sn} = {}^*G_{Sn} + 3900 - 4.4 \times T,\ G_{In} = {}^*G_{In} + 533 - 0.69 \times T,$	This work
${}^1L_{Mg,Sn} = 48116,$	[95]
${}^0L_{Mg,In} = -28451 + 6.09 \times T,\ {}^1L_{Mg,In} = -10460 + 5.44 \times T$	[97]
${}^0L_{Ag,Sn} = -6024.9 + 10.96 \times T,\ {}^1L_{Ag,Sn} = 43095.2 - 3.56 \times T$	This work
${}^0L_{Ag,In} = -15815.5 + 15.23 \times T,\ {}^1L_{Ag,In} = 74140.5 - 11.84 \times T,\ {}^2L_{Ag,In} = 46233.2 - 6.28 \times T$	This work
${}^0L_{Ag,Mg} = -33472.0 - 2.09 \times T,\ {}^1L_{Ag,Mg} = 15899.2$	This work
${}^0L_{Ag,Mg,Sn} = -142256.0 + 8.37 \times T,\ {}^1L_{Ag,Mg,Sn} = -148532.0 + 8.37 \times T,\ {}^2L_{Ag,Mg,Sn} = 41840.0$	This work
${}^0L_{Ag,Mg,In} = {}^1L_{Ag,Mg,In} = {}^2L_{Ag,Mg,In} = 29288.0$	This work
${}^0L_{Ag,In,Sn} = {}^1L_{Ag,In,Sn} = {}^2L_{Ag,In,Sn} = 71128.0 - 4.18 \times T$	This work
fcc_A1 phase, (Ag,In,Mg,Sn) :	
$G_{Mg} = {}^0G^{hcp}_{Mg} + 2600 + 0.90 \times T,\ G_{Ag} = {}^0G^{fcc}_{Ag}$	
$G_{In} = {}^*G_{In} + 123 - 0.30 \times T,\ G_{Sn} = {}^*G_{Sn} + 4150 - 5.2 \times T$	This work
${}^0L_{In,Sn} = 8368.0;\ {}^0L_{Ag,Sn} = -3138.0 + 10.04 \times T,\ {}^1L_{Ag,Sn} = 42258.4 - 7.53 \times T$	This work
${}^0L_{In,Mg} = -29915.6 - 1.88 \times T,\ {}^1L_{In,Mg} = -13723.5 - 1.46 \times T,\ {}^2L_{In,Mg} = -6276.0$	[97]
${}^0L_{Ag,In} = -18828.0 + 13.22 \times T,\ {}^1L_{In,Ag} = 36819.2 - 9.29 \times T$	This work
${}^0L_{Ag,Mg} = -52592.9 + 9.04 \times T,\ {}^1L_{Ag,Mg} = 29288.0 - 10.88 \times T,\ {}^2L_{Ag,Mg} = 3347.2 + 3.35 \times T$	This work
${}^0L_{Ag,Mg,Sn} = -20920 - 16.74 \times T;\ {}^1L_{Ag,Mg,Sn} = -8368 - 8.37 \times T;\ {}^0L_{Ag,Mg,Sn} = -54392.0 - 16.74 \times T$	This work
${}^0L_{Ag,In,Mg} = {}^1L_{Ag,In,Mg} = {}^2L_{Ag,In,Mg} = 41840.0$	
${}^0L_{Ag,In,Sn} = {}^1L_{Ag,In,Sn} = {}^2L_{Ag,In,Sn} = 43932.0 + 4.18 \times T$	This work
bct(Sn) phase, (Ag,In,Mg,Sn) :	
$G_{Mg} = {}^0G^{hcp}_{Mg} + 15000,\ G_{Ag} = {}^0G^{fcc}_{Ag} + 4184,$	This work
$G_{In:Va} = {}^*G_{In} + 2092, G_{Sn:Va} = {}^*G_{Sn}$	This work This work
${}^0L_{In,Sn:Va} = 460.2,\ {}^0L_{Ag,Sn:Va} = 18828.0$	
tet(In) phase, (Ag,In,Mg,Sn) :	
$G_{In} = {}^*G_{In}, G_{Sn} = {}^*G_{Sn} + 15000, G_{Mg} = {}^0G^{hcp}_{Mg} + 15000, G_{Ag} = {}^0G^{hcp}_{Ag} + 15000$	This work
${}^0L_{In,Sn} = 836.8 - 1.67 \times T,\ {}^0L_{In,Mg} = -26359.2 + 18.83 \times T$	
To be continued	

Table 7.7 (continued) Optimized model parameters for phases in the quaternary Mg-Sn-Ag-In system

Phase, model and thermodynamic parameters ($J \cdot mol^{-1}$ or $J \cdot mol^{-1} \cdot K^{-1}$)	Reference
β'' phase, (Mg,In)(Mg,In) :	
$G_{Mg:Mg} = {}^0G_{Mg}^{hcp} + 2600 + 0.90 \times T, G_{In:In} = {}^*G_{In} + 123 - 0.30 \times T,$	[97]
$G_{Mg:In} = G_{In:Mg} = {}^*G_{In} + {}^0G_{Mg}^{hcp} - 9204.8 - 0.60 \times T,$	[97]
${}^0L_{Mg,In:Mg} = {}^0L_{Mg:Mg,In} = -21756 - 0.63 \times T, {}^0L_{Mg,In:In} = {}^0L_{In:Mg,In} = 418.4 - 0.42 \times T,$	[97]
β', γ' phase, (Ag,Mg,In)$_3$(Ag,Mg,In) :	
$G_{Mg:Mg} = 4 \times {}^0G_{Mg}^{hcp} + 10400 + 3.6 \times T, G_{In:In} = 4 \times {}^*G_{In} + 492 - 1.20 \times T,$	[97]
$G_{Mg:In} = {}^*G_{In} + 3 \times {}^0G_{Mg}^{hcp} + 7923.0 \times +2.4T, G_{In:Mg} = 3 \times {}^*G_{In} + {}^0G_{Mg}^{hcp} - 35540.5 - 1.09 \times T$	[97]
${}^0L_{In:Mg,In} = -32049.4 + 2.93 \times T, {}^1L_{In:Mg,In} = 7949.6,$	[97]
$G_{Ag:Ag} = {}^0G_{Ag}^{fcc}, G_{Mg:Ag} = {}^0G_{Ag}^{fcc} + 3 \times {}^0G_{Mg}^{hcp} + 1751.0; G_{Ag:Mg} = {}^0G_{Mg}^{hcp} + 3 \times {}^0G_{Ag}^{fcc} - 53568 - 0.84 \times T$	This work
Ag_2In phase, (Ag,In,Sn)(Ag)$_2$:	
$G_{In:Ag} = 2 \times {}^0G_{Ag}^{fcc} + {}^*G_{In} - 21764.0 + 21.3 \times T, G_{Ag:Ag} = 3 \times {}^0G_{Ag}^{fcc}, G_{Sn:Ag} = 2 \times {}^0G_{Ag}^{fcc} + {}^*G_{Sn} - 4184.0$	This work
${}^0L_{Ag,In:Ag} = -4184.0, {}^0L_{Ag,Sn:Ag} = -3347.2 - 3.35 \times T$	This work
$AgMg_3$ phase, (Ag,In,Mg,Sn)(In,Mg,Sn)$_3$:	
$G_{Ag:Mg} = {}^0G_{Ag}^{fcc} + 3 \times {}^0G_{Mg}^{hcp} - 41492.7 + 1.17 \times T, G_{Mg:Mg} = 4 \times {}^0G_{Mg}^{hcp} + 16317.6;$	This work
$G_{Ag:In} = {}^0G_{Ag}^{fcc} + 3 \times {}^*G_{In} + 20920.0, G_{Mg:In} = {}^0G_{Mg}^{hcp} + 3 \times {}^*G_{In} + 418.5, G_{In:In} = 4 \times {}^*G_{In} + 418.5$	This work
$G_{In:Mg} = 3 \times {}^0G_{Ag}^{fcc} + {}^*G_{In} + 418.5, G_{Sn:Mg} = 3 \times {}^0G_{Mg}^{hcp} + {}^*G_{Sn}, G_{Mg:Sn} = {}^0G_{Mg}^{hcp} + 3 \times {}^*G_{Sn} + 4184.5$	This work
$G_{In:Sn} = {}^*G_{Sn} + 3 \times {}^*G_{In} + 4184.8, G_{Sn:In} = 3 \times {}^*G_{Sn} + {}^*G_{In} + 4184.5$	This work
$G_{Ag:Sn} = {}^0G_{Ag}^{fcc} + 3 \times {}^*G_{Sn} + 4184.8, G_{Sn:Sn} = 4 \times {}^*G_{Sn} + 4184.5$	This work
${}^0L_{Ag:Mg,Mg} = -17865.7 + 20.92, {}^0L_{Ag:In,Mg} = -119244, {}^0L_{Ag,In:Mg} = -35564$	This work
${}^0L_{Ag,Sn:Mg} = {}^0L_{Ag,Mg:Sn} = {}^0L_{Ag:Mg,Sn} = -112968.0 + 54.39 \times T$	This work
$Ag_{17}Mg_{54}$ phase, (Ag,Mg,Sn)$_{17}$(Mg)$_{54}$:	
$G_{Ag:Mg} = 17 \times {}^0G_{Ag}^{fcc} + 54 \times {}^0G_{Mg}^{hcp} - 569664.2 - 161.08 \times T; G_{Mg:Mg} = 71 \times {}^0G_{Mg}^{hcp} + 891192;$	This work
$G_{Sn:Mg} = 17 \times {}^*G_{Sn} + 54 \times {}^0G_{Mg}^{hcp}$	This work
${}^0L_{Ag,Mg:Mg} = -912112 + 209.2 \times T, {}^0L_{Ag,Sn:Mg} = -1317960.0 + 33.47 \times T$	This work
$\beta_1 (hR16)$ phase, (Mg,In)$_3$(Mg,In) :	
$G_{Mg:Mg} = 4 \times {}^0G_{Mg}^{hcp} + 6694.4, G_{In:In} = 4 \times {}^*G_{In},$	This work
$G_{Mg:In} = {}^*G_{In} + 3 \times {}^0G_{Mg}^{hcp} - 35145.6 + 3.18 \times T, G_{In:Mg} = 3 \times {}^*G_{In} + {}^0G_{Mg}^{hcp}$	This work
$\gamma (InSn)$ phase, (In,Sn) :	
$G_{In} = {}^*G_{In} + 10292.6 - 7.64 \times T, G_{Sn} = {}^*G_{Sn} + 924.7 - 1.76 \times T,$	[97]
${}^0L_{In,Sn} = -15480.8 + 18.74 \times T$	
$\beta (InSn)$ phase, (In,Sn) :	
$G_{In:Va} = {}^*G_{In}, G_{Sn:Va} = {}^*G_{Sn} + 5015.5 - 7.50 \times T,$	[97]
${}^0L_{In,Sn:Va} = 292 - 3.14 \times T, {}^1L_{In,Sn:Va} = 627.6 + 0.29 \times T$	
To be continued	

Table 7.7 (continued) Optimized model parameters for phases in the quaternary Mg-Sn-Ag-In system

Phase, model and thermodynamic parameters (J·mol^{-1} or J·mol^{-1}·K^{-1})	Reference
Mg_2Sn phase, $(Mg)_2(Sn)$:	
$G = -102589.8 + 367.5 \times T - 68.331 \times T \ln T - 0.0178986 \times T^2 + 3.33829 \times 10^{-7} \times T^3 + 95940/T$	[95]
bcc_A2 phase, (Ag,In,Mg,Sn)	
$G_{Mg} = {}^0G_{Mg}^{hcp} + 3100 - 2.1 \times T,\ G_{Ag} = {}^0G_{Ag}^{fcc} + 3400 - 1.1 \times T$	This work
$G_{Sn} = {}^*G_{Sn} + 4400 - 6.0 \times T,\ G_{In} = {}^*G_{In} + 1500$	This work
${}^0L_{Ag,In} = -16535.2 - 2.72 \times T,\ {}^1L_{Ag,In} = 26777.6,\ {}^0L_{Mg,Sn} = -4184.0$	This work
${}^0L_{Ag,Mg} = -45187.2 - 7.64 \times T,\ {}^1L_{Ag,Mg} = 20083.2 - 5.02 \times T,\ {}^2L_{Ag,Mg} = 23012$	This work
${}^0L_{Ag,Mg,Sn} = -92048,\ {}^1L_{Ag,Mg,Sn} = -125520.0 + 4.18 \times T,\ {}^2L_{Ag,Mg,Sn} = -29288.0 + 2.09 \times T$	This work
${}^0L_{Ag,In,Mg} = -83680 + 8.37 \times T,\ {}^1L_{Ag,In,Mg} = {}^2L_{Ag,In,Mg} = 62760$	This work
bcc_B2 phase, (Ag,In,Mg,Sn)(Ag,In,Mg,Sn)	
$G_{Mg:Ag} = G_{Ag:Mg} = -22593.6 + 3.82 \times T, G_{In:Ag} = G_{Ag:In} = 8267.6 + 1.36 \times T$	This work
$G_{Mg:In} = G_{In:Mg} = -2092 + 2.09 \times T$	This work
${}^0L_{Ag,Mg:Ag} = {}^0L_{Ag:Ag,Mg} = 37237.6 - 0.05 \times T, {}^0L_{Ag,Mg:Mg} = {}^0L_{Mg:Ag,Mg} = 8368 - 0.05 \times T$	This work
${}^1L_{Ag,Mg:Ag} = {}^1L_{Ag,Mg:Mg} = {}^1L_{Mg:Ag,Mg} = {}^1L_{Ag:Ag,Mg} = -4811.6 + 1.26 \times T$	This work
${}^0L_{Ag,In:Ag} = {}^0L_{Ag:Ag,In} = 28350.8 + 1.36 \times T, {}^0L_{Ag,In:In} = {}^0L_{In:Ag,In} = -11815.6 + 1.36 \times T$	This work
${}^1L_{Ag,In:Ag} = {}^1L_{Ag,In:In} = {}^1L_{In:Ag,In} = {}^1L_{Ag:Ag,In} = -6694.4$	This work
${}^0L_{Ag,Mg:In} = {}^0L_{In:Ag,Mg} = -33472 - 0.84 \times T$	This work
${}^0L_{Ag,Mg:Sn} = {}^0L_{Sn:Ag,Mg} = -48952.8, {}^0L_{Mg,Sn:Ag} = {}^0L_{Ag:Mg,Sn} = -50626.4$	This work
$AgMg_4$ phase, $(Ag)(In,Mg)_4$	This work
$G_{Ag:Mg} = 4 \times G_{Mg}^{hcp} + G_{Ag}^{fcc} - 55980 + 19.07 \times T, G_{Ag:In} = 4 \times {}^*G_{In} + G_{Ag}^{fcc}$	
Ag_3Sn phase, $(Ag,Mg,Sn)_3(Sn)$	This work
$G_{Ag:Sn} = 3 \times G_{Ag}^{fcc} + {}^*G_{Sn} - 18430.5 - 8.91 \times T, G_{Mg:Sn} = 3 \times G_{Mg}^{hcp} + {}^*G_{Sn}$	This work
$G_{Sn:Sn} = 4 \times {}^*G_{Sn} + 58576.0$	
$AgIn_2$ phase, $(Ag)(In)_2$: $G = G_{Ag}^{fcc} + 2 \times {}^*G_{In} -21764 + 21.3 \times T$	This work
Ag_3In phase, $(Ag)_3(Ag,In)$	
$G_{Ag:In} = 3 \times G_{Ag}^{fcc} + {}^*G_{In} - 30982.5, G_{Ag:Ag} = 4 \times G_{Ag}^{fcc}, {}^0L_{Ag:Ag,In} = -12296.8 + 71.55 \times T$	This work
Ag_2In phase, $(Ag)_2(Ag,In,Sn)$	
$G_{Ag:In} = 2 \times G_{Ag}^{fcc} + {}^*G_{In} - 23790.2 - 1.33 \times T, G_{Ag:Ag} = 3 \times G_{Ag}^{fcc}, G_{Ag:Sn} = 2 \times G_{Ag}^{fcc} + {}^*G_{Sn} - 4184.0$	This work
${}^0L_{Ag:Ag,In} = -4184.0, {}^0L_{Ag:Ag,Sn} = -5439.2 - 7.95 \times T$	This work
$InMg_2$ phase, $(In)(Mg)_2$: $G = 2 \times G_{Mg}^{hcp} + {}^*G_{In} -29022.64 + 1.09 \times T$	This work
In_2Mg_5 phase, $(In)_2(Mg)_5$: $G = 5 \times G_{Mg}^{hcp} + 2 \times {}^*G_{In} -65022.3 + 5.14 \times T$	This work

To be continued

Table 7.7 (continued) Optimized model parameters for phases in the quaternary Mg-Sn-Ag-In system

Phase, model and thermodynamic parameters ($J \cdot mol^{-1}$ or $J \cdot mol^{-1} \cdot K^{-1}$)	Reference
fcc_L12 phase, $(Ag,Mg)(Ag,Mg)_3$	
$G_{Mg:Ag} = 4184.0, G_{Ag:Mg} = -2092$	This work
${}^0L_{Ag:Ag,Mg} = -3430.9 + 27.87 \times T, {}^0L_{Mg:Ag,Mg} = 12259.1 + 36.23 \times T, {}^0L_{Ag,Mg:Ag} = 2343.0 + 12.64 \times T$	This work
${}^0L_{Ag,Mg:Mg} = -795.0 + 10.96 \times T, {}^1L_{Ag:Ag,Mg} = {}^1L_{Mg:Ag,Mg} = 43095.2 + 33.89 \times T$	This work

$${}^*G_{In} = \int {}^*Cp_{In}dt - T \times \int \frac{{}^*Cp_{In}}{T}dt, \qquad {}^*G_{Sn} = \int {}^*Cp_{Sn}dt - T \times \int \frac{{}^*Cp_{Sn}}{T}dt$$

$${}^*Cp_{Sn} = 25.858 - 0.0010237 \times T - 36880/T^{-2} + 1.9156602 \times 10^{-5} \times T^2 \qquad 249K<T<250K$$

$$= 15.961 + 0.0377404 \times T + 123920/T^{-2} - 1.8727002 \times 10^{-5} \times T^2 \qquad 251K<T<1000K$$

$$= 35.098 \qquad 506K<T<3000K$$

$${}^*C_p(In) = 21.8386 + 0.01145132 \times T + 45812 \times T^{-2} + 1.2721926 \times 10^{-5} \times T^2 \qquad 298K<T<429.78K$$

$$= 31.05 - 0.0001919 \times T - 312000 \times T^{-2} + 3.374 \times 10^{-8} \times T^2 \qquad 429.79K<T<3800K$$

The Ag-In system

The calculated phase diagram of the Ag-In binary system is shown in Fig. 7.8 along with the experimental data [39, 43, 47, 48]. The bcc, fcc, hcp, AgIn$_2$, Ag$_2$In, Ag$_3$In phases were taken into account according to the experimental results reported above. The Ag$_2$In phase was treated with a two sub-lattice model as (Ag, In) (Ag)$_2$ to reproduce its solid solubility and crystal structure.

The Ag$_3$In phase was calculated to decompose at $187\,^{\circ}$C following the peritectoid reaction hcp + fcc $\leftrightarrow$ Ag$_3$In, which is identical to the temperature measured by Weibke and Eggers [39] and Campbell and Wagemann [43]. All the invariant reactions in the calculated phase diagram of Ag-In binary system are listed in Table 7.8.

The calculated enthalpies of mixing of the liquid phase at 470, 755, 970 $^{\circ}$C are shown in Fig. 7.9 along with experimental data [50-53, 57]. As shown in the figure, data obtained by direct calorimetric measurements [52, 53, 57] are in reasonable agreement with each other. However, data derived from emf measurements [50, 51] do not agree very well with the data obtained by direct calorimetric measurements. Therefore, priority was given to the later during the optimization.
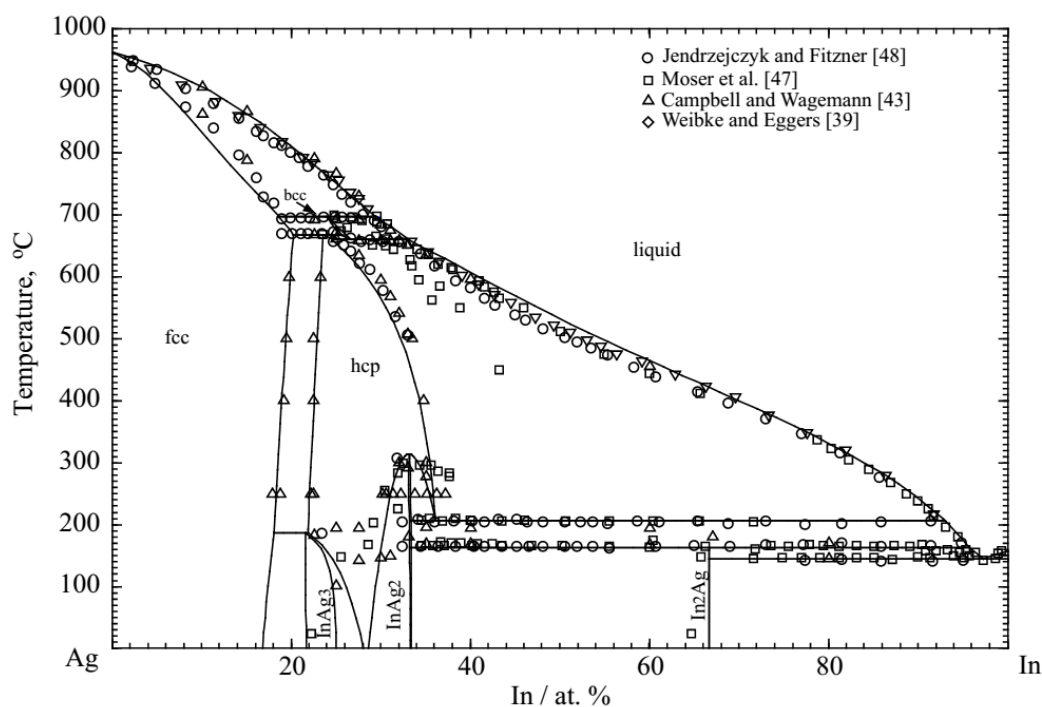
Figure 7.8 Calculated phase diagram of Ag-In system compared with experimental data [39, 43, 47, 48]

**Table 7.8** Calculated invariant reactions in the Ag-In system compared with experimental data

Reaction	Reaction type	Temperature (°C)	Composition (In at. %)			Reference
$hcp + fcc \leftrightarrow Ag_3In$	Peritectiod	187	20.0	-	-	[46]
		187	21.8	18.0	21.6	This work
$liquid + fcc \leftrightarrow bcc$	Peritectic	695	29.5	21	25.0	[46]
		697	29.4	18.6	24.0	This work
$fcc + bcc \leftrightarrow hcp$	Peritectiod	670	20.9	-	25.0	[46]
		667	20.2	25.3	23.6	This work
$bcc \leftrightarrow liquid + hcp$	Peritectiod	660	29.0	32.5	-	[46]
		660	26.7	33.4	24.6	This work
$hcp \leftrightarrow liquid + Ag_2In$	Peritectic	205	45.9	92.2	33.5	[46]
		205	36.1	93.1	33.3	This work
$liquid + Ag_2In \leftrightarrow AgIn_2$	Peritectic	166	-	33.5	-	[46]
		163	95.8	33.3	66.7	This work
$liquid \leftrightarrow AgIn_2 + tet(In)$	Eutectic	144	96.8	-	-	[46]
		144	97.2	66.7	100	This work
$hcp \leftrightarrow Ag_2In$	Congruent	312	-	-	-	[46]
		313	33.3	33.3	-	This work

The calculated activities of In in the liquid phase, collected between 727 and 1027 °C, are shown in Fig. 7.10 together with the experimental data discussed above [48, 50, 51, 54-56, 59]. The calculated enthalpies of formation of the solid phases at 25 °C are shown in Fig. 7.11 along with the experimental data of Kleppa [49] and Orr and Hultgren [58]. As we can see from the figures, our calculated results are in a good agreement with experimental data. All the parameters of the thermodynamic models are listed in Tables 7.6 and 7.7.
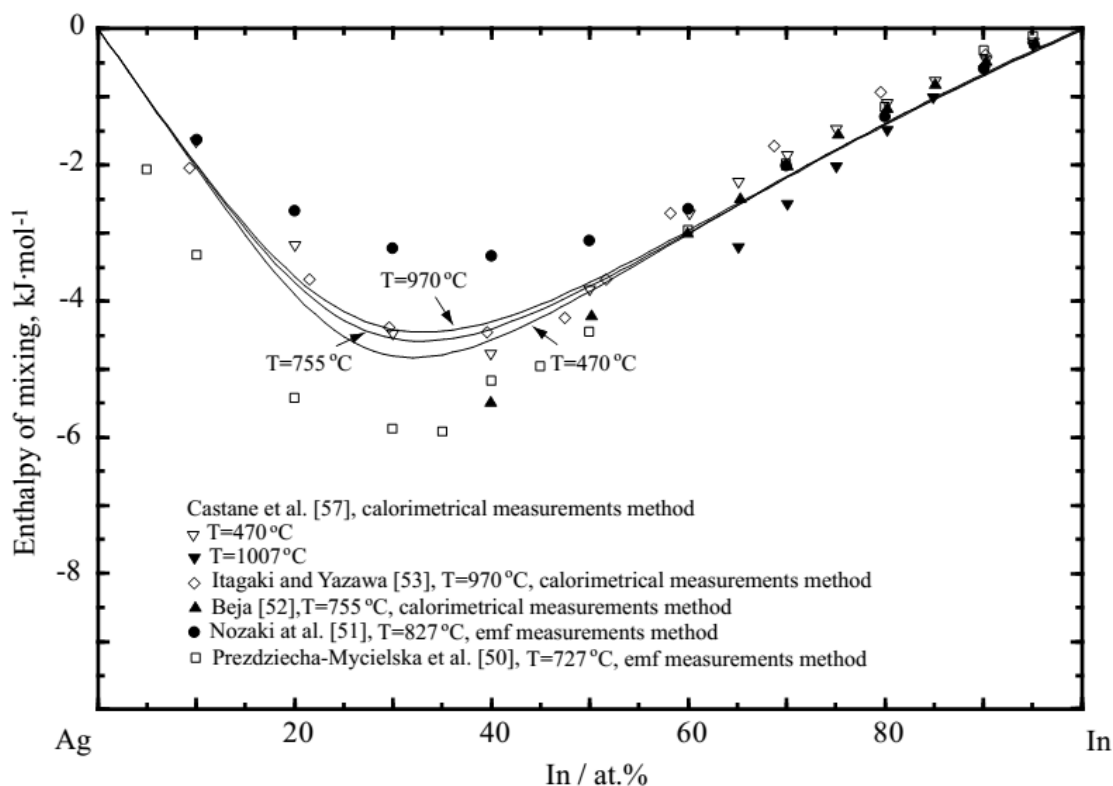
Figure 7.9 Calculated enthalpy of mixing of liquid phase at 470, 755 and 970 °C of Ag-In system compared with experimental data [50-53, 57]
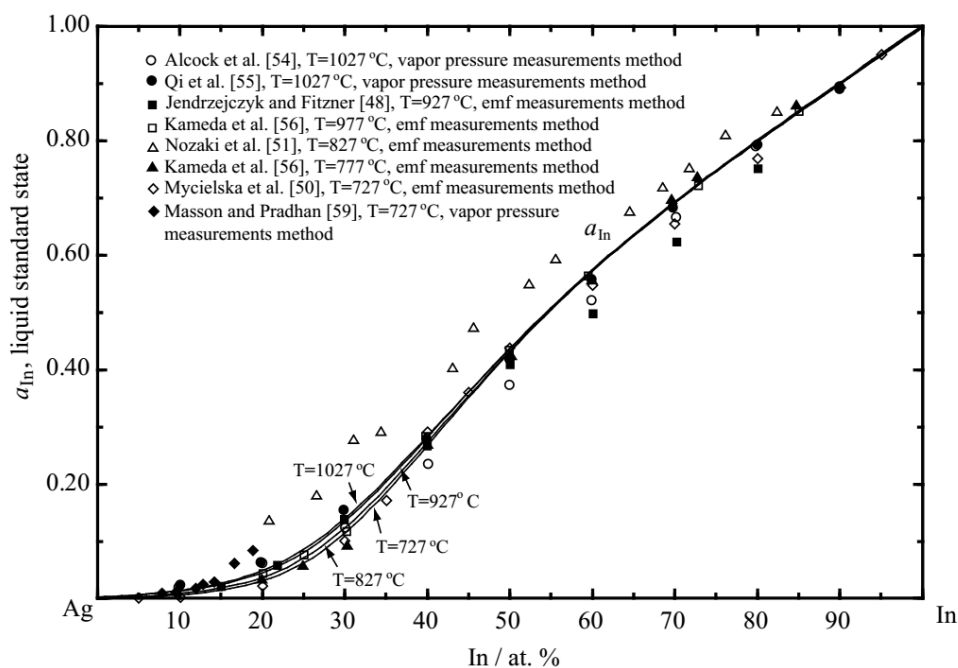
Figure 7.10 Calculated activity of In in the liquid phase in the temperature range of 727 °C to 1027 °C compared with experimental data [48, 50, 51, 54-56, 59]
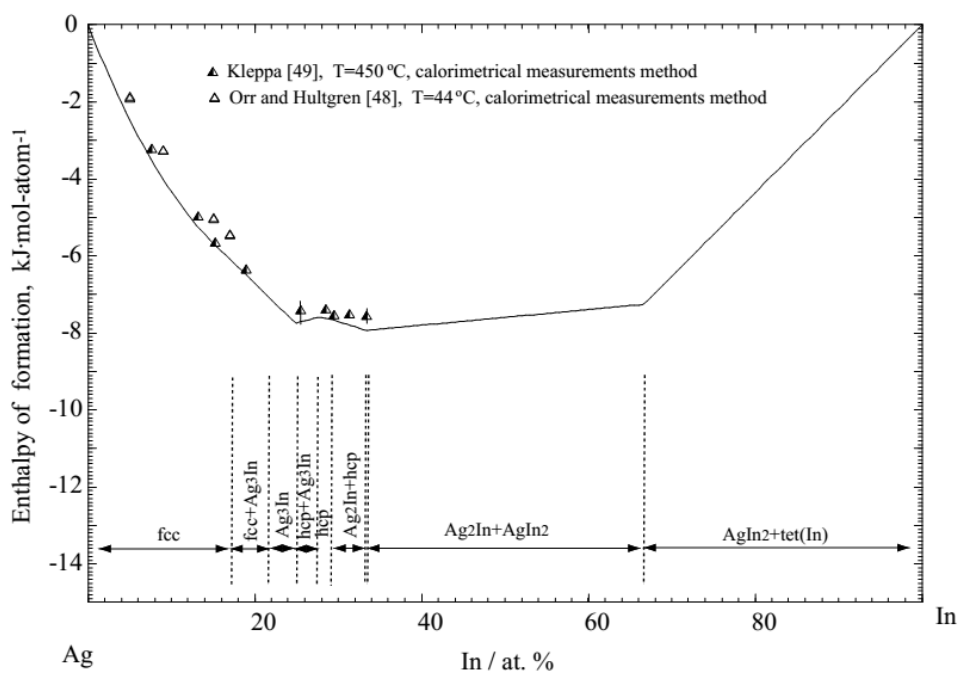
Figure 7.11 Calculated heat formation of solid phases of Ag-In system at 25 °C compared with experimental data [49, 48]

The Ag-Sn system

The calculated phase diagram of the Ag-Sn binary system is shown in Fig. 7.12 along with experimental data [62, 63, 65, 66, 68-71, 82]. According to our calculations, the hcp phase is formed from the peritectic reaction liquid + fcc ↔ hcp at 724 ^{o}C, which is identical to the experimental data reported by Murphy [65]. The Ag_3Sn binary compound was treated as a solid solution with a two sub-lattice model as $(Ag, Sn)_3 (Sn)$. It was calculated to form at 480 ^{o}C from the peritectic reaction liquid + hcp ↔ Ag_3Sn, which is in a good agreement with experimental data [63, 65]. All our calculated invariant reactions along with the compiled experimental data are listed in the Table 7.9.

The calculated enthalpy of mixing of the liquid phase at 1000 ^{o}C, the calculated activity of Sn in the liquid phase, and the calculated enthalpies of formation of the solid phases at 25 ^{o}C are shown along with experimental data in Figs. 7.13, 7.14, and 7.15, respectively. As we can see, all the data are in a reasonable agreement with each other and our optimization results agree well with the reported experimental data. All the thermodynamic parameters are listed in Tables 7. 6 and 7. 7.
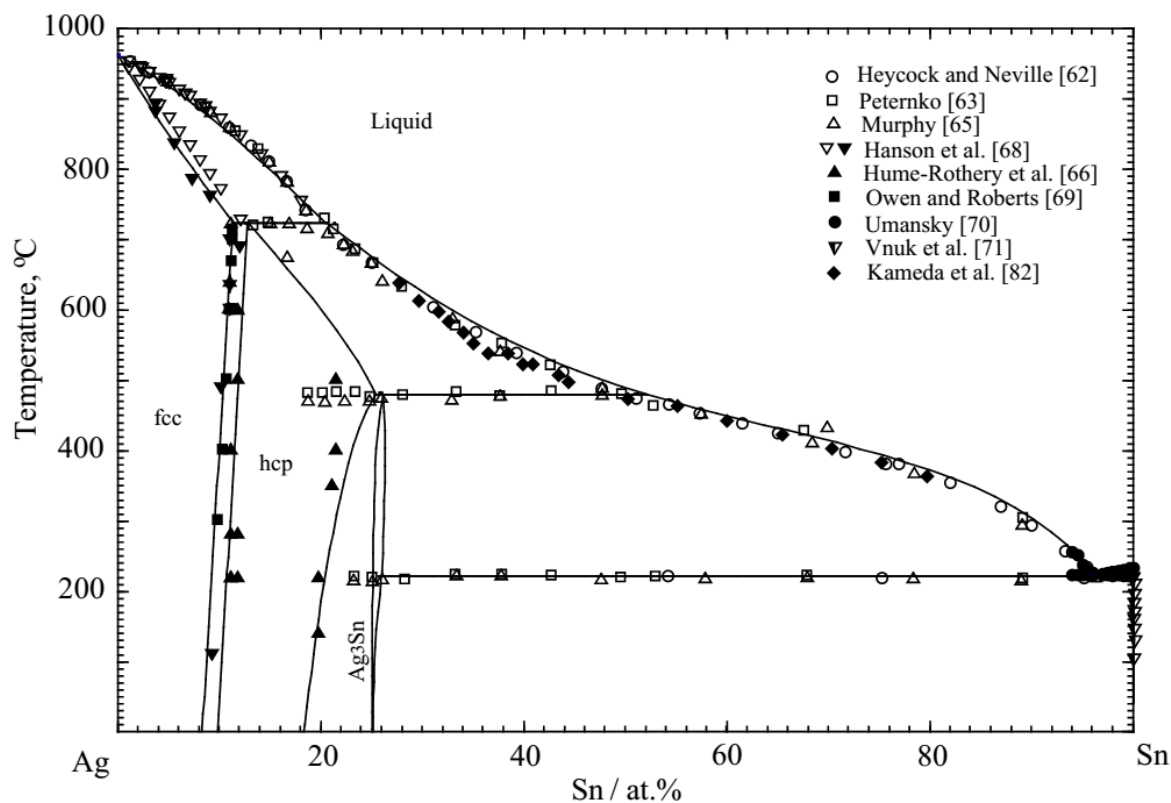
Figure 7.12 Calculated phase diagram of Ag-Sn system compared with experimental data [62, 63, 65, 66, 68-71, 82]

Table 7.9 Calculated invariant reactions in the Ag-Sn system compared with experimental data

Reaction	Reaction type	Temperature (°C)	Composition (Sn at. %)			Reference
$liquid + fcc \longleftrightarrow hcp$	Peritectic	724	19.5	11.5	13.0	[72]
		724	20.3	11.3	12.7	This work
$liquid + hcp \longleftrightarrow Ag_3Sn$	Peritectic	480	49.6	22.8	25.0	[72]
		480	52.1	25.3	26.0	This work
$liquid \longleftrightarrow Ag_3Sn + bct(Sn)$	Eutectic	221	96.2	25.9	99.91	[72]
		221	96.2	25.9	99.93	This work
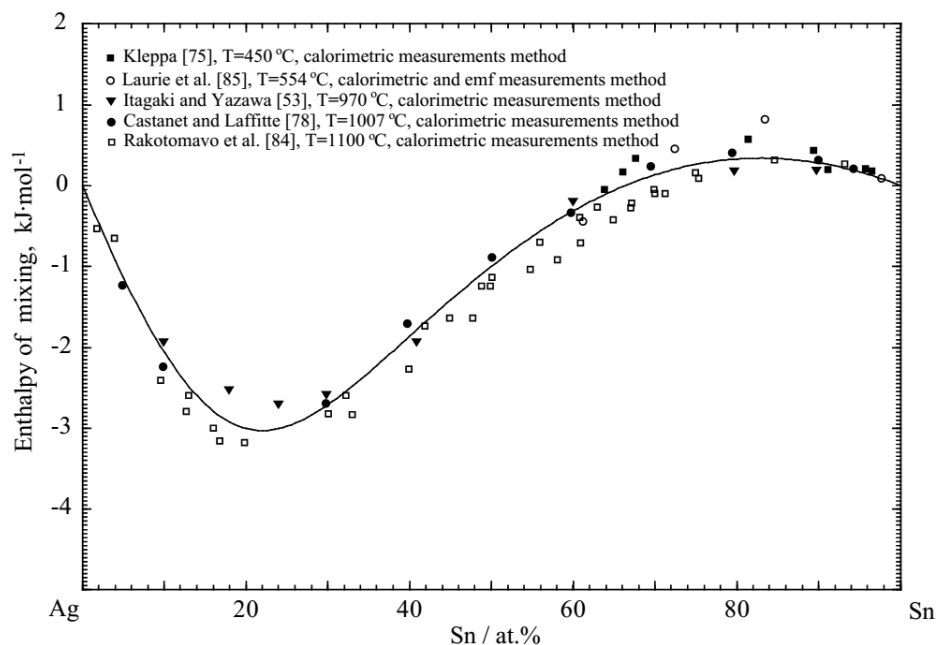
Figure 7.13 Calculated mixing of enthalpy of liquid phase of Ag-Sn system at 1000 $^{\circ}$C compared with experimental data [53, 75, 78, 84, 85]
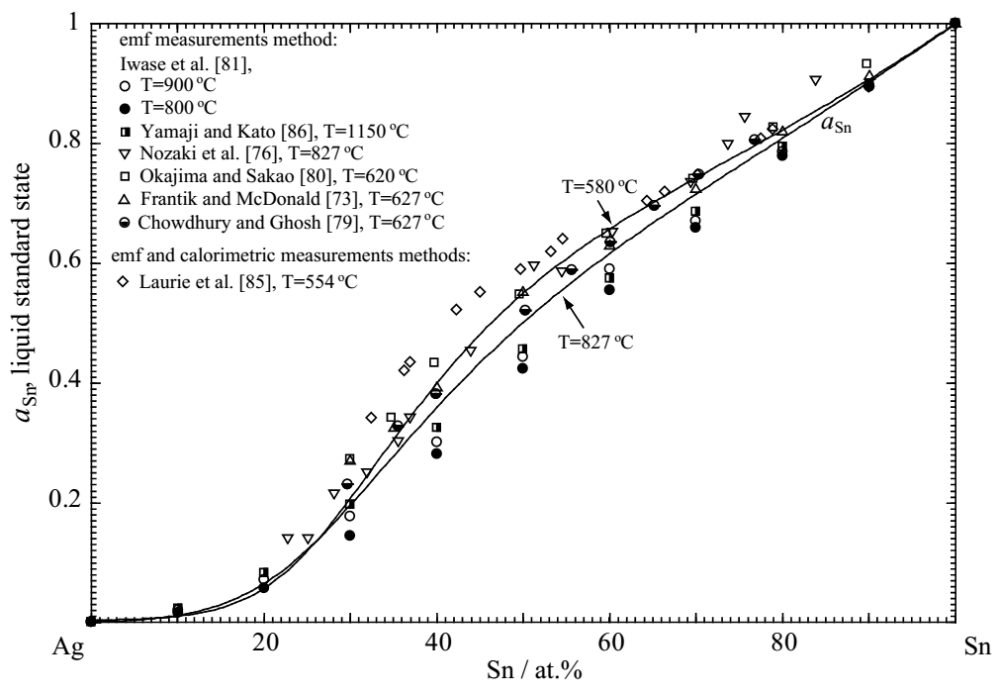
Figure 7.14 Calculated activity of Sn in liquid Ag-Sn alloys at 827 $^{\circ}$C and 580 $^{\circ}$C compared with experimental data [73, 76, 79-81, 85, 86]
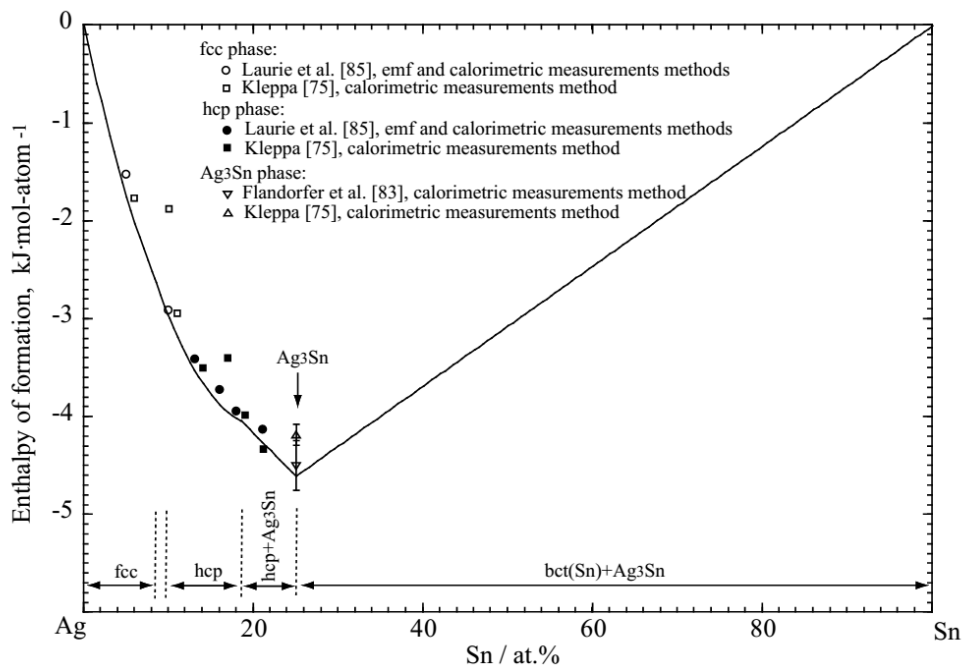
Figure 7.15 Calculated enthalpy of formation of compounds of Ag-Sn system at 25 ^{o}C compared with experimental data [75, 83, 85]

The Mg-Ag-In system

The Mg-In binary system was optimized in our previous work [97] and the Ag-Mg, and Ag-In in this one. The liquid phases of the Mg-In, Ag-Mg, and Ag-In binary systems have totally different thermodynamic properties; as a result, ternary parameters of the liquid phase of Mg-Ag-In system were modeled with the symmetric Kohler-like [107] approximation in the MQMPA.

The calculated isothermal section at 280 ^{o}C and the three ternary isopleths are shown in Figs. 7.16 and 7.17, respectively, along with experimental data [87]. As shown in Fig. 7.16, the calculated results are in a reasonable agreement with experimental data. However, the solubility limits of In and Ag in the terminal hcp (Mg) phase, as reported by Kolesnichenko [87], are different from the compiled data of Mg-Ag binary system [19] Consequently, new experimental data appear to be necessary here to resolve this issue.
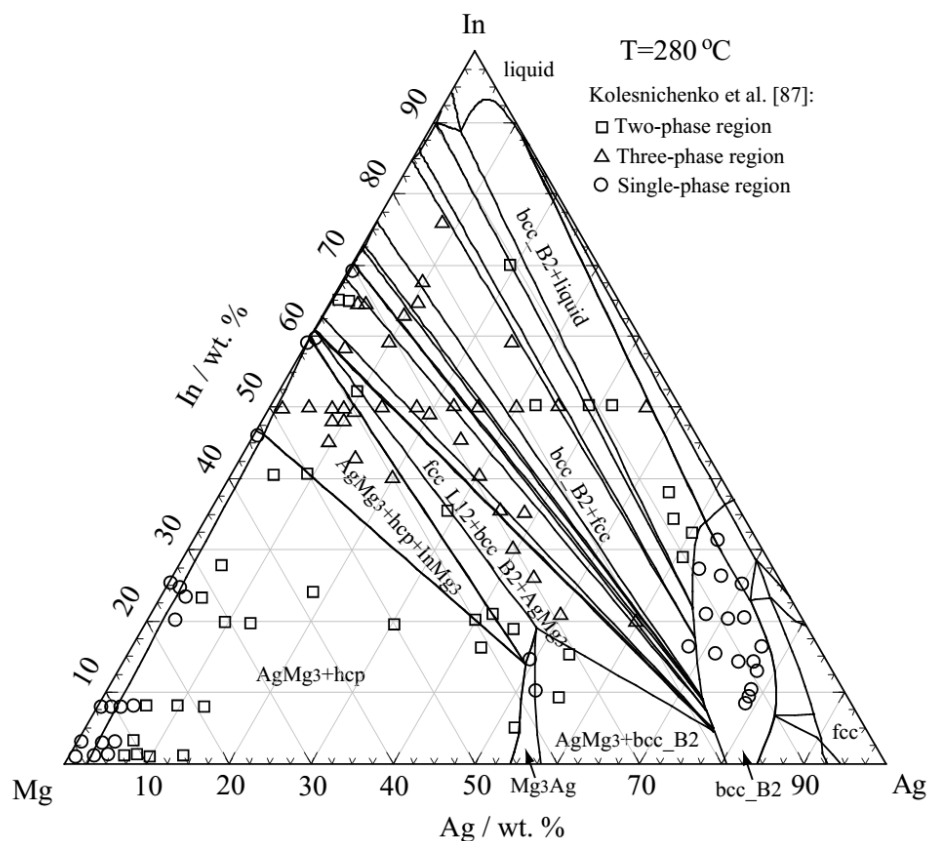
Figure 7.16 Calculated isothermal section of Mg-Ag-In ternary system at 280 °C along with experimental data [87]

The calculated liquidus projection of the Mg-Ag-In ternary system is shown in Fig. 7.18 and the calculated invariant reactions are listed in Table 7.10. All the thermodynamic parameters used are listed in the Tables 7.6 and 7.7.
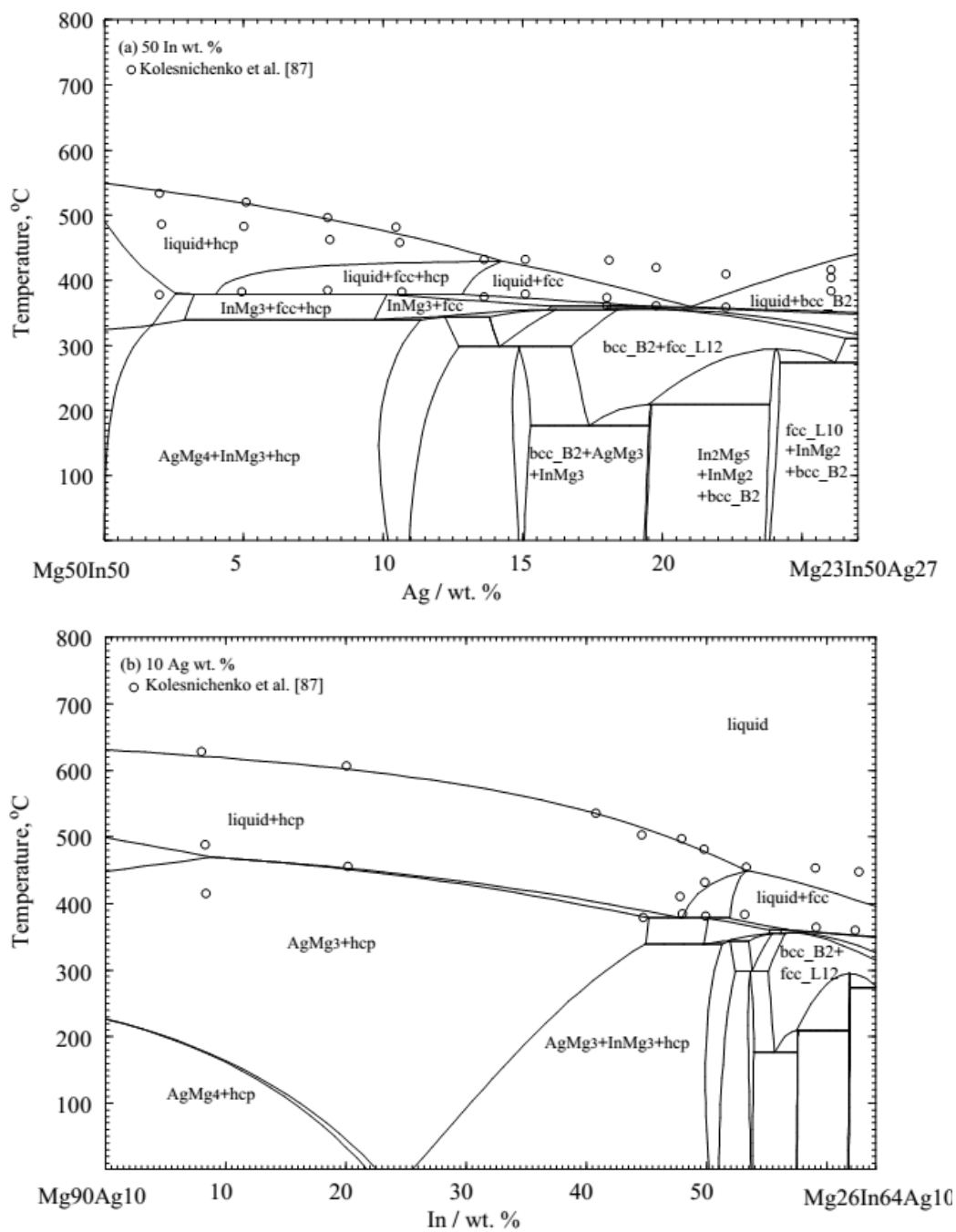
Figure 7.17 Calculated ternary isoplethal sections of the Mg-Ag-In system at (a) 50 In, (b) 10 Ag, and (c) 30 Mg (wt. %) along with the experimental data [87]
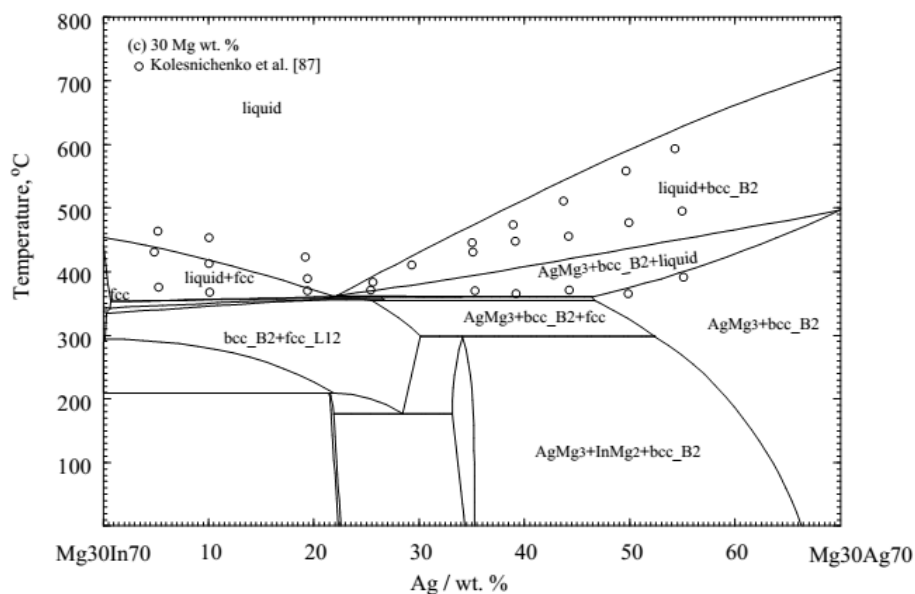
Figure 7.17 (Continued) Calculated ternary isoplethal sections of the Mg-Ag-In system at (a) 50 In, (b) 10 Ag, and (c) 30 Mg (wt. %) along with the experimental data [87]
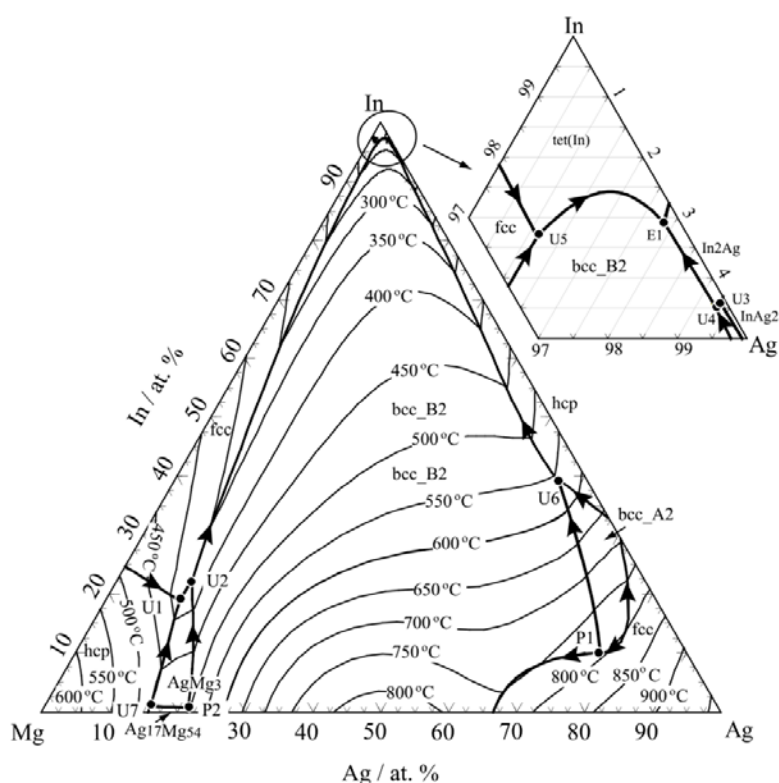
Figure 7.18 Calculated liquidus projection of the Mg-Ag-In ternary system

Table 7.10 Calculated invariant reactions in the liquidus projection of the Mg-Ag-In ternary system

Label	T (°C)	Reaction	Composition of liquid (at. %)		
			In	Mg	Ag
E1	145	$L \leftrightarrow tet(In) + bcc\_B2 + In_2Ag$	1.08	2.84	96.08
U1	377	$L + hcp \leftrightarrow AgMg_3 + fcc$	18.97	70.09	10.94
U2	360	$L + AgMg_3 \leftrightarrow fcc + bbc\_B2$	22.36	66.64	11.00
U3	162	$L + InAg_2 \leftrightarrow In_2Ag + hcp$	95.58	0.09	4.33
U4	161	$L + hcp \leftrightarrow bcc\_B2 + In_2Ag$	95.56	0.20	4.24
U5	156	$L + fcc \leftrightarrow tet(In) + bcc\_B2$	96.69	2.17	1.14
U6	557	$L + bcc\_A2 \leftrightarrow hcp\_A3 + bcc\_B2$	39.70	1.07	56.23
U7	468	$L + Ag_{17}Mg_{54} \leftrightarrow hcp\_A3 + AgMg_3$	0.86	83.09	16.05
P1	792	$L + fcc \leftrightarrow bcc\_A2 + bcc\_B2$	10.20	12.55	77.25
P2	491	$L + Ag_{17}Mg_{54} \leftrightarrow hcp\_A3 + AgMg_3$	0.54	78.36	21.10

The Mg-Ag-Sn system

All the available data from Raynor and Frost [88], Karonik *et al.* [89] and our current experimental data were taken into account in the present optimization. Since the liquid phases of the Ag-Mg, Ag-Sn, and Mg-Sn binary systems have totally different thermodynamic properties, the symmetric Kohler-like [107] extrapolation method was used for optimizing ternary liquid parameters of the Mg-Ag-Sn system within the MQMPA.

The calculated isothermal sections of the Mg-Ag-Sn ternary system are shown in Fig. 7.19 (a)-(d) along with experimental data from Raynor and Frost [88], Karonik *et al.* [89] and current experimental data.

The calculated ternary isoplethal sections with constant of 10 Sn and 10 Ag wt. % are depicted in Fig. 7.20 together with the experimental data of Karonik *et al.* [89]. The calculated ternary isopleths with constant value of 10 Sn and 30 Ag at. % are shown in Fig. 7.21 and compared with our new experimental data. As it can be seen, our calculated results are in reasonable agreement with the reported experimental data expect the two singles from sample Mg88Sn10Ag2 and Mg80Sn10Ag10. The unexpected singles observed at about 525-540 oC may due to the oxidation

and reaction with Al2O3 crucible problem, which needs to be verified with the further experiment. The calculated liquidus projection of the Mg-Ag-Sn system is shown in Fig. 7.22 and the calculated invariant reactions are listed in Table 7.10. All the thermodynamic parameters used are listed in the Tables 7.6 and 7.7.
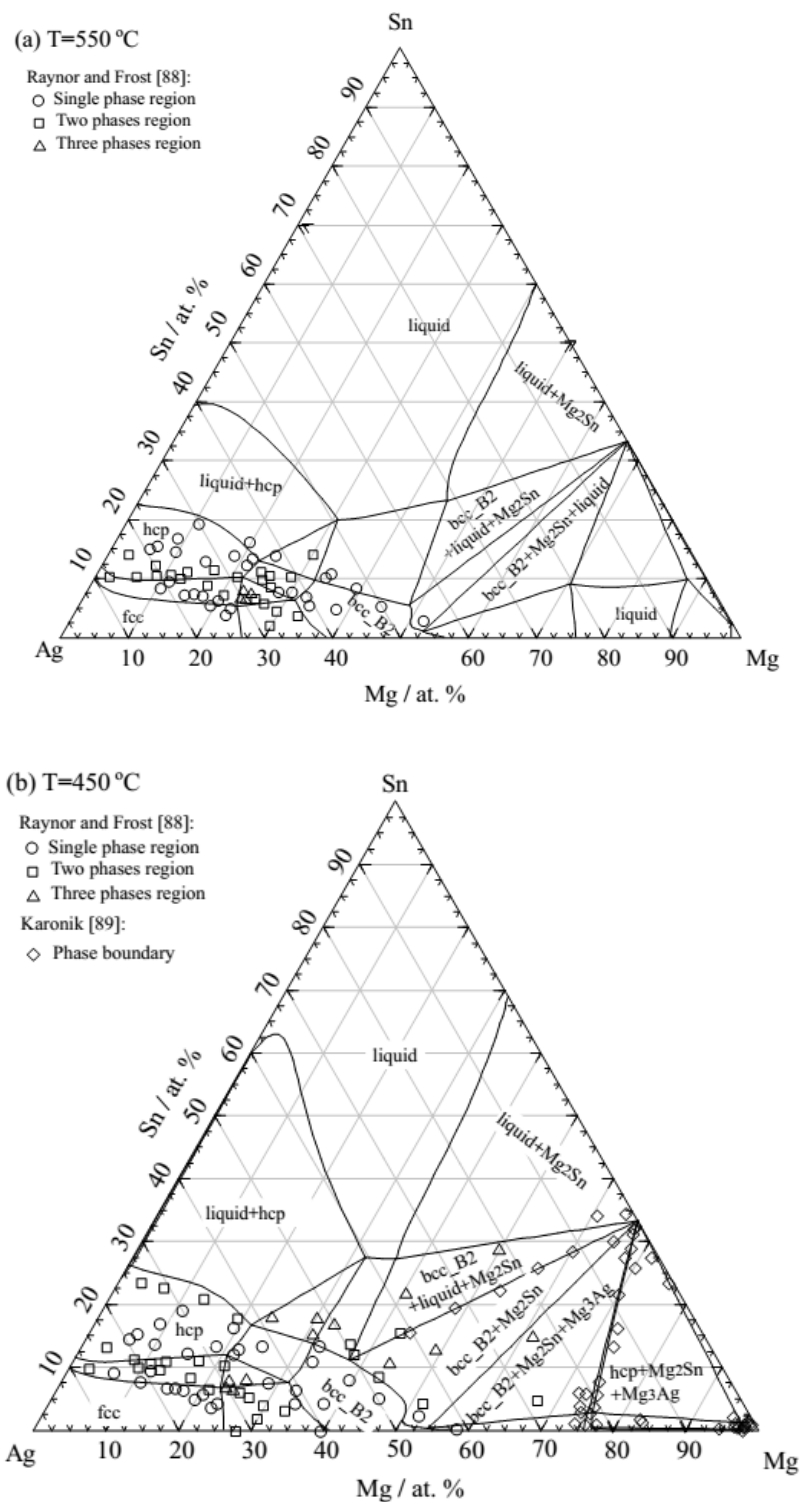
Figure 7.19 Calculated isothermal sections of the Mg-Ag-Sn ternary system at (a) 550 °C, (b) 450 °C, (c) 415 °C, and (d) 350 °C along with experimental data from present work and previous reported [88]
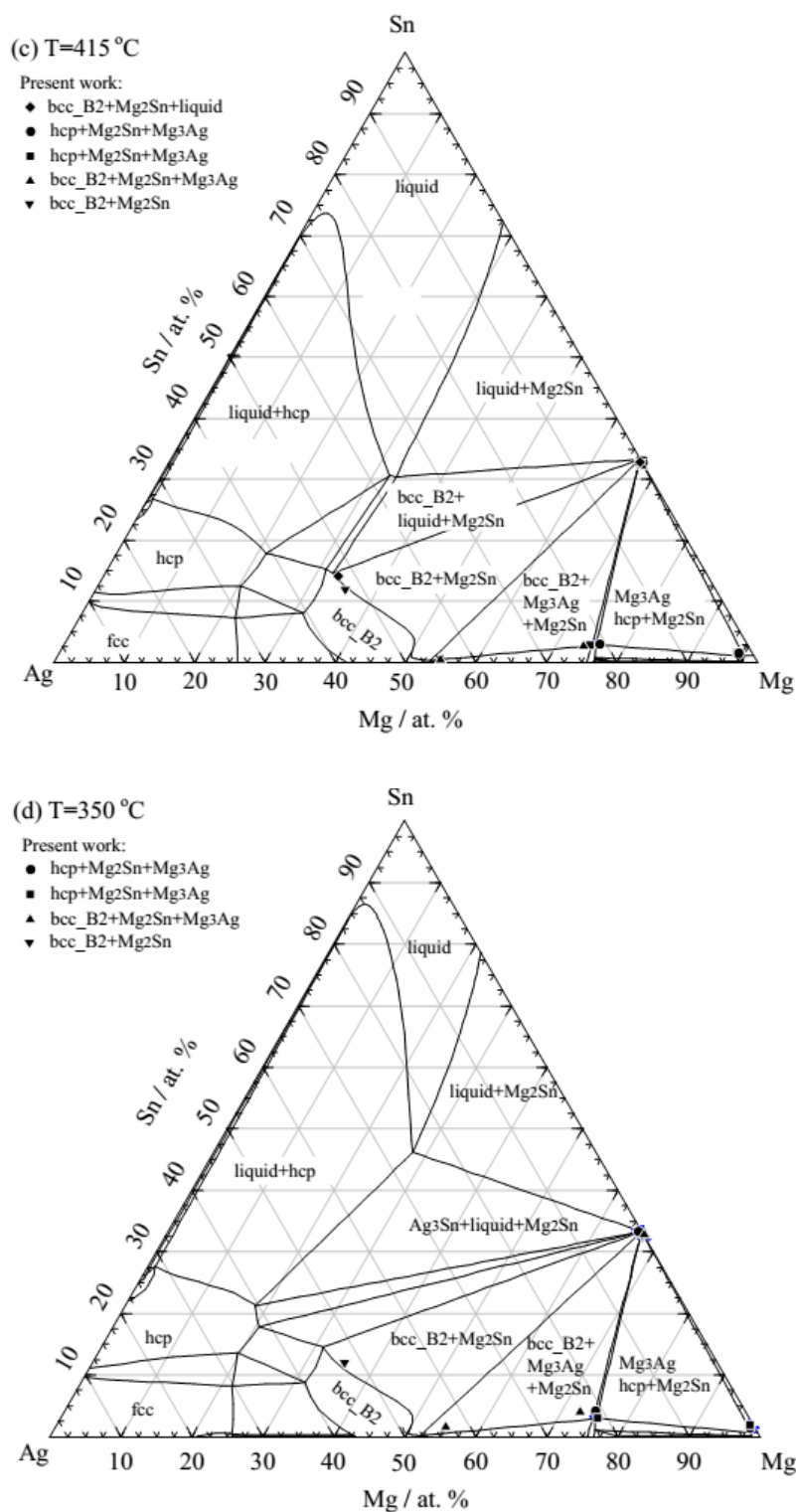
Figure 7.19 (Continued) Calculated isothermal sections of the Mg-Ag-Sn ternary system at (a) 550 °C, (b) 450 °C, (c) 415 °C, and (d) 350 °C along with experimental data from present work and previous reported [88]
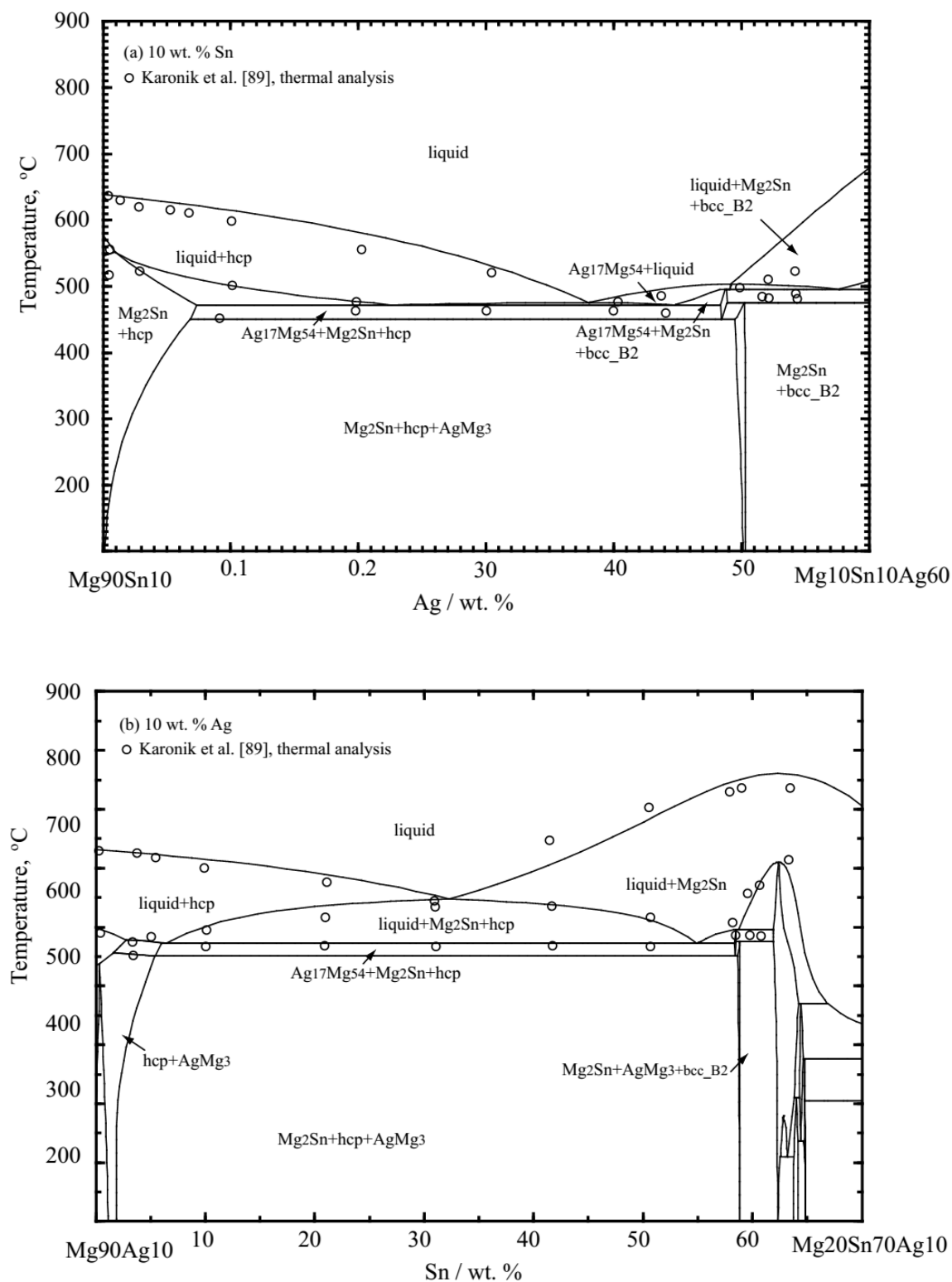
Figure 7.20 Calculated isoplethal sections of the Mg-Ag-Sn system at (a) 10 Sn and (b) 10 Ag (wt. %) compared with experimental data [89]
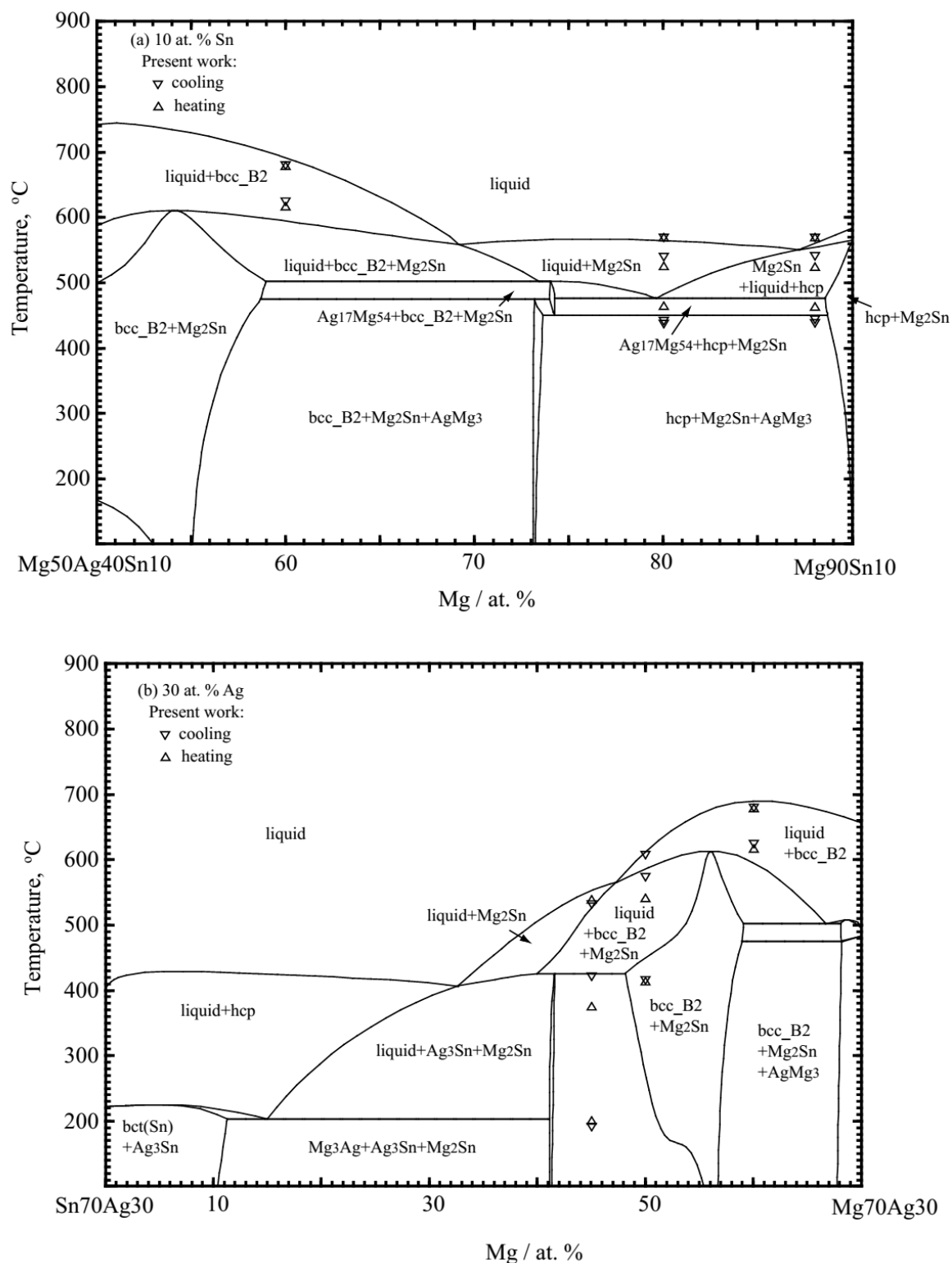
Figure 7.21 Calculated isoplethal sections of the of Mg-Ag-Sn system at (a) 10 Sn and (b) 30 (at. %) along with experimental data from present work
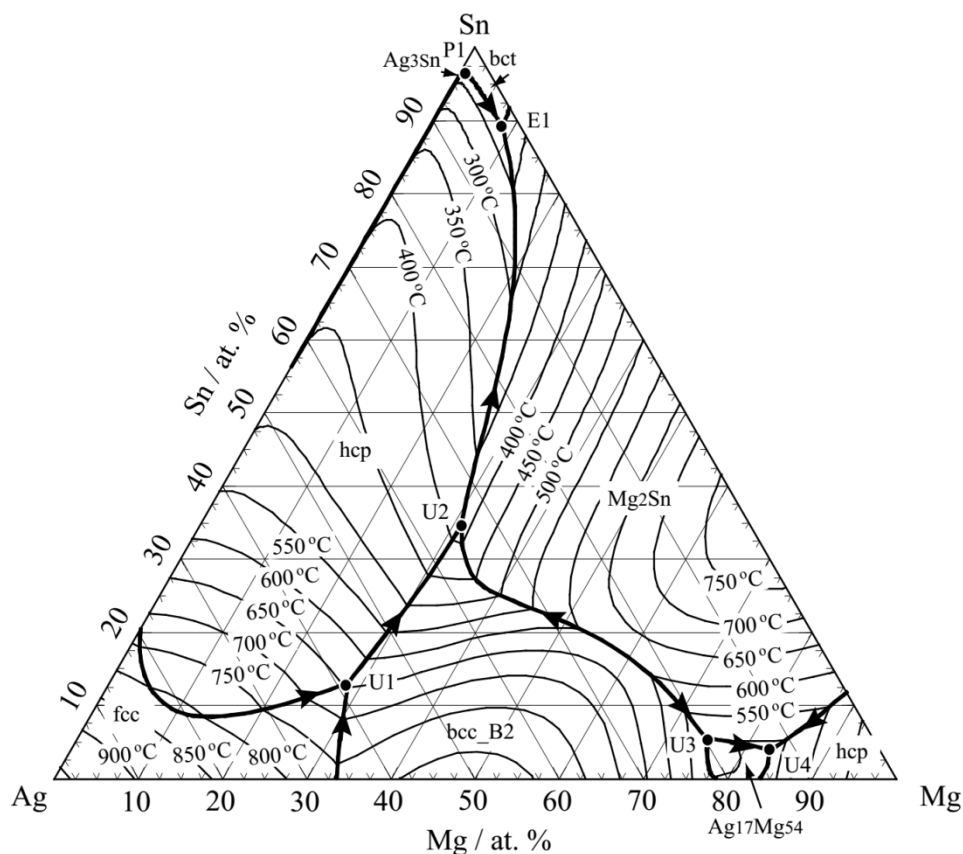
Figure 7.22 Calculated liquidus projection of the Mg-Ag-Sn ternary system

Table 7.11 Calculated invariant reactions in the liquidus projection of the Mg-Sn-Ag ternary system

Label	T (°C)	Reaction	Composition of liquid (at. %)		
			Mg	Ag	Sn
P1	221	$L + hcp \leftrightarrow bct + Ag_3 Sn$	0.01	3.85	96.13
E1	200	$L \leftrightarrow bct + Mg_2 Sn + hcp$	8.66	2.18	89.16
U1	641	$L + fcc \leftrightarrow hcp + bcc\_B2$	28.39	58.46	13.15
U2	382	$L + bcc\_B2 \leftrightarrow hcp + Mg_2 Sn$	30.99	34.34	34.67
U3	503	$L + bcc\_B2 \leftrightarrow Mg_{54} Ag_{17} + Mg_2 Sn$	74.87	19.73	5.39
U4	476	$L \leftrightarrow hcp + Mg_{54} Ag_{17} + Mg_2 Sn$	83.07	13.06	3.87

The Ag-In-Sn system

The In-Sn binary system was optimized in our previous work [97]. Zivkovic *et al.* [108] performed a comparative thermodynamic study of the Ag-In-Sn system and pointed out that the Toop-like model [107] is the most accurate method to calculate ternary liquid mixing parameters assuming Ag as an asymmetric component; Kohler and Toop [107] extrapolation techniques were both tested and Toop-like was found to be the best method to model the ternary liquid phase, which is in agreement with the suggestion from Zivkovic *et al.* [108].

The calculated isothermal sections at 180, 250, 400, and 600 $^{\circ}$C and isoplethal sections are shown in Figs. 7.23 and 7.24, respectively, along with experimental data [91]. Comparison of the measured [94] and calculated enthalpy of mixing of the liquid phase with different In/Sn atomic ratios is presented in Fig. 7.25. As it can be seen, the calculated results agree relatively well with experimental data. All the thermodynamic parameters used are listed in the Tables 7.6 and 7.7.
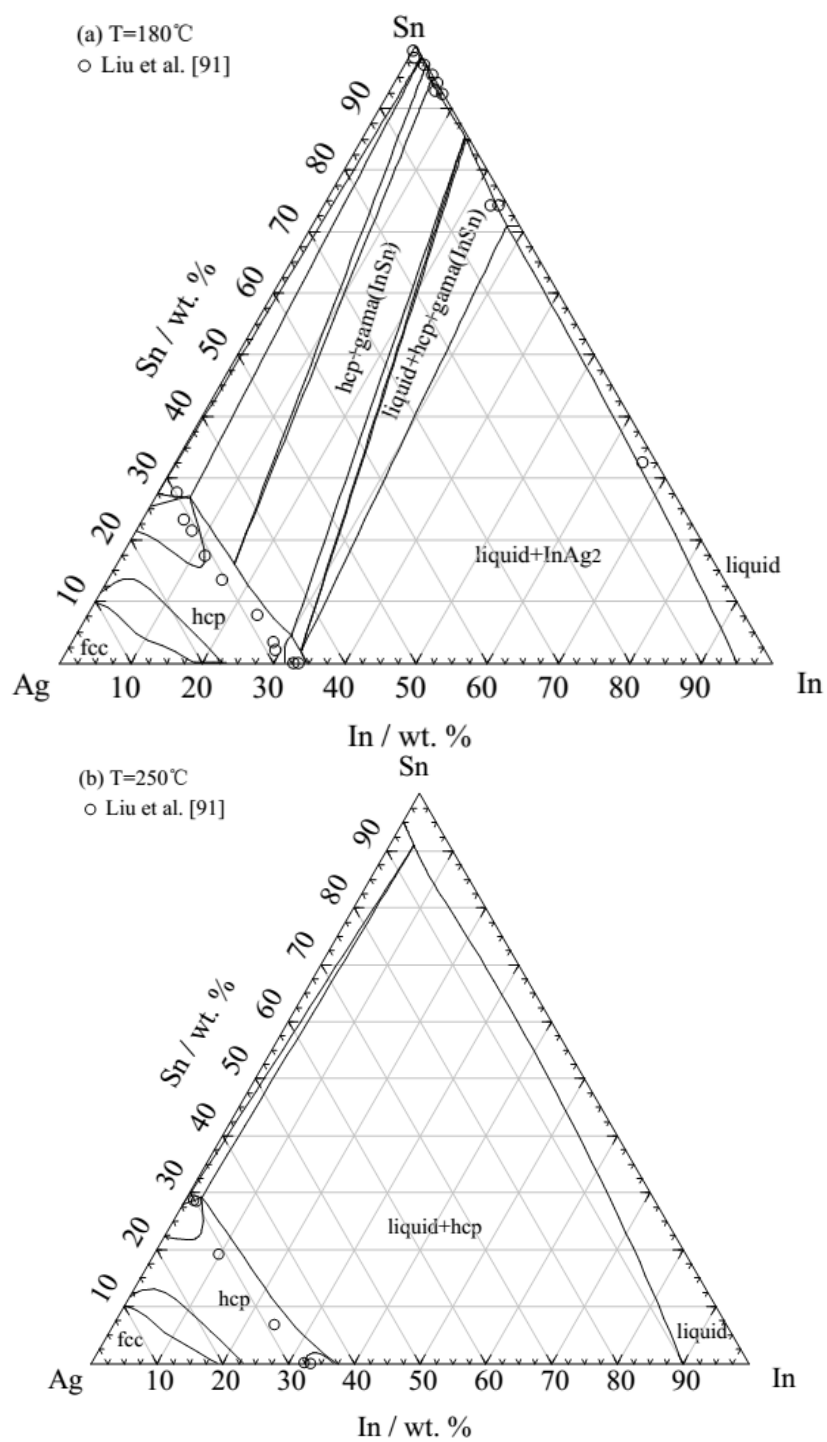
Figure 7.23 Calculated isothermal sections of the Ag-In-Sn ternary system at (a) 180 °C, (b) 250 °C, (c) 400 °C, and (d) 600 °C along with experimental data [91]

Figure 7.23 Calculated isothermal sections of the Ag-In-Sn ternary system at (a) 180 $^{\circ}$C, (b) 250 $^{\circ}$C, (c) 400 $^{\circ}$C, and (d) 600 $^{\circ}$C along with experimental data [91]
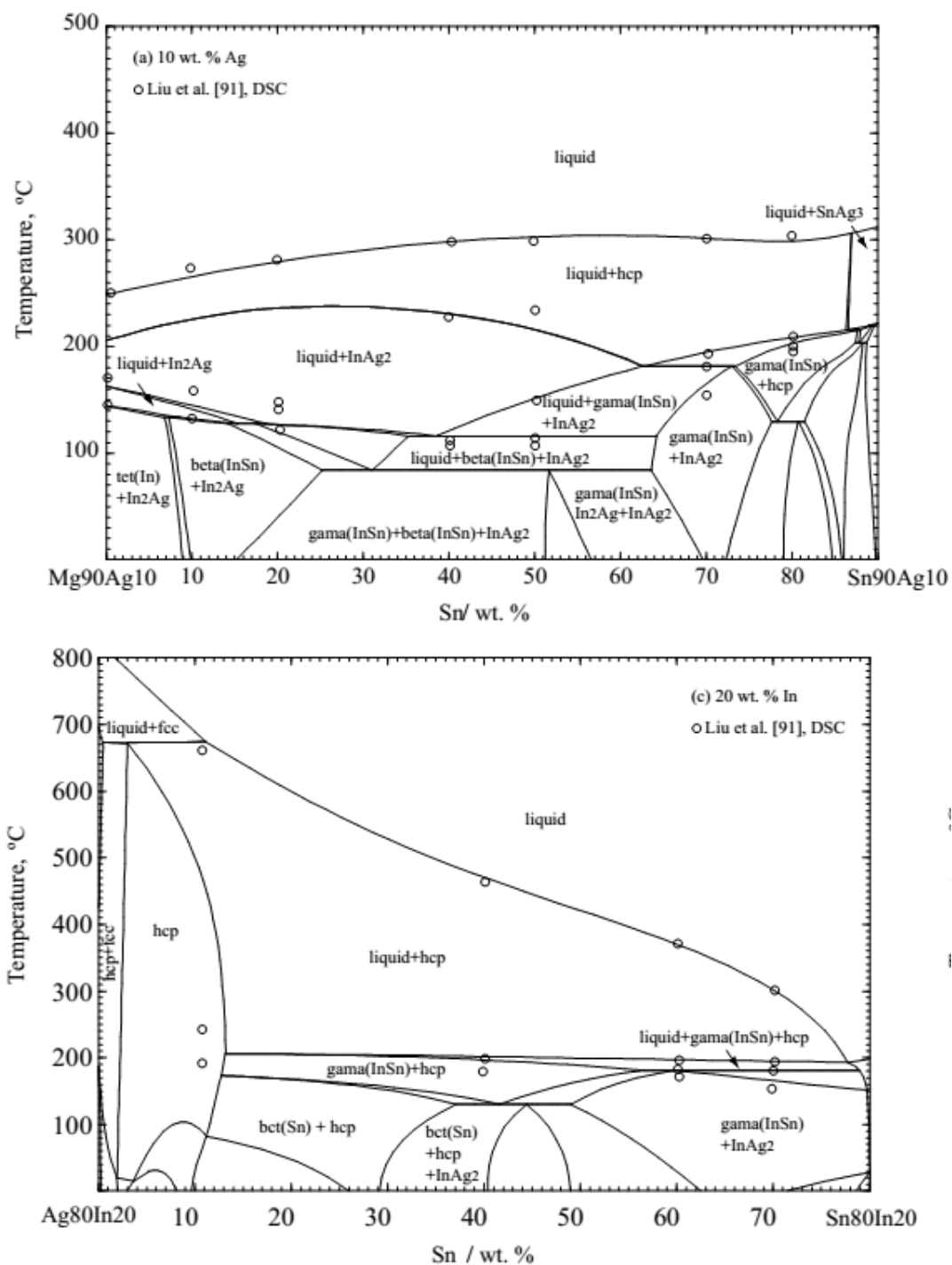
Figure 7.24 Calculated isoplethal sections of the Ag-In-Sn system at (a) 10 Ag, (b) 20 Ag, (c) 20 In, (d) 40 In (wt. %) in comparsion with experimental data [91]
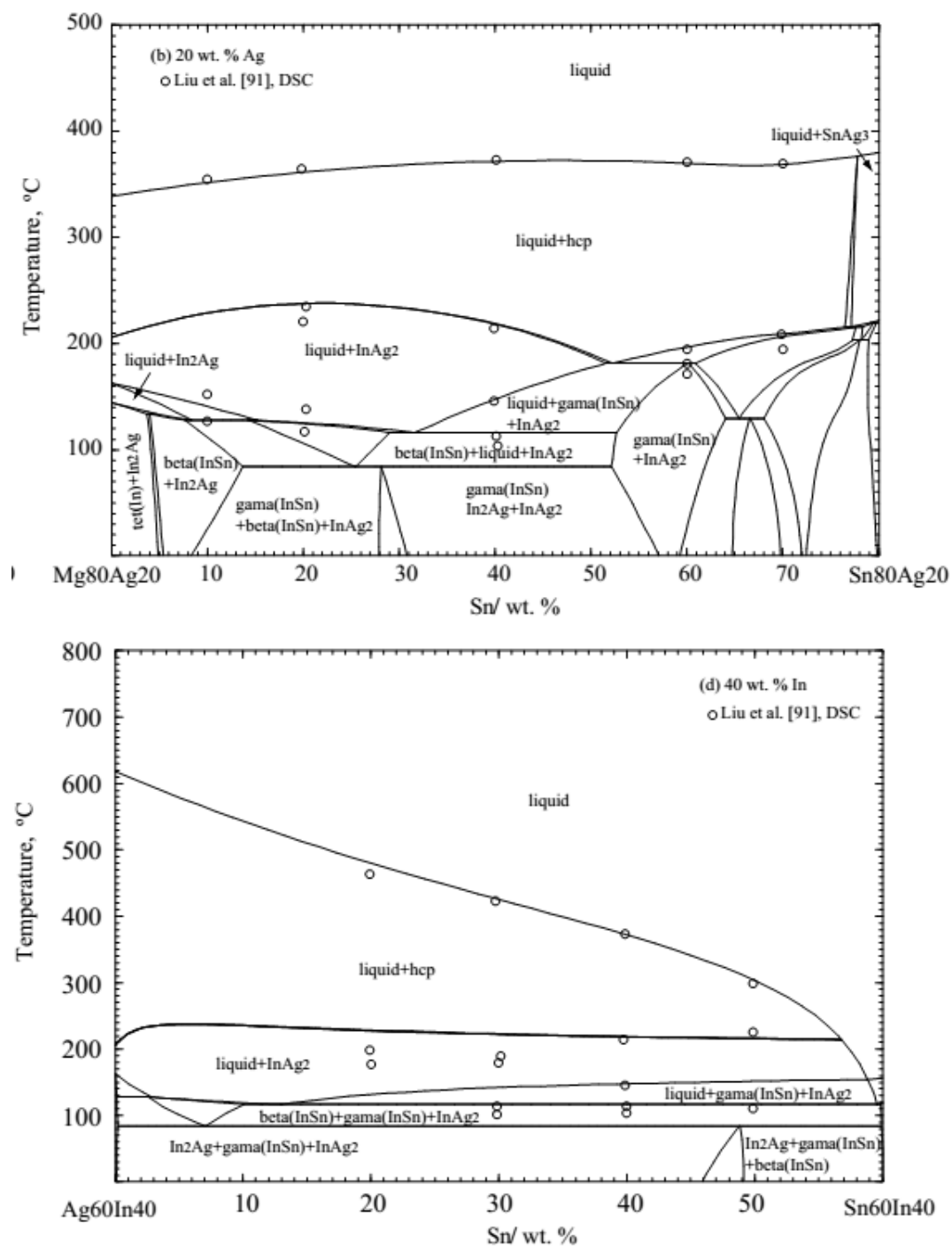
Figure 7.24 Calculated isoplethal sections of the Ag-In-Sn system at (a) 10 Ag, (b) 20 Ag, (c) 20 In, (d) 40 In (wt. %) in comparsion with experimental data [91]
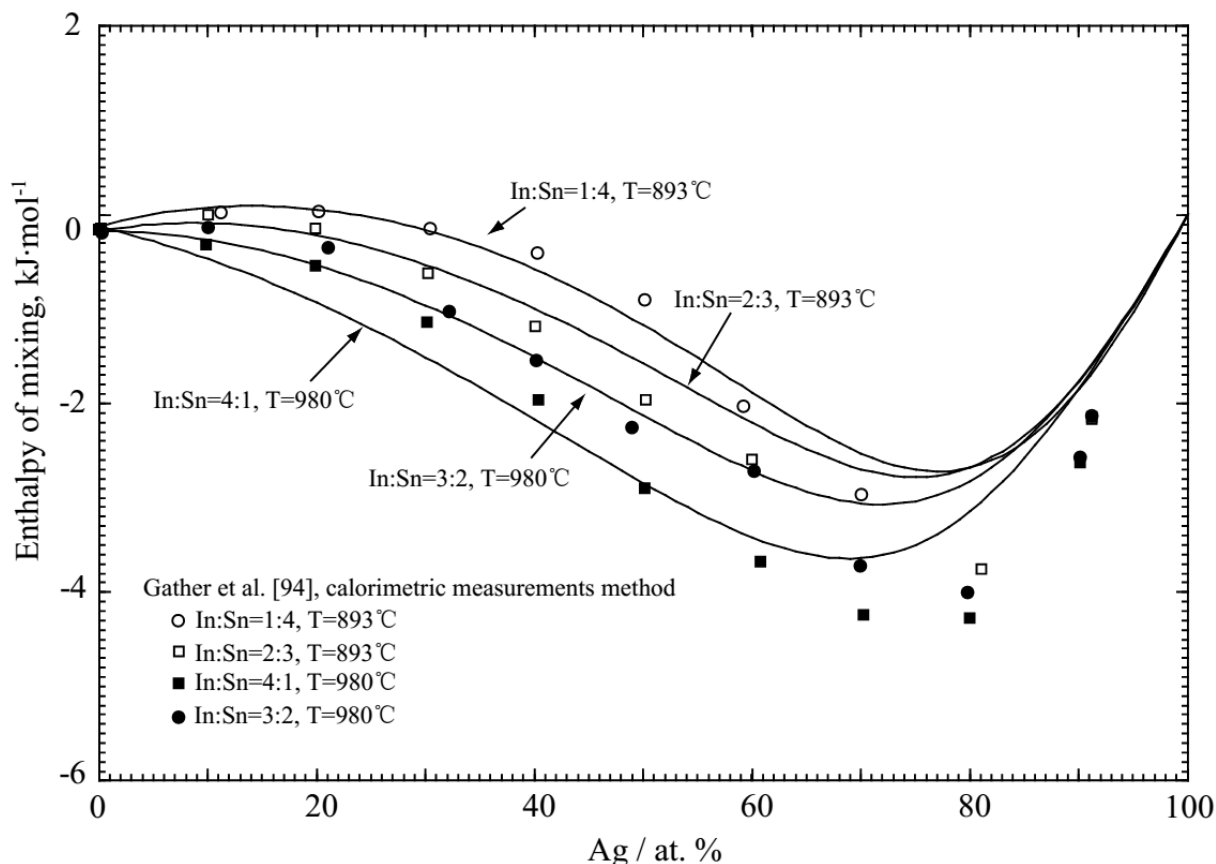
Figure 7.25 Measured and calculated enthalpy of mixing of the Ag-In-Sn liquid alloys for different In/Sn atomic ratios [94]

The Mg-Sn-Ag-In system

Phase equilibria in the Mg-rich portion of the Mg-Sn-Ag-In quaternary system at 300 and 450 $^{\circ}$C were investigated by Kolesnichenko *et al.* [109] by electrical conductivity, optical microscopy, and XRD. In the present optimization, the excess Gibbs energy contribution from the binary and ternary subsystems of the Mg-Sn-Ag-In quaternary system was interpolated using the method introduced by Pelton and Chartrand in reference [110]. The same method and notation were used in the present work, and no additional model parameters were added. The calculated isothermal sections at 300 and 450 $^{\circ}$C are shown in Fig. 7.26 along with the experimental data reported by Kolesnichenko *et al.* [109]. As we can see, the current optimization gives satisfactory results when compared with experimental data.
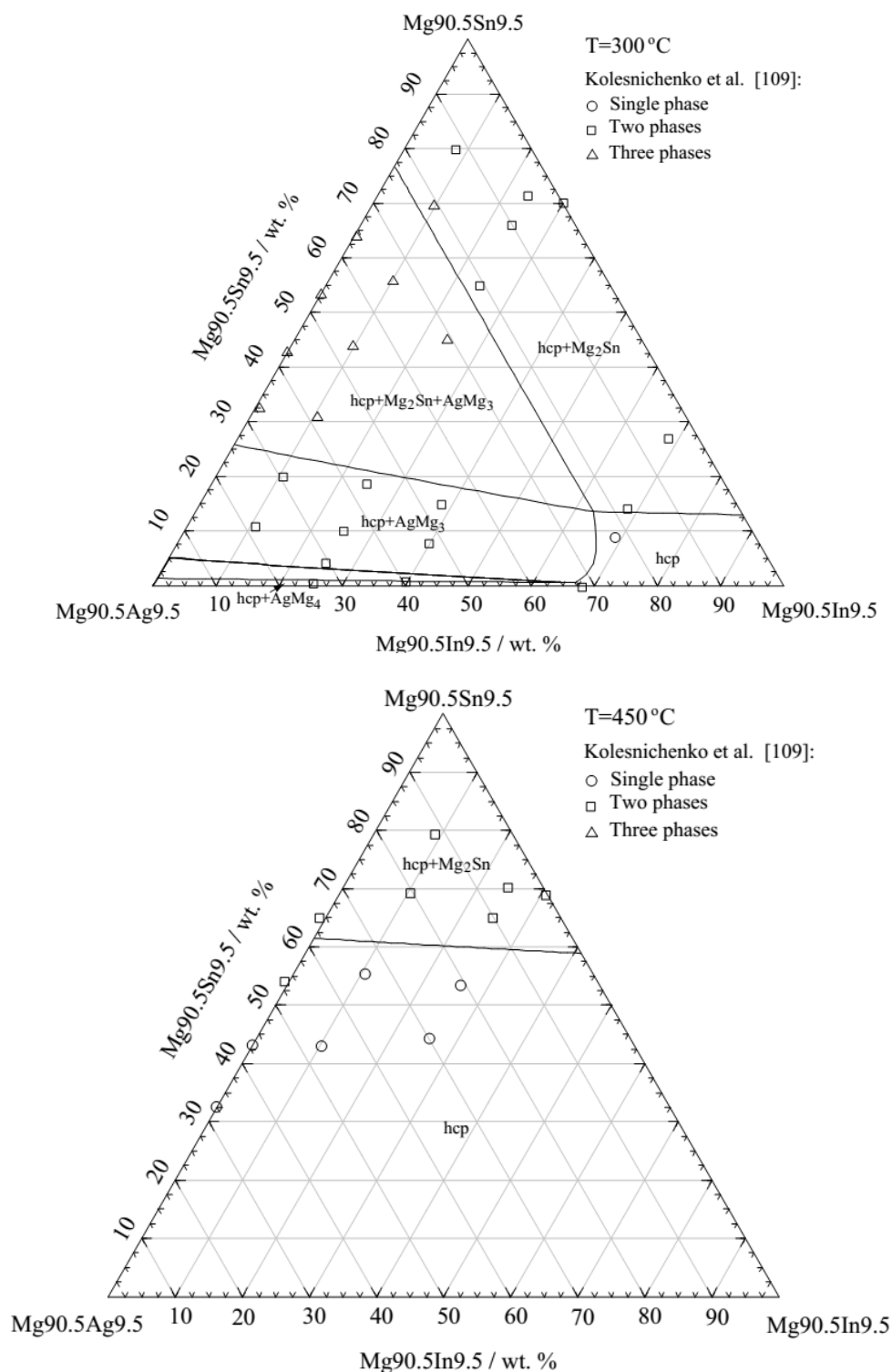
Figure 7.26 Calculated isothermal sections of the Mg-Sn-Ag-In ternary system at (a) 300 $^{\circ}$C and (b) 450 $^{\circ}$C... along with experimental data [109]

Solidification calculations with the Scheil cooling technique for Mg96Sn3Ag1, Mg95Sn3Ag1In1, Mg93Sn6Ag1, and Mg92Sn6Ag1In1 (wt. %) alloys are shown in Fig. 7.27 (a-d). As depicted in Fig.27(a) and (c), the secondary $Mg_{54}Ag_{17}$ phase will appear in the final solidification microstructure of Mg-Sn based alloys with addition of 1 wt. % Ag, which may improve mechanical properties. Compared to Ag addition alone, the combined addition of Ag and In (Fig.27 (b) and (d)) gives some interesting indications to improve the mechanical properties of Mg-Sn based alloys.
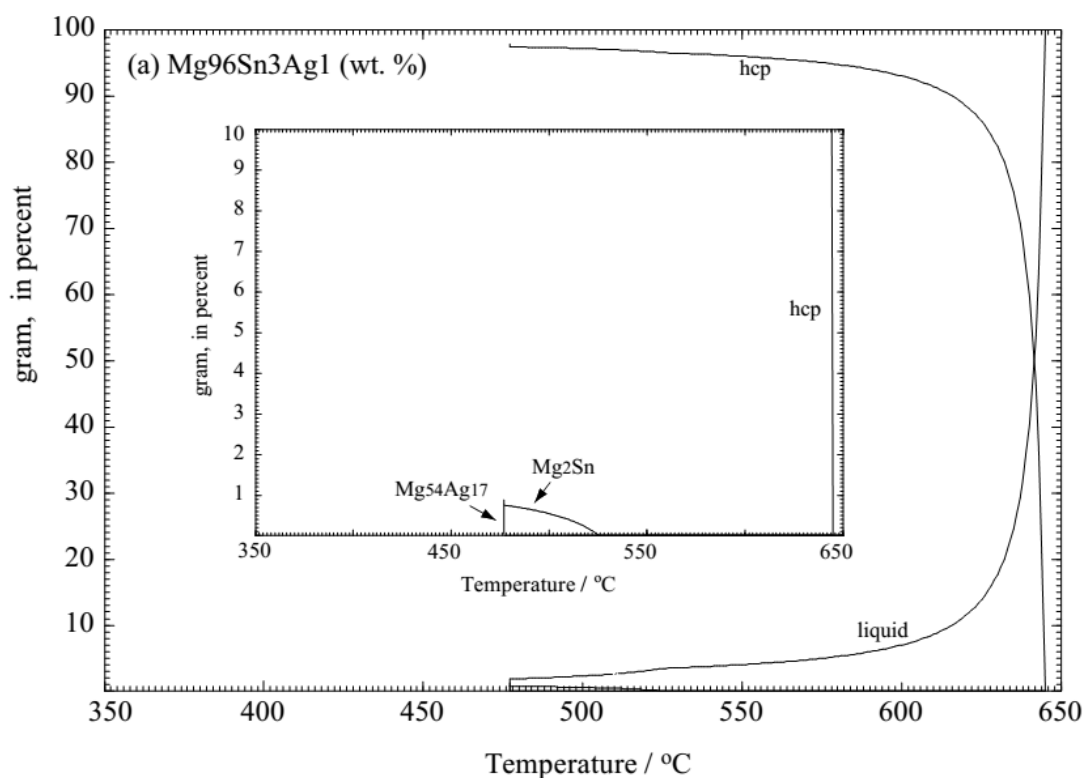
Figure 7.27 Calculated solidification phase proportions (weight basis) using the Scheil cooling method for Mg-Sn-Ag and Mg-Sn-Ag-In alloys: (a) 96Mg3Sn1Ag, (b) 95Mg3Sn1Ag1In, (c) 93Mg6Sn1Ag, (d) 92Mg6Sn1Ag1In (wt. %)

Figure 7.27 (Continued) Calculated solidification phase proportions (weight basis) using the Scheil cooling method for Mg-Sn-Ag and Mg-Sn-Ag-In alloys: (a) 96Mg3Sn1Ag, (b) 95Mg3Sn1Ag1In, (c) 93Mg6Sn1Ag, (d) 92Mg6Sn1Ag1In (wt. %)

Figure 7.27 (Continued) Calculated solidification phase proportions (weight basis) using the Scheil cooling method for Mg-Sn-Ag and Mg-Sn-Ag-In alloys: (a) 96Mg3Sn1Ag, (b) 95Mg3Sn1Ag1In, (c) 93Mg6Sn1Ag, (d) 92Mg6Sn1Ag1In (wt. %)

7.6 Discussions and conclusions

Phase relations in the Mg-rich portion of the Mg-Sn-Ag system at 350 and 415 ^{o}C were determined by the quenching method, XRD, and EPMA. No ternary compound was found in the isothermal sections. The solid solubility of Ag in Mg_2Sn at 350 and 415 ^{o}C is very limited, less than 0.1 at. % (Since these values are within the error limits of the EPMA measurements, the solubilities are considered negligible), while the solubility of Sn in Mg_3Ag is quite large as 3±0.5 at. %, which is in good agreement with the experimental data reported by Karonik et al. [89]. The ternary isoplethal sections with constant value of 10 Sn and 30 Ag at. % for Mg-Sn-Ag ternary system were also determined by DSC measurements.

A critical evaluation and thermodynamic assessment of the Ag-Mg, Ag-In and Ag-Sn binary systems, Mg-Ag-In, Mg-Ag-Sn and Ag-In-Sn ternary systems, and Mg-Sn-Ag-In quaternary

system was carried out by the CALPHAD method. The Gibbs energy of the liquid phase was optimized with the Modified Quasichemical Model in pair approximation (MQMPA) and the solid solutions and intermetallic compounds were described with the sub-lattice model.

For the Ag-Mg binary system, ordering of the bcc (bcc_A2 and bcc_B2) and fcc (fcc_A1 and fcc_L12) phases was modeled with two sublattices and the symmetry of the crystal structure was taken in consideration. Moreover, all the phases and solid solubility limits reported in previous works were considered. $AgMg_3$ and $Mg_{54}Ag_{17}$ were also modeled with distinct sublattices according to their crystal structures in contrast with Lim et al. [30], who treated them as single phases. Our optimized phase diagrams and thermodynamic properties are in better agreement with experimental data than Lim et al. [30], especially for the description of the solidus curve of hcp(Mg) above the eutectic temperature (see Fig. 7.28) which is very important for the investigation of Mg alloys.
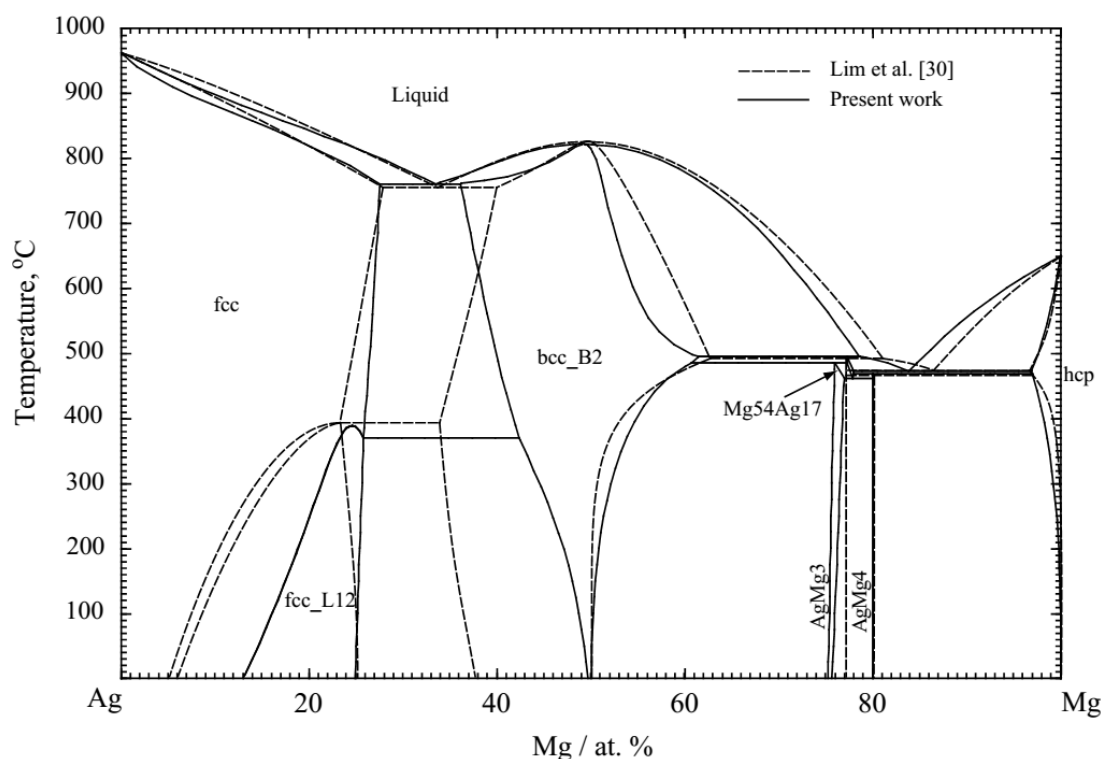
Figure 7.28 Calculated phase diagram of the Ag-Mg system in the present work in comparsion with the previous optimzation by Lim *et al.* [30]

Although the thermodynamic optimization of the Ag-In binary system was carried out numerous times [49, 91], it still lacks accuracy. For instance, the high temperature stable phases bcc_A2, and InAg$_3$ were always ignored. In the present work, after a critical evaluation of all the available experimental data, a strict thermodynamic re-optimization on the Ag-In binary system was performed using all experimental data, and all the existing phases were considered (see Fig. 7. 26).

Phase relations in the Mg-Ag-In, Mg-Sn-Ag and Ag-In-Sn ternary systems were optimized using all available experimental data. As shown in Fig. 7.16, the solid solubility of In in AgMg$_3$ and bcc_B2 is quite important. However, due to the lack of experimental data, the ternary solid solubility of Ag in Mg-In compounds was not considered in the present work. Consequently, to obtain better optimization results for the Mg-Ag-In ternary system, new experimental data are clearly needed, especially at low Ag concentrations.

The current optimization of the Mg-Sn-Ag ternary system is in good agreement with the current experimental data and the previous ones [88, 89]. The calculated liquidus projection (see Fig.22) indicates the presence of a stable ternary peritectic reaction with a high Mg component at the end of the solidification process (see Fig. 27).

In the Ag-Sn-In ternary system, which is part of the lead-free solder thermodynamic database, experimental and thermodynamic data are quite numerous. In the present work, all these data are in good agreement with the current optimization.

By combining all these results with our previous thermodynamic optimization of the Mg-In-Sn ternary system [97], a self-consistent thermodynamic database for the Mg-Sn-Ag-In quaternary system was constructed despite the limited experimental data [109] available. As shown in Fig. 7.27, solidification calculations with the Scheil cooling technique for the Mg-Sn based alloys with Ag and In additives give interesting indications to improve the mechanical properties of these alloys. With the combining addition of Ag and In to Mg-xSn (x = 3 or 6 wt. %) alloys, the final solidification microstructures become more complex, as they include secondary phases such as Mg$_{54}$Ag$_{17}$, Mg$_3$Ag, and fcc. The appearances of these secondary phases during the cooling process will improve grain refinement in Mg$_2$Sn and hcp phases.

Acknowledgements

References

[1] Y. Kojima, Platform science and technology for advanced magnesium alloys, Mater. Sci. Forum, 2000, pp. 3-18.

[2] M.A. Gibson, X. Fang, C.J. Bettles, C.R. Hutchinson, The effect of precipitate state on the creep resistance of Mg-Sn alloys, Scripta Mater., 63 (2010) 899-902.

[3] D.H. Kang, S.S. Park, Y.S. Oh, N.J. Kim, Effect of nano-particles on the creep resistance of Mg-Sn alloys, Mater. Sci. Eng. A, 449-451 (2007) 318-321.

[4] T.A. Leil, Y.D. Huang, H. Dieringa, N. Hort, K.U. Kainer, J. Buršík, Y. Jirásková, K.P. Rao, Effect of Heat Treatment on the Microstructure and Creep Behavior of Mg-Sn-Ca Alloys, Mater. Sci. Forum, 2007, pp. 69-72.

[5] N. Hort, Y. Huang, T. Abu Leil, P. Maier, K.U. Kainer, Microstructural investigations of the Mg-Sn-xCa System, Adv. Eng. Mater., 8 (2006) 359-364.

[6] T.A. Leil, N. Hort, W. Dietzel, C. Blawert, Y. Huang, K.U. Kainer, K.P. Rao, Microstructure and corrosion behavior of Mg-Sn-Ca alloys after extrusion, T. Nonferr. Metal. Soc., 19 (2009) 40-44.

[7] K. Van der Planken, Solution hardening of lead single crystals at liquid air temperature, J. Mater. Sci., 4 (1969) 927.

[8] C.L. Mendis, C.J. Bettles, M.A. Gibson, C.R. Hutchinson, An enhanced age hardening response in Mg–Sn based alloys containing Zn, Mater. Sci. Eng. A, 435-436 (2006) 163-717.

[9] C.L. Mendis, C.J. Bettles, M.A. Gibson, S. Gorsse, R. Hutchinson, Refinement of precipitate distributions in an age-hardenable Mg-Sn alloy through microalloying, Phil. Magazin. Lett., 86 (2006) 443-456.

[10] T.T. Sasaki, K. Oh-ishi, T. Ohkubo, K. Hono, Enhanced age hardening response by the addition of Zn in Mg-Sn alloys, Scripta Mater., 55 (2006) 251-254.

[11] S. Fang, X. Xiao, L. Xia, W. Li, Y. Dong, Relationship between the widths of supercooled liquid regions and bond parameters of Mg-based bulk metallic glasses, J. Non-Cryst. Solids, 321 (2003) 120-125.

[12] G. Liang, Synthesis and hydrogen storage properties of Mg-based alloys, J. Alloy. Comp., 370 (2004) 123-128.

[13] G. Ben-Hamu, D. Elizer, A. Kaya, Y.G. Na, K.S. Shin, Microstructure and corrosion behavior of Mg-Zn-Ag alloys, Mater. Sci. Eng. A, 435-436 (2006) 579-587.

[14] C.L. Mendis, K. Oh-ishi, K. Hono, Enhanced age hardening in a Mg-2.4 at. % Zn alloy by trace additions of Ag and Ca, Scripta Mater., 57 (2007) 485-488.

[15] H.T. Son, D.G. Kim, J.S. Park, Effects of Ag addition on microstructures and mechanical properties of Mg-6Zn-2Sn-0.4Mn-based alloy system, Mater. Lett., 65 (2011) 3150-3153.

[16] N. Saunders, A.P. Miodownik, CALPHAD (Calculation of Phase Diagrams): A Comprehensive Guide, Pergamon, 1998.

[17] H. Ohtani, K. Ishida, Application of the CALPHAD method to material design, Thermochim. Acta, 314 (1998) 69-77.

[18] J.C. Zhao, B.P. Bewlay, M.R. Jackson, L.A. Peluso, Structural Intermetallics 2001 TMS, Warrendale PA, 2001, pp. 483.

[19] A.A. Nayeb-Hashemi, J.B. Clark, The Ag-Mg system, Bulletin of Alloy phase diagrams, 5 (1984) 348-354.

[20] S.F. Zemczuznyj, On the alloys of Magnesium with silver, Z. Anorg. Allg. Chem., 49 (1906) 400-411.

[21] K.W. Andrews, W. Hume-Rothery, The constitution of Silver-magnesium alloys in the region 0-40 atomic precent magnesium, J. Inst. Met., 69 (1943) 485-493.

[22] R.J.M. Payne, J.L. Haughton, Alloys of magnesium. Part IV the constitution of the magnesium-rich alloys of Mg and Ag, J. Inst. Met., 60 (1937) 351-363.

[23] W. Hume-Rothery, E. Butchers, The solubility of Silver and Gold in solid magnesium, J. Inst. Met., 60 (1937) 345-350.

[24] N.V. Ageew, V.G. Kunezow, Izv. Akad. nauk SSSR Otd. Nauk, (1937) 289-309.

[25] H.R. letner, S.S. Sidhu, An x-ray diffraction study of the silver-magnesium alloys system, J. Appl. Phys., 18 (1947) 833-837.

[26] S. Goldsztaub, P. Michel, Preparation of silver-magnesium alloys in thin layers by the simultaneous evaporation of these constituents in vacuum, Compt. Rend., 232 (1951) 1843-1845.

[27] S. Nagashima, X-ray study of Guinier-preston zones fored in ager Magesium-rich, Magesium-silver alloys, J. Jpn. Inst. Met., 23 (1959) 381-384.

[28] M.V. Prokofev, V.E. Kolesnichenko, V.V. Karonik, Izv. Akad. nauk. SSSR Neorg. Mater., 21 (1985) 1332-1334.

[29] V.E. Kolesnichenko, V.V. Karonik, S.N. Tsyganova, T.A. Kupriyanova, L.N. Sysoeva, Phase equilibria in the Mg-Ag system in the eta phase region, Izv. Akad. nauk. SSSR Neorg. Mater., 5 (1988) 186-191.

[30] M. Lim, J.E. Tibballs, P.L. Rossiter, Thermodynamic assessment of Ag-Mg binary system, Z. Metallkd., 88 (1997) 160-167.

[31] A. Gangulee, M.B. Bever, The silver rich silid solid solutions in the system Ag-Mg, Trans. Am. Inst. Min. Meta.Petro.Eng., 242 (1968) 272-278.

[32] M. Kawakami, A further investigation of the heat of mixture in molten metals, Sci. Rep. Res. Inst. Tohoku Univ., 7 (1930) 351-364.

[33] J. Gran, M. Song, D. Sichen, Acitivity of Magnesium in liquid Ag-Mg alloys, CALPHAD, 36 (2012) 89-93.

[34] S. Kachi, Thermodynamic properties of Hume-rothery type Ag-Mg alloy, J. Jpn. Inst. Met., 19 (1955) 318-322.

[36] P.M. Robinson, M.B. Bever, The heat of formation of the intermetallic compound AgMg as a function of composition, Trans. Metal.Soci. AIME, 230 (1964) 1487-1488.

[37] A.K. Jena, M.B. Bever, On the temperature dependence of the heat of formation of the compound AgMg, Trans. Metal.Soci. AIME, 242 (1968) 2367-2369.

[38] W. Trzebiartowski, J. Terpilowski, Thermodynamic properties of the Ag-Zn system and the related beta-AgMg phase, Bull. Acad. Polon. Sci. Tech. Sco, 3 (1955) 391-395.

[39] F. Weibke, H. Eggers, The composition diagram of the system silver-indium Z. Anorg. Allg. Chem., 222 (1935) 145.

[40] W. Hume-rothert, G. W. Mabbott, K. M. Channel-evans, Phil. Trans. Roy. Soc. London A, (1934) 1.

[41] E.A. Owen, E.W. Roberts, Factors affecting the limit of solubility of elements in copper and silver, Phil. Magazin., 27 (1939) 294-327.

[42] V.E. Hellner, The binary system silver-indium, Z. Metallkd., 42 (1951) 17-19.

[43] A.N. Campbell, R. Wagemann, R.B. Ferguson, The Silver-Indium system: thermal analysis, photomicrography, electron microprobe, and X-ray powder diffraction results, Can. J. Chem., 48 (1970) 1703-1715.

[44] O. Uemura, I. Satow, Order-disorder transition of silver-indium (Ag3In) alloy, Trans. Jpn. Inst. Met., 14 (1973) 199-201.

[45] T. Satow, O. Uemura, S. Yamakawa, X-ray diffraction and electrical resistivity study of silver-indium (Ag2In) and high temperature Ag3In phases, Trans. Jpn. Inst. Met., 15 (1973) 253-255.

[46] M.R. Barren, Ag-In (silver-indium), in: H.O. C. E. T. White (Ed.) phase diagrams of Indium alloys and their engineering applications, ASM international, 1992, pp. 15-19.

[47] Z. Moser, W. Gasior, J. Pstrus, W. Zakulski, I. Ohnuma, X.J. Liu, Y. Inohana, K. Ishida, Studies of the Ag-In phase diagram and surface tension measurements, J. Electron. Mater., 30 (2001) 1120-1128.

[48] D. Jendrzejczyk, K. Fitzner, Thermodynamic Properties of liquid silver-indium alloys determined from emf measurements, Thermochim. Acta, 433 (2005) 66-71.

[49] O.J. Kleppa, Heat of formation of solid and liquid alloys in the systems Ag-Cd, Ag-In and Ag-Sb at 450c, J. Phys. Chem., 60 (1956) 846-852.

[50] E. Prezdziecka-Mycielska, J. Terpilowski, K. Strozecka, Thermodynamic properties of liquid metallic solutions. XI. The Ag-In system, Archi. Hutnictwa, 2 (1963) 85-101.

[51] T. Nozaki, M. Shimoji, K. Niwa, Thermodynamic properties of Ag-In liquid phase, Trans. Jpn. Inst. Met., 30 (1966) 7-10.

[52] R. Beja, C. R. Acad. Sci., 267 (1968) 123.

[53] K. Itagaki, A. Yazawa, Measurements of heats of mixing in liquid Ag binary alloys, Trans. Jpn. Inst. Met., 32 (1968) 1294-1300.

[54] C.B. Alcock, R. Sridhar, R.C. Svedberg, A mass spectrometric study of the binary liquid alloys, Ag-In and Cu-Sn, Acta Metall. Mater., 17 (1969).

[55] G.J. Qi, H. Mitsuhisa, A. Takeshi, Thermodynamic study of liquid silver-indium and silver-gallium alloys with a Knudsen cell-mass spectrometer, Mater. Trans., JIM, 30 (1989) 575-582.

[56] K. Kameda, Y. Yoshida, S. Sakairi, Activities of Liquid Silver-Indium Alloys by emf Measurements Using Zirconia Solid and Fused Salt Electrolytes, Trans. Jpn. Inst. Met., 45 (1981) 614-620.

[57] R. Castanet, Y. Claire, M. Laffitte, Thermodynamic properties of liquid Ag-In solutions, J. Chim. Phys.Physico-chim.Biolog., 67 (1970) 789-793.

[58] L.R. Orr, R. Hultgren, Heat formation of α-phase silver-indium alloys,, J. Phys. Chem., 65 (1961) 378-380.

[59] D.B. Masson, S.S. Pradhan, Measurement of vapor pressure of indium over a Ag-In using atomic absorption, Metall. Mater. Trans. A, 4 (1973) 991-995.

[60] C.T. Heycock, F.H. Neville, The molecular weights of metals when in solution, J. Chem. Soc., 57 (1890) 373-393.

[61] C.T. Heycock, F.H. Neville, The freezing point of triple alloys, J. Chem. Soc., 65 (1894) 65-76.

[62] C.T. Heycock, F.H. Neville, Complete Freezing point curves of binary alloys containing silver or copper, Phil. Trans.Roy. Soc. A, 189 (1897) 25-69.

[63] G.J. Peternko, On the alloyingof silver with lead and tin, Z. Anorg. Allg. Chem., 56 (1907) 20-22.

[64] N. Puschin, Das potential die chemiusche konstitution der metalllegierunge, Z. Anorg. Allg. Chem., 56 (1908) 1-45.

[65] A.J. Murphy, The constitution of the alloys of silver and tin, J. Inst. Met., 35 (1926) 107-129.

[66] W. Hume-Rothery, G.W. Mabbot, K.M. Channel-Evans, The freezing points, melting points and solid solubility limits of the alloys of Silver and copper with the elements of the sub-groups, Phil. Trans.Roy. Soc. A, 233 (1934) 1-97.

[67] W. Hume-Rothery, P.W. Reynolds, The accurate determination of the freezing points of alloys and a study of valency effects in certain alloys of silver, Proc. R. Soc. London A, 160 (1937) 282-303.

[68] D. Hanson, E.J. Stand, H. Syevens, Some properties of tin comtaining small amounts of Silver, iron, nickel or copper, J. Inst. Met., 55 (1934) 115-133.

[69] A. E. Owen, E.W. Roberts, Facts affecting the limit of solubility of elements in copper and silver, Philos. Mag., 27 (1939) 294-327.

[70] M.M. Umansky, Diagram of the alloy silver-tin, Zhurnal Fiz. Khim., 14 (1940) 846-849.

[71] F. Vnuk, M.H. Ainsley, R.W. Smith, The solid solubility of silver, gold and zinc in metallic tin, J. Mater.Sci., 16 (1981) 1171-1176.

[72] I. Karakaya, W.T. Thompson, The Ag-Sn system, Bulletin of Alloy phase diagrams, 8 (1987) 340-347.

[73] R.O. Frantik, H.J. McDaonald, Thermodynamic study of the Tin-Silver system, Trans. Electrochem. Soc., 88 (1945) 253-262.

[74] J.A. Yanko, A.E. Drake, F. Hovorka, Thermodynamic studies of dilute solutions in molten binary alloys, Trans. Electrochem. Soc., 89 (1946) 357-372.

[75] O.J. Kleppa, A calorimetric investigation of the system Ag-Sn at 450 $^{\circ}$C, Acta Metall., 3 (1955) 255-259.

[76] T. Nozaki, M. Shimoji, K. Niwa, Thermodynamic properties of Ag-Sn and Ag-Sb liquid alloys, Beri. Bun. Gesellscha., 70 (1966) 207-214.

[77] R.B. Elliott, J.F. Lemons, Activites of molten tin alloys from emf measurements, J. Electrochem. Soc., 114 (1967) 935-937.

[78] R. Castanet, M. Laffitte, Enthalpie de formation a 1280 K d'alliages liquides argent-etain et argent-germanium, C. R. Acad. Sci. Paris. C, 267 (1968) 204-206.

[79] P.J.R. Chowdhury, A. Ghosh, Thermodynamic measurements in liquid Sn-Ag alloys, Metall. Trans., 2 (1971) 2171-2174.

[80] K. Okajima, H. Sakao, Tie measurements on the activities of the Ag-Sb, Ag-Pb and Ag-Sn molten alloys, Trans. JIM, 15 (1974) 52-56.

[81] M. Iwase, M.O. Yasuda, S.I. Miki, A thermodynamic study of liquid Ag-Sn alloys by means of solid-oxide galvanic cell, Trans. JIM, 19 (1978) 654-660.

[82] K. Kameda, Y. Yoshida, S. Sakairi, Thermodynamic properties of liquid Ag-Sn alloys, J. Jpn. Inst. Met., 44 (1980) 858-863.

[83] H. Flandorfer, U. Saeed, C. Luef, A. Sabbar, H. Ipser, Interfaces in lead-free solder alloys: Enthalpy of formation of binary Ag-Sn, Cu-Sn and Ni-Sn intermetallic compounds, Thermochim. Acta, 459 (2007) 34-39.

[84] J. Rakotomavo, M. Gaune-Escard, J.P. Bros, P. Gaune, Enthalpies of formation at 1373 K of the liquid alloys Ag-Au, Ag-Sn,and A-Au-Sn, Ber. Bunssenges. , 88 (1974) 663-670.

[85] G.H. Laurie, A.H. Morris, J.N. Pratt, Electromotive force and calorimetric studies of thermodynamic properties of solid and liquid Ag-Sn alloys, Trans. Metall. AIME, 236 (1966) 1390-1395.

[86] T. Yamaji, E. Kato, Mass spectrometric study of the thermodynamic properties of the Ag-Sn system, Metall.Mater. Trans. B, 3 (1972) 1002-1004.

[87] V.E. Kolesnichenko, M.A. Komapoba, B.B. kapohhk, Study of the magnesium-silver-indium phase diagram, Izv. Akad. nauk SSSR Neorg. Mater., 5 (1982) 225-229.

[88] G.V. Raynor, B.R.T. Frost, The system Ag-Mg-Sn with reference to the theory of ternary alloys, J. Inst.Met., 75 (1949) 777-808.

[89] V.V. Karonik, V.E. Kolesnichenko, A.A. Shepelev, G.I. Kandyba, Magnesium-silver-tin phase diagram, Metalloved. Splavov na Osnove Tsv. Met. M., (1983) 78-84.

[90] T.M. Korhonen, J.K. Kivilahti, Thermodynamics of the Sn-In-Ag solder system, J. Electron. Mater., 27 (1998) 149-158.

[91] X.J. Liu, Y. Inohana, Y. Takaku, I. Ohnuma, R. Kainuma, K. Ishida, Z. Moser, W. Gasior, J. Pstrus, Experimental determination and thermodynamic calculation of the phase equilibira and surface tension in the Sn-Ag-In system, J. Electron. Mater., 31 (2002) 1139-1151.

[92] G. Vassilev, E.S. Dobrev, J.C. Tedenac, Experimental study of the Ag-Sn-In phase diagram, J. Alloy. Comp., 399 (2005) 118-125.

[93] T. Miki, N. Ogawa, T. Nagasaka, M. Hino, Activity measurement of the constituents in molten Sn-Ag-In and Sn-Zn-Mg ternary lead free solder alloys by mass spectrometry, Metall. Mater..Proc. Prin.Tech., 1 (2003) 405-415.

[94] B. Gather, P. Schroeter, R. Blachnik, Heats of mixing in the silver-indium-tin, silver-tin-antimony, silver-indium-antimony, and indium-lead-antimony ternary systems, Z. Metallkd., 78 (1987) 280-285.

[95] I.-H. Jung, D.H. Kang, W.J. Park, N.J. Kim, S.H. Ahn, Thermodynamic modeling of the Mg-Si-Sn system, CALPHAD, 31 (2007) 192-200.

[96] P. Ghosh, M.D. Mezbahul-Islam, M. Medraj, Critical assessment and thermodynamic modeling of Mg-Zn, Mg-Sn, Sn-Zn and Mg-Sn-Zn system, CALPHAD, 36 (2012) 28-43.

[97] J. Wang, I.H. Jung, P. Chartrand, M. Medraj, Experimental and thermodynamic studying on Mg-Sn-In-Zn system, J. Alloy. Comp., 588 (2013) 75-95.

[98] S.C. Oh, J.H. Shim, B.J. Lee, D.N. Lee, Thermodynamic study on the Ag-Sb-Sn system, J. Alloy. Comp., 238 (1996) 155-166.

[99] F. Meng, J. Wang, L. Liu, Z. Jin, Thermodynamic modeling of the Mg-Sn-Zn ternary system, J. Alloy. Comp., 508 (2010) 570-581.

[100] A.T. Dinsdale, SGTE data for pure elements, CALPHAD, 15 (1991) 317-425.

[101] C.W. Bale, P. Chartrand, S.A. Degterov, G. Eriksson, K. Hack, R. Ben Mahfoud, J. Melancon, A.D. Pelton, S. Petersen, Factage thermochemical software and databases, CALPHAD, 26 (2002) 189-228.

[102] H. Kopp, Investigations of the specific heat of solid bodies, Phil. Trans. Roy. Soc. A, 155 (1865) 71-202.

[103] M. Hillert, The compound energy formalism, J. Alloy. Comp., 320 (2001) 161-176.

[104] N. Dupin, I. Ansara, On the sublattice formalism applied to the B2 phase, Z. Metallkd., 90 (1999) 76-85.

[105] A. D. Pelton, P. Chartrand, The modified quasi-chemical model: Part II. Multicomponent solutions, Metall. Mater. Trans. A, 32 (2001) 1355-1360.

[106] A. D. Pelton, S. A. Degterov, G. Eriksson, C. Robelin, Y. Dessureault, The modified quasichemical model I-binary solutions, Metall. Mater. Trans. B, 31 (2000) 651-659.

[107] A.D. Pelton, A general "geometric" thermodynamic model for multicomponent solutions, CALPHAD, 25 (2001) 319-328.

[108] D. Zivkovic, A. Milosavljevic, A. Mitovski, B. Marjanovic, Comparative thermodynamic study and characterization of ternary Ag-In-Sn alloys, J. Therm. Anal. Calorim., 89 (2007) 137-142.

[109] V.E. Kolesnichenko, I.M. Khatsernov, V.V. Karonik, Phase composition of magnesium-silver-indium-tin alloys in the magnesium-rich region, Izv. Akadem. nauk. SSSR Metall., 2 (1989) 219-221.

[110] A. Pelton, P. Chartrand, The modified quasi-chemical model: Part II. Multicomponent solutions, Metall. Mater. Trans. A, 32 (2001) 1355-1360.

CHAPITRE 8   EXPERIMENTAL AND THERMODYNAMIC STUDY OF THE MG-SN-CA-LI-SR QUINARY SYSTEM

8.1   Introduction

Significant improvements of the binary Mg-Sn and ternary Mg-Sn-Ca systems, in as-cast conditions, have been recently proposed to achieve the best combination of castability, creep and corrosion properties (Leil, et al., 2009; Hort, et al., 2006; Kozlov et al., 2008; Rao, et al., 2008). Additions of Ca have been found to improve creep resistance (Nayyeri & Mahmudi, 2011). Consequently, the Mg_2Sn, Mg_2Ca, and $Ca_{2-x}Mg_xSn$ phases have been investigated more recently (Hort, et al., 2006; Yang et al., 2010). Strontium is an important additive in magnesium based alloys used for improving mechanical properties. The alloying effects of strontium in Mg-Al based alloys have been found to be superior creep performance and excellent high-temperature properties (Baril, et al., 2003). Hirai et al. (Hirai, et al., 2005) reported that cast AZ91 magnesium alloys having excellent mechanical properties (such as high strength and high creep resistance) can be made by the addition of Ca and Sr. Also, Mg–Li alloys have benefited from Li addition because of the hcp-bcc phase transition. Futher, Li addition results in lower density (1.30–1.65 g/m^3), good electromagnetic properties and superior mechanical properties (Sharma, et al., 2001; Sharma, et al., 1993; Shao, et al., 2009). As reported by Mendis et al. (Mendis, et al., 2006) can potentially be an alloying element that improves precipitation hardening in Mg-Sn based alloys because there are many stable Li-Sn binary intermetallic phases and ternary intermetallics in Mg-Sn-Li (Gasior, et al., 1996; Sviderskaya, et al., 1972).

As mentioned above, superior mechanical properties have been obtained for Mg-Sn based alloys by additions of Li, Ca, and Sr. However, a systematic study of the mechanisms behind the properties improvements, as well as optimization of the best composition of Mg-Sn-Ca-Li-Sr quinary alloys have not yet been performed. To obtain such information solely through experiment is cumbersome and costly. Consequently, development of a thermodynamic database for phase equilibria calculations in the Mg-Sn-Ca-Li-Sr quinary system is necessary. Thus, with a few key experimental data will aid in understanding on the phase relationship and the design of new alloys.

In the present work, the thermodynamic modeling of the Mg-Sn-Ca-Li-Sr quinary system was carried out as part of the thermodynamic database development of the larger Mg-X (X: Ag, Ca, In, Li, Na, Sn, Sr, Zn) multi-component system.

8.2 Literature review

8.2.1 The Sn-Ca system

The phase diagram of Sn-Ca binary system was first studied by Hume-Rothery (Hume-Rothery, 1926) using thermal analysis, optical microscopy and X-ray analysis methods. Hansen and Anderko (Hansen & Anderko, 1958) compiled data on the Ca-Sn phase diagram and included compounds (Ca_2Sn, $CaSn$ and $CaSn_3$), based on the reported results of Hume-Rothery (Hume-Rothery, 1926). Later, Fornasini and Franceschi (Fornasini & Franceschi, 1977) added a new compound ($Ca_{31}Sn_{20}$) resulting from their X-ray diffraction analysis experiments (without any thermal stability information). Palenzona et al. (Palenzona, et al., 2000) re-investigated the Sn-Ca phase diagram for the whole composition range using thermal analysis, metallographic observation, and single-crystal and powder X-ray diffraction analysis techniques. Three new compounds (Ca_7Sn_6, $Ca_{36}Sn_{23}$ and Ca_5Sn_3) were reported, and the previously reported four compounds (Ca_2Sn, $CaSn$, $Ca_{31}Sn_{20}$ and $CaSn_3$) were also confirmed in their work (Palenzona, et al., 2000). It should be pointed out that the liquidus curve in the Ca-rich region and the melting temperature of Ca_2Sn reported by Palenzona et al. (Palenzona, et al., 2000) are quite different from those of Hume-Rothery (Hume-Rothery, 1926). The melting temperatures of Ca_2Sn differ by about 200 ^{o}C.

The partial enthalpy of Ca at infinitely dilution in the Ca-Sn liquid phase was studied by Bouirden (Bouirden, 1984), King and Kleppa (King & Kleppa, 1964), and Guadagno (Guadagno, et al., 1970) at different temperatures by calorimetry technique. Sudavtsova and Batalin (Sudavtsova & Batalin, 1988) and Bouirden (Bouirden, 1984) studied the partial and integral mixing enthalpy of liquid Ca-Sn alloys with calorimetry technique. The activity of Ca in the liquid phase was measured by Potard et al. (Potard, et al., 1969) by using a vapor pressure method, and by Delect et al. (Delcet, et al., 1979) by using an EMF technique.

The enthalpy of formation of the $CaSn_3$ compound was measured by Bouirden (Bouirden, 1984) at the melting point with a calorimetric technique. The enthalpy of formation of $CaSn$, $CaSn_3$ and

Ca$_2$Sn in the temperature range from 600 to 700 ^{o}C were measured by Kubaschewski and Villa (Kubaschewski & Villa, 1949) using an adiabatic calorimeter. Min and Sano (Min & Sano, 1988) derived the enthalpy of formation of the Ca$_2$Sn compound at 25 ^{o}C based on the experimental measurements of chemical equilibration reactions. Ohno et al. (Ohno, et al., 2006) and Yang et al. (Yang, et al., 2010) studied the enthalpy of formation of the Ca-Sn binary compounds with First-Principles calculations.

Okamoto (Okamoto, 2001) compiled the phase diagram of the Ca-Sn binary system with all the available experimental data. Ohno et al. (Ohno, et al., 2006) and Cartigny et al. (Cartigny, et al., 2005) optimized the Ca-Sn binary system with a Bragg-williams model (Dinsdale, 1991) for the liquid phase.

8.2.2 The Sn-Sr system

Phase equilibria of the Sn-Sr binary system were measured in the composition range 63-100 Sn at. % by Ray (Ray, 1930) using thermal analysis and optical microscopy methods. Two compounds, SrSn$_5$ and SrSn$_3$, were reported. Phase equilibria in the composition range from 65-100 Sn at. % were investigated by Marshall and Chang (Marshall & Chang, 1981) using differential thermal analysis, microprobe analysis, metallography and X-ray diffraction analysis techniques. Marshall and Chang (Marshall & Chang, 1981) found that the phase in equilibrium with Sn has the stoichiometry SrSn$_4$ instead of SrSn$_5$ reported by Ray (Ray, 1930). Widera and Schafer (Widera & Schäfer, 1981) investigated phase equilibria in the composition range 0-35 Sn at. % using thermal analysis and X-ray diffraction techniques. Two new compounds, SrSn and Sr$_2$Sn, were found. The existence of the Sr$_2$Sn, Sr$_5$Sn$_3$, SrSn and SrSn$_3$ phases were confirmed in their work (Widera & Schäfer, 1981). Allotropic transition of Sr$_2$Sn and SrSn were reported at 820 °C and 900 °C, resepectively. Zürcher et al. (Zurcher, et al., 2001) studied a new compound Sr$_3$Sn$_5$ using X-ray diffraction and thermal analysis methods. Sr$_3$Sn$_5$ was reported to decompose peritectically into liquid and SrSn at 810 °C, based on the thermal analysis results of Zürcher et al. (Zurcher, et al., 2001). Hoffman (Hoffmann, 2002) studied phase equilibria in the composition range 57-88.4 Sn at. % using thermal analysis method, and confirmed the existence of Sr$_3$Sn$_5$ reported by Zürcher et al. (Zurcher, et al., 2001). Palenzona and Pani (Palenzona & Pani, 2004) re-investigated the phase equilibria of the Sn-Sr binary system in the whole composition range by thermal analysis, X-ray analysis and optical microscopy techniques on several key alloys. The

consistent of all the previously reported intermediate phases were confirmed. These included Sr_2Sn ($PbCl_2$-type), Sr_5Sn_3 (Cr_5B_3-type), $SrSn$ (CrB-type), Sr_3Sn_5 (Pu_3Pd_5-type), and $SrSn_3$ ($PuGa_3$-type). A new compound ($SrSn_4$) was reported by Palenzona and Pani (Palenzona & Pani, 2004). Three eutectics in the Sn-Sr binary system were reported by Palenzona and Pani (Palenzona & Pani, 2004). These were 752 °C at liquid composition of 2.5 Sn at.%, 1100 °C at liquid composition of 45.5 Sn at.%, and 230 °C at liquid composition of about 99.0 Sn at.%.

Morozova et al. (Morozova, et al., 1959) estimated the enthalpy of formation of Sr_2Sn compound as -115.42 $kJ \cdot (mol\text{-}atom)^{-1}$ based on the measured enthalpy of the reaction $Sr_2Sn + 4.42HCl = 2SrCl_2 + 0.21SnCl_2 + 2.21H_2 + 0.79Sn$. In the same paper the enthalpy of formation of Sr_2Si was estimated as -126.9 $kJ \cdot (mol\text{-}atom)^{-1}$ with the same method. This is much more negative than the value obtained by Balducci et al. (Balducci et al., 2006), -39.7 $kJ \cdot (mol\text{-}atom)^{-1}$ from vapor pressure measurements. The enthalpy of formation of compounds was calculated by Zhao et al. (Zhao et al., 2011) from First-principles calculations. The enthalpy of formation of Sr_2Sn was reported as -63.4 $kJ \cdot (mol\text{-}atoms)^{-1}$ by Zhao et al. (Zhao, et al., 2011), which is a more reasonable value than previously reported by Morozova et al. (Morozova, et al., 1959). Thus, in the present optimizations, the data from Morozova et al. (Morozova, et al., 1959) was not used. In additional, Esin et al. (Esin, et al., 1985) measured the enthalpy of mixing in the liquid phase within the composition range 0-50 Sr at.% at 1500 °C using a high-temperature isothermal calorimeter. A method, based on the measured change of depolarization value in the deposition of Sr on the Sn–Sr system cathode, was used by Lebanov et al. (Lebanov, Tvaradze, & Morachevskii, 1985). They hence determined the Sr activity in Sn-Sr liquid phase at 627 °C in the Sn-rich region. The phase diagram of Sn-Sr was optimized by by Zhao et al. (Zhao, et al., 2011) using the BMW for the liquid phase.

8.2.3 The Ca-Li system

The phase equilibria of the Ca-Li binary system was investigated by Zamotorin (Zamotorin, 1938) with thermal analysis method. However, most of his results were not confirmed in later studies. The phase diagram in the Li-rich region was investigated by Wolfson (Wolfson, 1956) using thermal analysis and hardness measurements methods: a eutectic and a peritectic were reported at the temperatures of 141.8 °C and 230.9 °C, respectively. Kanda and Keller (Kanda & Keller, 1964) investigated the phase equilibria of the Ca-Li system in the whole composition

range using dilatometry and thermal analysis techniques. A compound $CaLi_2$ with laves_C14 crystal structure was reported by Kanda and Keller (Kanda & Keller, 1964). The temperatures of eutectic and peritectic reported by Wolfson (Wolfson, 1956) were confirmed in the work of Kanda and Keller (Kanda & Keller, 1964). Carfagno (Carfagno, 1966) re-investigated the phase diagram using thermal analysis and X-Ray analysis techniques, and his results are in good agreement with the reported data from Kanda and Keller (Kanda & Keller, 1964) and Wolfson (Wolfson, 1956). There are no experimental data reported for the thermodynamic properties of the liquid phase. Grobner et al. (Grobner, et al., 2002) studied the enthalpy of formation of $CaLi_2$ by drop calorimetry and optimized the phase diagram with the BWM for the liquid phase.

8.2.4 The Mg-Sn-Ca system

The composition and crystal structure of the ternary compound CaMgSn (orthorhombic Co_2Si-type) in the Mg-Sn-Ca ternary system was studied by Axel et al. (Axel, et al., 1969), which was expected to be related to the crystal structure of binary compound Ca_2Sn itself. Later, Ganguli et al. (Ganguli, et al., 2000) confirmed the existence of the CaMgSn compound and pointed out that the CaMgSn ternary phase is actually the ternary solid solution of Ca_2Sn with Mg substituting for one Ca. Also, a new ternary compound $Ca_{6.2}Mg_{3.8}Sn_7$ was synthesized by Ganguli et al. (Ganguli, et al., 1998).

Phase equilbria in the Mg-Sn-Ca ternary system were studied by Kozlov et al. (Kozlov, et al., 2008) by DSC/DTA, X-ray and metallurgical analysis methods, and the isoplethal sections of the Mg_2Sn-Mg_2Ca, $Mg-CaSn$, Mg_2Sn-Ca_2Sn, and Ca47Sn53-Mg were reported (Kozlov, Ohno, Arroyave, et al., 2008). The enthalpy of formation of MgSnCa and $Mg_{3.8}Sn_7Ca_{6.2}$ were calculated to be -56.8 $kJ \cdot (mol-atom)^{-1}$ at 298 K by Kozlov et al. (Kozlov, et al., 2008) and -56.9 $kJ \cdot (mol-atom)^{-1}$ at 0 K by Mantina et al. (Mantina, et al., 2008), respectively from First-principles calculations.

8.2.5 The Mg-Sn-Sr system

There is limited experimental information on phase equilibria or applications of the Mg-Sn-Sr ternary system. A ternary compound MgSnSr with ordered anti-$PbCl_2$-type structure was reported by Eisenmann et al. (Eisenmann, et al., 1972). Yang et al. (Yang, et al., 2012) reported a good grain refinement of the MgSnSr ternary precipitate in the Mg matrix with the additions of Ca. No

experimental data of phase equilibria or thermodynamic properties in the Mg-Sn-Sr ternary system have been reported.

8.2.6 The Mg-Ca-Sr system

The phase equilibira of Mg-Ca-Sr ternary system were studied by Janz and Schmid-Fetzer (Janz & Schmid-Fetzer, 2009) using differential thermal analysis, scanning electron microscopy, and electron probe microanalysis methods. No ternary compound was reported in the work of Janz and Schmid-Fetzer (Janz & Schmid-Fetzer, 2009), and the binary compounds $Mg_{17}Sr_2$ and $Mg_{38}Sr_9$ were reported with solid solubilities of Ca of about 2 and 1 wt. %, respectively. Aljarrah and Medraj (Aljarrah & Medraj, 2008b) and Zhong et al. (Zhong, et al., 2006) calculated the phase diagram information of the Mg-Ca-Sr ternary system from the thermodynamic parameters of binary sub-systems, respectively.

8.2.7 The Mg-Ca-Li system

Experimental information related to the phase equilibria and the thermodynamic properties of the Mg-Ca-Li system is quite limited. An extrapolation of the isothermal sections of this ternary system was reported by Hsu and Saboungi (Hsu & Saboungi, 1978) based on the thermodynamic parameters from the sub-binary systems. Recently, Grobner et al. (Grobner, et al., 2002) studied the Mg-Ca-Li ternary system by using calorimetry and X-ray analysis techniques. The isothermal section of 150 ^{o}C and ternary isoplethal sections of Mg_2Ca-Li_2Ca and constant of 13 Li at. % were reported in their work. Finally, a thermodynamic optimization was carried out with the BWM for the liquid phase (Grobner, et al., 2002).

8.3   Thermodynamic model

The present optimizations have been carried out by means of the FactSage thermodynamic software (Bale, et al., 2002). The thermodynamic parameters of the pure elements were taken from the SGTE database (Dinsdale, 1991), and the Cp of Li and Sn were modified as discussed in the previous chapters.

The MQM (Pelton & Chartrand, 2001; Pelton, et al., 2000) is used for the liquid solution modeling which is formulated to integrate the Bragg-Williams random mixing model within the framework of the Modified Quasichemical Model if the model parameters for the liquid of a

binary subsystem have been optimized with the BW approximation. A detailed description of the MQM and its associated notation is given by Pelton et al. (Pelton & Chartrand, 2001), the same notations are used in the present work.

In the present work all the solid solutions (hcp, bcc, fcc, and the intermetallic compounds) in the binary systems were modeled with the sub-lattice models based on the crystal structures and solid solutions. The Gibbs energy expressions are based on each sub-lattice model derived from the Compound Energy Formalism and on their crystal structures. The heat capacity functions of all stoichiometric compounds were evaluated using the Neumann-Kopp rule (Kopp, 1865). The details of model description have been given in previous chapters, and the same notations were used in the present chapter. All the phases modeled in the present work are listed in Table 8.1.

Table 8.1 Phases of the Mg-Ca-Li-Sn-Sr quinary system modeled in the present work

Phase	Pearson symbol	Strukturvricht designation	Space group	Prototype	Model[a]
Liquid	-	-	-	-	MQMPA
fcc	cF4	A1	$Fm\bar{3}m$	Cu	CEF
bcc_B2	cP2	B2	$Pm\bar{3}m$	CsCl	CEF
bcc_A2	cI2	A2	$Im\bar{3}m$	W	CEF
hcp	hP2	A3	$P6_3/mmc$	Mg	CEF
$Li_{22}Sn_5$	cF432		$F23$		CEF
Li_2Sn_5	tI4		P_4/mbm		ST
Li_8Sn_3	-	-	-	-	ST
Li_5Sn_2	hR7	$D8_i$	$R\bar{3}m$	Mo_2B_5	ST
To be continued					

Table 8.1 (continued) Phases of the Mg-Ca-Li-Sn-Sr quinary system modeled in the present work

Phase	Pearson symbol	Strukturvricht designation	Space group	Prototype	Model[a]
Li_7Sn_2	oC36		*Cmmm*		ST
Li_7Sn_3	mP20		$P2_1/m$		ST
$Li_{13}Sn_5$	hP18		$P\bar{3}m1$		ST
LiSn	mP6		$P2/m$		ST
Mg_2Sn	cF24		$Fd\bar{3}m$	-	CEF
Ca_2Sn	oP12	C23	*Pnma*	Co_2Si	CEF
Ca_5Sn_3	tI32	$D8_1$	$I4/mcm$	Cr_5B_3	CEF
$Ca_{36}Sn_{23}$	tP118	-	$P4/mbm$	Y36Sn23	ST
$Ca_{31}Sn_{20}$	tI204	-	$I4/mcm$	$Pu_{31}Rh_{20}$	ST
Ca_7Sn_6	oP52	-	*Pnma*	Ca_7Sn_6	ST
CaSn	oC8	Bf	*Cmcm*	CrB	CEF
$CaSn_3$	cP4	$L1_2$	$Pm\bar{3}m$	$AuCu_3$	ST
Sn_4Sr	oC20	-	*Cmcm*	-	ST
Sn_3Sr	hR48	-	$R\bar{3}m$	$PuGa_3$	ST
Sn_5Sr_3	oC32	-	*Cmcm*	Pu_5Pd_3	ST
SnSr	oC8	Bf	*Cmcm*	CrB	CEF
Sn_3Sr_5	tI32	$D8_1$	$I4/mcm$	Cr_5B_3	CEF
$SnSr_2$	oP12	C23	*Pnma*	Co_2Si	CEF
$Li_{23}Sr_6$	cF116	$D8_a$	$Fm3m$	$Mg_{23}Th_6$	CEF
Li_2Sr_3	pT	-	-	Al_2Zr_3	ST
Mg_2Ca	hP12	C14	$P6_3/mmc$	$MgZn_2$	CEF
$CaLi_2$	hP12	C14	$P6_3/mmc$	$MgZn_2$	CEF
$Mg_{17}Sr_2$	hP38	-	$P6_3/mmc$	$Ni_{17}Th_2$	CEF
$Mg_{38}Sr_9$	hP94	-	$P6_3/mmc$	$Mg_{38}Sr_9$	CEF
$Mg_{23}Sr_6$	cF116	$D8_a$	$Fm3m$	$Mg_{23}Th_6$	CEF
Mg_2Sr	hP12	C14	$P6_3/mmc$	$MgZn_2$	CEF
MgCaSn	oP12	C23	*Pnma*	Co_2Si	CEF
MgSnSr	oP12	C23	*Pnma*	Co_2Si	CEF
Mg_5Sn_3Sr	-	-	-	-	ST
$Mg_{25}Sn_{24}Sr_{14}$	-	-	-	-	ST
$Ca_{6.2}Mg_{3.8}Sn_7$	-	-	-	-	ST
Li_2MgSn	cF16		$Fm\bar{3}m$	-	CEF
Li_4MgSn	-	-		-	ST

[a] MQMPA: Modified Quasichemical Model in Pairs Approximation; CEF: Compound Energy Formalism; ST: Stoichiometric compound

8.4 Experimental procedures

The ternary Mg-Sn-Ca and Mg-Sn-Sr key ternary alloys were prepared by using pure Mg (99.8%), pure Sn (99.9%) pure Ca (99.9%), and pure Sr (99 %) in an induction furnace under flowing argon. A cube shaped crucible made with Ta foil (99.5 % purity, 0.15 mm thickness) was prepared. The key alloys were washed with methanol to remove dust and oil, and then were remelted three times in the crucible in order to maximize homogeneity. The overall mass losses were less than 5 wt. % for each sample. The melting procedure involved the fusion of Mg and Sn in a first step, before adding Sr and/or Ca, in order to reduce the exothermic effect of these elements with Sn. Then the Mg-Sn-Ca and Mg-Sn-Sr key alloys were sealed into quartz capsules under argon and annealed at 415 ^{o}C for 20 days and at 350 ^{o}C for 35 days, respectively. The microstructures and equilibrium compositions of the phases in each sample were investigated by SEM and EDS techniques within 2 minutes after the final polishing. The nominal compositions of the samples and of their constituent phases are summarized in Tables 8.2 and 8.3.

Table 8.2 Equilibirum compositions of the Mg-Sn-Ca key samples determined in the present work

Temp. (^{o}C)	Alloy Nominal comp. (at. %)	Phase equilibiria Phase 1/Phase 2/Phase 3	Composition (at. %) (balance=Ca)					
			Phase 1		Phase 2		Phase 3	
			Mg	Sn	Mg	Sn	Mg	Sn
415	65Mg20Sn15Ca	hcp (Mg)/Mg$_2$Sn/MgCaSn	98.86	1.11	66.21	33.12	34.17	32.98
	40Mg45Sn15Ca	Mg$_2$Sn/MgCaSn/CaSn$_3$	66.21	33.03	34.63	32.36	2.23	74.38
	30Mg60Sn10Ca	CaSn$_3$/liquid/Mg$_2$Sn	1.77	75.00	2.05	95.42	66.21	33.63
	65Mg10Sn25Ca	hcp (Mg)/Mg$_2$Ca/MgCaSn	97.25	0.38	67.51	0.17	28.22	32.19
350	65Mg20Sn15Ca	hcp (Mg)/Mg$_2$Sn/MgCaSn	96.89	2.84	67.76	30.42	33.25	29.72
	40Mg45Sn15Ca	Mg$_2$Sn/MgCaSn/CaSn$_3$	65.35	31.61	31.71	33.88	1.25	73.61
	30Mg60Sn10Ca	CaSn$_3$/liquid/Mg$_2$Sn	1.25	73.61	2.09	95.97	66.12	33.25
	65Mg10Sn25Ca	hcp (Mg)/Mg$_2$Ca/MgCaSn	96.27	0.19	66.90	0.09	26.73	32.01

Table 8.3 Equilibirum compositions of the Mg-Sn-Sr key samples determined in the present work

Temp. (°C)	Alloy Nominal comp. (at. %)	Phase equilibira Phase 1/Phase 2/Phase 3	Composition (at. %) (balance=Sr)					
			Phase 1		Phase 2		Phase 3	
			Mg	Sn	Mg	Sn	Mg	Sn
415	82Mg3Sn15Sr	$Mg_{17}Sr_2$/$Mg_{38}Sr_9$/MgSnSr	88.35	0.02	81.84	0.16	34.42	30.58
	65Mg30Sn5Sr	hcp(Mg)/Mg_2Sn/Mg_5Sn_3Sr	97.83	2.06	67.27	32.54	54.94	31.84
	70Mg20Sn10Sr	hcp(Mg)/MgSnSr	99.76	0.14	34.18	30.56	-	-
	53Mg38Sn9Sr	Mg_5Sn_3Sr/Mg_2Sn/liquid	56.16	33.78	66.38	33.41	2.55	96.18
	40Mg40Sn20Sr	Mg_5Sn_3Sr/$Mg_{25}Sn_{24}Sr_{14}$/liquid	55.11	35.25	38.02	40.19	2.14	86.79
	33Mg40Sn27Sr	$Mg_{25}Sn_{24}Sr_{14}$/liquid	39.69	38.43	2.64	83.69	-	-
	65Mg5Sn30Sr	MgSnSr/Mg_2Sr/$Mg_{23}Sr_6$	31.43	31.38	65.95	9.05	77.49	3.50
350	82Mg3Sn15Sr	$Mg_{17}Sr_2$/$Mg_{38}Sr_9$/MgSnSr	89.11	1.77	82.39	0.15	33.92	31.91
	65Mg30Sn5Sr	hcp(Mg)/Mg_2Sn/Mg_5Sn_3Sr	98.09	1.84	66.27	33.31	53.56	34.20
	70Mg20Sn10Sr	hcp(Mg)/MgSnSr	99.67	0.18	34.49	33.88	-	-
	53Mg38Sn9Sr	Mg_5Sn_3Sr/Mg_2Sn/liquid	56.81	33.16	67.09	32.62	2.88	96.14
	40Mg40Sn20Sr	Mg_5Sn_3Sr/$Mg_{25}Sn_{24}Sr_{14}$/liquid	55.90	34.09	40.48	38.46	1.86	83.33
	43Mg34Sn23Sr	Mg_5Sn_3Sr/$Mg_{25}Sn_{24}Sr_{14}$	34.28	32.95	42.58	36.91	-	-
	65Mg5Sn30Sr	MgSnSr/Mg_2Sr/$Mg_{23}Sr_6$	33.87 =	31.12	65.77	7.40	78.44	2.60

8.5   Results and discussions

8.5.1 Experimental results

The Mg-Sn-Ca system

Isothermal sections of the Mg-Sn-Ca ternary system in the Mg-rich region at 350 ^{o}C and 415 ^{o}C were determined in this work. All the phase equilibrium compositions measurements are summarized in Table 8.2. The presence of the ternary compound MgCaSn was confirmed in these two isothermal sections. As shown in Table 8.1, there is limited solid solubility of either Ca in Mg_2Sn, or of Sn in Mg_2Ca. Typical back-scattered electron (BSE) images of the Mg-Sn-Ca key alloys are shown in Figure 8.1 (a) and (b). Phase identification was based on the SEM and EDS analysis results. In the 65Mg20Sn15Ca (at. %) alloy quenched from 415 ^{o}C, a three-phase equilibria consisting of hcp(Mg) + Mg_2Sn + MgCaSn was observed (Figure 8.1 (a)). In the 65Mg10Sn25Ca alloy quenched from 350 ^{o}C, a three-phase equilibria consisting of hcp(Mg) + Mg_2Ca + MgCaSn was observed (Figure 8.1 (b)). Also we can see from Figure 9.1, that the Mg_2Ca and MgCaSn phases are easily oxidized. This renders the preparation of the samples and their analysis more difficult.

The Mg-Sn-Sr system

Isothermal sections of the Mg-Sn-Sr ternary system at 350 ^{o}C and 415 ^{o}C were determined in the present work. Two new ternary compounds Mg_5Sn_3Sr and $Mg_{25}Sn_{24}Sr_{14}$ were found in these isothermal sections. The existence of the MgSnSr ternary phase was confirmed in the present work in the two isothermal sections. Typical BSE images of the Mg-Sn-Sr key alloys are shown in Figure 8.1(c) and (d), and the phase identification was based on SEM and EDS analysis results. Similarly to Mg-Sn-Ca alloys, Mg-Sn-Sr samples are also very easily oxidized. Compositions of the phases at equilibrum are summarized in Table 8.3.
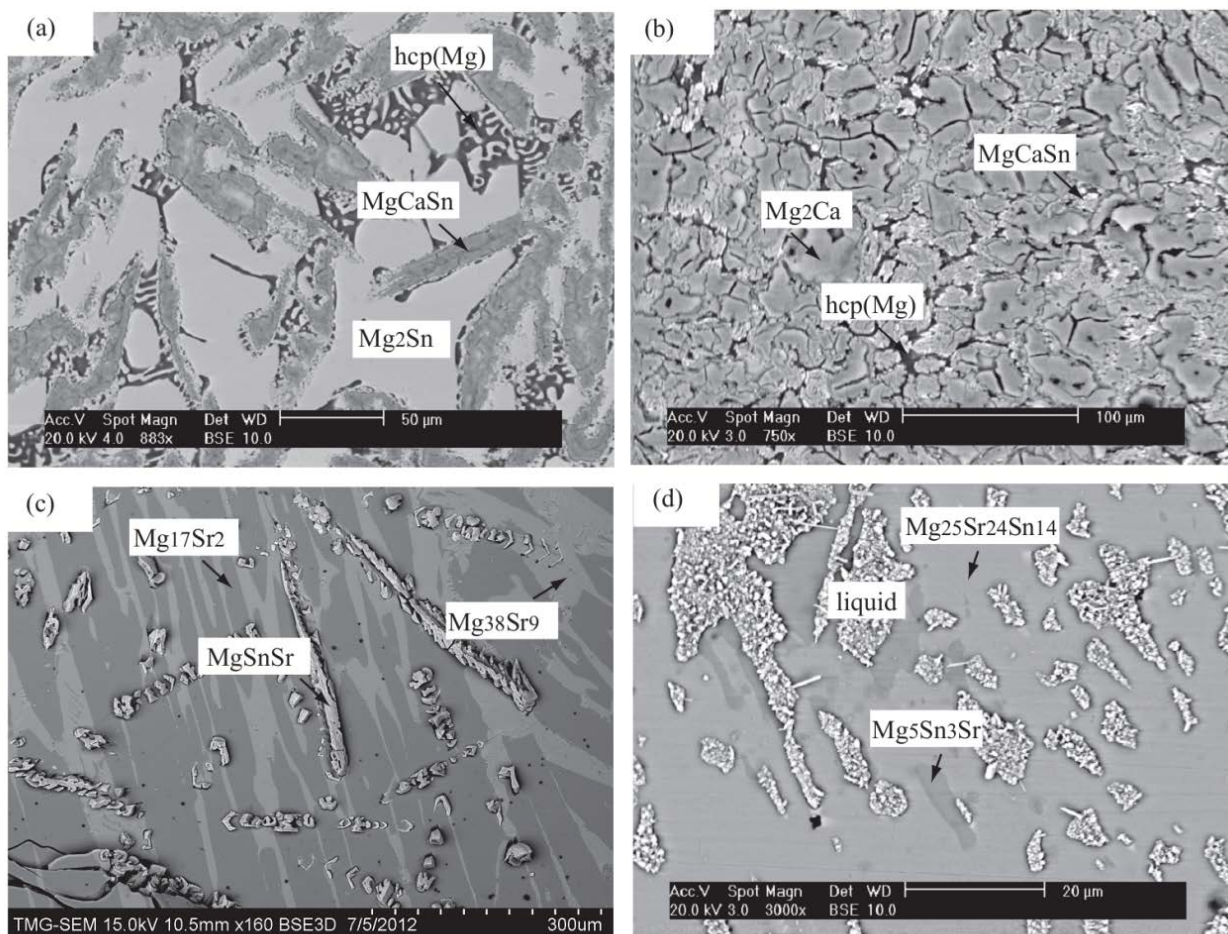
Figure 8.1 Typical ternary BSE images obatined from: (a) 65Mg20Sn15Ca, (c) 82Mg3Sn15Sr alloys annealed at 415 °C for 20 days, and (b) 65Mg10Sn25Ca, (d) 40Mg40Sn20Sr alloys (at. %) annealed at 350 °C for 35 days

8.5.2 Thermodynamic optimization

The phase diagram of the Mg-Sn (Jung, et al., 2007), Mg-Ca (Anctil, 2003), Mg-Li (P.J. Spencer, 2006), Mg-Sr (Aljarrah & Medraj, 2008a), Ca-Sr (Anctil, 2003), Ca-Sr (Aljarrah & Medraj, 2008a) and Li-Sr (Chartrand, 2003) binary systems have been critically evaluated and thermodynamic optimized using the MQMPA for the binary liquid solutions. In the present work, all the binary thermodynamic parameters were taken from their evaluations in the present optimization of the Mg-Sn-Ca-Li-Sr quinary system and their related subsystems. A critical

assessment and an optimization of the parameters of the thermodynamic models of phases of the Sn-Ca system were performed as part of the present work.

The Sn-Ca system

In the present work, the liquid phase of the Ca-Sn binary system was modeled with the Modified Quasichemical Model in the Pair Approximation (MQMPA) (Pelton & Chartrand, 2001; Pelton, et al., 2000). This was done because of the very negative experimental enthalpies of mixing and of formation of this system, suggesting strong level of short-range order in the liquid phase. The calculated enthalpies of mixing of the liquid phase at 615 ^{o}C, 644 ^{o}C and 748 ^{o}C are shown in Figure 8.2 with experimental data (Bouirden, 1984). Note that some points represent liquid in the presence of CaSn$_{3(s)}$.
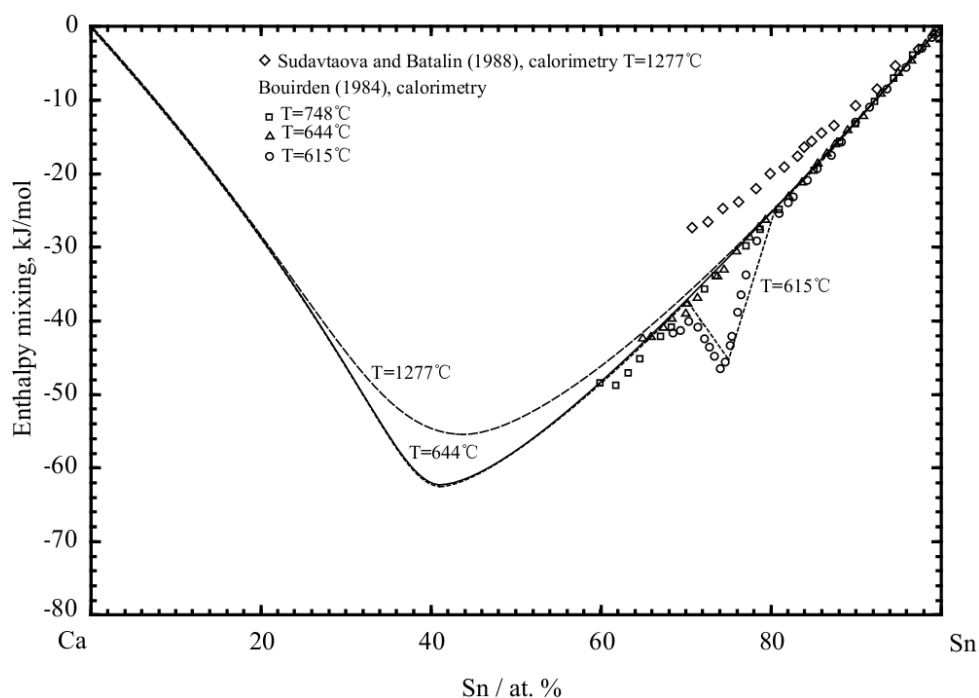
Figure 8.2 Calculated enthalpy mixing of stable and metastable liquid phase at 615, 644 and 1277 ^{o}C with experimental data (Bouirden, 1984; Sudavtsova & Batalin, 1988)

The calculated partial excess Gibbs energy curves of Ca and Sn in the liquid phase at 800 ^{o}C and 950 ^{o}C are shown in Figure 8.3 with the experimental data from Potard et al. (Potard, et al., 1969)

and Delect et al. (Delcet, et al., 1979). The reference states are pure liquid Ca and liquid Sn. As seen in Figure 8.3, a good agreement is seen between the present optimization results and experimental data from Delcet et al. (Delcet, et al., 1979), but not with the reported data from Potard et al. (Potard, et al., 1969). During the present optimization procedure, it was found that it is impossible to obtain a good fit with the reported data of Potard et al. (Potard, et al., 1969) while respecting other experimental data in the phase diagram. The experimental error of more than about 10 % in γ_{Ca} was mentioned by Potard et al. (Potard, et al., 1969). The calculated entropy of mixing of the Ca-Sn liquid phase at 1400 ^{o}C is shown in Figure 8.4 along with the previously calculated results by Ohno et al. (Ohno, et al., 2006) and Cartigny et al. (Cartigny, et al., 2005). The calculated results from present work and from Ohno et al. (Ohno, et al., 2006) are in more reasonable agreement compared with the results of Cartigny et al. (Cartigny, et al., 2005).
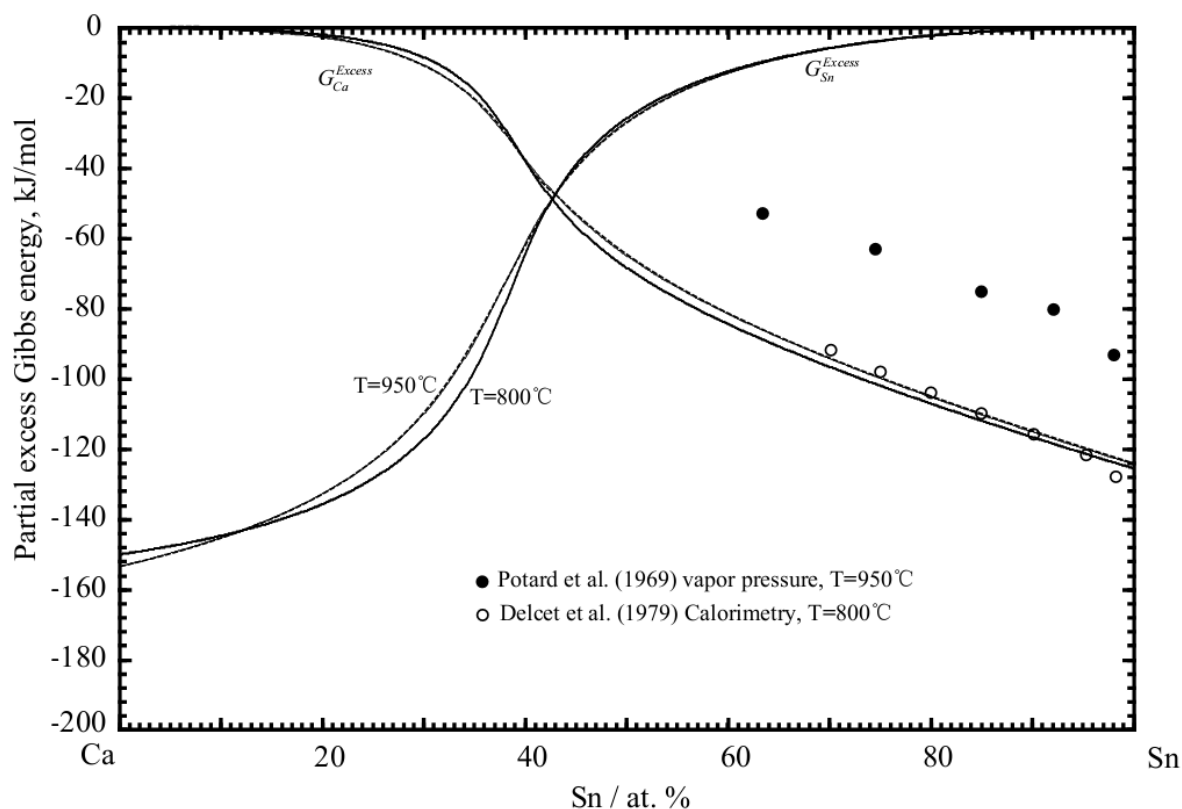
Figure 8.3 Calculated partial excess Gibbs energy of Ca and Sn in the liquid phase at 800 and 950 ^{o}C with experimental data (Delcet, et al., 1979; Potard, et al., 1969)
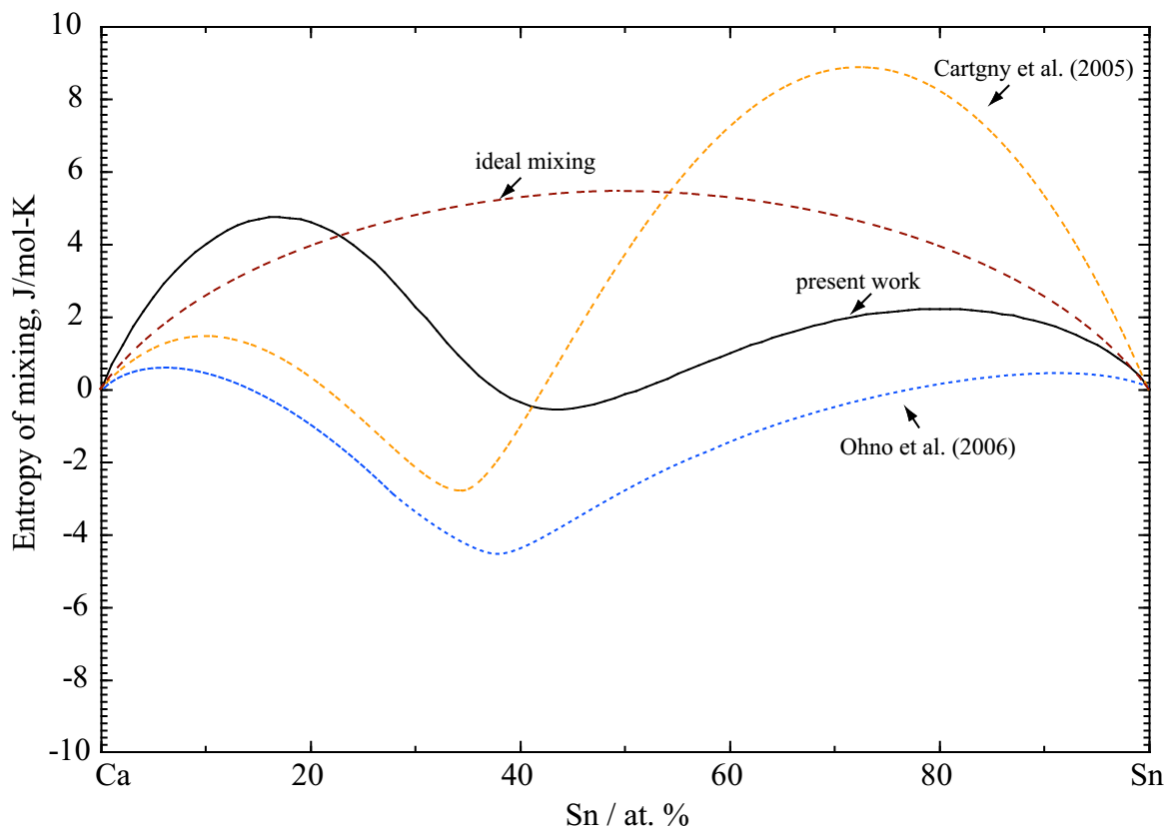
Figure 8.4 Calculated enropy of mixing of the Ca-Sn liquid phase at 1400 °C with previously calculated results (Ohno, et al., 2006, Cartigny, et al. 2005)

The calculated enthalpy of formation of compounds at 25 °C are shown in Figure 8.5 compared with the experimental data and data calculated from First-Principles calculations (Bouirden, 1984; Kubaschewski & Villa, 1949; Min & Sano, 1988; Ohno, et al., 2006; Yang, et al., 2010). The calculated phase diagram of the Ca-Sn binary system is shown in Figure 8.6 with the experimental data (Hume-Rothery, 1926; Palenzona, et al., 2000). The calculated invariant reactions are listed in Table 8.4 and compared with the compiled experimental data from Okamoto (Okamoto, 2001). As can be seen, all the calculated results are in good agreement with reliable experimental data. The thermodynamic parameters obatined in the present work are listed in Tables 8.5 and 8.6.

Table 8.4 Calculated invariant reactions in the Ca-Sn binary system from the present work compared with the compiled data (Okamoto, 2001)

Reaction	Reaction type	Temperature, ^{o}C	Composition at. % Sn			Reference
liquid $\longleftrightarrow$ Ca$_2$Sn+bcc	Eutectic	780	-	-	-	Okamoto, 2001
		780	4.8	33.3	100	This work
liquid $\longleftrightarrow$ Ca$_2$Sn	Congruent	1340	-	-	-	Okamoto, 2001
		1342	-	33.3	-	This work
liquid+Ca$_2$Sn $\longleftrightarrow$ Ca$_5$Sn$_3$	Peritectic	1130	-	-	-	Okamoto, 2001
		1130	42.1	33.3	37.5	This work
liquid+Ca$_5$Sn$_3$ $\longleftrightarrow$ Ca$_{36}$Sn$_{23}$	Peritectic	-	-	-	-	Okamoto, 2001
		1122	42.5	37.5	39.0	This work
liquid+Ca$_{36}$Sn$_{23}$ $\longleftrightarrow$ Ca$_{31}$Sn$_{20}$	Peritectic	-	-	-	-	Okamoto, 2001
		1111	42.9	39.0	39.2	This work
liquid+Ca$_{31}$Sn$_{20}$ $\longleftrightarrow$ Ca$_7$Sn$_6$	Peritectic	1000	-	-	-	Okamoto, 2001
		1000	46.5	39.2	46.2	This work
liquid $\longleftrightarrow$ Ca$_7$Sn$_6$+CaSn	Eutectic	995	-	-	-	Okamoto, 2001
		996	47.5	46.2	50.0	This work
liquid $\longleftrightarrow$ CaSn	Congruent	1010	-	-	-	Okamoto, 2001
		1012		50.0		This work
liquid $\longleftrightarrow$ CaSn+CaSn$_3$	Peritectic	610	-	-	-	Okamoto, 2001
		609	69.0	50.0	75.0	This work
liquid $\longleftrightarrow$ CaSn$_3$+bct	Eutectic	225	-	-	-	Okamoto, 2001
		231	99.7	75.0	100	This work
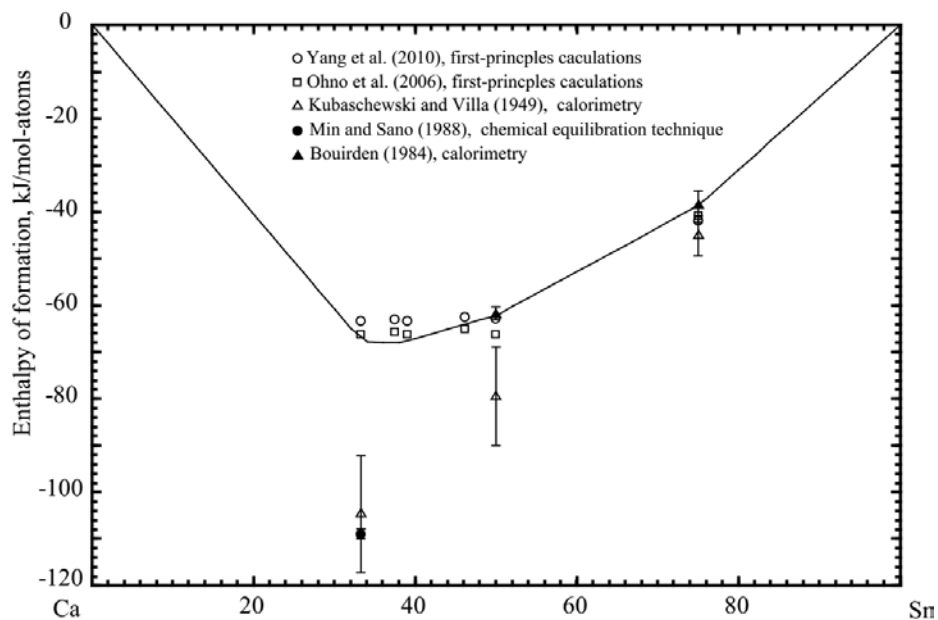
Figure 8.5 The calculated enthalpy formation of compounds at 25 °C compared with experimental data (Bouirden, 1984; Kubaschewski & Villa, 1949; Min & Sano, 1988; Ohno, et al., 2006; Yang, et al., 2010)
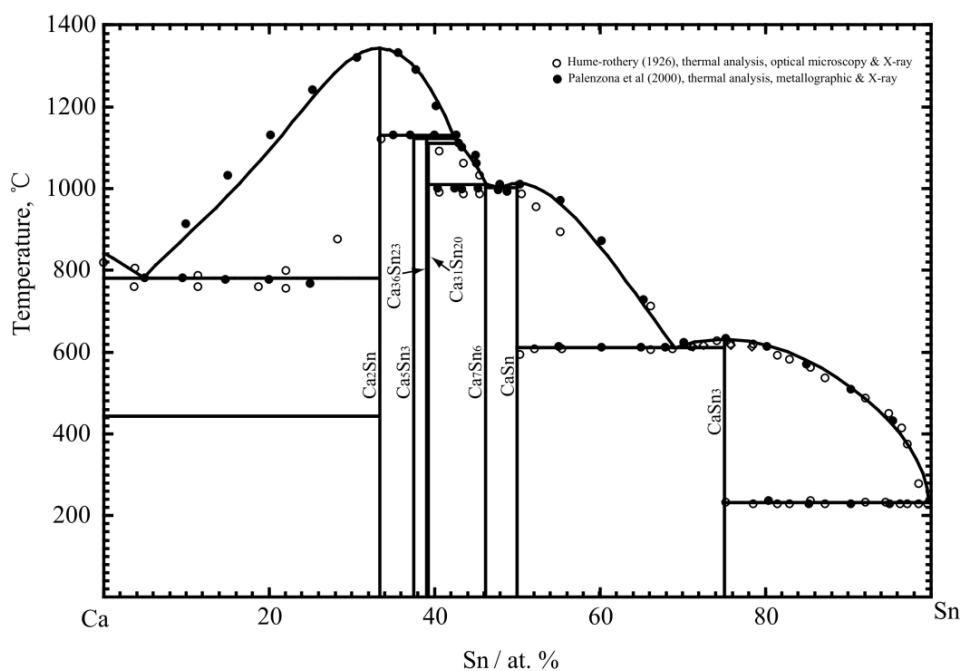
Figure 8.6 The calculated phase diagram of the Ca-Sn binary system with experimental data (Hume-Rothery, 1926; Palenzona, et al., 2000)

Table 8.5 Optimized parameters of the MQMPA for the Ca-Sn, Sn-Sr and Ca-Li binary liquid solutions

Coordination numbers [a]				Gibbs energies of pair exchange reactions (J·mol^{-1})
i	j	Z_{ij}^i	Z_{ij}^j	
Ca	Sn	4	6	$\Delta g_{Ca,Sn} = -54768.6 + 3.56 \times T + (12970.4 - 11.21 \times T)X_{CaCa} - (12342.8 - 0.46 \times T)X_{SnSn}$
Sn	Sr	6	4	$\Delta g_{SnSr} = -38513.7 - 0.84 \times T - (22175.0 + 0.88 \times T)X_{SnSn} + (5857.6 - 3.77 \times T)X_{SrSr}$
Ca	Li	6	6	$\Delta g_{Ca,Li} = -1213.4 - 1.30 \times T + 209.2 X_{CaCa}$
[a] For all pure elements (Ca, Li, Sr and Sn), $Z_{ij}^j = 6$				

Table 8.6 Optimized parameters for the Mg-Sn-Ca-Li-Sr quinary system ($^*Cp_{Sn}$ and $^*Cp_{Li}$ were modified in the present work)

Phase, model and thermodynamic parameters (J·mol^{-1}, or J· mol^{-1}·K^{-1})
liquid phase, (Ca, Li, Mg, Sn, Sr) :   Mg-Sn-Ca system : $q_{MgSn(Ca)=}^{001} = -34727.2 + 3.35 \times T$ $q_{SnCa(Mg)=}^{001} = -5522.9, q_{MgCa(Sn)=}^{001} = -30208.5$
bcc_A2 phase, (Ca, Li, Mg, Sn, Sr)(Va)$_3$: Li-Ca system: $L_{Li,Ca:Va} = 6568.9$
fcc_A1 phase, (Ca, Li, Mg, Sn, Sr)(Va)$_3$: Li-Ca system: $L_{Li,Ca:Va} = 7029.2$
hcp_A3 phase, (Ca, Li, Mg, Sn, Sr)(Va)$_3$: Li-Ca system: $L_{Li,Ca:Va} = 6276.0$
Bf_oC8 phase, (Ca,Sr)(Sn) : $G_{Ca:Sn} = G_{Ca} + {}^*G_{Sn} - 124409.5 + 6.17 \times T$,
Continued on next page

Table 8.6 (continued) The present optimized parameters for the Mg-Sn-Ca-Li-Sr quinary system ($^*Cp_{Sn}$ and $^*Cp_{Li}$ were modified in the present work)

Phase, model and thermodynamic parameters (J·mol⁻¹, or J· mol⁻¹·K⁻¹)
CaSn₃ phase, $(Ca)(Sn)_3$: $G_{Ca:Sn} = G_{Ca} + 3\times {}^*G_{Sn} - 154818.0 + 10.20\times T$
SrSn₃ phase, $(Sr)(Sn)_3$: $G_{Sn:Sr} = G_{Sr} + 3\times {}^*G_{Sn} - 134489.2 + 2.60\times T$
tI32_D8₁ phase, $(Sr,Ca)_5(Sn)_3$: $G_{Ca:Sn} = 5\times G_{Ca} + 3\times {}^*G_{Sn} - 545145.0 + 53.20\times T$ $G_{Sn:Sr} = 5\times G_{Sr} + 3\times {}^*G_{Sn} - 442601.0 + 32.02\times T$
oP13_C32 phase, $(Ca,Mg,Sr)_2(Sn)$: $G_{Ca:Sn} = 2\times G_{Ca} + {}^*G_{Sn} - 203227.0 + 20.55\times T$ $G_{Sr:Sn} = 2\times G_{Sr} + {}^*G_{Sn} - 104600.0$, $G_{Mg:Sn} = 2\times G_{Mg} + {}^*G_{Sn} - 25940.8 + 30.54\times T$ $L_{Ca,Mg:Sn} = -317565.6 + 117.15\times T$, $L_{Mg,Sr:Sn} = -343088.0 + 50.21\times T$
Laves_C14 phase, $(Ca,Li,Mg,Sn,Sr)_2(Ca,Li,Mg,Sn,Sr)$: $G_{Ca:Li} = 2\times G_{Ca} + {}^*G_{Li} + 15000.0$ $G_{Li:Ca} = G_{Ca} + 2\times {}^*G_{Li} - 4585.7 + 8.11\times T$, $G_{Li:Li} = 3\times {}^*G_{Li} + 15000$, $L_{Li:Mg,Ca} = -8368.0$
Ca₇Sn₆ phase, $(Ca)_7(Sn)_6$: $G_{Ca:Sn} = 7\times G_{Ca} + 6\times {}^*G_{Sn} - 833650.0 + 52.68\times T$
Ca₃₁Sn₂₀ phase, $(Ca)_{31}(Sn)_{20}$: $G_{Ca:Sn} = 31\times G_{Ca} + 20\times {}^*G_{Sn} - 3447839.0 + 310.70\times T$
Ca₃₆Sn₂₃ phase, $(Ca)_{36}(Sn)_{23}$: $G_{Ca:Sn} = 36\times G_{Ca} + 23\times {}^*G_{Sn} - 3993510.0 + 364.00\times T$
Sr₃Sn₅ phase, $(Sr)_3(Sn)_5$: $G_{Sr:Sn} = 3\times G_{Sr} + 5\times {}^*G_{Sn} - 358447.0 + 1.00\times T$
SrSn₄ phase, $(Sr)(Sn)_4$: $G_{Sr:Sn} = G_{Sr} + 4\times {}^*G_{Sn} - 137804.0 + 5.5\times T$
Mg₇Ca₁₂Sn₁₄ phase, $(Mg)_7(Ca)_{12}(Sn)_{14}$: $G_{Ca:Mg:Sn} = 7\times G_{Mg} + 12\times G_{Ca} + 14\times {}^*G_{Sn} - 2027060.8 + 189.97\times T$
Mg₅Sn₃Sr phase, $(Mg)_5(Sn)_3(Sr)$: $G_{Mg:Sn:Sr} = 5\times G_{Mg} + 3\times {}^*G_{Sn} + G_{Sr} - 305580.0 + 10.00\times T$
Mg₂₅Sn₂₄Sr₁₄ phase, $(Mg)_{25}(Sn)_{24}(Sr)_{14}$: $G_{Mg:Sn:Sr} = 25\times G_{Mg} + 24\times {}^*G_{Sn} + 14\times G_{Sr} - 2657860 + 70.00\times T$
Mg₁₇Sr₂ phase, $(Mg)_{17}(Ca,Sr)_2$: $G_{Mg:Ca} = 2\times G_{Ca} + 17\times G_{Mg} - 37656.0$
Continued on next page

Table 8.6 (continued) The present optimized parameters for the Mg-Sn-Ca-Li-Sr quinary system ($^*Cp_{Sn}$ and $^*Cp_{Li}$ were modified in the present work)

Phase, model and thermodynamic parameters (J·mol^{-1}, or J· mol^{-1}·K^{-1})
Mg$_{38}$Sr$_9$ phase, (Mg)$_{38}$(Ca,Sr)$_9$: $\quad G_{Mg:Ca} = 9 \times G_{Ca} + 38 \times G_{Mg} - 196648.0$
Sr$_2$Sn phase, (Sr)$_2$(Sn): $G_{Sr:Sn} = 2 \times G_{Sr} + {}^*G_{Sn} - 167023.3 + 15.76 \times T$
$^*G_{Li} = \int {}^*Cp_{Li}dt - T \times \int \dfrac{{}^*Cp_{Li}}{T}dt \qquad\qquad\qquad {}^*G_{Sn} = \int {}^*Cp_{Sn}dt - T \times \int \dfrac{{}^*Cp_{Sn}}{T}dt$ $\begin{aligned} {}^*Cp_{Sn} &= 25.858\text{-}0.0010237 \times T\text{-}36880/T^{-2} + 1.9156602E\text{-}5 \times T^2 & 249K<T<250K \\ &= 15.961 + 0.0377404 \times T + 123920/T^{-2}\text{-}1.8727002E\text{-}5 \times T^2 & 251K<T<1000K \\ &= 35.098 & 506K<T<3000K \end{aligned}$ $\begin{aligned} {}^*Cp_{Li} &= 38.940488\text{-}0.070933862 \times T\text{-}319988/T^{-2} + 0.000119218896 \times T^2 & 298K<T<454K \\ &= 32.94\text{-}0.0002179 \times T\text{-}598200/T^{-2} + 4.656E\text{-}8 \times T^2 & 455K<T<3000K \end{aligned}$

The Sn-Sr system

The present calculated phase diagram of the Sn-Sr binary system is shown in Figure 8.7 with the experimental data (Hoffmann, 2002; Marshall & Chang, 1981; Palenzona & Pani, 2004; Ray, 1930; Widera & Schäfer, 1981; Zurcher, et al., 2001) and the calculated results from Zhao et al. (Zhao, et al., 2011). All the calculated invariant reactions with phase compositions are listed in Table 8.7 compared with the experimental data (Marshall & Chang, 1981; Palenzona & Pani, 2004; Ray, 1930; Widera & Schäfer, 1981). The calculated enthalpy of mixing of liquid phase at 1500 °C is shown in Figure 8.8 with the experimental data from Esin et al. (Esin, et al., 1985). The calculated entropy of mixing of the Sn-Sr liquid phase at 1000 °C is shown in Figure 8.9 with the previously calculated results from Zhao et al. (Zhao, et al., 2011). As can be seen, the calculated results from Zhao et al. (Zhao, et al., 2011) are much more positive than the ideal mixing entropy; This is highly improbable in the system such as this.

Table 8.7 Calculated invariant reactions in the Sn-Sr binary system in the present work with experimental data (Marshall & Chang, 1981; Palenzona & Pani, 2004; Ray, 1930; Widera & Schäfer, 1981)

Reaction	Reaction type	Temperature °C	Composition (Sn at. %)			Reference
liquid ↔ Sr₂Sn	Congruent	1295±5	33.3	33.3		(Palenzona & Pani, 2004)
		1293	33.3	33.3		This work
liquid ↔ Sr₂Sn+bcc	Eutectic	752±5	2.5	-	-	(Palenzona & Pani, 2004)
		745	2.7	-	-	(Widera & Schäfer, 1981)
		750	2.1	33.3	0	This work
liquid+Sr₂Sn ↔ Sr₅Sn₃	Peritectic	1190±5	39.9	-	-	(Palenzona & Pani, 2004)
		1170	36.7	-	-	(Widera & Schäfer, 1981)
		1187	42.5	33.3	37.5	This work
liquid ↔ Sr₅Sn₃+SrSn	Eutectic	1100±5	45.6	-	-	(Palenzona & Pani, 2004)
		1080	46.1	-	-	(Widera & Schäfer, 1981)
		1114	46.3	37.5	50	This work
liquid ↔ SrSn	Congruent	1140±5	0.5	0.5	-	(Palenzona & Pani, 2004)
		1140	-	-	-	(Widera & Schäfer, 1981)
		910	-	-	-	(Zurcher, et al., 2001)
		1137	0.5	0.5	-	This work
liquid+SrSn ↔ Sr₃Sn₅	Peritectic	775±5	65.0	-	-	(Palenzona & Pani, 2004)
		780	-	-	-	(Hoffmann, 2002)
		810	-	-	-	(Zurcher, et al., 2001)
		775	66.9	50	62.5	This work
liquid+Sr₃Sn₅ ↔ SrSn₃	Peritectic	560±5	79.7	-	-	(Palenzona & Pani, 2004)
		563	-	-	-	(Hoffmann, 2002)
		598±1	75.1	-	-	(Marshall & Chang, 1981)
		561	78.7	62.5	75.0	This work
Continued on next page						

Table 8.7 (Continued) Calculated invariant reactions in the Sn-Sr binary system in the present work with experimental data (Marshall & Chang, 1981; Palenzona & Pani, 2004; Ray, 1930; Widera & Schäfer, 1981)

Reaction	Reaction type	Temp. °C	Composition (Sn at. %)			Reference
liquid+SrSn$_3$ ↔ SrSn$_4$	Peritectic	315±5	95.8	-	-	(Palenzona & Pani, 2004)
		316	-	-	-	(Hoffmann, 2002)
		338	95.1	-	-	(Ray, 1930)
		334±4	96.0	-	-	(Marshall & Chang, 1981)
		315	94.7	75.0	80.0	This work
liquid ↔ bct+SrSn$_4$	Eutectic	230±5	99.0	-	-	(Palenzona & Pani, 2004)
		232	99.7	-	-	(Widera & Schäfer, 1981)
		230±2	99.0	-	-	(Ray, 1930)
		226	98.4	100	80.0	This work
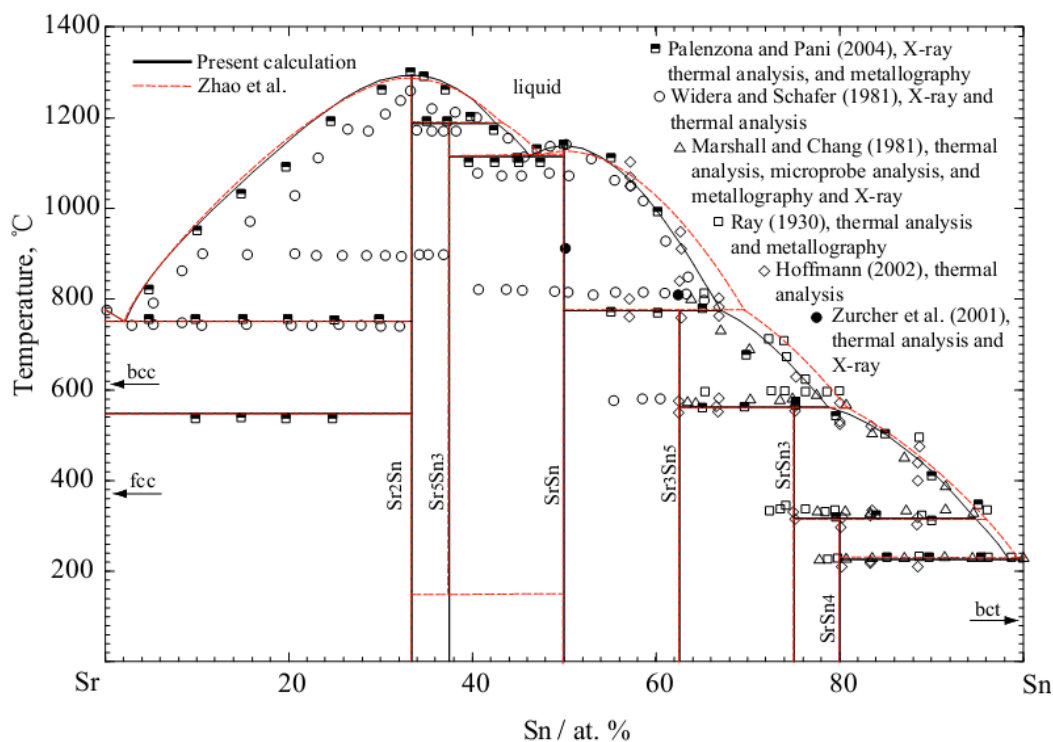
Figure 8.7 Calculated phase diagram of the Sn-Sr binary system with the experimental data
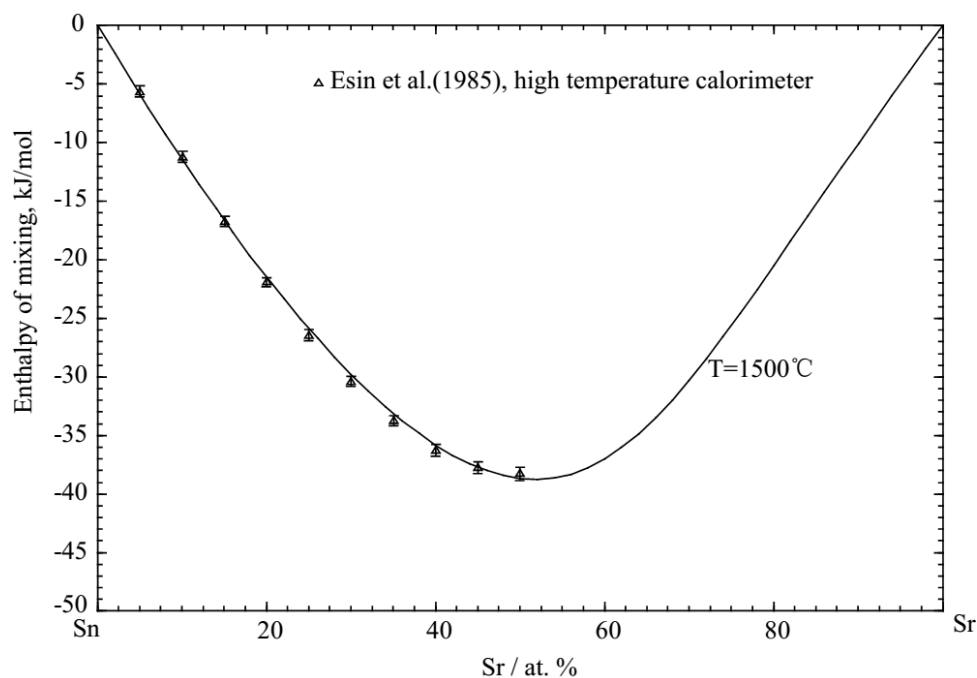
Figure 8.8 Calculated enthalpy of mixing of the liquid phase at 1500 ^{o}C with the experimental data (Esin, et al., 1985)
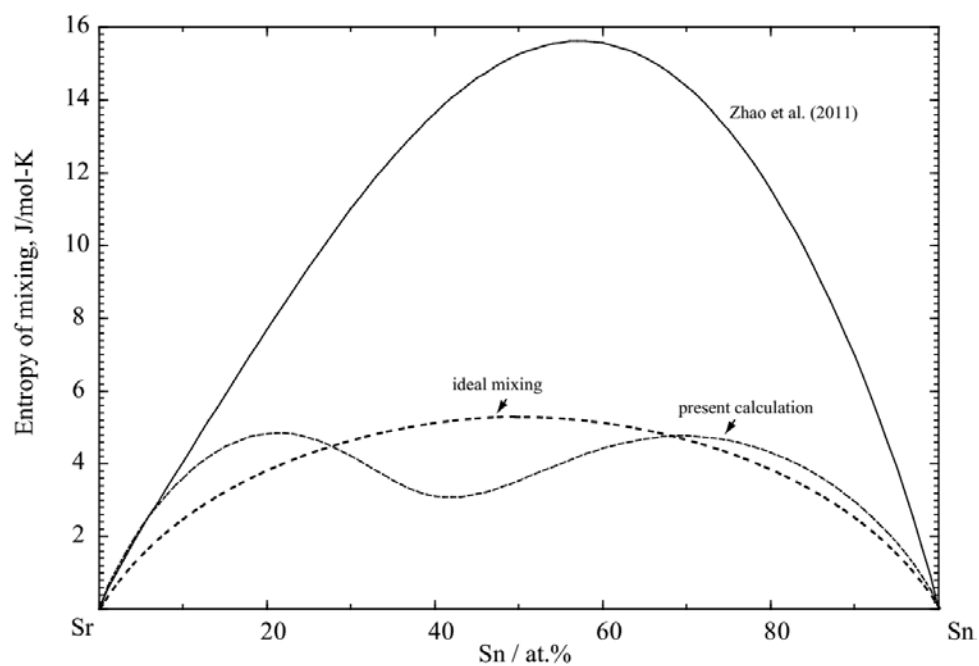

Figure 8.9 Calculated entropy of mixing of the Sn-Sr liquid phase at 1000 ^{o}C with the previously calculated results (Zhao, et al., 2011)
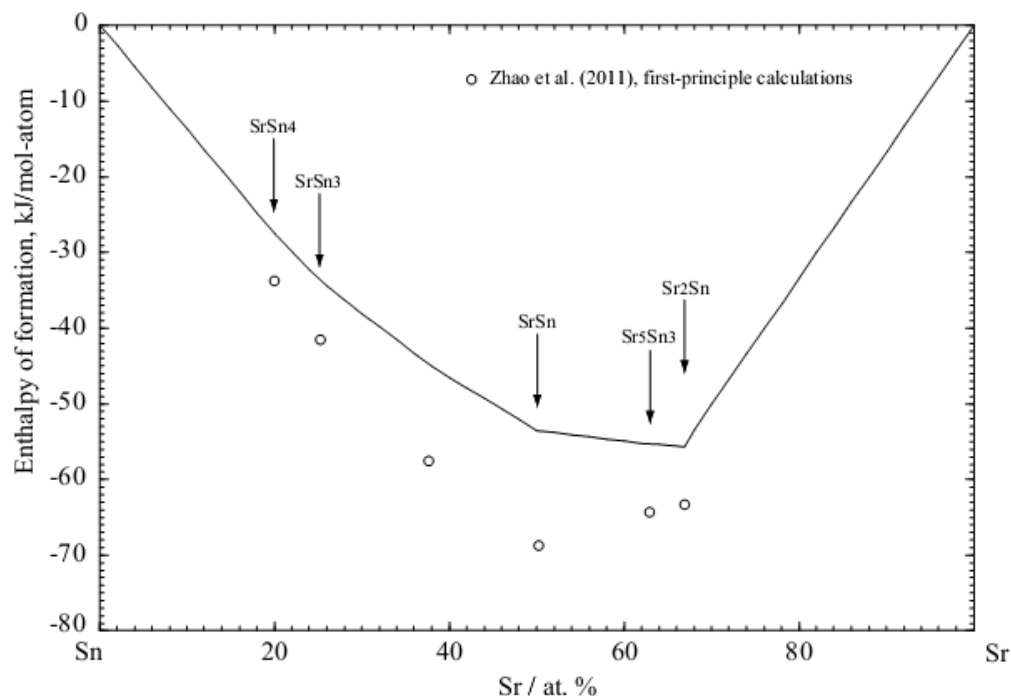
Figure 8.10 Calculated enthalpy of formation of solid phases at 25 °C with the previously calculated results (Zhao, et al., 2011)

The calculated enthalpy of formation of solid phases at 25 °C is shown in Figure 8.10 with the calculated results from Zhao et al. (Zhao, et al., 2011) from First-principles calculations. As seen in Figure 8.10, the present calculated results of enthalpy of formation of solid phases are slightly more positive than the First-principles calculations results of Zhao et al. (Zhao, et al., 2011). However, the present results are more consistent with a global fitting of both phase equilibrium and thermodynamic data. The thermodynamic parameters obtained in the present work are listed in Tables 8.5 and 8.6.

The Ca-Li system

The present calculated phase diagram of Ca-Li binary system is shown in Figure 8. 11 along with experimental data (Kanda & Keller, 1964; Wolfson, 1956). The calculated enthalpy of formation of solid phases at 25 °C in comparison with experimental data from Grobner et al. (Grobner, et al., 2002) is shown in Figure 8. 12. The calculated entropy of mixing of the Ca-Li liquid phase at

900 oC is shown in Figure 8.13 in comparison with the previous calculated results of Grobner et al. (Grobner, et al., 2002). All the thermal parameters obtained in the present work are listed in Tables 8.5 and 8.6.
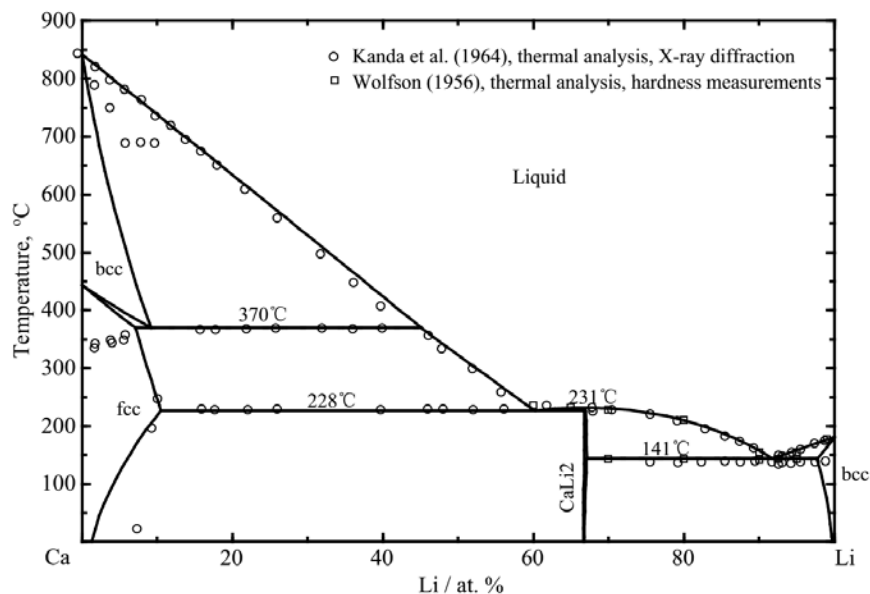
Figure 8.11 Calculated phase diagram of the Ca-Li system with the experimental data (Kanda & Keller, 1964; Wolfson, 1956)
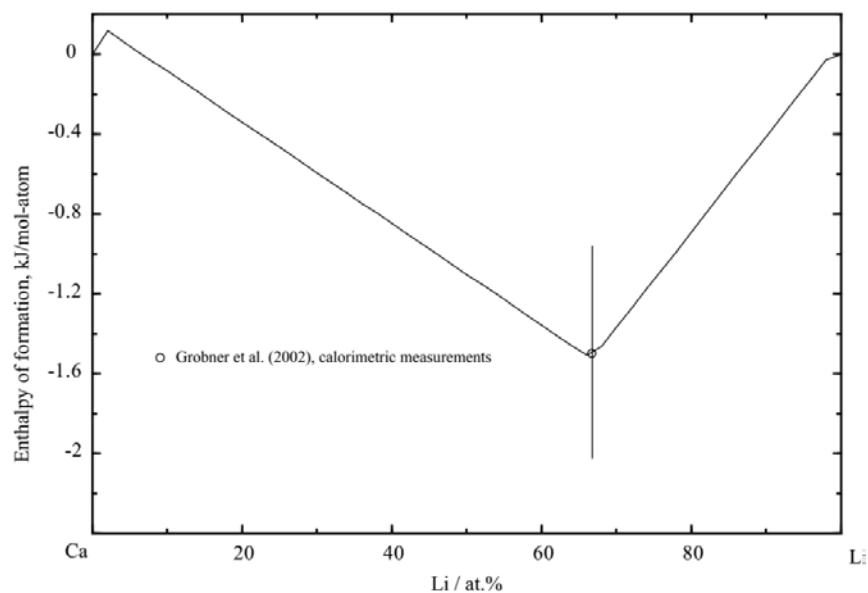
Figure 8.12 Calculated enthalpy of formation of the Ca-Li solid phases at 25 °C compared with experimental data (Grobner, et al., 2002)
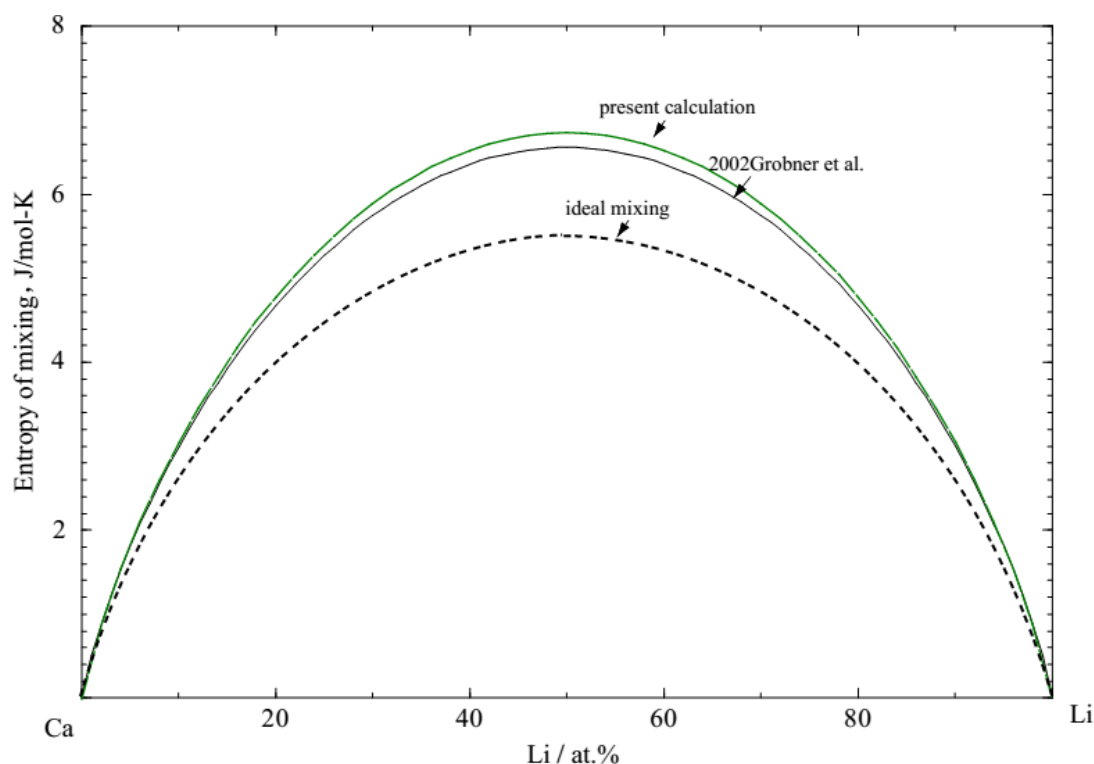
Figure 8.13 Calculated entropy of mixing of the Ca-Li liquid phase at 1000 $^{\circ}$C compared with the previously calculated results (Grobner, et al., 2002)

The Mg-Sn-Ca system

In the present work, the MgSnCa compound was modeled with two sublattices as $(Mg,Ca)_2(Sn)$ according to solid solubility and the crystal structure. The $Mg_{3.8}Sn_7Ca_{6.2}$ compound was treated as a stoichiometric phase and modeled with sublattices as $(Mg)_7(Ca)_{12}(Sn)_{14}$. The enthalpies of formation of the MgSnCa and $Mg_{3.8}Sn_7Ca_{6.2}$ compounds were fixed at -64.65 and -61.42 kJ·(mol-atom)$^{-1}$ respectively in the present work; These are in a reasonable agreement with calculated results from First-principles calculations (Kozlov, et al., 2008; Mantina, et al., 2008). The calculated isothermal sections of Mg-Sn-Ca ternary system at 350 $^{\circ}$C and 415 $^{\circ}$C are shown in Figure 8.14 with the experimental data obtained in the present work. As we can see, the calculated results are in a reasonable agreement with the experimental data. Due to the slow cooling rate during the quenching process (quenching samples into water with quartz tube), the liquid phase in the Sn-rich portion had changed into the final eutectic structure which makes it

difficult to measure the real composition of the equilibrated liquid phase. Thus the experimental data of the liquid phase were not considered in the present optimization.
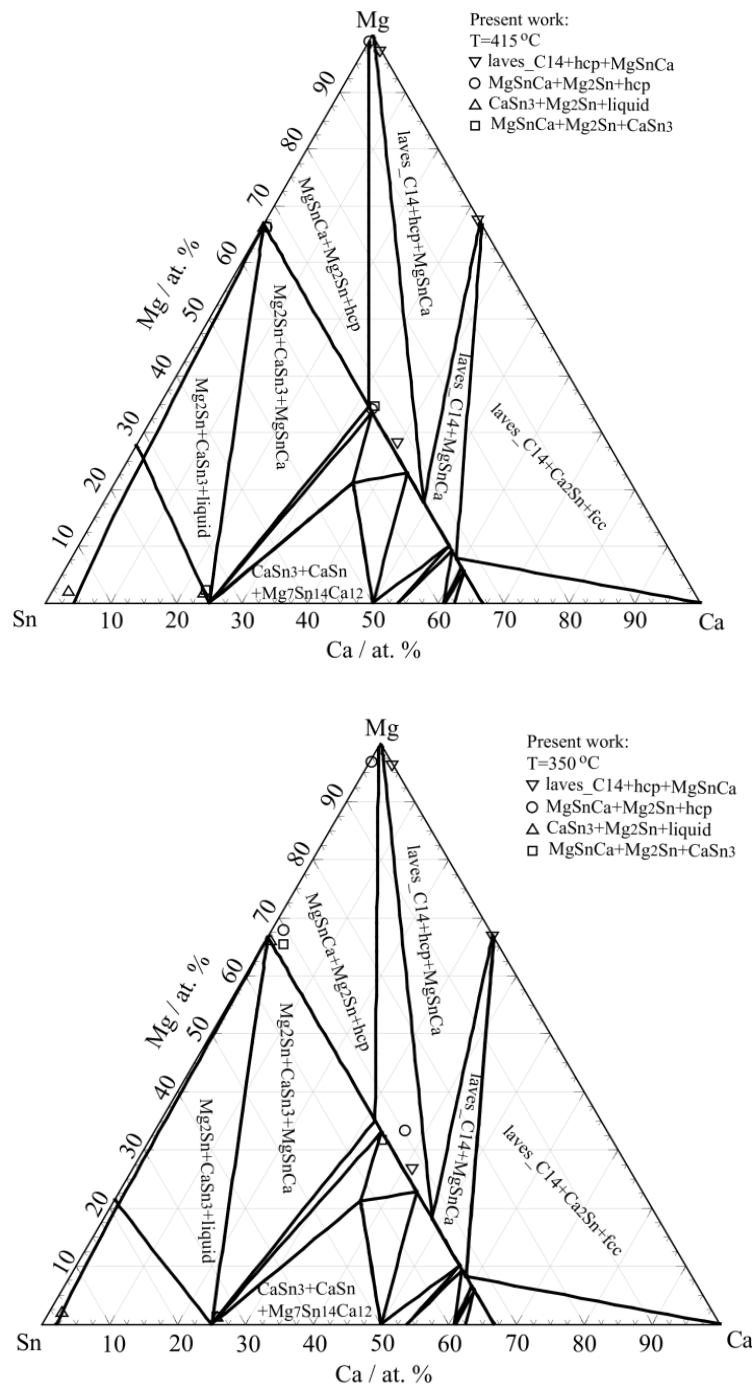
Figure 8.14 Calculated isothermal sections of Mg-Sn-Ca ternary system at 350 $^{\circ}$C and 415 $^{\circ}$C along with the experimental data obtained in the present work

The calculated isoplethal sections of Mg$_2$Sn-Mg$_2$Ca, Mg-CaSn , Mg$_2$Sn-Ca$_2$Sn, and 47Ca53Sn-Mg are shown in the Figure 8.15 with the experimental data from Kozlov et al. (Kozlov, et al., 2008). The calculated liquidus projection of the Mg-Sn-Ca ternary system in the Mg-rich region is shown in Figure 8.16. Evidently, the liquidus projection is dominated by the MgSnCa solid solution, which has a high melting temperature (liquidus) and a very negative enthalpy of formation from the elements. The precipitates in the Mg matrix of Mg-Sn based alloys will be changed into Mg$_2$Sn + MgSnCa or MgSnCa phase with small amounts of Ca additive. The optimizied thermodynamic parameters related to the ternary phases in the Mg-Sn-Ca obtained in the present work are listed in Tables 8.5 and 8.6.
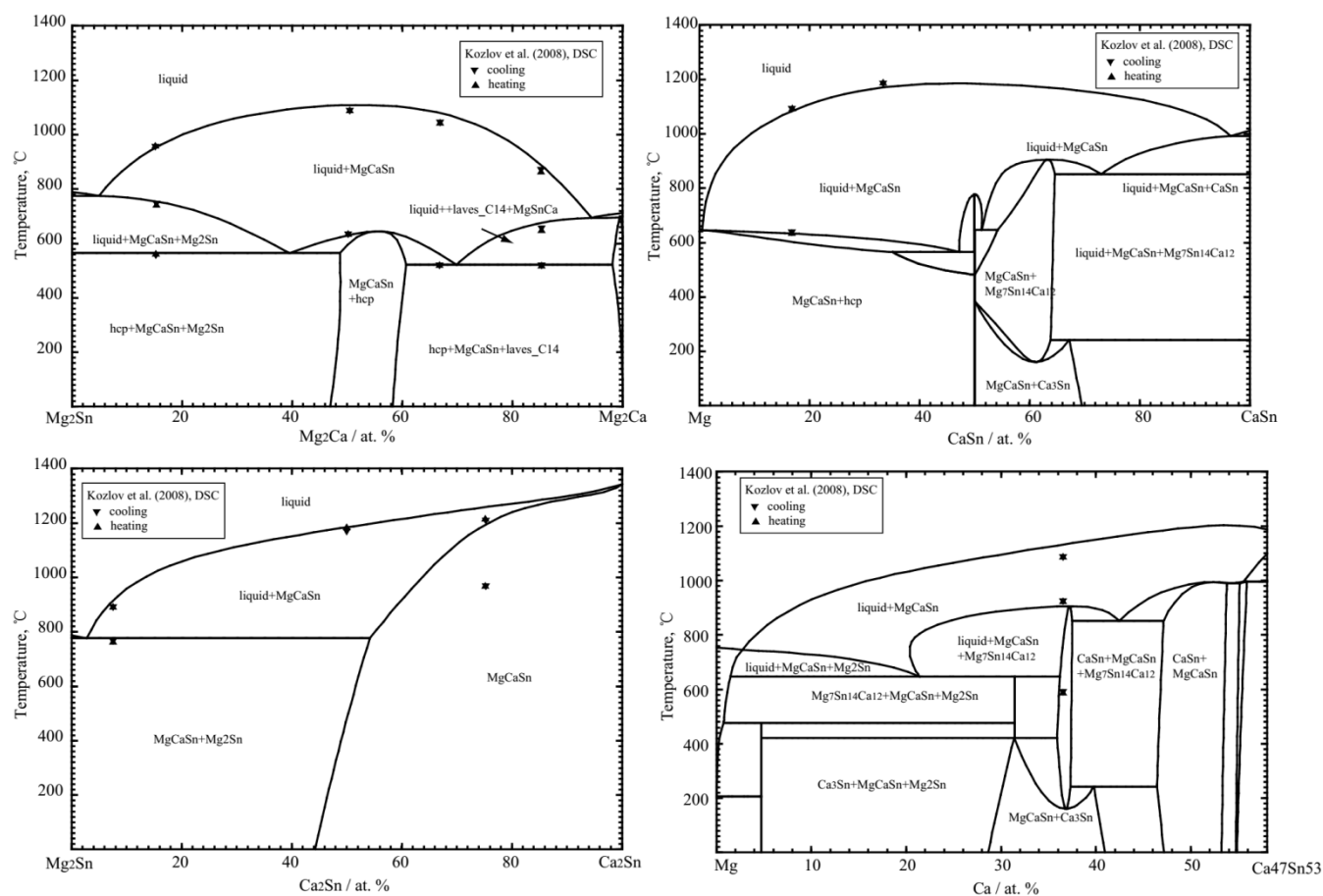
Figure 8.15 Calculated vertical sections of Mg$_2$Sn-Mg$_2$Ca, Mg-CaSn, Mg$_2$Sn-Ca$_2$Sn, and 47Ca53Sn-Mg with the experimental data from Kozlov et al. (Kozlov, et al., 2008).
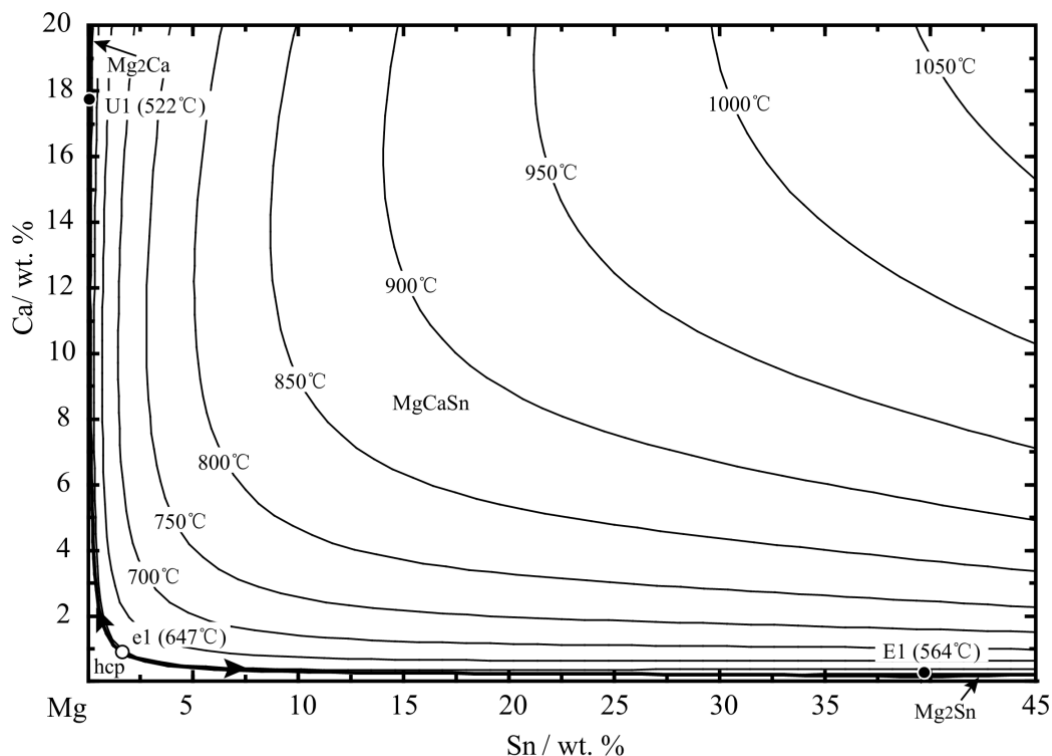
Figure 8.16 Calculated liquidus projection of the Mg-Sn-Ca ternary system in the Mg-rich region

The Mg-Sn-Sr system

The present thermodynamic optimization was based on phase equilibria data obtained form our experimental work. The ternary phases Mg_5Sn_3Sr and $Mg_{25}Sn_{24}Sr_{14}$ were treated as stoichiometric compounds and modeled with a three-sublattice structure as $(Mg)_x(Sn)_y(Sr)_z$. The MgSnSr ternary phase, which is described by the same sublattice as the MgSnCa phase, was modeled as $(Mg,Sr)_2(Sn)$. The calculated isothermal sections of Mg-Sn-Sr ternary system at 350 ^{o}C and 415 ^{o}C are shown in Figure 8.17 compared with experimental data obtained in the present work. It is similar to the Mg-Sn-Ca system. Because of the slow cooling rate during the quenching process (samples quenched into water with quartz tube), the liquid phase in the Sn-rich portion had changed into the final eutectic structure which makes it difficult to measure the real composition of the equilibrated liquid phase. Thus the experimental data of the liquid phase were not considered in the present optimization.
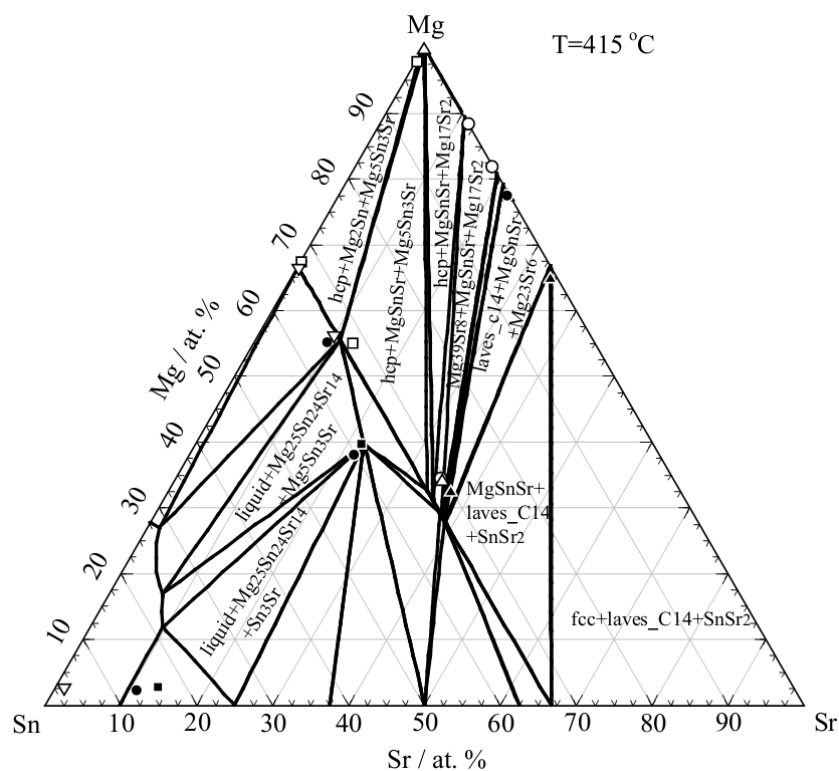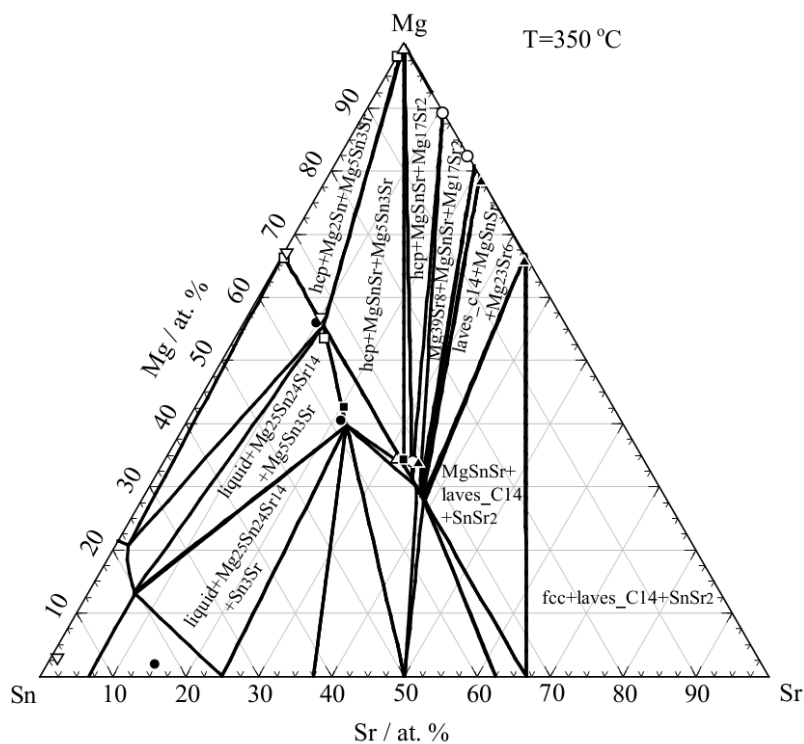
Figure 8.17 Calculated isothermal sections of the Mg-Sn-Sr ternary system at 350 ^{o}C and 415 ^{o}C along with the experimental data obtained in the present work

All the optimized thermodynamic parameters of the Mg-Sn-Sr ternary system in the present work are listed in Tables 8.5 and 8.6. In order to obtain a self-consistent thermodynamic description of the Mg-Sn-Sr ternary system, further experimental melting points (liquidus) and thermodynamic properties of ternary compounds are needed.

The Mg-Ca-Sr system

The calculated isothermal section of Mg-Ca-Sr ternary system at 500 $^{\circ}$C is shown in Figure 8.18 with the experimental from Janz and Schmid-Fetzer (Janz & Schmid-Fetzer, 2009). As seen in Figure 8.18, the present optimization results are in a reasonable agreement with the experimental data (Janz & Schmid-Fetzer, 2009). There is a slight translation of the experimental data for the laves_C14 phase compared with the real compositions of terminal binary systems. This may be due to easurement uncertainty. The difference between the calculated and experimental results were deemed to be within experimental error.
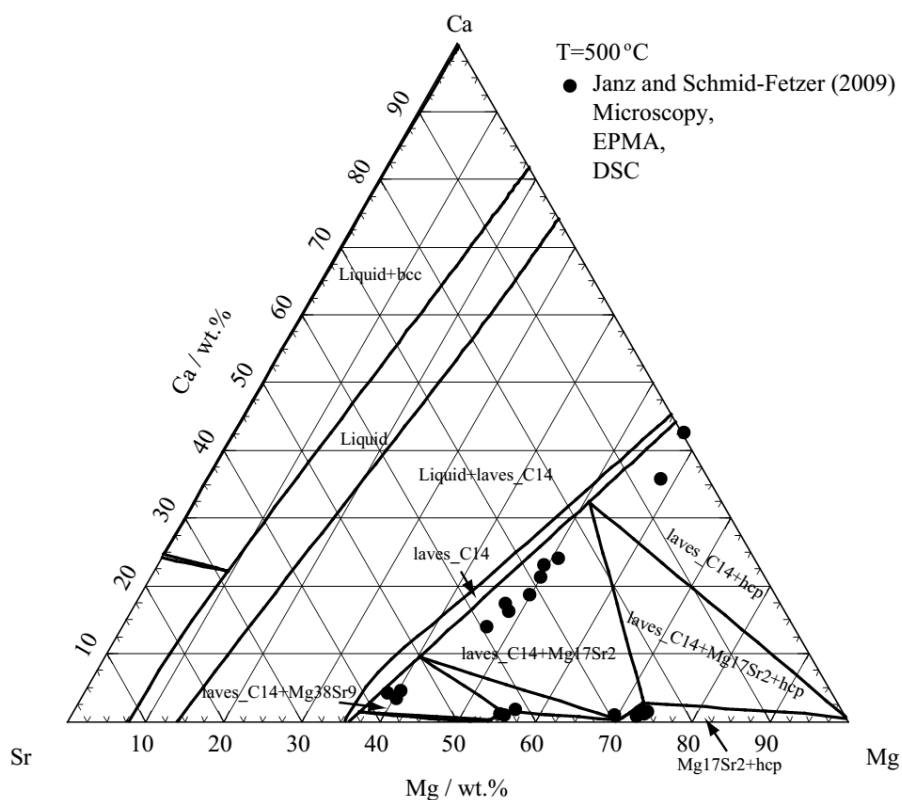
Figure 8.18 Calculated isothermal section of the Mg-Ca-Sr ternary system at 500 $^{\circ}$C along with the experimental data (Janz & Schmid-Fetzer, 2009)

The calculated isoplethal section of the 79.6Mg20.4Ca-53.7Mg46.3Sr (wt. %) is shown in figure 8.19 in comparison with the reported experimental data from Janz and Schmid-Fetzer (Janz & Schmid-Fetzer, 2009). There is good agreement between the present calculated results and experimental data. All the ternary thermodynamic parameters optimized of Mg-Ca-Sr ternary system in the present work are listed in Tables 8.5 and 8.6.
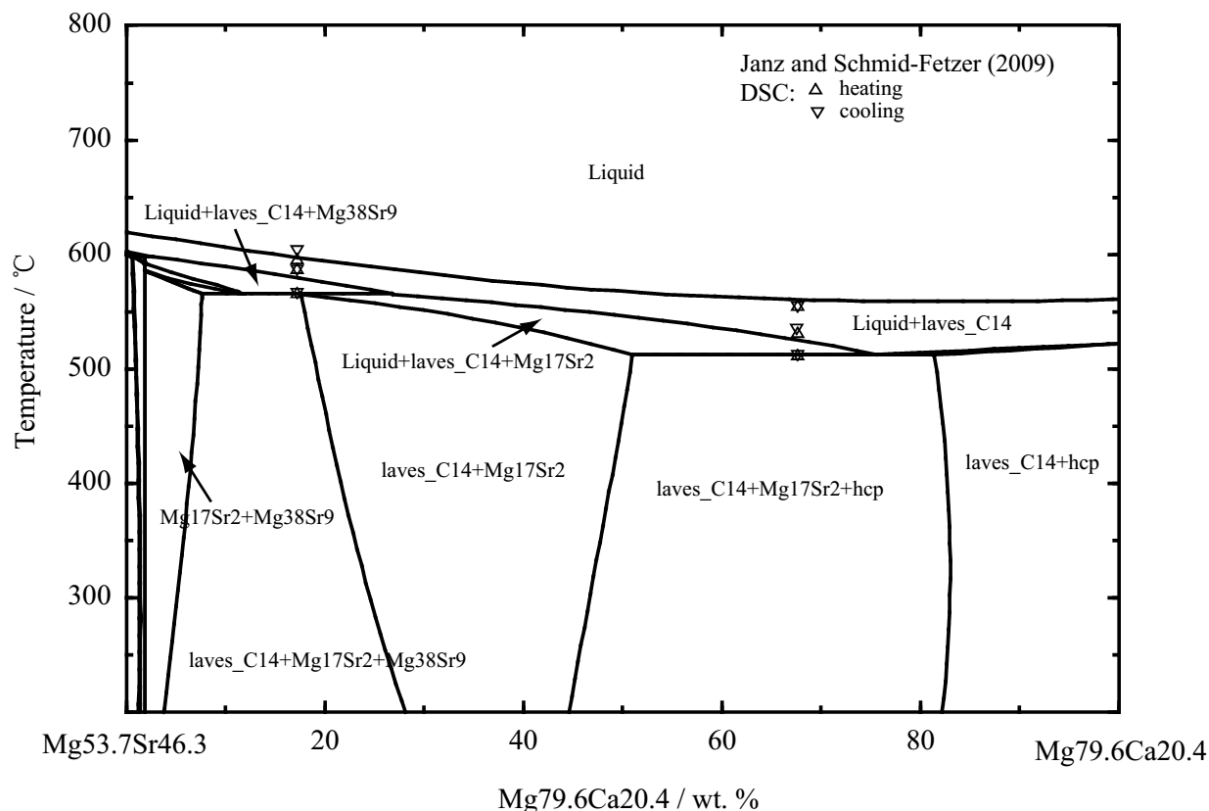
Figure 8.19 Calculated isopleth of the 79.6Mg20.4Ca-53.7Mg46.3Sr (wt. %) along with the experimental data (Janz & Schmid-Fetzer, 2009)

The Mg-Ca-Li system

In the present optimization, the liquid phase was modeled with MQM considering the short-range ordering behavior. The calculated isothermal section of 150 ^{o}C and the ternary isoplethal sections of Mg$_2$Ca-Li$_2$Ca and 13 Li (at. %) are shown in Figures 8.20 and 8.21 (a) and (b) in comparison with experimental data (Grobner, et al., 2002), respectively.

There is good agreement between the present calculated results and experimental data. All the ternary thermodynamic parameters optimized of Mg-Li-Ca ternary system in the present work are listed in Tables 8.5 and 8.6.
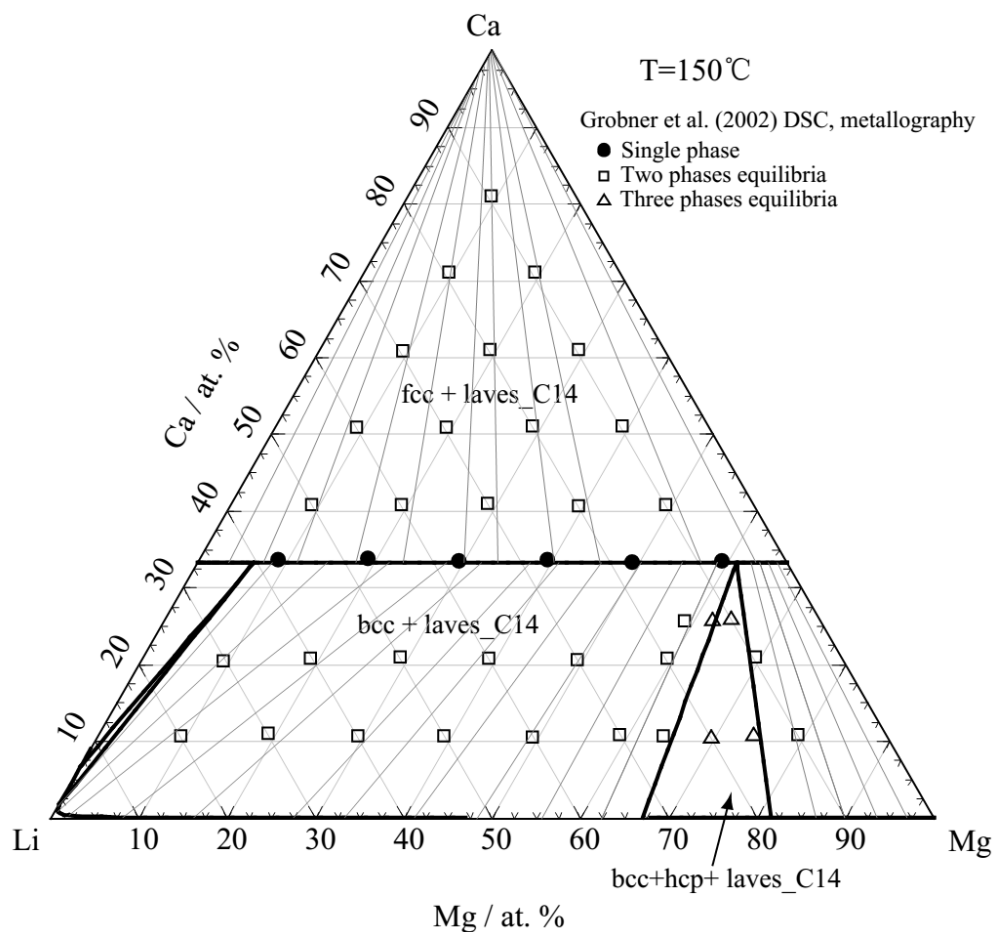
Figure 8.20 Calculated isothermal section of the Mg-Ca-Li ternary system at 150 °C along with the experimental data (Grobner, et al., 2002)
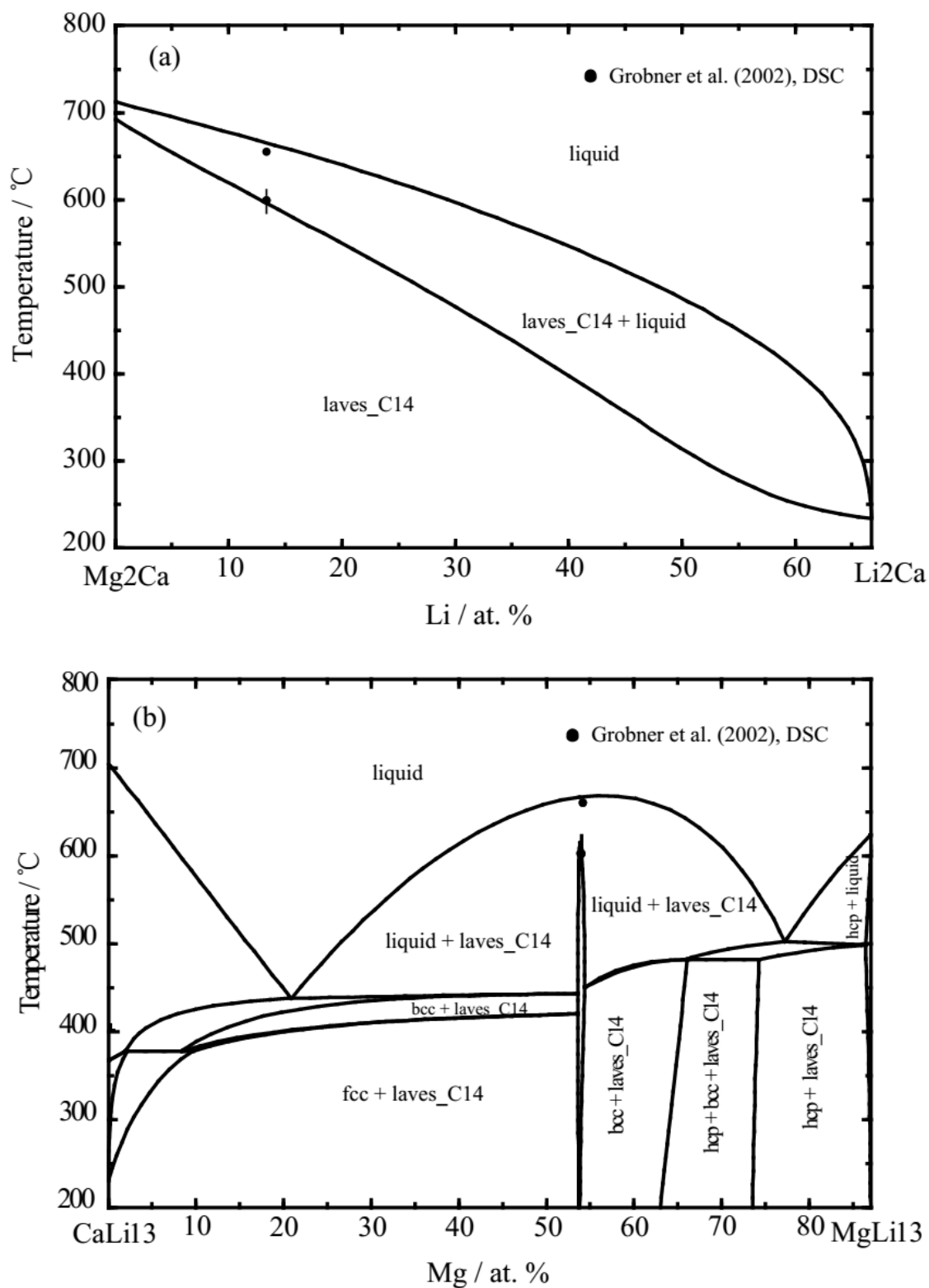
Figure 8.21 Calculated isoplethal sections of (a) Mg₂Ca-Li₂Ca and (b) CaMg-13Li (at. %) with the experimental data (Grobner, et al., 2002)

8.6   Conclusions

The phase equilibria of the Mg-Sn-Ca and Mg-Sn-Sr ternary systems in the Mg-rich range at 415°C and 350 ^{o}C were measured in the present work. The existence of the ternary phases MgSnCa and MgSnSr were confirmed in the present work. Two new ternary phases, Mg_5Sn_3Sr and $Mg_{25}Sn_{24}Sr_{14}$, were found in the Mg-Sn-Sr isothermal sections of 415 ^{o}C and 350 ^{o}C. Further experiment data are needed in determining the crystal structure and thermal stability of newly found compounds.

A systematic thermodynamic evaluation and optimization of the Sn-Ca, Sn-Sr and Ca-Li binary systems, and the Mg-Sn-Ca, Mg-Sn-Sr, Mg-Ca-Sr and Mg-Ca-Li ternary systems have been presented using the experimental data from the present work and from previously reported data literature. A thermodynamic database for the Mg-Sn-Ca-Li-Sr quinary system was developed in the present work, which is part of the project of developing Mg-X (X: Ag, Ca, Li, In, Na, Sr, Sn, and Zn) multi-component system for Mg-based alloys design.

CHAPITRE 9   THERMODYNAMIC OPTIMIZATION OF THE AG-X (X: CA, LI, ZN) AND CA-IN BINARY SYSTEMS

9.1 Introduction

Silver, as a trace additive for improving the mechanical properties of Mg-based alloys, has became a more and more interesting candidate for Mg-based alloys research (Fang, et al., 2003; Liang, 2004). The influence of Ag on Mg-based alloys was widely investigated recently, because Ag greatly affects the grain refinement and the corrosion resistance of Mg-based alloys (Ben-Hamu, et al., 2006; Mendis, et al., 2007). Furthermore, alloys with additions of Ag modify the age-hardening response which may result in enhanced mechanical properties. Son et al. (Son, et al., 2011) reported that the addition of Ag resulted in the formation of fine submicron-sized Mg–Ag particles, grain refinement, and weaker basal texture in the alloys, and the Ag-containing extruded alloys had better mechanical properties than the alloys without Ag.

Calcium is one of interesting additives for Mg-based alloys, which has distinct properties for improving the mechanical properties of these alloys. For examples, Ninomiya et al. (Ninomiya, et al., 1995) reported that Ca additions increased hardness at high temperature for the Mg-(3-9)Al (wt. %) alloys with the precipitation of the Mg_2Ca, laves_C14 and laves_C36 secondary phases. The addition of 0.1 to 1.0 wt. % Ca can improve the forming ability of Mg-9Li-2Zn (wt. %), while the ultimate tensile strength and yield strength can be raised by 28% and 25 %, respectively (Li, et al., 2006). While previously investigations of Mg-based alloys with added Ag and Ca have mainly addressed the effect of Ag and Ca additions on the microstructural variations and on hardness, sufficient data for Mg-(Zn, Sn)-based alloys with added Ag and Ca have not yet been reported.

Additions of microalloying elements such as Ag, Ca, Li, Na, Zn, Sr, In and rare-earth elements are widely used for improving the mechanical properties of Mg-based alloys (Mendis, et al., 2006; Sasaki, et al., 2006). In the case of In + Li additions, the increase in number density is closer to one order of magnitude and the hardening increment is about 150 % (270 % with Na) (Mendis, et al., 2006). A similar result has also been reported by Sasaki et al. (Sasaki, et al., 2006) for Na + Zn additions.

A systematic study of the Mg-(Zn, Sn)-X (X: Ag, Ca, In, Li, Na, Sr) system is necessary to design new Mg-based alloys. Thermodynamic modeling of the Ag-X (X: Ca, Li, and Zn) and the Ca-In systems was carried out as the part of the final thermodynamic database for the complete Mg-(Zn, Sn)-X (X: Ag, Ca, In, Li, Na, Sr) multi-component system.

9.2   Thermodynamic models

All the present optimizations have been carried out by means of the FactSage thermodynamic software (Bale, et al., 2002). The thermodynamic parameters of the pure elements were taken from the SGTE database (Dinsdale, 1991).

The liquid phase was modeled with the Modified Quasichemical Model in the Pair Approximation (MQMPA) (Pelton, et al., 2000), which is formulated to integrate the Bragg Williams random mixing model. This feature of the MQM provides great advantages for the construction of a multi-component database. A detailed description of the MQMPA and its associated notation is given by Pelton et al. (Pelton & Chartrand, 2001).

The Compound Energy Formalism (CEF) was introduced by Hillert (M. Hillert, 1998, 2001; M. Hillert & Jarl, 1978) to describe the Gibbs energy of solid phases with sub-lattices (long-range ordering), and ideal mixing on each sub-lattice is assumed. In the present work, all the solid solutions (hcp, tet, bcc, fcc, and the intermetallic compounds) in the binary systems were modeled with sub-lattice models, based on the crystal structures, using the CEF. The heat capacities of all the stoichiometric compounds were evaluated using the Neumann–Kopp rule (Kopp, 1865). Model description details have been given in previous chapters, and the same notations are used in the present chapter. All the phases considered in the present work are listed in Table 9.1.

Table 9.1 Phase structure information and thermodynamic models used in the present work

Phase	Pearson symbol	Strukturvricht designation	Space group	Prototype	Model[a]
Liquid	-	-	-	-	MQMPA
fcc	cF4	A1	$Fm\bar{3}m$	Cu	CEF
bcc_B2	cP2	B2	$Pm\bar{3}m$	CsCl	CEF
bcc_A2	cI2	A2	$Im\bar{3}m$	W	CEF
hcp	hP2	A3	$P6_3/mmc$	Mg	CEF
Ag_9Ca_2	-	-	-	-	ST
Ag_7Ca_2	hP18	-	$P6_3222$	-	ST
Ag_2Ca	oI12	-	$Imma$	-	ST
AgCa	oC8	Bf	$Cmcm$	CrB	ST
Ag_3Ca_5	tI32	D8l	$I4/mcm$	Cr_5B_3	ST
$AgCa_3$	-	-	-	-	ST
Li_2Ag	-	D83	$P\bar{4}3m$	Cu_9Al_4	CEF
Li_3Ag	-	-	-	-	CEF
Li_6Ag	-	-	-	-	CEF
AgZn	-	-	-	-	CEF
Ag_5Zn_8	cI52	D82	$I\bar{4}3m$	Cu_5Zn_8	CEF
Ca_3In	cF16	D0_3	$Fm\bar{3}m$	Bi_3F	ST
$CaIn_2$	hP6	-	$P6_3/mmc$	Ga_2Yb	ST
CaIn	cP2	B2	$Pm\bar{3}m$	CsCl	CEF

[a] MQMPA: Modified Quasichemical Model in Pairs Approximation; CEF: Compound Energy Formalism; ST: Stoichiometric compound

9.3   Critical evaluation and thermodynamic optimzation

9.3.1 The Ag-Ca system

Literature review

Phase equilibria in the Ag-Ca binary system was studied by Baar (Baar, 1911) by a thermal analysis method. Five compounds (Ag_4Ca, Ag_3Ca, Ag_2Ca, AgCa and $AgCa_2$) were reported (Baar, 1911). Alexander et al. (Alexander, et al., 1969) studied the whole composition range of

the Ag-Ca system by thermal analysis, X-ray diffraction, and metallographic analysis techniques. The presence of the compounds Ag_2Ca and $AgCa$, which were reported by Baar (Baar, 1911), was confirmed by Alexander et al. (Alexander, et al., 1969). Moreover, the compounds described as Ag_4Ca and Ag_3Ca (Baar, 1911) were found to be Ag_7Ca_2 and Ag_9Ca_2, respectively. Two definite new compounds Ag_3Ca_5 and $AgCa_3$, and a compound of uncertain stoichiometry containing 59 at. % Ca were also added to the Ag-Ca phase diagram by Alexander et al. (Alexander, et al., 1969). Due to the differing results of the previous work (Alexander, et al., 1969; Baar, 1911), Pascal et al. (Pascal, et al., 1970) re-investigated the phase equilibria of the Ag-Ca system for compositions lying in the range 50-100 at. % Ca by DTA and X-ray diffraction analysis techniques. Campbell et al. (Campbell, et al., 1970) investigated phase equilibria in the Ag-Ca system over the composition range 50-100 at. % Ca using differential thermal analysis and high temperature X-ray diffraction techniques. Their results are in a good agreement with the previous work of Pascal et al. (Pascal, et al., 1970), and the existence of Ag_3Ca_5, and $AgCa_3$ was confirmed. Pascal et al. (Pascal, et al., 1970) and Campbell et al. (Campbell, et al., 1970) pointed out that the uncertain compound of 59 at. % Ca reported by Alexander et al. (Alexander, et al., 1969) was not found in their work.

The activity of Ca in the liquid phase, the enthalpy of mixing, the Gibbs energy of mixing, and the entropy of mixing at 800 °C were reported by Delcet and Egan (J. Delcet & Egan, 1978) based on vapor pressure measurements. Fischbach (Fischbach, 1985) studied the activity of Ca in Ag-Ca liquid alloys by means of Knudsen effusion. Recently, Ivanov et al. (Ivanov, et al., 2009) measured the enthalpy of mixing of liquid Ag-Ca alloys at 1027 °C by isoperibolic calorimetry. The enthalpies of formation of compounds were determined by Notin and Hertz, and Notin et al. (Notin & Hertz, 1981; Notin, et al., 1995) from EMF measurements, and by Fischbach (Fischbach, 1985) by Knudsen effusion.

The Ag-Ca phase diagram was prepared by Baren (Baren, 1988) using the reported work in references (Alexander, et al., 1969; Baar, 1911; Campbell, et al., 1970; Pascal, et al., 1970). The accepted phase diagram of the Ag-Ca system is constituted by six intermetallic phases: Ag_3Ca_5, Ag_2Ca_9, Ag_2Ca_7, Ag_2Ca, $AgCa$ and $AgCa_3$, with Ag_2Ca_7 and $AgCa$ melting congruently. Huang et al. (Huang, et al., 2008) optimized this binary system using a Bragg-Williams model (Dinsdale, 1991) for the liquid phase. However, the optimized invariant reactions do not all correspond to the experimental data. For example, the peritectic reaction liquid + AgCa ↔

Ag$_9$Ca$_2$ was shown as a eutectic reaction liquid $\leftrightarrow$ Ag$_9$Ca$_2$ + AgCa in their work (Huang, et al., 2008).

Thermodynamic optimization results and discussions

The present calculated phase diagram of the Ag-Ca binary system with experimental data (Alexander, et al., 1969; Baar, 1911; Campbell, et al., 1970; Pascal, et al., 1970) is shown in Figure 9.1 and the calculated invariant temperatures are given in Table 9.1.
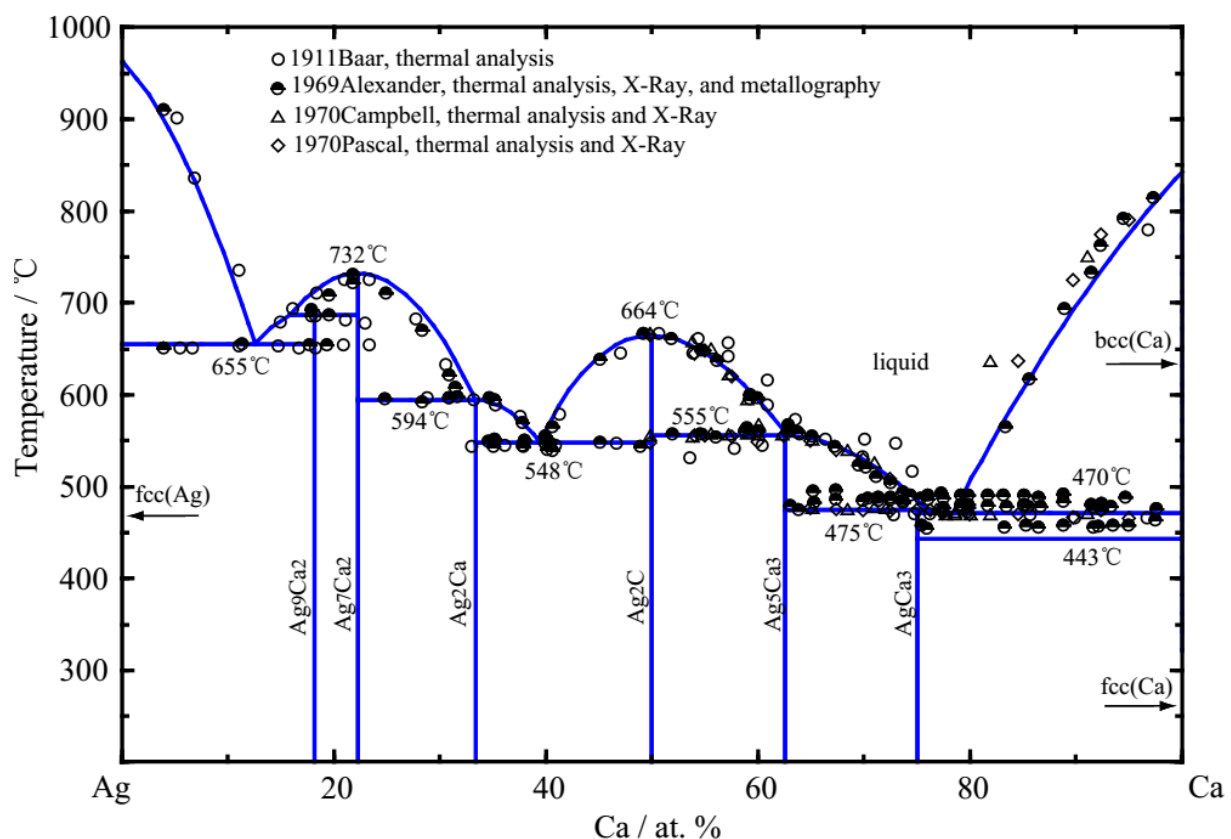
Figure 9.1 Calculated phase diagram of the Ag-Ca binary system with experimental data (Alexander, et al., 1969; Baar, 1911; Campbell, et al., 1970; Pascal, et al., 1970)

As shown in Figure 9.1, the experimental data from Baar (Baar, 1911) and Alexander et al . (Alexander, et al., 1969) are in a reasonable agreement in the composition range 0-50 at. % Ca. Alkali and alkaline-earth metallic elements are quite reactive toward moisture and oxgen, and

some (as for example Ca, Sr, Li and Na) are also reactive toward hydrogen. This increases difficulty of experimental measurement in these systems, especially in the alkali and alkaline-rich portions. In the Ag-Ca binary system, it can be seen that the experimental data are not consistent in the composition range 50-100 at. % Ca. This may due to the high reactivity of Ca with moisture and oxygen; experimental results would be affected by impurities from oxidation. All the calculated invariant reactions are listed in Table 9.1. As it can be seen, all calculated invariant reaction temperatures and congruent melting points are within 3 ^{o}C of the experimental data.

Table 9.2 Calculated invariant reactions of the Ag-Ca binary system in the present work compared with experimental data (Baren, 1988)

Reaction	Reaction type	Temperature, ^{o}C	Composition (Ca at. %)			Reference
$liquid \leftrightarrow fcc + Ag_9Ca_2$	Eutectic	655	14	0	18.2	Baren, 1988
		655	12.6	0	18.2	This work
$liquid + Ag_7Ca_2 \leftrightarrow Ag_9Ca_2$	Peritectic	687	18.2	22.2	18.2	Baren, 1988
		687	16.0	22.2	18.2	This work
$liquid \leftrightarrow Ag_7Ca_2$	Congruent point	731		22.2		Baren, 1988
		732		22.2		This work
$liquid + Ag_7Ca_2 \leftrightarrow Ag_2Ca$	Peritectic	597	33.3	22.2	33.2	Baren, 1988
		594	33.3	22.2	33.2	This work
$liquid \leftrightarrow Ag_2Ca + AgCa$	Eutectic	545	39.5	33.3	50	Baren, 1988
		548	39.4	33.3	50	This work
$liquid \leftrightarrow AgCa$	Congruent point	666		50		Baren, 1988
		664		50		This work
$liquid + AgCa \leftrightarrow Ag_3Ca_5$	Peritectic	555	62.5	50	62.5	Baren, 1988
		555	62.7	50	62.5	This work
$liquid + Ag_3Ca_5 \leftrightarrow AgCa_3$	Peritectic	475	75	62.5	75	Baren, 1988
		475	76	62.5	75	This work
$liquid \leftrightarrow AgCa_3 + bcc$	Eutectic	470	80	75	100	Baren, 1988
		470	78.4	75	100	This work
$bcc \leftrightarrow fcc$	Allotropic transformation	443		100		Baren, 1988
		443		100		This work

The calculated activity of Ca in the Ag-Ca liquid phase at 800 °C is shown in Figure 9.2 with experimental data from Delcet (Delcet & Egan, 1978) and Fischbach (Fischbach, 1985). The calculated enthalpy of mixing of liquid solutions at 1027 °C is shown in Figure 9.3 compared with experimental data (Ivanov, et al., 2009). The calculated enthalpy of formation of compounds at 557 °C are shown in Figure 9.4 with the experimental data from Notin and Hertz (Notin & Hertz, 1981). As can be seen, the calculated results are in a good agreement with reliable experimental data. The calculated entropy of mixing of the liquid phase at 1027 °C, compared with previously calculated results by Huang et al. (Huang, et al., 2008), is shown in Figure 9.5. The parameters of the thermodynamic models obtained in the present work are listed in Tables 9.2 and 9.3.
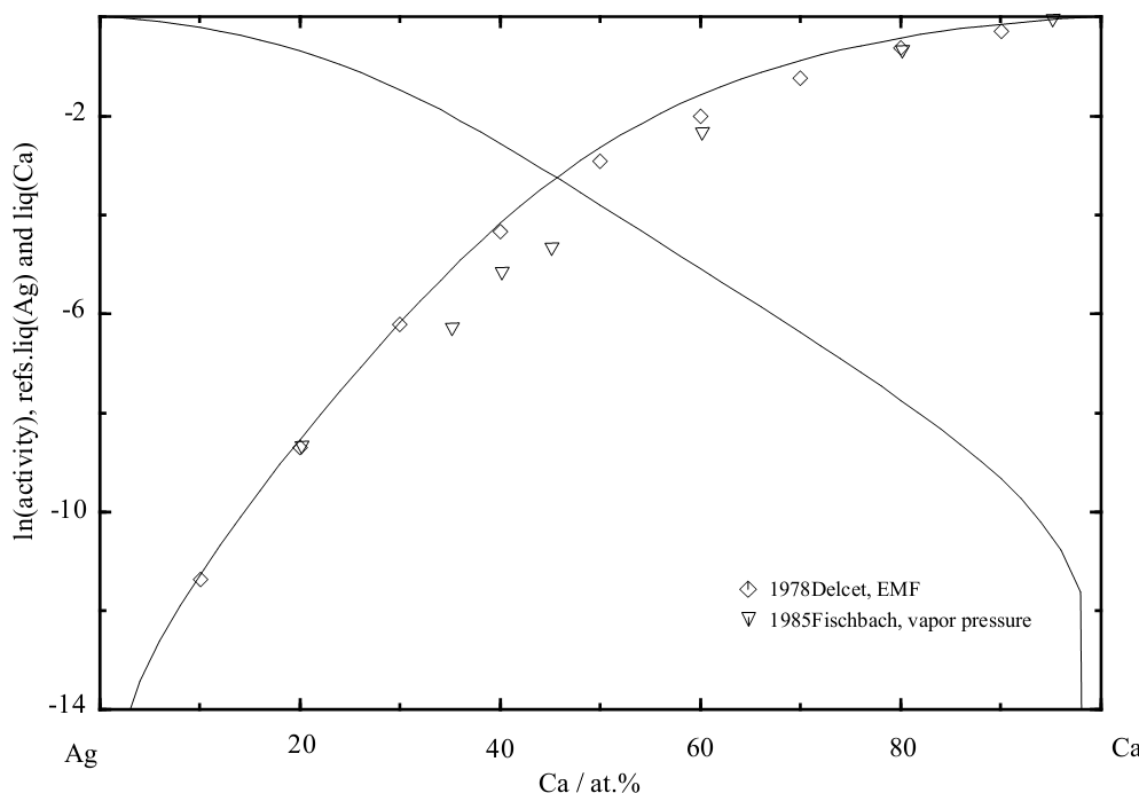
Figure 9.2 Calculated activity of Ca in Ag-Ca liquid solutions at 800 °C along with experimental data (Delcet & Egan, 1978; Fischbach, 1985). Reference states are pure liquids Ag and Ca
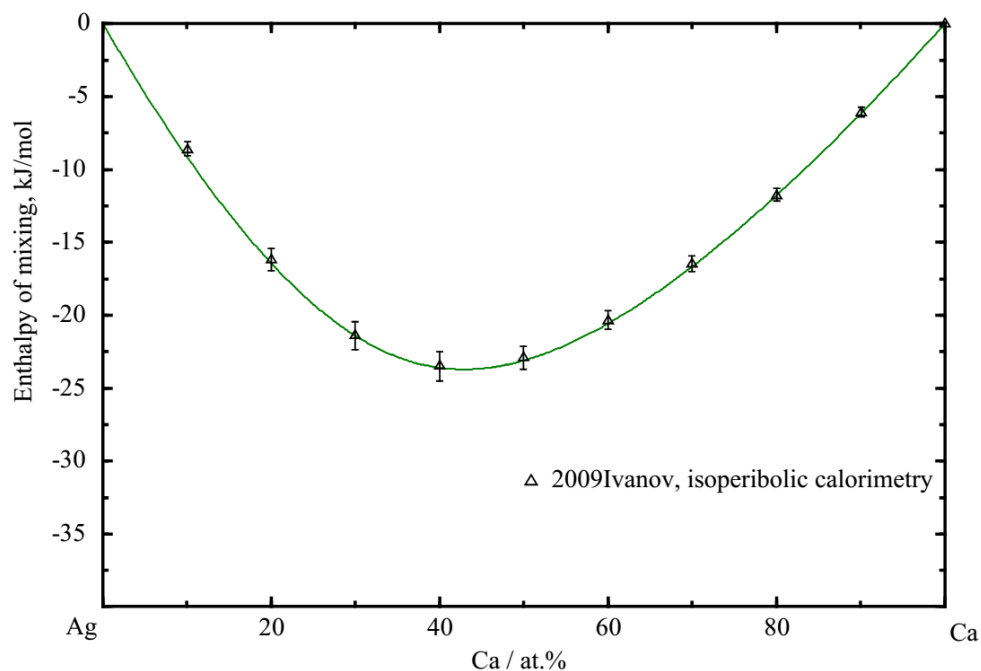
Figure 9.3 Calculated enthalpy of mixing of Ag-Ca liquid solutions at 1027 ^{o}C compared with experimental data (Ivanov, et al., 2009).
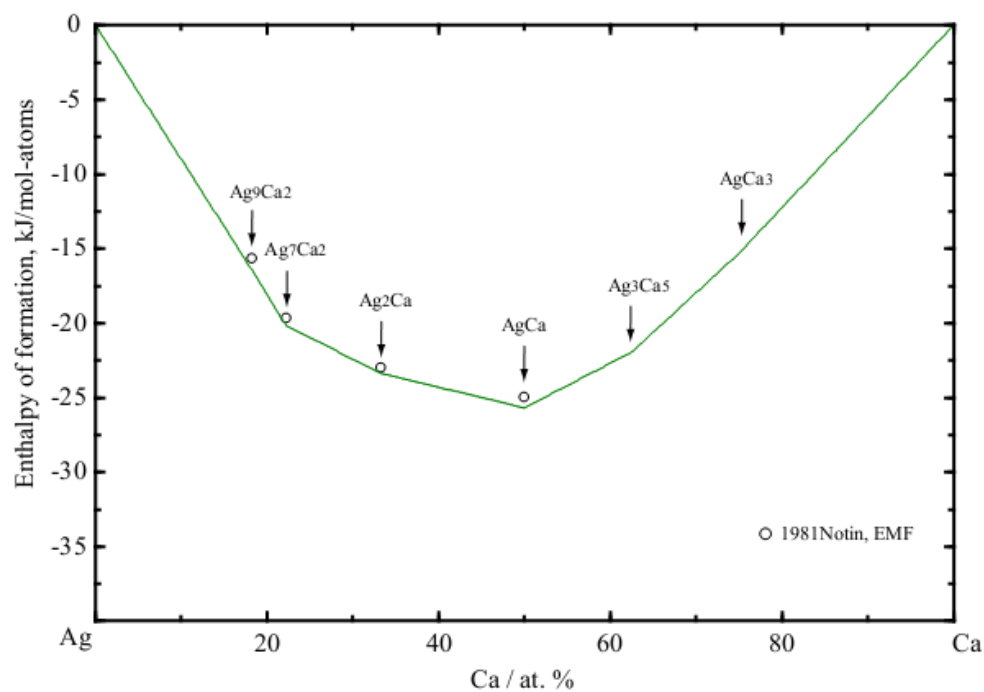
Figure 9.4 Calculated enthalpy of formation of compounds at 557 °C with experimental data (Notin & Hertz, 1981). Reference states are bcc(Ca) and fcc(Ag).
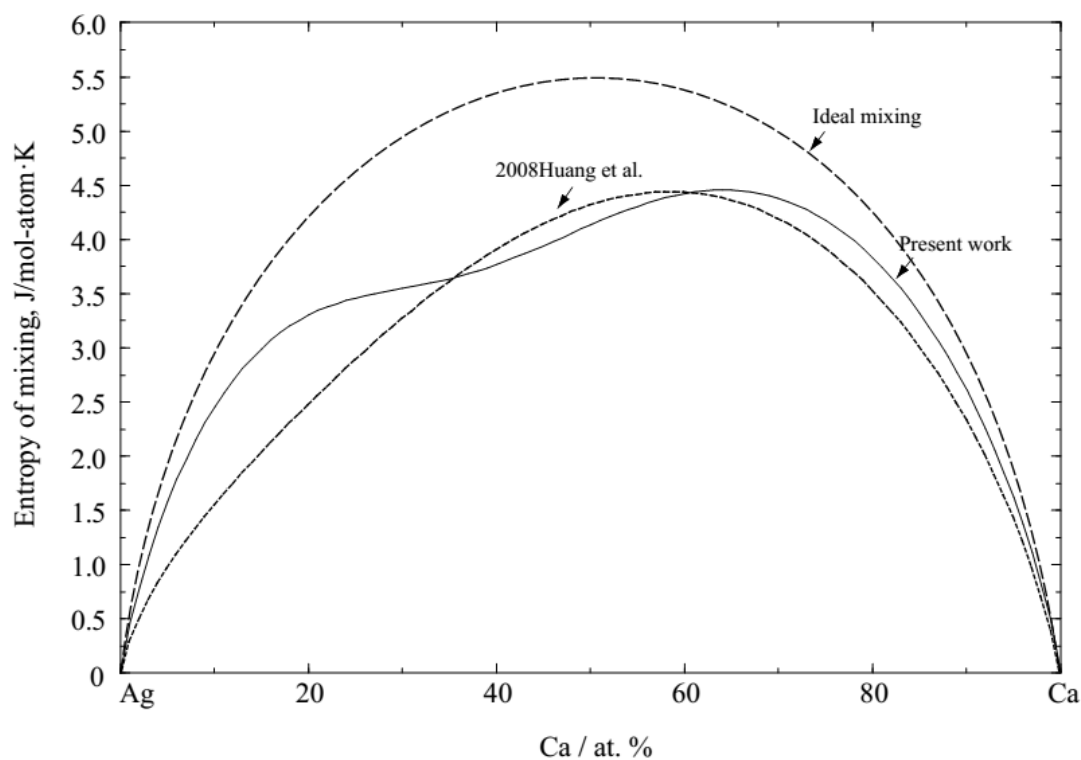
Figure 9.5 Calculated entropy of mixing of the Ag-Ca liquid phase at 1027 °C compared with the previously calculated results (Huang, et al., 2008)

Table 9.3 Optimized model parameters of the MQMPA for the liquid phase

Coordination numbers [a]				Gibbs energies of pair exchange reactions $(J \cdot mol^{-1}$, or $J \cdot mol^{-1} \cdot K^{-1})$
i	j	Z_{ij}^i	Z_{ij}^j	
Ag	Ca	4	6	$\Delta G = -24727.4 + 0.167 \times T - 3807.4 X_{AgAg} - 5020.8 X_{AgAg}^2 - 7447.5 X_{CaCa}$
Ag	Li	6	6	$\Delta G = -9706.9 - (2719.6 - 0.418 \times T) X_{AgAg} - (2238.4 - 0.418 \times T) X_{LiLi}^2$
Ag	Zn	6	6	$\Delta G = -5857.6 - 2510.4 X_{AgAg} - 209.2 X_{ZnZn}$
In	Ca	8	8	$\Delta G = -21756.8 - 2.218 \times T - (2217.5 - 3.012 \times T) X_{CaCa} - (3179.8 - 2.678 \times T) X_{Caca}^2 - (4443.4 + 0.837 \times T) X_{InIn}$

<div style="border:1px solid">

^{a} For all pure elements (Ag, Li, Ca, In and Zn), $Z_{ii}^{i} = 6$

</div>

Table 9.4 Optimized model parameters of the solid phases of Ag-X (X: Ca, Li, Zn) and Ca-In systems

Phase, model and thermodynamic parameters (J·mol^{-1}, or J· mol^{-1}·K^{-1})

fcc_A1 Phase, format $(Ag, Ca, In, Li, Zn)(Va)_3$

$G_{Ag:Va} = {}^{0}G_{Ag}^{fcc}$; $G_{In:Va} = {}^{*}G_{In} + 123 - 0.2988 \times T$; $G_{Li:Va} = {}^{*}G_{Li} - 108 + 1.3 \times T$; $G_{Zn:Va} = {}^{0}G_{Zn}^{hcp} + 2969.8 + 1.57 \times T$;

$G_{Ca:Va} = {}^{0}G_{Ca}^{fcc}$; ${}^{0}L_{Ag,Li:Va} = -34308.8 + 0.418 \times T$, ${}^{1}L_{Ag,Li:Va} = -5857.6 - 1.255 \times T$, ${}^{2}L_{Ag,Li:Va} = -6267$; ${}^{0}L_{Ag,Zn:Va} = -22593.6 - 0.481 \times T$;

bcc_A2 Phase, format $(Ag, Ca, In, Li, Zn)(Va)_3$

$G_{Ag:Va} = {}^{0}G_{Ag}^{fcc} + 3400 + 1.05 \times T$; $G_{Ca:Va} = {}^{0}G_{Ca}^{fcc} + 1405 + 2.25 \times T$; $G_{In:Va} = {}^{*}G_{In} + 800 - 0.8 \times T$; $G_{Li:Va} = {}^{*}G_{Li}$

$G_{Zn:Va} = {}^{0}G_{Zn}^{hcp} + 2886 - 2.5 \times T$; ${}^{0}L_{Ag,Zn:Va} = -28702.4 - 1.109 \times T$, ${}^{1}L_{Ag,Zn:Va} = 1673.6$;

${}^{0}L_{Ag,Li:Va} = -28409.4 + 2.552 \times T$; ${}^{1}L_{Ag,Li:Va} = -5355.5 - 1.464 \times T$, ${}^{2}L_{Ag,Li:Va} = 6108.6$; ${}^{0}L_{Ca,In:Va} = -4184$;

hcp_A3 Phase, format $(Ag, Ca, In, Li, Zn)(Va)_3$

$G_{Li:Va} = {}^{*}G_{Li} - 154 + 2 \times T$; $G_{In:Va} = {}^{*}G_{In} + 533 - 0.687 \times T$; $G_{Ag:Va} = {}^{0}G_{Ag}^{fcc} + 300 + 0.3 \times T$;

$G_{Zn:Va} = {}^{0}G_{Zn}^{hcp-Zn} + 2969 - 1.57 \times T$; $G_{Ca:Va} = {}^{0}G_{Ca}^{fcc} + 500 + 0.7 \times T$;

${}^{0}L_{Ag,Zn:Va} = -23012 + 2.301 \times T$, ${}^{1}L_{Ag,Zn:Va} = -24685 + 4.602 \times T$;

hcp_A3 (Zn) phase, format $(Ag, Ca, In, Li, Zn)(Va)_3$

$G_{Ag:Va} = {}^{0}G_{Ag}^{fcc} + 2000$; $G_{Ca:Va} = {}^{0}G_{Ca}^{fcc} + 2000$; $G_{Li:Va} = {}^{*}G_{Li} - 2 \times T$; $G_{In:Va} = {}^{*}G_{In} + 2000$; $G_{Zn:Va} = {}^{0}G_{Zn}^{hcp}$;

$L_{Ag,Zn:Va} = -16861.5 - 4.184 \times T$;

tet_A6 phase, format $(Ag, Ca, In, Li, Zn)(Va)_3$

$G_{Ag:Va} = {}^{0}G_{Ag}^{fcc} + 15000$; $G_{Ca:Va} = {}^{0}G_{Ca}^{fcc} + 15000$; $G_{In:Va} = {}^{*}G_{In}$; $G_{Li:Va} = {}^{*}G_{Li} + 15000$; $G_{Zn:Va} = {}^{0}G_{Zn}^{hcp} + 17505$

Ag_9Ca_2 phase, format $(Ag)_9(Ca)_2$: $G = 9 \times G_{Ag}^{fcc} + 2 \times G_{Ca}^{fcc} - 178920.9 + 0.197 * T$;

Ag_7Ca_2 phase, format $(Ag)_7(Ca)_2$: $G = 7 \times G_{Ag}^{fcc} + 2 \times G_{Ca}^{fcc} - 180109.9 + 5.023 * T$;

Ag_2Ca phase, format $(Ag)_2(Ca)$: $G = 2 \times G_{Ag}^{fcc} + G_{Ca}^{fcc} - 69360 + 0.621 * T$;

$AgCa$ phase, format $(Ag)(Ca)$: $G = G_{Ag}^{fcc} + G_{Ca}^{fcc} - 50571 + 0.33 * T$;

Ag_3Ca_5 phase, format $(Ag)_7(Ca)_2$: $G = 3 \times G_{Ag}^{fcc} + 5 \times G_{Ca}^{fcc} - 171400 + 6.901 * T$;

$AgCa_3$ phase, format $(Ag)(Ca)_3$: $G = G_{Ag}^{fcc} + 3 \times G_{Ca}^{fcc} - 58720 + 3.1 * T$;

Table 9.3 (continued) Optimized model parameters of the solid phases of Ag-X (X: Ca, Li, Zn) and Ca-In systems

Phase, model and thermodynamic parameters ($J \cdot mol^{-1}$, or $J \cdot mol^{-1} \cdot K^{-1}$)

Ca_3In phase, format $(In)(Ca)_3$: $G = {}^*G_{In} + 3 \times G_{Ca}^{fcc} - 104368.44$;

$CaIn_2$ phase, format $(In)(Ca)_3$: $G = 2 \times {}^*G_{In} + G_{Ca}^{fcc} - 128935.1 + 17.799 \times T$;

Li_2Ag phase, format $(Li, Ag)(Li)_2$: $G_{Li:Li} = 3 \times {}^*G_{Li} + 650$, $G_{Ag:Li} = G_{Ag}^{fcc} + 2 \times {}^*G_{Li} - 47488.4$;

Li_3Ag phase, format $(Li, Ag)(Li)_3$: $G_{Li:Li} = 4 \times {}^*G_{Li} + 520$, $G_{Ag:Li} = G_{Ag}^{fcc} + 3 \times {}^*G_{Li} - 48450.7$;

Li_6Ag phase, format $(Li, Ag)(Li)_6$: $G_{Li:Li} = 7 \times {}^*G_{Li} + 480$, $G_{Ag:Li} = G_{Ag}^{fcc} + 6 \times {}^*G_{Li} - 49162.0$;

$AgZn$ phase, format $(Ag, Zn)_2(Zn)$

$G_{Zn:Zn} = 3 \times G_{Zn}^{hcp\_Zn}$, $G_{Ag:Zn} = 2 \times G_{Ag}^{fcc} + G_{Zn}^{hcp\_Zn} - 21076.4 - 0.410 \times T$, ${}^0L_{Ag,Zn:Zn} = -32300.5$;

Ag_5Zn_8 phase, format $(Ag, Zn)_2(Ag)_2(Ag, Zn)_3(Ag, Zn)_6$

$G_{Ag:Ag:Ag:Ag} = 13 \times G_{Ag}^{fcc} + 239199.9 + 13.65 \times T$, $G_{Ag:Ag:Ag:Zn} = 7 \times G_{Ag}^{fcc} + 6 \times G_{Zn}^{hcp\_Zn} + 41116 - 7.65 \times T$,

$G_{Ag:Ag:Zn:Ag} = 10 \times G_{Ag}^{fcc} + 3 \times G_{Zn}^{hcp\_Zn} + 42658 + 3 \times T$, $G_{Ag:Ag:Zn:Zn} = 4 \times G_{Ag}^{fcc} + 9 \times G_{Zn}^{hcp\_Zn} + 39574 - 18.3 \times T$,

$G_{Zn:Ag:Ag:Ag} = 11 \times G_{Ag}^{fcc} + 2 \times G_{Zn}^{hcp\_Zn} + 43172 + 6.55 \times T$, $G_{Zn:Ag:Ag:Zn} = 5 \times G_{Ag}^{fcc} + 8 \times G_{Zn}^{hcp\_Zn} - 69783.84 - 54.456 \times T$,

$G_{Zn:Ag:Zn:Ag} = 8 \times G_{Ag}^{fcc} + 5 \times G_{Zn}^{hcp\_Zn} + 41630 - 4.1 \times T$, $G_{Zn:Ag:Zn:Zn} = 2 \times G_{Ag}^{fcc} + 11 \times G_{Zn}^{hcp\_Zn} - 10406.8 - 55.3156 \times T$

${}^0L_{Zn:Ag:Ag:Ag,Zn} = -71128 + 9.623 \times T$;

bcc_B2 phase, format $(Ag, Li, In, Ca)(Ag, In, Li, Ca)$

$G_{Ag:Ag} = G_{In:In} = G_{Li:Li} = G_{Ca:Ca} = 0$; $G_{Ag:Li} = G_{Li:Ag} = -14204.7 + 1.276 \times T$; $G_{Ca:In} = G_{In:Ca} = -178238.4 + 20.92 \times T$;

${}^0L_{Ag:Ag,Li} = {}^0L_{Ag,Li:Ag} = 15930.6 - 0.178 \times T$; ${}^0L_{Li:Ag,Li} = {}^0L_{Ag,Li:Li} = 7897.3 - 2.374 \times T$;

${}^1L_{Ag:Ag,Li} = {}^1L_{Ag,Li:Ag} = {}^1L_{Ag,Li:Li} = {}^1L_{Li:Ag,Li} = -1715.4 + 0.366 \times T$;

${}^0L_{In:Ca,In} = {}^0L_{In,Ca:Ca} = {}^0L_{Ca:In,Ca} = {}^0L_{Ca,In:Ca} = 2029$;

${}^*G_{In} = \int {}^*Cp_{In} dt - T \times \int \frac{{}^*Cp_{In}}{T} dt$, ${}^*G_{Li} = \int {}^*Cp_{Li} dt - T \times \int \frac{{}^*Cp_{Li}}{T} dt$

${}^*C_p(In) = 21.8386 + 0.01145132 \times T + 45812 \times T^{-2} + 1.2721926E-5 \times T^2$ 298K<T<429.78K

     $= 31.05 - 0.0001919 \times T - 312000 \times T^{-2} + 3.374E-8 \times T^2$ 429.79K<T<38000K

$$^{*}C_{p_{Li}} = 38.940488\text{-}0.070933862 \times T\text{-}319988 \times T^{-2} + 0.000119218896 \times T^2 \qquad 0\,K{<}T{<}454\,K$$

$$= 32.94\text{-}0.0002179 \times T\text{-}598200/T^{-2} + 4.656E\text{-}8 \times T^2 \qquad 455\,K{<}T{<}3000\,K$$

9.3.2 The Ag-Li system

Literature review

Pastorello (Pastorello, 1930) studied the phase equilibria in the Ag-Li binary system, and reported two stable compounds AgLi and AgLi$_3$. Later the phase equilibria of this system were more thoroughly studied by Freeth and Raynor (Freeth & Raynor, 1954). In the Freeth and Raynor work, alloys were melted in mild steel crucibles, and examined by chemical analysis. The techniques of thermal analysis, metallographic and X-ray diffraction analysis were used in phase equilibria measurements (Freeth & Raynor, 1954). Freeth and Raynor (Freeth & Raynor, 1954) did not find the two compounds AgLi and AgLi$_3$ reported by Pastorello (Pastorello, 1930). The assessed Ag-Li binary phase diagram containing seven phases (fcc, bcc, liquid, $\beta(bcc\_B2)$, γ_1 (Li$_2$Ag), γ_2 (Li$_3$Ag) and γ_3 (Li$_6$Ag)) was prepared by Pelton (Pelton, 1986) based on experimental results from Freeth and Raynor (Freeth & Raynor, 1954).

The enthalpy of mixing of the liquid phase at 977 ^{o}C and the enthalpy of formation of solid phases at 350 ^{o}C were measured by Predel et al. (Predel, et al., 1978) by solution calorimetry. The activity of Li in the liquid phase at 577 ^{o}C was reported by Becker et al. (Becker, et al., 1981) from EMF measurements.

Thermodynamic optimization

The calculated phase diagram of the Ag-Li binary system with experimental data of Freeth and Raynor (Freeth & Raynor, 1954) is shown in Figure 9.6. In the present work, the phase $\beta(bcc\_B2)$ was modeled with a two sub-lattice model as (Ag,Li)(Ag,Li) in its ordered bcc crystal structure. The calculated enthalpy of mixing of the liquid phase at 977 ^{o}C is shown in Figure 9. 7 compared with the experimental data from Predel et al. (Predel, et al., 1978).
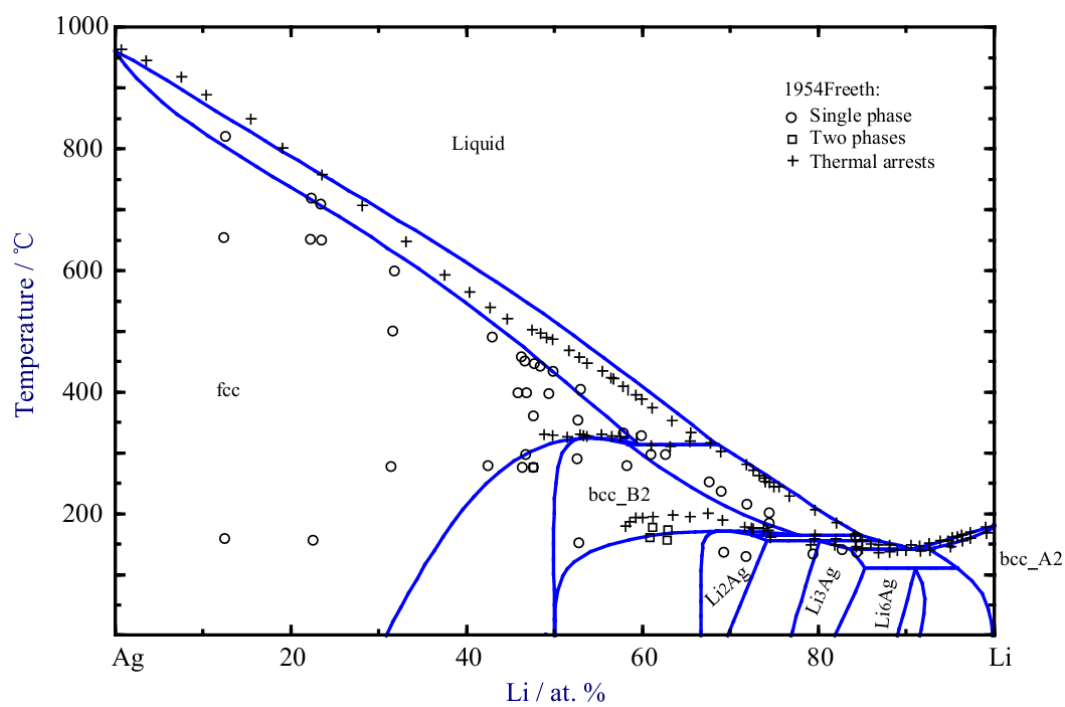
Figure 9.6 Calculated Ag-Li phase diagram with experimental data (Freeth & Raynor, 1954)
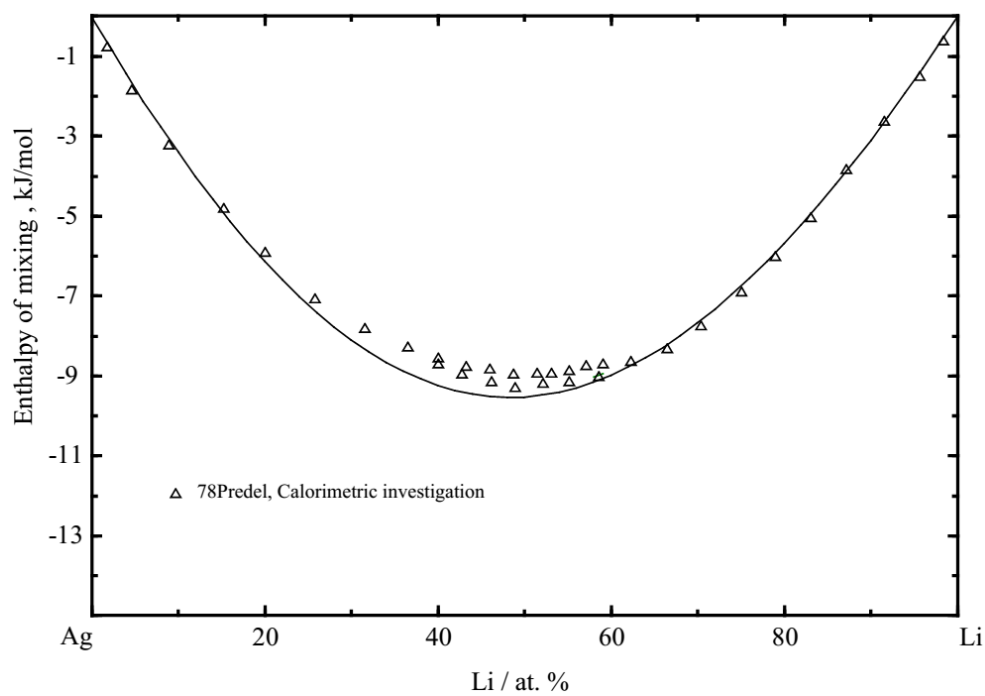
Figure 9.7 Calculated enthalpy of mixing of the liquid phase at 977 ℃ compared with experimental data (Predel, et al., 1978)

As shown in Figure 9. 6, the experimental data show that the minimum value of the enthalpy of mixing appears at around 50 at. % Li, which indicates a slight tendency to ordering in the liquid phase with maximum ordering near this composition. In the present work the coordination numbers of short-range ordering were given $Z_{AgLi}^{Ag} = 6$ and $Z_{AgLi}^{Li} = 6$ as shown in Table 9.2, fixing the composition of maximum SRO at 50 at. % Li. All the calculated invariant reaction temperatures in the Ag-Li binary system calculated in the present work are listed in Table 9.4. The calculated enthalpies of formation of solid phases (reference states. fcc (Ag) and liq (Li)) at 350 ^{o}C compared with experimental data (Predel, et al., 1978) are shown in Figure 9. 8. The calculated curve of the activity of Li in the liquid phase at 577 ^{o}C with experimental data is shown in Figure 9.9. The calculated results are in good agreement with the most reliable experimental data. The calculated entropy of mixing of the Ag-Li liquid phase at 1100 ^{o}C is shown in Fig. 9.10. The parameters of the thermodynamic models optimized in the present work are list in Tables 9. 2 and 9. 3.

Table 9.5 Calculated invariant reactions in the Ag-Li binary system compared with experimental data from Freeth (Freeth & Raynor, 1954)

Reaction	Reaction type	Temp. ^{o}C	Composition at. %			Reference
$liquid \leftrightarrow bcc\_A2 + Li_3Ag$	Eutectic	146	-	-	-	Freeth & Raynor, 1954
		143	90.6	92.5	83.6	This work
$bcc\_A2 + Li_3Ag \leftrightarrow Li_6Ag$	Peritectiod	-	-	-	-	Freeth & Raynor, 1954
		111	95.8	85.2	90.9	This work
$liquid + Li_2Ag \leftrightarrow Li_3Ag$	Peritectic	154	-	-	-	Freeth & Raynor, 1954
		156	86.8	74.1	80.1	This work
$bcc \leftrightarrow liquid + Li_2Ag$	Peritectic	164	-	-	-	Freeth & Raynor, 1954
		165	77.8	84.8	72.4	This work
$bcc \leftrightarrow Li_2Ag$	phase transformation	201	-	65.5	-	Freeth & Raynor, 1954
		171	-	68.7	-	This work
$fcc \leftrightarrow liquid + bcc\_B2$	Peritectic	-	-	-	60.8	Freeth & Raynor, 1954
		313	68.7	59.7	58.6	This work
$bcc\_B2 \leftrightarrow fcc$	phase transformation	330	-	-	-	Freeth & Raynor, 1954
		324	-	53.4	-	This work
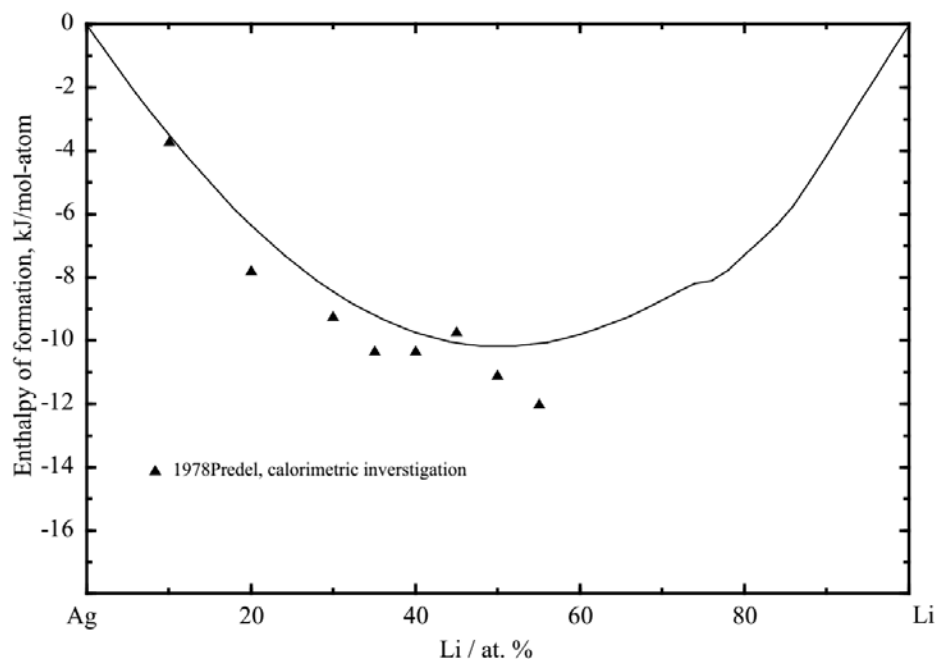
Figure 9.8 Calculated enthalpy of formation of solid phases at 350 ^{o}C compared with experimental data (Predel, et al., 1978)
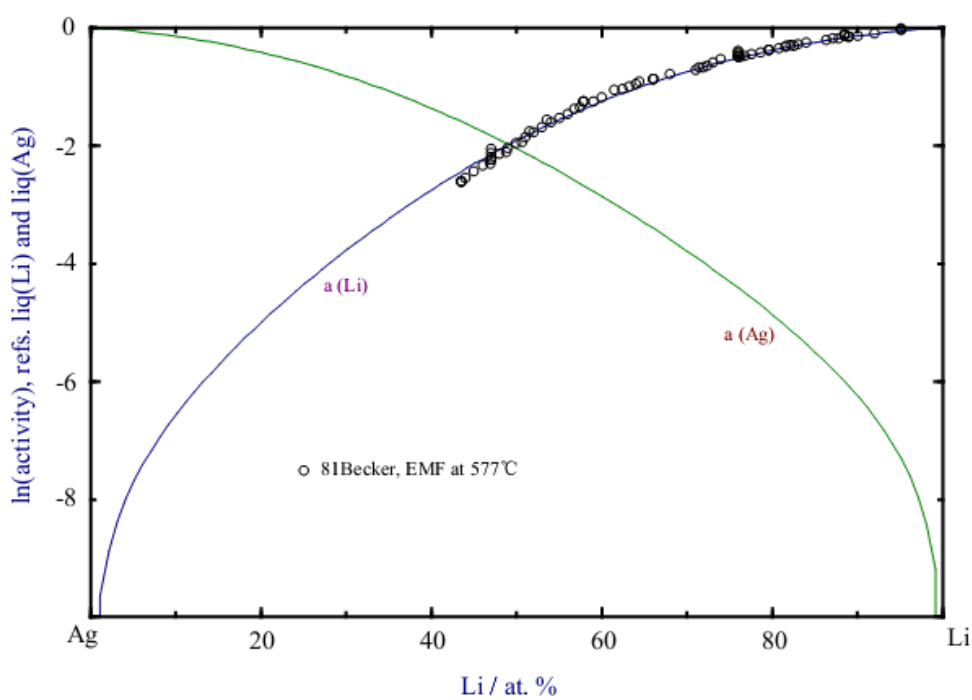
Figure 9.9 Calculated activity of Ag and Li in liquid solution at 577 ^{o}C compared with experimental data (Becker, et al., 1981)
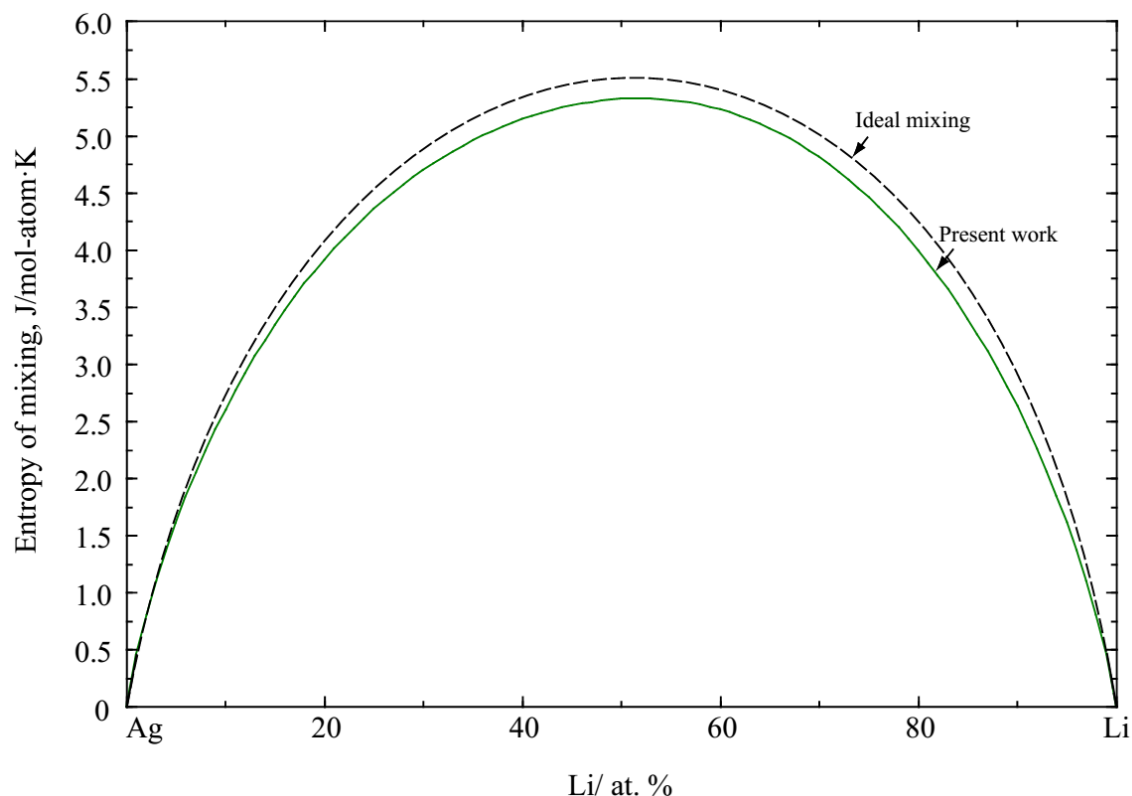
Figure 9.10 Calculated entropy of mixing of the Ag-Li liquid phase at 1100 $^{\circ}$C

9.3.3 The Ag-Zn system

Literature review

Heycock and Neville (Heycock & Neville, 1896) studied some freezing points of Ag-Zn alloys with a platinum resistance pyrometer method. Petrenko et al. (G. I. Petrenko, 1906; Petrenko & Petrenko, 1930) studied the phase equilibria and liquidus using thermal analysis and optical microscopy analysis techniques. The solid solubility of intermetallic phases was determined by Owen and Edmunds (Owen & Edmunds, 1935, 1938a, 1938b) by X-ray diffraction analysis. Andrews et al. (Andrews, et al., 1941) studied the phase equilibria of the Ag-Zn system over the whole composition range by thermal analysis, optical microscopy, and X-ray diffraction analysis. Hansen and Anderko (Hansen & Anderko, 1958) reviewed all experimental data on phase equilbira and thermodynamic properties of Ag-Zn binary system. The phase diagram of this

binary system is constituted by fcc (Ag), β(bcc_A2), γ(Ag$_5$Zn$_8$), ζ(AgZn), ε(hcp_A3) and hcp (Zn) phases.

Schneider and Schmid (Schneider & Schmid, 1942) derived the activity of Zn in solid and liquid phases at 677 ^{o}C from vapour pressures obtained from a dew point method. Kleppa and Thalmayer (Kleppa & Thalmayer, 1959), Yazawa and Gubcova (Yazawa & Gubcova, 1970), Gerling et al. (Gerling, Pool, & Predel, 1979), and Kameda (Kameda, 1987) obtained the thermodynamic properties of liquid Ag-Zn alloys from EMF measurements.

Birchenall and Cheng (Birchenall & Cheng, 1949), Underwood and Averbach (Underwood & Averbach, 1951), and Straalsund and Masson (Straalsund & Masson, 1968) studied the thermodynamic activity of zinc in solid phases by a dew point method. Scatchard and Westlund (Scatchard & Westlund, 1953) studied the activity of Zn in solid phases near the melting point and through the composition range 0-30 at. % Zn based on measurement of vapor pressures by absorption spectrophometry. Masson and Sheu (Masson & Sheu, 1970) measured the vapor pressure of Zn over moderately dilute solutions of the fcc phase by an isopiestic method. These reported activity values of Zn are in reasonable agreement, except those of Scatchard and Westlund (Scatchard & Westlund, 1953). The enthalpy of formation of the solid phases has been measured by Witting and Huber (Wittig & Huber, 1959), Hultgren et al.(Hultgren, Desai, Hawkins, Gleiser, & Kelley, 1973), Blair and Downie (Blair & Downie, 1970), and Orr and Rovel (Orr & Rovel, 1962) using calorimetry.

The phase diagram of the Ag-Zn binary system was optimized by the CALPHAD technique by Gomez-Acebo (Gomez-Acebo, 1998) using BMW for liquid phase.

Thermodynamic optimization

The calculated phase diagram of the Ag-Zn binary system is shown in Figure 9.11 with experimental data (Andrews, et al., 1941; Heycock & Neville, 1896; Owen & Edmunds, 1935, 1938a, 1938b; Petrenko, 1906; Petrenko & Petrenko, 1930). In the present work, the solid phase Ag$_5$Zn$_8$ was modeled with four sublattices: $(Ag,Zn)_2(Ag)_2(Ag,Zn)_3(Ag,Zn)_6$ according to its crystalline structure of $D8_2\_cI52\,(Cu_5Zn_8)$. The space group of the AgZn phase is $C\bar{3}$, and the unit cell contains nine atoms; three of the lattice positions are occupied almost exclusively by Zn atoms, and the remaining six lattice positions are occupied randomly by the remaining atoms.

Thus, the AgZn phase was modeled with a two-sublattice structure as $(Zn)(Ag,Zn)_2$ in the present work. As shown in Figure 9.11, both the invariant reactions and phase equilibria boundaries are well reproduced. All the calculated invariant reactions of the Ag-Zn binary system are listed in Table 9.6 compared with experimental data.

Table 9.6 Calculated invariant reactions of the Ag-Zn binary system compared with experimental data from Hansen and Anderko (Hansen & Anderko, 1958)

Reaction	Reaction type	Temp. ^{o}C	Composition at. %			Reference
$liquid + fcc \leftrightarrow bcc$	Peritectic	710	37.5	32.1	36.7	Hansen & Anderko 1958
		708	38.8	33.2	37.9	This work
$liquid + Ag_5Zn_8 \leftrightarrow hcp$	Peritectic	631	71	64.7	69.4	Hansen & Anderko 1958
		633	70.6	64.9	70.3	This work
$liquid + hcp \leftrightarrow hcp(Zn)$	Peritectic	431	98	89	95	Hansen & Anderko 1958
		430	97.8	86.8	96.3	This work
$liquid + bcc \leftrightarrow Ag_5Zn_8$	Peritectic	661	61.8	61	58.6	Hansen & Anderko 1958
		654	61.4	61.3	56.6	This work
$bcc \leftrightarrow fcc + AgZn$	Eutectoid	258	-	40.2	45.6	Hansen & Anderko 1958
		258	45.7	40.8	47.3	This work
$bcc + Ag_5Zn_8 \leftrightarrow AgZn$	Peritectoid	274	-	50.4	58.5	Hansen & Anderko 1958
		269	47.4	48.9	58.3	This work
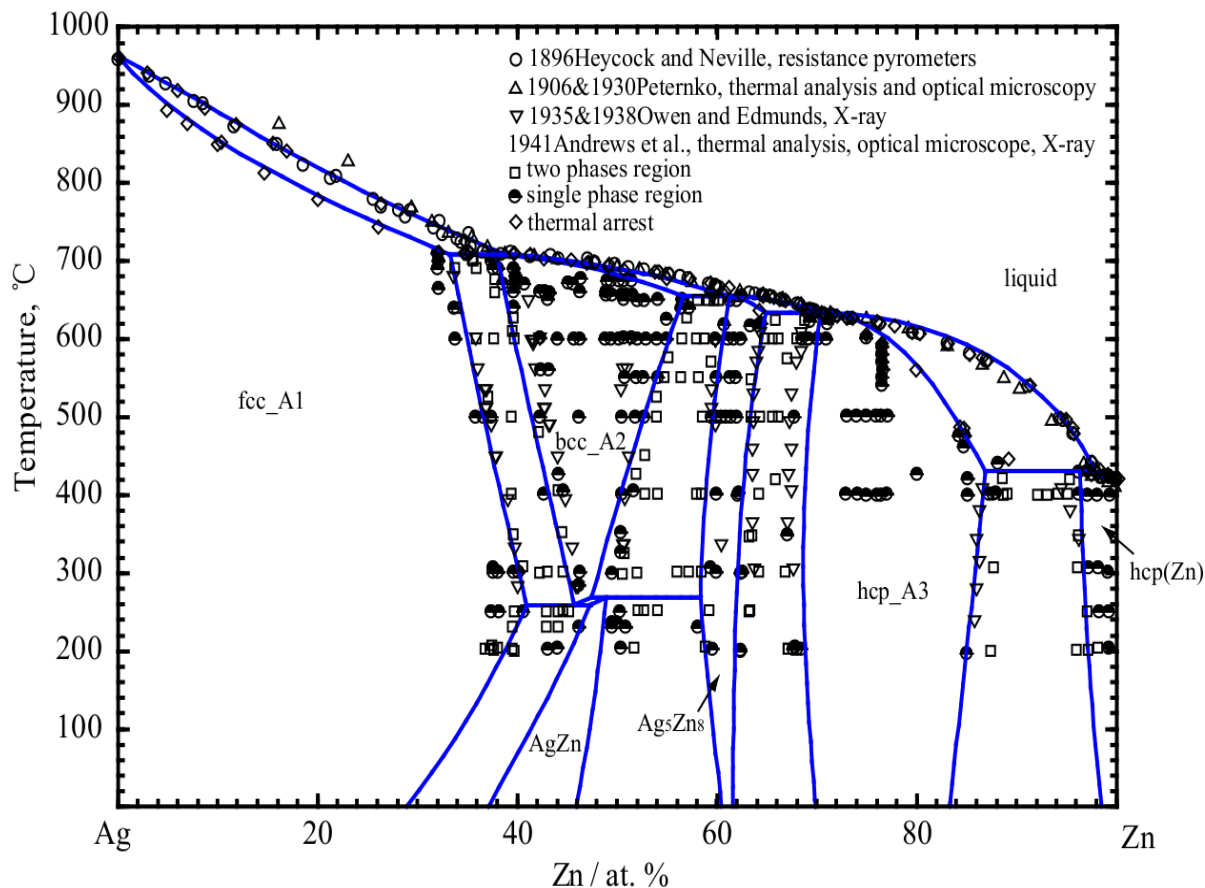
Figure 9.11 Calculated Ag-Zn phase diagram with experimental data (Andrews, et al., 1941; Heycock & Neville, 1896; Owen & Edmunds, 1935, 1938a, 1938b; Petrenko, 1906; Petrenko & Petrenko, 1930).

The calculated enthalpies of formation of solid phases at 350 ^{o}C are shown in Figure 9.12 compared with the reported experimental data (Blair & Downie, 1970; Hultgren, et al., 1973; Orr & Rovel, 1962). The calculated activities of Zn and Ag in the liquid solution at 677 ^{o}C and 800 ^{o}C are shown in Figure 9. 13 (a, b) along with experimental data (Birchenall & Cheng, 1949; Kameda, 1987; Masson & Sheu, 1970; Scatchard & Westlund, 1953; Schneider & Schmid, 1942; Yazawa & Gubcova, 1970). As shown in the Figure 9.13, the calculated results are in good agreement with the experimental data except the results from Scatchard and Westlund (Scatchard & Westlund, 1953), whose data differ markedly from the other reported data. The calculated entropy of mixing of the liquid phase at 1000 ^{o}C is shown in Figure 9.14. As can seen, the

previous calculated result from Gomez-Acebo (Gromez-Acebo, 1998) indicates a strong short range ordering behavior in the Ag-Zn solution. But according to the reported enthalpies of formation of Ag-Zn solid phases as shown in Figure 9.12, the Ag and Zn atoms would prefer to form ideal mixing rather than to form short range ordering pairs in liquid solution. The parameters of the thermodynamic models obtained in the present work are listed in Tables 9.2 and 9.3.
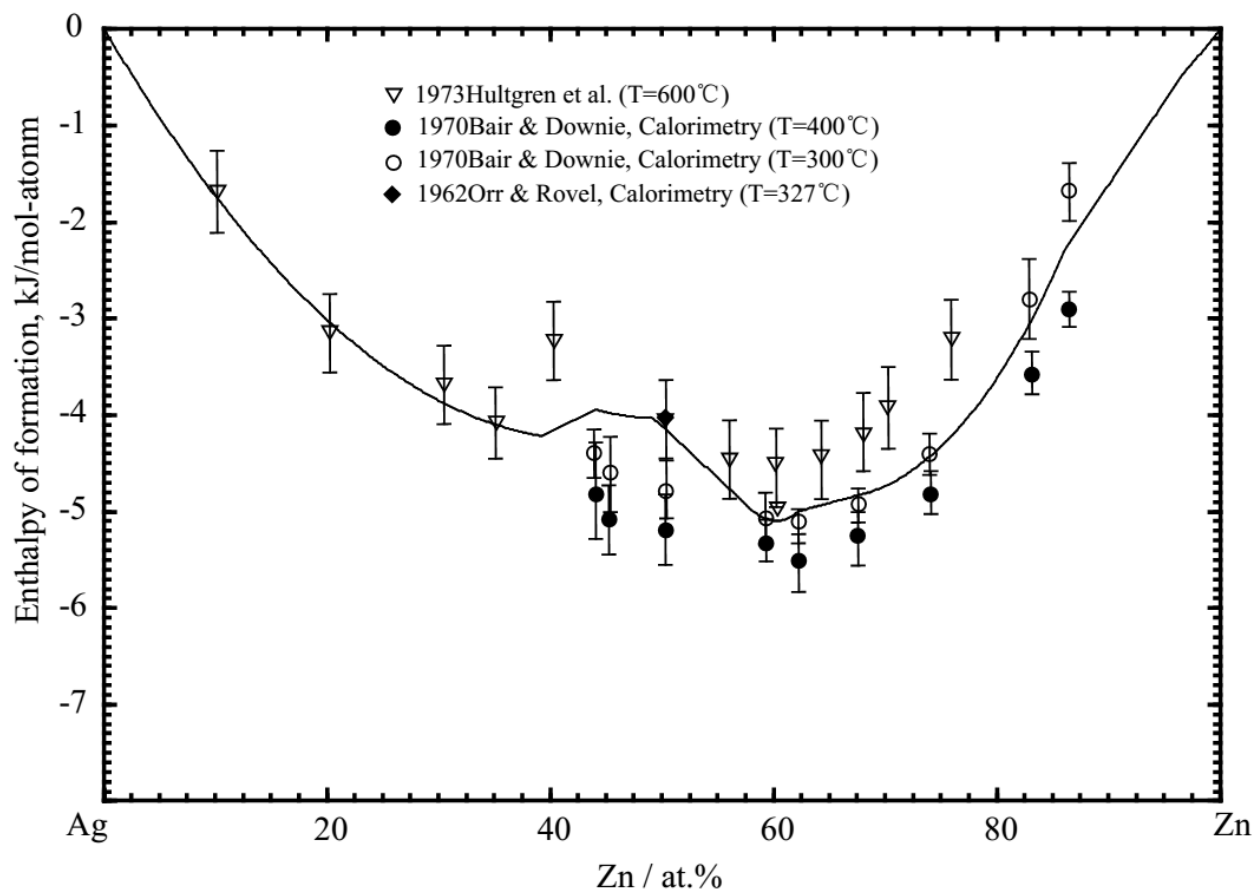
Figure 9.12 Calculated enthalpy of formation of solid phases at 350 $^{\circ}$C compared with the reported experimental data (Blair & Downie, 1970; Hultgren, et al., 1973; Orr & Rovel, 1962).
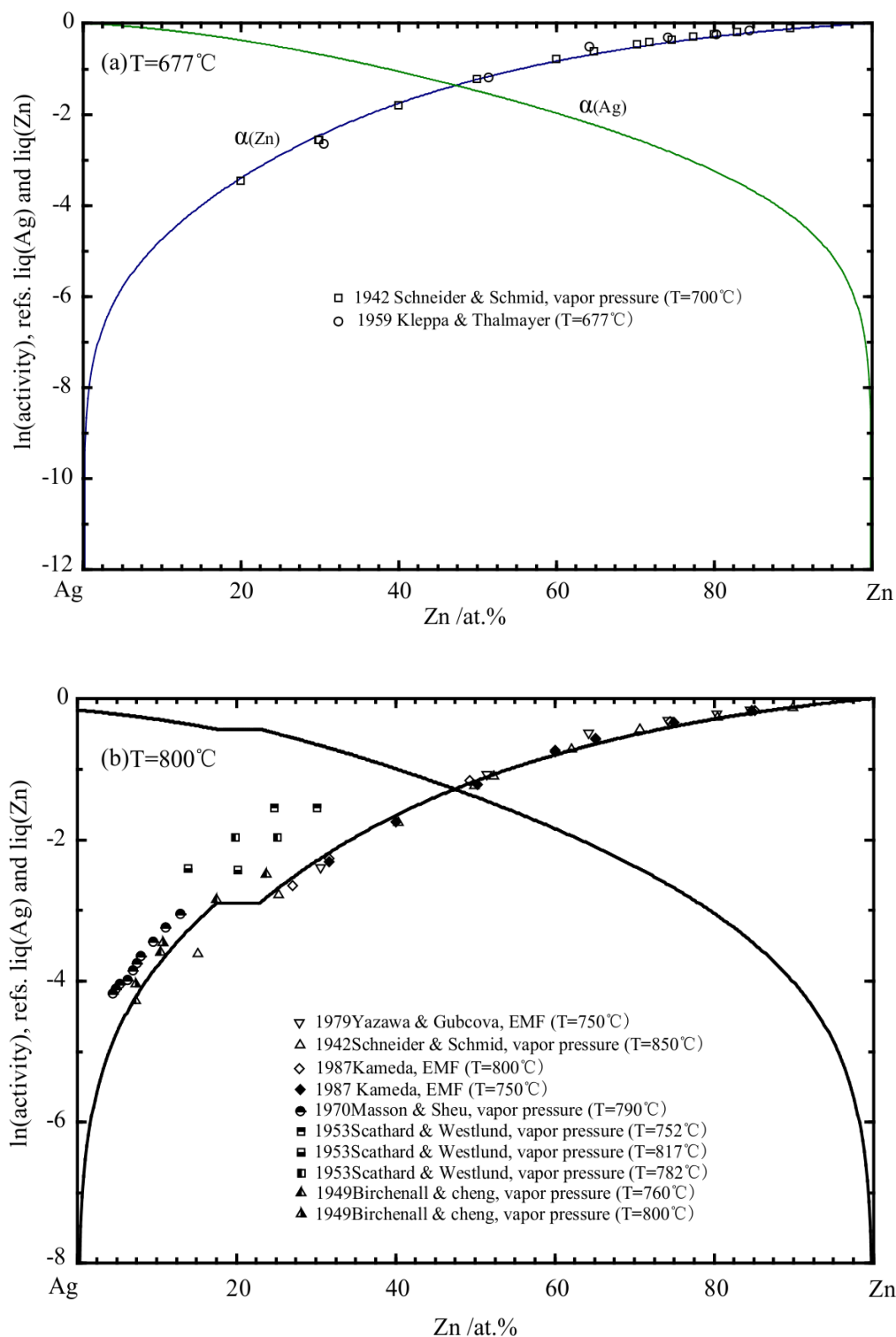
Figure 9.13 Calculated activity of Ag and Zn in the liquid solution at (a) 677°C and (b) 800°C along with experimental data (Birchenall & Cheng, 1949; Kameda, 1987; Masson & Sheu, 1970; Scatchard & Westlund, 1953; Schneider & Schmid, 1942; Yazawa & Gubcova, 1970)
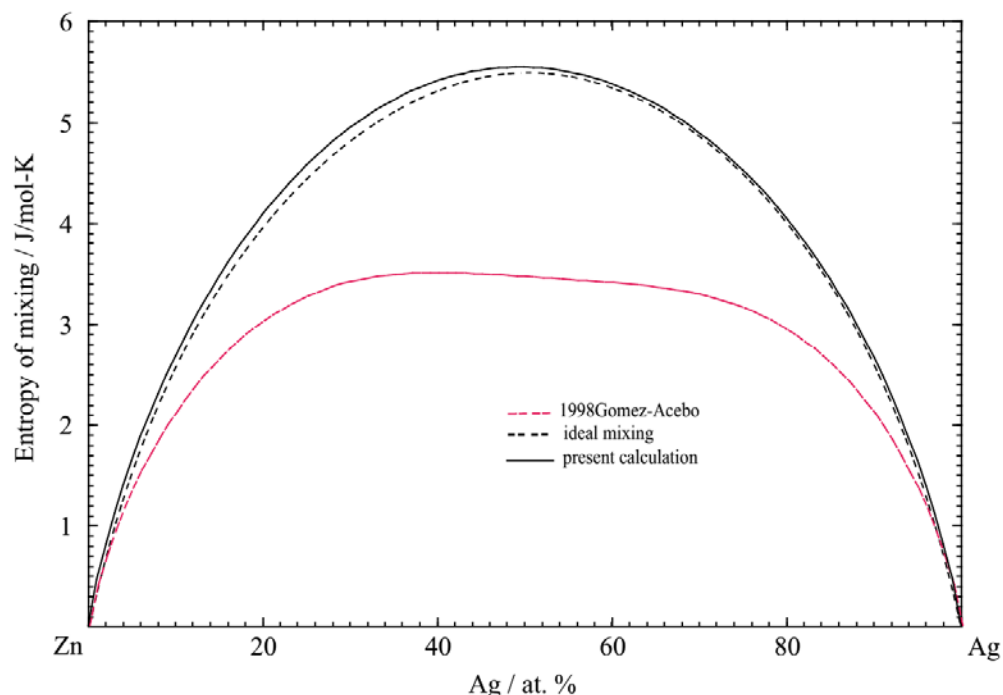
Figure 9.14 Calculated entropy of mixing of the Ag-Zn liquid phase at 1000 °C with the previously calculated result from Gomez-Acebo (Gromez-Acebo, 1998)

9.3.4 The Ca-In system

Literature review

The compound CaIn$_2$ was first identified by X-ray diffraction as reported by Landelli (Landelli, 1964). The phase equilibira in the Ca-In system was studied over the whole composition range by Bruzzone and Ruggiero (Bruzzone & Ruggiero, 1964) using X-ray diffraction, metallographic and thermal analysis methods. Three intermetallic phases (Ca_3In, $CaIn$, and $CaIn_2$) were found in this system, and congruent melting temperatures of Ca_3In, $CaIn$, and $CaIn_2$ were reported as 765 °C, 895 °C, and 835 °C respectively (G. Bruzzone & Ruggiero, 1964). No homogeneity solubility range was reported for the terminal solid solutions tet (In), fcc(Ca) and bcc(Ca) .

The thermodynamic properties of the liquid phase were determined by Delcet and Egan (J. Delcet & Egan, 1978) from EMF measurements with solid CaF$_2$ as electrolyte. The activity of Ca in the liquid phase, and the mixing free Gibbs energies of liquid solutions at 800 °C were derived by

Delcet and Egan (J. Delcet & Egan, 1978) from their EMF measurements. No experimental thermodynamic property data of solid phases was reported.

Thermodynamic optimization results

The calculated phase diagram is shown in Figure 9.15 compared with experimental data from Bruzzone and Ruggiero (Bruzzone & Ruggiero, 1964). The liquid was modeled using the Modified Quasichemical Model in the Pair Approximation (MQMPA), and the coordination numbers were fixed at $Z_{CaIn}^{Ca} = 6$ and $Z_{CaIn}^{In} = 6$ as shown in Table 9.2. All the calculated invariant reactions in the Ca-In binary system are listed in Table 9.7 compared with experimental data of Bruzzon and Ruggiero (Bruzzone & Ruggiero, 1964). The calculated Gibbs energy of mixing and the partial Gibbs energy of mixing of Ca in the liquid phase at 800 ^{o}C are shown in Figures 9.16 and 9.17 compared with the data derived by Delcet and Egan (Delcet & Egan, 1978). The calculated activity of Ca in the liquid phase at 800 ^{o}C with the experimental data (Delcet & Egan, 1978) are shown in Figure 9.18. The calculated entropy of mixing of the Ca-In liquid phase at 1000 ^{o}C is shown in Figure 9. 19, which shows strong short range ordering behavior in the liquid phase at 50 at. % Ca. All the calculated results are in a good agreement with the experimental data. The optimized parameters of the thermodynamic models of the present study are summarized in Tables 9.2 and 9.3.

Figure 9.15 Calculated phase diagram of the Ca-In system compared with experimental data of Bruzzone (Bruzzone & Ruggiero, 1964).

Table 9.7 Calculated invariant reactions in the Ca-In binary system compared with experimental data from Bruzzone (Bruzzone & Ruggiero, 1964)

Reaction	Reaction type	Temperature, °C	Composition at. %			reference
liquid ⟷ bcc_A2+Ca$_3$In	Eutectic	632	12.5	0	25	Bruzzone
		633	12.1	0	25	This work
liquid ⟷ Ca$_3$In+bcc_B2	Eutectic	660	35.5	25	50	Bruzzone
		661	35.1	25	50	This work
Continued to next page						

Table 9.7 (continued) Calculated invariant reactions in the Ca-In binary system compared with experimental data (Bruzzone & Ruggiero, 1964)

Reaction	Reaction type	Temp. °C	Composition at. %			reference
liquid ⟷ bcc_B2+CaIn₂	Eutectic	783	59	50	66.7	Bruzzone
		783	59.4	50	66.7	This work
liquid ⟷ bcc_B2+CaIn₂	Eutectic	156	100	66.7	100	Bruzzone
		155	99.4	66.7	100	This work
liquid ⟷ CaIn₂	Congruent	835	-	66.7	-	Bruzzone
		836		66.7		This work
liquid ⟷ Ca₃In	Congruent	765	-	25	-	Bruzzone
		763	-	25	-	This work
liquid ⟷ bcc_B2	Congruent	895	-	50	-	Bruzzone
		897	-	50	-	This work
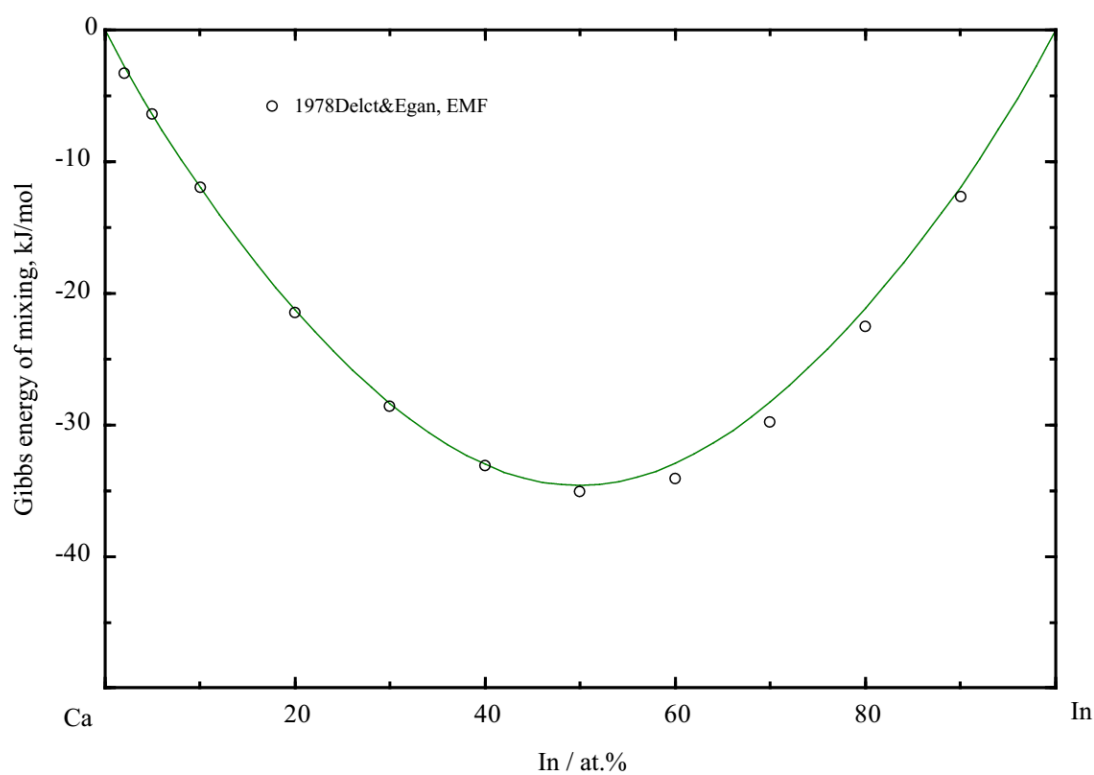
Figure 9.16 Calculated Gibbs energy of mixing of the liquid phase at 800 °C compared with reported data (Delcet & Egan, 1978)
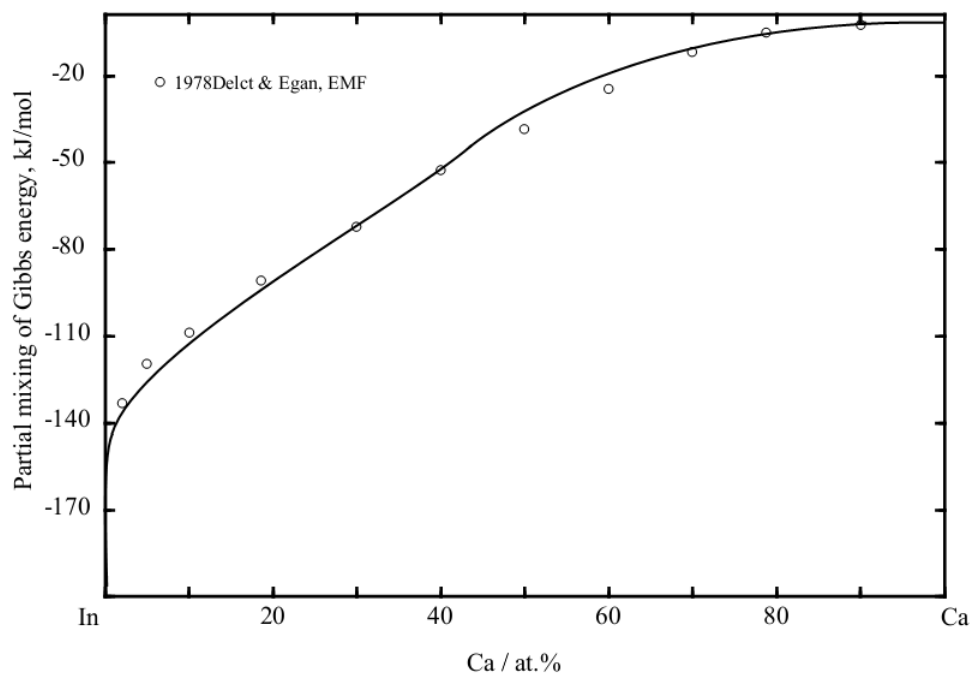
Figure 9.17 Calculated partial Gibbs energy of mixing of Ca in the liquid phase at 800 ^{o}C compared with reported data (Delcet & Egan, 1978)
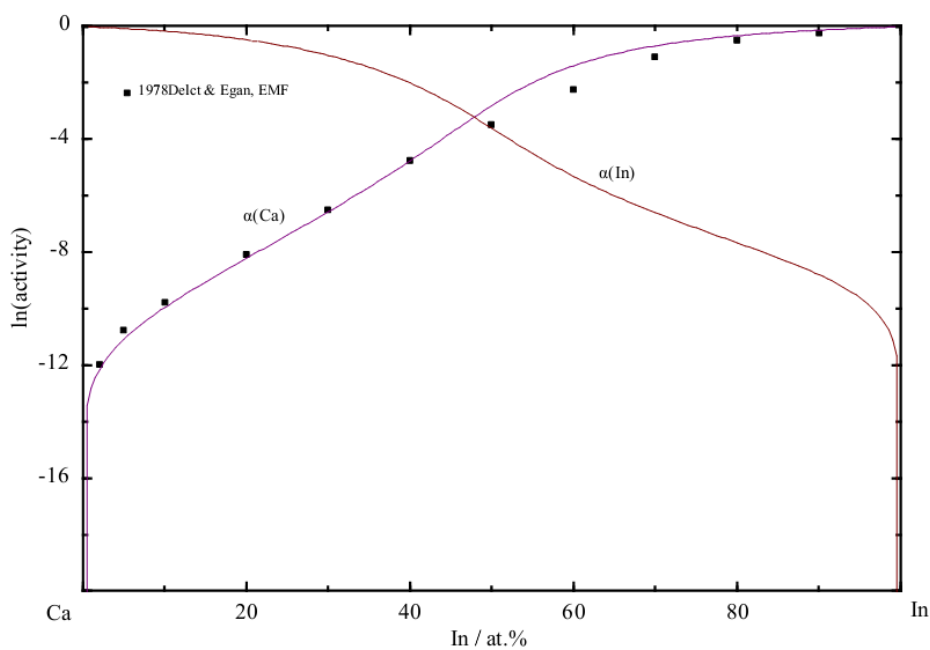
Figure 9.18 Calculated activity of Ca and In in the liquid phase at 800 ^{o}C compared reported data (Delcet & Egan, 1978)
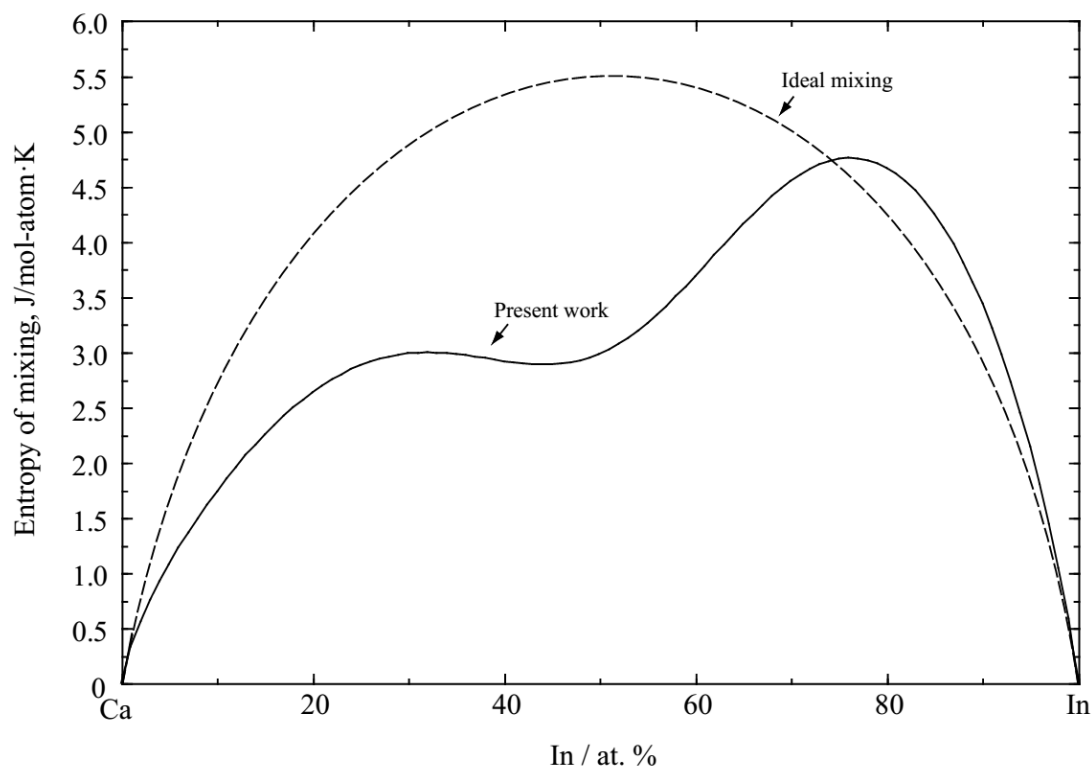
Figure 9.19 Calculated entropy of mixing of the Ca-In liquid phase at 1000 $^{\circ}$C

9.4   Conclusions

A critical evaluation and optimization of the Ag-X (X: Ca, Li, Zn) and Ca-In binary systems has been presented. The thermodynamic parameters of the Gibbs energy functions for all phases lead to reproduction, with good accuracy of the experimental data retained from critical evaluation. The thermodynamic database thus constituted is part of the project of developing a Mg-(Sn, Zn)-X (X: Ag, Ca, Li, In, Na, Sr) multi-component phase equilibrium model for design of Mg-based alloys.

CHAPITRE 10   GENERAL DISSCUSSION

This thermodynamic database of the Mg-Sn-Ag-Ca-In-Li-Na-Sr-Zn multi-component system has been constructed on the basis of all availavable experimental data. It is not yet completed as some binary and ternary systems are not fully evaluated: a complete analysis of the remaining sub-systems will be presented in the conclusion of this thesis, but the present calculations will not much be affected by these missing systems. Although it still requires further experimental and thermodynamic evaluation to complete the Mg-Sn-Ag-Ca-In-Li-Na-Sr-Zn multi-component database, it remains of great usefulness for the design of Mg-based alloys, especially for the Mg-Sn and Mg-Zn based alloys.

The final microstructure obtained at the end of the cooling process is very important for as-cast alloys investigation. The cooling process under local equilibrium conditions is quite complex. It is controlled by thermodynamic properties of the whole system, as well as solute diffusion in both liquid and solids. In order to simplify the cooling process and obtain an approximate results in convenient manner, time-consuming kinetic calculations were neglected in the cooling simulation process. There are two principle methods of equilibrium (lever-rule) and non-equilibrium (Scheil-Gulliver) (Gulliver, 1913; Scheil, 1942) are very often used for solidification simulations based on the thermodynamic aspect. The simulation processes of equilibrium (lever-rule) and non-equilibrium (Scheil-Gulliver) methods are given in Figure 10.1. During both sumilation processes, uniform solute distribution in the liquid solution is assumed (this is a reasonable approximation due to the large atomic mobility in the liquid solution). As for the solid phases, the uniform composition of the same solid phase is assumed in the lever-rule method, which is based on the assumption of infinite diffusion of solute. Actually, the solute diffusion, as substitutional solutes in the solid phases, is too slow to be neglected. Consequently, each infinitely small portion of the solids already formed during cooling is expected to retain the same composition thoroughout the whole solidification process. This is the basic assumption of the Scheil-Gulliver solidification simulation (Gulliver, 1913; Scheil, 1942) as shown in Figure 10.1. It is a simple but effective way to estimate with a rough kinetic approximation the as-cast microstructure from phase diagram (i.e. thermodynamic) information.

Within the FactSage^{TM} thermochemical software, the casting process can be simulated with both equilibrium or Scheil-Gulliver coolings (Gulliver, 1913; Scheil, 1942) and the annealing or

homogenization processes can be analyzed using multicomponent stable/metastable equilibrium and secondary phase precipitation calculations.
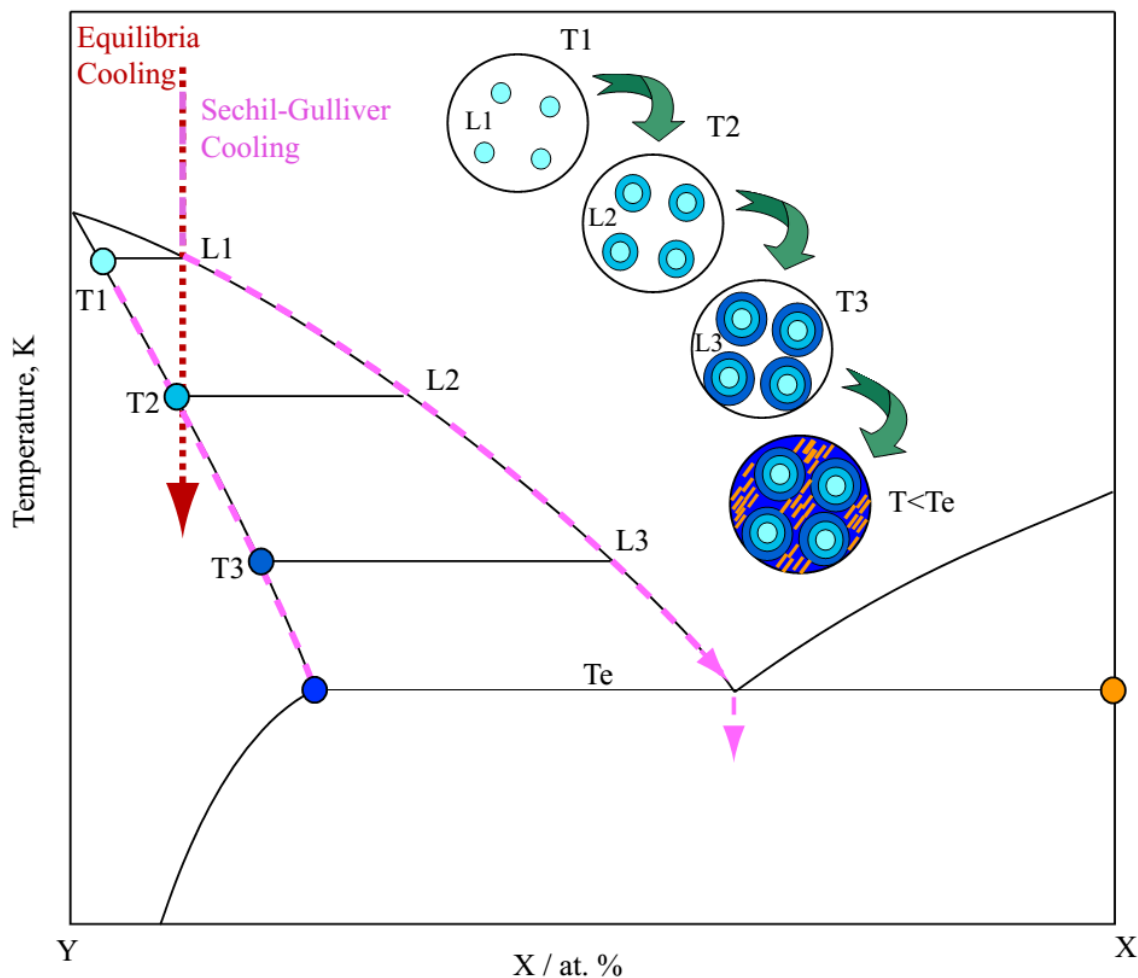
Figure 10.1 Simulation processes of equilibrium (lever-rule) and non-equilibrium (Scheil-Gulliver) methods applied to a simple hypothetical binary system

As mentioned in previous chapters, Mg alloys are widely used and have evident potential use as structural and sheet materials in the transportation applications. Due to shortcomings, as low creep resistance at high temperature, of the existing commercial alloys such as AZ91(Mg-9Al-1Zn), AM50 (Mg-5Al), AM60 (Mg-6Al) (wt. %), *etc*, the series of Mg-Sn based alloys has become of topical in interest the recent years. Mg-Sn based alloys maintain a stable microstructure and good mechanical properties at high temperatures due to the formation of the

thermally stable Mg$_2$Sn phase, which has the comparable or better creep resisitance properties than the AE42 alloy. However, Mg-Sn alloys require long aging times to reach their peak hardness. This is impractical for industrial applications (Van der Planken, 1969). Hence, it is necessary to improve these properties of Mg-Sn alloys. Microalloying potentially can achieve this goal with by means of alloying elements such as Ag, Ca, Li, Na, Zn, Sr, In, and rare-earth elements. In this section, the effect of Ag, Ca, Li, Na, Zn, Sr, and In on Mg-Sn based alloys was analyzed using thermodynamic calculations with the present database.

10.1 Design of wrought Mg-based alloys in the Mg-Sn-Li system

Typical fabrication processes of wrought Mg alloy products involves casting, solution treatment, rolling/extrusion, forming, and a final heat treatment. The secondary phases formed in dendrite (grain) boundary during the casting process should be dissolved back as much as possible into the Mg matrix during the solution treatment process. This minimizes defects and reduces deformation stress in the subsequent rolling/extrusion/forming process. Higher mechanical strengths of Mg-based alloys can be achieved with a more uniform distribution of fine precipitates in the Mg matrix during the final heat treatment process. In this way, Mg-Sn-Li can be a potential candidate for Mg alloy with high strength. As-cast microstructure can be estimated from Scheil-Gulliver cooling calculations (Gulliver, 1913; Scheil, 1942). The solution treatment and annealing processes can be approximated using equilibrium calculations applied to individual phases formed during the solidification path. Isothermal sections at 300, 400, 500 and 600 $^\mathrm{o}$C in the Mg-rich corner of the Mg-Sn-Li ternary system were calculated and are superimposed in Figure 10. 2.

According to Figure 10.2, Mg-Sn alloys containing about 0.5 wt.% Li can be solubilized at 500$^\mathrm{o}$C when Sn ≤ 3 wt. % and just above 500$^\mathrm{o}$C when 3 < Sn < 6 (wt. %). Then, if a Mg-Sn alloy containing 0.5 Li wt. % is annealed at about 300 or 400$^\mathrm{o}$C, most of the Li can be precipitated out as the Li$_2$MgSn ($cF16\_Fm\bar{3}m$) phase in the Mg matrix. There will also be some Mg$_2$Sn ($cF12\_Fm\bar{3}m$) for high Sn alloys (> 2 wt. %). Typically the precipitates formed during the thermomechanical process and final annealing can be finely distributed in Mg matrix phase, increasing the strength of the alloy. Of course, the precipitation strengthening is dependent on the (semi)coherency of the precipitates and the Mg matrix.
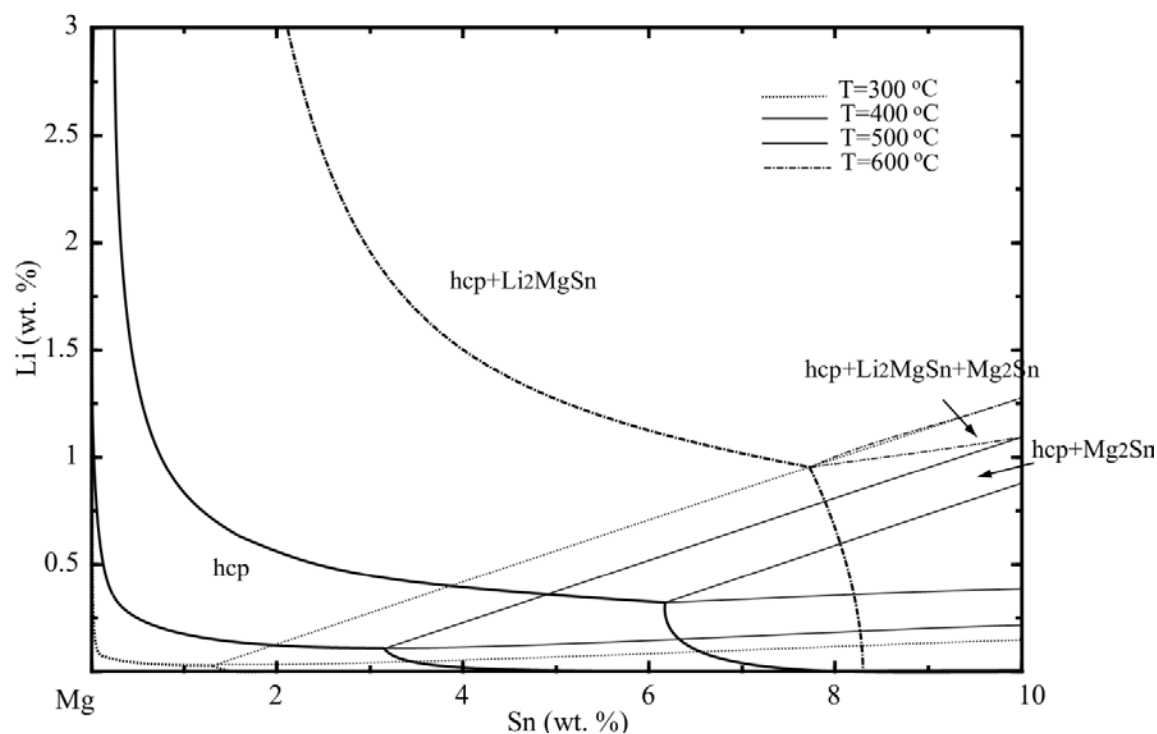
Figure 10.2 Calculated isothermal sections at $300\,^{\circ}$C, $400\,^{\circ}$C, $500\,^{\circ}$C and $600\,^{\circ}$C in the Mg-rich corner of the Mg-Sn-Li sysem

This is beyond the scope of the present study. The addition of Li at contents higher than 0.5 wt % in Mg-Sn alloys can be technically unrealistic due to the high tendency of oxidation of Li and difficulty in solubilization. The calculated liquidus projection in the Mg-rich corner of the Mg-Sn-Li system is shown in Figure 10.3.
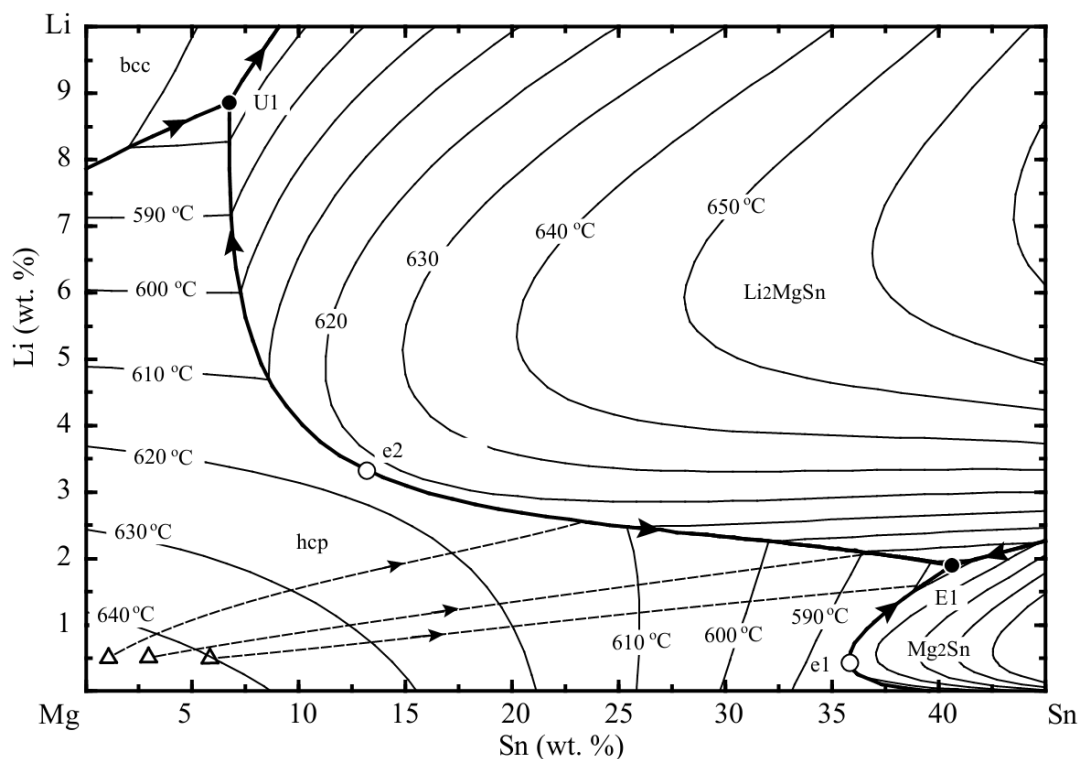
Figure 10.3 Calculated liquidus projection in Mg-rich corner of the Mg-Sn-Li system with the solidification trajectories of three Mg-Sn-Li alloys (Sn = 1, 3 and 6 wt. % with Li = 0.5 wt. %) calculated using the Scheil-Gulliver solidification method

The solidification trajectories of three Mg-Sn-Li alloys (Sn = 1, 3 and 6 wt. % with Li = 0.5 wt. %) calculated using the Scheil-Gulliver cooling (Gulliver, 1913; Scheil, 1942) method are also plotted in the figure. The amount of secondary phases formed during solidification of a 96.5Mg-3Sn-0.5Li (wt. %) alloy, calculated using the Scheil-Gulliver cooling (Gulliver, 1913; Scheil, 1942), is shown in Figure 10.4 (a). Figure 10.4 (b) shows the equilibrium calculation result of this same alloy. As can be seen in Figure 10.4(a), a small amount of the Li_2MgSn phase can form at the end of the solidification of 589 ^{o}C. The eutectic mixture of the Li_2MgSn and Mg_2Sn phases are formed at the end of the solidification at 576 ^{o}C. It is expected that all these second phases (total amount 0.8389 wt. %) can reside in the grain dendrite boundary. According to the equilibrium calculation for the same alloy, as shown in Figure 10.4(b), the alloy can be completely homogenized above 506°C (up to 570 ^{o}C). Then it can be thermomechanically processed at about 400 or 450 ^{o}C and annealed at ~300 ^{o}C. During the thermomechanical process,

partial precipitation can occur due to the large deformation energy; also, the rest of the precipitate can be formed in the final annealing process. The maximum amount of the precipitate (Li_2MgSn + Mg_2Sn) formed in this alloy would be about 4.0372 wt. % (~2.1 vol. %). The same procedure was performed for other alloys containing 1 and 6 % Sn and the results are summarized in Table 10.1. As shown in this Table, the maxium volume of precipitates can reach ~3.55 vol. % in the 96.5Mg-6Sn-0.5Li alloy, compared to ~2.86 vol. % for the 94Mg-6Sn alloy. With increasing Sn concentration, the Mg_2Sn phase can be formed during the solidification and also in the final annealing processes. According to the calculations, the Mg-Sn-0.5Li (wt. %) alloys with Sn up to 6 wt. % can be homogenized at 550 ^{o}C. Thus, a fine precipite formation is expected during the thermomechanical process. Final heat treatment will enhance Mg-Sn alloys strength by addition of Li.

Table 10.1 Calculated solidification and annealing data of selected Mg-0.5Li-xSn alloys

Alloys (wt. %)	Precipitate	Formation temperature upon cooling, (°C)	Amount of precipitates, (wt. %)					Total in matrix	Total in matrix, (Vol. %)[b]
			End of cooling	Annealing at 300°C					
				hcp#1	hcp#2	hcp#3	Total		
Mg-0.5Li-1Sn	Mg₂Sn	576	0.034	0 / 99.74 [a]	0 / 0.163 [a]	0.002 / 0.033 [a]	0.002	0.036	0.018
	Li₂MgSn	612	0.068	1.242 /99.738 [a]	0.015 / 0.163 [a]	0.002 / 0.033 [a]	1.260	1.328	0.689
Mg-0.5Li-3Sn	Mg₂Sn	576	0.598	0 / 98.016 [a]	0.016 / 0.349 [a]	0.049 / 0.795 [a]	0.065	0.663	0.330
	Li₂MgSn	589	0.241	3.068 /98.016 [a]	0.021 / 0.349 [a]	0.043 / 0.795 [a]	3.132	3.373	1.787
Mg-0.5Li-6Sn	Mg₂Sn	579	2.459	0 / 93.863 [a]	0.085 / 1.314 [a]	0.123 / 2.000 [a]	0.208	2.667	1.345
	Li₂Mgn	576	0.365	3.578/ 93.863 [a]	0.067 / 1.314 [a]	0.109 / 2.000 [a]	3.754	4.119	2.213

[a]amount of hcp phase; [b]From data of pure elements and compounds (Villars, & Cenzual, 2007)
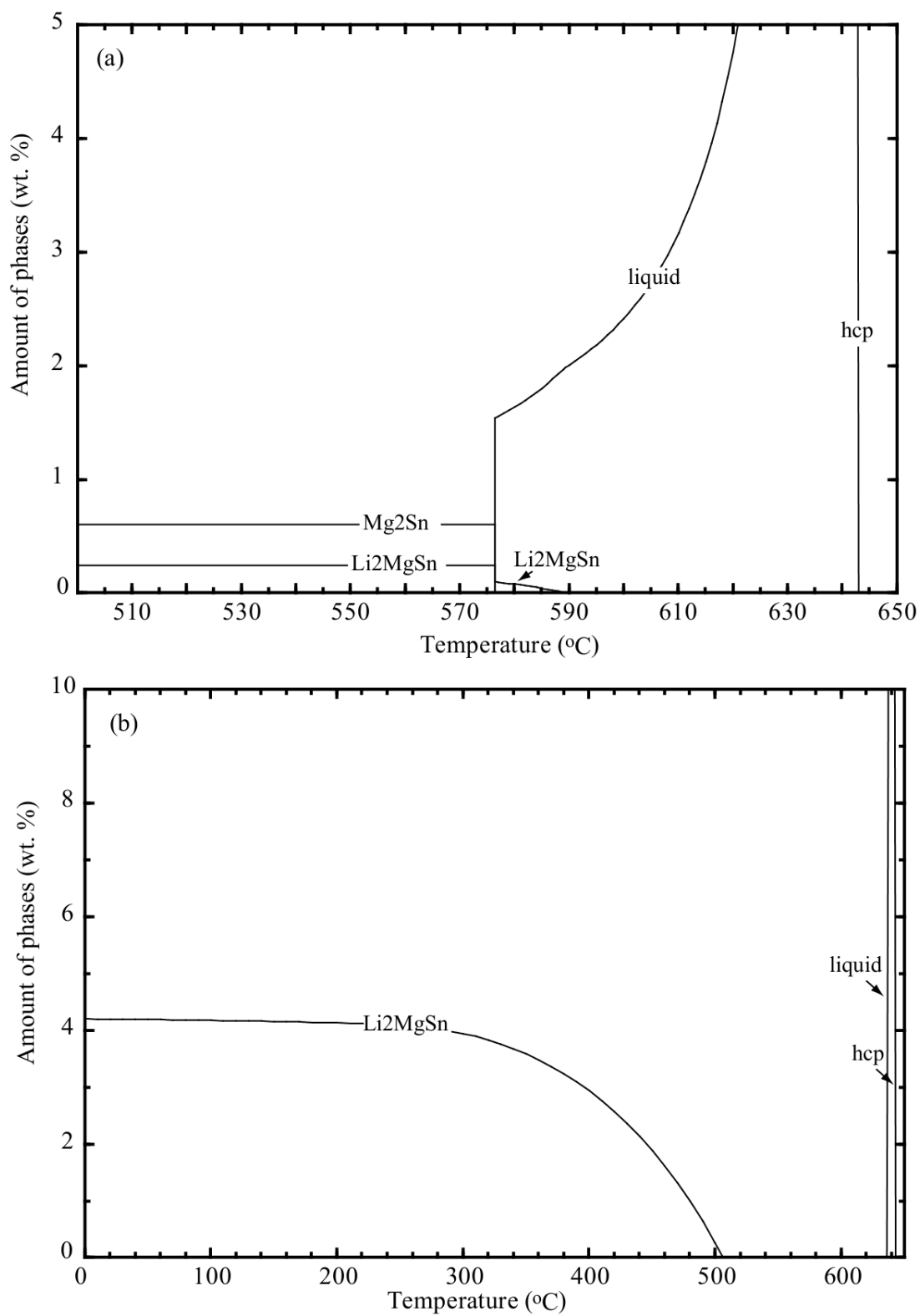
Figure 10.4 Calculated amounts of precipitates formed during solidification of a Mg-3Sn-0.5Li (wt. %) alloy using (a) Scheil-Gulliver solidification and (b) equilibrium calculations

10.2 The effect of In, Li, and Na on Mg-Sn based alloys

The hardness and microstructures of Mg-1.3Sn-0.13Na and Mg-2Sn-0.48Li-0.53In (at. %) alloys were studied by Mendis et al. (Mendis, et al., 2006) after an isothermal-ageing process, which showed superhardness in comparison with the Mg-Sn binary alloys as shown in Figure 10.5.
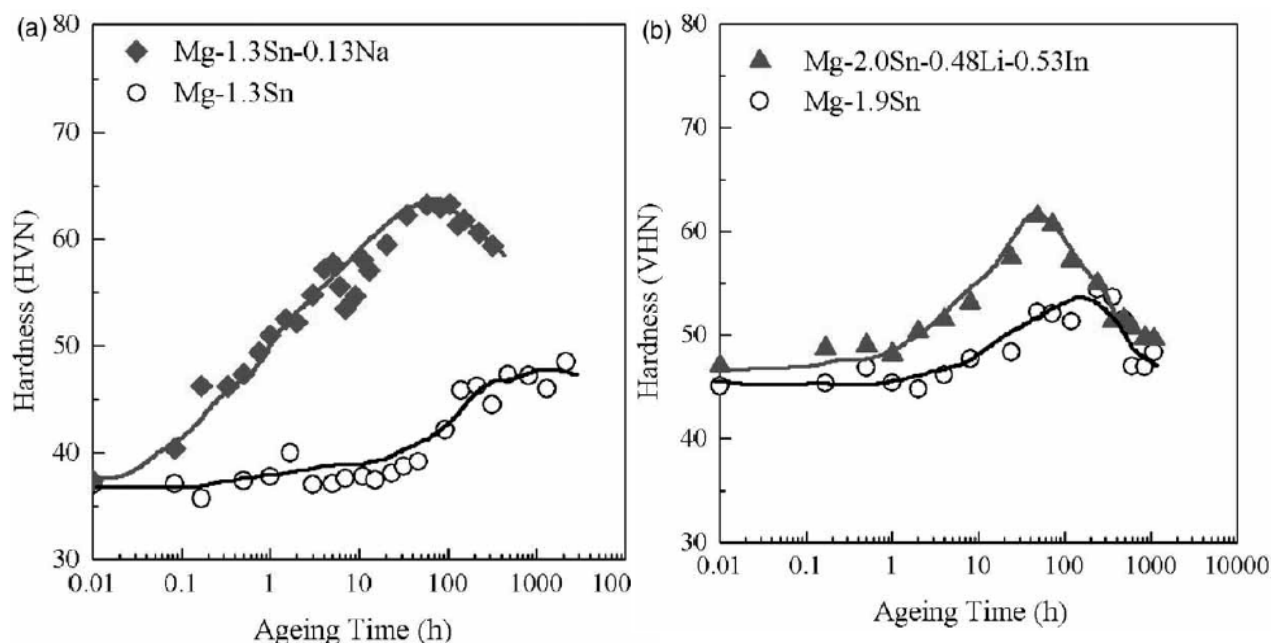
Figure 10.5 Measured room-temperature hardness as a function of the isothermal ageing time at 200 ^{o}C for (a) Mg-1.3Sn and Mg-1.3Sn-0.13Na and (b) Mg-1.9Sn and Mg-2.0Sn-0.48Li-0.53In (at. %) alloys. (Mendis, et al., 2006)

The calculated phase diagrams of (a) Mg-Sn (Jung, et al., 2007), (b) Mg-Na (Spencer, 2006), (c) Mg-Li (Spencer, 2006), and (d) Mg-In binary systems are shown in Figure 10.6. Sn, Li and In have large solid solubility limits in hcp (Mg) phase. In the Mg-Sn binary system, there is only one stable intermetallic phase, Mg_2Sn, with a melting temperature of 787 ^{o}C. The maximum solid solubility limit of Na in the hcp (Mg) phase is estimated at less than 0.5 at. % (Pelton, 1984).

The calculated Na-Sn phase diagram is shown in Figure 10.7. Intermediate phases in the Na-Sn binary system have very negative Gibbs energies of formation, and many intermetallic phases are formed (Chapter 4). Thus, it may be possible for Na to form Na_xSn_y binary compounds at

ambient temperature in a Mg-Sn alloy, as a tentative explanation for the hardness increase observed by Mendis et al. (Mendis, et al., 2006). The Scheil-Gulliver cooling simulation (Gulliver, 1913; Scheil, 1942) of the (a) Mg-1.3Sn and (b) Mg-1.3Sn-0.13Na alloys as calculated by the present thermodynamic database using the EQUILIB module of FactSage is shown in Figure 10.8. It is assumed here no ternary compound exists in the Mg-Sn-Na ternary system.

As shown in Figure 10.8 the final products at the end of the Scheil-Gulliver cooling process (Gulliver, 1913; Scheil, 1942) show small differences between the Mg-1.3Sn-0.13Na alloy and the Mg-1.3Sn (at. %) alloy. The developed database predicts that there are two extra precipitates (the bcc (Na) and the $Na_{15}Sn_4$ compound), in small proportion (~0.1 wt.%) at the end of the casting process with 0.13 Na additions. Although the amount of these extra precipitates is very small, they may have a large effect on the alloy. Precipitates of bcc(Na) obtained in the Scheil-Gulliver cooling process will be remelted during the ageing process (above 100 ^{o}C). This will speed up the diffusion of the elements reducing the time of phases to reach equilibria status. And also the high Na containing liquid phase will absorbe Sn to form Na-Sn binary compounds at the end of ageing following the quenching process. Thus, more secondary precipitates may be obtained around and inside of hcp grains which can result in better mechanical properties.

In order to evaluate the details of the heat treatment of Mendis et al. (Mendis, et al., 2006) (homogeneous at 500 ^{o}C for 6 h, and then ageing at 200 ^{o}C), calculated phase equilibrium data of the Mg-Sn-Na ternary system at 500 ^{o}C and 200 ^{o}C were obtained as listed in Table 10.2. According to the calculated equilibrium at 500 ^{o}C, the equilibrium phases of the Mg-1.3Sn-0.13Na (at. %) alloy are hcp(Mg) (99.937 wt. %) and liquid (0.063 wt. %). Consequently, the precipitates of Mg_2Sn, bcc (Na rich) and $Na_{15}Sn_4$ obtained at the end of casting process will be re-dissolved during the homogenization treatment at 500 ^{o}C. During the second heat treatment stage of ageing at 200 ^{o}C, Mg_2Sn will precipitate from the oversaturated hcp (Mg) matrix, for which the kinetics should be greatly improved by the presence of the small amount of liquid (Na-rich) phase (0.02769 wt. % at 200 ^{o}C). Being different from the ageing process of the Mg-1.3Sn alloy (Na-free), the appearance of a liquid (Na-rich) phase in the annealing process shall be the main effect to improve the precipitation of Mg_2Sn and its resulting positive impact on the room-temperature hardness (of course no liquid will be present at room temperature). It should be noted however that benefits obtained in harndness at ambient temperature with Na additions may cause

material failure at high temperatures (above the melting point of Na, 97.8 ^{o}C) in working conditions due to the formation of liquid Na phase.

Table 10.2 Calculated phase equilibrium data of the Mg-1.3Sn-0.13Na (at. %) alloy at 500 ^{o}C and 200 ^{o}C

Equilibrated phases	500 ^{o}C				200 ^{o}C			
	Total amount, (wt.%)	Composition, (wt. %)			Total amount, (wt.%)	Composition, (wt. %)		
		Mg	Sn	Na		Mg	Sn	Na
hcp	99.937	93.895	6.043	0.062	94.084	97.945	2.047	0.008
liquid	0.063	4.224	8.036	87.739	0.113	1.024	2.063	96.912
Mg$_2$Sn	0	-	-	-	5.803	66.667	33.333	0

Two contradictory results can be seen from the previous analysis: 1) For good ageing results in Mg-Sn based alloys, a very small amount of liquid (Na-rich) phase at ageing temperatures usually (150-250 ^{o}C,) should be present in order to improve the diffusion of solutes into the hcp phase and to reach near equilibrium conditions more quickly (usually a homogenisation time of 1 h-10 h is not enough for the alloy to reach the near equilibrium state at 500 ^{o}C if there is no liquid phase present); and 2) the appearance of a liquid phase in alloys should be prevented under their working temperature (25-150 ^{o}C). These two results seem incompatible from a thermodynamic point of view. However, as-cast alloys, simulated by a Scheil-Gulliver cooling process (Gulliver, 1913; Scheil, 1942), are in a metastable state, while the ageing process is the equilibrium path. Hence, one can design an alloy with a small amount of liquid phase resulting from the solidification process, which will slowly disappear, but still be temporarily present, during the beginning of the ageing process. To illustrate this result, Fig. 10.8 shows that at 580°C, a small amount of liquid phase is present after solidification (from a Scheil Gulliver calculation), and is not stable under annealing conditions (equilibrium) at the same temperature. However, the

presence of this liquid phase at the initial state of the ageing process may lead to improved kinetics of ageing. The objective is now to fine-tune the amont of Na added to Mg-Sn alloys in order, 1) to obtain a small amount of liquid (Na-rich) at 150°C from a Scheil-Gulliver calculation (simulating the as-cast microstructure), and 2) no liquid resulting from the full equilibrium calculation at the same temperature. The modification of the total amount of Na in Mg-Sn alloys is very important. The calculated amount of liquid phase with the addition of Na in Mg-6Sn and Mg-3Sn alloys at 150, 200 and 350 $^{\circ}$C are shown in Figure 10.9. As shown in this Figure, the calculated optimal composition ranges for Na additions are 0.8-4.2 ppm for Mg-3Sn, and 2.5 to 4.2 ppm for Mg-6Sn. The resulting amounts of liquid are very low (a few 10^{-6} g/g) and is clearly impractical. This approach is therefore not promising.
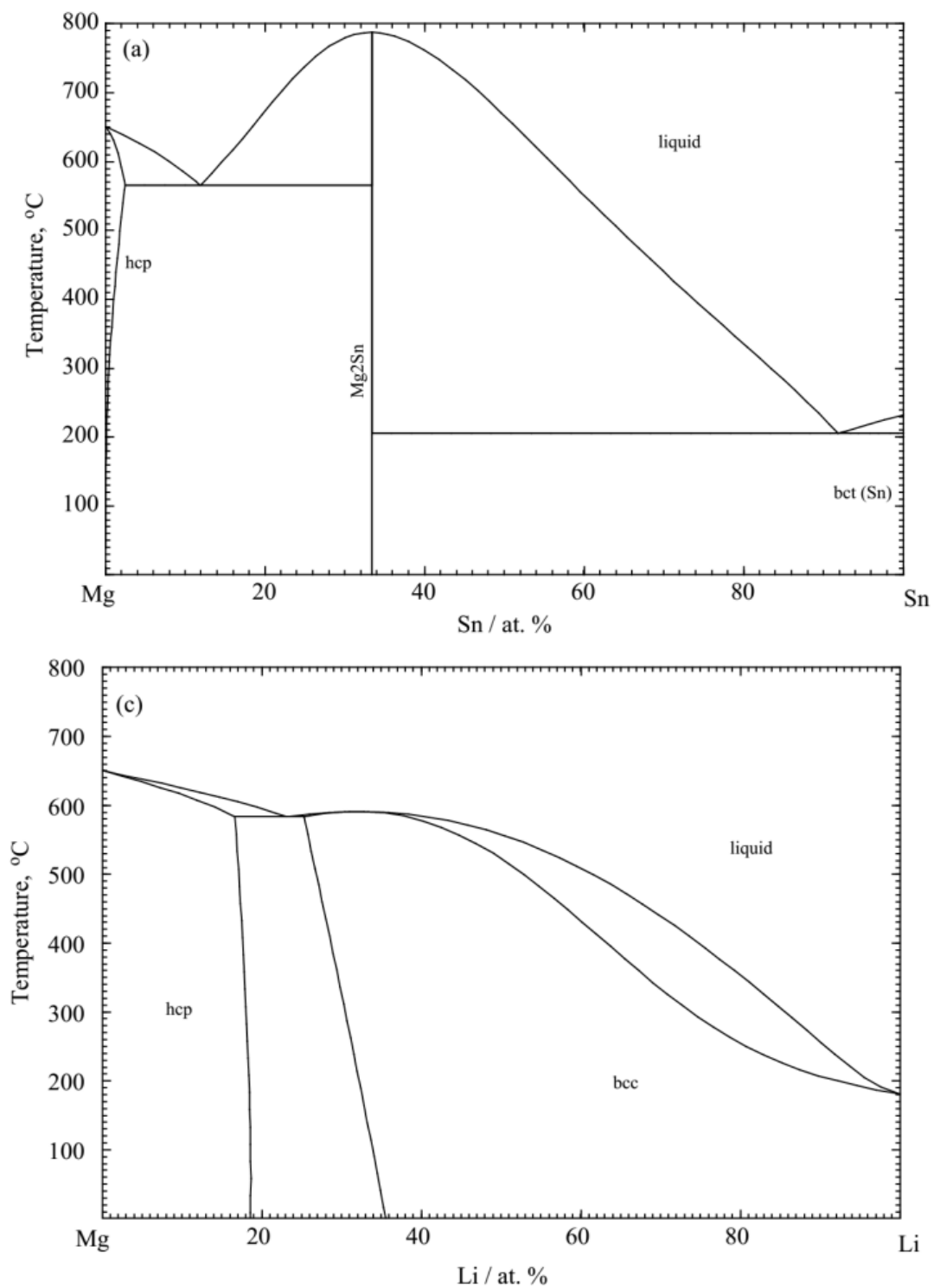
Figure 10.6 Calculated (a) Mg-Sn (Jung, et al., 2007), (b) Mg-Na (Spencer, 2006), (c) Mg-Li (Spencer, 2006), and (d) Mg-In (present work) phase diagrams
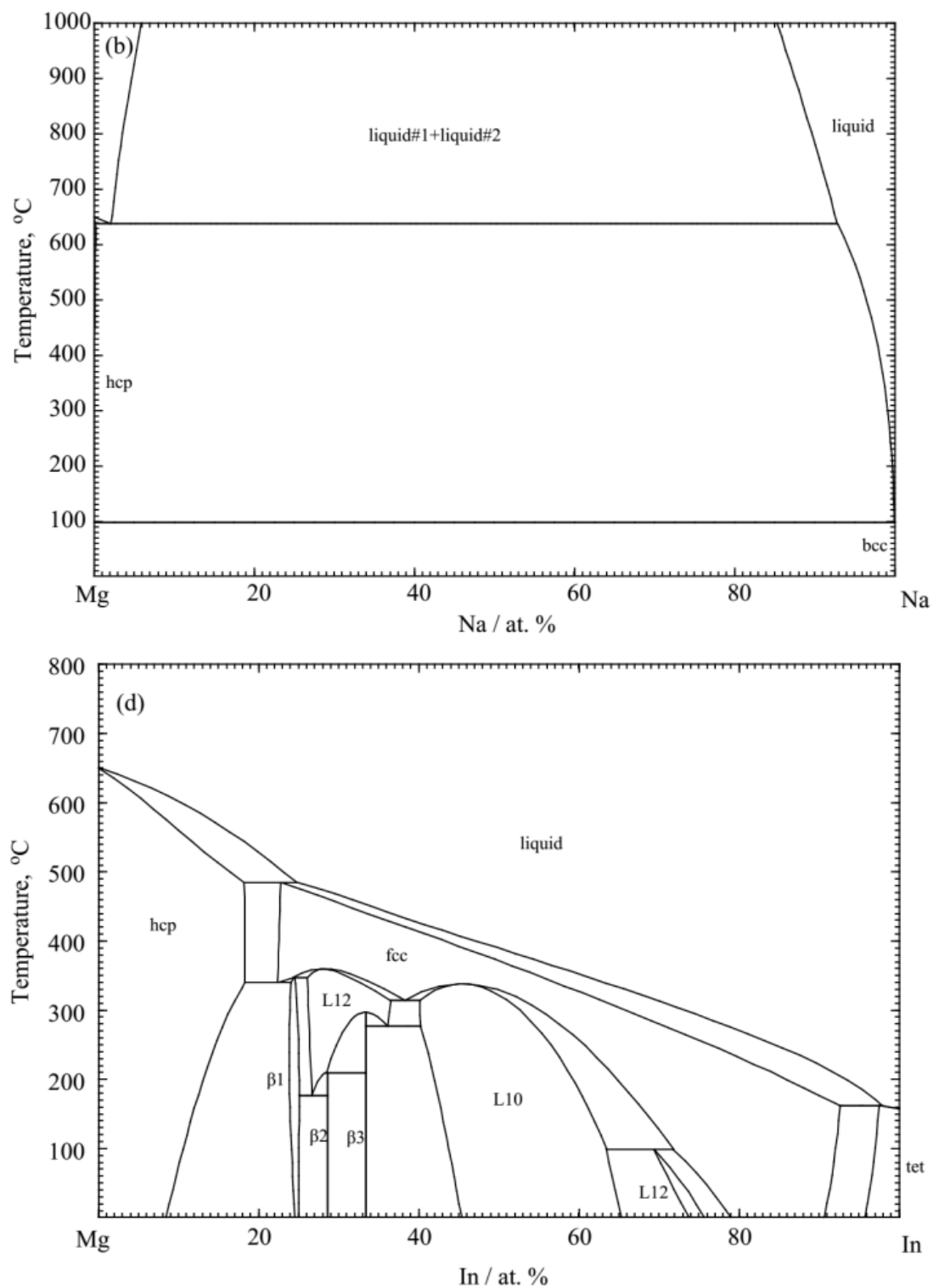
Figure 10.6 Calculated (a) Mg-Sn (Jung, et al., 2007), (b) Mg-Na (Spencer, 2006), (c) Mg-Li (Spencer, 2006), and (d) Mg-In (present work) phase diagrams
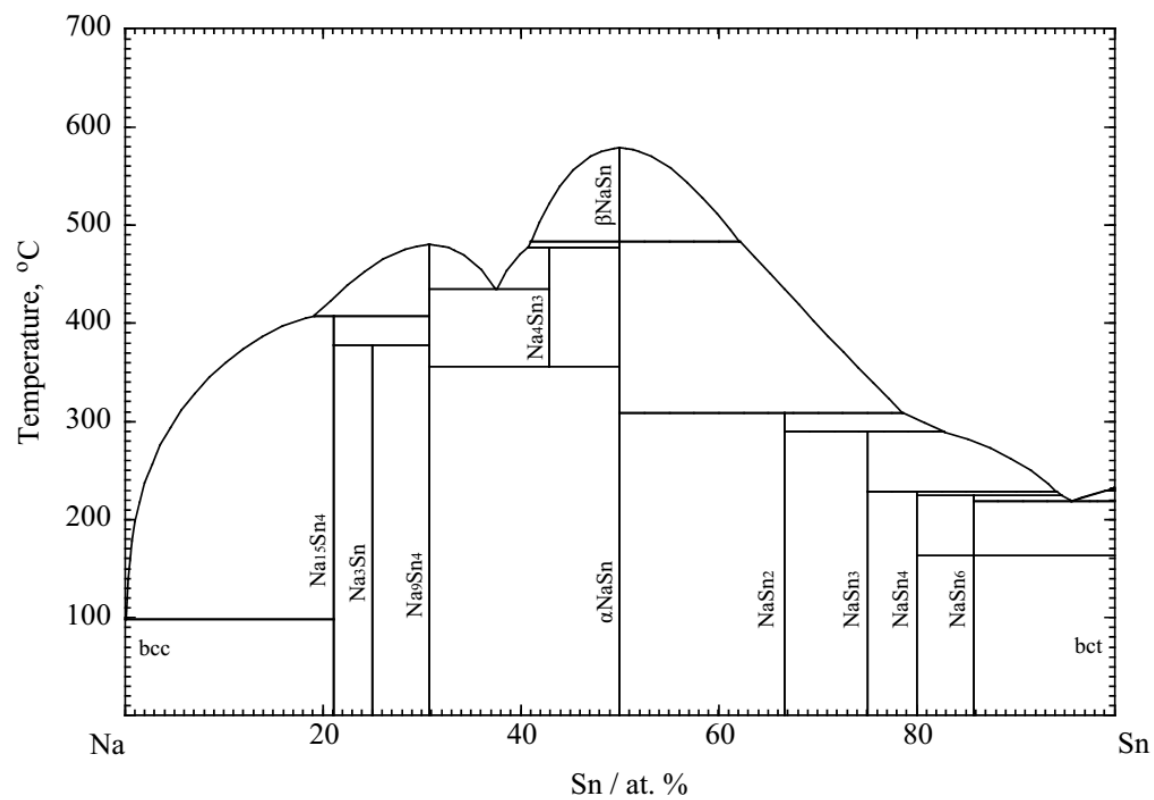
Figure 10.7 Calculated Na-Sn phase diagram (present work)
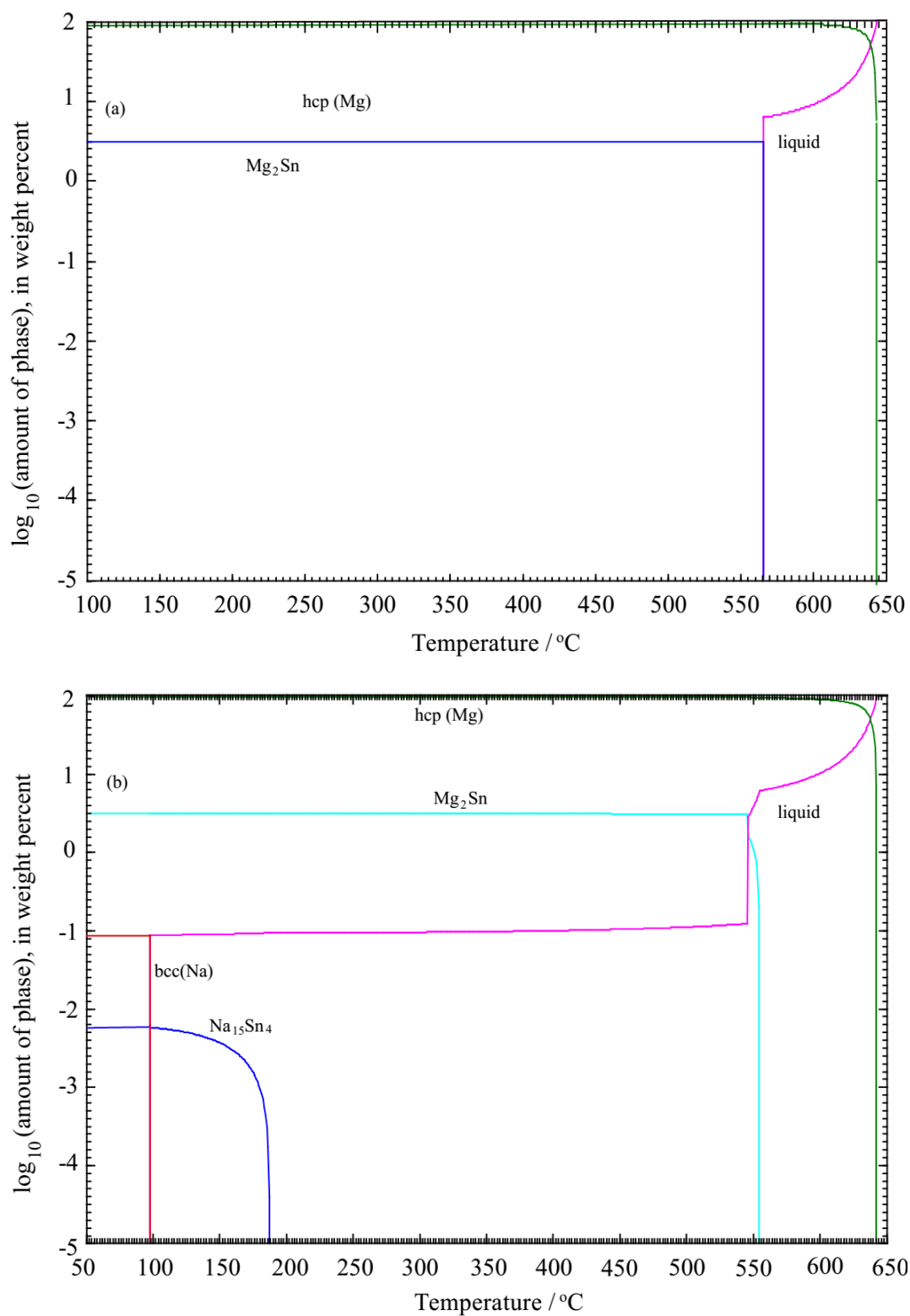
Figure 10.8 Scheil-Gulliver cooling simulation of (a) Mg-1.3Sn and (b) Mg-1.3Sn-0.13Na (at. %) with present thermodynamic database
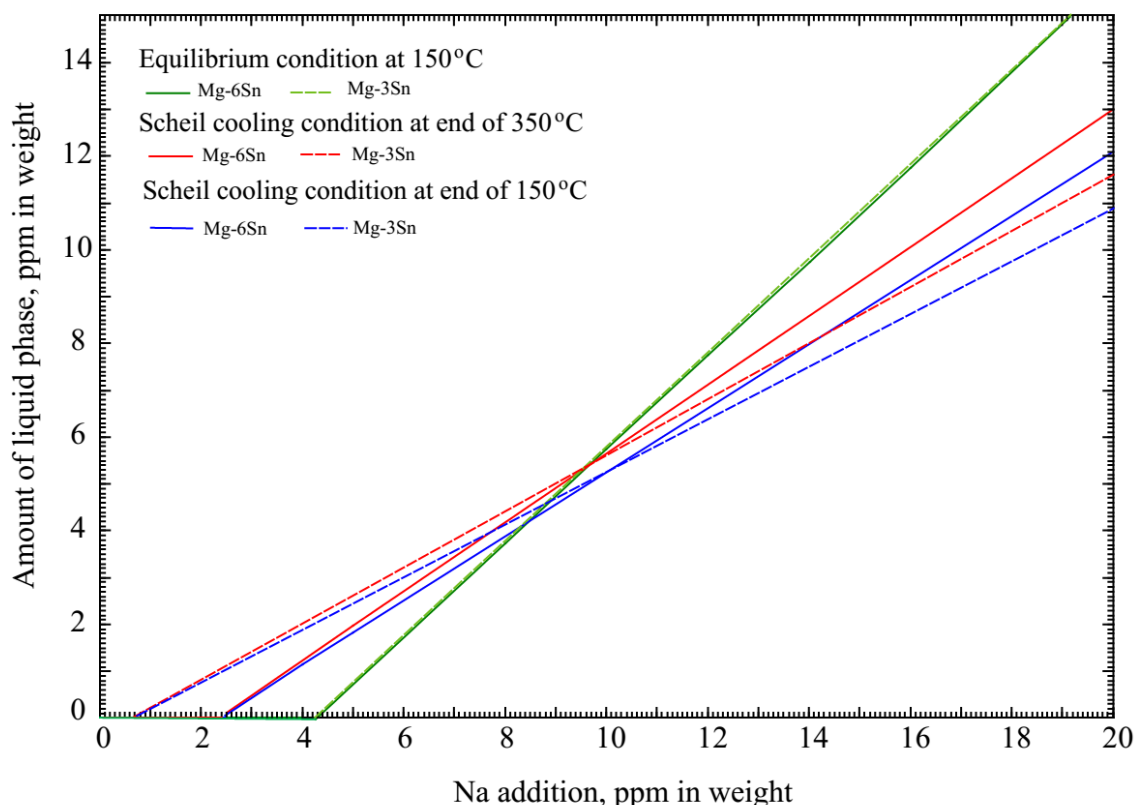
Figure 10.9 Calculated of the amount of liquid phase with the addition of Na in Mg-6Sn and Mg-3Sn alloys

Although the proposed approach leads to impractical additions of Na to Mg-Sn alloys, it may lead to better results in Mg-Sn alloys with Li-In additions (Mendis, et al., 2006). The Scheil-Gulliver cooling simulation (Gulliver, 1913; Scheil, 1942) of a Mg-2Sn-0.48Li-0.53In (at. %) alloy calculated in the EQUILIB module of FactSage with the present thermodynamic database is shown in Figure 10.10. According to the results, the Mg_2Sn phase will be formed from 578 ^{o}C, and then two more phases, fcc and tet(In), are formed from 474 ^{o}C and 159 ^{o}C separately.

The isothermal sections of the Mg-Sn-Li-In quaternary system in the Mg-rich region at 500 ^{o}C and 200 ^{o}C are shown in Figure 10.11. According to these calculated isothermal sections, the phase equilibrium in a Mg-2Sn-0.48Li-0.53In (at. %) alloy at 500 ^{o}C is constituted by the Mg_2Sn + hcp(Mg) phases. Then, if this alloy is annealed at about 200 ^{o}C after the heat treatment at 500 ^{o}C, most of Li will be precipitated out as the Li_2MgSn phase in the hcp(Mg) matrix. The final precipitate of metastable tet(In) obtained during the casting process will be changed into a liquid

phase during the heat treatment process. This should improve the mechanical via modification of the secondary precipitates. According the calculations as shown in Figure 10.11, there is no stable liquid phase in the Mg-rich region. This indicates that the In addition can improve the mechanical properties without the concern of high termperature failure with Na addition.
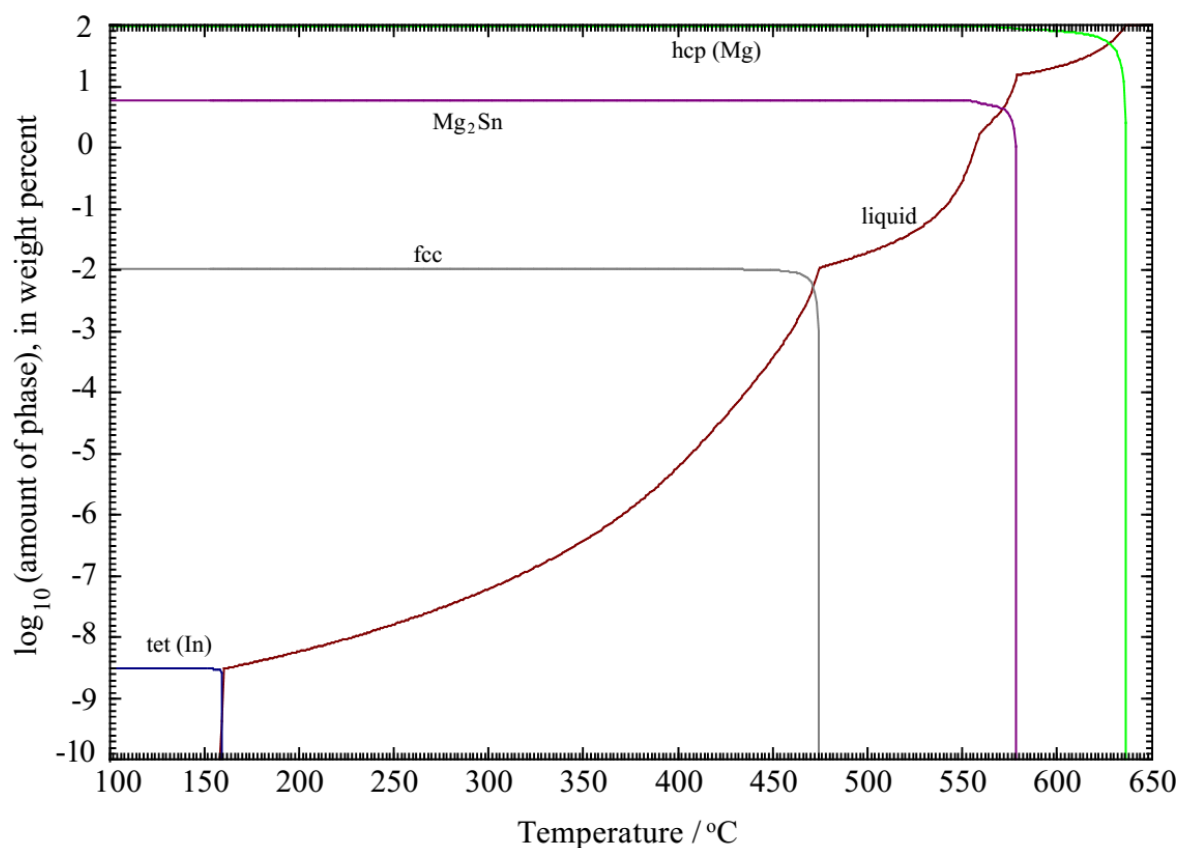
Figure 10.10 Scheil-Gulliver cooling simulation of Mg-2Sn-0.48Li-0.53In (at. %) calculated with the present thermodynamic database
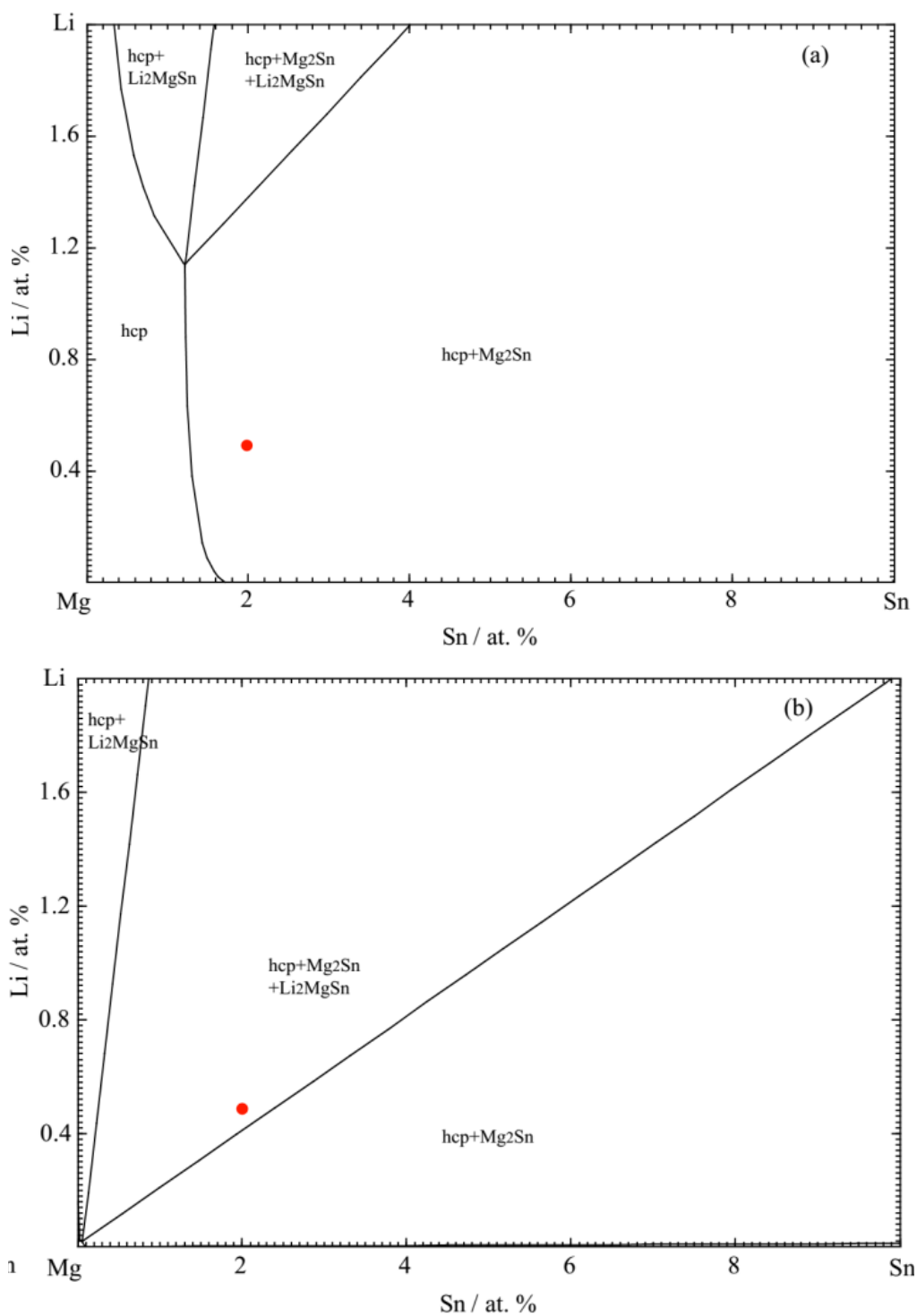
Figure 10.11 The calculated isothermal sections of Mg-Sn-Li-In quaternary system with constant 0.53 at. % In in Mg-rich region at (a) 500 $^{\circ}$C and (b) 200 $^{\circ}$C

The calculation results for the liquid phase with the addition of In to Mg-6Sn and Mg-3Sn alloys at 200 and 350 °C are shown in Figure 10.12. As shown in this Figure, the liquid phase can be obtained at the ageing temperature with In additions, but there is no liquid phase at equilibrium at the working temperature (up to around 150 °C). There should hence be advantages in using additions of In instead of Na for Mg-Sn based alloys. However, as seen in Figure 10.14, the total amount of liquid, with In addition, at the ageing temperature is very small in comparsion with these of Na, which will affect the modification result. In order to improve the amount of liquid phase at ageing temperature, Li-In additions are considered.
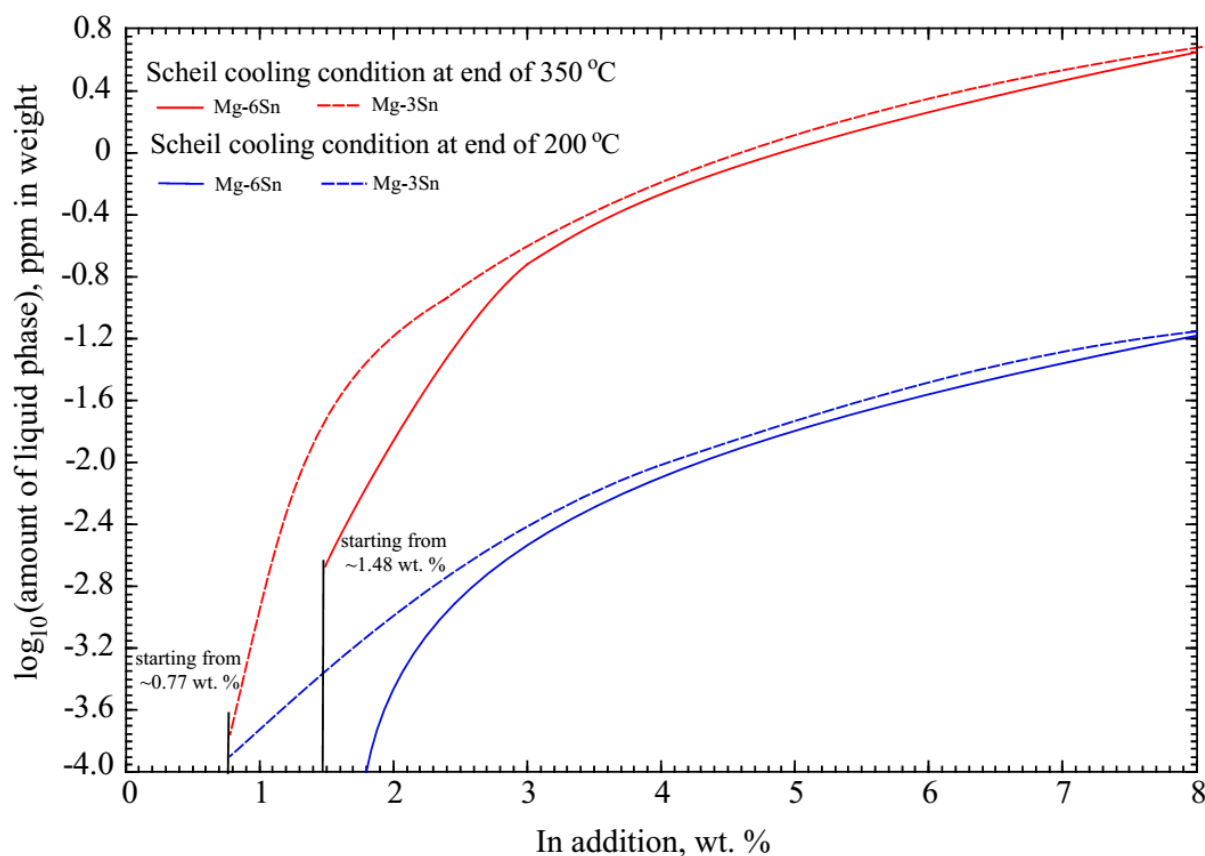
Figure 10.12 Calculated of the amount of liquid phase with the addition of In in Mg-6Sn and Mg-3Sn alloys

The calculated results for the liquid phase with the addition of Li to Mg-3Sn-mIn (m: 0.15, 1 and 3) (wt. %) alloy 350 °C and 200 °C are shown in Figure 10.13. As shown in this figure, the total

amount of the liquid phase at 350 $^{\circ}$C are increased obviously which is about 1000 times than orginal one just with 0.1-0.4 wt. % Li addition. The amount of liquid phase can be obtained by varying the amount of In added. According to present calculations, a comparative amount of liquid phase can be obtained in the Mg-3Sn-1In (wt. %) alloy more than 0.2 wt. % added Li.
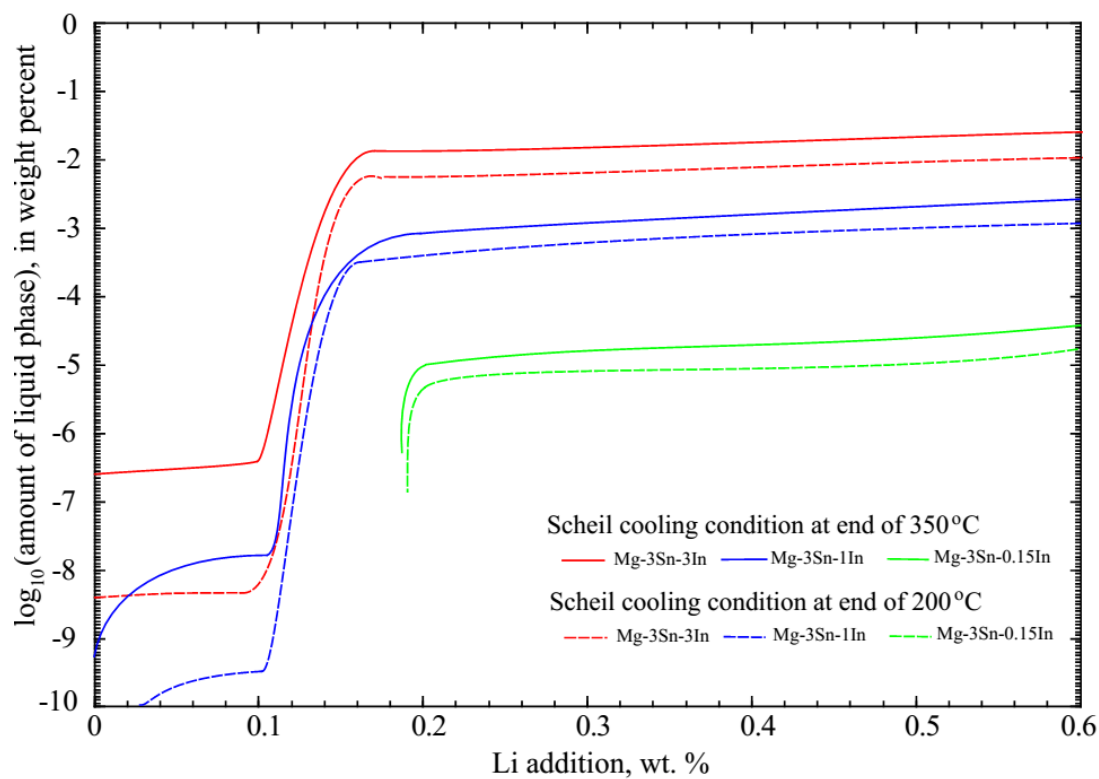
Figure 10.13 Calculated amounts of liquid phase with the addition of Li in Mg-3Sn-xIn (x:0.15, 1, and 3) (wt. %) alloy 350 $^{\circ}$C and 200 $^{\circ}$C resulting from Scheil-Gulliver cooling.

10.3 Design of aged hardening Mg-based alloys in the Mg-X (X: Ag, Ca, In, Li, Sn, Sr, and Zn) multi-component system

As discussed in the previous section, the most effective way of improving the mechanical properties of wrought Mg-based alloys is to increase the amount of secondary pricipitates. In particularly, the soluble alloying elements can be precipitated as fine intermetallic phases during the ageing process. Thus, the design of age hardening alloys can be done by two steps: (i) finding alloys with maximum solute solubility; (ii) maximizing the precipitates formation at the ageing temperature (usually ≤ 200 ^{o}C for Mg-based alloys). It is relatively easy to analyze the solid solubility limits of solutes and calculate the amount of precipitates in the hcp (Mg) phase for a binary or a ternary system from the experimental and calculated phase equilibria.But it is very hard to analyze them in multicomponent systems. In order to calculate the alloy compositions with maximum solubility of solutes X (X: Ag, Ca, In, Li, Sn, Sr, and Zn) in the hcp (Mg) phase and the maximum amount of precipitates in the Mg matrix at the end of ageing process, a systematic analysis on Mg-X multi-component system was carried out by using the Fact-Optimal module in the Factsage^{TM} thermodynamic software with present thermodynamic database.

It should be noted that the important factor in the strengthening of alloys is the increase of the volume percent of secondary precipitates, not mass or mole percentages. Unfortunately, the present thermodynamic database does not contain volumetric data for all compounds and solid solutions. This makes it impossible to maximize the calculated volume percent of precipitates. Because of the large differences in the density of the alloying elements (*eg.* 534 kg/m^3 for Li, 7310 kg/m^3 for In), the maximizing of molar fraction of elemental solutes in hcp (Mg), which should result in high volume fraction of precipitates during annealing, is the best second choice in the present optimizations. The temperature of the homogenization heat treatmeant for Mg based alloys is usually selected at around 350-450 ^{o}C, thus the annealing temperature of 400 ^{o}C was chosen in the present work.

The operation steps, input conditions and calculated results with Fact Optimal module are shown in Figure 10.14a-d. The maximum input amounts (Figure 10.14b) of each element X were set according to their current cost (www. metalprices.com, accessed October 2013) and solid solubility in the hcp(Mg) phase was optimized for the related Mg-X binary systems. The maxium total amount of alloying elements was fixed at 15 at. % (Figure 10.14c). The final optimized

alloy composition Mg-X that maximized the elemental solubility of alloying elements in hcp (Mg) phase at 400 ^{o}C was found to be 95.5929Mg - 2.9039Zn - 0.8331In - 0.1385Ag - 0.0046Sn - 0.0315Ca - 0Sr - 0.4955Li at. % (referred to QZ71-X in present section) using the Fact Optimal module (Figure 10.14d). The limited solid solubility in hcp (Mg) and the strong tendency to form very stable compounds with other additives (as MgSnSr, Mg$_{92-y}$Sr$_8$Zn$_y$) reduce the amount of Sr to less than 0.0001 at. %. According to the calculated phase equilibria at 330 ^{o}C of QZ71-X alloy with present thermodynamic database, the solid solubilities of additions are 3.6768 In, 0.1322 Li, 0.000009 Ca, 0.021 Sn, 6.7029 Zn and 0.55533 Ag (wt. %) respectively. This means that amount of additions can be dissolved into hcp (Mg) during the solutionizing process at 330 ^{o}C ideally. The total amount of precipitates remaining in the solutionizing process are listed in Table 10. 3
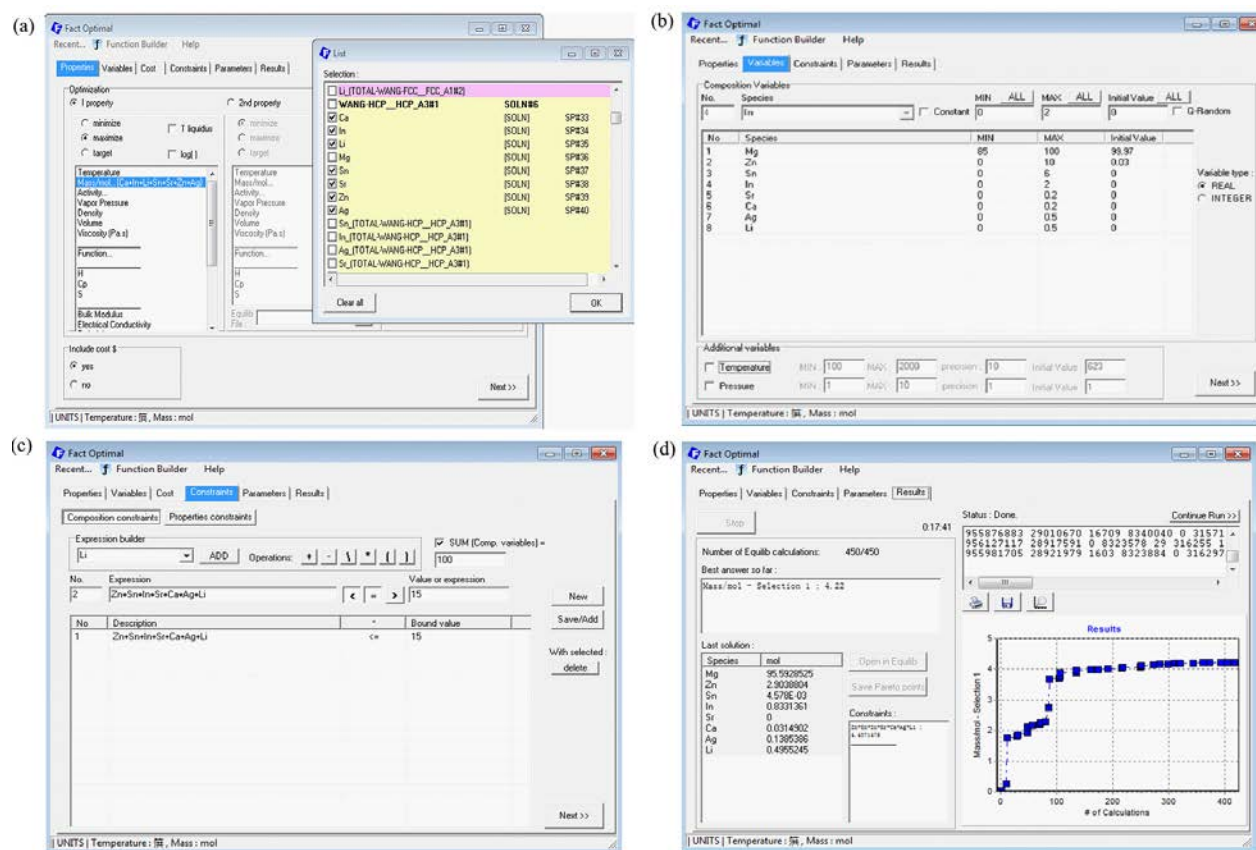
Figure 10.14 Operation steps, input conditions and calculated results of the maximization of molar elemental solubilities of alloying elements at 400°C using the Fact Optimal module

Table 10.3 Calculated amount of precipitates of selected alloy QZ71-X

Precipitates	Amount of precipitates, (wt. %)			
	Scheil cooling	Solutionizing at 330 ^{o}C	annealing at 300 ^{o}C	annealing at 200 ^{o}C
laves_C14 (Mg$_2$(Ca,Zn))	5.0049	0.8203	0.0585	0.1200
laves_C14#2 (Zn$_2$(Mg,Ag))	0.0007	0.2381	0.0242	0.0014
Li$_2$MgSn	0.0058	0	0.0045	0.0214
Zn$_3$Li$_2$	0.2924	0	0.0368	0.3740
Mg$_{12}$Zn$_{13}$	2.1603	0	0	0

In order to evaluate the as-cast products, a Scheil-Gulliver cooling simulation was performed with the chosen alloy QZ71-X as shown in Figure 10.15. The laves_C14 (Mg$_2$(Ca, Zn)) phase starts to solidify from 522 ^{o}C with the eutectic reaction *liquid→laves_C14 + hcp*, and Li$_2$MgSn starts to precipitate at 342 ^{o}C with the ternary eutectic reaction *liquid→laves_C14 + laves_C14#2* (Zn$_2$(Mg, Ag)) *+ hcp + Li$_2$MgSn*. The final reaction in the cooling process gives laves_C14 (Mg$_2$(Ca, Zn)), Li$_2$MgSn, Zn$_3$Li$_2$, Mg$_{12}$Zn$_{13}$ and laves_C14#2 (Zn$_2$(Mg, Ag)). The calculated solidification and annealing data of selected alloy QZ71-X are listed in Table 10.4. As shown in this Table, the total amount of precipitates can be obtained as 7.588 wt. % (~ 4.04 vol. %) and in the QZ71-X alloy at the end of annealing process, annealed at 300 ^{o}C, compared to the Mg-6Sn-0.5Li alloy of 6.786 wt. % (~3.55 vol. %).
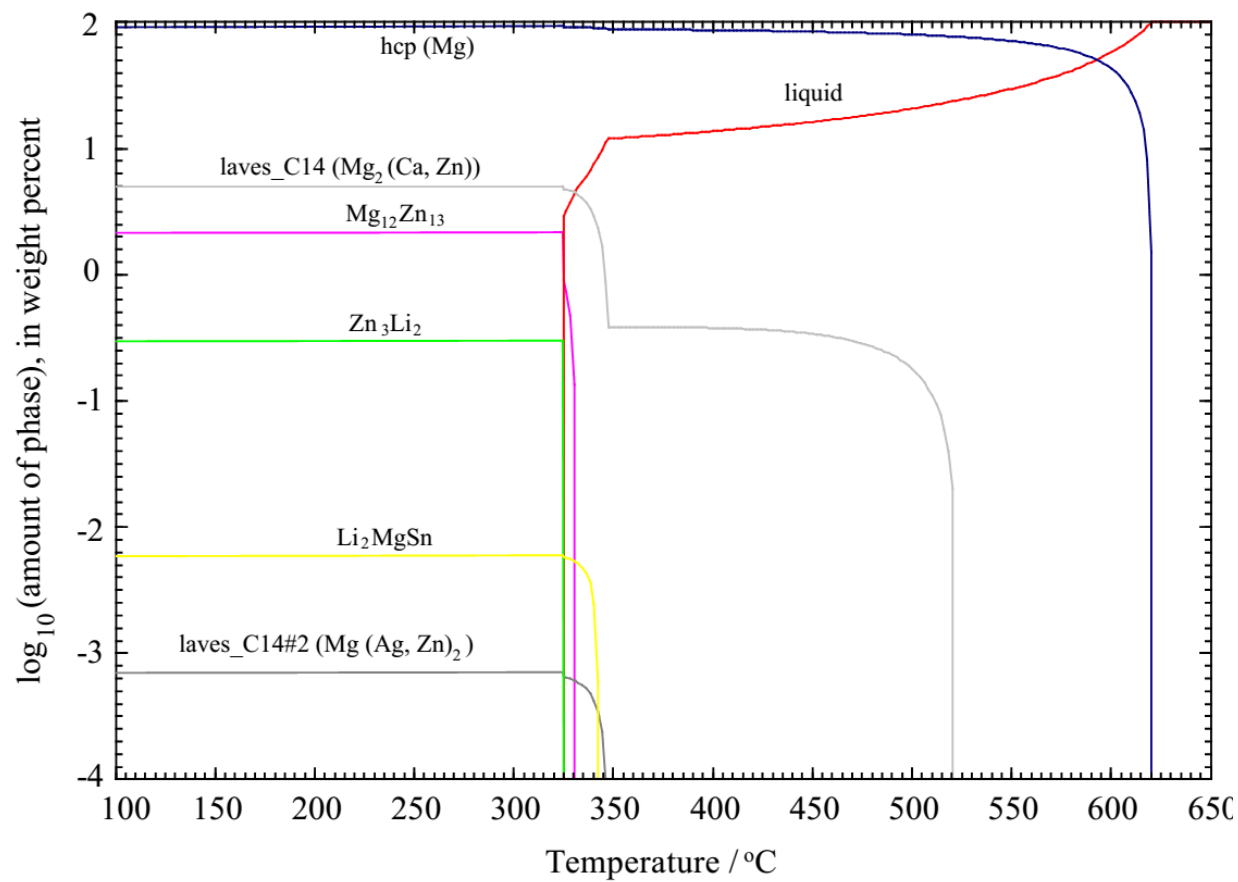
Figure 10.15 Scheil-Gulliver cooling simulation of QZ71-X alloy with the present thermodynamic database

Table 10.4 Calculated solidification and annealing data of the selected alloy QZ71-X

Precipitates	Formation temperature upon cooling, (^{o}C)	End of cooling	Amount of precipitates, (wt. %)							Total in matrix	Total in matrix, (Vol. %)[a]
			Annealing at 300°C						Total		
			hcp#1	hcp#2	hcp#3	hcp#4	hcp#5	hcp#6			
			76.232	11.511	1.416	1.762	0.629	0.987			
laves_C14 (Mg$_2$(Ca,Zn))	522	5.0049	0	0	0.0279	0.0306	0	0	0.0585	5.0634	2.818
laves_C14#2 (Zn$_2$(Mg,Ag))	347	0.0007	0.0229	0.0013	0	0	0	0	0.0242	0.0249	0.009
Li$_2$MgSn	342	0.0058	0	0.0031	0.0008	0.0006	0	0	0.0045	0.0103	0.006
Zn$_3$Li$_2$	330	0.2924	0	0	0	0	0.0114	0.0254	0.0368	0.3292	0.225
Mg$_{12}$Zn$_{13}$	325	2.1603	0	0	0	0	0	0	0	2.1603	0.980
[a]Data taken from pure elements and compound (Villars, & Cenzual, 2007).											

CONCLUSIONS AND FUTURE DIRECTIONS

CONCLUSIONS

The objective of the present work was to construct a critically evaluated thermodynamic database of optimized model parameters for the Mg-X (X: Ag, Ca, In, Li, Na, Sn, Sr, and Zn) multicomponent system, and to design new Mg-based alloys with the aid of this database. Five main aspects include 1) Critical evaluation of experimental data and thermodynamic description of 19 binary systems Mg-In, Mg-Ag, Ag-Zn, Ag-Ca, Ag-Li, In-Na, Na-Sn, Li-Sn, Na-Zn, In-Zn, Sn-Sr, Ca-Li, Ca-Sn, In-Sn, Ca-In, Ca-Na, Ag-In, Ag-Na and Ag-Sn; 2) Experimental measurements on five ternary systems Mg-Sn-X (X: Ag, In, Zn, Ca, and Sr); 3) Thermodynamic description of 12 ternary systems Mg-Sn-X (X: Ag, In, Li, Zn, Ca, and Sr), Mg-Zn-In, Mg-Ag-In, Mg-Ca-Li, Mg-Ca-Sr, Mg-Sn-In, and In-Sn-Zn; 4) Use of the thermodynamic database for calculations to analyze the solidification behavior of selected Mg-Sn based alloys at elevated temperatures; 5) Alloy design for Ag, Li, Ca, In, Sr, Sn, and Zn additions to Mg-based alloys have been carried out with the present thermodynamic database. The In-Sr and Li-In binary systems lack experimental data to be optimized, and hence are not included in this thesis. All remaining binary sub-systems and some selected important ternary sub-systems of the Mg-X multicomponent system were systematically evaluated and optimized. The updated optimization status of the sub-systems of the multicomponent system are listed in Tables C.1 and C.2. All available thermodynamic and phase equilibria data were evaluated in order to obtain a self-consistent thermodynamic database. The Modified Quasichemical Model, which takes short-range ordering into account, was systematically used for the liquid phase and the Compound Energy Formalism (CEF) was used with appropriate sublattice structures and species for each solid solutions in the binary and ternary systems.

The main contributions of the present thesis relevant to materials engineering research include:

1. An experimental study of the phase equilibria in the Mg-rich region of the five ternary systems Mg-Sn-Ag, Mg-Sn-In, Mg-Sn-Zn, Mg-Sn-Ca, and Mg-Sn-Sr:

Phase equilibria of isothermal sections of the Mg-Sn-Ag (350 and 415 ^{o}C) in the Mg-rich area were measured. No ternary compound was found in these sections. The solubility of Ag in Mg_2Sn at 415 and 350 ^{o}C is very limited, being less than 0.1 at. %. The solubility of Sn in Mg_3Ag

at 415 and 350 °C is about 2.5 to 3 at. %. Ternary isoplethal sections at constant composition of 10 Sn and 30 Ag at. % were measured by means of DSC.

Phase equilibria in the Mg-rich portion of the Mg-Sn-In ternary system at 415 and 330 °C, and the Mg-Sn-In ternary isoplethal sections at 10 Sn and 5 In (at. %) were investigated. No evidence for the existence of ternary compounds was found. The present results show that the solid solubilities of In in the Mg$_2$Sn phase and of Sn in the Mg-In binary intermetallic phases are very limited.

Phase equilibria in the Mg-rich portion of the Mg-Sn-Zn ternary system at 300 °C have been measured in the present work. They are similar to those of Mg-Sn-In ternary system, and no stable ternary compound was found in the isothermal section studied. There is limited solid solubility in all the terminal binary sub-compounds. A ternary isoplethal section of Mg-Sn-Zn at 10 Sn at. % has been measured using DSC. All reported experimental results from previous investigators and the present work are in reasonable agreement.

Table C.1 The updated optimization status of the binary sub-systems of Mg-X multicomponent system

System	Experimental data	Thermodynamic optimization	System	Experimental data	Thermodynamic optimization
Mg-Ca	Y	MQM	Ag-Ca	Y	MQM (This work)
Mg-Li	Y	MQM	Ag-Li	Y	MQM (This work)
Mg-Na	Y	MQM	In-Na	Y	MQM (This work)
Mg-Sn	Y	MQM	Na-Sn	Y	MQM (This work)
Mg-Sr	Y	MQM	Li-Sn	Y	MQM (This work)
Mg-Zn	Y	MQM	Na-Zn	Y	MQM (This work)
Ca-Sr	Y	MQM	In-Zn	Y	MQM (This work)
Ca-Zn	Y	MQM	Sn-Sr	Y	MQM (This work)
Li-Na	Y	MQM	Ca-Li	Y	MQM (This work)
Li-Sr	Y	MQM	Ca-Sn	Y	MQM (This work)
Na-Sr	Y	MQM	In-Sn	Y	MQM (This work)
Sr-Zn	Y	MQM	Ca-In	Y	MQM (This work)
Li-Zn	Y	MQM	Ca-Na	Y	MQM (This work)
Sn-Zn	Y	MQM	Ag-Na	Y	MQM (This work)
Ag-Sr	Y	MQM	Ag-Sn	Y	MQM (This work)
Mg-Ag	Y	MQM (This work)	Ag-In	Y	MQM (This work)
Ag-Zn	Y	MQM (This work)	In-Li	N/A	N
Mg-In	Y	MQM (This work)	In-Sr	N/A	N

Table C.2 The updated optimization status of the ternary Mg-containing sub-systems of Mg-X multicomponent system

System	Experimental data		Thermodynamic optimization
Mg-Li-Sn	[a]IS	370 ^{o}C	*MQM
	[b]VS	Li:Sn (1:1, 3:1, 9:1), Mg97Li3-Mg4Sn (wt. %)	
Mg-Zn-Sn	IS	*300 ^{o}C, 400 ^{o}C	*MQM
	VS	*10 at. % Sn; Mg$_2$Sn-MgZn$_2$, Mg$_2$Sn-Zn, *etc.*	
Mg-Li-Ca	IS	150 ^{o}C	*MQM
	VS	Mg$_2$Ca-Li$_2$Ca, CaMg-13Li (at. %)	
Mg-Ca-Sn	IS	*350 ^{o}C, *415 ^{o}C	*MQM
	VS	Mg$_2$Sn-Mg$_2$Ca, Mg-CaSn, Mg$_2$Sn-Ca$_2$Sn, 7Ca53Sn-Mg	
Mg-Zn-Li	IS	300 ^{o}C	*MQM
	VS	N/A	
Mg-Zn-Sr	IS	*300 ^{o}C	*MQM
	VS	N/A	
Mg-Sn-Sr	IS	*350 ^{o}C; *415 ^{o}C	*MQM
	VS	N/A	
Mg-Ca-Sr	IS	500 ^{o}C	*MQM
	VS	79.6Mg20.4Ca-53.7Mg46.3Sr (wt. %)	
Mg-Sn-In	IS	*330 ^{o}C; *415 ^{o}C	*MQM
	VS	*10 Sn, *5 In (at. %)	
Mg-Sn-Ag	IS	*330 ^{o}C; *415 ^{o}C, 550 ^{o}C, 450 ^{o}C	*MQM
	VS	*10 Sn, *30 Ag (at. %); 10 Sn, 10 Ag (wt. %)	
Mg-Ag-In	IS	280 ^{o}C	*MQM
	VS	50 In, 10 Ag, 30 Mg (wt. %)	
Mg-Ca-Zn	IS	300 ^{o}C	[c] MQM
	VS	2 Ca, 4Ca, Zn$_2$Mg-Mg$_2$Ca, *etc.* (at. %)	
Mg-Ag-Ca	N/A		[c] MQM
Mg-Sn-Na	N/A		[c] MQM
Mg-Zn-Na	N/A		[c] MQM
Mg-Ag-Sr	N/A		[c] MQM
Mg-Sr-Na	N/A		[c] MQM
Mg-Sr-Li	N/A		[c] MQM
Mg-Sr-In	N/A		[c] MQM
Mg-Na-Li	N/A		[c] MQM
Mg-Na-In	N/A		[c] MQM
Mg-Li-In	N/A		[c] MQM
Mg-Ca-In	N/A		[c] MQM
Mg-Ca-Na	N/A		[c] MQM
Mg-Zn-In	N/A		[c] MQM
Mg-Ag-Zn	N/A		[c] MQM
Mg-Ag-Li	N/A		[c] MQM
Mg-Ag-Na	N/A		[c] MQM

* This work, [a] Isothermal section, [b] Vertical section, [c] Extrapolated from binary sub-systems

Phase equilibria of the Mg-Sn-Ca and Mg-Sn-Sr ternary systems in the Mg-rich region at 350 and 415 ^{o}C were measured. The existence of the MgSnCa and MgSnSr ternary phases was confirmed.

Two new ternary phases Mg_5Sn_3Sr and $Mg_{25}Sn_{24}Sr_{14}$ were found in the Mg-Sn-Sr isothermal sections at 350 ^{o}C and 415 ^{o}C.

2. Thermodynamic descriptions of 19 critically evaluated binary systems, (Mg-In, Mg-Ag, Ag-Zn, Ag-Ca, Ag-Li, In-Na, Na-Sn, Li-Sn, Na-Zn, In-Zn, Sn-Sr, Ca-Li, Ca-Sn, In-Sn, Ca-In, Ca-Na, Ag-In, Ag-Na, Ag-Sn) were obtained using the CALPHAD approach.This included the MQMPA for the liquid phase, and six systems (Mg-In, Ag-Li, In-Na, Na-Sn, Ca-In, and Ag-Na) systems were optimized for the first time. The remaining 13 binary systems were critically evaluated from the reported experimental and calculated data. They were thermodynamically re-optimized in the present work. Comparisons of optimizations between present and previous work were made. This has highlighted the important advantages of the MQM for modeling thermodynamic properties of liquid solutions, particularly of high-order systems.

 3. The critical evaluation of experimental data and thermodynamic optimization on 12 selected ternary systems Mg-Sn-X (X: Ag, In, Li, Ca, Sr, Zn), Mg-Ag-In, Mg-Ca-Li, Mg-Ca-Sr, Mg-Sn-In, In-Sn-Zn and Ag-In-Sn have been performed. Reasonable agreement was obtained between the optimizations and experimental data.

4. A self-consistent thermodynamic database of the Mg-X (X: Ag, Ca, In, Li, Na, Sn, Sr, and Zn) multicomponent system was constructed. This facilitates the development of Mg alloys for practical industrial purposes.

5. The application of the present thermodynamic database for Mg alloys design was investigated in the present work. Secondary precipitates of Mg-Sn alloys with Li addition were studied with the Scheil-Gulliver simulation module. In the 93.5Mg-6Sn-0.5Li wt. % alloy, a maximum 3.55 vol. % of precipitates in the hcp (Mg) matrix was found. The Mg-6Sn alloy showed ~2.86 vol. % precipitates, by comparsion. Composition design in the Mg-X multicomponent system was carried out with the present thermodynamic database. An alloy QZ71-X with the composition 95.5929Mg-2.9039Zn-0.8331In-0.1385Ag-0.0046Sn-0.0315Ca-0Sr-0.4955Li (at. %) was found with the Fact Optimal module. The maximum volume of precipitates was found to be ~4.04 vol. % for this QZ71-X alloy. Finally, the effect of In, Li, and Na on Mg-Sn based alloys was studied. The 96Mg3Sn1In wt. % alloy with Li additions more than 0.2 wt. % may be interesting for Mg-based alloy design.

From part of the present thesis, two paper has been published, another one was accepted for publication. Two more publications are under review.

Phase equilibrium measurements on the Mg-Zn-Sr system at 300 ^{o}C were carried out with the collaboration of Mr. Yi-Nan Zhang of Concordia University. These measurements were done at 300 ^{o}C in the 0-30 at. % Sr range with key-sample and the diffusion-couple methods. Four new ternary compounds were found in this isothermal section. The glass formability of two series of Mg-Zn-Sr alloys, of compositions of $Mg_{88-x}Zn_xSr_2$ ($28 \leq x \leq 38$) and $Mg_{85-y}Zn_ySr_5$ ($23 \leq y \leq 37$), were studied experimentally and compared with calculated predictions.

Some difficulties during the experiments and the thermodynamic optimizations in the present work should be noted. Li composition cannot be measured by EPMA and EDS, which led to inaccuracies in determining Mg-Sn-Li phase equilibria. Phase equilibria measurements for the Mg-Sn-Na system were not successful due to the reactions of Na and its alloys with moisture and oxgen. The protection of samples containing Ca, Sr, Li and Na (especially at high content) from oxidation remains crucial. Thermodynamic description of the order-disorder phase transition (*eg.* bcc_A2↔bcc_B2) remains problematical in present optimization work. These are limits of present techniques, which requires future remediation.

FUTURE DIRECTIONS

This work has built a critically assessed thermodynamic database of model parameters for the Mg-X (X: Ag, Ca, In, Li, Na, Sn, Sr, and Zn) multicomponent system, which provides a foundation for the study of multicomponent Mg-based alloys. Good agreement and self-consistency among experimental and thermodynamic optimization results were attained. Improvements are possible by further experimental and thermodynamic studies to refine the quality of the database and its applications.

The following recommendations are made:

1. In the present work, the phase equilibria of Mg-Sn-X (X: Ag, In, Zn, Ca and Sr) ternary systems in the Mg-rich region were measured experimentally for the first time. These experimental results provided useful information for thermodynamic optimization in Mg-based alloys design. It should be noted that, due to difficulties in preparing and analyzing Mg-Sn-Sr and Mg-Sn-Ca key samples, the crystal structure of the ternary compounds Mg_5Sn_3Sr and $Mg_{25}Sn_{24}Sr_{14}$ could not be established. Information on the thermal stability of these ternary compounds is still lacking. This information is pivotal in obtaining the best possible thermodynamic optimization results for these ternary systems. Thus crystal structures and thermal stability limits should be studied for the newly found compounds in these ternary systems.

2. 19 binary systems (Mg-In, Mg-Ag, Ag-Zn, Ag-Ca, Ag-Li, In-Na, Na-Sn, Li-Sn, Na-Zn, In-Zn, Sn-Sr, Ca-Li, Ca-Sn, In-Sn, Ca-In, Ca-Na, Ag-In, Ag-Na, and Ag-Sn), were optimized in the present work, with the MQM for the liquid phase. All reported available experimental data are reproduced well. However, phase equilibria measurements and thermodynamic properties of the In-Sr and In-Sr binary systems are necessary for complete thermodynamic optimization. Experimental measurements or first-principles calculations are needed for the thermodynamic properties of solid compounds in the Mg-In, Ca-In, and Ag-Li binary systems. These better input data will improve the predictive accuracy of calculations with the multicomponent database.

3. 13 ternary sub-systems (Mg-Sn-X, X: Ag, In, Li, Ca, Sr, Zn, Mg-Ag-In, Mg-Ca-Li, Mg-Ca-Sr, Mg-Sn-In, In-Sn-Zn and Ag-In-Sn) were selected and have been optimized in the present work.

Present optimization results are in good agreement with the reported experimental data. Never the less, further experimental phase equilibrium measurements (isothermal and isoplehal sections) and thermodynamic properties (enthalpies formation of compounds) are needed to improve the quality of the database. For example, there is only one isothermal section and two experimental points in the vertical section of the Mg-Ca-Li ternary, which limits the completion of the optimization.

4. The multicomponent Mg-X thermodynamic database has been constructed. Experimental and thermodynamic studies on the remaining unfinished ternary systems are suggested in order to complete parameterization of the entire multicomponent system. This applies particularly to the Mg-containing sub-systems Mg-Zn-Ag, Mg-Zn-In, Mg-Ca-In, Mg-Ca-Ag, *etc*.

5. The study of glass formability and mechanical properties of Mg-Zn-X (X: Ag, Sr, Ca, Y, In, etc) appears promising for applications in biodegradable alloys. The present database can be used for selecting key alloy compositions.

6. Applications of Mg-Zn-Ca-Sr based alloys can be investigated with the advent of future experimental data and thermodynamic optimization results.

The thermodynamic database (19 binary and 13 ternary systems) obtained in this thesis will be integrated into Factsage^{TM} software and distributed to Factsage^{TM} users at an early date. For example, the addition of the optimized Na-Sn binary system parameters makes possible the extrapolation of the Mg-Na-Sn ternary from previous data of the Mg-Na and Mg-Sn binary systems within the FTlite database (Bale, et. al., 2009). The Mg-Zn-Li-Sn quaternary system can be parameterized more precisely with the present optimized Li-Sn, Mg-Li-Sn, and Mg-Zn-Sn sub-systems. This futher advances the development and design of new Mg-based alloys.

REFERENCES

Adhikari, D., Singh, B. P., & Jha, I. S. (2012). Structural and energetic anomaly in liquid Na-Sn alloys. *Journal of molecular liquids, 167*, 52-56.

Agarwal, R., Fries, S. G., Lukas, H. L., Petzow, G., Sommer, F., Chart, T. G., & Effenberg, G. (1992). The Mg-Zn system. *Zeitschrift fuer Metallkunde, 83*, 216-223.

Ageew, N. V., & Kuznezow, V. G. (1937). X-ray diffraction study of the Ag_3Mg compound, *Izv. Akad. nauk SSSR Otd. Nauk*, 289-309.

Akinlade, O. (1996). Segregation and local order in sodium-indium liquid alloys. *Zeitschrift fuer Metallkunde, 85*(7), 487-491.

Akinlade, O. (2006). Ordering Phenomena in Na-Ga and Na-Sn Molten Alloys. *Physics and Chemistry of Liquids: An International Journal , 29*(1), 9-21.

Alblas, B. P., Van der Lugt, W., Dijkstra, J., Geertsma, W., & Van Dijk, C. (1983). Structure of liquid Na-Sn alloys. *Journal of Physics F: Metal Physics, 13*(12), 2465-2470.

Alblas, B. P. , Van der Lugtt, W., Dijkstra, J. , & Van Dijk, C. (1984). Structure of liquid Li-Sn alloys. *Journal of Physics F: Metal Physics, 14*, 1995-2006.

Alcock, C. B. , Sridhar, R., & Svedberg, R. C. (1969). A mass spectrometric study of the binary liquid alloys: Ag-In and Cu-Sn. *Acta Metallurgica Et Materialia, 17,* 840-844.

Alexander, W. A., Calvert, L. D., Desaulniers, A., Dunsmore, H. S., & Sargent, D. F. (1969). The silver-calcium phase diagram. *Canadian Journal of chemistry, 47,* 611-614.

Aljarrah, M., Aghaulor, U., & Medraj, M. (2007). Thermodynamic assessment of the Mg-Zn-Sr system. *Intermetallics, 15*(2), 93-97.

Aljarrah, M., & Medraj, M. (2008a). Thermodynamic assessment of the phase equilibria in the Al-Ca-Sr system using the modified quasichemical model. *The Journal of Chemical Thermodynamics, 40*(4), 724-734.

Aljarrah, M., & Medraj, M. (2008b). Thermodynamic modelling of the Mg-Ca, Mg-Sr, Ca-Sr and Mg-Ca-Sr systems using the modified quasichemical model. *CALPHAD: Computer Coupling of Phase Diagrams and Thermochemistry, 32*(2), 240-251.

Alpaut, O., & Heumann, T. (1965). Thermodynamic properties of solid indium-tin alloys. *Acta Metallurgica, 13*(5), 543-548.

Alqasmi, R. , & Egan, J. J. (1983). Thermodynamics of liquid sodium-tin alloys using calcium fluoride solid electrolytes. *Berichte Der Bunsen-Gesellschaft fur physikalische chemie, 87*(9), 815-817.

Anctil, P. A. (2003). Ca-Mg system. *Thermodynamic database*, CRCT (Ed.), Montreal.

Andersson, J. O., Jansson, B., & Sundman, B. (1985). THERMO-CALC: a data bank for equilibria and phase diagram calculations. *CODATA Bulletin* (58), 31-35.

Andersson, J. O., Helander, T., Höglund, L., Shi, P. F., & Sundman, Bo. (2002). Thermo-Calc & DICTRA, computational tools for materials science. *CALPHAD: Computer Coupling of Phase Diagrams and Thermochemistry, 26*(2), 273-312.

Andrews, K .W., Davies, H. E., Hume-Rothery, W., & Oswin, C. R. (1941). The equilibrium diagram of the system silver-zinc. *Proc. Roy. Sco., A177*, 149-167.

Andrews, K. W., & Hume-Rothery, W. (1943). The constitution of silver-magnesium alloys in the region 0-40 atomic precent magnesium. *Journal Institute of Metals, 69*, 485-493.

Anres, P., Alaoui-elbelghiti, M., Gambino, M., & Bros, J. P. (2000). Enthalpy of formation of the In-Sn-Zn liquid system. *Thermochimica Acta, 346*, 49-56.

Axel, H., Eisenmann, B., Schaefer, H., & Weiss, A. (1969). Ternary E-phases of main group elements. I. CaMgSi, CaMgGe, and CaMgSn. *Zeitschrift für Naturforschung B, 24*, 815-817.

Baar, N. (1911). Alloys of molybdenum with nickel, manganese with thallium, and calcium with magnesium, thallium, lead, copper and silver. *Zeitschrift fuer Anorganische Chemie, 70*, 352-394.

Bailey, D. M. , Skelton, W. H. , & Smith, J. E. (1979). Li-Sn Phase Relationships between Li_7Sn_2 and LiSn. *Journal of the Less-common Metals, 64*(2), 233-240.

Balducci, G., Brutti, S., Ciccioli, A., Gigli, G., Trionfetti, G., Palenzona, A., & Pani, M. (2006). Vapor pressures and thermodynamic properties of strontium silicides. *Intermetallics, 14*(5), 578-583.

Bale, C. W., Bélisle, E., Chartrand, P., Decterov, S. A., Eriksson, G., Hack, K., & Pelton, A. D. (2009). FactSage thermochemical software and databases-recent developments. *CALPHAD: Computer Coupling of Phase Diagrams and Thermochemistry, 33*(2), 295-311.

Bale, C. W., Chartrand, P., Degterov, S. A., Eriksson, G., Hack, K., Ben Mahfoud, R., Petersen, S. (2002). FactSage thermochemical software and databases-recent developments. *CALPHAD: Computer Coupling of Phase Diagrams and Thermochemistry, 26*, 189-228.

Baradel, P., Vermande, A., Ansara, I., & Desre, E. (1971). Thermodynamic investigation of liquid Li-Sn alloys. *Rev. Int. Hautes Temp. Refract., 8*(3-4), 201-204.

Baren, M. R. (1988). The Ag-Ca system. *Bulletin of Alloy phase diagrams, 9*(3), 228-231.

Baril, E., Labelle, P., & Pekguleryuz, M. (2003). Elevated temperature Mg-Al-Sr: creep resistance, mechanical properties, and microstructure. *JOM: Journal of the Minerals, Metals and Materials Society, 55*(11), 34-39.

Baroni, A. (1932). Alloys of Li, thermal and X-ray analysis of the system Li-Sn. *Atti rend. Accad. Lincei, Roma, 16*(6), 153-158.

Barren, M. R., (Ed.). (1992). Ag-In (silver-indium). ASM international.

Barsoum, M. W., & Lukas, H. L. (1988). Thermodynamics of molten lithium-tin alloys. *Metallurgical Transactions A: Physical Metallurgy and Materials Science, 19*(3), 637-644.

Bartlett, H. E., Neethling, A. J., & Crowther, P. (1970). Thermodynamic properties of sodium-cadmium and sodium-indium liquid alloys from electromotive. *Journal of Chemical Thermodynamics, 2*(4), 523-534.

Becerra, A., & Pekguleryuz, M. (2009). Effects of zinc, lithium, and indium on the grain size of magnesium. *Journal of Materials Research, 24*(5), 1722-1729.

Becker, W., Schwitzgebel, G., & Ruppersberg, H. (1981). Thermodynamic investigations of liquid Li-Pb and Li-Ag alloys: A comparative study. *Zeitschrift fuer Metallkunde, 72*, 186-190.

Beja, R., & Laffitte, M. (1968). The enthalpy of mixture of liquid silver-gallium alloys at 500 C. *CR Acad. Sci., Paris C, 267*, 123-126

Ben-Hamu, G., Elizer, D., Kaya, A., Na, Y. G., & Shin, K. S. (2006). Microstructure and corrosion behavior of Mg-Zn-Ag alloys. *Materials Science Engineering A, 435-436*, 579-587.

Biltz, V. W. (1937). The heats of formation of intermetallic compounds. *Zeitschrift Fuer Metallkunde, 29*, 72-79.

Biltz, V. W., & Holverscheit, W. (1924). The systematic affinity principle. XXX, the heats of formation of intermetallic compounds. VI. Tin alloys. *Zeitschrift Fur Anorganische Und Allgemeine Chemie, 140*, 261-267.

Birchenall, C. E., & Cheng, C. H. (1949). The vapor pressures of zinc and cadmium over some of their silver alloys. *Transactions of the American Institute of Mining, Metallurgical, and Petroleum Engineers Incorporated, 1*(7), 428-434.

Blöchl, P. E. (1994). Projector augmented-wave method. *Physical Review B, 50*(24), 17953-17979.

Blair, G. R., & Downie, D. B. (1970). Calorimetric study of silver-zinc and copper-zinc alloys. *Metal science journal, 4*, 1-5.

Bohl, R. W., & Hildebrandt, V. D. (1957). Electrode potential studies of liquid-solid equilibrium in Zn-Cd and Zn-In alloys. *Journal of the American Chemical Society, 79*, 2711-2727.

Bouirden, L. (1984). Doctoral thesis, University of Nancy I, Nancy.

Bros, J. P., & Laffitte, M. (1970). Enthalpies of formation of In-Sn alloys in the liquid state. *Journal of chemical thermodynamics, 2*, 151-152.

Bushmanov, V. D., & Yatsenko, S. P. (1981). Thermodynamic properties of binary systems of lithium, sodium, and potassium with aluminum, gallium, indium, and thallium. *Zhurnal Fizicheskoi Khimii, 55*(11), 2951-2952.

Cakir, O., & Alpaut, O. (1988). Thermodynamic properties of solid In-Sn alloys. *Journal of the Less-common metals, 141*(1), 11-27.

Campbell, A. N., Wagemann, R., & Ferguson, R. B. (1970). The silver-indium system: thermal analysis, photomicrography, electron microprobe, and X-ray powder diffraction results. *Candian Journal of Chemistry, 48*, 1703-1715.

Cao, G., & Kou, S. (2006a). Hot cracking of binary Mg-Al alloy castings. *Materials Science and Engineering A: Physical Metallurgy and Materials Science, 417*(1-2), 230-238.

Cao, G., & Kou, S. (2006b). Hot tearing of ternary Mg-Al-Ca alloy castings. *Metallurgical and Materials Transactions A: Physical Metallurgy and Materials Science 37*(12), 3647-3663.

Carfagno, D. G. (1966). The Ca-Li equilibirum system. Doctoral thesis, Syracuse University, Syracuse, NY.   (35891)

Cartigny, Y., Fiorani, J. M., Maitre, A., & Vilasi, M. (2005). Thermodynamic assessment of the Ca-Sn system. *Zeitschrift Fur Metallkunde, 96*(11), 1308-1313.

Castanet, R., Claire, Y., & Laffitte, M. (1970). Thermodynamic properties of liquid Ag-In solutions. *Journal de chimie physique et physico-chimie biologique, 67*(4), 789-793.

Castanet, R., & Laffitte, M. (1968). Enthalpie de formation a 1280 K d'alliages liquides argent-etain et argent-germanium. *CR Acad. Sci. Paris. C, 267*, 204-206.

Cetin, H., & Ross, R. G. (1991). The phase diagram of Na-Zn system. *Journal of Phase Equilibria and Diffusion, 12*(1), 6-9.

Chartrand, P. (2003). Li-Sr system. *Thermodynamic database*, CRCT (Ed.). Montreal.

Chartrand, P., & Pelton, A. D. (2000a). On the choice of "geometric" thermodynamic models. *Journal of Phase Equilibria, 21*(2), 141-147.

Chartrand, P., & Pelton, A. D. (2000b). Thermodynamic evaluation and optimization of the LiCl-NaCl-KCl-RbCl-CsCl-MgCl$_2$-CaCl$_2$-SrCl$_2$ system using the modified quasichemical model. *Canadian Metallurgical Quarterly, 39*(4), 405-420.

Chen, S. L., Daniel, S., Zhang, F., Chang, Y. A., Yan, X. Y., Xie, F. Y., Oates, W. A. (2002). The PANDAT software package and its applications. *CALPHAD: Computer Coupling of Phase Diagrams and Thermochemistry, 26*(2), 175-188.

Chevalier, P. -Y. (1988). A thermodynamic evaluation of the Ag-Sn system. *Thermochimica Acta, 136*, 45-54.

Chirulli, G., Ferro, D., & Piacente, V. (1983). Magnesium activity in liquid In-Mg alloy from vapour pressure measurements. *Thermochimica Acta, 62*(2), 171-177.

Chou, C. -Y., Kim, H., & Hwang, G. S. (2011). A comparative first-principles study of the structure, energetics, and properties of Li-M (M= Si, Ge, Sn) alloys. *The Journal of Physical Chemistry C, 115*(40), 20018-20026.

Chowdhury, P. J. R., & Ghosh, A. (1971). Thermodynamic measurements in liquid Sn-Ag alloys. *Metalllurgical transactions, 2*, 2171-2174.

CompuTherm, LLC. (2008). Pandat 8.0-phase diagram calculation software for multi-component systems. *CompuTherm LLC, Madison, WI, USA*.

Courtney, I. A., Tse, J. S., Mao, O., Hafner, J., & Dahn, J. R. (1998). Ab initio calculation of the lithium-tin voltage profile. *Physical Review B, 58*(23), 15583.

Cui, Y., Liu, X.J., Ohnuma, I., kainuma, R., Ohtani, H., & Ishida, K. (2001). Thermodynamic calculation of the In-Sn-Zn ternary system. *Journal of Alloys and Compounds, 320*, 234-241.

Dadd, A. T., Hubberstey, E. , & Roberts, E. G. (1982). Solutions of group IV elements in liquid Li. *Journal of the Chemical Society, Faraday Transactions 1, 78*(9), 2735-2741.

Darken, L. S. (1967). Thermodynamics of binary metallic solutions. *Transactions of the metallurgical society of AIME , 239*(1), 80-89.

Davies, H. A. (1967). The solubility of In in liquid Na. *Transactions of the metallurgical society of AIME., 239*, 928-929.

Davies, R. H., Dinsdale, A. T., Gisby, J. A., Robinson, J. A. J., & Martin, S. M. (2002). MTDATA-thermodynamic and phase equilibrium software from the national physical laboratory. *CALPHAD: Computer Coupling of Phase Diagrams and Thermochemistry, 26*(2), 229-271.

Delcet, J., & Egan, J. J. (1978). Thermodynamics of liquid Ca-Ag and Ca-In alloys. *Journal of Less-common Metals, 59*(2), 229-236.

Delcet, J., Delgado-Brune, A., & Egan, J. J. (1979). Coulometric titrations using calcium fluoride and barium fluoride solid electrolytes to study alloy phases. Report: BNL-26264; CONF-790910-2 , Brookhaven National Lab. Upton, NY (USA).

Delimarskii, Y. K., & Konomuu, A. A. (1954). Electrochemical study of the system tin-sodium. *Zhurnal Fizicheskoi Khimii, 28*(7), 1169-1173.

Dinsdale, A. T. (1991). SGTE data for pure elements. *CALPHAD: Computer Coupling of Phase Diagrams and Thermochemistry, 15*, 317-425.

Du, Z. M., Jiang, Z. Q., & Guo, C. P. (2006). Thermodynamic optimizing of the Li-Sn system. *Zeitschrift fuer Metallkunde, 97*(1), 10-16.

Dupin, N., & Ansara, I. (1999). On the sublattice formalism applied to the B2 phase. *Zeitschrift Fur Metallkunde, 90*(1), 76-85.

Dutkiewicz, J., & Moser, Z. (1983). *Bull. Acad. Polon. Sci. Tech. Sco, 31*, 27.

Dutkiewicz, J., & Zakulski, W. (1984). The In-Zn system. *Bulletin of Alloy phase diagrams, 5*(3), 284-289.

Ehrlich, K. (1965). Doctoral thesis, Ludwig-maximilians university, Munchen.

Eisenmann, B., Schäfer, H.t, & Weiss, A. (1972). Der Übergang vom geordneten" Anti-PbCl$_2$-Gitter zum Anti-PbFCl-Gitter: ternäre phasen ABX der erdalkalimetalle mit elementen der 4. hauptgruppe (A = Ca, Sr, Ba; B = Mg; X = Si, Ge, Sn, Pb). *Zeitschrift Fur Anorganische Und Allgemeine Chemie, 391*(3), 241-254.

Elliott, R. B., & Lemons, J. F. (1967). Activites of molten tin alloys from EMF measurements. *Journal of The Electrochemical Society, 114*(9), 935-937.

Esin, Y., Litovskii, V. V., Demin, S. E., & Petrushevskii, M. S. (1985). Partial and integral enthalpies of formation of liquid alloys of strontium and barium with tin. *Zhurnal Fizicheskoi Khimii, 59*(3), 766-767.

Evans, D. S., & Prince, A. (Eds.). (1983). *Materials research society symposium proceeding 19*. North-holland: Elsecier.

Fürtauer, S., Tserenjav, E., Yakymovych, A., & Flandorfer, H. (2013). Calorimetric studies of Cu-Li, Li-Sn, and Cu-Li-Sn. *The Journal of Chemical Thermodynamics, 61*(0), 105-116.

Fang, Q., & Wendt, H. (1996). Performance and thermodynamic properties of Na-Sn and Na-Pb molten alloy electrodes foe alkali metal thermoelectric converter. *Journal of Applied Electrochemistry, 26*, 343-352.

Fang, S. S., Xiao, X. S., Xia, L., Li, W. H., & Dong, Y. D. (2003). Relationship between the widths of supercooled liquid regions and bond parameters of Mg-based bulk metallic glasses. *Journal of Non-Crystalline Solids, 321*(1), 120-125.

Ferro, D., Nappi, B. M., Piacente, V., & Cignini, P. L. (1978). Znic activity in In-Zn alloys measured by the Knudsen Torsion-effusion method. *High Temperature Science, 10*, 131-142.

Feschotte, P. (1976). The Mg-In binary system. *Journal of the Less-common metals, 46*(1), 51-54.

Fiorani, J. M., Naguet, C., Hertz, J., Bourkba, A., & Bouirden, L. (1997). *Zeitschrift fuer Metallkunde, 88*, 711.

Fischbach, H. (1985). Determination of the thermodynamic properties of liquid Ca-Ag alloys. *Journal of the Less-common metals, 108*, 151-162.

Fischer, A. K., & Johnson, S. A. (1972). Liquid-vapor equilibria and thermodynamics of Li-Sn System. *Journal of Chemical & Engineering Data, 17*(3), 280-283.

Flandorfer, H., Saeed, U., Luef, C., Sabbar, A., & Ipser, H. (2007). Interfaces in lead-free solder alloys: Enthalpy of formation of binary Ag-Sn, Cu-Sn and Ni-Sn intermetallic compounds. *Thermochimica Acta, 459*(1-2), 34-39.

Fornasini, M. L., & Franceschi, E. (1977). The crystal structure of calcium-tin ($Ca_{31}Sn_{20}$). *Acta Crystallogr., Sect. B, B33*, 3476-3479.

Foster, M. S., Crouthamel, C. E., & Wood, S. E. (1966). Thermodynamics of binary aAlloys. II. The Li-Sn System. *Journal of Physical Chemistry, 70*(10), 3042-3045.

Frank, U., & Muller, W. (1975). Preparation and crystal structure of Li_3Sn_5 and the structural relations between the phases of the systems Li-Sn and Li-Pb. *Zeitschrift für Naturforschung B, 30*(3), 316-322.

Frank, U., Muller, W., & Schafer, H. (1975a). The crystal structure of Li_5Sn_2. *Zeitschrift für Naturforschung B, 30*(1-2), 1-5.

Frank, U., Muller, W., & Schafer, H. (1975b). The crystal structure of Li_7Sn_2. *Zeitschrift für Naturforschung B, 30*(1-2), 6-9.

Frantik, R. O., & McDaonald, H. J. (1945). Thermodynamic study of the Tin-Silver system. *Transactions electrochemical society, 88*, 253-262.

Freeth, W. E., & Raynor, G. V. (1954). The constitution of the system Ag-Li. *Journal Institute of Metals, 82*, 569-574.

G. Bruzzone, & Ruggiero, A. F. (1964). The equilibrium diagram of the Ca-In system. *Journal of the Less-common metals, 7*, 368-372.

Gangulee, A., & Bever, M. B. (1968). The silver rich silid solid solutions in the system Ag-Mg. *Transaction of American Institute of Mining, Metallurgical, and Petroleum Engineers. 242*(2), 272-278.

Ganguli, A. K., Corbett, J. D., & Koeckerling, M. (1998). Mixed cations for the stabilization of new features. $Ca_{6.2}Mg_{3.8}Sn_7$, a phase with planar zigzag chains of interlinked square-planar tin units. *Journal of the American Chemical Society, 120*, 1223-1229.

Ganguli, A. K., Guloy, A. M., & Corbett, J. D. (2000). Concerning the $Ca_{2-x}Mg_x$ Tt Systems, Tt = Sn, Pb. *Journal of Solid State Chemistry, 152*, 474-477.

Gao, X., & Nie, J. F. (2007). Characterization of strengthening precipitate phases in a Mg-Zn alloy. *Scripta Materialia, 56*(8), 645-648.

Gasior, W., Moser, Z., & Zakulski, W. (1996). Thermodynamic studies and the phase diagram of the Li-Sn system. *Journal of Non-Crystalline Solids. 205-207*, 379-382.

Gasior, W., Moser, Z., Zakulski, W., & Schwitzgebel, G. (1996). Thermodynamic studies and the phase diagram of the Li-Mg system. *Metallurgical and Materials Transactions A: Physical Metallurgy and Materials Science, 27*(9), 2419-2428.

Gather, B., Schroeter, P., & Blachnik, R. (1987). Heats of mixing in the silver-indium-tin, silver-tin-antimony, silver-indium-antimony, and indium-lead-antimony ternary systems. *Zeitschrift fuer Metallkunde, 78*(4), 280-285.

Gerling, U., Pool, M. J., & Predel, B. (1979). On the thermodynamic properties of liquid Ag-Zn alloys. *Zeitschrift fuer Metallkunde, 70*(4), 224-229.

Ghosh, P., Mezbahul-Islam, M. D., & Medraj, M. (2012). Critical assessment and thermodynamic modeling of Mg-Zn, Mg-Sn, Sn-Zn and Mg-Sn-Zn system. *CALPHAD: Computer Coupling of Phase Diagrams and Thermochemistry, 36*, 28-43.

Gibbs, J. W. (1948). *The Collected Works: Thermodynamics*. Yale University Press.

Gibson, M. A., Fang, X., Bettles, C. J., & Hutchinson, C. R. (2010). The effect of precipitate state on the creep resistance of Mg-Sn alloys. *Scripta Materialia, 63*(8), 899-902.

Gladyshevskii, E. I. , Oleksiv, G. I. , & Kripyakevich, P. I. (1964). New examples of the structural type $Li_{22}Pb_5$. *Kristallografiya, 9*(3), 338-341.

Gladyshevsky, E. I., & Cherkashin, E. E. (1959). Solid solutions based on metallic compounds. *Zhurnal Neorganicheskoi Khimii 1*, 1394-1401.

Godecke, T., & Sommer, F. (1994). Stable and metastable phase equilibria in $MgZn_2$-Zn and Mg_2Sn-$MgZn_2$-Sn-Zn alloys. *Zeitschrift fuer Metallkunde, 85*, 683-691.

Goldsztaub, S., & Michel, P. (1951). Preparation of silver-magnesium alloys in thin layers by the simultaneous evaporation of these constituents in vacuum. *Comptes Rendus, 232*, 1843-1845.

Gomez-Acebo, T. (1998). Thermodynamic assessment of the Ag-Zn system. *CALPHAD: Computer Coupling of Phase Diagrams and Thermochemistry, 22*(2), 203-220.

Goward, G. R, Taylor, N. J., Souza, D. C. S., & Nazar, L. F. (2001). The true crystal structure of $Li_{17}M_4$ (M= Ge, Sn, Pb)–revised from $Li_{22}M_5$. *Journal of Alloys and Compounds, 329*(1), 82-91.

Graham, J. , & Raynor, G. V. (1957). Indium-rich indium-magnesium and indium-lithium alloys. *Philosophical Magazine, 2*(23), 1354-1363.

Gran, J., Song, M., & Sichen, D. (2012). Acitivity of magnesium in liquid Ag-Mg alloys. *CALPHAD: Computer Coupling of Phase Diagrams and Thermochemistry, 36*, 89-93.

Grobner, J., Schmid-Fetzer, R., Pisch, A., Colinet, C., Pavlyuk, V. V., Dmytriv, G. S., Bodak, O. I. (2002). Phase equilibira, calorimetric study and thermodynamic modeling of Mg-Li-Ca alloys. *Thermochica Acta, 389*, 85-94.

Grube, G., & Meyer, E. (1934). Electrical conductivity and phase diagram of binary alloys 16 the Li-Sn. *Zeitschrift für Elektrochemie, 40*(11), 771-777.

Guadagno, J. R. , Pool, M. J., & Shen , S. S. (1970). Thermodynamic investigation of liquid Ca-Sn, Sr-Sn, and Ba-Sn alloys. *Metallurgical Transactions, 1*(6), 1779-1780.

Gulliver, G. M. (1913). The quantitative effect of rapid cooling upon the constitution of binary alloys. The *Journal of the Insitute Metals, 9*, 120-157.

Gukov, O. Y., & Gukova, Y. Y., (1980). Intermentallic compounds in the Na-Sn system. *Deposited document SPSTL 777 Khp-D80*.

Hagiwara, H., Sugino, S., & Fujiwara, H. (1974). Thermodynamic properties of liquid In-Zn solutions. *Bulletin University Osaka, 23*(1), 41-50.

Hancke, W. (1938). Alloys of magnesium with gallium, indium and thallium. *Naturwissenschaften, 26*, 577-578.

Hansen, D. A., & Chang, L. J. (1969). Crystal structure of Li_2Sn_5. *Acta Crystallographica B, 25*(11), 2392-2395.

Hansen, M., & Anderko, K. (1958). *Constitution of Binary Alloys*. New York: McGraw-Hill.

Hanson, D., Stand, E. J., & Syevens, H. (1934). Some properties of tin comtaining small amounts of Silver, iron, nickel or copper. *Journal Institute of Metals, 55*, 115-133.

Hao, D., Bu, M., Wang, Y., Tang, Y., Gao, Q., Wang, M., Du, Y. (2012). Thermodynamic modeling of the Na-X (X= Si, Ag, Cu, Cr) systems. *Journal of Mining and Metallurgy, Section B: Metallurgy, 48*(2), 273-282.

Hauffe, K., & Vierk, A. L. (1948). Activity measurements in liquid sodium-sodium alloys with wide departure from ideal behavior. *Zeitschrift Fur Elektrochemie und angewandte physikalische Chemie, 53*(3), 151-191.

Hausler, W. (1960). The activity og sodium in molten Sodium zinc alloys at 600 ^{o}C. *Zeitschrift Fuer Metallkunde, 51*, 95.

Heberlein, Max F. W. (1952). Discussion of a paper on the In-Sb system. *Transactions ASM, 44*, 545-548.

Hellner, V. E. (1951). The binary system silver-indium. *Zeitschrift fuer Metallkunde, 42*, 17-19.

Heumann, T., & Alpaut, O. (1964). The phase diagram of In-Sn. *Journal of the Less-common metals, 6*(2), 108-117.

Heycock, C. T., & Neville, F. H. (1897). Complete freezing point curves of binary alloys containing silver or copper. *Philosophical Transactions of the Royal Society A, 189*, 25-69.

Heycock, C. T., & Neville, F. H. (1896). The freezing points of alloys containing Zinc and another metal. *Journal of the Chemical Society, 71*, 383-422.

Heycock, C. T., & Neville, F. H. (1894). The freezing point of triple alloys. *Journal of the Chemical Society, 65*, 65-76.

Heycock, C. T., & Neville, F. H. (1890). The molecular weights of metals when in solution. *Journal of the Chemical Society, 57*, 373-393.

Hillert, M. (2001). Compound energy formalism model, *Journal of Alloys and Compounds, 320*, 161-176.

Hillert, M. (1981). Some viewpoints on the use of a computer for calculating phase diagrams. *Physica B+ C, 103*(1), 31-40.

Hillert, M., & Jarl, M. (1978). A model for alloying in ferromagnetic metals. *CALPHAD: Computer Coupling of Phase Diagrams and Thermochemistry, 2*(3), 227-238.

Hiraga, K., Koiwa, M., & Hirabayashi, M. (1968). Constitution of the indium-rich portion of the indium-magnesium system. *Journal of the Less-common metals, 15*(2), 109-118.

Hirai, K., Somekawa, H., Takigawa, Y., & Higashi, K. (2005). Effects of Ca and Sr addition on mechanical properties of a cast AZ91 magnesium alloy at room and elevated temperature. *Materials Science and Engineering: A, 403*(1), 276-280.

Hoffmann, S. (2002). Darstellung, Struktur und Eigenschaften von Stanniden sowie Tetrelid-Silicaten und Silicaten. Diss., Naturwissenschaften ETH Zürich, Nr. 14941, 2003.

Hollrigl-Rosta, F., Just, E., Kohler, J., & Melzer, H. J. (1980). Magnesium in volkswagen. Paper presented at the 37th annual world conference on magnesium [Proc. Conf.], Salt Lake City, Utah, U. S. A., June 1980.

Hort, N., Huang, Y., Leil, T. A., Maier, P., & Kainer, K. U. (2006). Microstructural investigations of the Mg-Sn-xCa System. *Advanced Engineering Materials, 8*(5), 359-364.

Hsu, C. C., & Saboungi, M. L. (1978). Calculation of isothermal sections of the calcium-lithium-magnesium system. *Zeitschrift fuer Metallkunde, 69*, 581-586.

Huang, G. X., Liu, L. B., Jia, B. R., Zhang, L. G., & Jin, Z. P. (2008). Thermodynamic modeling of the Ca-Ag binary system. *Journal of Alloys and Compounds, 460*, 375-378.

Hubberstey, P., (1972). Thermodynamic properties of solutions of Group IV metals dissolved in liquid sodium. *Journal of The Electrochemical Society, 110*(7), 967-970.

Hubberstey, P., & Pulham, R. J. (1974). Solubility of Sn and Ge in liquid Na. *Journal of the Chemical Society Dalton Transactions, 14*, 1541-1544.

Hultgren, R., Desai, P. D., Hawkins, D. T., Gleiser, M. , & Kelley, K. K. (1973). Selected vaules of the thermodynamic properties of binary alloys *American Society for Metals.* Metals Park, Ohio.

Hume-Rothery, W. (1926). The nature, properties and conditions of formation of intermetallic compounds with special reference to certain compounds of tin. I-V. *Journal Institute of Metals*, 54 pp.

Hume-Rothery, W. (1928). The system sodium-tin. *Journal of Chemical Social Faraday Trans. 1*, 947-963.

Hume-Rothery, W., Mabbot, G. W., & Channel-Evans, K. M. (1934). The freezing points, melting points and solid solubility limits of the alloys of silver and copper with the elements of the sub-groups. *Philosophical Transactions of the Royal Society A, 233*, 1-97.

Hume-Rothery, W., & Butchers, E. (1937). The solubility of silver and gold in solid magnesium. *Journal Institute of Metals, 60*, 345-350.

Hume-Rothery, W., & Raynor, G. V. (1938). The constitution of the magnesiym-rich alloys in the systems Al-Mg, Ga-Mg, In-Mg, and Tl-Mg. *Journal of Institute Metals, 63*, 204-216.

Hume-Rothery, W., & Reynolds, P. W. (1937). The accurate determination of the freezing points of alloys and a study of valency effects in certain alloys of silver. *Proc. Roy. Soc. London A, 160*, 282-303.

Iandelli, A. (1964). MX2-Verbindungen der erdalkali- und seltenen erdmetalle mit gallium, indium und thallium. *Zeitschrift für Anorganische und Allgemeine Chemie, 330*(3-4), 221-234.

Ino, N., Hirabayashi, M., & Ogawa, S. (1965). X-ray and thermal analysis of the ordered-disordered transition in Mg-In alloys. *Transactions of the Japan Institue of Metals, 6*, 172-178.

Itagaki, K., & Yazawa, A. (1968). Measurements of heats of mixing in liquid Ag binary alloys. *Transactions of the Japan Institute of Metals, 32*(12), 1294-1300.

Itoh, M., & Kozuka, Z. (1991). Thermodynamic investigations of liquid Bi-Na and Sn-Na alloys by coulometric titration using beta-alumina. *Journal of materials science, 26*, 5221-5228.

Ivanov, M. I., Berezutski, V. V., & Usenko, N. I. (2009). Mixing enthalpies in Ag-Ca, Ag-Eu and Ag-Yb liquid alloys. *International Journal of Materials Research, 100*(7), 1001-1004.

Iwase, M., Sugino, S., & Ichise, E. (1985). Application of Na$^+$ -ion-conducting b-Al$_2$O$_3$ to thermodynamic studies of liquid sodium-based alloys: xNa+(1-x)Cd, xNa+(1-x)In, xNa+(1-x)Sn. *Journal of Chemical Thermodynamics, 17*, 601-609.

Iwase, M., Yasuda, M. O., & Miki, S. I. (1978). A thermodynamic study of liquid Ag-Sn alloys by means of solid-oxide galvanic cell. *Trans. JIM, 19*, 654-660.

Janz, A., & Schmid-Fetzer, R. (2009). Thermodynamics and constitution of Mg-Al-Ca-Sr-Mn alloys: Part I. Experimental investigation and thermodynamic modeling of subsystems Mg-Ca-Sr and Al-Ca-Sr. *Journal of Phase Equilibria and Diffusion, 30*(2), 146-156.

Jena, A. K., & Bever, M. B. (1968). On the temperature dependence of the heat of formation of the compound AgMg. *Transactions of the metallurgical society of AIME, 242*, 2367-2369.

Jenckel, E., & Roth, L. (1938). The solubility of several metals in Sn and their influence on the recovery temperature. *Zeitschrift fuer Metallkunde, 30*, 135-144.

Jendrzejczyk, D., & Fitzner, K. (2005). Thermodynamic properties of liquid silver-indium alloys determined from EMF measurements. *Thermochimical Acta, 433*, 66-71.

Jin, L. L., Kang, Y. -B., Chartrand, P., & Fuerst, C. D. (2010). Thermodynamic evaluation and optimization of Al-Gd, Al-Tb, Al-Dy, Al-Ho and Al-Er systems using a modified quasichemical model for the liquid. *CALPHAD: Computer Coupling of Phase Diagrams and Thermochemistry, 34*(4), 456-466.

Jin, L. L., Kang, Y. -B., Chartrand, P., & Fuerst, C. D. (2011). Thermodynamic evaluation and optimization of Al-La, Al-Ce, Al-Pr, Al-Nd and Al-Sm systems using the modified quasichemical model for the liquid. *CALPHAD*: *Computer Coupling of Phase Diagrams and Thermochemistry, 35*(1), 30-41.

Jung, I. -H. , Kang, D. H. , Park, W. J., Kim, N. J, & Ahn, S. H. (2007). Thermodynamic modeling of the Mg-Si-Sn system. *CALPHAD: Computer Coupling of Phase Diagrams and Thermochemistry, 31*(2), 192-200.

Jung, W.G. (2005). Activity measurement in liquid Zn-(In,Sn) alloy using EMF method. *Korean Journal of Materials research, 15*(1), 47-54.

Kachi, S. (1955a). Thermodynamic properties of Hume-rothery type Ag-Mg alloys. *Journal of The Japan Institute of Metals, 19*(6), 378-382.

Kachi, S. (1955b). Thermodynamic properties of Hume-rothery type Ag-Mg alloy. *Journal of The Japan Institute of Metals, 19*(6), 318-322.

Kainer, K. U., & Kaiser, F. (2003). Magnesium alloys and technology. Wiley Online Library.

Kameda, K. (1987). Activies of liquid Au-Zn and Ag-Zn binary alloys by EMF measurements using zirconia solid electrolyte cells. *Transactions of the Japan Institute of Metals, 28*(1), 41-47.

Kameda, K., Yoshida, Y., & Sakairi, S. (1980). Thermodynamic properties of liquid Ag-Sn alloys. *Journal of The Japan Institute of Metals, 44*(8), 858-863.

Kameda, K., Yoshida, Y., & Sakairi, S. (1981). Activities of liquid silver-indium alloys by EMF measurements using zirconia solid and fused salt electrolytes. *Transactions of the Japan Institute of Metals, 45*(6), 614-620.

Kanda, Frank A., & Keller, D. V. (1964). Phase equilibria and specific volumes of liquid metals and alloys (pp. 36). Syracuse University.

Kang, D. -H., Park, S. S., Oh, Y. S., & Kim, N. J. (2007). Effect of nano-particles on the creep resistance of Mg-Sn alloys. *Materials Science and Engineering: A, 449-451*, 318-321.

Kang, Y. -B. , Pelton, A. D., Chartrand, P., & Fuerst, C. D. (2008). Critical evaluation and thermodynamic optimization of the Al-Ce, Al-Y, Al-Sc and Mg-Sc binary systems. *CALPHAD: Computer Coupling of Phase Diagrams and Thermochemistry, 32*, 413-422.

Kang, Y. -B., & Pelton, A. D. (2010). Modeling short-range ordering in liquids: The Mg-Al-Sn system. *CALPHAD: Computer Coupling of Phase Diagrams and Thermochemistry, 34*(2), 180-188.

Kaplun, A. B. (1983). Phase transformations near the liquidus temperature in the indium-tin system. Paper presented at the Teplofiz. Svoistva Rastvorov.

Karakaya, I., & Thompson, W. T. (1987). The Ag-Sn system. *Bulletin of Alloy phase diagrams, 8*(4), 340-347.

Karonik, V. V., Kolesnichenko, V. E., Shepelev, A. A., & Kandyba, G. I. (1983). Magnesium-silver-tin phase diagram. *Metalloved. Splavov na Osnove Tsv. Met., M.*, 78-84.

Kattner, U. R. (1997). The thermodynamic modeling of multicomponent phase equilibria. *JOM: Journal of the Minerals, Metals and Materials Society, 49*(12), 14-19.

Kaufman, L, & Bernstein, H. (1970). Computer Calculations of Phase Diagrams. *New York: Academic*.

Kaufman, L., Turchi, P. E. A., Huang, W., & Liu, Z. K. (2002). *CALPHAD: Computer Coupling of Phase Diagrams and Thermochemistry, 25*, 419.

Kawakami, M. (1930). A further investigation of the heat of mixture in molten metals. *Sci. Rep. Res. Inst. Tohoku Univ., 7*, 351-364.

Kienast, G., & Verma, J. (1961). The behavior of the alkali metals toward copper, silver, and gold. *Zeitschrift fuer Anorganische und Allgemeine Chemie, 310*, 143-169.

King, R. C., & Kleppa, O. J. (1964). A thermochemical study of some selected Laves phases. *Acta Metallurgica, 12*, 87-97.

Kinzhibalo, V. (1981). Ternary systems of magnesium with elements of groups IIIA-VA. *Fazovye ranovesiya metallicheskikh splavakh, 6*, 73-78.

Kleinsteuber, T. (1961). The mixing enthalpy of Na and K with B-metals. Doctoral thesis, Ludwig-maximilian university, Munich, Germany.

Kleppa, O. J. (1958). Thermodynamic analysis of binary liquid alloys of Group IIB metals. I. The systems zinc-cadmium, zinc-gallium, zinc-indium, and zinc-tin. *Acta Metallurgica, 6*, 225-232.

Kleppa, O. J. (1956a). A calorimetric investigation of some binary and ternary liquid alloys rich in tin. *Journal of Physical Chemistry B, 60*, 842-846.

Kleppa, O. J. (1956b). Heat of formation of solid and liquid alloys in the systems Ag-Cd, Ag-In and Ag-Sb at 450 ^{o}C. *Journal of Physical Chemistry, 60*, 846-852.

Kleppa, O. J. (1955). A calorimetric investigation of the system Ag-Sn at 450 ^{o}C. *Acta Metallurgica, 3*, 255-259.

Kleppa, O. J., & Thalmayer, C. E. (1959). An EMF investigation of binary liquid alloys rich in Zinc. *Journal of Physical Chemistry, 63*(1953-1958).

Kohler, F. (1960). Estimation of the thermodynamic data for a ternary system from the corresponding binary systems. *Monatsh. Chem., 91*, 738-740.

Kohn, W., & Sham, L. J. (1965). Self-consistent equations including exchange and correlation effects. *Physical Review B, 140*(4A), 1133-1138.

Kojima, Y. (2000). Platform science and technology for advanced magnesium alloys. *Materials Science Forum.* 350-351, 3-18.

Kolesnichenko, V. E., Khatsernov, I. M., & Karonik, V. V. (1989). Phase composition of magnesium-silver-indium-tin alloys in the magnesium-rich region. *Izvestiya Akademii Nauk SSSR, Metally, 2*, 219-221.

Kolesnichenko, V. E., Komapoba, M. A., & kapohhk, B. B. (1982). Study of the magnesium-silver-indium phase diagram. *Izv. Akad. nauk SSSR Neorg. Mater., 5*, 225-229.

Kolesnichenko, V. E., Karonik, V. V., Tsyganova, S. N., Kupriyanova, T. A., & Sysoeva, L. N. (1988). Phase equilibria in the Mg-Ag system in the eta phase region. *Izv. Akad. nauk SSSR Neorg. Mater., 5*, 186-191.

Kopp, H. (1865). Investigations of the specific heat of solid bodies. *Philosophical Transactions of the Royal Society A, 155*, 71-202.

Korhonen, T. M., & Kivilahti, J. K. (1998). Thermodynamics of the Sn-In-Ag solder system. *Journal of Electronic Materials, 27*(3), 149-158.

Kozlov, A., Ohno, M., Arroyave, R., Liu, Z. K., & Schmid-Fetzer, R. (2008). Phase equilibria, thermodynamics and solidification microstructures of Mg-Sn-Ca alloys, Part 1: Experimental investigation and thermodynamic modeling of the ternary Mg-Sn-Ca system. *Intermetallics, 16*(2), 299-315.

Kozlov, A., Ohno, M., Leil, T. A., Hort, N., Kainer, K. U., & Schmid-Fetzer, R. (2008). Phase equilibria, thermodynamics and solidification microstructures of Mg-Sn-Ca alloys, Part 2: Prediction of phase formation in Mg-rich Mg-Sn-Ca cast alloys. *Intermetallics, 16*(2), 316-321.

Kresse, G., & Joubert, D. (1999). From ultrasoft pseudopotentials to the projector augmented-wave method. *Physical Review B, 59(3)*, 1758-1775.

Kresse, G., & Furthmüller, J. (1996a). Efficiency of ab-initio total energy calculations for metals and semiconductors using a plane-wave basis set. *Computational Materials Science, 6*(1), 15-50.

Kresse, G., & Furthmüller, J. (1996b). Efficient iterative schemes for ab initio total-energy calculations using a plane-wave basis set. *Physical Review B, 54*(16), 11169-11186.

Kubaschewski, O., & Seith, W. (1938). Heats of formation of nonferrous alloys. *Zeitschrift fuer Metallkunde, 30*, 7-9.

Kubaschewski, O., & Villa, H. (1949). Heat of formation of binary alkaline earth compounds. *Zeitschrift fur Angewandte Physik und Chemie, 53,* 32-40.

Kulekci, M. K. (2008). Magnesium and its alloys applications in automotive industry. *The International Journal of Advanced Manufacturing Technology, 39*(9-10), 851-865.

Lamprecht, G. J., & Crowther, P. (1969). The systems Na-In and Li-In. *Journal of Inorganic and Nuclear Chemistry, 31*, 925-931.

Lamprecht, G. J. , Crowther, P., & Kemp, D. M. (1967). Solubility of metals in liquid Na. The Na-Sn system. *The journal of Physical Chemistry, 71*(13), 4209-4212.

Lamprecht, G. J., & Crowther, P. (1968). solubility of metals in liquid Na: The systems Na-Ag, Na-Zn and Na-Ce. *Transaction of American Institute of Mining, Metallurgical, and Petroleum Engineers, 242*, 2169-2171.

Lantratov, M. F., Morachevskii, A. G., & Antonova, M. I. (1963). The thermodynamic properties of liquid alloys in the Na-Zn system. *Zhurnal Prikladnoi Khimii, 36*(6), 1278-1283.

Larose, S., & Pelton, A. D. (1991). The In-Na system. *Journal of Phase Equilibria and Diffusion, 12*(3), 371-376.

Laurie, G. H., Morris, A. H., & Pratt, J. N. (1966). Electromotive force and calorimetric studies of thermodynamic properties of solid and liquid Ag-Sn alloys. *Transactions of the metallurgical society of AIME, 236*, 1390-1395.

Lebanov, E. B., Tvaradze, O. O., & Morachevskii, A. G. (1985). Activity of strontium in molten alloys with tin. *Sov. Non-Ferrous Metal Research, 13*(5), 419-421.

Lee, B. -J. (1996). Thermodynamic assessments of the Sn-Zn and In-Zn binary systems. *CALPHAD: Computer Coupling of Phase Diagrams and Thermochemistry, 24*(4), 471-480.

Lee, B. -J., Oh, C. -S., & Shim, J. -H. (1996). Thermodynamic assessments of the Sn-In and Sn-Bi binary systems. *Journal of Electronic Materials, 25*(6), 983-991.

Leil, T. A., Hort, N., Dietzel, W., Blawert, C., Huang, Y., Kainer, K. U., & Rao, K. P. (2009). Microstructure and corrosion behavior of Mg-Sn-Ca alloys after extrusion. *Transactions of Nonferrous Metals Society of China, 19*(1), 40-44.

Leil, T. A., Huang, Y. D., Dieringa, H., Hort, N. , Kainer, K. U. , Buršík, J., Rao, K. P. (2007). Effect of heat treatment on the microstructure and creep behavior of Mg-Sn-Ca alloys. *Materials Science Forum.* 546-549, 69-72

letner, H. R., & Sidhu, S. S. (1947). An x-ray diffraction study of the silver-magnesium alloys system. *Journal of Applied Physics, 18*, 833-837.

Li, H. B., Yao, G. C., Guo, Z. Q., Liu, Y. H., & Ji, H. B. (2006). Microstructure and mechanical properties of Mg-Li alloys with Ca addition. *Acta Metallurgica Sinica, 19*(5), 335-361.

Liang, G. (2004). Synthesis and hydrogen storage properties of Mg-based alloys. *Journal of Alloys and Compounds, 370*(1), 123-128.

Lim, M., Tibballs, J. E., & Rossiter, P. L. (1997). Thermodynamic assessment of Ag-Mg binary system. *Zeitschrift fuer Metallkunde, 88*(2), 160-167.

Liu, X. J., Inohana, Y., Takaku, Y., Ohnuma, I., Kainuma, R., Ishida, K., Pstrus, J. (2002). Experimental determination and thermodynamic calculation of the phase equilibira and surface tension in the Sn-Ag-In system. *Journal of Electronic Materials, 31*(11), 1139-1151.

Liu, Y. J., & Liang, D., (2006). Thermodynamic modeling of the Ag-Sr system. *Journal of Alloys and Compounds, 407*(1), 74-77.

Lorenz, R., & Winzer, R. (1929a). Das zustandsdiagramm calcium-natrium. *Zeitschrift Fur Anorganische Und Allgemeine Chemie, 179*(1), 281-286.

Lorenz, R., & Winzer, R. (1929b). Gleichgewichte zwischen metallen und salzen im schmelzfluß. Nr.17. das gleichgewicht zwischen calcium und natrium mit ihren chloriden. *Zeitschrift Fur Anorganische Und Allgemeine Chemie, 181*(1), 193-202.

Lukas, H. L., Fries, S. G., & Sundman, Bo. (2007). Computational thermodynamics: the CALPHAD method, Cambridge University Press.

Lukas, H. L., Weiss, J., & Henig, E. T. (1982). Straegies for the calculation of phase diagrams. *CALPHAD: Computer Coupling of Phase Diagrams and Thermochemistry, 6*(3), 229-251.

Lupu, C., Mao, J. G., Rabalais, J. W., Guloy, A. M., & Richardson, J. W. (2003). X-ray and neutron diffraction studies on "Li$_{4.4}$Sn". *Inorganic Chemistry, 42*(12), 3765-3771.

Maiorova, E., & Morachevskii, A. G. (1976). Thermodynamic properties of dilute sodium slutions in molten tin. *Zhurnal Prikladnoi Khimii, 49*(11), 2537-2539.

Mantina, M., Wang, Y., Arroyave, R., Chen, L. Q., Liu, Z. K., & Wolverton, C. (2008). First-principles calculation of self-diffusion coefficients. *Physical Review Letters, 100*(21), 215901.

Marshall, D., & Chang, Y. A. (1981). Constitution of the tin-strontium system up to 35 at.% Sr. *Journal of the Less-Common Metals, 78*(1), 139-145.

Masing, G., & Tammann, G. (1910). Bechavior of Li toward Na, K, Sn, Cd, and Mg. *Zeitschrift Fur Anorganische Und Allgemeine Chemie, 67*(2), 193-199.

Masson, D. B., & Sheu, J. L. (1970). Variations in the composition dependence of the activity coefficient in terminal solid solutions of silver-zinc, silver-cadmium, and copper-zinc. *Metallurgical Transactions, 1*(11), 3005-3009.

Masson, D. B., & Pradhan, S. S. (1973). Measurement of vapor pressure of indium over a Ag-In using atomic absorption. *Metallurgical and Materials Transactions A: Physical Metallurgy and Materials Science, 4*(4), 991-995.

Masumoto, T., Inoue, A., Odera, K., & Oguchi, M. (1994). *European Patent No. EP 0339676.* Munich, Germany: European Patent Office.

Mathewson, C. H. (1911). Sodium-silver alloys. *Int. Z. Metallogro., 1*, 51-63.

Mathewson, C. H. (1906). Na-Al, Na-Mg and Na-Zn alloys. *Zeitschrift Fur Anorganische Chemie, 48*, 195-200.

Mathewson, C. H. (1905). Alloys of sodium and tin. *Zeitschrift Fur Anorganische Chemie, 46*, 94-112.

Mckisson, R. L., & Bromley, L. A. (1952). Heats of formation of sodium tin alloys determined with a new high temperature calorimeter. *Transaction of American Institute of Mining, Metallurgical, and Petroleum Engineers 4*(1), 33-38.

Mendis, C. L., Bettles, C. J., Gibson, M. A., Gorsse, S., & Hutchinson, R. (2006). Refinement of precipitate distributions in an age-hardenable Mg-Sn alloy through microalloying. *Philosophical Magazine Letters, 86*(7), 443-456.

Mendis, C. L., Bettles, C. J., Gibson, M. A., & Hutchinson, C. R. (2006). An enhanced age hardening response in Mg-Sn based alloys containing Zn. *Materials Science and Engineering: A, 435-436*(5), 163-717.

Mendis, C. L., Oh-ishi, K., & Hono, K. (2007a). Enhanced age hardening in a Mg-2.4 at. % Zn alloy by trace additions of Ag and Ca. *Scripta Materialia, 57(6)*, 485-488.

Meng, F. G., Wang, J., Liu, L. B., & Jin, Z. P. (2010). Thermodynamic modeling of the Mg-Sn-Zn ternary system. *Journal of Alloys and Compounds, 508*(2), 570-581.

Miki, T., Ogawa, N., Nagasaka, T., & Hino, M. (2003). Activity measurement of the constituents in molten Sn-Ag-In and Sn-Zn-Mg ternary lead free solder alloys by mass spectrometry. *Metallurgical and Materials Processing: Principles and Technologies,* 1(1), 405-415.

Min, D. J., & Sano, N. (1988). Determination of standard free energies of formation of calcium phosphide (Ca_3P_2) and calcium-tin (Ca_2Sn) at high temperatures. *Metallurgical and Materials Transactions B: Process Metallurgy and Materials Processing Science, 19B*, 433-439.

Mingolo, M., Arcondo, B., Nassif, E., & Sirkin, H. (1986). Changes in the glass forming ability of MgZnSn alloys due to the presence of an intermetallic compound. *Zeitschrift fuer Naturforschung A, 41*, 1357-1360.

Monkhorst, H. J., & Pack, J. D. (1976). Special points for Brillouin-zone integrations. *Physical Review B, 13(12)*, 5188-5192.

Moon, K. -W., Boettinger, W. J., Kattner, U. R., Biancaniello, F. S., & Handwerker, C. A. (2000). Experimental and thermodynamic assessment of Sn-Ag-Cu solder alloys. *Journal of Electronic Materials, 29*(10), 1122-1136.

Morachevskii, A. G., Bykova, M. A., & Maiorova, E. A. (1971). Thermodynamic properties of sodium-indium molten alloys. *Zhurnal Prikladnoi Khimii, 44*(10), 2317-2319.

Morachevskii, A. G., & Lantratov, M. F. (1959). Enthalpy of mixing in the system Sodium Tin. *Zhurnal Obshchei Khimii, 29*, 2109-2113.

Morachevskii, A. G., Maiorova, E. A., & Vorobeva, O. I. (1982). Thermodynamic properties of dilute sodium solutions in liquid Zinc. *Elektrokhimiya, 18*(1), 148-150.

Morachevskii, A. G., Gerasimenko, L. N., Demidov, A. I., & Drozdova, O. A. (1972). Thermodynamic properties of molten Li-Sn alloys. *Elektrokhimiya, 8*(11), 1622-1624.

Morozova, M. P., Bol'shakova, G. A., & Lukinykh, N. L. (1959). Enthalpy of formation of compounds of sodium with elements of the main subgroup of Group V. *Zhurnal Obshchei Khimii, 29*, 3144-3145.

Moser, Z. (1974). Thermodynamic studies of the Zn-Sn-In System in dilute liquid solutions. *Zeitschrift fur MetaIlkunde, 65*(2), 106-111.

Moser, Z. (1971). Determination of the thermodynamic properties in Zn-In liquid solutions. *Revue Roumaine de Chimie, 16*, 327-341.

Moser, Z., & Castanet, R. (1979). Thermodynamic studies on liquid Mg-In-Sn ternary solutions (pp. 263-271). INKA-confi.-79-003-023, IAEA-Sm-236/35.

Moser, Z., & Castanet, R. (1979a). EMF and calorimetric measurements on the Mg-In liquid solutions. *Metallurgical and Materials Transactions B: Process Metallurgy and Materials Processing Science, 10*, 483-487.

Moser, Z., & Castanet, R. (1977). EMF and calorimeteric measurements of the Mg-In liquid solutions. *Czech. Conf. Calorimetry, Inst, Inorg. Chem., Czech. Acad. Sci. Prague, A3*, 1-4.

Moser, Z., Gasior, W., Pstrus, J., Zakulski, W., Ohnuma, I., Liu, X.J., Ishida, K. (2001). Studies of the Ag-In phase diagram and surface tension measurements. *Journal of Electronic Materials, 30*(9), 1120-1128.

Moser, Z., Gasior, W., Sommer, E, Schwitzgebel, G., & Predel, B. (1986). Calorimelric and EMF studies on liquid Li-Sn alloys. *Metallurgical and Materials Transactions B: Process Metallurgy and Materials Processing Science, 17*(4), 791-796.

Muller, W., (1974). Preparation and crystal structure of Li_7Sn_3. *Zeitschrift für Naturforschung B, 29*(5-6), 304-307.

Muller, W., & Schiifer, H. (1973). The Crystal Structure of LiSn. *Zeitschrift für Naturforschung B, 28*(5-6), 246-248.

Muller, W., & Volk, K. (1975). Crystal structure of $Na_{3.7}Sn$ or $Na_{17}Sn_4$. *Zeitschrift für Naturforschung B, 30*(7-8), 494-496.

Muller, W., & Volk, K. (1978). Structures of Na_9Sn_4 and $Na_{15}Sn_4$. *Zeitschrift für Naturforschung B, 33*(3), 709-710.

Murphy, A. J. (1926). The constitution of the alloys of silver and tin. *Journal Institute of Metals, 35*, 107-129.

Muthmann, W., Weiss, L., & Metzger, J. (1907). Versuche über darstellung von metallen der seltenen erden und erdsäuren und deren verwendung IV. Ueber calciummetall. *Justus Liebigs Annalen der Chemie, 355*(2), 137-143.

Nagashima, S. (1959). X-ray study of Guinier-preston zones fored in ager magesium-rich, magesium-silver alloys. *Journal of The Japan Institute of Metals, 23*(7), 381-384.

Nakamura, Y., Shimoji, M., & Niwa, K. (1964). Thermodynamic studies on liquid ternary Zn-In-Sn solutions. *Transactions of the Japan Institue of Metals, 5*, 28-32.

Nakaura, Y., Watanabe, A., & Ohori, K. (2006). Effects of Ca, Sr additions on properties of Mg-Al based alloys. *Materials Transactions, 47*(4), 1031.

Nayeb-hashemi, A. A., & Clark, J. B. (1985). The In-Mg system. *Bulletin of Alloy phase diagrams, 6*(2), 149-160.

Nayeb-Hashemi, A. A., & Clark, J. B. (1984). The Ag-Mg system. *Bulletin of Alloy phase diagrams, 5*(4), 348-354.

Nayyeri, G., & Mahmudi, R. (2011). Effects of Ca additions on the microstructural stability and mechanical properties of Mg-5% Sn alloy. *Materials & Design, 32*(3), 1571-1576.

Nebell, H. (1970). Thermodynamic properyies of liquid Mg-Pb, Mg-In and Mg-Ga alloys. *Revue Roumaine de Chimie, 15*, 59-65.

Neething, A. J. (1974) Thermodynamic properties and phase diagram of ternary Na alloys. *S.A.A.E.B. Report (Ed.).* PEL230, Pretoria, Pelindaba. 21.

Ninomiya, R., Ojiro, T., & Kubota, K., (1995). Improved heat resisitance of Mg-Al alloys by the Ca addition. *Acta metallurgica et materialia*, *43(2),* 669-674.

Nishimura, G. S., Fidler, R. S., M., Ronald, T., & William, S. R. (1969). Classification of the indium-zinc eutectic. *Canadian Metallurgical Quarterly, 8*(4), 319-322.

Niu, C. J., Li, C. R., Du, Z. M., Guo, C. P., & Chen, S. C. (2012). A thermodynamic assessment of the Bi-Mg-Sn ternary system. *CALPHAD: Computer Coupling of Phase Diagrams and Thermochemistry, 39*, 37-46.

Notin, M., & Hertz, J. (1981). Potentiometric study of the thermodynamic properties of some Ag-Ca alloys. *Journal of the Less-common metals, 80*(1), 1-8.

Notin, M., Mejbar, J., Bouhajib, A., Charles, J., & Hertz, J. (1995). The thermodynamic properties of Ca intermetallic compounds. *Journal of Alloys and Compounds, 220*, 62-75.

Nozaki, T., Shimoji, M., & Niwa, K. (1966a). Thermodynamic properties of Ag-In liquid phase. *Transactions of the Japan Institute of Metals, 30*(1), 7-10.

Nozaki, T. , Shimoji, M. , & Niwa, K. (1966b). Thermodynamic properties of Ag-Sn and Ag-Sb liquid alloys. *Berichte der bunsen gesellschaft, 70*(2), 207-214.

Oelsen, W., & Zuhlke, E. A. (1956). The calorimetry and thermodynamics of the In-Zn system. *Archiv fuer das Eisenhuettenwesen, 27*, 743-752.

Oh, C. -S., Shim, J. -H., Lee, B. -J., & Lee, D. N. (1996). A thermodynamic study on the Ag-Sb-Sn system. *Journal of Alloys and Compounds, 238*(1), 155-166.

Ohno, M., Kozlov, A., Arroyave, R., Liu, Z. K., & Schmid-Fetzer, R. (2006). Thermodynamic modeling of the Ca-Sn system based on finite temperature quantities from first-principles and experiment. *Acta Materialia, 54*(18), 4939-4951.

Ohtani, H., & Ishida, K. (1998). Application of the CALPHAD method to material design. *Thermochimica Acta, 314*(1-2), 69-77.

Okajima, K., & Sakao, H. (1974). Tie measurements on the activities of the Ag-Sb, Ag-Pb and Ag-Sn molten alloys. *Materials Transactions JIM, 15*, 52-56.

Okamoto, H. (2001). Ca-Sn (Calcium-Tin). *Journal of Phase Equilibria and Diffusion, 22*(5), 589-590.

Orr, L. R., & Hultgren, R. (1961). Heats of formation of α-phase Ag-In alloys. *Journal of Physical Chemistry, 65*(2), 378-380.

Orr, R. L., & Rovel, J. (1962). Thermodynamics of the structural modifications of AgZn. *Acta Metallurgica, 10*(10), 935-939.

Otani, B. (1933). Constitution of the phase equilibrium diagram of the magnesium-zinc-tin system. *Tetsu to Hagane, 19*(7), 566-574.

Owen, E. A., & Edmunds, I. G. (1935). The determination of cetain phase boundaries in the silver-zinc thermal diagram by X-ray analysis. *Journal of the Institute of Metals, 57*(706), 297-306.

Owen, E. A., & Edmunds, I. G. (1938a). Silver-Zinc equilibrium diagram and the structure of the beta phase. *Journal of the Institute of Metals, 63*(291-301).

Owen, E. A., & Edmunds, I. G. (1938b). X-ray study of silver-zinc alloys rich in silver above the beta-transformation temperature. *Journal of the Institute of Metals, 62*(801), 266-278.

Owen, E. A., & Roberts, E. W. (1939). Factors affecting the limit of solubility of elements in copper and silver. *Philosophical Magazine, 27*, 294-327.

Ozisik, H. B., Colakoglu, K., Deligoz, E., & Ozisik, H. (2011). Structural and lattice dynamical properties of Zintl NaIn and NaTl compounds. *Computational Materials Science, 50*(3), 1070-1076.

Padezhnova, E. M., & Guzei, L. S. (1971). Magnesium-based solid solutions in the magnesium-lithium-tin system. *Strukt. Svoistva Legk. Splavov*, 11-16.

Palenzona, A., Manfrinetti, P., & Fornasini, M. L. (2000). Phase diagram of the Ca-Sn system. *Journal of Alloys and Compounds, 312*, 165-171.

Palenzona, A., & Pani, M. (2004). The phase diagram of the Sr-Sn system. *Journal of Alloys and Compounds, 384*(1), 227-230.

Park, S. C., Lim, J. D., Eliezer, D., & Shin, K. S. (2003). Microstructure and mechanical properties of Mg-Zn-Ag Alloys. *Materials Science Forum, 419-422*, 159-164.

Pascal, B., Caillet, M., & Allibert, M. (1970). Differential thermal analysis of the silver-calcium system in the calcium-rich region. *Comptes Rendus des Seances de l'Academie des Sciences, Serie C: Sciences Chimiques, 270*(6), 520-522.

Pastorello, S. (1930). Rovrddotontgenographic analysis of the system: lithium-silver. *Gazzetta Chimica Italiana, 60*, 493.

Payne, R. J. M., & Haughton, J. L. (1937). Alloys of magnesium. Part IV the constitution of the magnesium-rich alloys of Mg and Ag. *Journal Institute of Metals, 60*, 351-363.

Pelton, A. D., Degterov, S. A., Eriksson, G., Robelin, C., & Dessureault, Y. (2000). The modified quasichemical model I: binary solution. *Metallurgical and Materials Transactions B: Process Metallurgy and Materials Processing Science, 31*, 651-659.

Pelton, A. D. (2001). A general "geometric" thermodynamic model for multicomponent solutions. *CALPHAD: Computer Coupling of Phase Diagrams and Thermochemistry, 25*(2), 319-328.

Pelton, A. D. (1986). The Au-Na system. *Bulletin of Alloy phase diagrams, 7(2),* 136-139.

Pelton, A. D. (1986a). The Ag-Li system. *Bulletin of Alloy phase diagrams, 7*(3), 223-228.

Pelton, A. D. (1986b). The Ag-Na system. *Bulletin of Alloy phase diagrams, 7(2)*, 133-136.

Pleton, A. D. (1986c). The Na-Cu system. *Bulletin of Alloy phase diagrams, 7(1),* 25-27.

Pelton, A. D. (1985). The Ca-Na (Calcium-Sodium) system. *Journal of Phase Equilibria and Diffusion, 6*(1), 35-37.

Pelton, A. D. (1984). The Mg-Na system*, Bulletin of Alloy phase diagrams, 5(5)*, 454-456.

Pelton, A. D., & Chartrand, P. (2001). The modified quasi-chemical model: Part II. multicomponent solutions. *Metallurgical and Materials Transactions A: Physical Metallurgy and Materials Science, 32*(6), 1355-1360.

Perdew, J. P., & Wang, Y. (1992). Accurate and simple analytic representation of the electron-gas correlation energy. *Physical Review B, 45*(23), 13244-13249.

Perdew, John P., Burke, K., & Ernzerhof, M. (1996). Generalized gradient approximation made simple. *Physical Review Letters, 77*(18), 3865-3868.

Peternko, G. J. (1907). On the alloying of silver with lead and tin. *Zeitschrift Fur Anorganische Und Allgemeine Chemie, 56*, 20-22.

Petrenko, G. J. (1906). Over zinc silver alloys. *Zeitschrift für anorganische und allgemeine Chemie, 48*, 347-363.

Petrenko, G. J., & Petrenko, B. G. (1930). Zur frage des aufbaus der γ-Phase in den legierungen Ag-Zn. *Zeitschrift für anorganische und allgemeine Chemie, 185*(1), 96-100.

Pickwick, K. M., Alexander, W. A., & Gamble, E. H. (1969). The constitution of In-Mg alloys containing 23-100 atomic pre cent Indium. *Canadian Journal of chemistry, 47*, 3417-3427.

Pokrovskii, N. L., & Smirnova, T. G. (1961). Effects of additions of Na and Zn on the structure and microhardness of Sn. *Phys. Met. Metallog. USSR, 12*(5), 751-780.

Polmear, I. J. (1994). Magnesium alloys and applications. *Materials Science and Technology, 10*(1), 1-16.

Potard, C., Schaub, B., & Desre, P. (1970). Thermodynamical activity of calcium in liquid tin-calcium and beryllium-calcium alloys, *Nuclear Science Abstract*, *24(16),* 32437

Predel, B., & Godecke, T. (1975). Das dreistoffsystem zinn-indium-thallium. *Zeitschrift fuer Metallkunde, 66*, 654.

Predel, B., Oehme, G., & Vogelbein, W. (1978). Calorimetric studies of solid and liquid Ag-Li-Pb alloys. *Zeitschrift fuer Metallkunde, 69*, 163-166.

Prezdziecka-Mycielska, E., Terpilowski, J., & Strozecka, K. (1963). Thermodynamic properties of liquid metallic solutions. XI. The Ag-In system. *Archiwum hutnictwa, 2*, 85-101.

Prokof'ev, M. V., Kolesnichenko, V. E., & Karonik, V. V. (1985). Composition and structure of the Mg--Ag system in the vicinity of Mg_3Ag. *Izv. Akad. Nauk SSSR, Neorg. Mater.*, *8*(21), 1332-1334.

Puschin, N. (1908). Das potential die chemiusche konstitution der metalllegierunge. *Zeitschrift Fur Anorganische Und Allgemeine Chemie, 56*, 1-45.

Qi, G. J., Mitsuhisa, H., & Takeshi, A. (1989). Thermodynamic study of liquid silver-indium and silver-gallium alloys with a Knudsen cell-mass spectrometer. *Materials Transactions, JIM, 30*(8), 575-582.

Quercigh, E. (1910). On the equilibria diagram of Ag-Na alloys. *Zeitschrift Fur Anorganische Und Allgemeine Chemie, 68*, 301-306.

Rais, A., Cusack, N. E., & Neale, F. E. (1982). Simultaneous measurement of resistivity and thermodynamic properties of liquid binary alloys application to Na-In, Na-Sn. *Journal of Physics F: Metal Physics, 12*, 1091-1100.

Rakotomavo, J., Gaune-Escard, M., Bros, J. P., & Gaune, P. (1974). Enthalpies of formation at 1373 K of the liquid alloys Ag-Au, Ag-Sn,and Ag-Au-Sn. *Ber. Bunssenges., 88*, 663-670.

Rao, K. P., Prasad, Y., Hort, N., & Kainer, K. (2008). Hot workability characteristics of cast and homogenized Mg-3Sn-1Ca alloy. *Journal of Materials Processing Technology, 201*(1), 359-363.

Ray, K. W. (1930). Properties of strontium-tin Alloys. *Industrial & Engineering Chemistry, 22*(5), 519-522.

Raynor, G. V. (1948). The constitution of the In-Mg alloys in the region 20 to 50 atomic precent of In. *Transactions of the faraday society, 44*, 15-28.

Raynor, G. V., & Frost, B. R. T. (1949). The system Ag-Mg-Sn with reference to the theory of ternary alloys. *Journal Institute of Metals, 75*, 777-808.

Rechchach, M. , Sabbar, A. , Flandorfer, H. , & Ipser, H. (2010). Enthalpies of mixing of liquid In-Sn and In-Sn-Zn alloys *Thermochimica Acta, 502*(1-2), 66-72.

Rhines, F. N., & Grobe, A. (1944). Constitution of the system In-Zn. *Transactions of the metallurgical society of AIME, 156*, 253-262.

Rinck, A., Kaempf, E., & Steinmann, A. (1931). Zur direkten Berechnung des Saccharose- und Milchzuckergehaltes in Milchschokoladen. *Zeitschrift fur Analytische Chemie, 83*(1-2), 67-70.

Rivier, M., & Pelton, A. D. (1978). Thermodynamic properties of liquid Sn-Na alloys by EMF measurements with beta alumina electrolytes. *Journal of The Electrochemical Society, 125*(9), 1377-1382.

Robinson, P. M., & Bever, M. B. (1964). The heat of formation of the intermetallic compound AgMg as a function of composition. *Transactions of the metallurgical society of AIME, 230*, 1487-1488.

Roozeboom, H. W. B., & Ramser, H. (1900). The Heterogeneous Equilibria from the Standpoint of the Phase Rule (book); Translated from the German by H. Ramser, 546 pp..

Sabbar, A., Zrineh, A., Gambino, M., Bros, J. P., & Arcondo, B. (2001). Contribution a l'etude du diagramme d'equilibre des phases du systeme ternaire indium-etain-zinc. *Thermochimica Acta, 369(1-2)*, 125-136.

Saboungi, M. L., & Corbin, T. P. (1984). Dilute solution of sodium in molted bismuth and tin: EMF measurement and interpretation. *Journal of Physics F: Metal Physics, 14*, 13-21.

Sangster, J. , & Bale, C. W. (1998a). The Li-Sn system. *Journal of Phase Equilibria and Diffusion, 19*(1), 70-75.

Sangster, J. , & Bale, C. W. (1998b). The Na-Sn system. *Journal of Phase Equilibria and Diffusion, 19*(1), 76-80.

Sasaki, T. T., Oh-ishi, K., Ohkubo, T., & Hono, K. (2006). Enhanced age hardening response by the addition of Zn in Mg-Sn alloys. *Scripta Materialia, 55*(3), 251-254.

Satow, T., Uemura, O., & Yamakawa, S. (1973). X-ray diffraction and electrical resistivity study of silver-indium (Ag_2In) and high temperature Ag_3In phases. *Transactions of the Japan Institute of Metals, 15*(4), 253-255.

Saunders, N. (1990). A review and thermodynamic assessment of the Al-Mg and Mg-Li Systems. *CALPHAD: Computer Coupling of Phase Diagrams and Thermochemistry, 14*(1), 61-70.

Saunders, N., & Miodownik, A. P. (1998). *CALPHAD (Calculation of Phase Diagrams): A Comprehensive Guide* (Vol. 1): Pergamon.

Scatchard, G., & Westlund, R. A. (1953). Equilibrium of solid α-silver-zinc alloys with zinc vapor. *Journal of the American Chemical Society, 75*, 4189-4193.

Scheil, E. (1942). Bemerkungen zur schichtkristallbildung. *Zeitschrift für Metallkunde*, *34*(3), 70-72.

Schneider, A., & Schmid, H. (1942). Metal vapor pressures. III. The vapor pressures of Zn and Cd over their binary alloys with Cu, Ag and Au. *Zeitschrift fuer Elektrochemie und Angewandte Physikalische Chemie, 48*(11), 627-639.

Sevov, S. C., & Corbett, J. D. (1993). Synethesis, characterization, and bonding of Indium cluster phases: $Na_{15}In_{27.4}$, Na_2In. *Journal of solid state chemistry, 103*, 114-130.

Shao, Y.W., Huang, H., Zhang, T., Meng, G. Z., & Wang, F. H. (2009). Corrosion protection of Mg-5Li alloy with epoxy coatings containing polyaniline. *Corrosion Science 51*, 2906-2915.

Sharma, A. K., Rain, R. U., Bhojaraj, H., & Narayanamurthy, H. (1993). *Journal of Applied Electrochemistry, 23*, 500-507.

Sharma, A. K., Rain, R. U., & Mayanna, S. M. (2001). Thermal studies on electrodeposited black oxide coating on magnesium alloys. *Thermochimical Acta, 376*, 67-75.

Shi, Z. Z., & Zhang, W. Z. (2013). Enhanced age-hardening response and microstructure study of an Ag-modified Mg-Sn-Zn based alloy. *Philosophical Magazine Letters*, 1-8.

Singh, R. N., & Sommer, F. (1992). Temperature dependence of the thermodynamic functions of strongley interacting liquid alloys. *Journal of Physics: Condensed Matter, 4*, 5345-5358.

Sirkin, H., Mingolo, N., Nassif, E., & Arcondo, B. (1987). Increase of the glass-forming composition range of Mg-based binary alloys by addition of tin. *Journal of Non-Crystalline Solids, 93*, 323-330.

Slaby, H., & Terpilowski, J. (1965). Thermodynamic properties of liquid Mg-In solutions. *Bull. Acad. Polon. Sco., XIII*, 319-322.

Smith, J. F., & Moser, Z. (1975). Thermodynamic properties of binary Li systems. *Journal of Nuclear Materials, 95*(2), 158-174.

Sommer, E., Fischer, B., & Predel, B. (Eds.), (1982). *Determination of the Formarion Enthalpies of Na Alloys o f Li with In, Tl, Sn, Pb and Bi* (Vol. 395-400). New York: Plenum Press.

Son, H. T., Kim, D. G., & Park, J. S. (2011). Effects of Ag addition on microstructures and mechanical properties of Mg-6Zn-2Sn-0.4Mn-based alloy system. *Materials Letters, 65*(19-20), 3150-3153.

Spencer, P. J. (2006). Mg-Li system. *Thermodynamic database*, CRCT (Ed.). Montreal.

Spencer, P. J., Pelton, A. D., Kang, Y. -B., Chartrand, P., & Fuerst, C. D. (2008). Thermodynamic assessment of the Ca-Zn, Sr-Zn, Y-Zn and Ce-Zn systems. *CALPHAD: Computer Coupling of Phase Diagrams and Thermochemistry, 32*(2), 423-431.

Straalsund, J. L., & Masson, B. (1968). Influence of the density of states on the thermodynamic acitivity of zinc in the epsilon phase of the silver-zinc system. *Transactions of the American Institute of Mining, Metallurgical and Petroleum Engineers, 242*(2), 190-195.

Sudavtsova, V. S., & Batalin, G. I. (1988). Thermodynamic properties of binary melts of the systems calcium-silicon (tin). *Izv. Akad. Nauk SSSR, Neorg. Mater., 24*, 1578-1580.

Sviderskaya, Z. A., Padezhnova, E. M., & Guzei, L. S. (1972). Phase diagram of the magnesium-lithium-tin system in the magnesium-rich region. *Metalloved. Tsvet. Metal. Splavov*, 48-52.

Svirbely, W.T., & Selis, S. M. (1953). A thermodynamic study of the Zn-In system. *Journal of the American Chemical Society, 75*, 1532-1535.

Tamaki, S., Ishiguro, T., & Takeda, S. (1982). Thermodynamic properties of liquid Na-Sn alloys. *Journal of Physics F: Metal Physics, 12*, 1613-1624.

Terpilowski, J., & Prezdziecka-Mycielska, E. (1960). Thermodynamic properties of liquid metallic solutions. IV. The system In-Sb. *Archiv Hutnictwa, 5*, 281-290.

Terpilowski, J., & Slaby, H. (1967). Thermodynamic properties of liquid Mg-In solutions. *Roczniki, Chem. Ann. Soc. Chim. Polon, 41*, 1845-1855.

Teslyuk, M. Y., Mel'nik, E. V., Malinkovich, A. N., & Mitrofanova, M. F. (1969). Magnesium-lithium-tin ternary system in the 0-50 atom percent tin region, *Visnik L'vivs'kogo Derzhavnogo Universitetu, Seriya Khimichna, 11*, 25-30.

Thummel, R., & Klemm, W. (1970). The Behavior of alkali metals towards metals of group IIIB. *Zeitschrift Fur Anorganische Und Allgemeine Chemie, 376*, 44-63.

Toop, G. W. (1965). Predicting ternary activities using binary data. *Trans. TMS-AIME, 223*, 850-855.

Trzebiartowski, W., & Terpilowski, J. (1955). Thermodynamic properties of the Ag-Zn system and the related beta-AgMg phase. *Bull. Acad. Polon. Sci. Tech. Sco, 3*(7), 391-395.

Tung, H. K. K., Lai, D. C. F., Wong, M., & Stephen, N. G. (2012). Newton–Raphson method. *Professional Financial Computing Using Excel and VBA*, 59-66.

Uemura, O., & Satow, I. (1973). Order-disorder transition of silver-indium (Ag_3In) alloy *Transactions of the Japan Institute of Metals, 14*(3), 199-201.

Umansky, M. M. (1940). Diagram of stte of the alloy silver-tin. *Zhurnal Fizicheskoi Khimii, 14*, 846-849.

Underwood, E. E., & Averbach, B. L. (1951). Vapor pressures of zinc over silver-zinc alloys. *Journal of Metals, 3*, 1198-1202.

Valentiner, V. S. (1943). On the In-Zn and In-Cd system. *Zeitschrift fuer Metallkunde, 35*, 250-253.

Van der Marel, C., Van Oosten, A. B., Geertsma, W., & Van der Lugt, W. (1982). The electrical resistivity of liquid lithium-tin, sodium-tin, and sodium-lead alloys: Strong effects of chemical interactions. *Journal of Physics: F Metal Physics, 12*, 2349-2361.

Van der Planken, K. (1969). Solution hardening of lead single crystals at liquid air temperature. *Journal of Materials Science, 4(6)*, 499-508.

Vassilev, G., Dobrev, E. S., & Tedenac, J. C. (2005). Experimental study of the Ag-Sn-In phase diagram. *Journal of Alloys and Compounds, 399*, 118-125.

Vassiliev, V., Feutelais, Y., Sghaier, M., & Legendre, B. (1998). Liquid state electrochemical study of the system In-Sn. *Thermochimica Acta, 315*, 129-134.

Villars, P, & Cenzual, K., (2007). Pearson's crystal data, crystal structure database for inorganic compounds. *Materials Park (OH): ASM International*.

Vnuk, F., Ainsley, M. H., & Smith, R. W. (1981). The solid solubility of silver, gold and zinc in metallic tin *Journal of Material science 16*(5), 1171-1176.

Wang, J., Jung, I. H., Chartrand, P., & Medraj, M. (2013). Experimental and thermodynamic studying on Mg-Sn-In-Zn system. *Journal of Alloys and Compounds (accepted)*.

Wang, P. S., Du, Y., & Liu, S. H. (2011). Thermodynamic optimization of the Li-Mg and Al-Li-Mg systems. *CALPHAD: Computer Coupling of Phase Diagrams and Thermochemistry, 35*(4), 523-532.

Wasiur-Rahman, S., & Medraj, M. (2009). Critical assessment and thermodynamic modeling of the binary Mg-Zn, Ca-Zn and ternary Mg-Ca-Zn systems. *Intermetallics, 17*(10), 847-864.

Watanabe, Y. (1975). Consititution og the Mg-In system near the composition of Mg_3In and phase transition of beta1 phase. *Acta Metallurgica, 23*, 691-696.

Weeks, J. R. (1969). Liquidus of the Na-Ag system: 0 to 6 at. % Ag. *Trans. ASM, 62*, 304.

Weibke, F., & Eggers, H. (1935). The composition diagram of the system silver-indium *Zeitschrift Fur Anorganische Und Allgemeine Chemie, 222*, 145.

Wen, C. J., & Huggins, R. A. (1981). Thermoodynamic study of the Li-Sn System. *Journal of The Electrochemical Society, 128*(6), 1181-1187.

Widera, A., & Schäfer, H. (1981). Das Zustandsdiagramm Sr-Sn und die verbindung $Sr_3 SnO$. *Journal of the Less-common Metals, 77*(1), 29-36.

Willars, P. (1997). Pearson's handbook desk edition. Materials park, OH: ASM international.

Wilson, C. L., & Peretti, E. A. (1936). Zn-In alloy system. *Ind. Eng. Chem. Process des. Develop., 26*, 204-205.

Wittig, F. E., & Huber, F. (1959). Energetics of metallic systems. XII. The heats of formation in the system silver-zinc at 475°C. *Zeitschrift fuer Elektrochemie und Angewandte Physikalische Chemie, 63*(8), 994-1001.

Wittig, F. E., & Muller, E. (1960). The heats of mixing of the binary liquid systems of Znic and cadmium with indium and thallium. *Zeitschrift fuer Metallkunde, 51*, 226-238.

Wittig, F. E., & Scheidt, P. (1961). Energetics of metallic systems. XIV. Heats of mixing in the binary systems of indium and thallium with tin and lead. *Zeitschrift fuer Physikalische Chemie, 28*, 120-142.

Wojtaszek, Z., & Kuzyk, H. (1974). Phase digram of the In-Sn system in the range 60-100 atomic % tin. *Zeszyty Naukowe Uniwersytety Jagiellonskiego, Prace Chemiczne, 19*, 281-287.

Wojtaszek, Z., & Kuzyk, H. (1976). Phase digram of the In-Sn system in the range 0-60 atomic per cent of tin. *Zeszyty Naukowe Uniwersytety Jagiellonskiego, Prace Chemiczne, 21*, 27-32.

Wolfson, M. R. (1956). Phase relations of the calcium-lithium system. *Trans. Am. Soc. Met., Preprint No. 44*, 10 pp.

Xie, Y., Qiao, Z. Y., & Mikula, A. (2001). The Sn-In-Zn system. *CALPHAD: Computer Coupling of Phase Diagrams and Thermochemistry, 25*(1), 3-10.

Xie, Y., Schicketanz, H., & Mikura, A. (1998). The In-Sn-Zn system. *Berichte der Bunsen-Gesellschaft für Physikalische Chemie, 102*(9), 1334-1338.

Yamaji, T., & Kato, E. (1972). Mass spectrometric study of the thermodynamic properties of the Ag-Sn system. *Metallurgical and Materials Transactions B, 3*(4), 1002-1004.

Yang, M. B., Pan, F. S., Li, H. L., Guo, T. C., Qin, C. Y., Li, H., Zhou, T. (2012). CN102392151A.

Yang, Y. W., Shi, D. M., Wen, B., Melnik, R., Yao, S., & Li, T. J. (2010). First-principle studies of Ca-X (X=Si, Ge, Sn, Pb) intermetallic compounds. *Journal of Solid State Chemistry, 183*(1), 136-143.

Yanko, J. A., Drake, A. E., & Hovorka, F. (1946). Thermodynamic studies of dilute solutions in molten binary alloys. *Transaction electrochemical socity, 89*(1), 357-372.

Yatsenko, S. E., & Saltykova, E. A. (1979). Thermodynamic properties of alloys of the Li-Sn System. *Khim. Thermodin. Termokhim.*, 190-191.

Yazawa, A. , & Gubcova, A. (1970). Thermodynamic studies of liquid Au-Zn and Ag-Zn system. *Transaction of American Institute of Mining, Metallurgical, and Petroleum Engineers, 11*, 419-423.

Yazawa, A., Kawashima, T., & Itagaki, K. (1968). Measurements of heats of mixing in molten alloys with the adiabatic calorimeter. *Nippon Kinzoku Gakkaishi, 32*(12), 1281-1287.

Yin, F. C., Su, X. P., Li, Z., & Wang, J. H. (2005). Thermodynamic assessment of the Li–Sn (Lithium–Tin) system. *Journal of Alloys and Compounds, 393*, 105-108.

Yoon, S. W., Soh, J. R., Lee, H. M., & Lee, B. -J. (1997). Thermodynamics-aided alloy design and evaluation of Pb-free solder, SnBiInZn system. *Acta Materialia, 45*(3), 951-960.

Yoon, S. W., Soh, J. R., Lee, B. -J., & Lee, H. M. (Eds.). (1997). *Design and reliability of solders and solders interconnections*: The Mineral, Metals and Materials Society.

Ypma, T. J. (1995). Historical development of the Newton-Raphson method. *SIAM Review, 37*(4), 531-551.

Yuan, D., & Kroger, F. A. (1969). The sodium activity in liquid sodium tin alloys. *The journal of Physical Chemistry, 73*(7), 2390-2492.

Zakulski, W. , Moser, Z. , & Sommer, F. (1997). Thermodynamic study of liquid Mg-In-Sn alloys. *Journal of Phase Equilibria and Diffusion, 18*(2), 122-127.

Zamotorin, M. I. (1938). The equilibrium diagram of calcium-lithium alloys. *Metallurg (Leningrad), 13*, 96-99.

Zemczuznyj, S. F. (1906). On the alloys of Magnesium with silver. *Zeitschrift Fur Anorganische Und Allgemeine Chemie, 49*, 400-411.

Zhang, S. J., Shin, D. W., & Liu, Z. K. (2003). Thermodynamic modeling of the Ca-Li-Na system. *CALPHAD: Computer Coupling of Phase Diagrams and Thermochemistry, 27*(2), 235-241.

Zhao, J. –C., Bewlay, B. P., Jackson, M. R., & Peluso, L. A. (2001). Structural Intermetallics 2001 TMS, Warrendale PA.

Zhao, J. R., Du, Y., Zhang, L. J., Wang, A. J., Zhou, L. C., Zhao, D. D., & Liang, J. L. (2011). Thermodynamic assessment of the Sn-Sr system supported by first-principles calculations. *Thermochimica Acta, 529*, 74-79.

Zhong, Y., Sofo, J. O., Luo, A. A., & Liu, Z. K. (2006). Thermodynamics modeling of the Mg-Sr and Ca-Mg-Sr systems. *Journal of Alloys and Compounds, 421*(1), 172-178.

Zintl, E., & Haucke, W. (1937). Constitution of the metallic phases $NaZn_{13}$, KZn_{13}, KCd_{13} and $CsCd_{13}$. *Acta crystallographica, 5*, 637-644.

Zivkovic, D., Milosavljevic, A., Mitovski, A., & Marjanovic, B. (2007). Comparative thermodynamic study and characterization of ternary Ag-In-Sn alloys. *Journal of Thermal Analysis and Calorimetry, 89*(1), 137-142.

Zivkovic, D., Mitovski, A., Balanovic, L., manasujevic, D., & Zivkovic, Z. (2010). Thermodynamic analysis of liquid In-Sn alloys using Oelsen calorimetry. *Journal of Thermal Analysis and Calorimetry, 102*, 827-830.

Zurcher, R., Nesper, R., Hoffmann, S., & Fassler, T. F. (2001). Novel Arachno-type X56-Zintl anions in Sr_3Sn_5, Ba_3Sn_5, and Ba_3Pb_5 and charge influence on Zintl. *Zeitschrift Fur Anorganische Und Allgemeine Chemie, 627*(9), 2211-2219.

APPENDIX 1 EXPERIMENTAL STUDY ON PHASE EQUILIBRIA OF MG-ZN-SR SYSTEM AND ITS APPLICATION FOR METALLIC GLASS

1. Introduction

Strontium, acting as an important additive in Mg-based alloys for improving high-T mechanical properties, has drawn much attention in recent years. Ca which is in part detrimental due to hot-cracking effects (Hollrigl-Rosta, et al., 1980), can be combined with Sr additions to help to reduce the hot-cracking effect of Ca. Baril et al. reported that (Baril, et al., 2003) the micro-alloying element of strontium in magnesium alloys (e.g. Mg–Al based alloys) displays superior creep performances and excellent high-temperature properties. Hirai et al. (Hirai, et al., 2005) reported that a cast AZ91 magnesium alloy having excellent mechanical properties (as high strength, high creep resistance) was developed by additional elements Sr.

In order to understand the alloying effects of Zn and Sr in the Mg-based alloys on the improvement of mechanical properties, a comprehensive study of the phase equilibria in the Mg-Zn-Sr ternary is necessary. The phase equilibria in the composition range from 0 to 33 Sr at. % was measured with EPMA, EDS, DSC, and X-ray techniques, and a thermodynamic optimization of the ternary Mg-Zn-Sr system was carried out in the present work.

Amorphous Mg-based alloys become a hot topic because of their high strength, good anti-corrosion properties, *etc* (Wang, et al., 2011; Yang, 2009). Since Calka et al. (Calka, et al., 1977) got the first Mg-based amorphous alloys with a rapid cooling method (Mg + 20-30 wt. % Zn) in 1977, the Mg-Zn based metallic glasses have been found to have good biological properties for use as bone replacement and other medical devices (He, et al., 2010; He et al., 2009; Sun, et al., 2012). Recently, Mg-Zn-Sr alloys were found to have a low degradation rate and moderate mechanical properties which makes them potential biodegradable alloy candidates (Brar, et al., 2012). Consequently, the investigation of the glass formablity of Mg-Zn-Sr alloys shall be of interest for the development of metallic glasses with good mechanical properties. In the present work, the phase equilibria of Mg-Zn-Sr ternary system at 300 ^{o}C was measured first, and a thermodynamic optimization on Mg-Zn-Sr ternary system was carried out. Finally, the glass formablity of selected Mg-Zn-Sr alloys were studied according to the prediction from present thermodynamic optimized results.

2. Literature review

The phase diagrams of the Mg-Sr (Chartrand, & Pelton 1994), Mg-Zn (Spencer, 2006) and Zn-Sr (Spencer, et al., 2008) binary systems have been critically evaluated and parameters of their thermodynamic models have been optimized previously using the MQMPA for the liquid solutions. In the present work, all the binary thermodynamic parameters were taken from their work in the present optimization of the Mg-Zn-Sr ternary system. The calculated Mg-Sr, Mg-Zn and Zn-Sr binary systems with the parameters from the previous work (Chartrand, & Pelton 1994; Spencer, 2006; Spencer, et al., 2008) are shown in Fig. A1.1. There is no reported experimental information on phase equilibria and glass forming ability of Mg-Zn-Sr alloys.
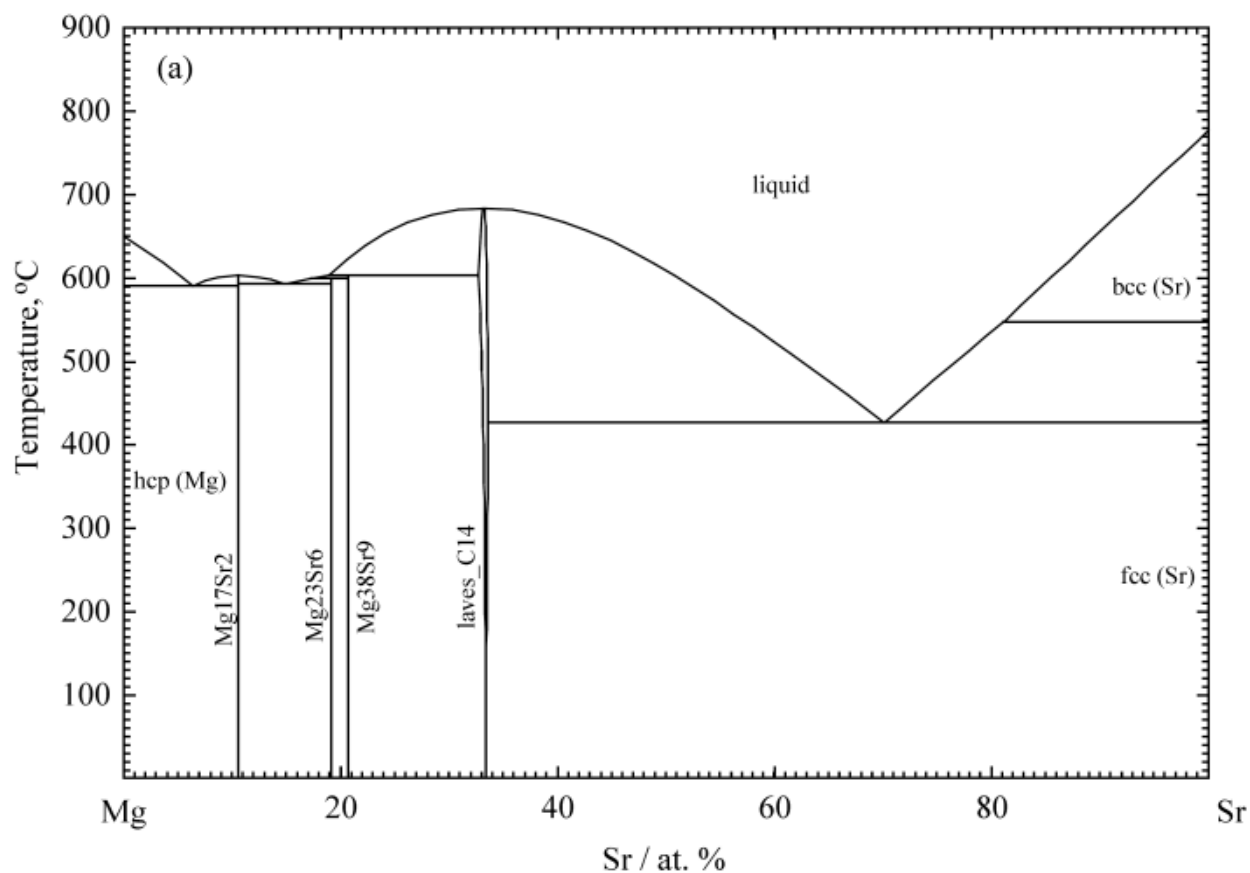
Figure A1.1 Calculated (a) Mg-Sr, (b) Mg-Zn and (c) Zn-Sr binary systems with the parameters from previous work (Chartrand, & Pelton 1994; Spencer, 2006; Spencer, et al., 2008)
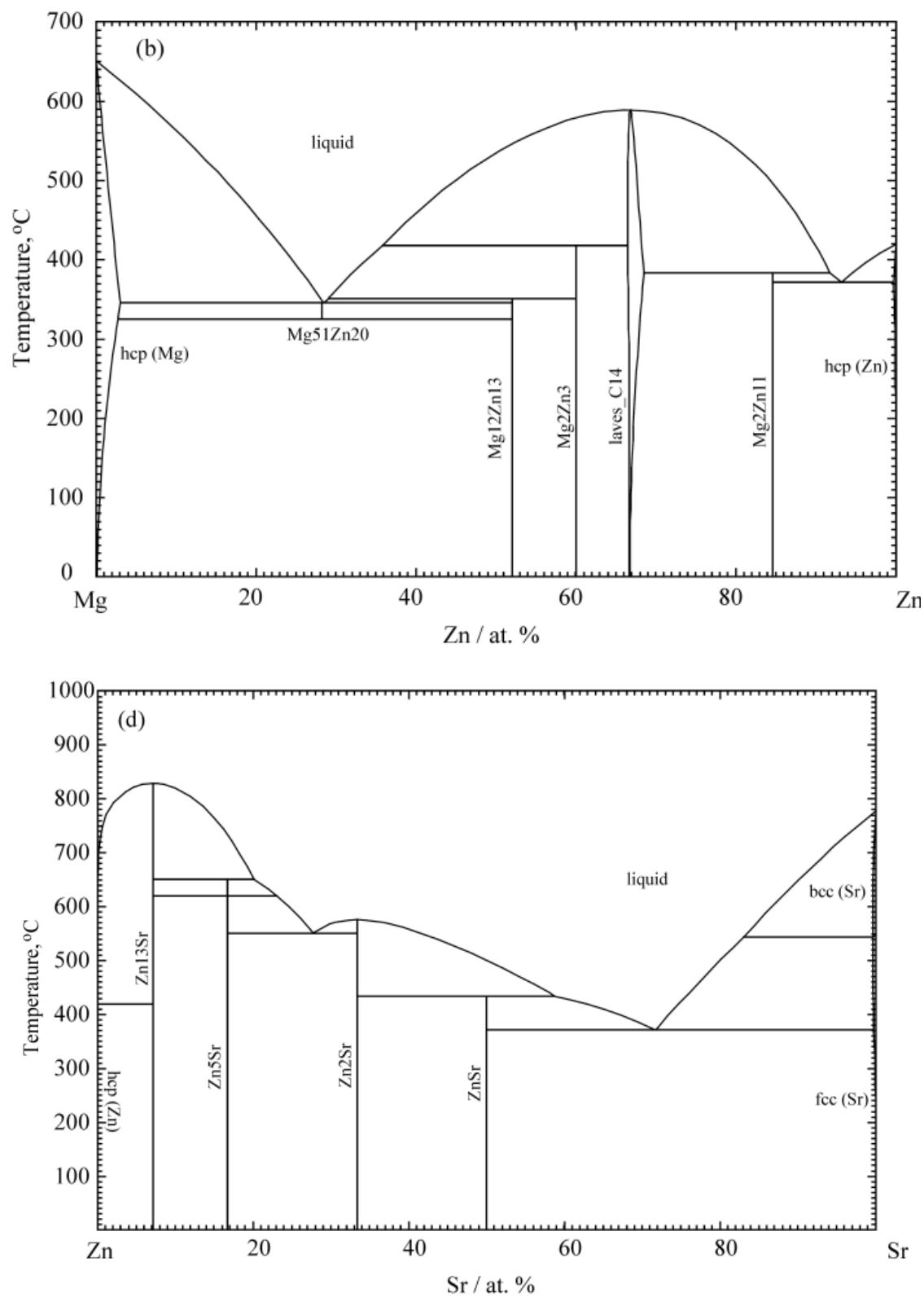
Figure A1.1 (Conntinued) Calculated (a) Mg-Sr, (b) Mg-Zn and (c) Zn-Sr binary phase diagrams from Spencer et al. (Spencer, et al., 2008)

3. Experiment procedure

The starting materials are high-purity Mg ingot of 99.8%, Sr ingot with a purity of 99%, and Zn pieces with a purity of 99.99%. The purity of the Ta foil used for protecting the samples is 99.5 % (with 0.15 mm thickness). All investigated samples were prepared in an induction furnace. Before melting, all the pure metals were washed with diluted hydrochloric acid (~1% HCl) for removing the oxidation layer, and then were flushed with acetone. All the samples were melted in a cubic shaped Ta foil crucible under an argon atmosphere and re-melted at least 3 times to get a good homogeneity. The melting losses of the elements with high vapor pressures were been estimated during the samples weighting, and the melting losses were controlled at less than 5 wt. % for each sample. After melting, key samples were cut into several pieces, and sealed into quartz tubes wrapped in Ta foils under argon protection gas. The sealed samples were put into heat furnaces at 300^oC for 30 days for annealing. All the samples were quenched into cold water with the quartz tube after the end of the annealing period.

The microstructure and phase composition of Mg-Zn-Sr samples were analyzed using Diffusion couples and key samples have been experimentally investigated using SEM (Scanning Electron Microscopy), Electron Probe Microanalysis (EPMA) with Wavelength Dispersive X-Ray Spectrometry (WDS), Electron Backscattered Diffraction (EBSD), X-ray Diffraction (XRD) as well as Transmission Electron Microscopy (TEM). The error limits of the EPMA measurement is estimated to be about ±3 at. %, and of the EDS is about ±5 at. %. X-ray diffraction is used for phase analysis and determination of the solubility limits in the key alloys. The XRD patterns are obtained using PANanalytical Xpert Pro powder X-ray diffractometer with a CuKα radiation at 45kV and 40mA. The XRD spectrum is acquired from 20 to 120º 2θ with a 0.02º step size. X-ray diffraction study of the samples is carried out using X'Pert HighScore Plus Rietveld analysis software in combination with Pearson's crystal database.

10 key samples were prepared with the same methods as phase equilibira measurements process, and then each of these samples were crushed into apropriate size for single-roller melt-spinning (Masumoto, et al., 1994). The melt-spinning process was carried out under high purity helium protection atmosphere with a wheel tangential speed of 50 m/s.

The XRD technique was used to verify the amorphous state on the free side of each ribbon. The thermal stability and glass transition were studied by calibrated non-isothermal DSC under a

continuous flow of purified argon. All the samples were tested in a graphite crucible covered with lid at the heating and cooling rates of 5, 10, 20 and 40 K/min.

4. Results and discussions

4.1 Phase equilibria of Mg-Zn-Sr ternary system

The isothermal section of the Mg-Zn-Sr ternary system at 300°C in the portion of 0 to 33 Sr (at. %) was investigated in the present work by using diffusion couples and key-sample methods. Two diffusion couples (wthe end members of Zn - Mg75Sr12.5Zn12.5 and Mg - Mg25Zn55Sr20 at. %) were prepared and annealed at 300 $^{\circ}$C for three weeks. The BSE (back-scattered electron) images of the Zn-Mg75Sr12.5Zn12.5 diffusion couple obtained by SEM is shown in Fig. A1.2. As shown in Fig. A1.2(a), a new solution with a stoichiometry of $Mg_{84-x}Sr_{16}Zn_x$ is in equilibrium with the $Mg_{17}Sr_2$ phase, and was observed in the end member alloy Mg75Sr12.5Zn12.5 (at. %). The other new ternary phase found is $Mg_{92-y}Sr_8Zn_y$ with a large solid solubility in this diffusion couple (Figs. A1.2(a)-(d)). The diffusion path of the Zn-Mg75Sr12.5Zn12.5 diffusion couple is $Mg_{84-x}Sr_{16}Zn_x+ Mg_{17}Sr_2 \leftrightarrow Mg_{92-y}Sr_8Zn_y + MgZn_2 \leftrightarrow Zn_{13}Sr \leftrightarrow Zn$ (hcp) based on the present observed result.

The BSE (back-scattered electron) of the Mg-Mg25Sr20Zn55 diffusion couple obtained by SEM is shown in the Fig. A1.3. The new ternary phase $Mg_{84-x}Sr_{16}Zn_x$ was also observed in the end member alloy of Mg25Sr20Zn55 (at. %) equilibrated with Zn_2Sr phase (see Fig. 0.3(a)). The three-equilibrated-phase microstructure $Mg_{84-x}Sr_{16}Zn_x+ Mg_{92-y}Sr_8Zn_y+ Mg_{17}Sr_2$ was found in the Mg-Mg25Sr20Zn55 diffusion couple. According to the present result, the diffusion paths of the Mg-Mg25Sr20Zn55 diffusion couple are $Mg_{84-x}Sr_{16}Zn_x \leftrightarrow Mg_{92-y}Sr_8Zn_y \leftrightarrow Mg_{17}Sr_2 \leftrightarrow Mg$ (hcp) and $Mg_{84-x}Sr_{16}Zn_x \leftrightarrow Mg_{17}Sr_2 \leftrightarrow Mg$ (hcp) (as shown in Fig. A1.3 (b)). The line scaning on the elements components of diffusion layers are shown in Fig. A.3 (d).
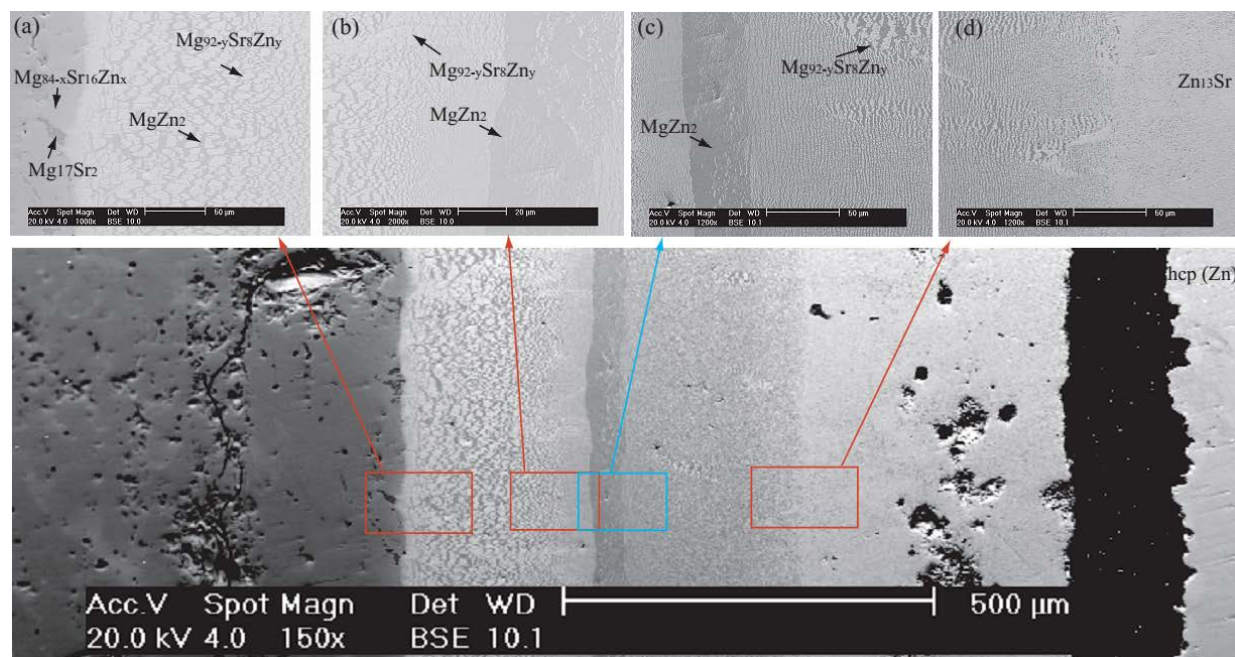
Figure A1.2 The BSE (back-scattered electron) images of the Zn-Mg75Sr12.5Zn12.5 diffusion couple annealed at 300 ^{o}C for three weeks with increased magnification of the area of interest
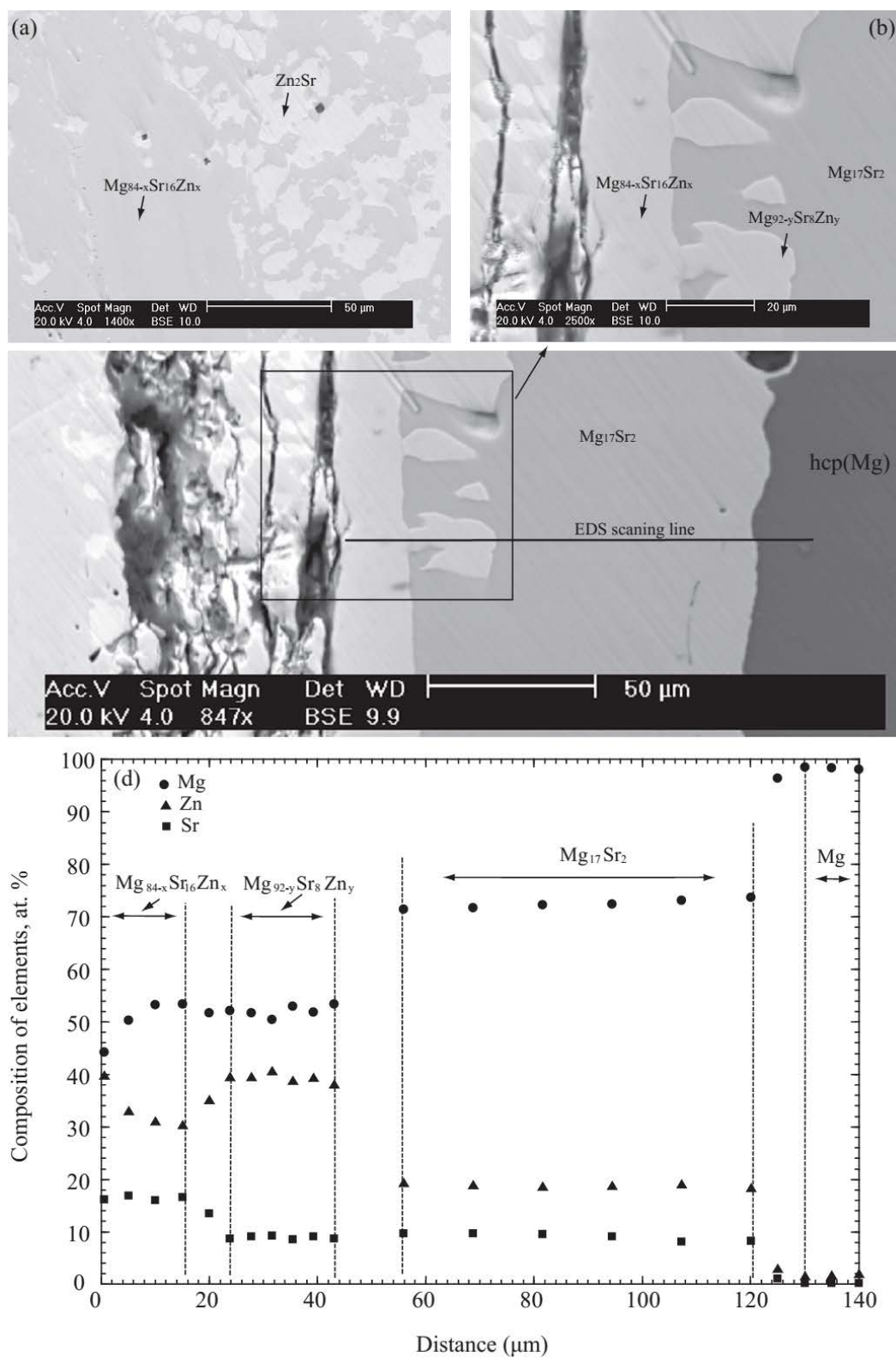
Figure A1.3 The BSE (back-scattered electron) images of the Mg-Mg25Sr20Zn55 diffusion couple annealed at 300 °C for three weeks with increased magnification of the area of interest

The BSE images of a typical ternary Mg-Zn-Sr alloys are shown in Fig. A1.4 (a)-(h). In the Zn-rich portion, the three- phase microstructure $MgZn_2+Zn_{13}Sr+Mg_2Zn_{11}$ was observed in the key sample Mg5Sr5Zn90 (Fig. A1.4 (a)). In the key samples Mg3Sr10Zn87 and Mg16Sr4Zn80 (Fig. A1.4 (b) and (c)), three-phase microstructures were observed, and the new ternary compound $Mg_{92-y}Sr_8Zn_y$ was comfirmed in the equilibrated key sample. According to the present EPMA measurement results based on the equilibrated three- phase microstructure $Zn_5Sr+Zn_{13}Sr+Mg_{92-y}Sr_8Zn_y$ in key sample Mg3Sr10Zn87, the maxmiun solid solubility of Zn in the new phase was measured as 91.7 at. % (thus this new compound was named as $Mg_{92-y}Sr_8Zn_y$).

In the key sample Mg35Sr10Zn55, another new compound $Mg_{33.8}Zn_{49.5}Sr_{16.7}$ was found as shown in Figure A1.4 (d), which was named as $Mg_{84-x}Sr_{16}Zn_x$ in the present work. And this phase is also observed in the other key samples (such as Mg78Sr15Zn7 as shown in Figure A1.4 (h)). And in the key sample Mg45Sr4Zn51 (Figure A1.4 (e)), an equilibrated three- phase microstructure is observed with a third new ternary compound $Mg_{55.5}Sr_{1.6}Zn_{42.9}$, which was named as $Mg_{55}Sr_2Zn_{43}$.

The observation of the equilibrated three-phase microstructures of $hcp+Mg_{55}Sr_2Zn_{43}+Mg_{92-y}Sr_8Zn_y$ and $hcp+Mg_{17}Sr_2+Mg_{92-y}Sr_8Zn_y$ in the key samples Mg45Sr4Zn51 and Mg80Sr5Zn15 (Figure A1.4 (e) and (f)) fixes the maxium solid solubility of Mg as 48.1 at. % in the compound of $Mg_{92-y}Sr_8Zn_y$.
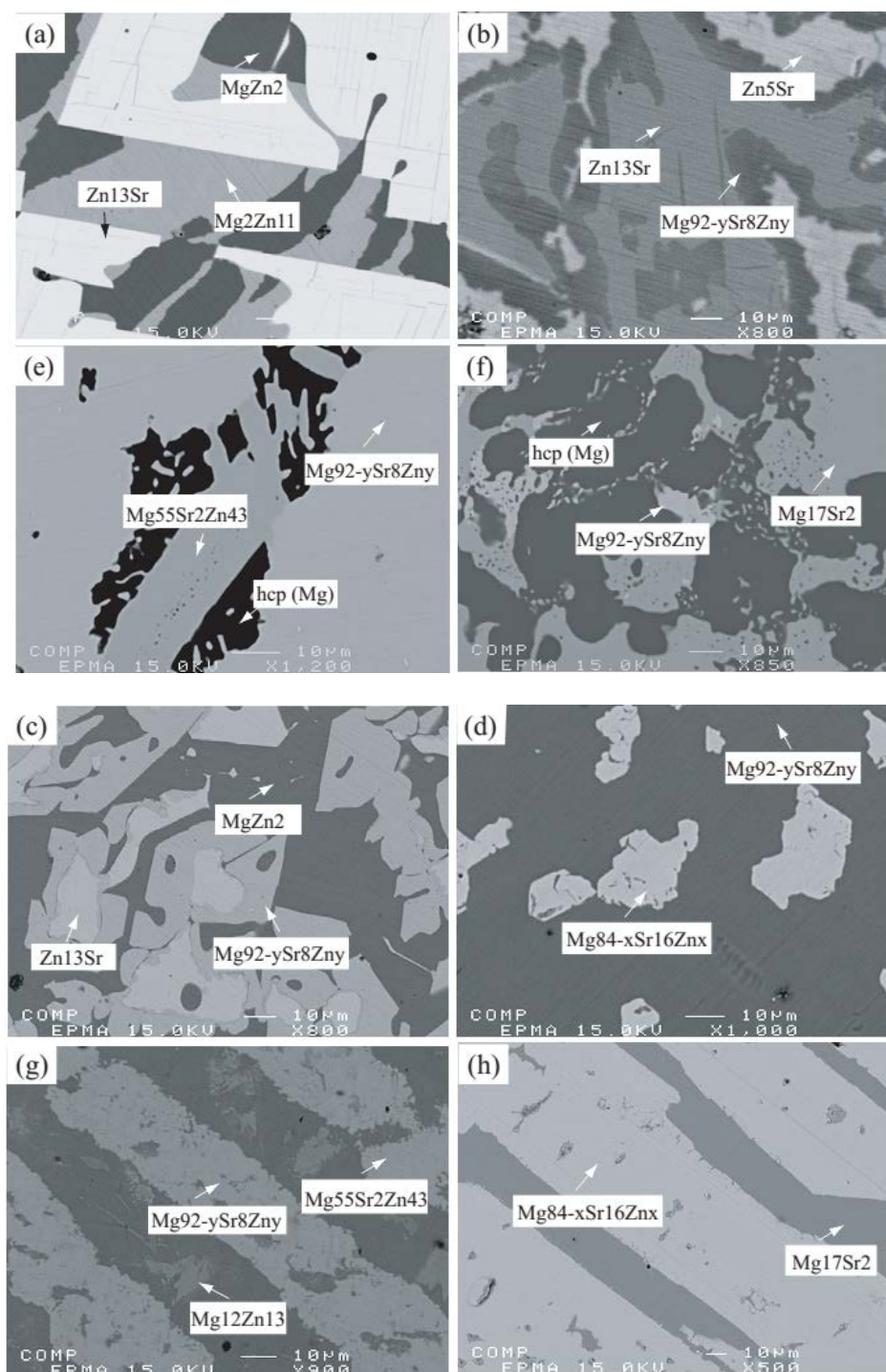
Figure A1.4 The BSE (back-scattered electron) images of typical ternary Mg-Zn-Sr alloys: (a) Mg5Sr5Zn90, (b) Mg3Sr10Zn87, (c) Mg16Sr4Zn80, (d) Mg35Sr10Zn55, (e) Mg60Sr5Zn35, (f) Mg80Sr5Zn15, (g) Mg45Sr4Zn5, (h) Mg78Sr15Zn7 annealing at 300 ^{o}C for 30 days.

The measured Mg-Sr-Zn isothermal section at 300 $^{\circ}$C is shown in Fig. A1.5. Four new ternary compounds $Mg_{20}Sr_{18}Zn_{62}$, $Mg_{84-x}Sr_{16}Zn_x$ ($60 \geq x \geq 3$), Mg_{92-y} Sr_8Zn_y ($85 \geq y \geq 42$) and $Mg_{55}Sr_2Zn_{43}$ (at. %) were observed in this isothermal section. $Mg_{17}Sr_2$ was found to have a ~20 Zn at. % ternary solubility with Zn substituting Mg. There is a limited ternary solubility of Sr in the hcp(Mg) phase, hcp(Zn) phase and Mg-Zn sub-binary compounds. The ternary solubility limits of Mg in Zn_2Sr and Zn_5Sr compounds were observed at about 3.5 and 3 at. %, respectively, and the solubility limit of Mg in the $Zn_{13}Sr$ compound is very limited, at less than 0.1 at. %. All the phase equilibria information obtained in the present work is listed in Table A1.1.
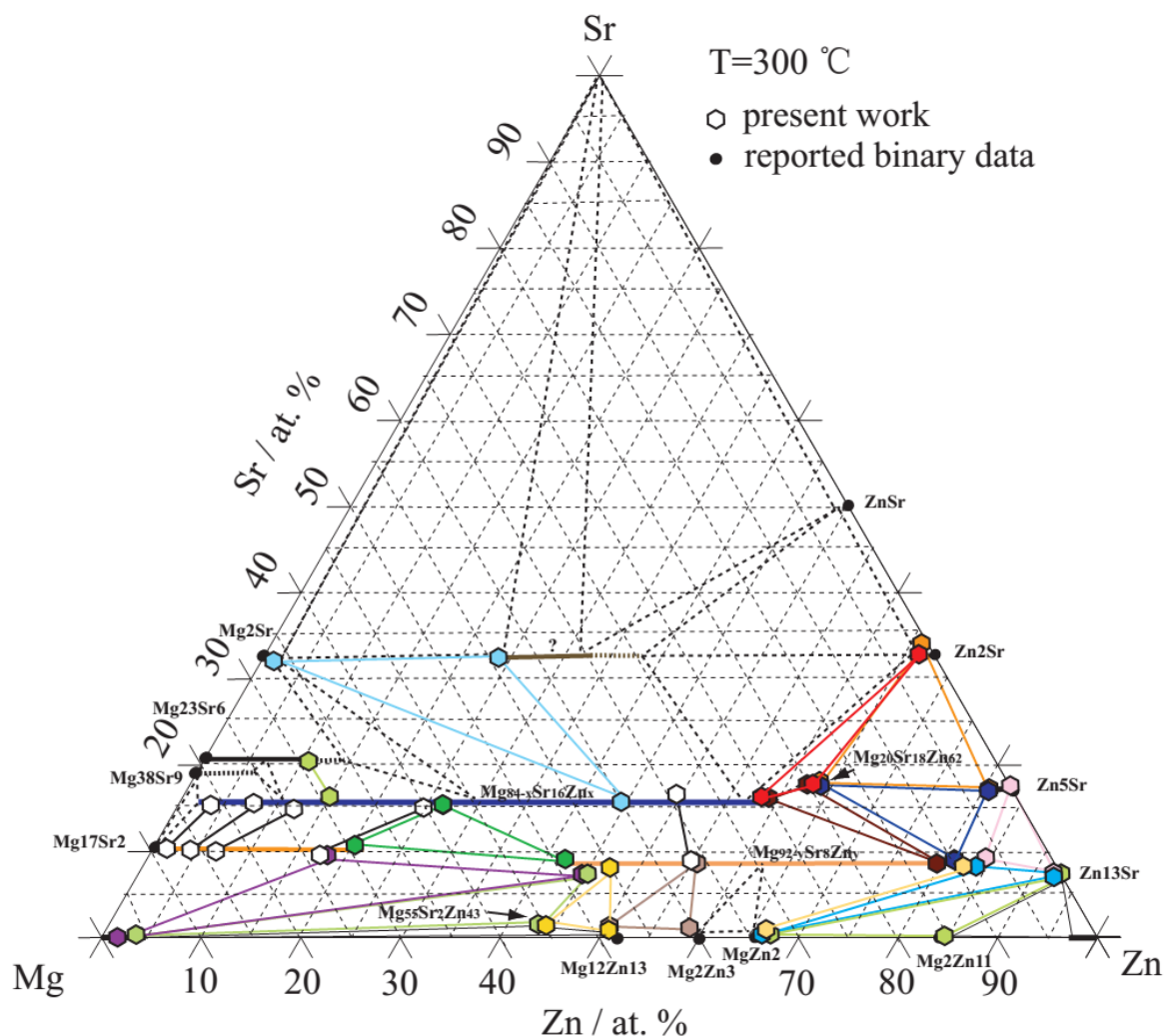
Figure A1.5 Isothermal section of Mg-Zn-Sr ternary system determined experimentally at 300 $^{\circ}$C

Table A.1 Equilibrium compositions in the Mg-Zn-Sr ternary system at 300°C as determined in the present work

Samples Nominal comp. (at. %)	Phase equilibria Phase1/ Phase2/ Phase3	Measured compositions (at. %) (balance is Sr)					
		Phase 1		Phase 2		Phase	
		Mg	Zn	Mg	Zn	Mg	Zn
Mg3Sr10Zn87	$Zn_5Sr/Zn_{13}Sr/Mg_{92-y}Sr_8Zn_y$	0.04	82.59	0.69	91.72	6.60	84.19
Mg5Sr5Zn90	$Mg_2Zn_{11}/Zn_{13}Sr/ Mg_2Zn$	15.33	84.51	0.23	92.66	32.61	67.07
Mg16Sr4Zn80	$MgZn_2/Zn_{13}Sr/Mg_{92-y}Sr_8Zn_y$	33.45	66.23	1.01	92.04	8.07	83.70
Mg5Sr15Zn80	$Mg_{92-y}Sr_8Zn_y /Zn_5Sr/Mg_{20}Sr_{18}Zn_{62}$	9.76	81.19	2.58	80.45	19.07	63.32
Mg10Sr25Zn65	$Zn_2Sr/Zn_5Sr/ Mg_{20}Sr_{18}Zn_{62}$	0.60	65.31	2.06	80.49	18.68	63.22
Mg20Sr15Zn65	$Mg_{92-y}Sr_8Zn_y / Mg_{84-x}Sr_{16}Zn_x$	11.83	79.61	24.89	58.79	20.39	61.84
Mg35Sr10Zn55	$Mg_{92-y}Sr_8Zn_y / Mg_{84-x}Sr_{16}Zn_x$	36.31	54.80	33.84	49.52	—	—
Mg40Sr5Zn55	$Mg_{92-y}Sr_8Zn_y / Mg_2Zn_3/ Mg_{12}Zn_{13}$	35.83	55.44	40.33	58.54	48.37	50.33
Mg45Sr4Zn51	$Mg_{92-y}Sr_8Zn_y / Mg_{55}Sr_2Zn_{43}/ Mg_{12}Zn_{13}$	44.98	46.94	54.60	43.95	48.62	50.58
Mg60Sr5Zn35	$Mg_{92-y}Sr_8Zn_y / Mg_{55}Sr_2Zn_{43}/ hcp$	47.54	45.02	55.49	42.89	96.48	3.20
Mg80Sr5Zn15	$Mg_{92-y}Sr_8Zn_y / Mg_{17}Sr_2/ hcp$	48.11	44.46	72.41	18.06	98.52	1.32
Mg82Sr15Zn3	$Mg_{84-x}Sr_{16}Zn_x / Mg_{17}Sr_2$	81.40	3.25	88.39	1.27	—	—
Mg78Sr15Zn7	$Mg_{84-x}Sr_{16}Zn_x / Mg_{17}Sr_2$	76.98	7.51	86.09	3.73	—	—
Mg83Sr10Zn7	$Mg_{84-x}Sr_{16}Zn_x / Mg_{17}Sr_2$	73.24	11.89	83.65	6.34	—	—
Mg70Sr10Zn20	$Mg_{84-x}Sr_{16}Zn_x / Mg_{17}Sr_2$	60.05	24.76	73.16	17.14	—	—
Mg65Sr10Zn25	$Mg_{92-y}Sr_8Zn_y / Mg_{84-x}Sr_{16}Zn_x /$	48.98	41.98	58.07	26.42	69.18	20.16
Mg70Sr15Zn25	$Mg_{23}Sr_6 / Mg_{84-x}Sr_{16}Zn_x$	69.01	10.47	69.01	14.67	—	—
Mg40Sr15Zn45	$Mg_{84-x}Sr_{16}Zn_x / ?/ Mg_2Sr$	40.06	44.26	43.91	23.46	66.70	1.15
Mg20Sr18Zn62	$Zn_2Sr / Mg_{20}Sr_{18}Zn_{62} /Mg_{84-x}Sr_{16}Zn_x$	1.59	65.45	19.61	62.46	25.88	57.81

4.2 Metallic glass forming ability of selected Mg-Zn-Sr alloys

One of the ways to predict the possible bulk glass composition is the phase diagram calculation with suspending of the formation of intermetallic phases which do not formed congruently. The formation of stoichiometric intermetallic compounds which have the ordered structure of atoms into specific lattice sites needs time for the rearrangement of atoms from the liquid state. Thus, the formation of intermetallic compounds can be suppressed during the fast solidification process normally applied to bulk glass production. The congruent melting compound usual has more negative Gibbs energy, and the cluster composition in liquid solution is close to the composition of congruent melting compound. Consequently, it may be supposed that the formation of congruent melting compound from the liquid solution would be easier than others. In the present work, the congruently melting compounds will be kept in the prediction calculations. Figure A1.6 shows the calculated metastable phase diagram of the Mg-Zn system suppression of incongruent compounds ($Mg_{12}Zn_{13}$, $Mg_{51}Zn_{20}$, Mg_2Zn_3 and Mg_2Zn_{11}) compared with the reported experimental data of glass forming range (Altounian, et al., 1982; Giessen, et al., 1977; Matsuda & Mizutani, 1982). In Figure A1.6, the compostion ranges of the metallic glass formation range are highligthed with colors (below $450^{\circ}C$).

The calculated metastable liquid regions of the Mg-Zn-Sr ternary system at $350^{\circ}C$ and $450^{\circ}C$ is show in Figure A1.7 with the same method as for Mg-Zn binary system with the suspension of the stability of the incongruent phases. Because there is no phase transformation information for the new found tenary compounds, these tenary compounds were suspended in the present calculation.

As shown in Fig. A1.7, the range of stability of the liquid under metstable conditions decreases quickly from 450 $^{\circ}C$ to 350 $^{\circ}C$ at low Sr composition range. From the calculated stable liquid compostion range, one can conclude that the glass forming region will be increased by increasing the Sr content without considering any ternary phases. In fact, two new compounds with large solid solubility were identified, as discussed in section 4.1. Consequently, the possible glass formation range should be limited to 0 to 8 at. % Sr, and to 25 to 40 Zn at.%.

In the present work, 10 samples with the nominal compositions at 2 at.% Sr as $Mg_{88-x}Zn_xSr_2$ ($28 \leq x \leq 38$) and at 5 at.% Sr as $Mg_{85-y}Zn_ySr_5$ ($23 \leq y \leq 37$) (Fig. A1.8) were selected. The XRD
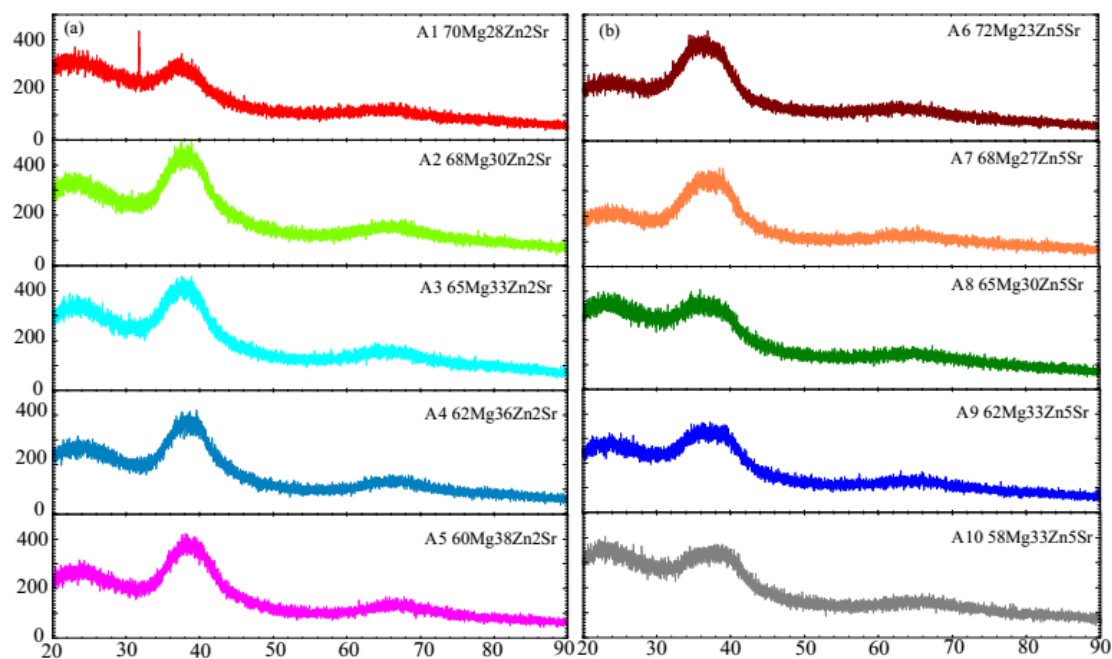
patterns of free side parts of the as-quenched Mg-Zn-Sr metallic glasses obtained by the melt-spinning method are shown in Figure A1.8 (a) and (b). The absence of detectable crystalline diffraction peaks, together with the broad scattering peaks around 37° and 67°, confirmed the amorphous nature of these samples except the sample A1 (70Mg28Zn2Sr). In Figure A1.8, the broad scattering maxima shifts slightly towards higher diffraction angles due to the fact that Zn atoms have a smaller atomic radius than Mg atoms.
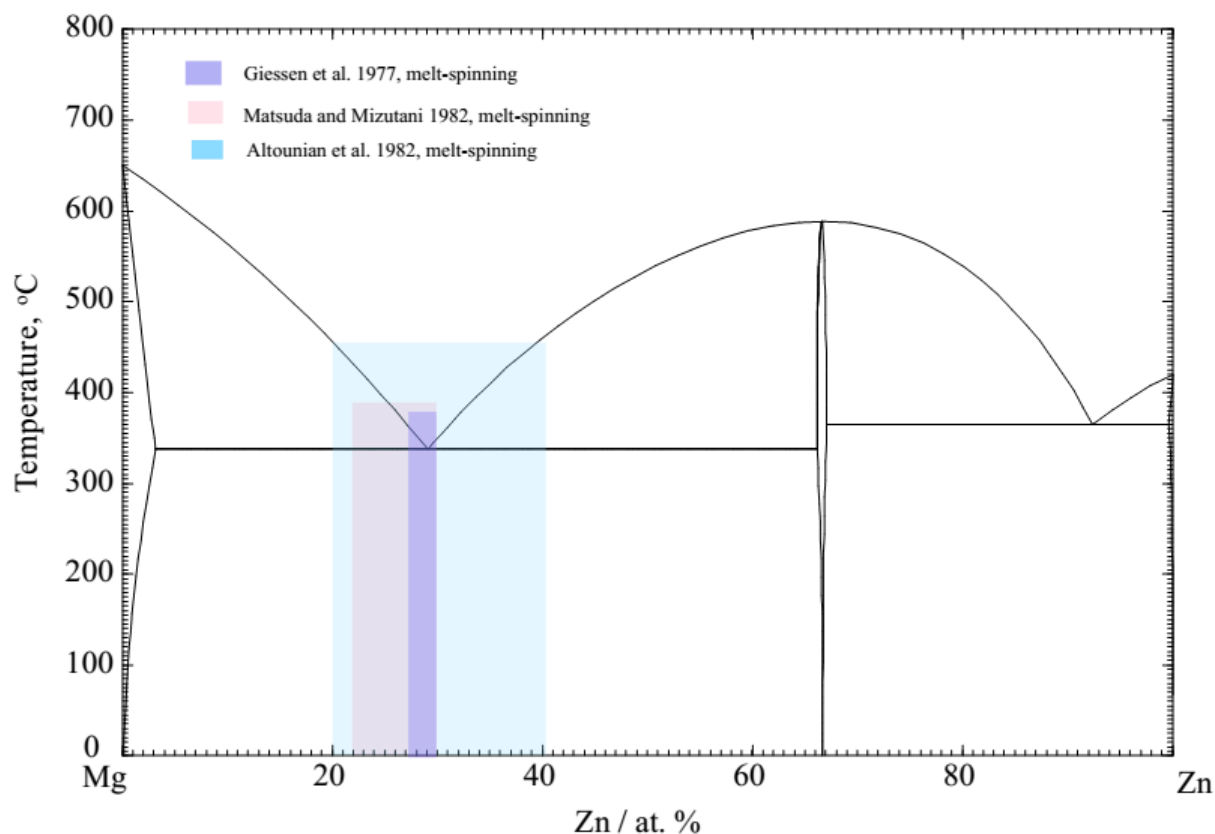
Figure A1.6 Calculated metastable phase diagram of the Mg-Zn system suppression of incongruent compounds ($Mg_{12}Zn_{13}$, $Mg_{51}Zn_{20}$, Mg_2Zn_3 and Mg_2Zn_{11}). The reported experimental data of the glass forming range are given (Altounian, et al., 1982; Giessen, et al., 1977; Matsuda & Mizutani, 1982)
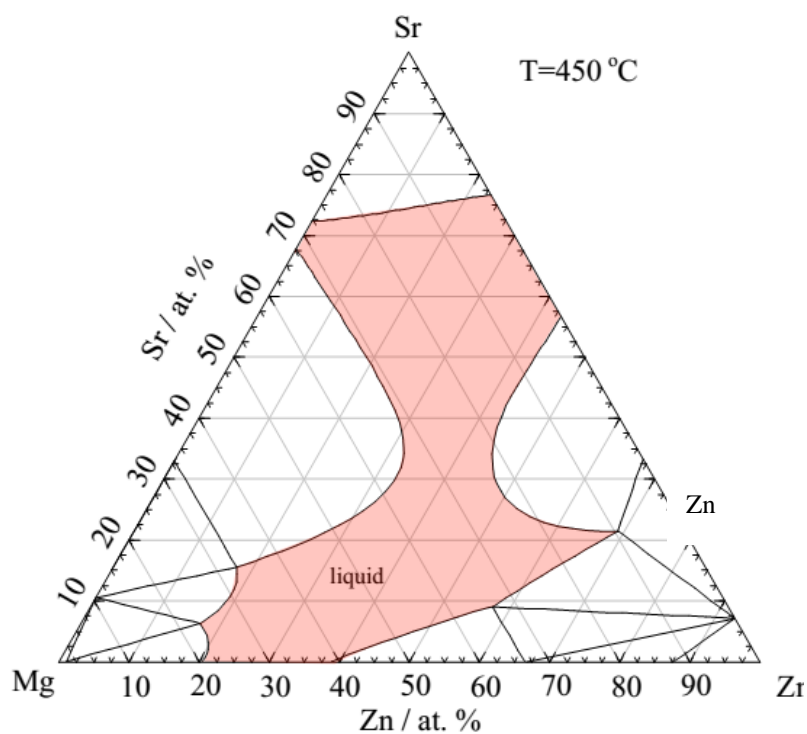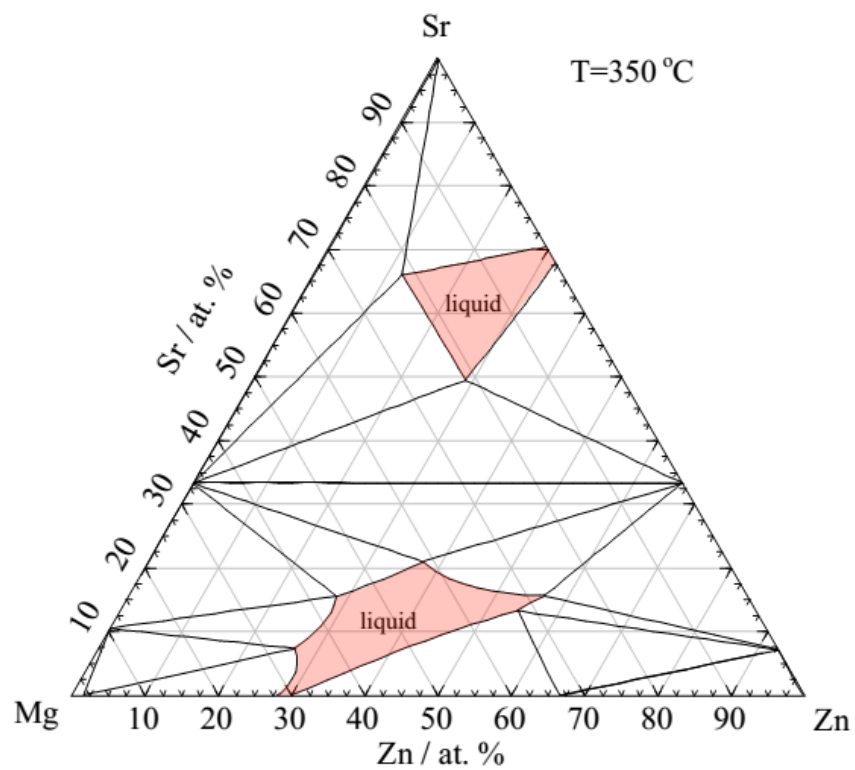
Figure A1.7 Calculated metastable phase diagram of the Mg-Zn-Sr system at 350 °C and 450 °C with the suspension of the formation of incongruent compounds

Figure A1.8 XRD patterns obtained from the free side of the as-quenched Mg-Zn-Sr metallic glasses after melt-spinning with the composition (a) $Mg_{88-x}Zn_xSr_2$ ($28 \leq x \leq 38$) and (b) $Mg_{85-y}Zn_ySr_5$ ($23 \leq y \leq 37$)

The glass transition temperatures and activation properties of the presnt samples were studied by DSC measurements. The composition dependence of the reduced glass transition temperature T_{rg} ($T_{rg}=T_g/T_M$, where T_g is the glass transition temperature, T_M is the melting temperature) of the two series metallic glass is shown in Figure A1.9. In Figure A1.9, the maximum of T_{rg} was found to be 28-32 Zn at. %. And the glass forming ability of the 5 at.% Sr series is better than 2 at.% Sr series.
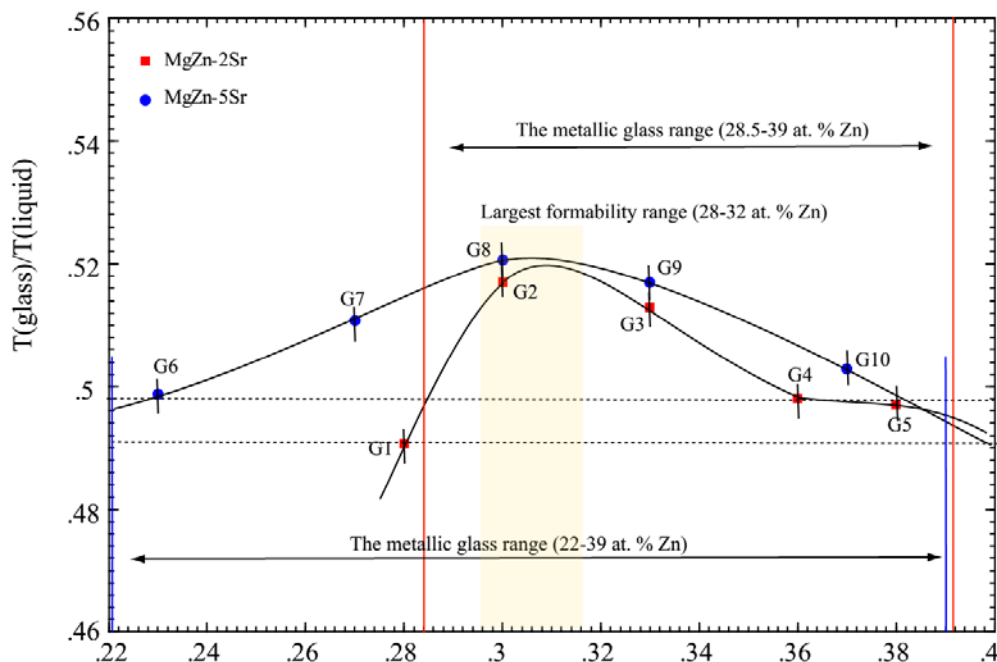
Figure A1.9 The measured composition dependence of the reduced glass transition temperature T_{rg} of the two series of metallic glasses (curves were extraplated from experimental points of G_1-G_{10})

5. Conclusions

Phase equilbria of the Mg-Zn-Sr system at 300 ^{o}C in the 0-30 at. % Sr range were measured in the present work with key-samples and the diffusion-couple method. Four new tenary compounds, $Mg_{20}Sr_{18}Zn_{62}$, $Mg_{84-x}Sr_{16}Zn_x$ ($60 \geq x \geq 3$), Mg_{92-y} Sr_8Zn_y ($85 \geq y \geq 42$) and $Mg_{55}Sr_2Zn_{43}$ (at. %), were found in this isothermal section.

The glass forming ability range of two series of Mg-Zn-Sr alloys at 2 and 5 at.% Sr with the composition within $Mg_{88-x}Zn_xSr_2$ ($28 \leq x \leq 38$) and $Mg_{85-y}Zn_ySr_5$ ($23 \leq y \leq 37$) were studied experimentally in the present work. According to the prediction from calculation, the possible glass formation range should be limited to 0 to 8 at. % Sr, and to 25 to 40 Zn at.%. The glass formation range according to the experimental results of T_{rg} was found to be about 28-32 at. %, which is in a reasonable agreement with the calculation prediction

APPENDIX 2 CLACULATED ENTROPY OF MIXING OF BINARY LIQUID SOLUTIONS IN THE MG-X (X: AG, CA, IN, LI, NA, SN, SR AND ZN) SYSTEM OPTMIZED IN THE PRESENT WORK

In the present work, binary liquid solutions in the Mg-X (X: Ag, Ca, In, Li, Na, Sn, Sr and Zn) multi-component system were modeled using the Modified Quasichemical Model in the Pair Approximation (MQM). The important advantages of MQM over typical Bragg-Williams (BWM) type of models for modeling the thermodynamic properties of liquid solutions, particularly in high-order systems, have been discussed (Sections 1.31, 2.1.2, 4.5, *etc.*) and demonstrated in the present work with comparisons to previous optimized results (with BWM). The MQM takes short-range ordering of atoms into account which allows to reproduce the typical "m" shape of the isothermal entropy of mixing curves, where it is not considered in the BWM. In this Appendix, the calculated entropy of mixing of all binary system optimized in the present work are shown (in figures A2.1 to A2.19) and compared with the previous optimized results (obtained with BWM).

1. Ag-Ca system
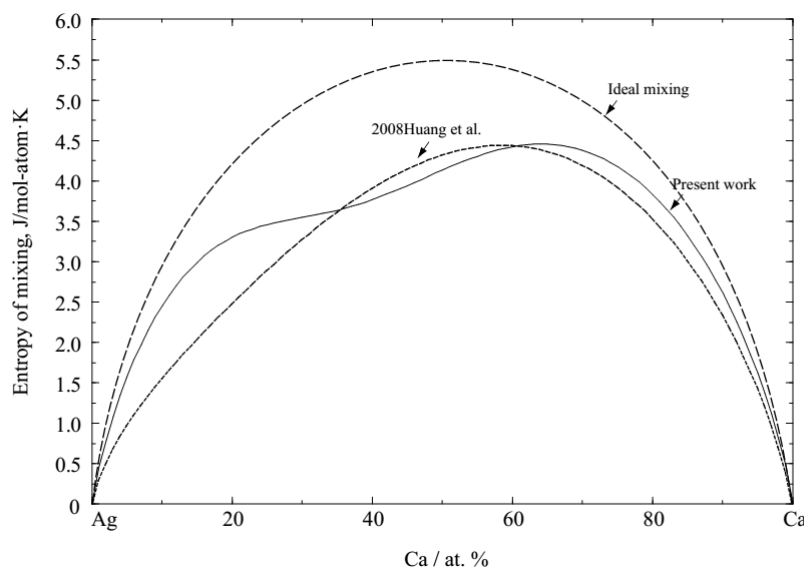
Figure A2.1 Calculated entropy of mixing of the Ag-Ca liquid phase at 1027 ^{o}C in comparsion with the previous calculated results by Huang et al. (Huang, et al., 2008)

2. Ag-In system
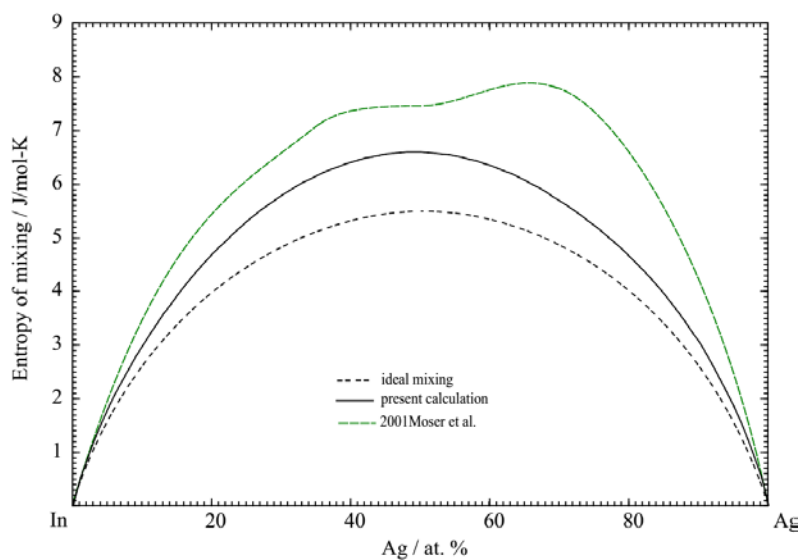
Figure A2.2 Calculated entropy of mixing of the Ag-In liquid phase at 1000 ^{o}C in comparsion with the previous calculated results by Moser et al. (Moser, et al. 2001)

3. Ag-Li system
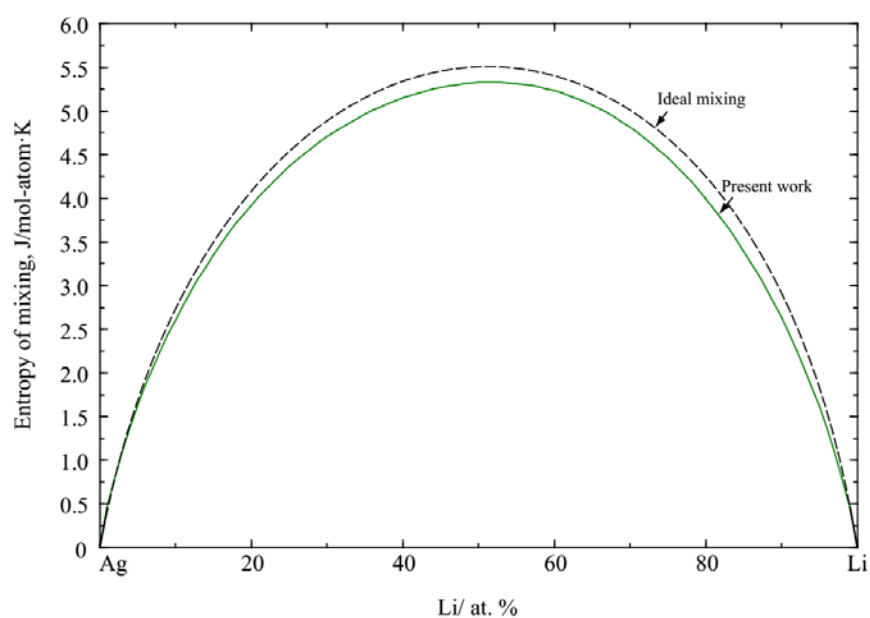
Figure A2.3 Calculated entropy of mixing of the Ag-Li liquid phase at 1100 ^{o}C
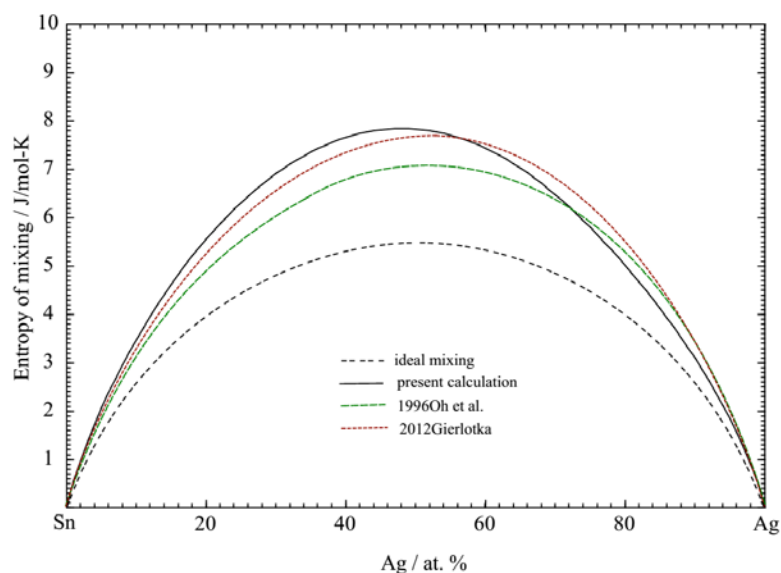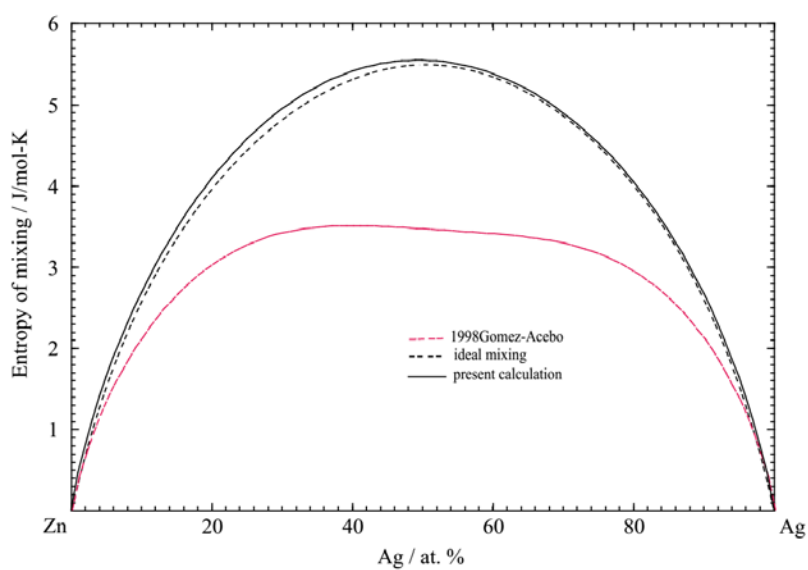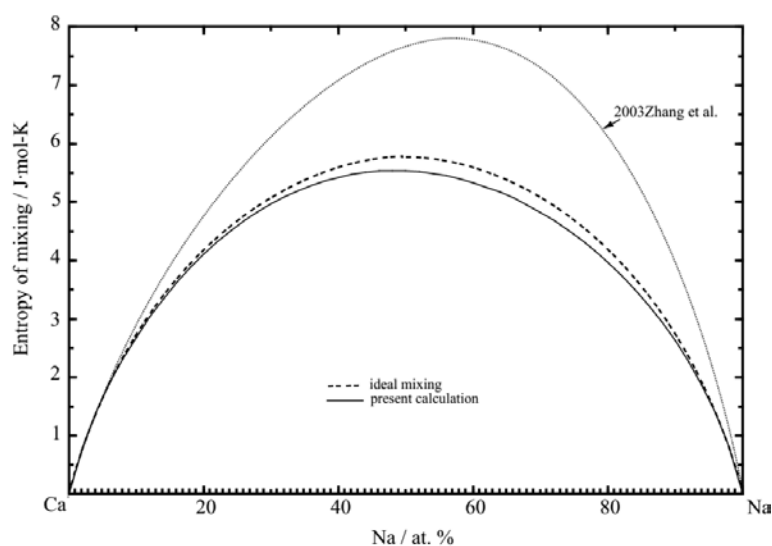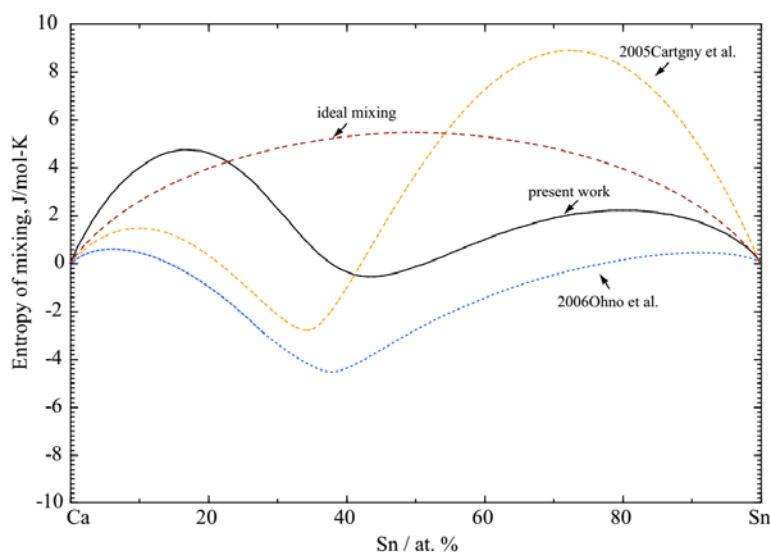
4. Ag-Mg system
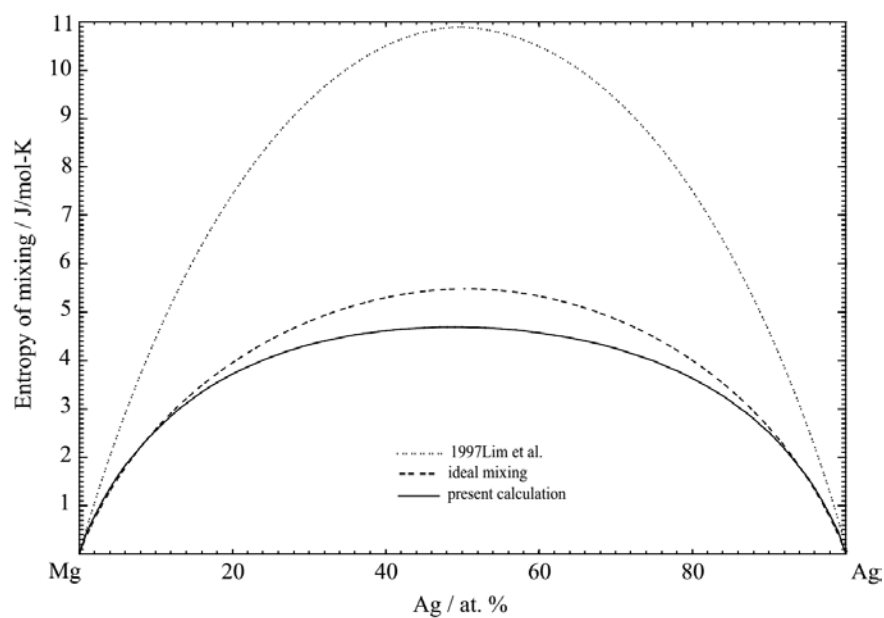
Figure A2.4 Calculated entropy of mixing of the Ag-Mg liquid solution at 1000 $^{\circ}$C with the previous calculated result from Lim et al. (Lim, et al. 1996)

5. Ag-Na system
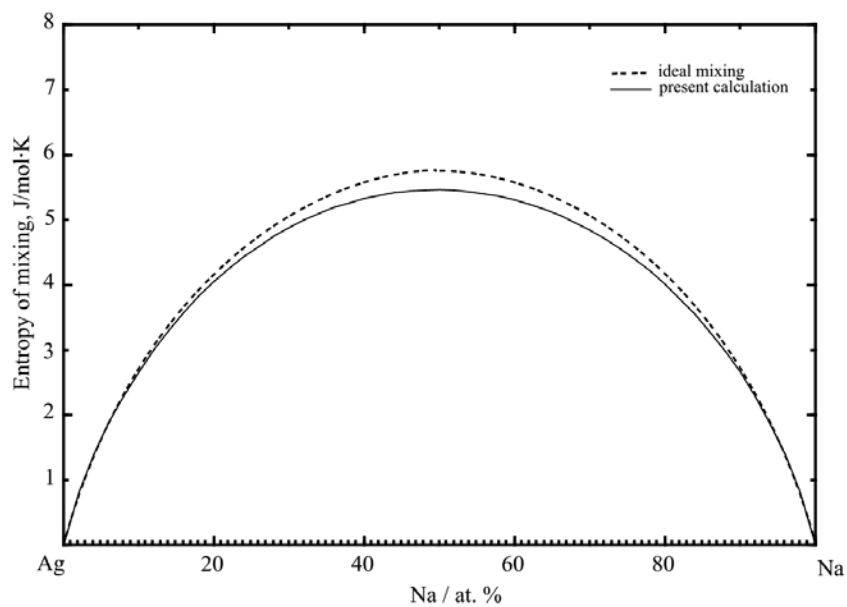
Figure A2.5 Calculated entropy of mixing of the Ag-Na liquid solution at 1000 $^{\circ}$C

6. Ag-Sn system
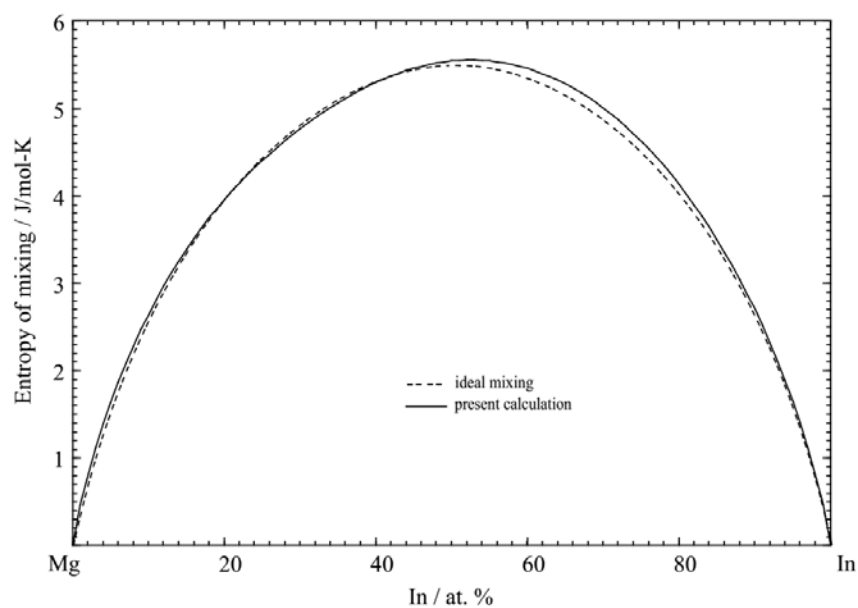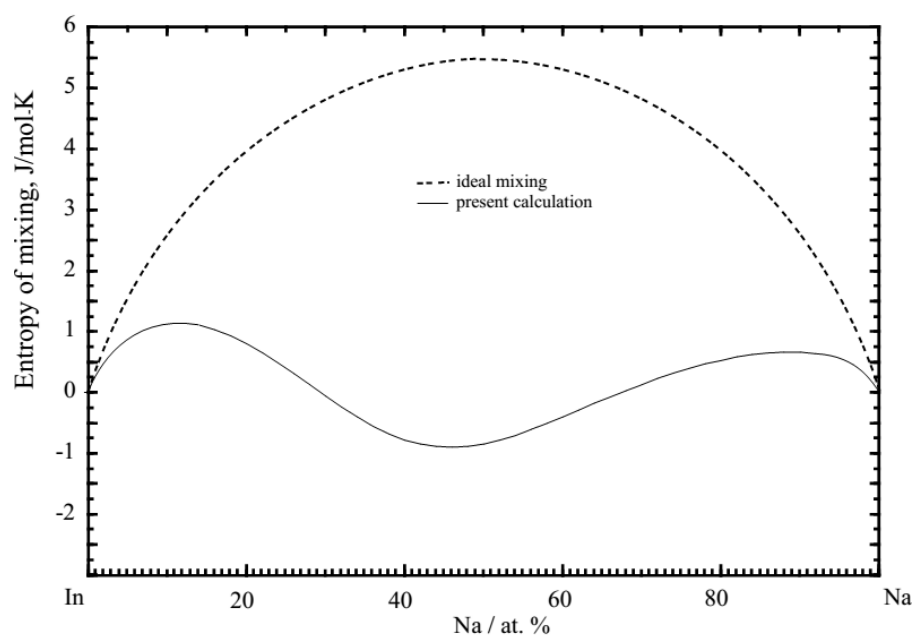

Figure A2.6 Calculated entropy of mixing of the Ag-Sn liquid solution at 1000 °C along with the previous calculated result from Oh et al. (Oh, et al. 1996) and Girlotka (Girlotka, 2012)

7. Ag-Zn system

Figure A2.7 Calculated entropy of mixing of the Ag-Zn liquid solution at 1000 °C along with the previous calculated result from Gomez-Acebo (Gromez-Acebo, 1998)

8. Ca-In system
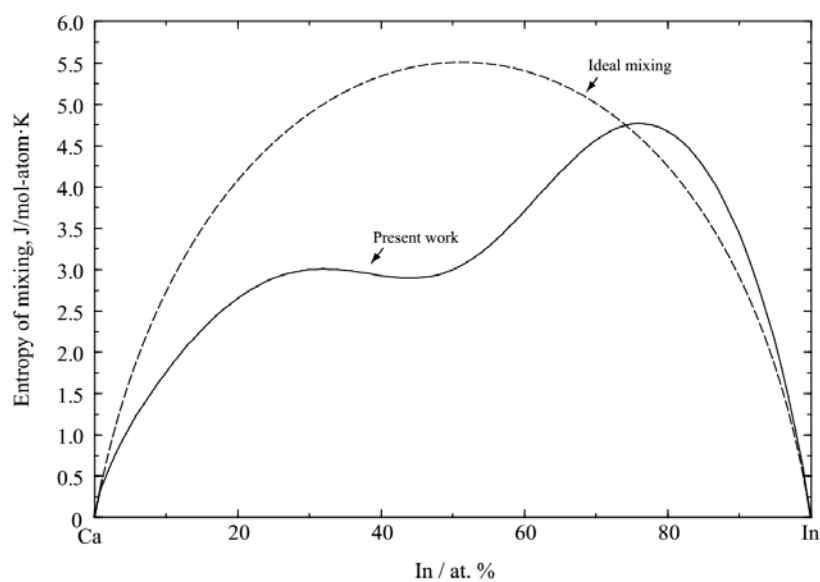
Figure A2.8 Calculated entropy of mixing of the Ca-In liquid solution at 1000 ^{o}C
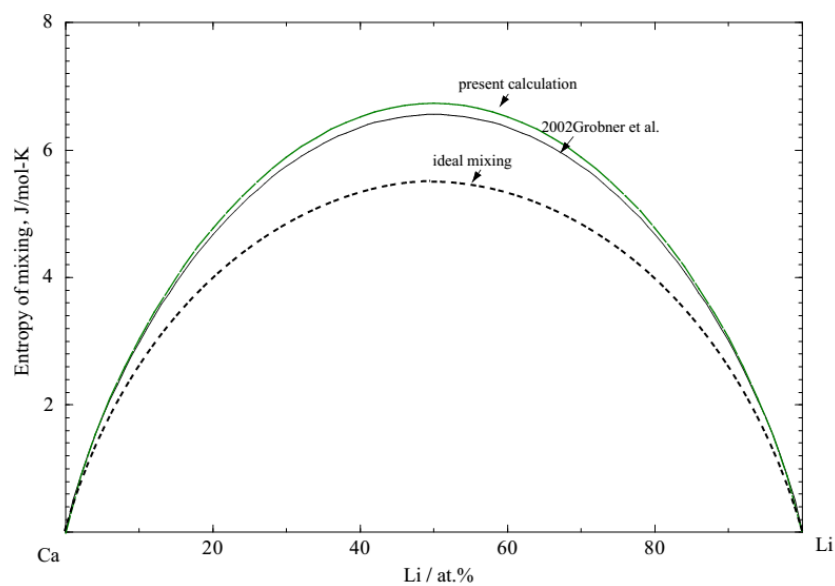
9. Ca-Li system

Figure A2.9 Calculated entropy of mixing of the Ca-Li liquid phase at 1000 ^{o}C in comparison with the previous calculated result from Grobner et al. (Grobner, et al., 2002)

10. Ca-Na system

Figure A2.10 Calculated entropy of mixing of the Ca-Na liquid solution at 1000 ^{o}C in comparison with the previous calculated result from Zhang et al. (Zhang, et al., 2003)

11. Ca-Sn system

Figure A2.11 Calculated entropy of mixing of Ca-Sn liquid phase at 1400 ^{o}C along with the previous calculated results by Ohno et al. (Ohno, et al., 2006) and Cartigny et al. (Cartigny, et al., 2005)

12. In-Mg system

Figure A2.12 Calculated entropy of mixing of the In-Mg liquid phase at 1000 °C

13. In-Na system

Figure A2.13 Calculated entropy of mixing of the In-Na liquid phase at 1000 °C
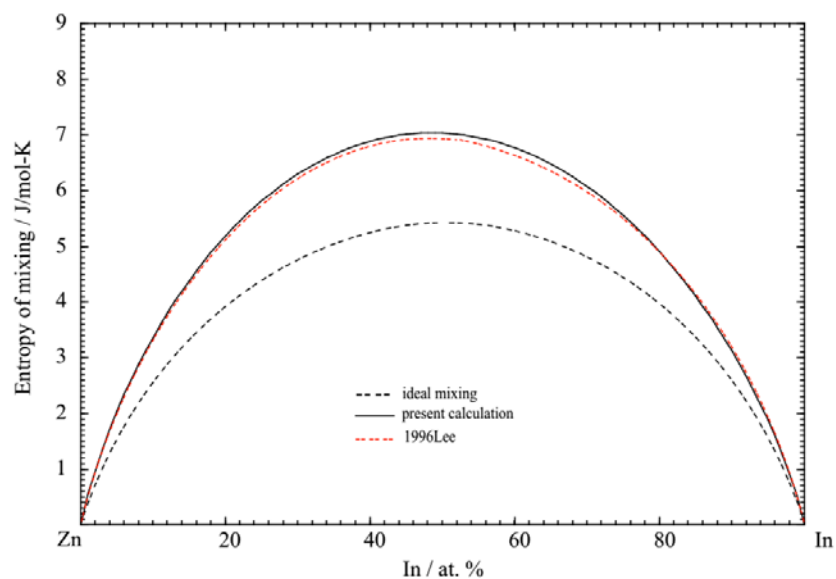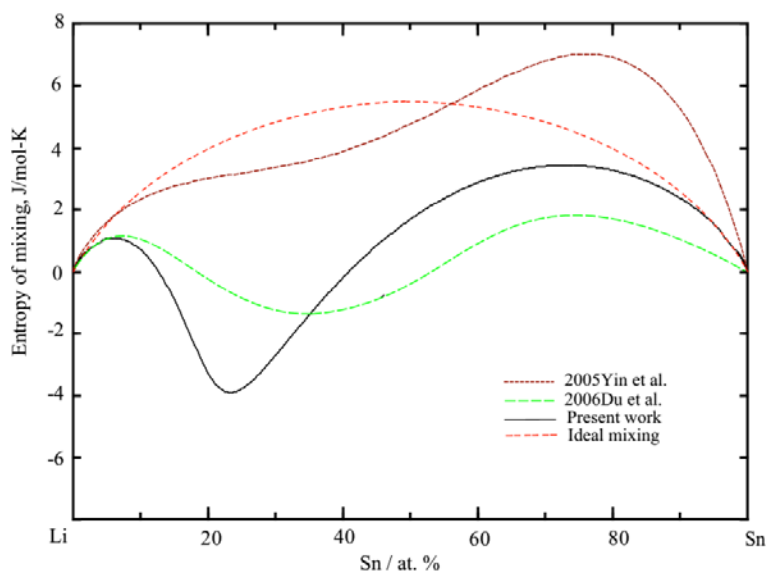
14. In-Sn system
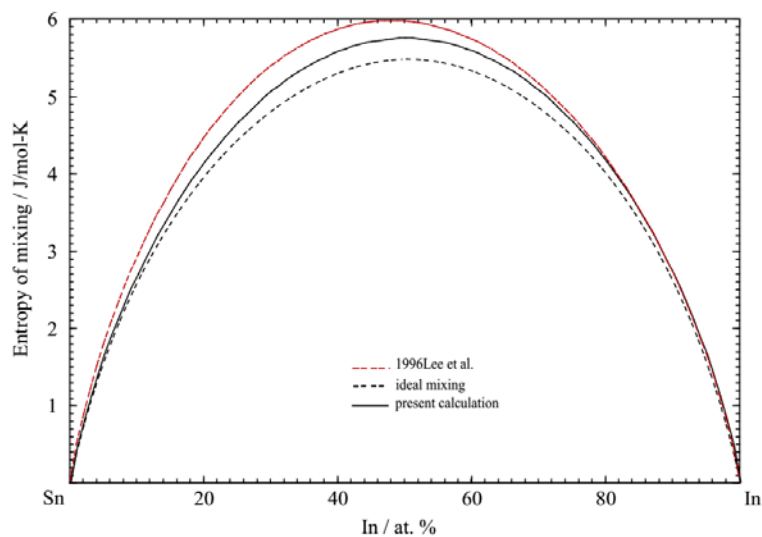
Figure A2.14 Calculated entropy of mixing of the In-Sn liquid phase at 500 ^{o}C with the previous calculated result from Lee et al. (Lee, et al. 1996)
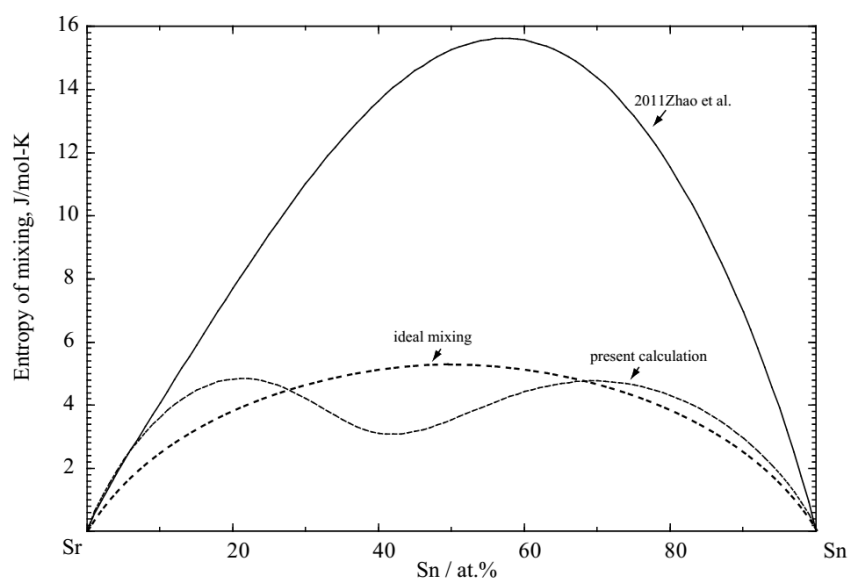
15. In-Zn system

Figure A2.15 Calculated entropy of mixing of the In-Zn liquid phase at 500 ^{o}C along with the previous calculated result from Lee (Lee, 1996)

16. Li-Sn system

Figure A2.16 Calculated entropy of mixing of the Li-Sn liquid phase at 800 $^{\circ}$C in comparison with the previous optimized work from Yin et al. (Yin, et al. 2005) and Du et al. (Du, et al. 2006)

17. Sn-Sr system

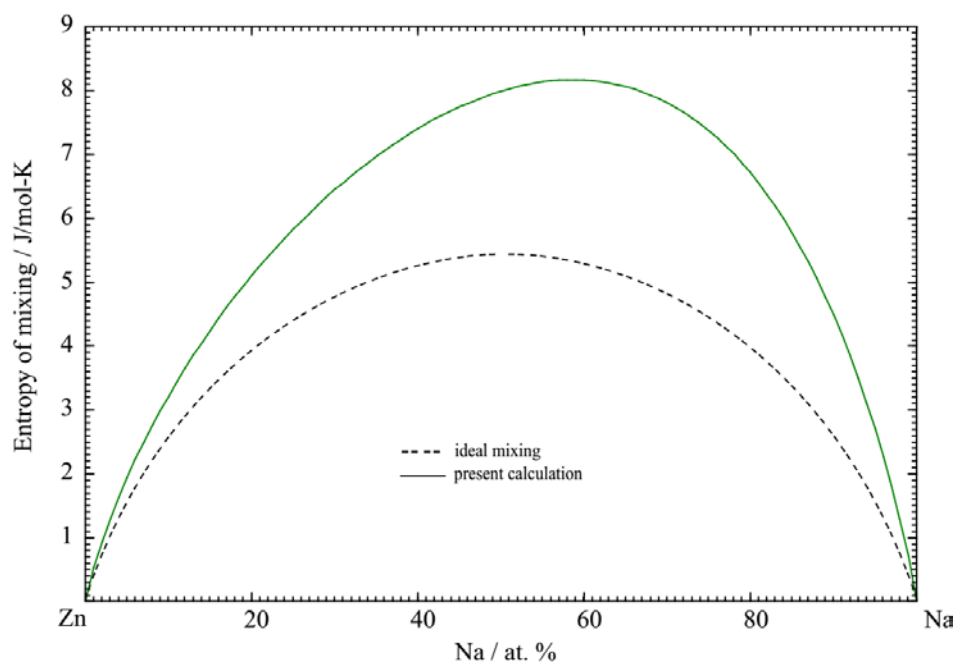**Figure A2.17** Calculated entropy of mixing of the Sn-Sr liquid phase at 1000 $^{\circ}$C along with the previous calculated results from Zhao et al. (Zhao, et al., 2011)

18. Na-Sn system
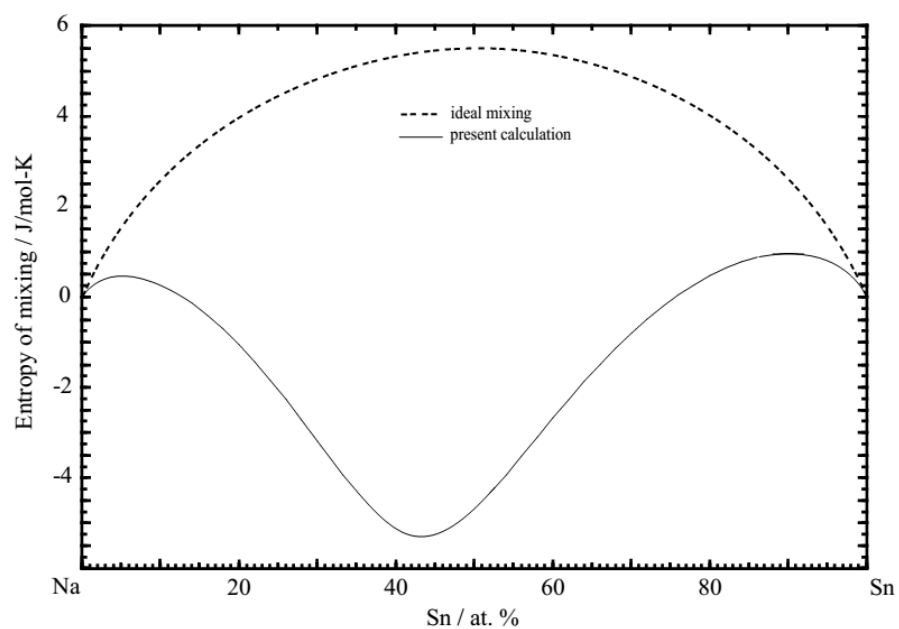
Figure A2.18 Calculated entropy of mixing of the Na-Sn liquid phase at 500 $^{\circ}$C

19. Na-Zn system

Figure A2.19 Calculated entropy of mixing of the Na-Zn liquid phase at 850 $^{\circ}$C